Interplay of Inhomogeneous Currents and Magnetization Textures

D i s s e r t a t i o n

zur Erlangung des Doktorgrades
des Department Physik
der Universität Hamburg

vorgelegt von

S t e l l a n B o h l e n s

aus Hamburg

Hamburg
2010

Gutachterin / Gutachter der Dissertation:	Prof. Dr. Daniela Pfannkuche Prof. Dr. Ulrich Merkt Prof. Dr. Rembert Duine
Gutachterin / Gutachter der Disputation:	Prof. Dr. Daniela Pfannkuche Prof. Dr. Michael Thorwart
Datum der Disputation:	05. Mai 2010
Vorsitzender des Prüfungsausschusses:	PD Dr. Alexander L. Chudnovskiy
Vorsitzender des Promotionsausschusses:	Prof. Dr. Jochen Bartels
Dekan der Fakultät für Mathematik, Informatik und Naturwissenschaften:	Prof. Dr. Heinrich Graener

Abstract

THIS THESIS DEALS with the mutual interaction of non-equilibrium conduction electrons and spatially inhomogeneous ferromagnetic order parameters. For this purpose non-collinear magnetotransport is studied within linear response theory by means of a semiclassical transport framework. Particular emphasis is attached on spin-dependent transport properties with the prospect of spintronics applications. The magnetic vortex is as a selected aspect investigated in detail concerning current-induced magnetization dynamics.

For the case of a magnetic vortex the distinct manipulation of the magnetization texture via the spin-transfer torque phenomenon is exploited in a proposal for an unambiguous writing and reading mechanism for a non-volatile magnetic memory device. A realization of a vortex random-access memory (VRAM) containing vortex cells that are controlled by alternating currents only is proposed. In a collinear electric current and magnetic field arrangement the dynamics of the vortex is entirely controlled by its handedness that is defined as the product of the vortex' boolean, topological quantities chirality and core polarization. The vortex handedness as a bit representation allows direct mechanisms for reading and writing the bit information. The proposed scheme allows transferring the vortex into an unambiguous binary state regardless of its initial state within a sub-nanosecond time scale.

The coupling of electric current and magnetization is investigated on two levels of abstraction. First, for the case of a magnetic vortex the mutual dynamical coupling of current and magnetization is investigated by means of classical electron transport theory with emphasis on non-linear effects. The anisotropic magnetoresistance effect is considered within a classical approach to electrical transport in terms off phenomenological transport coefficients that govern realistic current paths via macroscopic transport equation. This treatment covers the effect of spin-orbit interactions on electron transport and the spin-transfer torque on a macroscopic level. The mutual non-linear dependence of spin-polarized electric current and magnetization dynamics is considered numerically by self-consistently solving the constituting equations, the extended Landau-Lifshitz-Gilbert equation and Poisson's equation. Herefrom, a non-linear influence of the anisotropic magnetoresistance on the vortex gyration is deduced that results in a geometry-dependent renormalization of the spin-transfer torque coupling parameter.

Secondly, a semiclassical transport framework is developed that treats electron and spin transport on equal footing and allows for an accurate description of magnetotransport in spatially strongly varying magnetization textures. The formalism fully accounts for the quantum mechanical nature of the conduction electron's spin degree of freedom while it treats its spatial and momentum degrees of freedom quasiclassically. For general spatially slowly varying magnetization textures the transport coefficients for the charge current, the spin-transfer torque, and the spin-current tensor are derived in terms of microscopic scattering times. Concerning general, spatially slowly varying magnetization textures a

description of adiabatic non-collinear magnetotransport is proposed in terms of a *four channel model* that comprises additionally to the majority and minority spin-channels familiar from collinear magnetotransport, two transverse channels that are responsible for the spin-transfer torque. The resulting expression for the *degree of non-adiabaticity* identifies the intrinsic twist of spin channels in non-collinear magnetization textures as the origin of non-adiabaticity.

In the case of a domain wall the transport framework allows for the analytical computation of the spatially resolved spin-transfer torque, domain-wall resistivity and momentum transfer. They are identified as processes of successive order by a perturbative expansion of the kinetic equation in the magnetization twist. In narrow domain walls it turns out that the treatment of coupled charge and spin transport offers startling insight in fascinating physics in an intermediate transport regime that comprises diffusive charge transport and ballistic spin transport at the same time. In the case of ballistic spin transport the spin-transfer torque as well as the local degree of non-adiabaticity oscillate within the region of the domain wall. For narrow domain walls the degree of non-adiabaticity is strongly enhanced due to spin mistracking and exhibits a sign change in dependence on the domain-wall width that suggests the possibility for a geometrical control of domain wall dynamics and opens new perspectives for memory applications and domain-wall logic. The consistent treatment of charge and spin transport within the semiclassical framework discovers a natural connection between the non-adiabatic spin-transfer torque and the intrinsic domain-wall resistivity as well as the momentum transfer. In particular, the enhanced non-adiabaticity due to spin mistracking is unambiguously identified as the origin of domain-wall resistivity and momentum transfer. The oscillations in the spin-transfer torque, the domain-wall resistivity and the momentum transfer are of quantum origin and emphasize the particular role the spin degree of freedom of the conduction electrons takes with respect to non-collinear magnetotransport. A sign change with the domain-wall width stems from the enhanced coupling of conduction electron spin and local moments in narrow domain walls and sheds light on the long-standing controversy about the sign of the domain-wall resistivity. To observe a sign change a combination of three ingredients is required: consistent treatment of transverse degrees of freedom with respect to spin mistracking, spin-dependent impurity scattering such that the current is carried by the minority electrons, and ballistic spin transport to mediate the coherence within the spin sector.

Inhaltsangabe

Die vorliegende Arbeit befasst sich mit der wechselseitigen Abhängigkeit von Nicht-Gleichgewicht-Leitungselektronen und räumlich inhomogenen ferromagnetischen Ordnungsparametern. Hierzu wird innerhalb der Theorie der linearen Antwort nicht-kollinearer Magnettransport mittels einer halb-klassischen Transporttheorie untersucht. Besondere Beachtung wird dabei auf Spin-abhängige Transport-Phänomene gelegt, die geeignet erscheinen, Verwendung in spintronischen Bauteilen zu finden. Ferner wird der magnetische Vortex als ausgewählter Aspekt strominduzierter Magnetisierungsdynamik eingehend betrachtet.

Anhand der Manipulation der Magnetisierungstextur vermöge des Spin-Drehmoment-Übertrages wird für einen magnetischen Vortex der Vorschlag eines eindeutigen Lese- und Schreibmechanismus für eine nicht-flüchtige magnetische Speichereinheit herausgearbeitet. Eine Realisierung eines Vortex Random-Access Memory (VRAM) wird vorgeschlagen, das aus Zellen aufgebaut ist, die Vortizes enthalten, und einzig durch Wechselströme kontrolliert wird. Hierbei wird die Dynamik der Vortizes in einer kollinearen Anordnung von elektrischem Strom und magnetischem Feld mit Hilfe der Händigkeit des Vortex kontrolliert, die als Produkt der booleschen, topologischen Größen Chiralität und Kern-Polarisierung definiert ist. Die Händigkeit des Vortex bietet neben der Bit-Darstellung insbesondere die Möglichkeit eines direkten Schreib- und Auslese-Mechanismus der Bit-Information. Der vorgeschlagene Entwurf erlaubt es, den Vortex innerhalb einer Zeitskala, die sich unterhalb des Bereichs von Nanosekunden befindet, unabhängig von der Ausgangskonfiguration in einen eindeutigen Binärzustand zu versetzen.

Die Kopplung zwischen elektrischem Strom und Magnetisierung wird auf zwei Abstraktionsebenen betrachtet. Zuerst wird der Einfluss der wechselseitigen dynamischen Kopplung von Strom und Magnetisierung anhand des anisotropen Magnetwiderstandes auf die strominduzierte Vortex-Gyration mittels klassischem Elektronentransport untersucht, wobei besondere Beachtung nicht-linearen Effekten zukommt. Der anisotrope Magnetwiderstand findet in einer klassischen Herangehensweise an den elektrischen Transport vermöge phänomenologischer Transport-Koeffizienten Berücksichtigung, die auf Basis der makroskopischen Transportgleichung die Berechnung realistischer Strompfade regulieren. Der Einfluss der Spin-Bahn-Wechselwirkung auf den Elektronentransport und Spin-Drehmoment-Übertrag wird somit auf makroskopischer Ebene betrachtet. Die Behandlung der wechselseitigen, nicht-linearen Abhängigkeit von spin-polarisiertem Strom und Magnetisierungsdynamik erfolgt numerisch, indem die konstituierenden Gleichungen – die erweiterte Landau-Lifshitz-Gilbert und die Poisson Gleichungen – selbstkonsistent gelöst werden. Hieraus kann ein nicht-linearer Einfluss des anisotropen Widerstandes auf die Gyration des Vortex gefolgert werden, der in einer geometrieabhängigen Renormierung des Kopplungsparameters des Spin-Drehmoment-Übertrages resultiert.

Des Weiteren wird ein halbklassischer Transport-Formalismus entwickelt, der eine gleichberechtigte Behandlung von Elektron- und Spin-Transport und somit eine akkurate Beschreibung von Magnettransport in räumlich stark variierenden Magnetisierungtexturen erlaubt. Während der entwickelte Formalismus die quantenmechanische Natur des Spins des Ladungselektrons vollkommen berücksichtigt, werden räumliche und Impulsfreiheitsgrade quasi-klassisch behandelt. Für generelle, räumlich schwach variierende Magnetisierungstexturen werden die Transportkoeffizienten für den Ladungsstrom, den Spin-Drehmoment-Übertrag und den Tensor des Spin-Stromes in Abhängigkeit von mikroskopischen Streuzeiten berechnet. Soweit es generelle, räumlich langsam variierende Magnetisierungstexturen anbelangt, wird eine Beschreibung adiabatischen, nicht-kollinearen Magnettransports gemäß eines Vier-Kanal-Modells vorgeschlagen, das neben den Majoritäts- und Minoritäts-Spin-Kanälen des kollinearen Magnettransports zusätzlich zwei weitere transversale Kanäle aufweist, die den Spin-Drehmoment-Übertrag konstituieren. Der abgeleitete Ausdruck für den Grad der Nicht-Adiabatizität identifiziert die intrinsische Verdrehung der Spin-Kanäle als dessen mikroskopische Ursache.
Für den Fall einer Domänenwand erlaubt die entwickelte Transport-Umgebung die analytische Berechnung des räumlich aufgelösten Spin-Drehmoment-Übertrages, des Domänenwand-Widerstandes und des Impulsübertrages. Sie werden als Prozesse aufeinander folgender Ordnung einer Störungsentwicklung der kinetischen Gleichung in der Verdrehung durch die Magnetisierungtextur identifiziert. Für besonders schmale Wände stellt sich heraus, dass die gemeinsame Behandlung von gekoppeltem Ladungs- und Spin-Transport überraschende physikalische Einsichten nach sich zieht, sofern diffuser Ladungstransport und ballistischer Spin-Transport vorliegt. Im Falle ballistischen Spin-Transports oszilliert sowohl der lokale Spin-Drehmoment-Übertrag als auch der lokale Grad der Nicht-Adiabatizität innerhalb der Domänenwand. Aufgrund von Spin Mistracking erhöht sich der Grad der Nicht-Adiabatizität in schmalen Wänden drastisch und weist darüber hinaus einen Vorzeichenwechsel in Abhängigkeit der Domänenwandbreite auf, der die Möglichkeit der Kontrolle über die Domänenwanddynamik vermöge der Probengeometrie in Aussicht stellt und somit neue Perspektiven für Speicheranwendungen und Domänenwandlogik aufzeigt. Die konsistente Behandlung von Ladungs- und Spin-Transport innerhalb der geschaffenen halb-klassischen Transport-Umgebung enthüllt auf natürliche Art und Weise die Verbindung zwischen dem Nicht-Adiabatischen Spin-Drehmoment-Übertrag und dem intrinsischen Domänenwand-Widerstand beziehungsweise dem Impulsübertrag. Insbesondere wird die erhöhte Nicht-Adiabatizität aufgrund des Spin Mistracking eindeutig als Ursache des Domänenwand-Widerstandes und Impulsübertrages identifiziert. Die generisch auftretenden Oszillationen im Spin-Drehmoment-Übertrag, im Domänenwand-Widerstand und im Impulsübertrag finden somit ihre Ursache in der quantenmechanischen Natur des Spins und betonen die besondere Rolle, die dem Spin-Freiheitsgrad der Leitungselektronen in nicht-kollinearem Magnettransport zukommt. Die Gegenwart eines Vorzeichenwechsels in Abhängigkeit der Breite der Domänenwand resultiert aus der stark erhöhten Kopplung zwischen dem Spin des Leitungselektrons und der lokalen magnetischen Momente in schmalen Domänenwänden; insbesondere gibt sie Aufschluss über die lang währende Kontroverse um das Vorzeichen des Domänenwand-Widerstandes. Die Existenz eines Vorzeichenwechsels erfordert eine Kombination von drei Voraussetzungen: konsistente Behandlung von transversalen Freiheitsgraden aufgrund des Spin Mistrackings, spin-abhängige Streuung an Verunreinigungen, so dass der Strom hauptsächlich von den Minoritäts-Ladungsträgern getragen wird, und ballistischer Spin-Transport, auf Grund dessen die Kohärenz im Spin-Sektor gewährleistet ist.

Contents

Chapter 1

Introduction

SINCE THE DISCOVERY of the anisotropic magnetoresistance effect in 1856 [1], electron transport in ferromagnetic materials has constantly been a topic of interest. As an intrinsic property of elementary particles the electron possesses both a charge and a spin degree of freedom. In non-magnetic metals the spins of the electrons are usually randomly oriented and do not play a role with regard to transport. In ferromagnets the electric current becomes spin-polarized through spin-dependent electron scattering and magnetotransport in ferromagnetic metals exhibits a lot of features that are absent in non-magnetic metals. [2–4] The essential entrance to magnetotransport in ferromagnetic metals is to recognize the separation of the dynamics of itinerant electrons at the Fermi level from the collective dynamics of the localized moments that constitute the entire Fermi sea. [5] Accordingly, the interplay of currents and magnetization textures relies on an exchange interaction between the spin of the conduction electrons and the localized magnetic moments. In contrast to the elementary charge the spin takes on two possible configurations, up or down with respect to a quantization axis, for instance given by the magnetization. Consequently, transport properties in magnetic materials are spin dependent, i.e., they depend on the two possible configurations for the spin. The exchange interaction between the spin of the conduction electron and the local moments results in transport anomalies and macroscopic quantum effects that are not expected from classical electrodynamics and provide various novel perspectives, for instance for technical utilization or the study of non-equilibrium spin systems. The interdigitation of the charge and the spin degree of freedom of the conduction electron constitutes the central theme of spin electronics, i.e., *spintronics*, research. [6–11] From an application-oriented aspect the incorporation of the spin degree of freedom via the mutual exchange interaction of conduction electrons and local moments opens the way to either manipulate magnetization dynamics by means of an electric current or to alter the current flow by tuning the magnetic configuration. Both mechanisms are prime examples of the research field of spintronics, where the charge of the electron cannot be separated from its spin degree of freedom causing the interdependence of current and magnetization.

In mesoscopic ferromagnets, a multi-domain structure that consists of regions in which the magnetization points in different spatial directions is energetically more favorable than a monodomain. This is due to the long-range demagnetization energy that overcomes the short-range exchange energy in samples of considerable spatial extensions. The individual domains are separated by domain walls, i.e.,

localized topological defects in the magnetization texture, where the magnetization changes continuously. [12, 13] Owing to the exchange interaction, magnetotransport is sensitive to inhomogeneities in the magnetization texture, where a domain wall constitutes the simplest, non-trivial model system. A spin-polarized current traversing a non-collinear magnetization texture exerts a spin-transfer torque on the local magnetization, i.e., a direct transfer of spin-angular momentum between the conduction electrons and the local magnetization due to the exchange interaction. [14, 15] This provides the possibility to manipulate the magnetization configuration by means of a spin-polarized current. As the converse effect to the spin-transfer torque, domain walls are found to modify the electron transport due to their non-collinear magnetization texture. The adiabatic separation in majority and minority spin channels collinear with the local magnetization that applies to wide walls is no longer valid in narrow domain walls as the coupling between the spin of the conduction electron and the local magnetization gets drastically enhanced and the spin channels mix in the non-adiabatic regime. The charge of the electron cannot be separated from its spin degree of freedom and narrow domain walls alter the electrical transport significantly by introducing a contribution to the electrical resistance. It is of experimental evidence that the resistivity correction linked to a domain wall may enhance or decrease the electrical resistivity compared with the case without a domain wall. [16]

Today, the present information technology is based on magnetism and electron transport, whereas until recently the spin of the conduction electron has been ignored and did not receive an application. The discovery of the giant magnetoresistance effect by Grünberg and Fert in 1988 [17, 18], who shared the Nobel Prize for Physics in 2007, marked the dawn of spintronics and denoted a paradigm shift for the storage industry. [6, 7] By exploiting the spin degree of freedom the giant magnetoresistance effect led to a revolutionary increase in the storage capacity of hard disks. The giant magnetoresistance effect provides a read-out of the binary information by purely electronical means and thus replaced the conventional, well-established but inefficient read-out based on Faraday's law by means of an induction coil. [11] The commercial success of the giant magnetoresistance-based devices renewed the interest in the rather old research topic of magnetotransport owing to its technological relevance. In the way the giant magnetoresistance effect serves as the reading mechanism for today's memory devices, its inverse effect, the manipulation of the magnetization by means of the spin-transfer torque effect is a promising candidate to take over the role of the write mechanism in future memory devices. [6, 7, 19–21] Until recently the binary information was entirely written according to Ampère's law by means of the Oersted field accompanying a current flow. This indirect coupling of current and magnetization based on Maxwell's equations of classical electrodynamics faces the problem of scalability. Keeping the current density constant, the current decreases by decreasing the size of a device. The Oersted field whose task is to switch the magnetization within a storage cell is proportional to the current itself. Thus, a higher current density is needed to achieve the field strength necessary for switching. The situation is different concerning the direct manipulation of the magnetization via the current. The spin-transfer torque is proportional to the current density and thus the current needed for switching is reduced by shrinking the size of a device. Moreover, compared with a magnetic field, an electric current is much more appropriate to operate a device, since it can be handled with high precision and it can be spatially restricted. In addition, the employment of electric currents avoids the generic crosstalk between magnetic-based devices due to field leakages. [22, 23] Thus, higher storage

densities as well as shorter access times along with lower power consumption are possible in magnetic random access memories using the spin-transfer torque. Nowadays spin-transfer torque devices consist in the majority of cases of multilayer structures that are composed of magnetic and non-magnetic elements. However, devices with a similar functionality but relying on the displacement of domain walls announce more simplicity in the manufacturing process and, foremost, switching current densities that are up to two orders of magnitude smaller compared with multilayer devices. [24–28] The total current needed to induce domain-wall motion decreases with decreasing system size, whereas the equivalent magnetic field to achieve the same translation of a domain wall increases. [29] Besides being a candidate for information storage [19–21] current-induced domain-wall motion is considered as the future alternative to electronic logic circuits. [24, 28, 30] One utopia is a *chameleon processor* that combines storage and logic within one unit and allows for reconfigurable computing. [11, 24, 28, 31–33]

Due to enormous developments in the processing technology of nanostructures and experimental improvements stimulated by the perspective of technological applications under the advent of spintronics, non-collinear magnetotransport more and more turned into one of the most active research fields in the solid-state research community within the last few years. [16] Collinear magnetotransport is quite well understood since Mott's proposal in 1936 to divide the entire Fermi sea of electrons into two spin-dependent subsystems corresponding to the majority and minority charge carriers each contributing separately and in parallel to magnetotransport. [34] In contrast, the situation with non-collinear magnetotransport is less clear to date and its investigation is restricted to the near past. In the following we understand by non-collinear magnetotransport electron transport in an inhomogeneous, continuous ferromagnet that contains a non-collinear magnetization texture. From a fundamental point of view the interplay between electron transport and magnetization dynamics poses a theoretically appealing problem as it involves the interaction between the non-equilibrium conduction electrons and the localized magnetic moments. In non-collinear magnetization textures the spin degree of freedom of the electron gains importance due to the twist of spin channels in the presence of a spatially varying magnetization texture. This twist affects the electron transport as well as the local magnetization at the same time. Since the beginning there exist two distinct communities, who either focus on the modification of the electron transport or on the magnetization dynamics as induced by spin-polarized currents, although both phenomena are but different aspects of the same mutual exchange interaction. This thesis aims at a different approach: Both phenomena should be considered as being inverse to each other as a separated treatment obscures their intimate relation. By focusing on the response of the conduction electrons to an electric field in the presence of a spatially varying magnetization both phenomena turn out to be different aspects in an unifying treatment. This perspective not only enables the explicit calculation of the spin-transfer torque and the domain-wall resistivity for a given magnetization texture but also provides a natural explanation of both phenomena by mutually causing each other.

It dates back to 1973 when Berger was the first to realize that an electric current provides the possibility of a distinct control of the magnetization. [35] By theoretical considerations he addressed the possibility to drive a domain wall by means of an electrical current. In 1984 it was again Berger who investigated the effect of the force that arises from the reflection of the conduction electrons at

the domain wall. [2] The effect is nowadays referred to as *momentum transfer* and originates from the sd exchange interaction. Earlier in 1978, Berger predicted that the conduction electrons should exert a torque on the domain wall based on the sd exchange interaction that tends to cant the local spins. [3, 36, 37] In 1992 Berger showed that the torque that is nowadays called *spin-transfer torque* can result in a translation of the domain wall driven by a pulsed spin-polarized current. [38]
After the pioneering works of Berger, it lasted until 1996, when Slonczewski [14] and Berger [15] independently developed a theory of magnetization reversal by current in multilayer structures with non-collinear magnetic elements. This discovery paved the path for the distinct manipulation of the orientation of a ferromagnetic layer without the deployment of external magnetic fields. Though the spin-transfer torque responsible for the reversal was essentially the same torque as proposed by Berger in Ref. [38], the technologically appealing propose of magnetization reversal in small pillar structures drew the attention of many solid-state researchers on the topic and entailed extensive studies. [39–46] More and more sophisticated experiments on continuous magnetization textures demanded more elaborate theoretical studies. [5, 47–49] In 2004 Tatara and Kohno succeeded in the derivation of the equation of motions for a rigid domain wall under the influence of a current. [49] The equations of motions are essentially the ones proposed twenty years ago by Berger [2, 38], but are derived from a microscopic theory without phenomenological assumptions and ambiguities. [49, 50] It also dates to 2004, that, after preliminary works by Bazaliy et al. [47] and Fernández-Rossier et al. [51], Zhang and Li proposed the macroscopic description of the spin-transfer torque for general, continuously slowly varying magnetization textures based on the sd exchange interaction. [5] Since then the impact of spin-polarized currents on the dynamics of continuous magnetization textures is described by the meanwhile established concept of the transfer of spin-angular momentum from the conduction electrons to the local magnetization. The seminal work of Ref. [5] featured the introduction of the non-adiabatic spin-transfer torque that accounted for the experimental mystery about the terminal velocity in current-induced domain-wall motion. [26, 52] The phenomenology of the non-adiabatic spin-transfer torque relates the terminal domain-wall velocity to a phenomenologically introduced, constant material parameter, the *degree of non-adiabaticity*, and its relation to the Gilbert-damping. [5] The most remarkable consequence of this proposal is the independence of the degree of non-adiabaticity and thus the terminal domain-wall velocity with respect to the characteristics of the domain wall, i.e., the width and the type of the domain wall. [5, 48] However, the phenomenological introduction of the spin-transfer torque raised the question for its microscopic origin and strength. Accordingly, the microscopic derivation of the phenomenological parameters, the spin-transfer torque coupling coefficient and the degree of non-adiabaticity, is currently one of the most urgent theoretical issues in current-induced magnetization dynamics. [5, 48, 53–60]
The validity of the phenomenological spin-transfer torque as proposed by Ref. [5] is limited to adiabatic magnetotransport through wide domain walls. The adiabatic approximation results in a spatially independent response that provides constant coupling coefficients, which can be regarded as material parameters independent of the details of the magnetization texture. The situation is different in narrow domain walls. As a consequence of the strong spatial variations of the local moments the mixing of spin channels in narrow domain walls allow the anticipation of a spatially inhomogeneous response of the conduction electrons that significantly affects the magnetotransport and the dynamics of narrow domain walls. While in bulk ferromagnets the typical width of a domain wall is determined by the

properties of the material, in ferromagnetic nanowires the transition from wide to narrow domain walls takes place smoothly. Here, the width of a domain wall depends additionally on the sample geometry and can be experimentally tailored. A consistent theory of spin-transfer torque that is also applicable to the technologically relevant narrow domain walls is still missing and the impact of the spin-transfer torque in narrow domain walls, for instance on the equilibrium configuration or on the dynamic of narrow domain walls, is not assessable to date. High precision experiments and the perspective of technological usability substantiates the need for a tractable transport framework that interconnects both impacts of the exchange interaction, the spin-transfer torque and the domain-wall resistivity. Insofar a sophisticated approach to non-collinear magnetotransport is necessary that considers electron and spin transport on equal footing and allows the microscopic derivation of the spin-transfer torque and the electrical resistivity for general magnetization textures. The development of such a transport framework constitutes an essential step towards a consistent description of non-collinear magnetotransport in accordance with current-induced magnetization dynamics.

In this thesis, a transport framework is developed that operates on the interface between spin-transfer torque and domain-wall resistivity and facilitates the description of non-collinear magnetotransport in narrow domain walls. By treating charge and spin transport on equal footing the open gap between the phenomena of spin-transfer torque and domain-wall resistivity is closed. The framework provides explanations for urgent questions, for instance as it concerns the degree of non-adiabaticity or the sign of the intrinsic domain-wall resistivity, and is employed to study the variation of transport coefficients and coupling constants that occur during the crossover from the adiabatic to the non-adiabatic transport regime. This thesis is subdivided into three main parts.

After a short introduction in chapter 2 to the fields of magnetism, current-induced magnetization dynamics and electron transport in non-magnetic metals, chapter 3 presents a memory device that is based on the handedness of a magnetic vortex, which is defined as the product of the intrinsic vortex properties chirality and core polarization. The handedness as a bit representation allows for a writing process that requires no preceding reading operation. The concrete application of current-induced magnetization dynamics in a spintronic device serves as a motivation for the rest of this thesis.

Chapter 4 investigates by numerical simulations the current-driven gyroscopic motion of a magnetic vortex in square thin-film elements in the presence of an inhomogeneous current flow due to the anisotropic magnetoresistance. The consideration of realistic current distributions due to magnetoresistance effects in the resistivity tensor of Ohm's law allows for the self-consistent computation of current-induced magnetization dynamics. A numerical study of the non-linear response of the magnetic vortex with respect to the applied current density is reported.

Chapter 5 is devoted to non-collinear magnetotransport and lays the theoretical foundation for the phenomenological theory as employed in the preceding chapters. First, a general kinetic equation is derived that takes into account coupled charge and spin transport. For the case of general, spatially slowly varying magnetization textures a non-equilibrium solution is presented. Finally, the kinetic

equation is solved perturbatively for the case of an one-dimensional domain wall, which allows for the spatially resolved computation of the spin-transfer torque, the domain-wall resistivity and the momentum transfer.

This thesis ends in chapter 6 and 7 with a conclusion and an outlook.

Chapter 2

Electron transport and magnetism

THIS CHAPTER PROVIDES a basic introduction to the fields of magnetism, current-induced magnetization dynamics and electron transport in non-magnetic metals.

2.1 The sd model of ferromagnetism

A ferromagnet is characterized by undergoing a phase transition at a critical temperature (the Curie temperature T_C). Below T_C the ferromagnet enters an ordered magnetic phase and exhibits a macroscopic magnetic moment. Ferromagnetism is a correlated state in which the spin-rotational symmetry is broken spontaneously due to the exchange interaction. The exchange interaction is an effective spin-dependent interaction that is of purely quantum mechanical origin: Below T_C the electrons within a ferromagnet collectively align their spins and form a macroscopic magnetization in order to reduce the strong Coulomb repulsion between the electrons. [61, 62] Accordingly, ferromagnetism is a collective many-body phenomenon. The Pauli principle requires that the many-body wave function is antisymmetric under particle-permutations due to the fermionic nature of the electrons. The Coulomb repulsion between individual electrons can be reduced by an enhanced spatial separation of the electrons due to a reduction of the overlap of their wave functions. This requires the spatial part of the wave function to be antisymmetric. Due to the Pauli principle this forces the spin part of the wave function in turn to be symmetric and the electrons collectively align their spins and form the macroscopic moment. The order parameter associated with the spontaneous symmetry-breaking is the magnetization $\vec{m}(\vec{r}, t)$.
In ferromagnets the time-reversal symmetry is broken due to the exchange interaction. In theoretical models of ferromagnetism the magnetization is modeled by a Zeeman-like mean field $\vec{m}(\vec{r}, t)$ that acts on the spin of the electrons comparable to an external background magnetic field. [12] The magnetic field analogy is justified through the pseudovector character of the magnetization that is odd under time-reversal.

As proposed by Refs. [2, 3, 5, 49, 63] spin-dependent transport phenomena as the spin-transfer torque and magnetoresistive effects can be understood by recognizing two different kinds of electrons that exhibit a separated dynamic. In a certain class of ferromagnets the dynamics of the itinerant conduction electrons, which carry the electric current and stem from the Fermi surface can be separated

from the localized moments that constitute the local magnetization and originate from the entire Fermi sea. Both kinds of electrons, itinerant s electrons and localized d electrons participate in a mutual sd exchange interaction. In the course of this thesis it will be shown that domain-wall resistivity and spin-transfer torque can be interpreted as different aspects of this exchange interaction. In the sd model of ferromagnetism the electrons are separated into itinerant s electrons that do not contribute to the magnetization and localized d electrons that constitute the local magnetic moments. [64] The sd picture is motivated by the specific band-structure of a certain class of ferromagnets. [34] The d electrons possess quite flat bands that constrain their mobility due to a large effective mass. The flat bands prevent the d electrons from participating in transport. In turn, transport is entirely ascribed to the itinerant s electrons whose interaction with each other is negligible compared to the interaction with the d electrons. Whether the validity of a such model with a separated dynamic is applicable for a given ferromagnet or not must be decided by ab-initio band-structure calculations. [65]
A point of view opposite to the sd model is the picture of an itinerant ferromagnet, where all electrons contribute to the magnetization. [66] Both scenarios, itinerant and sd model, provide extreme cases that do not hold for actual ferromagnets. A realistic ferromagnet is somewhere in between these models. In real materials the hybridization of the d bands with the s band can be quite strong and thus their distinct treatment is often not well justified. [67] However, it turned out that most physical properties of the ferromagnet do not depend essentially on the nature of the employed model. [68]
In the sd model the d electron shells are treated as local moments $\vec{S}$ that interact with the spin of the conduction electrons $\vec{s}$ through the local sd exchange integral $\tilde{J}_{\text{sd}}$

$$\mathcal{H}_{sd} = -\frac{2\tilde{J}_{\text{sd}}}{\hbar}\vec{S}\cdot\vec{s}, \tag{2.1}$$

where $\tilde{J}_{\text{sd}}$ is a measure of orbital overlap between s and d electrons.
The separation in two kinds of electrons is motivated by the different response of the conduction electron $\vec{s}$ and the local moments $\vec{S}$ with respect to an external electric field. While the magnetotransport is provided by fast s electrons close to the Fermi surface, the collective magnetization dynamics involve d electrons from the entire Fermi sea whose response to an electric field is negligible. The high mobility of the s electrons can be understood in terms of that the tunneling matrix element for s electrons is much larger than for d electrons. [69, 70] The itinerant s electrons are delocalized and their extended wave function interacts with a large number of localized moments. Mesoscopic magnetotransport deals with the interaction between conduction electrons and topological defects in the magnetization texture, i.e., domain walls (cf. section 2.4 and 5.1.1 for a detailed discussion of length scales). A domain wall comprises numerous d electrons and constitutes in this sense a macroscopic object. In order to consider the effect of spin relaxation and non-adiabaticity correctly, the spin of the conduction electrons $\vec{s}$ must be treated fully quantum mechanically. [71] The spin of the conduction electron $\vec{s}$ sees a large number of localized moments and only the mean field created by the local moments affects the dynamics of the conduction electrons. Due to strong ferromagnetic correlations between the local moments $\vec{S}$, their collective dynamic is much slower than the dynamics of the spin of the conduction electrons $\vec{s}$. Accordingly, the local moments $\vec{S}$ can be treated as a classical molecular field

$$\langle\vec{S}\rangle = -S\vec{m}(\vec{r},t), \tag{2.2}$$

which neglects quantum fluctuations ΔS of the local moments $\vec{S}$. Equation (2.2) yields usually a very good approximation, as the localized d orbital electron spins $\vec{S}$ possess a very large net spin $S \gg \Delta S$ and exhibit strong ferromagnetic correlations that efficiently suppress quantum fluctuations. This results in much slower semiclassical dynamic of the local moments compared with the dynamic of the spin of the conduction electron $\vec{s}$. [5, 72] The mean-field description as provided by Eq. (2.2) is in accordance with the collective magnetization dynamics in terms of the micromagnetic model as will be discussed in section 2.2 and perfectly suited for the description of mesoscopic magnetotransport (cf. section 2.4 for a detailed discussion). A description of the magnetization dynamics by means of the classical Landau-Lifshitz-Gilbert equation focuses on the long wavelength dynamics and neglects quantum fluctuations that occur on a much shorter time scale.
By considering Eq. (2.2) the sd Hamiltonian of Eq. (2.1) can be rewritten as

$$\mathcal{H}_{sd} = J_{\text{sd}} \vec{\sigma} \cdot \vec{m}(\vec{r}, t), \tag{2.3}$$

where we introduced half the exchange splitting $J_{\text{sd}} := S\tilde{J}_{\text{sd}}$ and employed the representation of spins via Pauli matrices $\vec{s} = \hbar/2\vec{\sigma}$. The sd Hamiltonian in Eq. (2.3) destroys the time-reversal symmetry within the electron system and causes an exchange splitting of the previously degenerate energy levels. Choosing the effective sd Hamiltonian in Eq. (2.3) as a starting point for the derivation of a transport equation, we are not concerned about the microscopic origin of the dynamical, inhomogeneous magnetization $\vec{m}(\vec{r}, t)$. It is sufficient just to assume its existence.

2.2 Micromagnetic model

At long wavelengths the dynamics concerning the ferromagnetic order parameter is phenomenologically described by the micromagnetic model in terms of the Landau-Lifshitz-Gilbert (LLG) equation. [73] The micromagnetic model is a semiclassical continuum model that serves for the description of magnetization dynamics in a certain class of ferromagnets, for instance the transition metal ferromagnets Co, Fe, Ni. Instead of focusing on individual atoms, the micromagnetic model adopts a continuum description of the microscopic spin system in terms of a smooth vector field $\vec{m}(\vec{r}, t)$ that captures the collective, slow magnetization dynamics at mesoscopic length scales. The micromagnetic model is designed to describe magnetization processes, such as magnetic hysteresis and domain-wall motion. In this sense the micromagnetic model provides the link between microscopic quantum theory by containing a continuum expression of the quantum mechanical exchange interaction [74] and the macroscopic theory of Maxwell's electrodynamics. It is an experimentally well justified fact, that along with a small set of parameters the Landau-Lifshitz-Gilbert equation provides an adequate way to describe the spatially non-uniform magnetization dynamics of a ferromagnet in the sub-micrometer regime. The classical mean-field treatment of the magnetization neglects quantum and short-time fluctuations, such as magnetic noise. Owing to the continuum approximation, the micromagnetic model is limited to the description of smooth magnetization textures. This precludes strongly inhomogeneous magnetic configurations on the atomic scale.

An arbitrary magnetic configuration is associated with a distinct free energy. The sum of all pos-

sible magnetic configurations constitutes the free energy functional

$$F[\vec{m}(\vec{r})] = F_{\text{exchange}} + F_{\text{anisotropy}} + F_{\text{Zeeman}} + F_{\text{demagnetization}}, \tag{2.4}$$

of the spatially inhomogeneous magnetic configuration $\vec{m}(\vec{r})$. At temperatures well below the Curie temperature T_C the free energy functional in Eq. (2.4) attains a minimum at a finite magnetization ($\vec{m}(\vec{r}) \neq 0$) that points in an arbitrary direction. The free energy in Eq. (2.4) consists of several contributions that possess clear physical interpretations while their mathematical form can be deduced by symmetry arguments. The micromagnetic model treats the long-ranged magnetic dipole interaction, the strayfield within a ferromagnet, as well as local magnetic interactions such as the Zeeman interaction explicitly while it employs a gradient expansion for the short-ranged quantum mechanical interactions. Zeroth-order gradients in the energy functional are the magnetic or crystalline anisotropy interaction due to spin-orbit interactions and the Zeeman interaction with an external magnetic field. The anisotropy energy sums up band structure effects induced by spin-orbit interaction that try to correlate the direction of the magnetization with the underlying atomic lattice. The leading gradient term that is allowed by spatial inversion symmetry is of second order and is the quantum mechanical exchange energy. The exchange interaction takes into account energy variations due to magnetization gradients and is characterized by the exchange constant A, also called spin stiffness that is a well known material parameter. [72] The microscopic origin of the exchange interaction is the strong Coulomb repulsion between electrons (cf. discussion in section 2.1). Below the Curie temperature the parallel alignment of the electron spins is energetically more favorable for the individual electrons and the exchange interaction reflects the decrease of energy that occurs for a parallel orientation of the magnetic moments. [61, 72]
The different interactions that are associated with the individual contributions to the free energy in Eq. (2.4) act on different length scales. A striking consequence is that for larger samples sizes the magnetic ground state is in general spatially non-uniform. At a certain size of the specimen it is energetically more favorable to divide the whole ferromagnet in magnetic domains with different spatial orientation. [72, 75] The formation of domains is a bulk effect that becomes energetically more favorable with increasing sample size. The separation in magnetic domains reduces the long-range dipolar energy for all spins comprised within the specimen. In contrast, the cost in exchange energy concerns solely the spins at the boundaries of the domains that form the domain wall. [76] Though the magnetic dipole interaction is much weaker than the exchange energy, the dipolar bulk effect prevails at a certain sample size over the expense in exchange energy due to the large number of involved spins. Possible outcomes are highly non-trivial magnetization patterns in dependence of the geometry of the specimen, for instance a domain wall or a magnetic vortex. [77–79]

The formation and time-evolution of a magnetization texture is described by the Landau-Lifshitz-Gilbert equation. It is governed by the effective field that is determined as the thermodynamically conjugate with respect to the magnetization

$$\vec{H}_{\text{eff}} = -\frac{1}{\mu_0 M_s} \frac{\delta F[\vec{m}(\vec{r})]}{\delta \vec{m}(\vec{r})}, \tag{2.5}$$

with constant saturation magnetization M_s. In equilibrium the general form of a dynamic equation for the magnetization that is in accordance with symmetry considerations leads to a Bloch equation

$$\frac{d\vec{m}(\vec{r},t)}{dt} = -\gamma\vec{m}(\vec{r},t) \times \vec{H}_{\text{eff}} + \alpha\vec{m}(\vec{r},t) \times \frac{d\vec{m}(\vec{r},t)}{dt}. \tag{2.6}$$

Equation (2.6) is referred to as the Landau-Lifshitz-Gilbert equation [74, 80] and determines the time-evolution of the magnetization within a ferromagnet, where γ is the gyromagnetic ratio and α is the phenomenological Gilbert damping. [80, 81] In this sense the free energy in Eq. (2.4) allows via Eq. (2.5) and Eq. (2.6) the phenomenological description of the collective magnetization dynamics without dissipation ($\alpha = 0$).

The Landau-Lifshitz-Gilbert equation (2.6) preserves the magnitude of the magnetization at any point in space $\vec{r}$ and time t

$$\begin{aligned}\frac{1}{2}\frac{d}{dt}\left(\vec{m}(\vec{r},t)\right)^2 &= \vec{m}(\vec{r},t) \cdot \frac{d\vec{m}(\vec{r},t)}{dt} \\ &= \vec{m}(\vec{r},t) \cdot \left(-\gamma\vec{m}(\vec{r},t) \times \vec{H}_{\text{eff}} + \alpha\vec{m}(\vec{r},t) \times \frac{d\vec{m}(\vec{r},t)}{dt}\right) \\ &= 0. \end{aligned} \tag{2.7}$$

Accordingly, the magnetization constitutes therefore an unimodular vector field $||\vec{m}(\vec{r},t)|| = 1$ or $\vec{m}(\vec{r},t) = \vec{M}(\vec{r},t)/M_s$, respectively. As a consequence the micromagnetic model is unable to describe abrupt magnetization textures with a strong canting of the local moments on an atomic length scale. Instead, the mesoscopic description of magnetization dynamics via Eq. (2.6) is suited to describe macroscopic magnetization configurations and is thus in accordance with the mesoscopic approach to electron transport as pursued in this thesis (cf. section 2.4).

The first term in the Landau-Lifshitz-Gilbert equation (2.6) describes the precession of the magnetic moments around the effective field that is defined in Eq. (2.5). It points perpendicular to the magnetization and the precession term preserves the energy. To account for dissipation, which is generically present at the macroscopic level, a damping term ($\propto \alpha$) is usually added. The second term in Eq. (2.6) is of phenomenological origin and accounts in a local and isotropic manner for a relaxation mechanism that tends to align the magnetization in equilibrium with the effective field. The Gilbert damping parametrizes a dynamic correction to the instantaneous effective field that accounts for the finite time delay that is needed for all relevant microscopic degrees of freedom to relax to the local magnetization.

Let us prove that the Gilbert damping causes energy dissipation. The rate of change of the total energy reads

$$\frac{1}{\mu_0 M_s}\frac{dF[\vec{m}(\vec{r}),t]}{dt} = \frac{1}{\mu_0 M_s}\int d^3r\, \frac{\delta F[\vec{m}(\vec{r})]}{\delta\vec{m}(\vec{r})}\frac{d\vec{m}(\vec{r},t)}{dt} = -\frac{\alpha}{\gamma}\int d^3r \left(\frac{d\vec{m}(\vec{r},t)}{dt}\right)^2, \tag{2.8}$$

where we employed the Landau-Lifshitz-Gilbert equation (2.6) in the second step in Eq. (2.8). As $\alpha > 0$, it follows from Eq. (2.8) that the change in energy is negative and the Gilbert damping transfers energy from the magnetic system to the lattice. We note that the Gilbert-term is dissipative in the sense that it violates the time-reversal symmetry of the Landau-Lifshitz-Gilbert equation (2.6).

Though this is not part of this thesis, a few remarks concerning the phenomenological damping term are required. First, the assumption of a single scalar damping parameter α instead of a damping tensor that accounts for anisotropic energy relaxation is surely a simplification of the problem. In a huge class of problems this does not matter, as many magnetic quasi-static properties, for instance a magnetic hysteresis, are not sensitive to the damping parameter. In contrast to quasi-static processes, the nature of the damping becomes essential in the investigation of dynamical magnetization processes, for instance domain-wall motion. The introduction of several phenomenological damping constants is not satisfying from a theoretical point of view, as the damping mechanism is under strong debate. [80, 82–91] However, recently a microscopic derivation of the Gilbert damping from relativistic origins succeeded. [92] In particular for conducting ferromagnets, Ref. [93] proposes a spatially dependent damping tensor by assuming that in current-induced magnetization dynamics the main source of energy relaxation is due to Joule heating of the conduction electrons. Due to the spatial dependence of the damping tensor, this can modify the dynamics of narrow domain walls in an essential manner and requires a reexamination of micromagnetic simulations in the case of current-induced magnetization dynamics.

2.3 Spin-transfer torque and transport properties

In conducting ferromagnets the electric current density constitutes a new dynamical variable concerning the manipulation of domain walls. The mutual interaction of the spin of the conduction electron with the domain wall results in a novel class of phenomena. Among these, two complementary mechanisms are commonly accepted to induce domain-wall motion by means of an electric current. Both effects are entirely different in their mode of operation, though both arise from the interaction between the local magnetization and the spin of the conduction electrons. The first effect, the spin-transfer-torque effect, is most important for spatially slowly varying magnetization textures and is proportional to the spin polarization of the current as it transfers spin-angular momentum from the non-equilibrium conduction electrons to the spatially inhomogeneous magnetization texture. The second effect, momentum transfer, takes into account the partial reflection of the conduction electrons at the magnetization texture and is proportional to the charge current that is altered due to the extra resistivity caused by a spatially strongly inhomogeneous magnetization texture. A conduction electron that is reflected by the domain wall transfers its linear momentum to the wall, which results in domain-wall motion. The momentum transfer effect is usually of minor importance except for the case of very narrow domain walls. In this thesis we exclusively investigate domain walls with widths larger than the Fermi wavelength. In this regime the semiclassical description of magnetotransport is valid.

In this section, we will give an introduction to the spin-transfer torque phenomenon, that constitutes the most important and interesting manifestation of the impact of the current onto the magnetization for continuous, spatially slowly varying magnetization textures. We follow the historical development of the spin-transfer-torque effect and start from the idea of angular momentum conservation. By generalizing the spin-transfer torque to situations where angular momentum conservation fails, we arrive at the most recent and most general picture of current-induced torques as caused by current-carrying quasiparticles. We will discuss the proposed mechanisms responsible for the spin-transfer torque and

report about the ongoing controversy that concerns a non-adiabatic contribution to the spin-transfer torque.

In ferromagnetic materials the electric current is spin-polarized due to spin-dependent scattering. This gives rise to the possibility that the spin-angular momentum, as carried by the spin-polarized conduction electrons, is transferred from the non-equilibrium conduction electrons to the local moments, which results in a spin-transfer torque on the local magnetization. Responsible for the transfer of spin-angular momentum is the exchange interaction between the conduction electrons and localized d electrons of the ferromagnet. Without spin-orbit interactions, there are two necessary requirements for the presence of the spin-transfer-torque: a non-equilibrium situation, i.e., a current flow and the presence of a non-collinear magnetization texture.

In 1996 Slonczewski [14] proposed a spin-transfer torque for magnetic, non-magnetic multilayer, for instance F(erromagnet)1/M(etal)/F(erromagnet)2 hybrid systems (spin valves)

$$\vec{\tau}_{\text{Slonczewski}} = -\frac{a_{\text{j}}(\measuredangle(\vec{M},\vec{M}_{\text{P}}))}{M_s}\vec{M}\times(\vec{M}\times\vec{M}_{\text{P}}). \tag{2.9}$$

In the following we denote current-induced torques that can be added to the Landau-Lifshitz-Gilbert equation (2.6) by $\vec{\tau}$. The applicability of Eq. (2.9) is restricted to multilayer systems and can be viewed as the inverse of the giant magnetoresistance effect. The main idea behind Eq. (2.9) rests on the concept of conservation of spin-angular momentum. A net flux of spin current into a volume of magnetic material results in a torque that acts on the same volume. Equation (2.9) is a macrospin equation and $\vec{M} = M_s\vec{m}$ represents the uniform magnetization of the free ferromagnetic layer F2 with saturation magnetization M_s, while $\vec{M}_{\text{P}}$ symbolizes the magnetization of the fixed layer that acts as a spin-polarizer for the electric current traversing the multilayer structure. The macrospin approximation assumes that spatial variations in the magnetization texture within a sample are frozen out. Then, the magnetization remains spatially homogeneous within each layer and can be treated as one macrospin. a_{j} is a model-dependent function proportional to the current density, which depends on the relative orientation between the fixed and the free layer.
It took about two years from the proposal and mathematical formulation of the spin-transfer torque in magnetic multilayers [14] to its generalization for arbitrary, spatially slowly varying magnetization textures by Bazaliy et al. in 1998. [47] Guided by the idea that there must exist a general counteraction of the current onto the magnetization, Ref. [47] proposed a continuum generalization of the spin-transfer torque within a ballistic transport model for half-metallic materials. [14, 15, 36] Later in 2003, Fernández-Rossier et al. [51] recognized that it is the spin current rather than the charge current that affects the magnetization dynamics. In this manner, Ref. [51] generalizes the result of Ref. [47] from half-metallic to arbitrary ferromagnets. Taking both findings together, this results in a straightforward manner in the final form of what is nowadays called the adiabatic spin-transfer torque

$$\vec{\tau}_{\text{ad}}(\vec{r}) = -\frac{\mu_{\text{B}}P}{eM_s}\vec{M}(\vec{r})\times(\vec{M}(\vec{r})\times(\vec{j}_{\text{e}}(\vec{r})\cdot\vec{\nabla}_{\vec{r}})\vec{M}(\vec{r})). \tag{2.10}$$

Here P is the diffusive spin polarization of the electric current $\vec{j}_{\text{e}}(\vec{r})$ that links the charge current to the spin current.

It is worth noting, that the adiabatic spin-transfer torque of Eq. (2.10) and the Slonczewski torque for multilayer structures in Eq. (2.9) exhibit similar mathematical forms. Due to the double cross product both kinds of spin torque have in common that the resulting torque on the magnetization vanishes when the magnetization texture is collinear. A closer examination reveals, that the Slonczewski torque in Eq. (2.9) is a special case of the adiabatic spin-transfer torque in Eq. (2.10) that is valid for continuous slowly varying magnetization textures: Integration of Eq. (2.10) across the layers by assuming a homogeneous monodomain for each layer, as required by the macrospin approximation, directly recovers Eq. (2.9) from Eq. (2.10). But caveat, as the strength of the Slonczewski torque in multilayers is mainly determined by the non-magnetic interface, the spacer layer, the prefactor a_{j} in Eq. (2.9) cannot be identified with the diffusive spin polarization P of the bulk ferromagnet. Moreover, it can be orders of magnitude larger in dependence on the properties of the interface. [94, 95]

In the adiabatic regime it is assumed that the magnetization varies spatially slowly and thus the spin direction of the non-equilibrium conduction electrons follows the magnetization adiabatically. This situation holds for continuous ferromagnets with wide domain walls, such that the spin of the conduction electrons has enough time to comply with the local magnetization. As addressed by Li and Zhang [94, 96], the adiabatic spin-transfer torque in Eq. (2.10) follows directly from the adiabatic approximation that the polarization of the spin current is aligned with the local magnetization. In this case the spin-current tensor can be assumed to be the tensor product of the flow direction of the conduction electrons $\vec{j}_{\mathrm{e}}(\vec{r})$ and the local magnetization $\vec{m}(\vec{r})$ [94, 96]

$$\hat{J}_{\mathrm{ad}}(\vec{r}) := \frac{\mu_{\mathrm{B}} P}{e M_s} \vec{j}_{\mathrm{e}}(\vec{r}) \otimes \vec{m}(\vec{r}). \tag{2.11}$$

At this point of the discussion, we will focus on the idea of conservation of spin-angular momentum [95] that allows computing the spin torque by considering the net change in spin current before and after the interaction with the magnetization of the ferromagnet. The argument of angular momentum conservation serves to relate the spin-transfer torque directly to the angular momentum as lost or gained by means of the spin current. This is sometimes referred to as the *bookkeeping* theory of spin-transfer. [95] Whenever the flow of spin-angular momentum has sources or sinks, the spin current is not conserved and spin-transfer torque arises due to the transfer of spin-angular momentum. A necessary condition for a non-conserved spin current are inhomogeneities in the magnetic configuration. In spatially varying magnetization textures, $\vec{\nabla}_{\vec{r}} \vec{m}(\vec{r}) \neq 0$, the spin current in Eq. (2.11) is not conserved. The prime examples are either a non-collinear magnetization configuration in a multilayer structure, for instance a spin valve, where the spin current is filtered by the adjacent ferromagnetic layer oriented non-collinear to the first layer or an extended domain wall as a special case of a spatially inhomogeneous magnetization pattern. In both cases the flow of spin-angular momentum is altered by the magnetization that exerts a torque on the spins of the conduction electrons in order to reorient them. Vice versa, due to conservation of angular momentum the non-equilibrium conduction electrons exert an opposite torque of equal strength on the magnetization of the ferromagnet – the spin-transfer torque.

A torque is the time rate of change of angular momentum and by conservation of angular momentum, the spin torque can thus be related to the loss or gain of the spin-angular momentum of the spin current. To capture these ideas more quantitatively, let us define the spin-current density $\hat{J}_{\vec{k}}(\vec{r})$ as in

Eq. (2.11) by a tensorial quantity, which has both, a direction of flow in real space and a direction in spin space. Relying on conservation of angular momentum, the spin-transfer torque acting on the magnetization of a small volume of the ferromagnet is determined by the net flux of non-equilibrium spin current through the surface of the small volume V

$$\vec{T}_{\text{STT}} = -\int_{\partial V} d^2r\, \hat{\vec{n}}\hat{J}(\vec{r}), \tag{2.12}$$

where $\vec{r}$ is the spatial position and $\hat{\vec{n}}$ is the interface normal for each surface of the volume V. Due to the theorem of Gauß, Eq. (2.12) is equivalent to the volume integral over the divergence of the spin-current density within the small volume

$$\vec{T}_{\text{STT}} = -\int_{V} d^3r\, \vec{\nabla}_{\vec{r}}\hat{J}(\vec{r}). \tag{2.13}$$

Due to the tensorial nature of the spin-current density $\hat{J}_{\vec{k}}(\vec{r})$, its spatial divergence is a vector in spin space. However, the magnetization dynamics is governed by the spin-torque density. [5] From the differential form of Eq. (2.13) it follows that the spin-torque density is given by the divergence of the spin-current density [94]

$$\vec{\nabla}_{\vec{r}}\hat{J}_{\text{ad}}(\vec{r}) = \frac{\mu_{\text{B}}P}{eM_s}\vec{\nabla}_{\vec{r}}(\vec{j}_{\text{e}}(\vec{r}) \otimes \vec{M}(\vec{r})) = \frac{\mu_{\text{B}}P}{eM_s}(\vec{j}_{\text{e}}(\vec{r}) \cdot \vec{\nabla}_{\vec{r}})\vec{M}(\vec{r}), \tag{2.14}$$

where we considered local charge neutrality $\vec{\nabla}_{\vec{r}}\vec{j}_{\text{e}}(\vec{r}) = 0$ in the second step of Eq. (2.14). The torque in Eq. (2.14) is exactly the adiabatic spin-transfer torque of Eq. (2.10) as derived by Refs. [47, 49, 51, 94, 96, 97].

The situation sketched thus far is known as the *bookkeeping* theory of the spin-transfer torque, where it is assumed that the total spin-angular momentum is entirely transferred from the spin current to the local magnetization. In the course of time, discrepancies between theory and experiment required the development of a more general concept of the spin-transfer-torque. [5] From a theoretical point of view, according to Ref. [95], the main obstacles with the *bookkeeping* theory are:

- In the *bookkeeping* theory of the spin-transfer, the distinct difference between the conduction electrons and the localized electrons that constitute the magnetization is not obvious. In particular for transition metal ferromagnets it is well known that both kinds of electrons participate in transport (cf. section 2.1).

- The *bookkeeping* theory of spin-transfer is based on conservation of spin-angular momentum. The question at hand is, whether spin-transfer also occurs in systems with strong spin-orbit interaction where the spin-angular momentum is not conserved.

These inconveniences have been resolved by the introduction of a more general concept of the spin-transfer torque [5, 48, 49]: The current-induced torques arise from a misalignment between the current-carrying quasiparticles, the induced magnetization of the non-equilibrium conduction electrons and the collective degrees of freedom comprised within the ferromagnetic order parameter. At

this point it is necessary to briefly comment on the concept formation for the current-carrying quasiparticles. Within the giant magnetoresistance or tunneling magnetoresistance community the out-of equilibrium magnetization of the conduction electrons is called spin accumulation in diffusive systems, whereas it is called spin density in ballistic systems. As this is not a standardized denotation we decide to refer simply to the magnetization of the conduction electrons and hope that this will not create much confusion.
In situations, where the spin is (approximately) conserved the concept of current-induced torques reduces to the *bookkeeping* theory and the idea that the spin-transfer torque arises from the spin current. [95] Thus the current-induced torque picture can be seen as a generalization of the *bookkeeping* theory. The benefit of the current-induced torque picture rests on the fact that it can be applied to systems where the spin is not conserved, for instance to systems with spin-orbit interaction. Moreover, it explains the fact that the spin-transfer torque acts on the antiferromagnetic order parameter, even though there exists no relation between the spin-transfer torque and the total spin. [95]

The picture of current-induced torques exhibits some subtleties that we will discuss in the following. This picture is of particular importance for this thesis, as we will adopt the more general picture of current-induced torques along with a linear response calculation of the magnetization of the conduction electrons in section 5 of this thesis. The spin-transfer torque arises from the misalignment of the non-equilibrium transverse magnetization of the conduction electrons with the local moments. The determination of the spin-transfer torque then reduces to the task of estimating the transverse non-equilibrium magnetization of the conduction electrons in the presence of a given non-collinear magnetization texture.

The current-induced torque picture started out in 2004, when Zhang and Li [5] recognized that besides the adiabatic spin-transfer torque a second torque perpendicular to the adiabatic spin-transfer torque in Eq. (2.10) must be present to lift the mystery about experimentally observed velocities in current-induced domain-wall motion. [26] The adiabatic torque of Eq. (2.10) predicts a vanishing terminal velocity for a domain wall, as the energy due to the current is pumped continuously into the rotation of the wall and is thus no longer available for a translational motion. [5, 48, 52, 96] By adopting a phenomenological spin-diffusion equation that relaxes the transverse magnetization of the conduction electrons to the local magnetization by means of spin-flip processes, they took into account a finite lag of the magnetization of the conduction electrons due to non-conserved spins. In addition to the adiabatic torque in Eq. (2.14) they derived a non-adiabatic spin-transfer torque that originates from the counteraction of the non-conserved non-equilibrium magnetization of the conduction electrons on the local magnetization. The non-adiabatic component of the spin-transfer torque is taken into account by adding the term

$$\vec{\tau}_{\text{non-ad}}(\vec{r}) = -\frac{\mu_{\text{B}} P \xi}{e M_s} \vec{M}(\vec{r}) \times (\vec{j}_{\text{e}}(\vec{r}) \cdot \vec{\nabla}_{\vec{r}}) \vec{M}(\vec{r}), \tag{2.15}$$

to the Landau-Lifshitz-Gilbert equation (2.6). The non-adiabatic torque in Eq. (2.15) points perpendicular to the adiabatic torque in Eq. (2.10) and the local magnetization $\vec{M}(\vec{r})$ and describes in general the mistracking between the conduction electron spin and the local magnetization. The mechanism for the mistracking can be either spin relaxation that is always present as long as the spin is not completely conserved or the spin mistracking due to the non-adiabaticity as induced by a spatially

strongly varying magnetization texture. The magnitude of the non-adiabatic torque is parametrized by the non-dimensional *degree of non-adiabaticity* ξ that is defined as the ratio of the non-adiabatic and the adiabatic torque and is sensitive to microscopic characteristics. Affected by the phenomenological nature of their spin-diffusion equation, Zhang and Li intuitively claimed that the predominant mechanism to relax the transverse magnetization of the conduction electrons is spin-flip scattering and consequently their proposed value for the degree of non-adiabaticity reads

$$\xi^{\mathrm{ZL}} = \frac{\tau_{\mathrm{sd}}}{\tau_{\mathrm{sf}}^{\mathrm{ZL}}}. \tag{2.16}$$

In Eq. (2.16), $\tau_{\mathrm{sf}}^{\mathrm{ZL}}$ is the phenomenologically introduced spin flip-relaxation time that serves as a spin sink and relaxes the macroscopic transverse magnetization of the conduction electrons to the local magnetization. τ_{sd} is the precession time of the conduction electrons around the local magnetization associated with the sd interaction. Zhang and Li estimated a value of $\xi^{\mathrm{ZL}} \approx 10^{-2}$ that corresponds to a value of $\tau_{\mathrm{sf}}^{\mathrm{ZL}} \approx 10^{-12}$ s without microscopically specifying the mechanism that relaxes the transverse magnetization of the conduction electrons. Typically all kinds of spin-flip scattering processes with or without momentum conservation contribute to the relaxation of the out-of-equilibrium magnetization of the conduction electrons. [98] Due to spin-orbit scattering by impurities and defects $\tau_{\mathrm{sf}}^{\mathrm{ZL}}$ is expected to be non-zero at zero temperature and could obtain additional contributions at finite temperatures from electron-magnon scattering. However, we will confirm in section 5 that the phenomenologically introduced transverse relaxation time $\tau_{\mathrm{sf}}^{\mathrm{ZL}}$, which is responsible for the relaxation of the transverse conduction electron magnetization, turns out to arise in our kinetic approach from longitudinal relaxation times, familiar from collinear magnetotransport, due to the twist of spin channels in non-collinear magnetization textures.

The most general spin-transfer torque valid for spatially slowly magnetization textures can be expressed as the leading order terms of a spatial gradient expansion linear in the current density $\vec{j}_{\mathrm{e}}(\vec{r})$ [95, 99]

$$\vec{\tau}_{\mathrm{STT}}(\vec{r}) = \vec{\tau}_{\mathrm{ad}}(\vec{r}) + \vec{\tau}_{\text{non-ad}}(\vec{r}) = \frac{\mu_{\mathrm{B}} P}{e M_s}(\vec{j}_{\mathrm{e}}(\vec{r}) \cdot \vec{\nabla}_{\vec{r}})\vec{M}(\vec{r}) - \frac{\mu_{\mathrm{B}} P \xi}{e M_s}\vec{M}(\vec{r}) \times (\vec{j}_{\mathrm{e}}(\vec{r}) \cdot \vec{\nabla}_{\vec{r}})\vec{M}(\vec{r}). \tag{2.17}$$

We note that both terms in Eq. (2.17), the adiabatic $\vec{\tau}_{\mathrm{ad}}(\vec{r})$ and the non-adiabatic $\vec{\tau}_{\text{non-ad}}(\vec{r})$ spin-transfer torque, constitute the only two possible terms linear in current and first order in spatial derivatives of the magnetization and are therefore quite general.[1] Both torques are generated by the sd interaction. While the prefactor of the adiabatic torque $\vec{\tau}_{\mathrm{ad}}(\vec{r})$ is determined by spin-angular momentum considerations as discussed above, the strength of the non-adiabatic torque $\vec{\tau}_{\text{non-ad}}(\vec{r})$ is at this phenomenological stage arbitrary. Its strength depends on microscopic details and is here parametrized phenomenologically by the *degree of non-adiabaticity* ξ. The non-adiabatic torque is in general smaller than the adiabatic torque and its existence requires an additional microscopic mechanism that remains to be

[1] Strictly speaking the terminology that distinguishes between the adiabatic and the non-adiabatic torque is incorrect, since both terms belong to the same order of a gradient expansion in the magnetization. Throughout this thesis, we decided to adopt this terminology to avoid confusion, since it is well established within the magnetic community. As will be elaborately discussed in section 5.5 the non-adiabatic spin-transfer torque in Eq. 2.15 competes with other, true non-adiabatic contributions for the dynamics of narrow domain walls. [58, 71]

identified. [100] The most commonly accepted mechanisms are either spin relaxation [5] or spin mistracking [2]. At this point of the discussion we like to mention that the adiabatic torque can be derived as a reactive term from an energy functional, whereas the non-adiabatic torque is dissipative. [47, 49, 51, 95]
A very remarkable point is that the spin-transfer torque in Eq. (2.17) as well as the *degree of non-adiabaticity* ξ applies to any spatially slowly varying magnetization texture and does not depend on details of the magnetization texture as long as we stay in the adiabatic transport regime. This implies that the terminal velocity of a domain wall is independent of the type of the domain wall, for instance Bloch, Néel or vortex wall.
The adiabatic and non-adiabatic spin-transfer torque terms are fully characterized by means of three parameters: the diffusive spin polarization P of the electric current, the saturation magnetization M_s and the degree of non-adiabaticity ξ. [99] If we add the spin-transfer torque in Eq. (2.17) to the Landau-Lifshitz-Gilbert equation (2.6), we note that odd spatial gradients appear that were absent in equilibrium. This is conceivable as the presence of the current breaks the spatial inversion symmetry. In the absence of currents, it is the exchange contribution that is of second order in the spatial derivatives (cf. section 2.2) that constitutes the leading order term in the gradient expansion.
The microscopic origin as well as the macroscopic properties of the spin-transfer torque are currently under strong debate. In particular the non-adiabatic spin-transfer torque is strongly debated, as its value differs by orders of magnitude in theoretical predictions and in measurements. [5, 53–55, 101–110] The phenomenological explanation for non-adiabaticity is the following: Since the exchange interaction J_{sd} is not infinite, the conduction electron spin does not perfectly align with the local magnetization and the total spin is not entirely conserved. For exchange interactions large compared with transverse spin relaxation $\hbar/J_{\mathrm{sd}} \gg \tau_{\mathrm{sf}}^{\mathrm{ZL}}$ this effect becomes negligible and the total spin can be regarded as conserved within a good approximation. This general spin misalignment dephases with a characteristic relaxation time and acts as a correction to the adiabatic spin-transfer torque. The feature of non-adiabaticity is not accessible in the *bookkeeping* picture, which assumes the total conservation of spin.

The applicability of the presented theory concerning the spin-transfer-torque is restricted to spatially slowly varying magnetization textures. In the non-adiabatic regime associated with a spatially strongly varying magnetization the spins of the conduction electrons cannot follow the local magnetization. Here, the spin-transfer torque should depend on the detailed structure of the magnetization texture. If the spatial gradient of the magnetization across the wall becomes too large, a finite angle due to spin mistracking between conduction electron spins and local magnetization arises and introduces a spatially dependent non-adiabatic pressure on the wall. The relative importance of these non-adiabatic corrections depend crucially on the width of the domain wall. [58, 59, 111]
Thus far, a consistent theory that mediates between both, the adiabatic transport regime through wide domain walls and the non-adiabatic regime of narrow walls is missing and both regimes are strictly disconnected in the treatments of the spin-transfer torque. Section 5 of this thesis is concerned with the derivation of a general theory that allows for the computation of the spin-transfer torque in strongly varying magnetization textures. Already at this point some features of a general theory can be anticipated. In narrow domain walls the direction of the torque should be given by a spin accumulation

that is not linked to the local magnetization. Therefore we expect spatially dependent transport coefficients. Furthermore, the spin should be treated accurately in a quantum mechanical manner and not in the diffusive approximation. The quantum interference in the spin sector should cause interesting spin-angular momentum physics in narrow domain walls, if the spin transport takes place in the ballistic regime.

In conclusion, in a continuous ferromagnet the influence of a spin-polarized current on the time evolution of the magnetization is considered within the extended Landau-Lifshitz-Gilbert equation [5]

$$\begin{aligned}\frac{d\vec{M}(\vec{r},t)}{dt} =& -\gamma\vec{M}(\vec{r},t)\times\vec{H}_{\text{eff}}(\vec{r},t)+\frac{\alpha}{M_s}\vec{M}(\vec{r},t)\times\frac{d\vec{M}(\vec{r},t)}{dt}\\ &-\frac{b_j}{M_s^2}\vec{M}(\vec{r},t)\times\Big(\vec{M}(\vec{r},t)\times(\vec{j}(\vec{r},t)\cdot\vec{\nabla}_{\vec{r}})\vec{M}(\vec{r},t)\Big)\\ &-\xi\frac{b_j}{M_s}\vec{M}(\vec{r},t)\times(\vec{j}(\vec{r},t)\cdot\vec{\nabla}_{\vec{r}})\vec{M}(\vec{r},t),\end{aligned} \tag{2.18}$$

where $b_j := P_j\mu_B/[eM_s(1+\xi^2)]$ is the coupling constant between current and magnetization, P_j is the diffusive spin polarization, M_s is the saturation magnetization, α is the Gilbert damping parameter and ξ is the degree of non-adiabaticity. Note that a factor ξ^2 appears in the denominator of the coupling constant between current and magnetization according to Ref. [5]. As usually $\xi \ll 1$, this factor is too small to be of practical importance and thus has been neglected in the course of this section (cf. section 5.4 for a discussion concerning its physical meaning).

2.4 Electron transport in non-magnetic materials – the kinetic equation

This section introduces the semiclassical description of electron transport in terms of the kinetic equation, the Boltzmann equation. Transport is a branch of non-equilibrium thermodynamics. The charge carriers are not isolated from their environment and continuously gain energy due to the acceleration by an external electric field. At the same time scattering limits the motion of the charge carriers by dissipating energy to the lattice. The randomly distributed impurities within a sample as well as lattice vibrations in terms of phonons cause deviations from the strict periodicity of the lattice. This results in scattering of the charge carriers. Irreversible processes establish and maintain thermal equilibrium. For a dc electric field the acceleration is exactly balanced by collisions, such that a steady current flow arises. Up to date an a priory theory of transport is missing in the sense that the macroscopic transport equations have never been rigorously deduced from microscopic equations of motions. [112] Microscopic collisions introduce irreversibility on the macroscopic level though the underlying microscopic laws are invariant with respect to time-reversal.
Electron transport in non-magnetic metals based on the Drude form of conductivity [113] has been successful in predicting transport properties in terms of the relaxation-time approximation. [76, 114] The most important quantity concerning the relaxation-time approximation is the mean free path of the electrons. The mean free path is given by the distance that an electron travels as a free particle between adjacent collisions. In non-magnetic metals the Fuchs-Sondheimer theory serves to experimentally determine the mean free path of the conduction electrons. [115, 116] Here, the resistance is measured with a concomitant variation of the thickness of the thin film.

Table 2.1: Different levels of abstraction concerning electron transport in ferromagnetic metals.

Level of description	microscopic	mesoscopic	macroscopic
Hierarchy of length scales	$k_{\mathrm{F}}^{-1} \ll l_{\mathrm{ex}} < \lambda$ (atomic distances below the exchange length – end of micromagnetic continuum model)	λ (width of a domain wall)	$\gg \lambda$ (domain structures)
Governing equations	Schrödinger eq.	kinetic eq. (Boltzmann eq.)	macroscopic transport eq. (Ohm's law)

An approach to transport depends crucially on the involved length or time scales of the system. The main task is to employ suitable simplified models that capture the essential physics. Transport in general constitutes a complicated non-equilibrium many-body problem. In principal a formal solution of the Schrödinger equation would equip us with all the necessary correlation functions of the interacting many-body system. However, as it concerns mesoscopic transport the explicit knowledge of all the microscopic details is not required focusing on the dynamics that happen on a distinct time and length scale, for instance as set by the external perturbations.
Table 2.1 depicts the hierarchy of length scales in descending order. Irreversibility appears at the transition from the microscopic to the kinetic level. Throughout this thesis we pursue the kinetic method that is most appropriate for a description of electron transport on mesoscopic length scales. Here, the spatial and momentum degrees of freedom can be treated classically as the microscopic dynamics that takes place on the much smaller length scale of the Fermi wavelength can be disregarded. The kinetic description of transport in terms of the distribution function is referred to as semiclassical as the quantum mechanical non-locality is integrated out. It is assumed that the position and the momentum of the charge carriers are simultaneously well defined in analogy to a localized wavepacket. In this sense coherence effects are neglected and the description is restricted to the mesoscopic level. A benefit of semiclassical transport results is that they yield quantitative results in terms of microscopic scattering times that can be compared with results from full quantum mechanical techniques.
The focus of this thesis rests on mesoscopic transport in inhomogeneous, mesoscopic ferromagnets. A semiclassical formulation of transport requires the smooth variation of the involved transport fields on atomic length scales, i.e., a slow variation compared to the Fermi wavelength of the conduction electrons. In the case of magnetotransport this poses a constraint on the spatial variation of the electric field and the macroscopic magnetization $\vec{m}(\vec{r})$ (cf. section 5.1.2). The relevant length scale of magnetotransport exceeds the Fermi wavelength $|\vec{\nabla}_{\vec{r}}\vec{m}(\vec{r})| \sim \lambda^{-1} \ll k_{\mathrm{F}}$. Therefore, it is appropriate to treat the spatial and the momentum degrees of freedom semiclassically in magnetotransport.
The important parameter for transport in narrow domain walls is the spatial variation of the magnetization texture (cf. section 5.5) and the kinetic method is adequate to properly take this into account. Moreover, the kinetic method provides accurate results for ballistic as well as diffusive transport. This is important for non-collinear magnetotransport as spin transport takes place either in the ballistic or

the diffusive regime (cf. section 5.1.2), in particular the kinetic approach provides the possibility to study transitions between both transport regimes.

2.4.1 Semiclassical theory of electron transport

Throughout the following we restrict ourselves to one single band and therefore drop any reference to a band index for convenience. Conduction electrons in metals constitute a highly degenerate fermionic system that must be described by quantum statistics. In thermal equilibrium the average occupation number of an electron in the state $\vec{k}$ with energy $\epsilon_{\vec{k}}$ is given by the Fermi function

$$f^0(\epsilon_{\vec{k}}) = \frac{1}{e^{\beta(\epsilon_{\vec{k}}-\mu_0)}+1}, \tag{2.19}$$

with temperature $\beta = 1/k_{\mathrm{B}}T$ and equilibrium chemical potential μ_0. The deployment of the Fermi function takes into account the statistical nature of the charge carriers as indistinguishable fermions.
When treating electron transport one has to consider that electrons in solids are band particles. The group velocity of a wavepacket of Bloch states describes the electrons in the periodic potential of the lattice. It is determined by the slope of the band dispersion

$$\vec{v}_{\vec{k}} \equiv \vec{\nabla}_{\vec{k}} \frac{\epsilon_{\vec{k}}}{\hbar}. \tag{2.20}$$

Equation (2.20) states that the velocity of a semiclassical electron is given in terms of the group velocity of the underlying wavepacket. [76] For a gas of free and independent electrons $\epsilon_{\vec{k}} = \hbar^2\vec{k}^2/(2m)$ and the kinetic expression (2.20) reflects that there is no interaction between the electrons. Interactions between the conduction electrons would modify the energy $\epsilon_{\vec{k}}$ and thus the Bloch velocity in Eq. (2.20).
The effective mass tensor is defined according to

$$\frac{1}{\hbar^2}\frac{\partial^2\epsilon_{\vec{k}}}{\partial k_i \partial k_j} = \frac{1}{\hbar}\frac{\partial v^i_{\vec{k}}}{\partial k_j} = [M^{-1}_{\vec{k}}]_{ij}. \tag{2.21}$$

It governs the inertia response of the charge carriers with respect to a force. [112] The sign of the effective mass tensor (2.21) determines the nature of the charge carriers: for positive values the transport is carried by electrons, for negative values holes dominate the transport.
The semiclassical equations of motions for electron transport read [76]

$$\frac{\partial\vec{r}}{\partial t} = \vec{v}_{\vec{k}}, \tag{2.22}$$

$$\hbar\frac{\partial\vec{k}}{\partial t} = -e\vec{E}(\vec{r}) - e\vec{v}_{\vec{k}} \times \vec{B}(\vec{r}). \tag{2.23}$$

Equations (2.22) and (2.23) describe the dynamics of Bloch electrons in weak electromagnetic fields. [76] The semiclassical relations (2.22), (2.23) hold for sufficiently weak external electromagnetic fields, such that interband tunneling is absent. [76]

2.4.2 The Boltzmann equation

The kinetic description of transport in terms of the Boltzmann equation is a quasiclassical theory that combines the quantum mechanical nature of the electronic structure (cf. Eq. (2.20)) with a classical description of transport. In the periodic potential of the lattice the electron states are Bloch states with wave functions $\Psi_{\vec{k}}(\vec{r}) = u_{\vec{k}}(\vec{r})e^{i\vec{k}\vec{r}}$. The Bloch momentum is not a good quantum number and therefore not appropriate for a description of electron transport. Instead wave packets can be constructed from the Bloch states. These wave packets move with group velocity $\vec{v}_{\vec{k}}$ as it is given by Eq. (2.20). In analogy to elementary wave mechanics the wave packets can be treated as particles that are accelerated due to the electric field and scattered at crystal imperfections and enable a local description of transport. The central quantity in the kinetic method is the probability distribution function $f_{\vec{k}}(\vec{r},t)$ that measures the number of electrons in the $\vec{k}$-th state in a small neighborhood of $\vec{r}$ at time t. All macroscopic quantities of interest can be directly computed from the distribution function. The distribution function obeys a flow equation, the kinetic or Boltzmann equation that describes a non-equilibrium problem in response to arbitrary, external fields. It determines the phase-space trajectory of the distribution function $f_{\vec{k}}(\vec{r},t)$.
The equation of motion for the distribution function can either be derived classically from the Liouville theorem that states the conservation of probability or quantum mechanically from the one-particle density matrix. [117] The quantum mechanical approach serves in section 5.1 for the derivation of the kinetic equation for ferromagnets with a non-collinear magnetization texture. At this point we pursue the classical derivation. The Liouville theorem implies a conservation law for the distribution function. The phase-space density, i.e., the distribution function, is conserved in the absence of collisions. This corresponds to the vanishing of the total derivative with respect to time

$$0 = \frac{df_{\vec{k}}(\vec{r},t)}{dt} = \frac{\partial f_{\vec{k}}(\vec{r},t)}{\partial t} + \frac{\partial \vec{r}}{\partial t}\vec{\nabla}_{\vec{r}} f_{\vec{k}}(\vec{r},t) + \frac{\partial \vec{k}}{\partial t}\vec{\nabla}_{\vec{k}} f_{\vec{k}}(\vec{r},t). \tag{2.24}$$

2.4.2.1 Steady state Boltzmann equation for electrons

The kinetic equation for electron transport in metals follows from the combination of Eq. (2.24) with the semiclassical equations of motions for electron transport (2.22) and (2.23)

$$\frac{\partial f_{\vec{k}}(\vec{r},t)}{\partial t} + \vec{v}_{\vec{k}}\vec{\nabla}_{\vec{r}} f_{\vec{k}}(\vec{r},t) - \frac{e}{\hbar}\left(\vec{E}(\vec{r}) + \vec{v}_{\vec{k}} \times \vec{B}(\vec{r})\right)\vec{\nabla}_{\vec{k}} f_{\vec{k}}(\vec{r},t) = 0. \tag{2.25}$$

Equation (2.25) constitutes the deterministic flow part of the kinetic equation for electron transport in non-magnetic metals. The deterministic flow part of the Boltzmann equation (2.25) determines the phase-space trajectory of the distribution function $f_{\vec{k}}(\vec{r},t)$. The acceleration due to the presence of external forces is balanced by microscopic collisions to maintain a steady current flow. The microscopic collisions are usually modeled in terms of a collision integral that is added phenomenologically to the r.h.s. of the Boltzmann equation (2.25). This is the point, where irreversibility comes into play. The statistical character of the collision term breaks the time-reversal symmetry of the Boltzmann equation. Though the flow part as well as the underlying microscopic laws are invariant with respect to time-reversal, the collisions break the time-reversal symmetry on the mesoscopic level thereby introducing irreversibility to the kinetic description. As a consequence the resulting full Boltzmann

equation turns into an integro-differential equation for the distribution function $f_{\vec{k}}(\vec{r},t)$. The individual parts of the Boltzmann equation possess clear physical interpretations. The distribution function changes with time t in the neighborhood of $\vec{r}$ through the following mechanisms: [112]

- Diffusion: The spatial motion with Bloch velocity $\vec{v}_{\vec{k}}$ causes electrons to enter (leave) the region $d\vec{r}$ from (to) neighbouring regions. In the presence of spatial fluctuations the distribution function varies from point to point due to diffusion processes

$$\frac{\partial f_{\vec{k}}(\vec{r},t)}{\partial t}|_{\text{diffusion}} := -\vec{v}_{\vec{k}}\,\vec{\nabla}_{\vec{r}} f_{\vec{k}}(\vec{r},t). \tag{2.26}$$

- External fields: The charge carriers are driven by external fields. This changes the occupation number of the Bloch state $\vec{k}$ according to

$$\frac{\partial f_{\vec{k}}(\vec{r},t)}{\partial t}|_{\text{field}} := \frac{e}{\hbar}\left(\vec{E}(\vec{r}) + \frac{1}{c}\vec{v}_{\vec{k}}(\vec{r}) \times \vec{B}(\vec{r})\right)\vec{\nabla}_{\vec{k}} f_{\vec{k}}(\vec{r},t). \tag{2.27}$$

  A steady current flow requires the presence of an external field.

- Scattering: Besides the acceleration due to external fields the wave packets of Bloch electrons are scattered incoherently by impurities within the sample. Scattering causes relaxation of the distribution function and is qualitatively a different feature compared with the coherent acceleration due to external fields. Scattering results from deviations of the strict periodicity of the lattice and can be considered by the introduction of a correction term. The collision term

$$\frac{\partial f_{\vec{k}}(\vec{r},t)}{\partial t}|_{\text{col}}, \tag{2.28}$$

  resembles the difference between the gain and loss rate for the state $\vec{k}$ at a time t. Collisions are responsible for thermal equilibrium. Let us restrict ourselves to elastic impurity scattering and inelastic electron-phonon scattering. Electron-electron scattering becomes only important at low temperatures and is therefore disregarded. [117] The focus of this thesis rests on transport in ferromagnets at ambient temperatures that is dominated by electron-phonon scattering. [76, 117]
  For our purpose it is sufficient to treat elastic scattering from state $\vec{k} \to \vec{k}'$ at a fixed time $t = t_0$. If $\vec{k}'$ lies in the range $d\vec{k}'$, the probability of a transition into the state $\vec{k}$ is given by

$$\wp_{\vec{k},\vec{k}'}(\vec{r})d\vec{k}' = f_{\vec{k}}(\vec{r})(1 - f_{\vec{k}'}(\vec{r}))P_{\vec{k},\vec{k}'}d\vec{k}', \tag{2.29}$$

  where $P_{\vec{k},\vec{k}'}$ is the transition rate from $\vec{k} \to \vec{k}'$. The weighting factor $f_{\vec{k}}(\vec{r})\,(1-f_{\vec{k}'}(\vec{r}))$ takes into account the probability that the initial state $\vec{k}$ is occupied (that the final state $\vec{k}'$ is not occupied). The factor $1 - f_{\vec{k}'}(\vec{r})$ is due to the fermionic nature of the conduction electrons and accounts for Pauli's exclusion principle that considers that the final state $\vec{k}'$ is not occupied and thus available for the scattering process.
  The inverse process reads

$$\wp_{\vec{k}',\vec{k}}(\vec{r})d\vec{k}' = f_{\vec{k}'}(\vec{r})(1 - f_{\vec{k}}(\vec{r}))P_{\vec{k}',\vec{k}}d\vec{k}'. \tag{2.30}$$

Summation over all initial and final states $\vec{k'}$ yields the collision integral

$$\frac{\partial f_{\vec{k}}(\vec{r})}{\partial t}|_{\text{col}} = \int d^3k' P_{\vec{k},\vec{k'}} f_{\vec{k'}}(\vec{r})(1 - f_{\vec{k}}(\vec{r})) - \int d^3k' P_{\vec{k'},\vec{k}} f_{\vec{k}}(\vec{r})(1 - f_{\vec{k'}}(\vec{r})). \tag{2.31}$$

The collision probabilities $P_{\vec{k},\vec{k'}}$ depend at low temperatures on the impurity potential as well as the density of states and can be evaluated according to *Fermi's Golden Rule*

$$P_{\vec{k},\vec{k'}} = \frac{2\pi}{\hbar} \nu_{\text{imp}} N(\epsilon_{\text{F}}) |T_{\vec{k},\vec{k'}}|^2 \delta(\epsilon_{\vec{k}} - \epsilon_{\vec{k'}}), \tag{2.32}$$

where ν_{imp} is the impurity concentration, $N(\epsilon_{\text{F}})$ denotes the density of states taken at the Fermi level (the density of states is usually constant in the relevant energy range), the δ-function considers elastic scattering and $T_{\vec{k},\vec{k'}}$ is the transition matrix element that characterizes the scattering process

$$T_{\vec{k},\vec{k'}} = \frac{1}{V} \int d^3r \, \Psi_{\vec{k}}(\vec{r}) \hat{V} \Psi_{\vec{k'}}(\vec{r}). \tag{2.33}$$

Equation (2.33) describes the transition of an electron from the initial state $\Psi_{\vec{k}}(\vec{r})$ to the final state $\Psi_{\vec{k'}}(\vec{r})$ in the presence of the quantum mechanical scattering potential $\hat{V}$. We note that in ferromagnets all quantities become additionally spin-dependent.
According to the principle of microscopic reversibility - follows for elastic impurity scattering from Eqns. (2.32) and (2.33)) directly from the fact that $\hat{V}$ is hermitian - the intrinsic transition rates are symmetric

$$P_{\vec{k},\vec{k'}} = P_{\vec{k'},\vec{k}}, \tag{2.34}$$

and Eq. (2.31) simplifies accordingly to

$$\begin{aligned} \frac{\partial f_{\vec{k}}(\vec{r})}{\partial t}|_{\text{col}} &= \int d^3k' P_{\vec{k},\vec{k'}} \left[f_{\vec{k'}}(\vec{r})(1 - f_{\vec{k}}(\vec{r})) - f_{\vec{k}}(\vec{r})(1 - f_{\vec{k'}}(\vec{r})) \right] \\ &= \int d^3k' P_{\vec{k},\vec{k'}} \left[f_{\vec{k'}}(\vec{r}) - f_{\vec{k}}(\vec{r}) \right]. \end{aligned} \tag{2.35}$$

Equation (2.35) marks the final expression for the collision integral.

The interplay of the contributions (2.26), (2.27) and (2.28) determines the Boltzmann equation

$$\frac{\partial f_{\vec{k}}(\vec{r},t)}{\partial t} = \frac{\partial f_{\vec{k}}(\vec{r},t)}{\partial t}|_{\text{diffusion}} + \frac{\partial f_{\vec{k}}(\vec{r},t)}{\partial t}|_{\text{field}} + \frac{\partial f_{\vec{k}}(\vec{r},t)}{\partial t}|_{\text{col}}. \tag{2.36}$$

In the steady state the left hand side of Eq. (2.36) vanishes and Eq. (2.36) reduces to

$$-\frac{\partial f_{\vec{k}}(\vec{r})}{\partial t}|_{\text{diffusion}} - \frac{\partial f_{\vec{k}}(\vec{r})}{\partial t}|_{\text{field}} = \frac{\partial f_{\vec{k}}(\vec{r})}{\partial t}|_{\text{col}}. \tag{2.37}$$

Equation (2.37) explicitly states that the changes due to diffusion and external fields are balanced by collisions. Inserting the expressions (2.26), (2.27) and (2.31) in Eq. (2.37) and disregarding the magnetic field ($\vec{B} = 0$) we arrive at the Boltzmann equation for electron transport in non-magnetic materials

$$\vec{v}_{\vec{k}} \vec{\nabla}_{\vec{r}} f_{\vec{k}}(\vec{r}) - \frac{e}{\hbar} \vec{E}(\vec{r}) \vec{\nabla}_{\vec{k}} f_{\vec{k}}(\vec{r}) = \int d^3k' P_{\vec{k},\vec{k'}} \left[f_{\vec{k'}}(\vec{r}) - f_{\vec{k}}(\vec{r}) \right]. \tag{2.38}$$

The validity of the Boltzmann equation assumes that the distribution function $f_{\vec{k}}(\vec{r})$ varies slowly compared to the Fermi wavelength or atomic distances. This is fulfilled when the mean free path of the electrons is large compared to the Fermi wavelength $l_{\text{mfp}} \gg k_{\text{F}}^{-1}$. Then the quasi-momentum $\vec{k}$ of the Bloch state is a good quantum number and serves for an appropriate description of transport. At interfaces, appropriate boundary conditions must be chosen to match the piecewise solutions of Eq. (2.38).

2.4.2.2 Linearized Boltzmann equation for electrons

When considering electron transport in metals or good conducting semiconductors, the full Boltzmann equation is unnecessarily complicated. In this case it is sufficient to focus on the linear response of the charge carriers with respect to the electric field. As long as deviations from Ohm's law can be neglected, transport is described appropriately by focusing on the linearized Boltzmann equation with respect to the external field. In the case of small applied field strengths transport in metals takes place close to equilibrium and can be described by a field-induced small shift of the Fermi sphere, i.e., transport at considerably low temperatures with respect to the Fermi energy is dominated by electrons at the Fermi surface. The occupancy of states far away from the Fermi energy does not change, as these states do not participate in the transport. A scattering process can only take place when the transfered energy lasts for the electron to leave the Fermi sphere. At low temperatures all states within the Fermi sphere are occupied and all scattering events that would scatter an electron inside the Fermi sphere are forbidden due to the Pauli exclusion principle.
In linear response, deviations from the spatially homogeneous equilibrium distribution function $f^0(\epsilon_{\vec{k}})$ (cf. Eq. (2.19)) are parametrized by the non-equilibrium distribution function $g_{\vec{k}}(\vec{r})$

$$f_{\vec{k}}(\vec{r}) = f^0(\epsilon_{\vec{k}}) + g_{\vec{k}}(\vec{r})\frac{\partial f^0(\epsilon_{\vec{k}})}{\partial \epsilon_{\vec{k}}}. \tag{2.39}$$

Inserting the ansatz (2.39) into the Boltzmann equation (2.38) leads to

$$\begin{aligned} &\vec{v}_{\vec{k}}\left(\vec{\nabla}_{\vec{r}} g_{\vec{k}}(\vec{r})\right)\left(\frac{\partial f^0(\epsilon_{\vec{k}})}{\partial \epsilon_{\vec{k}}}\right) - e\vec{E}(\vec{r})\vec{v}_{\vec{k}}\frac{\partial f^0}{\partial \epsilon_{\vec{k}}} \\ &= \int d^3k' P_{\vec{k},\vec{k}'}\left[\left(g_{\vec{k}'}(\vec{r})\frac{\partial f^0(\epsilon_{\vec{k}'})}{\partial \epsilon_{\vec{k}'}} - g_{\vec{k}}(\vec{r})\frac{\partial f^0(\epsilon_{\vec{k}})}{\partial \epsilon_{\vec{k}}}\right) + \left(f^0(\epsilon_{\vec{k}'}) - f^0(\epsilon_{\vec{k}})\right)\right], \end{aligned} \tag{2.40}$$

where we neglect the term proportional to $\partial\left(g_{\vec{k}}(\vec{r})\frac{\partial f^0(\epsilon_{\vec{k}})}{\partial \epsilon_{\vec{k}}}\right)/\partial_{\epsilon_{\vec{k}}}$ as a term of second order in the electric field. Note that the non-equilibrium distribution itself is linear in the electric field $g_{\vec{k}}(\vec{r}) \propto \vec{v}_{\vec{k}}\vec{E}(\vec{r})$. A term of higher order in the electric field $\vec{E}(\vec{r})$ results in deviations from Ohm's law. The equilibrium distribution function $f^0(\epsilon_{\vec{k}})$ in the state $\vec{k}$ depends solely on the energy $\epsilon_{\vec{k}}$. As we are dealing with elastic impurity scattering, which does not change the energy of the particle the equality $f^0(\epsilon_{\vec{k}'}) = f^0(\epsilon_{\vec{k}})$ holds. Moreover, it follows directly from the Boltzmann equation (2.38) in the absence of external fields that the scattering term (2.31) vanishes in equilibrium

$$\frac{\partial f^0_{\vec{k}}(\vec{r})}{\partial t}|_{\text{col}} = 0. \tag{2.41}$$

With these considerations, we arrive at the linearized Boltzmann equation

$$\vec{v}_{\vec{k}}\vec{\nabla}_{\vec{r}}g_{\vec{k}}(\vec{r}) - e\vec{E}(\vec{r})\vec{v}_{\vec{k}} = \int_{\mathrm{FS}} d^2k' P_{\vec{k},\vec{k}'}\left[g_{\vec{k}'}(\vec{r}) - g_{\vec{k}}(\vec{r})\right], \tag{2.42}$$

where the three dimensional $\vec{k}'$ integration is restricted to a surface integral over the Fermi surface. This reflects that only electrons in the vicinity of the Fermi surface participate in transport. The notation on the r.h.s. of Eq. (2.42) should be understood as follows

$$\int_{\mathrm{FS}} d^2k' P_{\vec{k},\vec{k}'}\left[f_{\vec{k}'}(\vec{r}) - f_{\vec{k}}(\vec{r})\right] := \int d^3k'\,\delta(\epsilon_{\vec{k}'} - \epsilon_{\mathrm{F}}) P_{\vec{k},\vec{k}'}\left[f_{\vec{k}'}(\vec{r}) - f_{\vec{k}}(\vec{r})\right], \tag{2.43}$$

where we employed the following property of the Fermi-function at low temperatures compared to the Fermi energy

$$-\frac{\partial f^0(\epsilon_{\vec{k}})}{\partial \epsilon_{\vec{k}}} = \delta(\epsilon_{\vec{k}} - \epsilon_{\mathrm{F}}). \tag{2.44}$$

2.4.2.3 Collision integral in the relaxation-time approximation

The remaining difficulty in solving the linearized Boltzmann equation (2.42) rests on the collision integral on its right hand side. In general, the Boltzmann equation is an integro-differential equation. A common simplification is to treat the collision integral within the relaxation-time approximation. In this case the discrete spectrum of the collision integral is substituted by one single, infinitely degenerate eigenvalue: a relaxation time τ. Descriptively, the relaxation-time approximation does not focus on the collisions themselves but on the mean free path of the electrons between adjacent collisions. In the relaxation-time approximation the Boltzmann equation (2.42) reduces to a differential equation that enables analytic solutions.

The relaxation-time approximation describes the collisions of the conduction electrons as random, uncorrelated effects and assumes that the precise form of the non-equilibrium distribution function $g_{\vec{k}}(\vec{r})$ is irrelevant for the scattering process. The relaxation-time approximation assumes that an electron experiences a collision in an infinitesimal time interval dt with probability dt/τ. We will treat the collision term in the simplest manner, by s-wave scattering, which results in a momentum-independent relaxation time. The collision integral in Eq. (2.31) consists of two terms. The incoming electrons

$$\frac{\partial f_{\vec{k}}(\vec{r})}{\partial t}|^{\mathrm{in}}_{\mathrm{col}} = \int d^3k' P_{\vec{k}',\vec{k}} f_{\vec{k}'}(\vec{r})(1 - f_{\vec{k}}(\vec{r})), \tag{2.45}$$

and the outgoing electrons

$$\frac{\partial f_{\vec{k}}(\vec{r})}{\partial t}|^{\mathrm{out}}_{\mathrm{col}} = -f_{\vec{k}}(\vec{r}) \int d^3k' P_{\vec{k},\vec{k}'}(1 - f_{\vec{k}'}(\vec{r})). \tag{2.46}$$

With the definition of the relaxation time

$$\frac{1}{\tau} := \int d^3k' P_{\vec{k},\vec{k}'}(1 - f_{\vec{k}'}(\vec{r})), \tag{2.47}$$

the relaxation-time approximation assumes that the incoming electrons in Eq. (2.45) can be associated with the equilibrium distribution [76]

$$\frac{\partial f_{\vec{k}}(\vec{r})}{\partial t}|^{\mathrm{in}}_{\mathrm{col}} = \frac{f^0(\epsilon_{\vec{k}})}{\tau}, \tag{2.48}$$

while due to Eq. (2.47) the outgoing electrons in Eq. (2.46) are determined by the full distribution function

$$\frac{\partial f_{\vec{k}}(\vec{r})}{\partial t}|_{\text{col}}^{\text{out}} = -\frac{f_{\vec{k}}(\vec{r})}{\tau}. \tag{2.49}$$

Combining Eqns. (2.45) and (2.46) yields the collision integral in the relaxation-time approximation

$$\frac{\partial f_{\vec{k}}(\vec{r})}{\partial t}|_{\text{col}} = -\frac{\left(f_{\vec{k}}(\vec{r}) - f^0(\epsilon_{\vec{k}})\right)}{\tau}. \tag{2.50}$$

Equation (2.50) causes the full distribution $f_{\vec{k}}(\vec{r})$ to relax towards the equilibrium distribution $f^0(\epsilon_{\vec{k}})$ within a characteristic time scale set by τ.

Chapter 3

The vortex random-access memory

This chapter has been published slightly modified in Ref. [118], S. Bohlens, B. Krüger, A. Drews, M. Bolte, G. Meier, and D. Pfannkuche, Current controlled random-access memory based on magnetic vortex handedness, Appl. Phys. Lett. **93***, 142508 (2008)*

THE THEORETICAL FOUNDATION for a non-volatile memory device based on magnetic vortices is presented. We propose a realization of a vortex random-access memory (VRAM) containing vortex cells that are controlled by alternating currents only. The proposed scheme allows to transfer the vortex into an unambiguous binary state regardless of its initial state within a sub-nanosecond time scale. The vortex handedness defined as the product of chirality and polarization as a bit representation allows for reading and writing of the bit information. The VRAM is stable at room temperature.

3.1 Motivation

The perception that magnetization dynamics is tunable by spin-polarized currents paves the path for the development of new kinds of memory devices. Its boolean topological quantities distinguish the magnetic vortex to be a natural candidate for memory application. In this chapter, we propose a realization of a vortex random-access memory (VRAM) that is controlled by alternating currents only. Due to alternating current excitations, the main benefit of the VRAM is the operation at a lower current density compared with domain-wall motion in racetracks [19] or the switching in multilayer as used in current magnetic random-access memories [25–28].

3.2 Equation of motion for the magnetic vortex

This section sketches the derivation of the equation of motion for a magnetic vortex confined in a square thin-film element for a collinear electric current and magnetic field arrangement. The vortex motion takes place in two spatial dimensions. It is characterized in terms of the collective coordinates (X, Y) that are canonically conjugated variables for the vortex. [71, 119] The equations of motion provide the analytical solution that serves as the basis for the memory proposal as outlined in the next

section.

Thiele recognized in 1973 [120, 121] that if it is plausible to assume that a magnetization pattern keeps its rigid shape during its motion, then the Landau-Lifshitz-Gilbert equation (2.6) can be rewritten in an equation for equivalent forces acting on a rigid magnetization pattern by replacing the time derivatives of the magnetization with its spatial gradients that move under a constant velocity $\vec{v} = (dX(t)/dt, dY(t)/dt)^T$

$$\frac{d\vec{M}(\vec{r},t)}{dt} = -\left(\vec{v}\,\vec{\nabla}_{\vec{r}}\right)\vec{M}(\vec{r},t). \tag{3.1}$$

The Thiele equation translates the torques on the local moments to equivalent forces on the whole rigid magnetization texture and thus introduces a description in which the static magnetization texture moves as a quasiparticle under the influence of external forces.

Thiaville et al. [48] extended the Thiele equation to take into account the influence of a spin-polarized current (cf. Eq. (2.18))

$$\vec{F} + \vec{G} \times \left(\vec{v} + b_j\vec{j}\right) + D\left(\alpha\vec{v} + \xi b_j\vec{j}\right) = 0. \tag{3.2}$$

For the case of a magnetic vortex, Eq. (3.2) describes the balance of forces acting on the vortex core that moves under the velocity $\vec{v}$. The Thiele equation (3.2) constitutes a system of two coupled first-order differential equations that can be decoupled to yield one equation of motion of second order. However, owing to the fact that the vortex is a topological object described by two conjugated spatial coordinates, the vortex responds instantaneously to an external perturbation and in this sense does not possess an inertia mass. This stands in contrast with an one-dimensional domain wall. Here, the conjugated variable is the out-of-plane tilting angle, which is able to store energy due to finite out-of-plane angles. The stored magnetic energy and the inert response gives rise to a finite domain wall mass. [122]

External driving mechanism as magnetic fields and spin-polarized currents cause a deflection of the vortex core from its equilibrium position $(X, Y) = (0, 0)$. The deflection is balanced by an internal force arising from a combination of the demagnetization and exchange fields due to the magnetostatic energy as caused by the deflected vortex. The restoring force arises from the confinement of the vortex within a thin-film element. The effective force $\vec{F}$ originates from the effective field H_{eff} and accounts for external forces, for instance an external applied Zeeman field, as well as internal forces, such as the restoring force due to the demagnetization and exchange fields. The gyrotropic force is associated with the gyrovector $\vec{G}$ and composed of a part that takes into account the motion of the vortex and a driving part due to the adiabatic spin-transfer torque that causes the vortex to move perpendicular to the direction of the current flow. The dissipation term D takes into account the dissipation due to the Gilbert damping $\propto \alpha\vec{v}$ and of the non-adiabatic spin-transfer torque $\propto \xi b_j\vec{j}$ that pushes the vortex in the direction of the current flow. The dissipative terms $\propto D$ depend on the magnetization texture that reads in spherical coordinates

$$\vec{M}(\vec{r}) = M_s \begin{pmatrix} \sin\theta\cos\phi \\ \sin\theta\sin\phi \\ \cos\theta \end{pmatrix}. \tag{3.3}$$

The profile of a vortex is parametrized by the out-of-plane angle θ and the in-plane angle

$$\phi = \beta + \frac{\pi}{2}c. \tag{3.4}$$

Here, β denotes the real space angle and c is the chirality of the vortex. [123] For a vortex in a thin-film element the stable chiralities are $c \pm 1$.
In the following, we apply the equation of motion (3.2) to a static vortex that moves with constant velocity $\vec{v}$. The motion of the rigid vortex is described in terms of collective, time-dependent coordinates $(X(t), Y(t))$ that determine the position of the vortex core. The equivalent force is given by

$$\vec{F} = -\mu_0 \int d^3r \left[(\vec{\nabla}_{\vec{r}}\theta)\frac{\partial}{\partial\theta} + (\vec{\nabla}_{\vec{r}}\phi)\frac{\partial}{\partial\phi} \right] (\vec{H}_{\text{eff}} \cdot \vec{M}). \tag{3.5}$$

Owing to its particular magnetization texture a vortex experiences a gyrotropic force perpendicular to its velocity. This unusual feature is related to the topological character of the magnetic vortex. [59] The gyrotropic force is controlled by the gyrovector

$$\vec{G} = -\frac{M_s\mu_0}{\gamma} \int d^3r \sin\theta (\vec{\nabla}_{\vec{r}}\theta \times \vec{\nabla}_{\vec{r}}\phi) = G_0\vec{e}_z, \tag{3.6}$$

that points out-of-plane (z direction) and the term $\vec{G}\times\vec{v}$ in Eq. (3.2) results in the in-plane precessional motion of the vortex. The dissipation tensor for the vortex takes the form

$$D = -\frac{M_s\mu_0}{\gamma} \int d^3r \, (\vec{\nabla}_{\vec{r}}\theta\vec{\nabla}_{\vec{r}}\theta + \sin^2\theta\vec{\nabla}_{\vec{r}}\phi\vec{\nabla}_{\vec{r}}\phi) = D_0 \begin{pmatrix} 1 & 0 & 0 \\ 0 & 1 & 0 \\ 0 & 0 & 0 \end{pmatrix}. \tag{3.7}$$

Considering the explicit shape of the gyrovector (3.6) and the dissipation-tensor (3.7) results in an equation for the velocity of the vortex-core [123]

$$\vec{v} = (G_0^2 + D_0^2\alpha^2)^{-1} \left[\vec{G} \times \vec{F} - D_0\alpha\vec{F} - (G_0^2 + D_0^2\alpha\xi)\tilde{b}_j\vec{j} + \tilde{b}_j D_0 \vec{G} \times \vec{j}(\xi - \alpha) \right]. \tag{3.8}$$

The equivalent force that acts on the vortex consists of two parts: the restoring force for the vortex due to the demagnetization and exchange fields that is of purely geometrical nature and the force due to the interaction of the external magnetic field with the homogeneous domains. The latter force is independent of the position of the vortex core. The sum of both forces reads

$$\vec{F} = -\vec{\nabla}_{\vec{r}} \left(E_{\text{zeeman}} + E_{\text{demag}} \right) = \mu_0 M_s H l t c \vec{e}_y - m\omega_r^2 \left(X\vec{e}_x + Y\vec{e}_y \right), \tag{3.9}$$

where l (t) is the sample length (thickness) and $m\omega_r^2$ parametrizes the restoring, harmonic potential. [123]

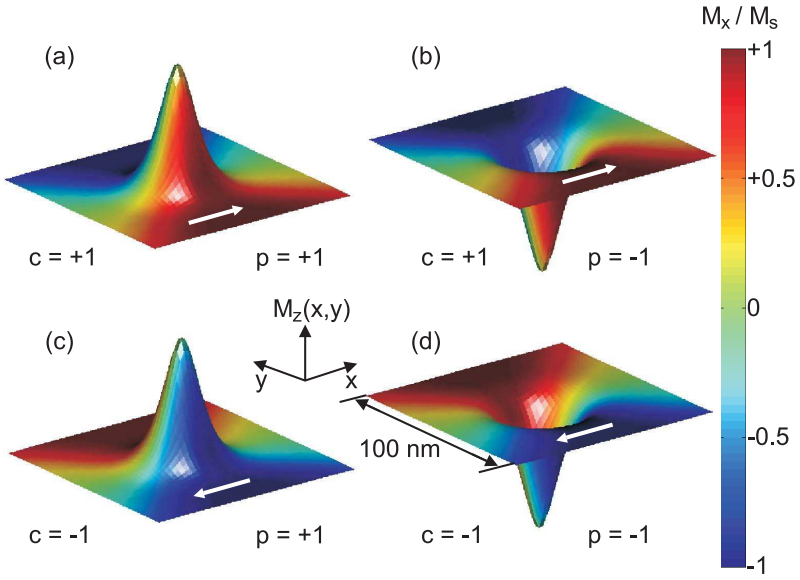

Figure 3.1: (Color online) The fourfold degenerate ground state of a magnetic vortex in a thin-film element with chirality $c = \pm 1$ and core polarization $p = \pm 1$. The white arrows illustrate the sense of rotation of the in-plane magnetization. The magnetization in the center points out of plane. The height indicates the out-of-plane magnetization M_z while the colors visualize the x component of the in-plane magnetization M_x normalized to the saturation magnetization M_s.

3.3 Current controlled random-access memory based on magnetic vortex handedness

The perception that magnetization dynamics is tunable by spin-polarized currents [14, 15] triggered an intensive investigation of applications within the last years. Compared with a magnetic field, an electrical current is much more appropriate to control a device, since it can be handled with high precision and can be spatially restricted. Recently, it has been suggested to employ the polarization of a magnetic vortex core for data storage. [124] This is motivated by the experimental discovery [125, 126] and numerical investigation [127, 128] of vortex-core switching in various scenarios. In a ferromagnetic thin-film element a vortex state with a core of a few nanometers [129] is formed due to the interplay of exchange and demagnetization energy. The in-plane magnetization curls around a sharp singularity in the center, where the magnetization is forced out of plane to minimize exchange energy. Despite its complex structure the magnetic vortex in many ways behaves as a quasiparticle only characterized by the polarization p, the chirality c, and the coordinates X and Y of the vortex core in the sample plane as illustrated in Fig. 3.1.

The vortex core pointing up (down) denoted by the polarization $p = +1$ ($p = -1$) provides a basis for a binary logic. The chirality characterizes the sense of rotation of the in-plane magnetization. For $c = +1$ ($c = -1$) the magnetization curls counterclockwise (clockwise) around the core. In a ferromagnetic square or circular thin-film element with no crystalline anisotropy, e.g., made of permalloy (Py=$Ni_{80}Fe_{20}$), the vortex state constitutes the energetic ground state, which is fourfold degenerate

due to the combinations of chirality and polarization (cf. Fig. 3.1). To change its polarization, the vortex has to overcome an energy barrier, which is of the order of ten electronvolts. [130] Hence, the vortex core is quite stable against thermal fluctuations at room temperature or magnetic stray fields in the millitesla regime. The benefit of using magnetic vortices in a memory device is their innate smallness and their generic existance. Therefore, the vortex is appropriate to serve as a non-volatile storage device.
We present a memory device based on the magnetic vortex handedness defined as the product cp of chirality and core polarization. The application of the handedness as a bit representation allows bit writing without the knowledge of the initial magnetization state as well as a direct reading of the bit information. Consequently, a main advantange is that the writing process requires no preceding reading operation.

Recently, it has been shown that a vortex confined in a thin-film element performs elliptical rotations around its equilibrium position when excited by an alternating current [123, 126, 131–135] or magnetic field [123, 131, 136]. We propose that a collinear arrangement of electrical current density and magnetic field as depicted in Fig. 3.2 (a) yields a way to employ the magnetic vortex as a storage device.
A possible technical realization of the vortex random-access memory (VRAM) is shown in Fig. 3.2 (b), where the ferromagnetic cells are aligned on a strip line. Each storage cell contains a vortex. The injected current splits up in two parts: one flowing in x direction through a distinct cell and the other flowing in y direction underneath the cell array. While the first part of the current flows straight through the ferromagnetic material of the selected VRAM cell, the second part of the current passes by the VRAM cells in a strip-line beneath the cells. The current in x direction is the writing current, which excites the vortex of a single cell due to the spin-torque effect. [5, 132] The role of the second current is to create an alternating, spatially homogeneous Oersted field in the cell above it, which results in a precession of the vortices in the cells (cf. Fig. 3.2 (b)). Thus, the scheme proposed in Fig. 3.2 (a) provides a parallel arrangement of electrical current density and magnetic field. For a current density $\vec{j} = j\vec{e}_x$ and a magnetic field $\vec{H} = H\vec{e}_x$ the equation of motion for the quasiparticle vortex reads [123]

$$\begin{pmatrix} \dot{X} \\ \dot{Y} \end{pmatrix} = \begin{pmatrix} -\Gamma & -p\omega \\ p\omega & -\Gamma \end{pmatrix} \begin{pmatrix} X \\ Y \end{pmatrix} + \begin{pmatrix} -v_\mathrm{j} - \frac{\Gamma^2}{\omega^2+\Gamma^2}\frac{\xi-\alpha}{\alpha}v_\mathrm{j} \\ \frac{p\omega\Gamma}{\omega^2+\Gamma^2}\frac{\xi-\alpha}{\alpha}v_\mathrm{j} \end{pmatrix} + \frac{v_\mathrm{H}\omega c}{\omega^2+\Gamma^2}\begin{pmatrix} p\omega \\ \Gamma \end{pmatrix}. \tag{3.10}$$

The equation of motion (3.10) follows from substituting the gyrovector (3.6) and the expression for the force (3.9) into Eq. (3.8). The free angular frequency $\omega = -pG_0 m\omega_r^2/(G_0^2 + D_0^2\alpha^2)$ and the damping constant $\Gamma = -D_0\alpha m\omega_r^2/\left(G_0^2+D_0^2\alpha^2\right)$ (cf. Eq. (3.9)). [123] The driving velocity due to the magnetic field H is $v_\mathrm{H} = \gamma H l/(2\pi)$ with the edge length l of the cell. The driving velocity of the current is $v_\mathrm{j} = b_j j$. The coupling constant between the current and the magnetization is $b_j = P_j\mu_B/[eM_s(1+\xi^2)]$, where P is the spin polarization, M_s the saturation magnetization, ξ the degree of non-adiabaticity, [5] and α the phenomenological Gilbert-damping parameter. The resonance frequency of the vortex due to the demagnetizing field [123] is ω_r, and G_0 (3.6) and D_0 (3.7) are constants of the gyrovector and dissipation tensor, [120] respectively. A special feature of Eq. (3.10) is that a parallel or antiparallel arrangement of current density and Oersted field leads to either an enhancement or a quenching of the

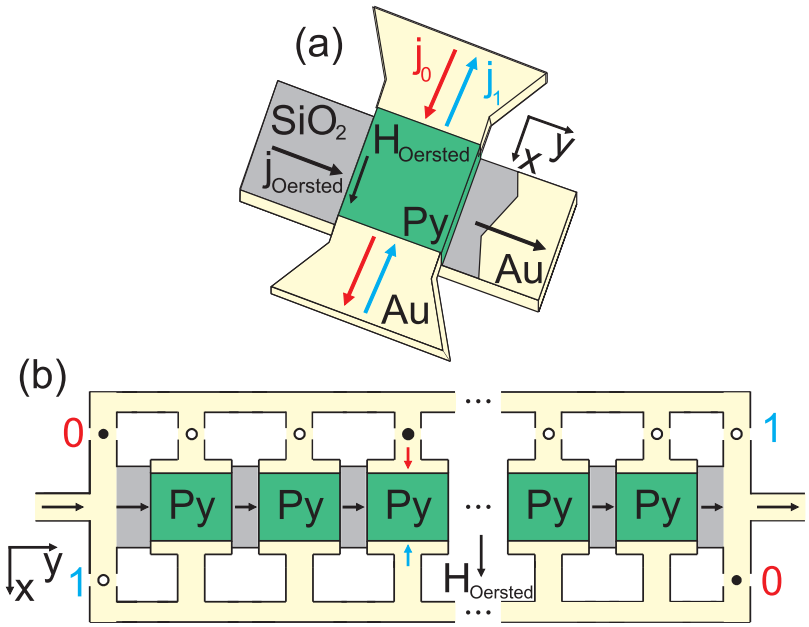

Figure 3.2: (Color online) (a) A single vortex random-access memory (VRAM) cell with collinear current and Oersted field. (b) Possible technical realization of a VRAM. The cells are arranged in a two-dimensional array from which one row is depicted. The high-ohmic permalloy squares constitute the memory cells while the gold strip lines supply the read-write current. Open (filled) circles symbolize open (closed) switches that are used to store information in an individual cell. The numbers 0 and 1 denote the switches, which have to be activated to write the according bit in the activated cell. The configuration shown here writes a binary "zero" into the third cell (red arrow).

gyration amplitude of vortex motion in agreement with the results for antivortices. [137] The steady-state solution of Eq. (3.10) with harmonic current excitation for which the magnetic field and the electrical current density are of the form $H(t) = H_0 e^{i\Omega t}$ and $j(t) = j_0 e^{i\Omega t}$ yields [123]

$$\begin{pmatrix} X \\ Y \end{pmatrix} = \frac{e^{i\Omega t}}{\omega^2 + (i\Omega + \Gamma)^2} \begin{pmatrix} -\frac{\Gamma}{\omega}\frac{\xi}{\alpha} v_\mathrm{j}\omega & + & \left(v_\mathrm{H} cp - v_\mathrm{j}\right) i\Omega \\ \left(v_\mathrm{H} cp - v_\mathrm{j}\right) p\omega & + & \frac{\Gamma}{\omega}\left(v_\mathrm{H} cp + \frac{\xi-\alpha}{\alpha} v_\mathrm{j}\right) ip\Omega \end{pmatrix}, \tag{3.11}$$

under the assumption that the squared Gilbert-damping parameter is small ($\alpha^2 \ll 1$), and thus the damping constant is small compared to the frequency ($\Gamma^2 \ll \omega^2$). At resonance ($\Omega = \omega$) and for weak damping ($\Gamma \ll \omega$) the steady-state vortex motion is a circle with radius

$$R(v_\mathrm{H}, v_\mathrm{j}, \Gamma, cp) = \sqrt{(\Re X)^2 + (\Re Y)^2} = \frac{|v_\mathrm{H} cp - v_\mathrm{j}|}{2\Gamma}, \tag{3.12}$$

which depends on the vortex handedness cp. When the driving velocities of field and current are equal ($|v_\mathrm{H}| = |v_\mathrm{j}|$), Eq. (3.12) yields a doubling or a quenching of the gyration amplitude dependent on the handedness.

The key mechanism of the VRAM is to employ that the gyration amplitude behaves oppositely for the cases $cp = 1$ and $cp = -1$ without the need to determine the absolute values of c or p separately. From the viewpoint of binary logic the proposed arrangement reduces the fourfold degenerate vortex ground state to two distinct cp states with two representations representing the single bit. In the following let us define the "zero" ("one") by cp positive (cp negative).

Recent numerical investigations of the vortex-core switching have shown that the switching depends only on the velocity of the vortex [138, 139] and thus on the radius of gyration. Furthermore, the critical velocity for switching was found to be an intrinsic parameter and hence does not depend on specific properties of the driving force. [138] There exist theories about the critical velocity for switching. [126, 139] For permalloy Guslienko et al. estimated $v_\mathrm{switch} \approx 320$ m/s while Yamada et al. found $v_\mathrm{switch} \approx 250$ m/s "regardless of the excitation current density" (cf. Ref. [126]). According to Guslienko et al., [139] the critical velocity is proportional to the saturation magnetization or the square root of the exchange constant. Thus for permalloy structures (exchange constant of $A = 13 \cdot 10^{-12}$ J/m, lateral sample size of 200 nm, and a thickness of 20 nm), the critical current density is $1.3 \cdot 10^{11}$ A/m^2 for pure current excitation and a critical velocity of $v_\mathrm{switch} \approx 320$ m/s. This corresponds to a current of ≈ 0.5 mA and an absorbed power of 2.7 μW. Thus, if for $|v_\mathrm{H}| = |v_\mathrm{j}|$ the current amplitude is tuned to more than half of its critical value that is defined as the current amplitude needed for switching the vortex due to current alone, the vortex ends up with a distinct handedness. In the case of current parallel to field, a quenching of the vortex motion occurs for positive cp (cf. Eq. (3.12)) and the values of c and p remain the same. For negative cp, a doubling of the gyration amplitude and therefore a switching of the vortex occurs, since the radius attains the critical value. While the polarization changes during the switching process, the chirality is conserved. After the switching the vortex comes to rest being now in the opposite cp state, which immediately leads to cancellation of the driving forces. The subsequent free damped oscillation results in a quenching of the vortex rotation. Irrespective of the starting configuration, this writing process leads to the defined property $cp = +1$ representing the binary value "zero". Accordingly to write the binary "one" $cp = -1$, the direction of the spin-torque has to be inverted. This can be achieved by reversing the direction of the current flowing in opposite x direction through the cell ($v_\mathrm{j} \to -v_\mathrm{j}$) as shown in Fig. 3.2 (b). The information

is permanently stored in the magnetic-vortex configuration cp even when the current is switched off. Instead of using an alternating current it is possible to operate the VRAM with short current pulses $v_{\mathrm{H}}^{\mathrm{p}}$ and $v_{\mathrm{j}}^{\mathrm{p}}$. Numerical investigations have shown that pulses offer the advantage of vortex switching that is up to one order of magnitude faster than switching by alternating currents. [127, 140] If we choose a collinear arrangement for current and field and consider that the damping constant is small compared with the frequency of the free vortex ($\Gamma \ll \omega$), Eq. (3.10) reduces to

$$\begin{pmatrix} \dot{X} \\ \dot{Y} \end{pmatrix} = \begin{pmatrix} -\Gamma & -p\omega \\ p\omega & -\Gamma \end{pmatrix} \begin{pmatrix} X \\ Y \end{pmatrix} + \begin{pmatrix} v_{\mathrm{H}}^{\mathrm{p}} cp - v_{\mathrm{j}}^{\mathrm{p}} \\ 0 \end{pmatrix}. \tag{3.13}$$

The last term is the driving force. Equation (3.13) states that the action of short current and magnetic field pulses compensate or amplify each other depending on the handedness of the vortex.
In principle, a vortex excitation in a collinear alignment of current and field could be replaced by a rotating magnetic field making use of the polarization p instead of the combined quantity cp. [141, 142] However, a setup with a rotating field requires two currents with a phase shift of $\pi/2$ (cf. Ref. [142]). We want to point out that a main advantage of our concept is to use one current only.
For the reading mechanism it is necessary to determine the product cp as the bit information is encoded in the handedness. If current and field are aligned parallel, the binary value "zero" ("one") corresponds to a resting (rotating) vortex. In the absence of current and field, precession or cessation of precession of the vortex holds no information about the actual memory state of the VRAM cell. Thus a small reading current, together with the magnetic field in the collinear arrangement, is needed to determine the cp state. For parallel current and field, reading collimates in the task of distinguishing a vortex at rest ($cp = +1$) from a rotating vortex ($cp = -1$). The proposed VRAM realization in Fig. 3.2 consists of a two-dimensional array of permalloy cells. The rotating vortex creates a time-varying magnetic flux that can be measured by placing a pickup coil (induction loops) above the storage cell or by detecting resistance changes. [143, 144] To read out the information a lower current density compared to the writing current density has to be used. A current density less than half of the critical current density has neither an influence on the polarization nor on the chirality. Thus, the VRAM cell can be read out an infinite number of times without affecting its binary state.

In conclusion we propose a magnetic vortex random-access memory (VRAM). In a collinear current and field arrangement, we established an one-to-one correspondence of the vortex handedness to the binary values "zero" and "one". The VRAM needs not be read or erased preceding the writing and, in general, allows an infinite number of read and write operations. This is an advantage compared with existing memory technologies, such as the FLASH memory, which requires a slow erasing procedure of the present memory state. [145, 146] The VRAM concept is non-volatile and fulfills the stability requirements for a memory device, since the vortex state is stable against temperature and magnetic fields as long as they remain in the millitesla regime. The VRAM shows a good scaling behavior, in general no material fatigue, and is foremost a fast memory concept.

Chapter 4

Influence of inhomogeneous current distribution on vortex motion

THE INFLUENCE OF inhomogeneous current paths on the gyroscopic motion of current-driven magnetic vortices in small thin-film elements is investigated by numerical simulations. It is found that the deflection of the gyrating vortex scales quadratically with the ratio of the anisotropic magnetoresistance. The enhancement of the gyration amplitude scales with the fundamental ratio between the dissipation tensor and the gyrovector and is determined by the lateral sample size and the sample thickness. The counteraction of the magnetization to the current manifests itself in a geometry-dependent renormalization of the spin transfer-torque coupling parameter.

4.1 Anisotropic magnetoresistance

Transport in ferromagnetic metals exhibits remarkable features compared with transport in non-magnetic metals. The oldest known phenomenon is the anisotropic magnetoresistance at small magnetic fields ($\leq$ 1 T). [1] Applying a magnetic field parallel (perpendicular) to the direction of the current flow results in a hysteretic behavior of the resistance. The electric resistivity is governed by the magnetization within the sample that corresponds in ferromagnetic metals to field strength up to ≈ 1 T and thus usually dominates the external applied field. Nevertheless, the magnetization configuration of the sample is controlled by the external field. It turns out that for transition metals the resistance of the sample is higher for a parallel alignment of current and magnetization and accordingly lower for a perpendicular orientation of both. The total sample resistivity obeys the relation

$$\rho = \rho_{\perp} + \Delta\rho \, \langle \cos^2(\measuredangle(\vec{j}, \vec{M})) \rangle, \tag{4.1}$$

where $\rho_{||}$ ($\rho_{\perp}$) are the resistances for the sample being saturated due to an external magnetic field parallel (perpendicular) to the current flow and $\Delta\rho = \rho_{||} - \rho_{\perp} > 0$ measures the anisotropy in the resistivity. [147, 148] Thus, the anisotropic magnetoresistivity depends on the mutual angle $\measuredangle(\vec{j}, \vec{M})$ that encloses the electric current with the local magnetization, which in turn depends on the direction of the external magnetic field. The brackets in Eq. (4.1) denote an averaging over the sample, where a constant current density throughout the sample is assumed.

A microscopic explanation of the AMR effect dates back to 1951 [149] and 1974 / 75 [147, 148]:

The conduction electrons are coupled to the local magnetization by means of spin-orbit interactions via scattering processes. The individual scattering events give rise to a spin asymmetric lifetime, whereas the asymmetry depends on the angle between current and magnetization. [147, 148] The conduction electrons possess a larger scattering cross section for collinear alignment of conduction-electron spin and magnetization and a smaller scattering cross section for transverse alignment due to an asymmetric density of states. We note at this point that the precise mechanism for the AMR effect in transition metals is still elusive and a matter of current research. [150, 151]

4.2 Influence of inhomogeneous current distributions on the motion of magnetic vortices

4.2.1 Introduction

Today's interest in spin-transfer torque phenomena can be traced back to its technological importance with the perspective of being the future in magnetic technology. At the same time spin-transfer torque poses a theoretically appealing problem as it involves the interaction of non-equilibrium conduction electrons with the ferromagnetic order parameter, i.e., the magnetization. An understanding of the mutual interplay of both, current and magnetization, allows for a controlled manipulation of magnetization reversal and thus paves the path for current-controlled magnetic storage devices. Considering the mutual influence of electrical current and magnetization on equal footing provides the basis to a variety of fascinating non-linear spin-dependent phenomena. While the torque of a spin-polarized current influences the local magnetization [14, 15], vice versa the magnetization influences the current flow via the anisotropic magnetoresistance (AMR). [1] The microscopic origin of the AMR is spin-orbit coupling. [148] Due to an asymmetric density of states the conduction electrons possess a larger scattering cross section for collinear alignment of conduction-electron spin and magnetization and consequently a smaller scattering cross section for transverse alignment. Classically spin-orbit coupling results in local resistance variations. [147] A transfer of spin-angular momentum from itinerant s-like conduction electrons to localized d electrons (spin-transfer torque) emerges in non-collinear magnetization patterns. It is accompanied by local resistance changes due to the AMR effect. An increase of the resistivity leads to a local reduction of the current density. This causes a locally reduced spin-transfer torque acting on the magnetization dynamics. In turn, the magnetization influences the local resistivity. As a result, the mutual influence of current and magnetization causes non-linear effects in the linear regime of electron transport.

Due to the non-collinearity, but high symmetry of its magnetization pattern and its quasiparticle-(soliton)-like behavior, the magnetic vortex in a micro- or nanostructured thin-film element is a prime example to study the interplay of electrical current and magnetization. Vortices are flux-closured states where the in-plane magnetization curls around a few nanometer large center region [129] to minimize the overall energy. Large angles between neighboring magnetic moments lead to a drastic increase of the exchange energy. [152] To overcome this situation the magnetization is forced out-of-plane forming the vortex core in the center of the thin-film element. In ferromagnetic square thin-film elements the vortex constitutes the energetic groundstate being fourfold degenerate due to the boolean vortex properties chirality and core polarization. Chirality and core polarization are topological quantities

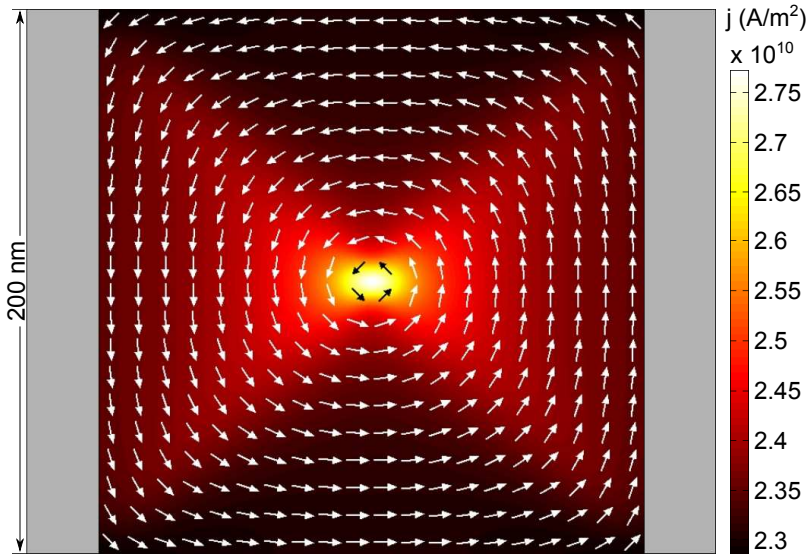

Figure 4.1: (Color online) Inhomogeneous current distribution of a magnetic vortex in a $200 \times 200 \times 20\,\mathrm{nm}^3$ permalloy square. The arrows sketch the in-plane magnetization while the color (dark to bright) scales with the current density. The current flowing from left to right tends to flow through the vortex core. The gray areas indicate the non-magnetic ohmic contacts.

that characterize a vortex. A chirality of $+1$ (-1) denotes a counterclockwise (clockwise) curling of the magnetization around the vortex core while a polarization of $+1$ (-1) labels the out-of plane direction of the magnetization in the vortex core, up (down) respectively. Recent experiments showed that spin-polarized electric currents cause the vortex to precess. [126, 135, 138, 153] Hitherto, analytical expressions as well as micromagnetic simulations confirming the elliptical gyration of vortex cores, take a homogeneous current flow into account neglecting the effect of inhomogeneous current paths occurring in real samples due to the AMR. The process of vortex-core switching is of fundamental interest and still an open question. Moreover it is of general interest, as vortex-core switching is the key ingredient in recent memory device proposals. [118, 154] Thus for both, a detailed understanding of current-driven vortex dynamics and the purpose of technical utilization, it is crucial to consider realistic current paths.

In this chapter we investigate the current-driven gyroscopic motion of a magnetic vortex in square thin-film elements in the presence of an inhomogeneous current flow exemplarily depicted in Fig. 4.1. In the case of a homogeneous current the vortex gyration is topological in nature as the gyrotropic force that acts on the vortex and is responsible for its gyration solely depends on the vortex' polarization but is independent of the size of the vortex core. [120] We conclude that in the case of a vortex the non-linear effect of the counteraction of the magnetization on the current leads to an enhancement of the gyration amplitude while it does not affect the quasiparticle like behavior of the vortex at all, e.g., no shape deformations are visible. As a consequence, the consideration of realistic current distributions leads to a geometry-dependent correction of the vortex' motion.
This chapter is organized as follows: In section 4.2.2 we explain how to consider inhomogeneous

current paths due to non-collinear magnetization textures in the time-evolution of the magnetization. Section 4.2.3 investigates the gyroscopic motion of magnetic vortices and compares the homogeneous with the inhomogeneous case. Section 4.2.4 yields a theoretical explanation of the simulated findings. Section 4.2.5 summarizes our findings of the amplitude enhancement in an analytical expression for the renormalized spin-transfer torque coupling parameter. Section 4.2.6 attends to the highly non-linear regime of vortex-core switching. This chapter ends in Section 4.2.7 with a conclusion.

4.2.2 Numerical simulations

In a continuous ferromagnet the influence of a spin-polarized current on the time-evolution of the magnetization $\vec{M}(\vec{r},t)$ is considered by the extended Landau-Lifshitz-Gilbert equation (cf. section 2.2 and 2.3) [5]

$$\begin{aligned}\frac{d\vec{M}(\vec{r},t)}{dt} =& -\gamma\vec{M}(\vec{r},t)\times\vec{H}_{\text{eff}}(\vec{r},t)+\frac{\alpha}{M_s}\vec{M}(\vec{r},t)\times\frac{d\vec{M}(\vec{r},t)}{dt}\\ &-\frac{b_j}{M_s^2}\vec{M}(\vec{r},t)\times\Big(\vec{M}(\vec{r},t)\times(\vec{j}(\vec{r},t)\cdot\vec{\nabla}_{\vec{r}})\vec{M}(\vec{r},t)\Big)\\ &-\xi\frac{b_j}{M_s}\vec{M}(\vec{r},t)\times(\vec{j}(\vec{r},t)\cdot\vec{\nabla}_{\vec{r}})\vec{M}(\vec{r},t),\end{aligned} \tag{4.2}$$

where $b_j = P_j\mu_B/[eM_s(1+\xi^2)]$ is the coupling constant between current and magnetization, P is the absolute value of the spin polarization and M_S is the saturation magnetization. The terms containing the Gilbert damping α and the degree of non-adiabaticity ξ are dissipative in the sense that they break the time-reversal symmetry of the Landau-Lifshitz-Gilbert equation, i.e., they are odd under time-reversal transformation $t\to -t, \vec{H}_{\text{eff}}\to -\vec{H}_{\text{eff}}, \vec{j}\to -\vec{j}, \vec{M}\to -\vec{M}$. [155]
The electronic transport is treated classically and calculated quasi-statically from a local version of Ohm's law

$$\vec{j}(\vec{r}) = \sigma(\vec{r})\vec{E}(\vec{r}), \tag{4.3}$$

while local charge neutrality is considered, $\vec{\nabla}_{\vec{r}}\vec{j}(\vec{r}) = -\frac{\partial}{\partial t}\rho(\vec{r}) = 0$,

$$\vec{\nabla}_{\vec{r}}\vec{j}(\vec{r}) = \vec{\nabla}_{\vec{r}}\Big[\sigma(\vec{r})\vec{\nabla}_{\vec{r}}\,\Phi(\vec{r})\Big] = 0. \tag{4.4}$$

The influence of the magnetization on the current flow is incorporated in Eq. (4.4) via a magnetization-dependent conductivity tensor $\sigma(\vec{r}) = \sigma(\vec{M}(\vec{r}))$. The shape of the conductivity tensor accounts for the AMR, such that the resistivity locally obeys the relation

$$\rho = \rho_\perp + \Delta\rho\cos^2(\measuredangle(\vec{j},\vec{M})), \tag{4.5}$$

which reflects the $\cos^2$-resistance dependence on the angle between local current and magnetization. The AMR ratio in thin-film elements

$$\rho_{\text{AMR}} = \frac{\rho_{||}-\rho_\perp}{\rho_{||}+\rho_\perp} \equiv \frac{\Delta\rho}{\rho_{||}+\rho_\perp}, \tag{4.6}$$

characterizes the strength of the AMR effect. The material parameters $\rho_{||}$ ($\rho_\perp$) are the resistances for the sample being saturated due to an external magnetic field parallel (perpendicular) to the current

flow. Thus, the anisotropic magnetoresistivity $\Delta\rho$ is the change in resistance between a parallel and a perpendicular directed magnetization with respect to the applied current.
In order to compute realistic current paths that take into account the anisotropic magnetoresistance, we now derive the general shape for the conductivity tensor in arbitrary magnetization textures. In the local reference frame of the magnetization, the resistivity tensor is diagonal (cf. section C)

$$\rho = \begin{pmatrix} \rho_\perp & 0 & 0 \\ 0 & \rho_\perp & 0 \\ 0 & 0 & \rho_{||} \end{pmatrix}, \tag{4.7}$$

where we let the magnetization w.l.o.g. point in z direction. The two different elements of the resistivity tensor in Eq. (4.7) are the phenomenological resistivities introduced in Eq. (4.1) and take into account that the resistivity is different for a parallel compared to a perpendicular alignment of current and magnetization. The next step is to perform a local rotation from the reference frame of the magnetization to the laboratory frame. This transformation is most easily carried out by decomposing Eq. (4.7) according to

$$\rho = \rho_\perp \mathbb{1} + \left(\rho_{||} - \rho_\perp\right) \begin{pmatrix} 0 & 0 & 0 \\ 0 & 0 & 0 \\ 0 & 0 & 1 \end{pmatrix}. \tag{4.8}$$

The first part in Eq. (4.8) is manifest invariant with respect to rotations and the second part can be transformed by introducing the laboratory basis elements with respect to the magnetization, which point in the cartesian directions of the laboratory frame

$$\vec{e}_{m_i} = \begin{pmatrix} \cdots \\ \cdots \\ m_i \end{pmatrix}, \quad i = x, y, z. \tag{4.9}$$

The precise shape of the first two components are not important and thus neglected in Eq. (4.9). By a projection of Eq. (4.8) on the laboratory basis as provided by Eq. (4.9)

$$\Delta\rho\, \vec{e}_{m_i} \cdot \begin{pmatrix} 0 & 0 & 0 \\ 0 & 0 & 0 \\ 0 & 0 & 1 \end{pmatrix} \cdot \vec{e}_{m_j} = \Delta\rho\, m_i m_j, \quad i, j = x, y, z. \tag{4.10}$$

we attain the shape of the resistivity tensor in the laboratory frame $\tilde{\rho}_{ij} = \rho_\perp \delta_{ij} + \Delta\rho\, m_i m_j, \quad i, j = x, y, z$

$$\tilde{\rho} = \rho_\perp \mathbb{1} + \Delta\rho \begin{pmatrix} m_x^2 & m_x m_y & m_x m_z \\ m_x m_y & m_y^2 & m_y m_z \\ m_x m_z & m_y m_z & m_z^2 \end{pmatrix}. \tag{4.11}$$

With the help of the identity $m_x^2 + m_y^2 + m_z^2 = 1$, the general resistivity tensor in Eq. (4.11) can be written as

$$\tilde{\rho} = \begin{pmatrix} \rho_\perp(m_y^2 + m_z^2) + \rho_{||} m_x^2 & \Delta\rho\, m_x m_y & \Delta\rho\, m_x m_z \\ \Delta\rho\, m_x m_y & \rho_\perp(m_x^2 + m_z^2) + \rho_{||} m_y^2 & \Delta\rho\, m_y m_z \\ \Delta\rho\, m_x m_z & \Delta\rho\, m_y m_z & \rho_\perp(m_x^2 + m_y^2) + \rho_{||} m_z^2 \end{pmatrix}. \tag{4.12}$$

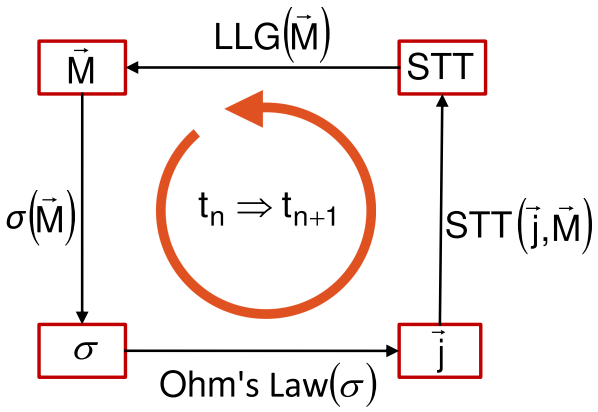

Figure 4.2: (Color online) Self-consistency loop for the numerical computation of current-induced magnetization dynamics. The physical quantities in the boxes are solutions of the equations as denoted by the arrows. The anisotropic magnetoresistance is considered within a magnetization-dependent conductivity tensor $\sigma(\vec{M}(\vec{r}))$. The current paths $\vec{j}(\vec{r})$ are obtained from Ohm's law and are incorporated via the spin-transfer torque (STT) in the Landau-Lifshitz-Gilbert (LLG) equation.

The final shape of the resistivity tensor reads with $\vec{M} = M_s\vec{m}$

$$\tilde{\rho} = \frac{1}{M_s^2}\begin{pmatrix} \rho_\perp(M_y^2+M_z^2)+\rho_{||}M_x^2 & \Delta\rho M_xM_y & \Delta\rho M_xM_z \\ \Delta\rho M_xM_y & \rho_\perp(M_x^2+M_z^2)+\rho_{||}M_y^2 & \Delta\rho M_yM_z \\ \Delta\rho M_xM_z & \Delta\rho M_yM_z & \rho_\perp(M_x^2+M_y^2)+\rho_{||}M_z^2 \end{pmatrix}. \tag{4.13}$$

Owing to the local form of the resistivity tensor in Eq. (4.13), the corresponding conductivity tensor is obtained by inverting Eq. (4.13)

$$\tilde{\sigma} = \tilde{\rho}^{-1}. \tag{4.14}$$

It follows from Eq. (4.5) or (4.13) that for non-collinear magnetization textures the magnetization influences the current via the anisotropic magnetoresistance by a spatially varying conductance. Figure 4.1 depicts the solution of the current density for a current passing a magnetic vortex structure in a permalloy square. The arrows sketch the in-plane magnetization of the vortex curling counterclockwise around the vortex core in the center. The sample dimensions are 200×200 nm^2 with a thickness of 20 nm. Dirichlet boundary conditions are imposed on the current biased probes (gray bars on the left and right hand side in Fig. 4.1) to fix the potential of the probes. Von Neumann boundary conditions ensure that no current leaves the sample through the upper or lower sample boundaries. Thus the current flows from left to right. The current favors the vortex core resulting in a higher local current density (bright color). In areas where the current is aligned perpendicular to the magnetization the conductivity is higher than in areas where the current is aligned parallel to the magnetization.
In the numerical simulations the mutual influence of current and magnetization is taken into account by gradually plugging the numerical result for the magnetization from Eq. (4.2) into the conductivity tensor of Eq. (4.3), calculating the current from Eq. (4.3) for the desired time-step Δt of Eq. (4.2), and iterating this procedure. The self-consistent calculation scheme for the counteraction of the magnetization on the current is illustrated in Fig. 4.2. The approach is justified because the band structure

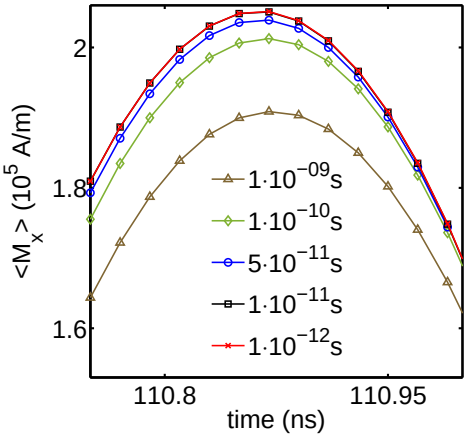

Figure 4.3: (Color online) Mean x component of the magnetization of a magnetic vortex in a $200 \times 200 \times 20\,\mathrm{nm}^3$ permalloy square versus time. The different lines are the average x component of the magnetization belonging to the indicated timestep for the calculation of the current paths.

responsible for the electronic transport relaxes orders of magnitude faster ($\tau_{\mathrm{bs}} \approx 10^{-14}\,\mathrm{s}$) than the typical time scale of magnetization dynamics that is set by the Larmor frequency $\omega = \gamma M_s$ and is on the order of $\tau_{\vec{M}} \approx 10^{-11} - 10^{-12}\,\mathrm{s}$. There exist a separation of time scales in the fast electronic dynamics of the conduction electrons and the comparatively slow collective dynamics of the localized d electrons that constitute the magnetization. [156] From the viewpoint of the time-evolution of the magnetization the current flow is always in its steady state and can be computed quasi-statically by means of Eq. (4.3). The spin-transfer torque on the contrary is locally modulated by the inhomogeneous current density $\vec{j}(\vec{r})$ and acts on spatial inhomogeneities of the magnetization texture (cf. Eq. (4.2)). The local conductivity $\sigma(\vec{M}(\vec{r}))$ and thus the inhomogeneous current is determined by the magnetization itself and therefore varies on the time scale of magnetization dynamics. Thus, to capture the effect of the AMR on the vortex motion it is sufficient to compute the current paths on the time scale of vortex dynamics. Figure 4.3 depicts the mean x component of the magnetization of a gyrating vortex in its steady state. The sample dimensions are $200 \times 200\ \mathrm{nm}^2$ with a thickness of 20 nm and an AMR ratio $\rho_{\mathrm{AMR}} = 0.5$. As long as the time interval for a new current path calculation is below $\Delta t = 10^{-11}\,\mathrm{s}$ the result for the gyration amplitude is not affected and the physical results are independent of the unphysical time-interval for the current path calculation. This observation is in agreement with the Larmor frequency that takes for permalloy (Py=$\mathrm{Ni}_{80}\mathrm{Fe}_{20}$) a value of $\omega_{\mathrm{Py}} = 1.77 \cdot 10^{11} s^{-1}$. Furthermore it is consistent with the adiabatic approximation that spin and charge currents are governed by the instantaneous magnetization that is implicitly assumed in the spin-transfer torque terms of Eq. (4.2).

In the case of harmonic excitations the vortex performs elliptical rotations. [123] At resonance the amplitude of the vortex core displacement in x and y direction is the same and the orbit is a circle. The ratio between the semi-axes is given by the ratio between the frequency of the excitation and the

resonance frequency. [123] The sense of rotation of the vortex is controlled by its polarization, i.e., $p = +1$ ($p = -1$) causes a counterclockwise (clockwise) gyration of the vortex core around its equilibrium position. The analytic equation of motion for an applied homogeneous current in x direction reads for the quasiparticle coordinates of the vortex core [123]

$$\begin{pmatrix} \dot{X} \\ \dot{Y} \end{pmatrix} = \begin{pmatrix} -\Gamma & -p\omega \\ p\omega & -\Gamma \end{pmatrix} \begin{pmatrix} X \\ Y \end{pmatrix} + \begin{pmatrix} -b_j j - \frac{\Gamma^2}{\omega^2+\Gamma^2} \frac{\xi-\alpha}{\alpha} b_j j \\ \frac{p\omega\Gamma}{\omega^2+\Gamma^2} \frac{\xi-\alpha}{\alpha} b_j j \end{pmatrix}. \tag{4.15}$$

The free angular frequency $\omega = -pG_0 m\omega_r^2/(G_0^2 + D_0^2\alpha^2)$ and the damping constant $\Gamma = -D_0\alpha m$ $\omega_r^2/(G_0^2 + D_0^2\alpha^2)$, as well as the constants G_0 of the gyrovector and D_0 of the dissipation tensor are defined in Ref. [123] (cf. section 3.2). Figure 4.4 depicts the analytical steady-state trajectory of a vortex according to Eq. (4.15). The snapshots are the spatially resolved magnetization patterns and their corresponding current densities in the sample plane for four exemplary positions.

4.2.2.1 Numerical discretization of the extended Landau-Lifshitz-Gilbert equation

An analytic solution of the Landau-Lifshitz-Gilbert equation (4.2) is possible only in low-dimensional scenarios that possess a high symmetry. In the general case, the continuum micromagnetic model must be solved numerically by means of a tempo-spatial discretization on a grid. In this thesis a finite-difference method-based Poisson solver in MATLAB has been developed. [157] The integration of the Poisson solver and the micromagnetic solver M^{3}S, written by Massoud Najafi in MATLAB, happened in close collaboration with Massoud Najafi.

In order to capture important dynamical effects in mesoscopic samples such as domain wall deformation or transformation, in particular the formation of vortex structures, it is important to treat the long-ranged magnetic dipole interaction accurately. In micromagnetic simulations the magnetic dipole interaction is treated in a mean-field way by a continuum limit of the dipole-dipole interaction between the individual discretization cells. [158] This involves an interaction between each discretization cell with every other cell and is thus computationally demanding.

As a classical continuum theory, the micromagnetic model possesses some limits concerning its range of applicability. First, by implication of the gradient approximation for the exchange energy (cf. section 2.2), large angles between the magnetization vectors of neighboring discretization cells are forbidden. This demands small discretization cells and thus limits the size of the samples that can be treated in a reasonable computational amount of time. More precisely, in order to resolve micromagnetic structures in micromagnetic simulations properly, the simulation cell size must significantly below the exchange length

$$L_{\text{ex}} = \sqrt{\frac{2A}{\mu_0 M_s^2}}, \tag{4.16}$$

that sets the relevant length scale in the micromagnetic model. Secondly, as a classical continuum theory, singularities such as Bloch points are forbidden, though they are allowed in lattice models. [159] Bloch points appear in micromagnetic simulations, for instance during the annihilation of vortex-antivortex pairs as an artifact of the spatial discretization.

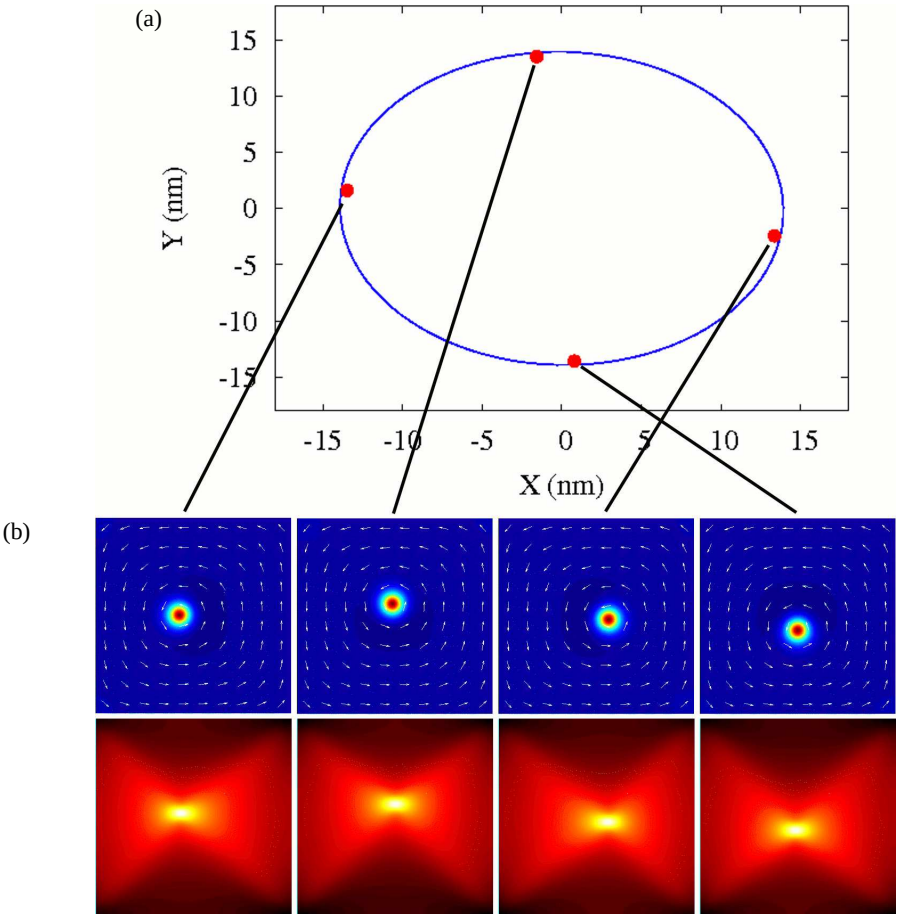

Figure 4.4: (Color online) Steady-state trajectory of a current-driven magnetic vortex in a $200 \times 200 \times 20\,\mathrm{nm}^3$ permalloy square. (a) The line represents the analytical trajectory. The dots mark the positions of the vortex core that corresponds to the particular inset. (b) The insets depict the numerical results of the self-consistently calculated mutual current and magnetization dynamics. The upper row shows the spatially resolved magnetization where the arrows indicate the in-plane magnetization. The lower row displays the current density with the same scale as in Fig. 4.1.

4.2.3 Numerical results for coupled current and magnetization dynamics

To investigate the influence of inhomogeneous current distributions on the magnetic vortex by means of the coupled Eqns. (4.2) and (4.3), we conduct micromagnetic simulations. We perform simulations for magnetic thin-film elements with different lengths l and thicknesses t for various current densities and AMR values. In the following, the parameters of polarization and chirality are not varied. It follows from symmetry considerations that they do not influence the current flow in perfect square elements. We use the material parameters of permalloy, i.e., an exchange constant of $A = 13 \cdot 10^{-12}$ J/m and a saturation magnetization of $M_s = 8 \cdot 10^5$ A/m. For the Gilbert damping we assume a value of $\alpha = 0.01$, which is affirmed by recent experiments. [160–162] The degree of non-adiabaticity ξ is set to be equal to α. [103, 163]
The simulation cells are chosen to be one cell of thickness t in z direction and 2 nm in x and y direction, which is well below the exchange length of permalloy. The position of the vortex is characterized by the maximum amplitude of the out-of-plane magnetization. It is determined by an interpolation with the Lagrange polynomial of second order of the respective simulation cell with maximum out-of-plane magnetization and its next neighbors.
To deduce the influence of inhomogeneous current paths on the vortex motion, alternating currents $P\vec{j}(\vec{r},t) = P\vec{j}(\vec{r})\cos\Omega t$ flowing spatially inhomogeneously in x direction are investigated. Even in simulations with idealized values of the AMR ratio ρ_{AMR} as high as 50% no deformation of the vortex structure is visible and no deviation from the quasiparticle behavior occurs. This suggests that the rigid particle model in Eq. (4.15) is sufficient to describe the vortex dynamics in the presence of inhomogeneous currents with a concomitant renormalization of the coupling parameters due to the counteraction of the magnetization by means of the AMR. To investigate the dependence of the gyration amplitude on the AMR ratio, we excite the magnetization in a $200 \times 200 \times 20$ nm^3 permalloy square for different current densities j at the vortex resonance frequency of 4.4 GHz in the vortex' gyrotropic mode. At about 100 ns the vortex gyration has reached its steady state and the amplitudes for different AMR ratios and current densities are compared. A variation of the AMR ratio is achieved by varying the parallel resistivity $\rho_{||}$ while fixing at the same time the perpendicular resistivity $\rho_\perp$.
The gyration amplitude depicted in Fig. 4.5 exhibits a quadratic amplitude enhancement with the AMR ratio and an offset of one (dashed red line). Similarly the total sample resistance R (solid blue line) increases quadratically. The mutual coupling of inhomogeneous current flow and magnetization dynamics leads to a non-linear response of the vortex motion and in terms of electron transport causes the vortex to act as a non-linear medium for the electric current. In the case of no AMR and a homogeneous current flow the gyration amplitude of the vortex scales with the current density.
However, instead of focusing on the AMR ratio, we decided to investigate the behavior of the gyration amplitude with the anisotropic resistivity $\Delta\rho$. Figure 4.6 depicts a linear increase of the gyration amplitude (dashed red line) as well as a concomitant linear increase of the total sample resistance R (solid blue line) with $\Delta\rho$

$$r_{\text{AMR}} = \left(a\frac{\Delta\rho}{\rho_\perp} + 1\right) r_{\text{hom}}, \tag{4.17}$$

where the free parameter a is the amplitude scaling and r_{hom} is the steady-state radius in the presence of a homogeneous current flow. Due to the inhomogeneous current flow an enhanced force acts on the vortex that causes a stronger deflection and an enhanced gyration amplitude compared to a homoge-

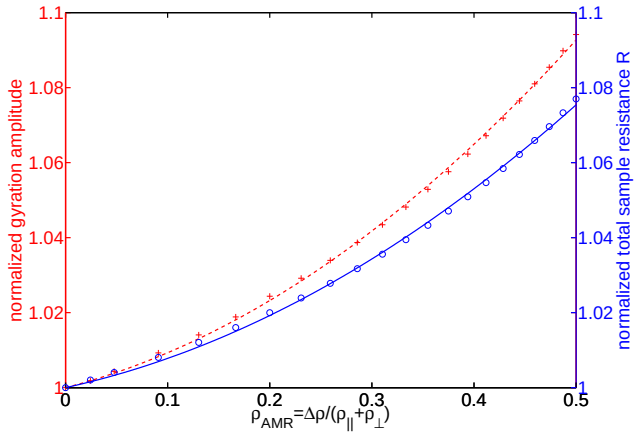

Figure 4.5: (Color online) Enhancement of the gyration amplitude of a vortex due to the anisotropic magnetoresistance ratio (dashed red line) for a current density of $2.5 \cdot 10^{10}$ A/m^2 in a $200 \times 200 \times 20$ nm^3 permalloy square. Increase of the total sample resistance versus the AMR (solid blue line). The symbols denote the numerical results while the lines are quadratic fits.

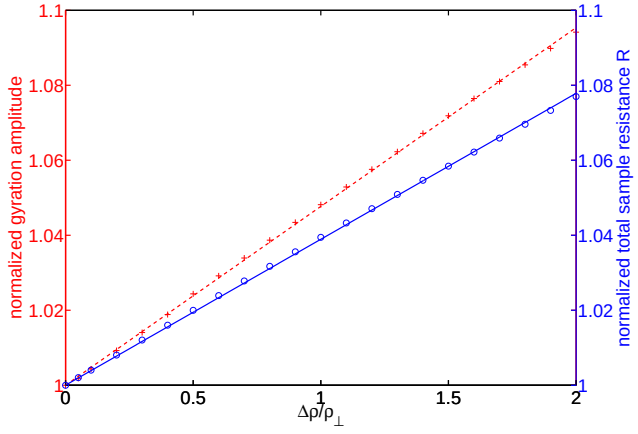

Figure 4.6: (Color online) Enhancement of the gyration amplitude of a vortex due to the anisotropic magnetoresistivity (dashed red line) for a current density of $2.5 \cdot 10^{10}$ A/m^2 in a $200 \times 200 \times 20$ nm^3 permalloy square. Increase of the total sample resistance versus the normalized anisotropic magnetoresistivity (solid blue line). The symbols denote the numerical results while the lines are linear fits.

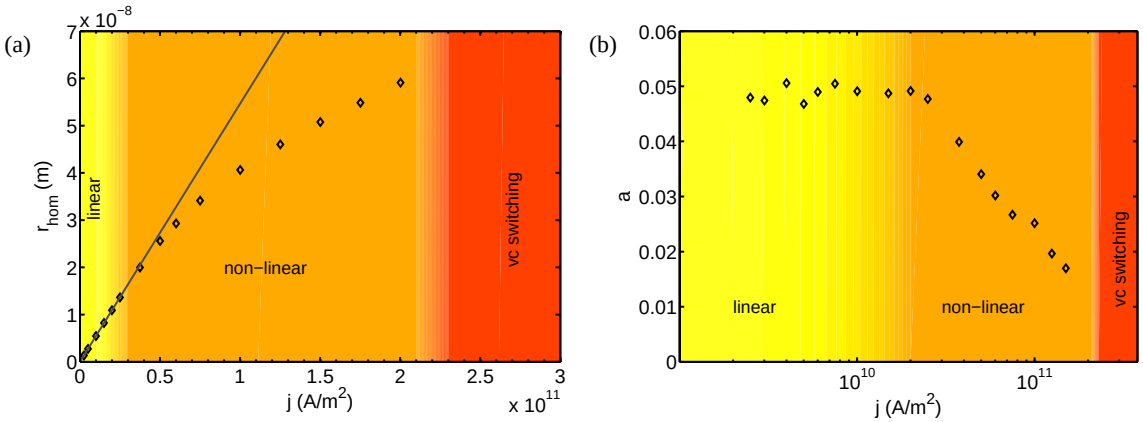

Figure 4.7: (Color online) Enhancement of the gyration amplitude of the vortex in the steady state for a $200 \times 200 \times 20$ nm^3 permalloy square. (a) Radius enhancement versus current density for a homogeneous current flow. (b) The amplitude scaling a of Eq. (4.17) in dependence of the current density.

neous current.

Next, we investigate the enhancement of the gyration amplitude with respect to the applied current density. Figure 4.7 (a) depicts the steady-state radii for a homogeneous current flow in a $200 \times 200 \times 20$ nm^3 permalloy square. There exist three regimes of translational vortex motion. These regimes depend on the applied current density and thus on the deflection of the vortex core from its equilibrium position. The vortex can be regarded as a quasiparticle that moves in a restoring potential (cf. section 3.2). [123] The restoring potential is caused by the demagnetization energy and the exchange energy due to the finite sample size and enhances with larger deflections of the vortex core from its equilibrium position. The linear regime with current densities of about $2.5 \cdot 10^9 - 2 \cdot 10^{10}$A/m^2 yields a linear increase of the steady-state amplitude with the applied current density. In the non-linear regime $2 \cdot 10^{10} - 2 \cdot 10^{11}$A/m^2 the amplitude increases in a sublinear manner. Finally there exists the highly non-linear regime of vortex-core switching, which starts at approximately $2 \cdot 10^{11}$A/m^2 with no steady-state radius due to multiple vortex-core switching. Every regime is characterized by a different dependence of the vortex motion on the applied current density. In the linear regime of the vortex gyration, the vortex moves in a parabolic potential and the enhancement of the steady-state amplitude scales linearly with the applied current density (indicated by the line in Fig. 4.7 (a)). At higher current densities the enhancement flattens due to steeper non-linearities in the restoring potential.
Figure 4.7 (b) depicts the amplitude scaling a due to the AMR as determined by Eq. (4.17) with the applied current density with the applied current density in reference to a homogeneous current flow. A variation of the applied current density leaves the linear dependence of the anisotropic magnetoresistivity unaffected but alters its slope, the amplitude scaling a, as illustrated in Fig. 4.7 (b). In the linear regime of vortex motion we find an almost constant amplitude scaling independent of the applied current density. The harmonic potential does not affect the amplitude scaling and it attains a

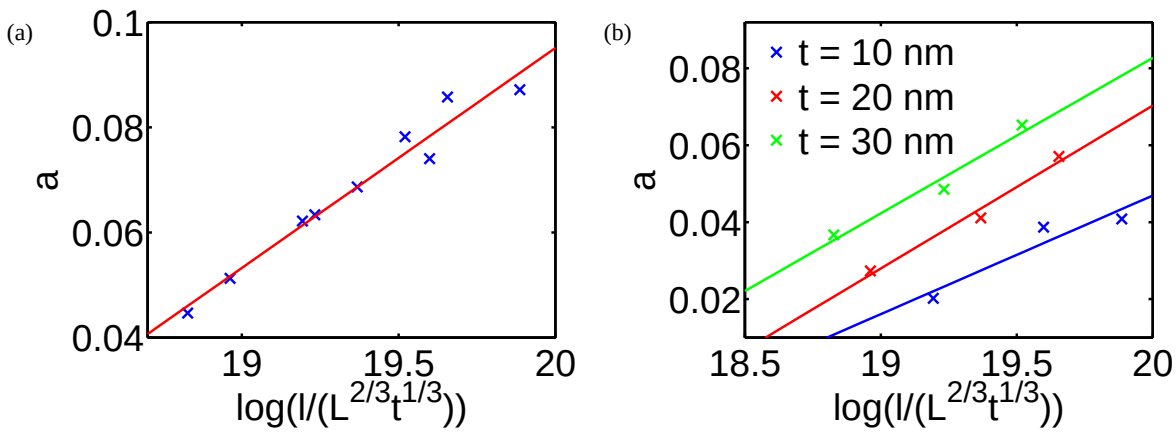

Figure 4.8: (Color online) Geometry dependence of the amplitude scaling (a) in the linear regime of vortex motion for a current density of $2.5 \cdot 10^9$ A/m^2 and (b) in the non-linear regime for a current density of $7.5 \cdot 10^{10}$ A/m^2. In the non-linear regime the geometry dependence of the amplitude scaling holds for different sample thicknesses t individually.

constant value. At about $2 \cdot 10^{10}$A/m^2 the vortex enters the non-linear regime of the vortex gyration and the amplitude scaling a decreases with increasing applied current density until the regime of vortex-core switching is reached (cf. Fig. 4.7 (b)). The decrease of the scaling is thus a direct consequence of the steeper confining potential: Due to a non-linear restoring force the amplitude scaling decreases along with the flattening of the amplitude enhancement in the non-linear regime of vortex motion. Besides the non-linear restoring force there is a second reason responsible for the decrease of the amplitude scaling. Micromagnetic simulations confirm a deformation of the vortex core in the non-linear regime of vortex motion due to the gyrotropic field [126, 139]. More precisely the vortex core shrinks with increasing applied current density. A smaller vortex core in the presence of an inhomogeneous current flow results in a lower increase of the gyrotropic force on the vortex and thus in a lower scaling (cf. section 4.2.4 for a detailed discussion). Note that the current dependence of $a(j)$ in the non-linear regime of the vortex gyration expresses directly the non-linear coupling of the current due to the counteraction of the AMR. These findings have an importance for experiments [132] and memory applications [118], since vortex-core switching depends critically on the radius of the vortex gyration. [164]

As with the current density, the geometry of the thin-film element affects the scaling of the gyration amplitude. To deduce the geometry dependence of a, we perform simulations on squares with various length l and thicknesses t. The value of the scaling a is the sole fit parameter and is thus a function of the applied current density and the sample geometry $a = a(j, l, t)$. Figure 4.8 (a) depicts a logarithmic geometry dependence of the scaling a for a current density of $2.5 \cdot 10^9$ A/m^2 and for sample lengths of $l = 200$, 300, 400 nm and thicknesses of $t = 10$, 20, 30 nm. Varying in turn the current density, the amplitude scaling always exhibits the functional behavior (cf. Fig. 4.8)

$$a(j, l, t) = \kappa(j, t) \log\left(\frac{\zeta(j, t)}{\sqrt[3]{L^2}} \frac{l}{\sqrt[3]{t}}\right), \tag{4.18}$$

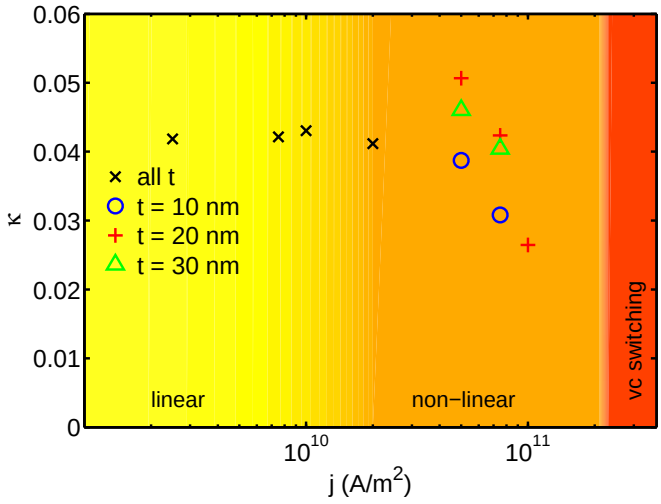

Figure 4.9: (Color online) Dependence of the fit parameter κ defined in Eq. (4.18) on the applied current density for the linear and non-linear regime of vortex motion.

where $\kappa(j,t)$ and $\zeta(j,t)$ are fit parameters and $L = \sqrt{2A/\mu_0 M_s^2}$ is the exchange length. The exchange length relates the exchange constant A to the saturation magnetization M_s and sets the relevant length scale in micromagnetism. While the parameter ζ is almost constant the run of κ with the current density is depicted in Fig. 4.9. Analogously to the situation illustrated in Fig. 4.7 (b) we find two different reaction regimes. The linear regime of vortex motion yields a constant parameter κ that is independent of the applied current density and the sample geometry. In the non-linear regime of vortex motion $\kappa(j,t)$ is decreasing with the applied current density and according to Fig. 4.8 (b) depends moreover on the sample thickness t (cf. section 4.2.4 for a detailed discussion).
In conclusion the transition in the vortex motion from the linear to the non-linear regime marks the transition from a linear transport regime with no explicit current dependence of $a(l,t)$ to a non-linear transport regime with $a(j,l,t)$ depending now explicitly on the current density. The logarithm of the ratio $l/\sqrt[3]{t}$ is proportional to the ratio of the constants belonging to the dissipation tensor and the gyrovector $D_0/G_0 \propto \log(l/\sqrt[3]{t})$ (cf. Ref. [164]). The ratio of dissipation tensor and gyrovector is in turn proportional to the ratio of damping Γ and the free frequency ω: $D_0/G_0 \propto \Gamma/\omega$. [123] Thus the geometric dependence in Eq. (4.18) is linked to characteristic quantities of the current-driven vortex.

4.2.4 Theoretical explanation

In this section we give a theoretical explanation why inhomogeneous current paths affect the gyration amplitude of the current-driven vortex. As confirmed by micromagnetic simulations, the vortex keeps its static structure and no deviation from the particle-like behavior occurs when excited with a spin-polarized current. Therefore, the static motion still can be described by the Thiele equation [120] with the expansion by Nakatani et al. [48] to include the action of a spin-polarized current

$$\vec{F} + \vec{G} \times (\vec{v} + b_j \vec{j}) + D(\alpha \vec{v} + \xi b_j \vec{j}) = 0. \tag{4.19}$$

Here, $\vec{F}$ is the restoring force due to the demagnetization and exchange fields that stems from the effective field, D is the diagonal dissipation tensor and $\vec{G}$ is the gyrovector (cf. section 3.2). Besides the gyrotropic force the gyrovector constitutes the driving force due to the current of Eq. (4.19), while the dissipation tensor resembles the loss of energy occurring in magnetic systems, which is referred to damping of the electron system. Note the two distinct origins of dissipation, the first term in the expression of the dissipation tensor of Eq. (4.19) is the usual Gilbert damping of the localized d electrons, while the second term describes spin relaxation of the itinerant s electrons parametrized by the degree of non-adiabaticity ξ. [5] The magnetization is a vector field of uniform length that can be expressed in dependence of two coordinates: for the vortex the polar angle θ changes in radial direction and the azimuthal angle ϕ characterizes the curling in-plane magnetization. Equation (4.19) represents an already integrated version of the Thiele equation that assumes no spatial dependence either of the velocity $\vec{v}$ nor of the current $\vec{j}$. Considering realistic current paths this assumption clearly does not hold and we have to consider the full integral Thiele equation [123]

$$\begin{aligned}
&-\mu_0 \int dV \left[(\vec{\nabla}_{\vec{r}}\theta)\frac{\partial}{\partial\theta} + (\vec{\nabla}_{\vec{r}}\phi)\frac{\partial}{\partial\phi} \right] (H_{\text{eff}} \cdot \vec{M}) \\
&-\frac{M_s\mu_0}{\gamma} \int dV \sin\theta (\vec{\nabla}_{\vec{r}}\theta \times \vec{\nabla}_{\vec{r}}\phi) \times (\vec{v} + b_j\vec{j}(\vec{r})) \\
&-\frac{M_s\mu_0}{\gamma} \int dV \, (\vec{\nabla}_{\vec{r}}\theta\vec{\nabla}_{\vec{r}}\theta + \sin^2\theta\vec{\nabla}_{\vec{r}}\phi\vec{\nabla}_{\vec{r}}\phi)(\alpha\vec{v} + \xi b_j\vec{j}(\vec{r})) \\
&= 0.
\end{aligned} \tag{4.20}$$

However, the simulations presented in section 4.2.3 indicate that a description of vortex motion in terms of collective coordinates by an integrated version of the Thiele equation still offers a good description for the case of inhomogeneous current paths. The employment of the integrated version of the Thiele equation is possible with a proper renormalization of one of the coupling parameters in Eq. (4.19). In a first approximation of homogeneous current paths, the vortex motion is independent of the size of the vortex core and thus considered to be of topological nature. [120] A spatial dependence of the current in the integrands of Eq. (4.20) requires corrections compared with the homogeneous case. As addressed in Ref. [165] the velocity in Eq. (4.19) must be modified to match with detailed micromagnetic simulations. For the case of a vortex confined in a thin-film element the rigid particle approximation is only approximatively fulfilled as the velocity within the vortex core is different compared to the velocity in the domains. There is no general rule how to treat modifications of the quasiparticle picture. In order to modify Eq. (4.19) as little as possible and to maintain a quasi-linear structure of the Thiele equation with respect to the current density, we decide to attribute the renormalization to the spin-transfer torque coupling parameter b_j whose derivation has been performed for a homogeneous current flow. [5] This approach is motivated by the following considerations. The gyrotropic force that arises due to the adiabatic current term (cf. Eq. (4.20)) reads for the case of a magnetic vortex [123]

$$\begin{aligned}
\vec{G} \times \tilde{b}_j\vec{j} &= -\frac{M_s\mu_0}{\gamma} \int dV \, \sin\theta (\vec{\nabla}_{\vec{r}}\theta \times \vec{\nabla}_{\vec{r}}\phi) \times b_j\vec{j}(\vec{r}) \\
&= -\frac{2\pi M_s\mu_0 p}{\gamma} t \, \vec{e}_z \times \tilde{b}_j\vec{j} \\
&= \tilde{b}_j G_0 \vec{e}_z \times \vec{j}.
\end{aligned} \tag{4.21}$$

Except for the small area of the vortex core, θ is almost constant and thus $\vec{\nabla}_{\vec{r}}\theta$ in the integrand of Eq. (4.21) vanishes. This restricts the integration to the region of the vortex core. Though defined as an integral over the whole sample the gyrovector is primarily located at the vortex core. Due to the spatial integration the renormalized spin-transfer torque coupling can be expected to depend on the set of all possible parameters $\tilde{b}_j = \tilde{b}_j(j, \rho_{||}, \rho_\perp, l, t)$.
If we rearrange the modified version of Eq. (4.19) as follows

$$\begin{aligned} G_0^2\vec{v} \approx (G_0^2 + D_0^2\alpha^2)\vec{v} = \vec{G} \times \vec{F} - D_0\alpha\vec{F} - (G_0^2 + D_0^2\alpha\xi)\tilde{b}_j\vec{j} \\ + \tilde{b}_j D_0 \vec{G} \times \vec{j}(\xi - \alpha) \\ \approx \vec{G} \times \vec{F} - D_0\alpha\vec{F} - G_0^2\tilde{b}_j\vec{j}, \end{aligned} \tag{4.22}$$

we deduce that the driving part proportional to the current $\tilde{b}_j\vec{j}$ is primarily given by the square of the gyrovector, where, as usually, we have assumed $\alpha, \xi \ll 1$. The influence of the cross product term in Eq. (4.22) can be disregarded, since we employed $\alpha \approx \xi$ in the simulations. [103] Note that in contrast to the gyrovector the dissipation tensor

$$D = -\frac{M_s\mu_0}{\gamma}\int dV\,(\vec{\nabla}_{\vec{r}}\theta\vec{\nabla}_{\vec{r}}\theta + \sin^2\theta\vec{\nabla}_{\vec{r}}\phi\vec{\nabla}_{\vec{r}}\phi), \tag{4.23}$$

attains its contributions mainly in the domains due to the change in the second term by the in-plane angle ϕ (cf. Eq. (3.4)), while the contribution from the vortex core is small. It is little affected by the current flow as it contributes to the driving force via the non-adiabatic spin-transfer torque and is thus suppressed by factors of $\alpha\xi$, α^2 and $D_0/G_0(\xi - \alpha)$ (cf. Eq. (4.22)).

To summarize, in the case of current excitations the driving force acts on the vortex core, while the energy dissipation mainly takes place in the domains of the Landau pattern as expressed by the second term on the right hand side of Eq. (4.22). These circumstances can also be directly understood from the Landau-Lifshitz-Gilbert equation (4.2). The spin-transfer torque is proportional to the spatial derivative of the magnetization, hence the spin transfer-torque contribution is located in the center region while its influence is negligible in the almost uniform domains. In discs the rotational symmetry does not allow internal domain walls and the vortex exhibits similar behavior. [166] Thus, the contribution to the spin-transfer torque of the four Néel walls is small. This reveals a striking difference between inhomogeneous current and magnetic field excitations. While inhomogeneous magnetic fields cause deformations of the vortex structure, the electrical current mainly affects the vortex core and the vortex structure is kept stable, even in the case of a strong inhomogeneous current flow. This contrasts with alternating, homogeneous field and current excitations that result for the vortex in similar magnetization dynamics.
Taking now the AMR effect into account the current tends to flow through the vortex core resulting in a locally higher current density compared with the homogeneous case. The occurrence of the locally higher current density in the vortex core coincides with the location of the gyrovector that constitutes according to Eq. (4.22) the driving force. An enhanced gyrotropic force acts on the vortex and a bigger amplitude results for the vortex gyration compared with a homogeneous current flow. The stability of the vortex during the motion must be addressed to the high symmetry of the vortex pattern, such that internal stresses compensate each other and the magnetic configuration as a whole is not affected.

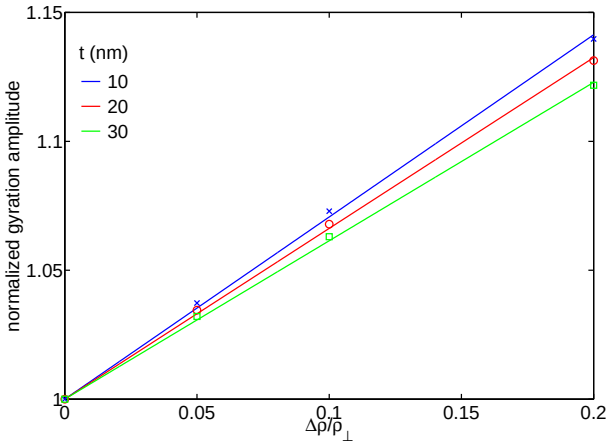

Figure 4.10: (Color online) Comparison of the enhancement slope for a sample size of $l = 300$ nm and three different thicknesses $t = 10, 20, 30$ nm for a current density of $j = 2.5 \cdot 10^{10}\mathrm{A/m}^2$.

As mentioned in the context of Eq. (4.21), in the case of inhomogeneous current paths the geometry of the thin-film element influences the coupling parameter $\tilde{b}_j$ and thus the amplitude scaling a. The numerical simulations in Fig. 4.8 exhibit for the amplitude scaling a a logarithmic geometry dependence proportional to the ratio of dissipation tensor and gyrovector: $D_0/G_0 \propto (\log l - const. \cdot \log t)$. Owing to the integration over the sample in the expression for the gyrovector (cf. Eq. (4.21)), the lateral size of the sample gains its importance for the vortex motion due to the inhomogeneity of the current flow. In the preceding section we have determined the exact geometry dependence from micromagnetic simulations. In samples with a larger sample length l the driving force is bigger resulting in an enhanced gyration amplitude ($\tilde{b}_j \propto \log l$). At the same time the amplitude scaling a increases with decreasing sample thickness t ($\tilde{b}_j \propto \log 1/t$). The connection of the increase in the gyration amplitude with decreasing sample thickness t is exemplarily depicted in Fig. 4.10 for a fixed sample length of $l = 300$ nm and a current density of $j = 2.5 \cdot 10^{10}\mathrm{A/m}^2$. For smaller t a higher gyrotropic force acts on the vortex caused by the AMR effect.

As discussed, it is the vortex core that controls the dynamic behavior of the vortex state in the case of excitation due to a spin-polarized electric current. With the particular role the vortex core takes in current-driven vortex dynamics, the origin of the decrease of the factor $\kappa(j,t)$ in the non-linear regime of vortex motion as depicted in Fig. 4.9 becomes comprehensible. The vortex core shrinks with increasing applied current density due to the non-linear restoring potential experienced by the vortex caused by larger displacements from the equilibrium position. To obtain the same amplitude scaling in the presence of the non-linear potential as compared to the linear case, the local current density within the core would have to become even more inhomogeneous than in the linear regime of vortex motion. As a consequence, the gyrotropic force on the vortex and thus $\kappa(j,t)$ decreases. In addition, the vortex reaches with smaller sample thickness t the non-linear regime for lower current densities or deflections from its equilibrium position. For small aspect ratios $t/l \ll 1$ the frequency of the vortex is approximately proportional to the aspect ratio itself $\omega \propto t/l$. [167] In turn, the vortex

displacement is inversely proportional to the aspect ratio $r \propto l/t$. This means that the non-linearities set in earlier with lower sample thickness t due to a larger displacement of the vortex. A change in the sample thickness t affects the shape of the non-linear potential. The consequence is the occurring thickness dependence of $\kappa(j,t)$ in the non-linear regime, while the sample length l plays a minor role. The observations of section 4.2.3 are a constant amplitude scaling κ in the linear regime of small deflections of the vortex core independent of the applied current density. In the non-linear regime $\kappa(j,t)$ decreases with higher current densities as a direct consequence of the non-linear potential felt by the vortex.

4.2.5 Renormalization of the spin-transfer torque coupling parameter

As discussed in the preceding sections, considering the influence of inhomogeneous current paths on the gyrotropic motion of a magnetic vortex modifies the spin-transfer torque coupling parameter b_j. The renormalization involves a dependence on the geometry, the electric current and on the parameters that characterize the AMR effect: $\tilde{b}_j(j, \rho_{||}, \rho_\perp, l, t)$. Note that the explicit current dependence of $\tilde{b}_j$ in the non-linear regime of vortex motion expresses the non-linear coupling of current and magnetization. The counteraction caused microscopically by spin-orbit interaction renormalizes the spin-transfer torque coupling parameter according to

$$\tilde{b}_j(j, \rho_{||}, \rho_\perp, l, t) = \left(a(j,l,t) \frac{\Delta\rho}{\rho_\perp} + 1 \right) b_j, \tag{4.24}$$

$$a(j,l,t) = \kappa(j,t) \log\left(\frac{\zeta(j,t)}{\sqrt[3]{L^2}} \frac{l}{\sqrt[3]{t}}\right). \tag{4.25}$$

With respect to a description of vortex motion in terms of collective coordinates, $\tilde{b}_j j$ acts as a renormalized velocity due to the current in the equations of motion (4.15). The counteraction of the magnetization by means of the anisotropic magnetoresistivity results for the current-driven vortex in a geometry-dependent renormalization of the spin-transfer torque coupling parameter and can be interpreted as a correction to the entirely topological motion of vortices in the presence of a homogeneous current flow. For small deflections in the linear regime of vortex motion the correction due to the AMR effect is small and the quasiparticle approximation remains applicable. The equations of motion keep their shape and maintain their validity as effective equations of motion comprising the counteraction of the magnetic vortex on the electric current via the AMR effect. For higher deflections, in particular in the regime of vortex-core switching (cf. next section), the counteraction of the AMR leads to non-linear effects that have to be identified by detailed self-consistent micromagnetic simulations.

4.2.6 Influence of the anisotropic magnetoresistance on the highly non-linear regime of vortex-core switching

If the vortex gyration exceeds a critical velocity (≈ 320 m/s for Py), the highly non-linear regime of vortex-core switching is entered. [126, 139] The vortex-core switching is accompanied by a halo formation – a region with opposite oriented out-of-plane magnetization is formed close to the vortex – and subsequent vortex-antivortex nucleation and annihilation. [139] Due to the non-trivial topology of the combined vortex-antivortex state it is crucial to consider realistic current paths. The gyrotropic

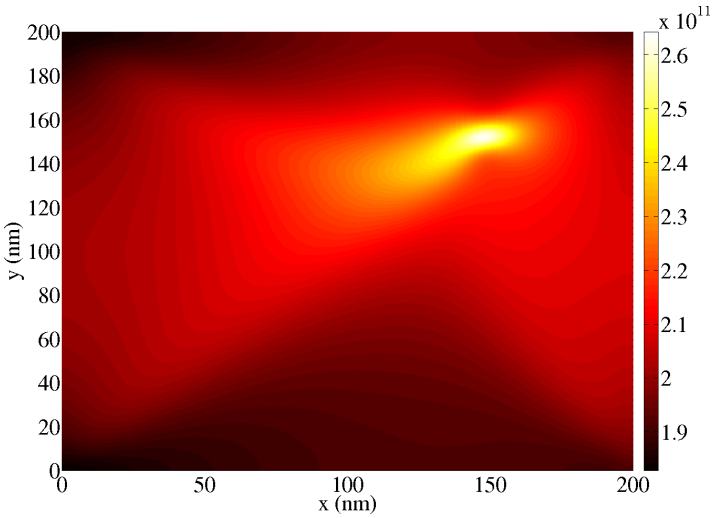

Figure 4.11: (Color online) Current density of a magnetic vortex in a $200 \times 200 \times 20\,\mathrm{nm}^3$ permalloy square at the critical velocity 320 m/s for vortex-core switching.

field responsible for the vortex-core distortion and the subsequent core-reversal at higher gyration amplitudes forms a dip with out-of-plane magnetization in the inside of the vortex' orbit. [139] An exemplary current density is depicted in Fig. 4.11 that reveals the complexity of the current paths in the regime of vortex-core switching as a direct consequence of the complex distorted magnetization texture. Thus far, we have considered the steady-state radius of the vortex. Let us now turn the attention to the time-domain. A question of experimental and applicational relevance is the time between excitation of the vortex and its switching. Figure 4.12 depicts the time required until the vortex reached its critical velocity for switching with respect to the AMR ratio. The particular point in time in Fig. 4.12 corresponds to the critical velocity (320 m/s relates to a radius of 72.8 nm at a frequency of 4.4 GHz) that was found to be the universal criterion for vortex-core switching. [139] A higher AMR ratio linearly reduces the time until vortex-core switching sets in.

4.2.7 Conclusion

In conclusion the counteraction of the magnetization on the current-driven magnetic vortex results in a geometry-dependent renormalization of the spin-transfer torque coupling parameter by means of the anisotropic magnetoresistivity. This can be interpreted as a correction to the topological motion of vortices in the presence of a homogeneous current flow. The renormalized coupling parameter depends on the ratio of the dissipation tensor and gyrovector that constitute intrinsic vortex' properties that are determined by the geometry of the thin-film element, namely its size and its thickness. In the non-linear regime of vortex motion the change in the shape of the vortex core explicitly introduces a non-linear dependence of the renormalized spin-transfer coupling parameter on the current density. The results are obtained by micromagnetic simulations taken the spin-transfer torque as well as the inhomogeneity of the current flow into account. Incorporating the counteraction of the magnetization onto the current flow provides a non-linear coupling of mutual current and magnetization dynamics.

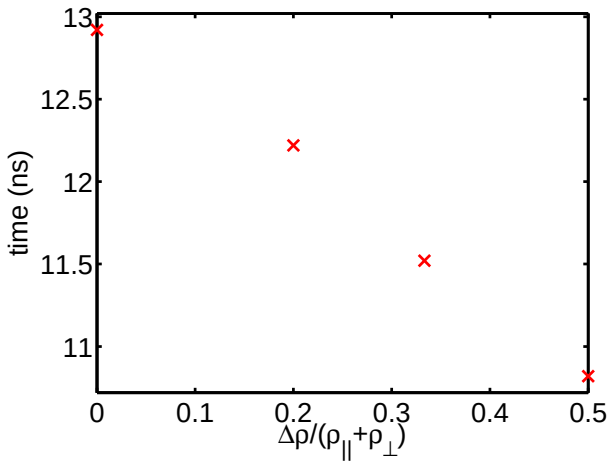

Figure 4.12: (Color online) Time until a critical velocity of 320 m/s is reached for a vortex in a $200 \times 200 \times 20\,\mathrm{nm}^3$ permalloy square in dependence of the AMR ratio.

For experimental and technical implications we identified the AMR as a candidate to reduce the time until the critical velocity for vortex-core switching is reached.

Chapter 5

Non-collinear magnetotransport

Parts of this chapter have been published slightly modified in Ref. [168], S. Bohlens and D. Pfannkuche, Width dependence of the nonadiabatic spin-transfer torque in narrow domain walls, Phys. Rev. Lett. **105**, *177201 (2010)*

IN THIS CHAPTER we generalize the kinetic equation to non-collinear magnetization textures and investigate some important aspects of non-collinear magnetotransport. The spin-dependent transport coefficients for the itinerant electrons are calculated by means of the non-equilibrium, linear response to a current-inducing electric field. To capture various spin-dependent transport phenomena, we develop in section 5.1 a formalism that treats electron and spin transport on equal footing. In section 5.2 we review collinear magnetotransport to get familiar with spin-dependent concepts in transport. In section 5.3 we derive a general equilibrium solution for non-collinear magnetization textures that serves as a starting point for the derivation of a general linear response kinetic equation. Section 5.4 exhibits the derivation of a general non-equilibrium solution for spatially slowly varying magnetization textures. This yields global transport coefficients such as the charge and spin current conductivity, as well as the spin-transfer torque and the degree of non-adiabaticity. This chapter closes with section 5.5 that provides an analytical solution of the generalized kinetic equation for the case of an one-dimensional domain wall and the derivation of the local spin-transfer torque, domain-wall resistivity and momentum transfer within the domain wall. It turns out that the treatment of coupled charge and spin transport offers startling insight into an intermediate transport regime that comprises diffusive charge transport and ballistic spin transport at the same time. In narrow domain walls the spin degree of freedom significantly influences the magnetotransport due to an enhanced coupling of the spin of the conduction electron with the local magnetization.

In monodomain ferromagnets with a collinear magnetization texture the magnetization distinguishes a natural global quantization axis. The spin of the conduction electron commutes with the total Hamiltonian and thus is a conserved quantity with respect to transport, if we neglect spin-flip scattering processes. In this case transport can be well described in terms of the majority and minority electrons with respect to the global quantization axis. This is the basic idea behind the *two-current model* [34, 169], where all physical quantities are spin dependent in terms of majority (minority), $\uparrow$ ($\downarrow$), charge carri-

ers. However, transport in non-collinear magnetization textures is more complicated. Here, a natural choice is to align the quantization axis with the local magnetization. The consequence of this choice is that the quantization axis now varies spatially. The majority or minority electrons are no longer eigenstates of the underlying Hamiltonian and the spin channels mix in the presence of an electric field. A key feature of non-collinear magnetotransport is that the channel mixing gives rise to transverse magnetization of the conduction electrons.

Compared to electron transport in non-magnetic materials, transport in ferromagnets with collinear magnetization patterns demands a doubling of the degrees of freedom due to the lifted spin degeneracy within a ferromagnet. In turn, transport in ferromagnets with a non-collinear magnetization texture requires the treatment of full Pauli spin space in terms of 2×2 spin $1/2$ density matrices. Compared with collinear magnetotransport, this corresponds to a further doubling of the degrees of freedom. The additional degrees of freedom take into account transverse spin dynamics.

Throughout this thesis, we restrict ourselves to stationary non-equilibrium problems, although our formalism can be easily extended to capture time-dependent phenomena. The distribution function in non-collinear magnetization textures $\hat{f}_{\vec{k}}(\vec{r})$ is a 2×2 matrix in Pauli spin space. Pauli spin space is the space of the Hermitian 2×2 matrices that is spanned by the four basis elements $\{\mathbb{1}, \vec{\sigma}\}$. Here, $\mathbb{1}$ is the unity matrix and $\vec{\sigma}$ is a vector that contains as components the three Pauli matrices σ_i, $i = x, y, z$ as defined in appendix A. We will refer to the subspace spanned by $\mathbb{1}$ as the charge subspace and the subspace spanned by $\vec{\sigma}$ as the spin subspace. Furthermore, we will refer to the expectation value of spin space as magnetization space. The off-diagonal elements of the distribution matrix $\hat{f}_{\vec{k}}(\vec{r})$ describe transverse spins that have to be taken into account, since the spin of the conduction electrons does not commute with the total Hamiltonian in non-collinear magnetization textures. [53] The connection with the *two-current model* is provided by the following: In collinear patterns the off-diagonal components vanish and the distribution matrix becomes diagonal in Pauli spin space. In this case the diagonal entries of the distribution function reduce to the majority (minority) distributions $f^{\uparrow}_{\vec{k}}(\vec{r})$ ($f^{\downarrow}_{\vec{k}}(\vec{r})$). These are the distribution functions familiar from collinear magnetotransport.

In general, the spin-dependent distribution matrix $\hat{f}_{\vec{k}}(\vec{r})$ can always be locally diagonalized by an unitary rotation in spin space $\hat{U}_{\vec{k}}(\vec{r})$. The magnetization is strong in ferromagnets, with corresponding field strengths up to ≈ 1 T and we can neglect a $\vec{k}$-dependence of $\hat{U}_{\vec{k}}(\vec{r})$. In this case the rotation is independent of the actual position on the Fermi surface. Then the general distribution function can be related to the majority ($f^{\uparrow}_{\vec{k}}(\vec{r})$) and minority ($f^{\downarrow}_{\vec{k}}(\vec{r})$) distribution functions that are locally well defined in the following manner

$$\hat{f}_{\vec{k}}(\vec{r}) = \hat{U}_{\vec{k}}(\vec{r}) \begin{pmatrix} f^{\uparrow}_{\vec{k}}(\vec{r}) & 0 \\ 0 & f^{\downarrow}_{\vec{k}}(\vec{r}) \end{pmatrix} \hat{U^{\dagger}}_{\vec{k}}(\vec{r}). \tag{5.1}$$

The difference between a collinear and a non-collinear magnetization texture is that in the collinear case the rotation $\hat{U}_{\vec{k}}(\vec{r})$ does not depend on position, whereas in the non-collinear case the rotation $\hat{U}_{\vec{k}}(\vec{r})$ depends explicitly on position. In this connection offdiagonal elements in the distribution matrix corresponds in the collinear case to additional gauge degrees of freedom that stem from an inappropriate choice of the quantization axis and can be gauged away by a global rotation $\hat{U}_{\vec{k}}(\vec{r})$ to the reference frame of the magnetization. In the non-collinear case the situation is distinct different: the local unitary rotation $\hat{U}_{\vec{k}}(\vec{r})$ does not commute with spatial derivatives or spin-dependent quantities and the off-diagonal elements are not dispensable degrees of freedom as in the collinear case.

Rather, they are needed for an appropriate description of non-collinear magnetotransport. However, the macroscopic observables are obtained by tracing out Pauli spin space. The transformation $\hat{U}_{\vec{k}}(\vec{r})$ solely acts on the spin subspace and the charge quantities are thus manifest invariant with respect to unitary transformations in Pauli spin space. Hence, the relation $f^0_{\vec{k}}(\vec{r}) = f^{\uparrow}_{\vec{k}}(\vec{r}) + f^{\downarrow}_{\vec{k}}(\vec{r})$ always holds for the charge distribution.
The macroscopic observables are given in terms of the ensemble averages of the distribution matrix. The expectation value with respect to momentum considers the many-body nature of transport. The charge density $n(\vec{r})$ and the local magnetization of the conduction electrons $\langle\hat{\vec{\sigma}}(\vec{r})\rangle$ are related to the zeroth moments of the distribution matrix

$$n(\vec{r}) = -e \int \frac{d^3k}{(2\pi)^3} \mathrm{Tr}\, \hat{f}_{\vec{k}}(\vec{r}), \tag{5.2}$$

$$\langle\hat{\vec{\sigma}}(\vec{r})\rangle = -\mu_\mathrm{B} \int \frac{d^3k}{(2\pi)^3} \mathrm{Tr}\, \hat{f}_{\vec{k}}(\vec{r})\vec{\sigma}, \tag{5.3}$$

while the charge $\vec{j}(\vec{r})$ and the spin current $\hat{J}(\vec{r})$ are given in terms of the first moments

$$\vec{j}(\vec{r}) = -e \int \frac{d^3k}{(2\pi)^3} \vec{v}_{\vec{k}} \mathrm{Tr}\, \hat{f}_{\vec{k}}(\vec{r}), \tag{5.4}$$

$$\hat{J}(\vec{r}) = -\mu_\mathrm{B} \int \frac{d^3k}{(2\pi)^3} \vec{v}_{\vec{k}} \otimes \mathrm{Tr}\, \hat{f}_{\vec{k}}(\vec{r})\vec{\sigma}. \tag{5.5}$$

The spin current in Eq. (5.5) is a tensorial quantity constructed by a tensor product between the spatial flow direction and the direction in magnetization space. The spatial divergence of the spin current tensor yields a vector in magnetization space.
The distribution matrix $\hat{f}_{\vec{k}}(\vec{r})$ can be represented in Pauli spin space according to

$$\begin{aligned}\hat{f}_{\vec{k}}(\vec{r}) &= \frac{1}{2}\left(f^0_{\vec{k}}(\vec{r})\mathbb{1} + f^x_{\vec{k}}(\vec{r})\sigma_x + f^y_{\vec{k}}(\vec{r})\sigma_y + f^z_{\vec{k}}(\vec{r})\sigma_z\right) \\ &= \frac{1}{2}\begin{pmatrix} f^0_{\vec{k}}(\vec{r}) + f^z_{\vec{k}}(\vec{r}) & f^x_{\vec{k}}(\vec{r}) - i f^y_{\vec{k}}(\vec{r}) \\ f^x_{\vec{k}}(\vec{r}) + i f^y_{\vec{k}}(\vec{r}) & f^0_{\vec{k}}(\vec{r}) - f^z_{\vec{k}}(\vec{r}) \end{pmatrix}.\end{aligned} \tag{5.6}$$

The separation of Pauli spin space into the charge subspace $\propto \mathbb{1}$ and the traceless spin subspace $\propto \vec{\sigma}$ becomes directly evident from Eq. (5.6). The transition from $\mathbb{R}^3$ to the $SU(2)$ spin subspace is carried out by expanding a vector $\vec{A} = (A_x, A_y, A_z)^T \in \mathbb{R}^3$ in terms of the Pauli matrices (cf. appendix A.1)

$$\vec{A}\cdot\vec{\sigma} = \sum_i A_i\sigma_i = A_x\sigma_x + A_y\sigma_y + A_z\sigma_z = \begin{pmatrix} A_z & A_x - iA_y \\ A_x + iA_y & A_z \end{pmatrix}. \tag{5.7}$$

The inverse mapping from Pauli spin space, the sum of the charge subspace and the $SU(2)$ spin subspace, to $\mathbb{R}^4$ is achieved by taking the trace with the corresponding Pauli matrix

$$f^\mu_{\vec{k}}(\vec{r}) = \mathrm{Tr}\, \hat{f}_{\vec{k}}(\vec{r})\sigma_\mu, \qquad \mu = 0, x, y, z, \tag{5.8}$$

where we employed the notation $\sigma_0 \equiv \mathbb{1}$. The transformations between $\mathbb{R}^4$ and Pauli spin space are unique as the directives (5.7) and (5.8) constitute bilinear maps.

In the decomposition (5.6) the distribution $f^0_{\vec{k}}(\vec{r})$ is the charge distribution function that counts the number of conduction electrons and accordingly, $f^0_{\vec{k}}(\vec{r})d^3rd^3k$ is the number of electrons in the semiclassical phase-space element d^3rd^3k about the point $(\vec{r},\vec{k})$. The vectorial distribution function $\vec{f}_{\vec{k}}(\vec{r}) = (f^x_{\vec{k}}(\vec{r}), f^y_{\vec{k}}(\vec{r}), f^z_{\vec{k}}(\vec{r}))^T$ is the macroscopic spin distribution function or the distribution function of the magnetization of the conduction electrons and $f^i_{\vec{k}}(\vec{r})d^3rd^3k$ is the expectation value for the spin in the spatial direction $i = x, y, z$ in the semiclassical phase-space element d^3rd^3k about the point $(\vec{r},\vec{k})$. In view of the statistical interpretation by means of Eq. (5.2), the distribution of the charge carriers $f^0_{\vec{k}}(\vec{r})$ must be positive and finite. To secure a positive definite charge subspace, the diagonal entries, i.e., the spin up and spin down distributions, must be positive definite $f^{\uparrow}_{\vec{k}}(\vec{r}), f^{\downarrow}_{\vec{k}}(\vec{r}) > 0$. In contrast, the spin distributions $f^i_{\vec{k}}(\vec{r})$ are real.

Let us now focus on the distribution matrix itself. Analogously to the density matrix, $\hat{f}_{\vec{k}}(\vec{r})$ must be Hermitian. Its norm is the charge distribution $\mathrm{Tr}\,\hat{f}_{\vec{k}}(\vec{r}) = f^0_{\vec{k}}(\vec{r})$. The most general ansatz for the Hermitian distribution function reads

$$\hat{f}_{\vec{k}}(\vec{r}) = \begin{pmatrix} f^{\uparrow\uparrow}_{\vec{k}}(\vec{r}) & (f^{\uparrow\downarrow}_{\vec{k}}(\vec{r}))^* \\ f^{\uparrow\downarrow}_{\vec{k}}(\vec{r}) & f^{\downarrow\downarrow}_{\vec{k}}(\vec{r}) \end{pmatrix}. \tag{5.9}$$

The spin distribution follows from Eq. (5.9) with the help of the relation (5.8)

$$\vec{f}_{\vec{k}}(\vec{r}) = \frac{1}{2}\begin{pmatrix} f^{\uparrow\downarrow}_{\vec{k}}(\vec{r}) + (f^{\uparrow\downarrow}_{\vec{k}}(\vec{r}))^* \\ i(f^{\uparrow\downarrow}_{\vec{k}}(\vec{r}) - (f^{\uparrow\downarrow}_{\vec{k}}(\vec{r}))^*) \\ f^{\uparrow\uparrow}_{\vec{k}}(\vec{r}) - f^{\downarrow\downarrow}_{\vec{k}}(\vec{r}) \end{pmatrix} = \begin{pmatrix} \Re f^{\uparrow\downarrow}_{\vec{k}}(\vec{r}) \\ -\Im f^{\uparrow\downarrow}_{\vec{k}}(\vec{r}) \\ \frac{1}{2}(f^{\uparrow\uparrow}_{\vec{k}}(\vec{r}) - f^{\downarrow\downarrow}_{\vec{k}}(\vec{r})) \end{pmatrix}. \tag{5.10}$$

The spin accumulation in Eq. (5.10) is obviously real, as required. A comparison of Eq. (5.9) and (5.10) illustrates that the complex off-diagonal entry of the transverse spin-distribution function $f^{\uparrow\downarrow}_{\vec{k}}(\vec{r})$ constitutes the transverse parts of the macroscopic spin distribution, the spin accumulation.

In the next section we will generalize the kinetic equation for general magnetization textures. This concerns the derivation of the deterministic flow part for the distribution matrix $\hat{f}_{\vec{k}}(\vec{r})$ and a generalization of the collision integral $\hat{\mathcal{I}}[\hat{f}_{\vec{k}}(\vec{r})]$. Throughout this thesis, we want to pursue a phenomenological parametrization of the collision integral in terms of relaxation times. In general, the relaxation times can exhibit a non-trivial spin structure and do not have to commute with the distribution matrix $[\hat{f}_{\vec{k}}(\vec{r}), \hat{\mathcal{I}}[\hat{f}_{\vec{k}}(\vec{r})]] \neq 0$. As we are dealing with spin-dependent particles, we focus on two different types of spin-dependent scattering at magnetic impurities: Spin-conserving scattering that preserves the spin but relaxes the momentum to the lattice and spin-flip scattering that flips the spin. The spin-flip scattering events are, e.g., due to spin-orbit interactions with magnetic impurities and conserve the momentum.

5.1 Derivation of the kinetic equation for general magnetization textures

This section sketches the derivation of the deterministic flow part of the kinetic equation for general, non-collinear magnetization textures. A rigorous definition of the distribution function follows from the one-particle density matrix $\hat{\tilde{\rho}}(\vec{r}_1, \vec{r}_2, t)$ that is defined as follows [114, 117]

$$\hat{\tilde{\rho}}(\vec{r}_1, \vec{r}_2, t) = \langle \Psi^\dagger(\vec{r}_2, t)\Psi^\dagger(\vec{r}_1, t)\rangle = \mathrm{Tr}\,\rho\Psi^\dagger(\vec{r}_2, t)\Psi^\dagger(\vec{r}_1, t), \tag{5.11}$$

where ρ is the full density matrix of the system and $\Psi^\dagger(\vec{r}, t)$, $\Psi(\vec{r}, t)$ are the creation and annihilation operators in the Heisenberg picture of second quantization. The one-particle density matrix can be expressed in relative $\vec{r}\,' = \vec{r}_1 - \vec{r}_2$ and center of mass $\vec{r} = (\vec{r}_1 + \vec{r}_2)/2$ coordinates

$$\hat{\tilde{\rho}}(\vec{r}_1, \vec{r}_2, t) = \hat{\tilde{\rho}}(\vec{r} + \frac{\vec{r}\,'}{2}, \vec{r} - \frac{\vec{r}\,'}{2}, t) = \hat{\rho}(\vec{r}, \vec{r}\,', t). \tag{5.12}$$

The spin is entirely a quantum mechanical concept that does not possess a classical analogue. The starting point for a derivation of a generalized kinetic equation that governs charge and spin transport must thus be an equation that governs quantum mechanical dynamics. The time evolution of the one-particle density matrix $\hat{\rho}$ obeys the quantum Liouville or the von Neumann equation [114]

$$i\hbar\frac{\partial\hat{\rho}(t)}{\partial t} = [\mathcal{H}, \hat{\rho}(t)]. \tag{5.13}$$

The total time derivative of the density matrix is always equal to zero, this reflects the conservation of probability.

The aim of this section is to derive an equation of motion for a semiclassical analogon of the quantum-mechanical density matrix, called the Wigner distribution, that reduces to the kinetic equation in the classical limit. [114] The resulting equation is a kinetic equation that will serve for the description of non-collinear magnetotransport. To attain a kinetic equation we perform a Wigner transform by separating the spatial and momentum degrees of freedom into slowly varying center of mass coordinates $\vec{r}$ and fast varying relative coordinates $\vec{r}\,'$. The fast varying relative coordinates $\vec{r}\,'$ that oscillate with the Fermi wavelength are integrated out by performing a Fourier transform with respect to $\vec{r}\,'$. This leaves a dependence on the slowly varying center of mass coordinates $\vec{r}$ and as a result of the Fourier transform on the momentum $\vec{k}$. [117, 170] The new coordinates $\vec{r}, \vec{k}$ allow for an expansion of quantum mechanical commutators in Poisson brackets that operate on classical phase space (cf. appendix B for details of the transformation). [170] As the Wigner transform acts only on the spatial and momentum operators, this method keeps the spin explicitly quantum mechanically. From this starting point the collision integral that is responsible for the irreversibility in the kinetic equation is purely phenomenological (cf. section 5.1.3).

The connection of the density matrix $\hat{\rho}$, a quantum mechanical operator on Hilbert space, with the Wigner distribution, a smooth function on classical phase space, is provided by the Wigner transform. In the semiclassical limit the Wigner function reduces to the distribution function for the kinetic equation $\hat{\rho} \xrightarrow{\text{W.T.}} \hat{f}_{\vec{k}}(\vec{r})$. According to the general definition of the Wigner transform given in Eq. (B.1) the distribution matrix is defined as

$$\hat{f}_{\vec{k}}(\vec{r}) = \int d^3r\,'\,\hat{\rho}(\vec{r} + \frac{\vec{r}\,'}{2}, \vec{r} - \frac{\vec{r}\,'}{2})e^{i\vec{k}\vec{r}\,'}. \tag{5.14}$$

The starting point for a derivation of a generalized kinetic equation is a microscopic Hamiltonian. We consider a sd-Hamiltonian (cf. section 2.1) for non-interacting conduction electrons that are coupled to the spatially varying ferromagnetic order parameter $\vec{m}(\vec{r},t)$ in the mean field approximation

$$\mathcal{H} = \left[\frac{\hbar^2}{2m}\vec{\nabla}_{\vec{r}}^2 + eV_{\text{ext}}(\vec{r},t)\right]\mathbb{1} + J_{\text{sd}}\vec{\sigma}\cdot\vec{m}(\vec{r},t). \tag{5.15}$$

$V_{\text{ext}}(\vec{r},t)$ is the electric potential that gives rise to an external electric field and J_{sd} is the sd exchange integral that equals half the exchange splitting. The Hamiltonian is a 2×2 matrix in Pauli spin space, the space of the Hermitian 2×2 matrices. The Hamiltonian (5.15) decomposes in three parts

$$\mathcal{H} = H_0 + H_{\text{V}} + H_{\text{sd}}. \tag{5.16}$$

The sd exchange interaction part H_{sd} of the Hamiltonian (5.15) can always be locally diagonalized by an unitary rotation in spin space $\hat{U}(\vec{r})$ (cf. Eq. (A.9)). The rotation $\hat{U}(\vec{r})$ corresponds to a gauge transformation in spin space[1] that aligns the quantization axis with the local moments. The spatial dependence in $\hat{U}(\vec{r})$ is entirely determined through the magnetization pattern ($\hat{U}(\vec{r}) \to \hat{U}(\vec{m}(\vec{r}))$). The difference between a collinear and a non-collinear magnetization texture is that in the collinear case the rotation $\hat{U}$ does not depend on position and commutes with the total Hamiltonian (5.15). Therefore $\hat{U}\mathcal{H}\hat{U}^\dagger$ diagonalizes the full Hamiltonian (5.15). In the non-collinear case the rotation $\hat{U}(\vec{m}(\vec{r}))$ depends on position due to the spatially varying magnetization $\vec{m}(\vec{r})$ and therefore does not commute with the kinetic term H_0 in the total Hamiltonian (5.16). As a consequence the Hamiltonian (5.15) is not diagonalized and spin-dependent gauge potentials appear in the transformed Hamiltonian as a consequence of the gauge transformation. [171] In an inhomogeneous ferromagnetic order parameter the gauge transformation $\hat{U}(\vec{m}(\vec{r}))$ maps the spins of the conduction electrons to conduction electrons spins in an uniform ferromagnet that are additionally interacting with spin-dependent gauge fields (cf. section 5.5.4 for further discussions).

5.1.1 Wigner transform and gradient expansion

In this section, we perform the Wigner transformation individually on all three terms of the Hamiltonian (5.16) to derive the deterministic flow part of a generalized kinetic equation. If we assume that the density matrix and transport fields vary slowly in space with respect to the Fermi wavelength, we can perform a gradient expansion to obtain the semiclassical equation of motion for the distribution function that is the kinetic equation. In inhomogeneous magnetization texture the most important interaction is the sd interaction that can be quite strong in ferromagnets $J_{\text{sd}}/\epsilon_{\text{F}} \sim \mathcal{O}(0.01-1)$. The strong exchange interaction between the local moments causes numerous localized d spins to be coupled within a length scale λ forming the macroscopic magnetization texture $\vec{m}(\vec{r},t)$. The typical length scale λ of the magnetization as well as the electric transport field vary spatially slowly compared with the Fermi wavelength that sets the length scale for the conduction electrons k_{F}^{-1}. Accordingly, a semiclassical treatment of the conduction electrons is well justified as long as the condition holds $k_{\text{F}}\lambda \gg 1$ (cf. section 2.4). The situation is different as it concerns the spin of the conduction electron. Here, the

[1] The gauge transformation as defined in Eq. (A.9) corresponds to a non-abelian $SU(2)$ gauge transformation that introduces in general three independent gauge fields (cf. comments in appendix A).

relevant length scale is determined by the precession length of the spins of the conduction electrons

$$\lambda_{\text{sd}} := \frac{\pi}{|k_F^{\uparrow} - k_F^{\downarrow}|} = \frac{\hbar v_{\text{F}}}{J_{\text{sd}}}. \tag{5.17}$$

In other communities λ_{sd} is also called the ferromagnetic coherence or transverse spin-dephasing length. [172–174] The precession length in Eq. (5.17) can be of the order as the length scale of the magnetization, for instance the width of a narrow domain wall $\lambda \gtrsim \lambda_{\text{sd}} \gg k_{\text{F}}^{-1}$ (cf. discussion in section 5.5). This demonstrates the need to consider the full quantum coherence concerning the spin degree of freedom. A spin state that is not collinear to the magnetization is not a majority, minority eigenstate of the ferromagnet that are associated with different Fermi wave vectors $k_F^{\uparrow}$, $k_F^{\downarrow}$. Instead, a Bloch state with arbitrary spin direction is composed of a coherent linear combination of majority, minority spin states. The linear coefficients of the majority and minority spins oscillate spatially as a function of position, which is equivalent to a precession around the local moments. When injecting a spin current that is composed of many majority and minority states with different Larmor frequencies with polarization non-collinear to the homogeneous ferromagnet they interfere destructively inside the homogeneous ferromagnet. As the macroscopic spin current is determined by all wave vectors at the Fermi energy, where each corresponds to a different precession length (5.17), this results in an efficient relaxation of the non-diagonal terms in the density matrix that are associated with transverse spins. The macroscopic spin current is given by the integral over the Fermi surface and the strongly oscillating integrand cancels out due to destructive interference caused by the sd exchange splitting except for the vicinity of the injection interface. Typically the transverse component of the incident spin currents are absorbed within the very short length scale λ_{sd}. [173, 175] In turn the absorbed angular momentum is transferred to the ferromagnet and acts as a spin-transfer torque on the homogeneous domain. This is the microscopic picture of the *bookkeeping* theory of spin-transfer torque (cf. discussion in section 2.3). In contrast, in normal metals the just mentioned dephasing mechanism of transverse spins is absent. Here, the spin part of the wave functions remain coherent on the length scale of the spin-diffusion length that is associated with weak spin-flip scattering and can be of $\mathcal{O}(\mu\text{m})$. [174]

However, to properly take into account the influence of the spin degree of freedom of the conduction electrons onto transport, the above stated arguments outline the need to treat the spin in a full quantum mechanical manner while we pursue a gradient expansion for the space and momentum variables. This approach treats the motion of the distribution matrix in phase space semiclassically while it keeps the spin degree of freedom fully quantum mechanically. Consequently, the spin variables $\uparrow, \downarrow$ remain discrete quantum mechanical variables and the 2×2 matrix structure of the Hamiltonian (5.15) and the density matrix (5.13) directly translates to the distribution matrix $\hat{f}_{\vec{k}}(\vec{r})$.

To perform a gradient expansion, we must establish a connection between a full quantum mechanical operator $\hat{O}(\vec{r}_1, \vec{r}_2)$ on Hilbert-space and a smooth function on classical phase space $O(\vec{r}, \vec{k})$. A connection is provided by the Weyl-Wigner transformation as defined in Eq. (B.1). [170] As demonstrated in appendix B, the Wigner transform of a product of two operators $\hat{A}$ and $\hat{B}$ leads to an expansion in phase space [170]

$$\hat{A}\hat{B} \xrightarrow{\text{W.T.}} A(\vec{r}, \vec{k})B(\vec{r}, \vec{k}) + \frac{1}{2i}\left(\vec{\nabla}_{\vec{r}} A(\vec{r}, \vec{k})\vec{\nabla}_{\vec{k}} B(\vec{r}, \vec{k}) - \vec{\nabla}_{\vec{k}} A(\vec{r}, \vec{k})\vec{\nabla}_{\vec{r}} B(\vec{r}, \vec{k})\right) + \dots . \tag{5.18}$$

$A(\vec{r},\vec{k})$, $B(\vec{r},\vec{k})$ are the Wigner transforms of the operators $\hat{A}$ and $\hat{B}$ that are defined according to Eq. (B.1). The r.h.s. of Eq. (5.18) constitutes a gradient expansion on classical phase space up to first order in the phase-space gradients. According to Eq. (5.18), a commutator is transformed as

$$\begin{aligned}[\hat{A},\hat{B}] &\xrightarrow{\text{W.T.}} [A(\vec{r},\vec{k}),B(\vec{r},\vec{k})] - i(\vec{\nabla}_{\vec{r}}A(\vec{r},\vec{k})\vec{\nabla}_{\vec{k}}B(\vec{r},\vec{k}) - \vec{\nabla}_{\vec{k}}A(\vec{r},\vec{k})\vec{\nabla}_{\vec{r}}B(\vec{r},\vec{k})) + ... \\ &= [A(\vec{r},\vec{k}),B(\vec{r},\vec{k})] - i\left\{A(\vec{r},\vec{k}),B(\vec{r},\vec{k})\right\}^{\text{Poisson}}_{\vec{r},\vec{k}} + ...\,, \end{aligned} \tag{5.19}$$

where the first term in the expansion 5.19 constitutes the commutator of two functions on phase space and we introduced the classical Poisson bracket

$$\left\{A(\vec{r},\vec{k}),B(\vec{r},\vec{k})\right\}^{\text{Poisson}}_{\vec{r},\vec{k}} := \vec{\nabla}_{\vec{r}}A(\vec{r},\vec{k})\vec{\nabla}_{\vec{k}}B(\vec{r},\vec{k}) - \vec{\nabla}_{\vec{k}}A(\vec{r},\vec{k})\vec{\nabla}_{\vec{r}}B(\vec{r},\vec{k}). \tag{5.20}$$

Usually, the ordinary commutator of two Wigner transforms as it appears on the r.h.s. of Eq. (5.19) is identical zero, as functions on phase space commute. Due to the spin structure of the distribution matrix, we cannot simply discard the zeroth-order terms of the gradient expansion (5.19). Aiming at the linear response of the system to an external electric field we disregard higher terms in the gradient expansion (5.18). Expressions indicated by dots in Eq. (5.19) would produce higher order terms in the electric field. Equipped with the identification Eq. (5.14) and the directive of the Wigner expansion (5.19), we are now able to perform the gradient expansion for the Hamiltonian (5.16).
As discussed above the dynamic of the conduction electrons takes place on much faster time-scales compared with the slow collective magnetization dynamics. [156] To capture the essential influence of magnetotransport on a mesoscopic time scale that determines the dynamics for the micromagnetic model, it is sufficient to consider magnetotransport in the steady state. Accordingly, in this thesis we are interested in stationary magnetotransport, i.e., we assume time-independent transport fields $\vec{m}(\vec{r},t) \to \vec{m}(\vec{r},t_0) := \vec{m}(\vec{r})$, $\vec{E}(\vec{r},t) \to \vec{E}(\vec{r},t_0) := \vec{E}(\vec{r})$, $\mathcal{H} \to \mathcal{H}^{\text{st}}$. Thus we consider Eq. (5.13) in the steady state

$$[\mathcal{H}^{\text{st}},\hat{\rho}^{\text{st}}] = 0. \tag{5.21}$$

We now perform the gradient expansion of Eq. (5.21) for the individual parts of the Hamiltonian (5.16)

$$\begin{aligned}[H_0,\hat{\rho}] &\xrightarrow{\text{W.T.}} \frac{\hbar^2}{2m}\underbrace{[-\vec{k}^2\mathbb{1},\hat{f}_{\vec{k}}(\vec{r})]}_{=0} - i\frac{\hbar^2}{2m}(\underbrace{\vec{\nabla}_{\vec{r}}(-\vec{k}^2)}_{=0}\vec{\nabla}_{\vec{k}}\hat{f}_{\vec{k}}(\vec{r}) - \vec{\nabla}_{\vec{k}}(-\vec{k}^2)\vec{\nabla}_{\vec{r}}\hat{f}_{\vec{k}}(\vec{r})) \\ &= -\frac{i\hbar^2}{m}\vec{k}\cdot\vec{\nabla}_{\vec{r}}\hat{f}_{\vec{k}}(\vec{r}) = -i\hbar\vec{v}_{\vec{k}}\cdot\vec{\nabla}_{\vec{r}}\hat{f}_{\vec{k}}(\vec{r}), \end{aligned} \tag{5.22}$$

$$\begin{aligned}[H_{\text{V}},\hat{\rho}] &\xrightarrow{\text{W.T.}} e\underbrace{[V\mathbb{1},\hat{f}_{\vec{k}}(\vec{r})]}_{=0} - ie(\vec{\nabla}_{\vec{r}}V(\vec{r})\vec{\nabla}_{\vec{k}}\hat{f}_{\vec{k}}(\vec{r}) - \underbrace{\vec{\nabla}_{\vec{k}}V(\vec{r})}_{=0}\vec{\nabla}_{\vec{r}}\hat{f}_{\vec{k}}(\vec{r})) \\ &= ie\vec{E}(\vec{r})\cdot\vec{\nabla}_{\vec{k}}\hat{f}_{\vec{k}}(\vec{r}), \end{aligned} \tag{5.23}$$

$$
\begin{aligned}
[H_{\text{sd}},\hat{\rho}] \xrightarrow{\text{W.T.}} & J_{\text{sd}}[\vec{\sigma}\cdot\vec{m}(\vec{r}),\hat{f}_{\vec{k}}(\vec{r})] - iJ_{\text{sd}}(\vec{\nabla}_{\vec{r}}(\vec{\sigma}\cdot\vec{m}(\vec{r}))\vec{\nabla}_{\vec{k}}\hat{f}_{\vec{k}}(\vec{r}) - \underbrace{\vec{\nabla}_{\vec{k}}(\vec{\sigma}\cdot\vec{m}(\vec{r}))}_{=0}\vec{\nabla}_{\vec{r}}\hat{f}_{\vec{k}}(\vec{r})) \\
&= \frac{J_{\text{sd}}}{2}\underbrace{[\vec{\sigma}\cdot\vec{m}(\vec{r}),f^0_{\vec{k}}(\vec{r})\mathbb{1}]}_{=0} + \frac{J_{\text{sd}}}{2}[(\vec{\sigma}\cdot\vec{m}(\vec{r})),(\vec{\sigma}\cdot\vec{f}_{\vec{k}}(\vec{r}))] - iJ_{\text{sd}}\vec{\nabla}_{\vec{r}}(\vec{\sigma}\cdot\vec{m}(\vec{r}))\vec{\nabla}_{\vec{k}}\hat{f}_{\vec{k}}(\vec{r}) \\
&= \frac{J_{\text{sd}}}{2}\sum_{i,j} f^i_{\vec{k}}(\vec{r})[\sigma_i,\sigma_j]m^j(\vec{r}) - iJ_{\text{sd}}\vec{\nabla}_{\vec{r}}(\vec{\sigma}\cdot\vec{m}(\vec{r}))\vec{\nabla}_{\vec{k}}\hat{f}_{\vec{k}}(\vec{r}) \\
&= iJ_{\text{sd}}\sum_{i,j,k}\epsilon_{ijk}f^i_{\vec{k}}(\vec{r})m^j(\vec{r})\sigma_k - iJ_{\text{sd}}\vec{\nabla}_{\vec{r}}(\vec{\sigma}\cdot\vec{m}(\vec{r}))\vec{\nabla}_{\vec{k}}\hat{f}_{\vec{k}}(\vec{r}) \\
&= iJ_{\text{sd}}\vec{\sigma}\left(\vec{f}_{\vec{k}}(\vec{r})\times\vec{m}(\vec{r})\right) - iJ_{\text{sd}}\vec{\nabla}_{\vec{r}}(\vec{\sigma}\cdot\vec{m}(\vec{r}))\vec{\nabla}_{\vec{k}}\hat{f}_{\vec{k}}(\vec{r}). \qquad (5.24)
\end{aligned}
$$

In Eq. (5.22) we employ $\vec{v}_{\vec{k}} = \hbar\vec{k}/m$ and that the Wigner transform of $\vec{\nabla}^2_{\vec{r}}$ is equal to $-\vec{k}^2$ due to the Fourier transform contained in the Wigner transform. In the upper last line of Eq. (5.24) the relation (A.2) comes into operation. Note that expression (5.24) holds for general spins, as we employ the fundamental commutation relations for spins, not just properties of spin 1/2 particles.
According to Eq. (5.13), the collection of the individual terms (5.22) - (5.24) constitutes the generalized flow part of the kinetic equation in the steady state ($\partial_t\hat{f}_{\vec{k}}(\vec{r}) = 0$)

$$
\begin{aligned}
0 = & -\frac{1}{i\hbar}\Big[- i\hbar\vec{v}_{\vec{k}}\cdot\vec{\nabla}_{\vec{r}}\hat{f}_{\vec{k}}(\vec{r}) + ie\vec{E}(\vec{r})\cdot\vec{\nabla}_{\vec{k}}\hat{f}_{\vec{k}}(\vec{r}) + iJ_{\text{sd}}\vec{\sigma}\left(\vec{f}_{\vec{k}}(\vec{r})\times\vec{m}(\vec{r})\right) \\
& - iJ_{\text{sd}}\vec{\nabla}_{\vec{r}}(\vec{\sigma}\cdot\vec{m}(\vec{r}))\vec{\nabla}_{\vec{k}}\hat{f}_{\vec{k}}(\vec{r})\Big] \\
= & \ \vec{v}_{\vec{k}}\cdot\vec{\nabla}_{\vec{r}}\hat{f}_{\vec{k}}(\vec{r}) - \frac{e}{\hbar}\vec{E}(\vec{r})\cdot\vec{\nabla}_{\vec{k}}\hat{f}_{\vec{k}}(\vec{r}) - \frac{J_{\text{sd}}}{\hbar}\vec{\sigma}\left(\vec{f}_{\vec{k}}(\vec{r})\times\vec{m}(\vec{r})\right) + \frac{J_{\text{sd}}}{\hbar}\vec{\nabla}_{\vec{r}}(\vec{\sigma}\cdot\vec{m}(\vec{r}))\vec{\nabla}_{\vec{k}}\hat{f}_{\vec{k}}(\vec{r}) \\
= & \ \vec{v}_{\vec{k}}\cdot\vec{\nabla}_{\vec{r}}\hat{f}_{\vec{k}}(\vec{r}) - \frac{J_{\text{sd}}}{\hbar}\vec{\sigma}\left(\vec{f}_{\vec{k}}(\vec{r})\times\vec{m}(\vec{r})\right) - \left(\frac{e}{\hbar}\vec{E}(\vec{r}) - \frac{J_{\text{sd}}}{\hbar}\vec{\nabla}_{\vec{r}}(\vec{\sigma}\cdot\vec{m}(\vec{r}))\right)\vec{\nabla}_{\vec{k}}\hat{f}_{\vec{k}}(\vec{r}). \qquad (5.25)
\end{aligned}
$$

The r.h.s. of Eq. (5.25) is the generalized flow part of the kinetic equation that serves for a semiclassical description of non-collinear magnetotransport.

5.1.2 Physical interpretation of the individual terms of the flow part of the generalized kinetic equation and an introduction to transport regimes

Compared with the flow part of the Boltzmann equation (2.25) that constitutes the kinetic equation for electron transport in non-magnetic materials, the deterministic flow part of the generalized kinetic equation (5.25) exhibits two extra terms in addition to the diffusion and the drift term

$$
\vec{v}_{\vec{k}}\cdot\vec{\nabla}_{\vec{r}}\hat{f}_{\vec{k}}(\vec{r}) + i\frac{J_{\text{sd}}}{\hbar}[\vec{\sigma}\cdot\vec{m}(\vec{r}),\hat{f}_{\vec{k}}(\vec{r})] - \frac{e}{\hbar}\vec{E}(\vec{r})\cdot\vec{\nabla}_{\vec{k}}\hat{f}_{\vec{k}}(\vec{r}) + \frac{J_{\text{sd}}}{2\hbar}\{\vec{\nabla}_{\vec{r}}(\vec{\sigma}\cdot\vec{m}(\vec{r})),\vec{\nabla}_{\vec{k}}\hat{f}_{\vec{k}}(\vec{r})\}. \quad (5.26)
$$

In the last term of Eq. (5.26) we employ the anticommutator. Due to the property (A.4) of the Pauli matrices, the last term in Eq. (5.25) contains an unphysical imaginary part. This inconvenience can be removed by taking the real part of Eq. (5.25). According to relation (A.3) this is equivalent to the anticommutator notation. The anticommutator provides a symmetrization of the product of two observables and presents the common way to quantize classical expressions. [176]

The physical meaning of the drift and diffusion term in Eq. (5.26) has already been discussed in section 2.4.2.1. Additionally, two new terms that are proportional to the magnetization occur in Eq. (5.26) due to the interaction of the conduction electron spin with the local moments. They stem from the commutator of the sd-Hamiltonian with the density matrix and express the impact of the non-collinear magnetization texture on transport.
The second term in Eq. (5.26) is a reformulation of the second term in Eq. (5.25) and describes a precession of the spin-dependent part of the distribution function around the local magnetization. The Larmor frequency of the precession is determined by the sd exchange interaction

$$\omega_{\text{sd}} = 1/\tau_{\text{sd}} = J_{\text{sd}}/\hbar. \tag{5.27}$$

The fourth term in Eq. (5.26) is proportional to the gradient of the magnetization. Mathematically this term exhibits the same structure as the drift term proportional to the electric field. Thus, the fourth term of Eq. (5.26) constitutes an additional drift term for the distribution function that drives charge and spin distributions in the presence of a non-collinear magnetization texture. A non-collinear magnetization texture acts as an effective transport field on the distribution matrix.

Let us expand Eq. (5.26) in terms proportional to $\mathbb{1}$ and $\vec{\sigma}$ to clarify the physical meaning of the two new terms. The expansion results in two separate equations for the charge distribution $f^0_{\vec{k}}(\vec{r})$ and the spin distribution $\vec{f}_{\vec{k}}(\vec{r})$

$$\vec{v}_{\vec{k}} \cdot \vec{\nabla}_{\vec{r}} f^0_{\vec{k}}(\vec{r}) - \frac{e}{\hbar}\vec{E}(\vec{r}) \cdot \vec{\nabla}_{\vec{k}} f^0_{\vec{k}}(\vec{r}) + \frac{J_{\text{sd}}}{\hbar}\left(\vec{\nabla}_{\vec{r}}\vec{m}(\vec{r})\right) \cdot \left(\vec{\nabla}_{\vec{k}}\vec{f}_{\vec{k}}(\vec{r})\right) = 0, \tag{5.28}$$

$$\vec{v}_{\vec{k}} \cdot \vec{\nabla}_{\vec{r}} \vec{f}_{\vec{k}}(\vec{r}) - 2\frac{J_{\text{sd}}}{\hbar}\left(\vec{f}_{\vec{k}}(\vec{r}) \times \vec{m}(\vec{r})\right) - \frac{e}{\hbar}\vec{E}(\vec{r}) \cdot \vec{\nabla}_{\vec{k}} \vec{f}_{\vec{k}}(\vec{r}) + \frac{J_{\text{sd}}}{\hbar}\left(\vec{\nabla}_{\vec{r}}\vec{m}(\vec{r})\right) \cdot \left(\vec{\nabla}_{\vec{k}} f^0_{\vec{k}}(\vec{r})\right) = 0. \tag{5.29}$$

The short hand notation that we employ in Eqns. (5.28) and (5.29) and throughout the rest of this thesis implies implicitly the following vector structure: $\left(\vec{\nabla}_{\vec{r}}\vec{m}(\vec{r})\right) \cdot \left(\vec{\nabla}_{\vec{k}}\vec{f}_{\vec{k}}(\vec{r})\right) = \sum_{i,j} \nabla^i_{\vec{r}} m^j(\vec{r}) \nabla^i_{\vec{k}} f^j_{\vec{k}}(\vec{r})$. Corresponding vector structures apply to similar terms. The charge distribution $f^0_{\vec{k}}(\vec{r})$ couples to the spin-distribution distribution $\vec{f}_{\vec{k}}(\vec{r})$ due to the non-vanishing magnetization gradient (cf. Eq. (5.28)), while the spin distribution in addition precesses around the local magnetization (cf. Eq. (5.29)). The last terms in Eqns. (5.28) and (5.29) vanish in collinear magnetization textures where charge and spin degree of freedom decouple in contrast to non-collinear magnetization textures.

In general, there are four independent length scales present in magnetotransport. With respect to mesoscopic magnetization textures as considered in this thesis the length scales read ordered in ascending sequence: the Fermi wavelength, the sd precession length or the mean free path and the characteristic length of the structure that is the geometric length (for instance the domain-wall width). The coupling of charge and spin transport as it results from Eqns. (5.28) and (5.29) introduces the possibility of new intermediate transport regimes that are absent in non-magnetic and collinear transport. Usually, there are two limiting regimes in transport. In ballistic systems the mean free path of the electron exceeds the system size and the transport properties are determined entirely by the geometry. In this case scattering processes are negligible concerning the resistance of the specimen and the

deterministic flow part of the kinetic equation governs the physics. In diffusive systems the mean free path is shorter than the system size, the geometry becomes negligible and the transport is dominated by impurity scattering comprised within the collision integral of the kinetic equation.
A new length scale emerges for spin transport from Eq. (5.29) due to the presence of the two new terms: the precession length of the spin around the local magnetization with the frequency set by the sd interaction defined in Eq. (5.27). According to Eq. (5.26) the precession is determined by the deterministic flow part. The mean free path is set by the relaxation times due to spin-dependent impurity scattering τ^s, $s =\uparrow, \downarrow$ that characterize the time between two adjacent scattering events for the two spin species. If the predominant time-scale for transport is given by the coherence time or Larmor precession τ_{sd}, we will refer to this transport regime as *ballistic spin transport*. More precisely $\tau_{\text{sd}}/\tau^s < 1$ applies to strong ferromagnets and designates the regime of ballistic spin transport where the spin has enough time to precess around the local magnetization between gradual collisions. $\tau_{\text{sd}}/\tau^s > 1$ distinguishes the diffusive spin transport regime of relatively dirty systems. Here the precession of the transverse magnetization is damped out due to relaxation. In contrast, the charge transport is entirely diffusive for the mesoscopic structures that our semiclassical transport formalism aims at. In this connection, the interesting possibility of an intermediate transport regime arises: *ballistic spin transport*, where the charge transport is diffusive while the spin transport is ballistic at the same time. Section 5.5 demonstrates that the regime of ballistic spin transport entails fascinating physical consequences for narrow domain walls.

Besides the common discrimination between diffusive and ballistic transport, non-collinear magnetotransport gives rise to two different transport regimes in discrimination of the magnetization texture itself. In the regime of *adiabatic* magnetotransport the magnetization varies slowly in space, such that the conduction electron spin precesses with small angle around the local magnetization. The spin of the conduction electron resides in its majority or minority spin state during the traversal of the magnetization texture. The conduction electron spin can follow the local magnetization and no scattering with the magnetization texture takes place. As a result, the adiabatic transport coefficients do not depend on the details of the magnetization texture. In the *non-adiabatic* transport regime, the magnetization varies strongly and the conduction electron spin cannot follow the local magnetization. During the traversal of spatially strongly inhomogeneous magnetization textures, the spin of the conduction electron resides in a coherent superposition of majority and minority states. In this case spin-mistracking occurs due to the mixing of spin channels. The transport coefficients attain an explicit dependence on the characteristics of the magnetization texture. While we focus in sections 5.4 entirely on adiabatic magnetotransport, the explicit solution of the kinetic equation for the case of a domain wall in section 5.5 grants an insight in the non-adiabatic regime, where such interesting phenomena as domain-wall resistivity and momentum transfer emerge due to the mixing of spin channels caused by the enhanced spatial variations of the magnetization texture.
In the case of *adiabatic* transport we expect to attain global transport coefficients. In this sense, the conduction coefficients are global as they do not depend on position. In the non-adiabatic case the transport coefficients depend on the characteristics of the magnetization texture and are therefore local.

At this point of the derivation, it is inevitable to check, whether the generalized flow part as given

in Eq. (5.26) reduces to the two-current model in collinear magnetization textures. In homogeneous ferromagnets the precession of non-equilibrium spins in the sd exchange field of the homogeneous magnetization $\vec{m}$ results in an effective relaxation of the transverse magnetization of the conduction electrons on the scale of the precession length (5.17). [174] Consequently, the spin part of the distribution matrix is aligned with the constant magnetization

$$\hat{f}_{\vec{k}}(\vec{r}) = \frac{1}{2}\left[f_{\vec{k}}^{\text{charge}}(\vec{r})\mathbb{1} + f_{\vec{k}}^{\text{spin}}(\vec{r})\,(\vec{\sigma}\cdot\vec{m})\right]. \tag{5.30}$$

In collinear magnetization textures, we can adjust the quantization axis with the local magnetization by a global unitary rotation $\hat{U}$ such that $\hat{U}\,(\vec{\sigma}\cdot\vec{m}(\vec{r}))\,\hat{U}^\dagger = \sigma_z$. If we apply the rotation to Eq. (5.26) and insert Eq. (5.30), the commutator vanishes and the last part is zero due to $\vec{\nabla}_{\vec{r}}(\vec{\sigma}\cdot\vec{m}(\vec{r})) = 0$. Accordingly, we obtain the flow part of the two-current model for collinear magnetization patterns (cf. section 5.2)

$$(\vec{v}_{\vec{k}}\cdot\vec{\nabla}_{\vec{r}})\hat{f}_{\vec{k}}^{\text{collinear}}(\vec{r}) - \frac{e}{\hbar}\vec{E}(\vec{r})\cdot\vec{\nabla}_{\vec{k}}\hat{f}_{\vec{k}}^{\text{collinear}}(\vec{r}). \tag{5.31}$$

with the diagonal distribution matrix that contains the majority, minority spin distributions

$$\hat{f}_{\vec{k}}^{\text{collinear}}(\vec{r}) = \frac{1}{2}\left[f_{\vec{k}}^{\text{charge}}(\vec{r})\mathbb{1} + f_{\vec{k}}^{\text{spin}}(\vec{r})\sigma_z\right] = \begin{pmatrix} f_{\vec{k}}^{\uparrow}(\vec{r}) & 0 \\ 0 & f_{\vec{k}}^{\downarrow}(\vec{r}) \end{pmatrix} := \hat{U}\hat{f}_{\vec{k}}(\vec{r})\hat{U}^\dagger. \tag{5.32}$$

Note that off-diagonal terms in the distribution matrix correspond in the collinear case to additional gauge degrees of freedom that must be only taken into account, when combining two homogeneous non-collinear ferromagnets, for instance within a spin valve, but are redundant in a homogeneous ferromagnet. [174]

5.1.3 Generalized collision integral in the relaxation-time approximation

The collision term bears a particular meaning in a kinetic description of transport as it governs the physics (cf. section 2.4). In the previous section, we generalized the flow part of the kinetic equation for non-collinear magnetization textures. The collision integral $\hat{\mathcal{I}}[\hat{f}_{\vec{k}}(\vec{r})]$ constitutes the r.h.s. of the kinetic equation (cf. section 2.4) and requires a generalization to Pauli spin space. In general, the collision integral exhibits a non-trivial spin structure, such that $[\hat{f}_{\vec{k}}(\vec{r}), \hat{\mathcal{I}}[\hat{f}_{\vec{k}}(\vec{r})]] \neq 0$, where the details depend on the specific microscopic model. The derivation of its actual form is subject to a microscopic theory, for instance a Keldysh approach and is beyond the scope of this thesis.
Instead of introducing a multitude of phenomenological relaxation times at this point, we refer to the comments in section 5.3.3 and restrict ourself throughout this thesis to neglect transverse spin relaxation and consider longitudinal spin relaxation only. Then, the collision integral is composed of a part due to momentum relaxation and due to spin flip: $\hat{\mathcal{I}}[\hat{f}_{\vec{k}}(\vec{r})] = \hat{\mathcal{I}}_{\text{mr}}[\hat{f}_{\vec{k}}(\vec{r})] + \hat{\mathcal{I}}_{\text{sf}}[\hat{f}_{\vec{k}}(\vec{r})]$. We limit ourselves to the simplest non-trivial form by parameterizing the collision integral in terms of three independent relaxation times: the momentum relaxation times τ^s, where $s = \{\uparrow,\downarrow\}$ denotes the relaxation of majority and minority charge carriers and a single scalar spin-flip relaxation time τ_{sf}.
Keeping the quantization axis parallel to the local magnetization allows us to replace the collision integral by a momentum relaxation-time matrix-approximation in spatially varying magnetization textures

$$\hat{\mathcal{I}}_{\text{mr}}[\hat{f}_{\vec{k}}(\vec{r})] := -\frac{1}{2}\{\hat{\tau}^{-1}(\vec{r}), (\hat{f}_{\vec{k}}(\vec{r}) - \hat{f}_{\text{eq}}(\vec{m}(\vec{r}),\epsilon))\}. \tag{5.33}$$

Note, however, that we account for a coherent spin rotation accordingly. $\hat{\tau}^{-1}(\vec{r})$ is the momentum relaxation-time matrix that preserves the spin in homogeneous ferromagnets. Due to the inherent spin structure, a symmetrization of the product of the relaxation-time matrix and the distribution matrix is required in Eq. (5.33). This avoids unphysical imaginary parts (cf. discussion in section 5.1.2). With this generalization the influence of the magnetization texture on the solution of the kinetic equation is twofold: first the magnetization appears directly in the flow part of the kinetic equation and second the magnetization determines the collision integral.
In addition, we introduce a scalar spin-flip relaxation time τ_{sf}, where it is assumed that no spin direction is preferred, i.e., the transition probability is the same from up to down and vice versa. We consider the spin-flip to be an elastic process, which does not transfer momentum. The generalization of the spin-flip part of the collision integral reads

$$\hat{\mathcal{I}}_{\text{sf}}[\hat{f}_{\vec{k}}(\vec{r})] := -\frac{{}^{\text{sf}}\hat{f}_{\vec{k}}(\vec{r}) - {}^{\text{sf}}\hat{f}_{\text{eq}}(\vec{m}(\vec{r}),\epsilon)}{\tau_{\text{sf}}}, \tag{5.34}$$

with the abbreviation [177]

$${}^{\text{sf}}\hat{f}_{\vec{k}}(\vec{r}) \equiv \frac{1}{2}\vec{\sigma}\text{Tr}\,\hat{f}_{\vec{k}}(\vec{r})\vec{\sigma} = \left(\hat{f}_{\vec{k}}(\vec{r}) - \mathbb{1}\frac{\text{Tr}\,\hat{f}_{\vec{k}}(\vec{r})}{2}\right). \tag{5.35}$$

The expression for the spin-flip in Eq. (5.35) is a projection on the $SU(2)$ spin subspace. In section 5.2, we show that the generalized collision integral given by (5.33) and (5.34) reduces to the collision term of the two-current model in collinear magnetization patterns. In particular, it will be discussed in section 5.2.2 that Eq. (5.35) constitutes an appropriate expression for the spin flip.

5.1.3.1 Inverse momentum relaxation-time matrix

As discussed in the last chapter we must generalize the spin-conserving relaxation times $\tau^{\uparrow}, \tau^{\downarrow}$ that are well defined in collinear magnetization patterns to non-collinear magnetization patterns. This can be achieved with the help of the unitary rotation (A.9). Keeping the quantization axis parallel to the local magnetization results for spatially varying magnetization textures in a momentum relaxation-time matrix

$$\hat{\tau} = \hat{U}(\vec{m}(\vec{r}))\hat{\tau}^{\text{diagonal}}\hat{U}^{\dagger}(\vec{m}(\vec{r})) = \hat{U}(\vec{m}(\vec{r}))\begin{pmatrix}\tau^{\uparrow} & 0\\ 0 & \tau^{\downarrow}\end{pmatrix}\hat{U}^{\dagger}(\vec{m}(\vec{r})). \tag{5.36}$$

Equation (5.36) generalizes the two-current model [34] for general magnetization textures. $\hat{U}(\vec{m}(\vec{r}))$ is the unitary rotation matrix as defined in Eq. (A.9). The spin-conserving relaxation-time matrix (5.36) is diagonal in the reference frame of the magnetization and therefore only takes longitudinal spin relaxation into account. An occupation of off-diagonal elements in the local reference frame of the magnetization would correspond to the introduction of transverse spin relaxation. With the magnetization angles θ, ϕ, as defined in Eqns. (A.7) and (A.8) the general result for Eq. (5.36) reads

$$\hat{\tau} = \begin{pmatrix}\frac{1}{2}\left(\tau^{\uparrow}+\tau^{\downarrow}+(\tau^{\uparrow}-\tau^{\downarrow})\cos\theta\right) & \frac{1}{2}e^{-i\phi}(\tau^{\uparrow}-\tau^{\downarrow})\sin\theta\\ \frac{1}{2}e^{i\phi}(\tau^{\uparrow}-\tau^{\downarrow})\sin\theta & \frac{1}{2}\left(\tau^{\uparrow}+\tau^{\downarrow}+(\tau^{\downarrow}-\tau^{\uparrow})\cos\theta\right)\end{pmatrix}. \tag{5.37}$$

The next step is to invert the magnetization dependent spin-conserving relaxation-time matrix in Eq. (5.37)

$$\hat{\tau}^{-1} = \frac{1}{2\tau^{\uparrow}\tau^{\downarrow}} \begin{pmatrix} \tau^{\uparrow} + \tau^{\downarrow} + (\tau^{\downarrow} - \tau^{\uparrow})\cos\theta & e^{-i\phi}(\tau^{\downarrow} - \tau^{\uparrow})\sin\theta \\ e^{i\phi}(\tau^{\downarrow} - \tau^{\uparrow})\sin\theta & \tau^{\uparrow} + \tau^{\downarrow} + (\tau^{\uparrow} - \tau^{\downarrow})\cos\theta \end{pmatrix}. \tag{5.38}$$

It is useful to decompose Eq. (5.38) into components

$$\hat{\tau}^{-1} = (\tau^0)^{-1}\mathbb{1} + \sum_i (\tau^i)^{-1}\sigma_i, \tag{5.39}$$

with

$$(\tau^0)^{-1} = \frac{1}{2}(\frac{1}{\tau^{\uparrow}} + \frac{1}{\tau^{\downarrow}}), \tag{5.40}$$

$$(\tau^x)^{-1} = \frac{1}{2}(\frac{1}{\tau^{\uparrow}} - \frac{1}{\tau^{\downarrow}})\sin\theta\cos\phi, \tag{5.41}$$

$$(\tau^y)^{-1} = \frac{1}{2}(\frac{1}{\tau^{\uparrow}} - \frac{1}{\tau^{\downarrow}})\sin\theta\sin\phi, \tag{5.42}$$

$$(\tau^z)^{-1} = \frac{1}{2}(\frac{1}{\tau^{\uparrow}} - \frac{1}{\tau^{\downarrow}})\cos\theta. \tag{5.43}$$

Note from Eqns. (5.40) to (5.43) that an inhomogeneous magnetization pattern solely influences the spin-dependent part of the relaxation-time matrix while the charge part $(\tau^0)^{-1}$ in Eq. (5.40) remains unaffected. Thus, the magnetization pattern leaves the total relaxation time for the electrons unchanged, but alters only the relaxation times of the different components of the spin distributions. Equations (5.40) to (5.43) explicitly refer to the magnetization in spherical coordinates. Alternatively, the spin-conserving relaxation time can be written in terms of the local magnetization

$$\begin{aligned} \hat{\tau}^{-1}(\vec{m}(\vec{r})) &= \frac{1}{2}\left[\left(\frac{1}{\tau^{\uparrow}} + \frac{1}{\tau^{\downarrow}}\right)\mathbb{1} + \left(\frac{1}{\tau^{\uparrow}} - \frac{1}{\tau^{\downarrow}}\right)(\vec{\sigma}\cdot\vec{m}(\vec{r}))\right] \\ &= \frac{1}{2}\left[\tau_c^{-1}\mathbb{1} + \tau_s^{-1}(\vec{\sigma}\cdot\vec{m}(\vec{r}))\right]. \end{aligned} \tag{5.44}$$

The inverse momentum relaxation-time matrix (5.44) generalizes the momentum conserving relaxation times $\tau^{\uparrow}$, $\tau^{\downarrow}$ to arbitrary non-collinear magnetization textures. We note that off-diagonal terms in the relaxation-time matrix (5.44) originate from the spatially varying magnetization. A future microscopic calculation of the collision integral is necessary to shed light on an appropriate form and to consider transverse relaxation. We just note here that the general intuition tells us that transverse relaxation times are associated with gradient corrections, because derivatives of the magnetization are perpendicular to the magnetization itself.

5.1.4 Generalized equilibrium kinetic equation

In the previous section we derived the generalized kinetic equation for charge and spin transport in continuous non-collinear magnetization textures[2]

$$\vec{v}_{\vec{k}}\vec{\nabla}_{\vec{r}}\hat{f}_{\vec{k}}(\vec{r}) + i\frac{J_{\text{sd}}}{\hbar}[\vec{\sigma}\vec{m}(\vec{r}), \hat{f}_{\vec{k}}(\vec{r})] - \frac{e}{\hbar}\vec{E}(\vec{r})\vec{\nabla}_{\vec{k}}\hat{f}_{\vec{k}}(\vec{r}) + \frac{J_{\text{sd}}}{2\hbar}\{\vec{\nabla}_{\vec{r}}(\vec{\sigma}\vec{m}(\vec{r})), \vec{\nabla}_{\vec{k}}\hat{f}_{\vec{k}}(\vec{r})\} = \hat{\mathcal{I}}[\hat{f}_{\vec{k}}(\vec{r})]. \tag{5.45}$$

$\hat{f}_{\vec{k}}(\vec{r})$ is the spin-dependent matrix distribution function that contains the charge distribution function and the three spin distributions. In equilibrium the collision integral $\hat{\mathcal{I}}[\hat{f}_{\vec{k}}(\vec{r})]$ and the electric field $\vec{E}$ vanish and Eq. (5.45) reduces to the equilibrium kinetic equation

$$\vec{v}_{\vec{k}}\vec{\nabla}_{\vec{r}}\hat{f}_{\text{eq}}(\vec{m}(\vec{r}), \epsilon) + i\frac{J_{\text{sd}}}{\hbar}[\vec{\sigma}\vec{m}(\vec{r}), \hat{f}_{\text{eq}}(\vec{m}(\vec{r}), \epsilon)] + \frac{J_{\text{sd}}}{2\hbar}\{\vec{\nabla}_{\vec{r}}(\vec{\sigma}\vec{m}(\vec{r})), \vec{\nabla}_{\vec{k}}\hat{f}_{\text{eq}}(\vec{m}(\vec{r}), \epsilon)\} = 0. \tag{5.46}$$

In the following sections the calculation of transport properties shall be performed in linear response to an external electric field by considering small deviations from the equilibrium. Hence, for expansions around the equilibrium the first task is to determine the equilibrium solution from Eq. (5.46). For this purpose, we will distinguish two different cases: first a homogeneous magnetization pattern with no spatial variations ($\vec{\nabla}_{\vec{r}}(\vec{\sigma}\vec{m}(\vec{r})) = 0$) in section 5.2 and secondly general non-collinear magnetization patterns ($\vec{\nabla}_{\vec{r}}(\vec{\sigma}\vec{m}(\vec{r})) \neq 0$) in section 5.4.

[2] Throughout the rest of this thesis we employ an implicit notation for scalar products for the sake of simplicity of notation.

5.2 Collinear magnetotransport – the two-current model

In the previous section we derived a generalized kinetic equation to extend magnetotransport to non-collinear magnetization textures. In order to understand the implications of the generalized kinetic equation (5.45) for non-collinear magnetotransport as it will be discussed in the following sections, it is instructive to first review collinear magnetotransport. This familiarizes us with spin-dependent concepts and facilitates the comprehension of non-collinear transport. In a ferromagnetic material most scattering events conserve the spin direction of the incident electrons at temperatures low compared with the Curie temperature. Relying on the proposal by Mott [178, 179] that dates back to 1936, majority and minority electrons can be treated independently as if they carry currents in parallel. Mott proposed that scattering from s to d bands dominates the transport in transition metals and as a consequence of the spin-splitting of the d states, he addressed the sd scattering to cause different mean free paths or relaxation times $\tau^{\uparrow}$ ($\tau^{\downarrow}$) for the majority (minority) charge carriers. [34, 180] The essence of the two-current model is to recognize that majority and minority spins contribute unequally to the electron transport because of two reasons: first the density of states of majority, minority spins at the Fermi level is usually different, and secondly, the mobility is usually different for the majority (minority) charge carriers due to different relaxation times $\tau^{\uparrow} \neq \tau^{\downarrow}$. The different density of states at the Fermi level is in ferromagnets due to a lifted degeneracy by means of the exchange interaction. Different relaxation times are either due to different scattering rates for majority, minority carriers as a consequence of asymmetric spin-dependent impurity scattering or are an indirect consequence of the different density of states. As it follows from *Fermi's golden rule* the relaxation times depend on the transition matrix elements as well as on the density of states (cf. Eq. (2.32) in section 2.4) and the dominating contribution depends on the material and the kind of impurities. In conclusion, the consequence of this view are different conductivities due to different band structures for majority and minority charge carriers. [181] The treatment of majority and minority electrons in individual channels is referred to as the *two-current model*. [34, 169, 180] The individual channels communicate by spin-flip processes. The distribution function $f^s_{\vec{k}}(\vec{r})$ obtains a spin index $s = \{\uparrow, \downarrow\}$ that labels the two possible spin directions and obeys a spin-generalized version of the Boltzmann equation for non-magnetic metals (2.42)

$$\vec{v}_{\vec{k}} \vec{\nabla}_{\vec{r}} f^s_{\vec{k}}(\vec{r}) - \frac{e}{\hbar} \vec{E}(\vec{r}) \vec{\nabla}_{\vec{k}} f^s_{\vec{k}}(\vec{r}) = \mathcal{I}[f^s_{\vec{k}}(\vec{r})]. \tag{5.47}$$

A coupling of the two spin channels in Eq. (5.47) is considered within the collision integral $\mathcal{I}[f^s_{\vec{k}}(\vec{r})]$ via spin-flip processes at magnetic impurities.

5.2.1 Equilibrium solution

In a homogeneous or monodomain ferromagnet the magnetization always points along a distinct direction. We will choose this axis as spin quantization axis

$$\vec{m} = \hat{e}_{m_z} = const.. \tag{5.48}$$

In equilibrium, the electric field $\vec{E}(\vec{r})$ and the collision integral $\mathcal{I}[f^s_{\vec{k}}(\vec{r})]$ vanish. In the case of a constant magnetization, the equilibrium kinetic equation (5.46) reduces to

$$i \frac{J_{\text{sd}}}{\hbar} [\sigma_z, \hat{f}^{\text{coll}}_{\text{eq}}(\epsilon)] = 0, \tag{5.49}$$

and constitutes a contraint on the equilibrium distribution $\hat{f}_{\text{eq}}^{\text{coll}}(\epsilon)$ in collinear magnetization textures. Condition (5.49) requires the equilibrium distribution to be diagonal in spin space

$$\hat{f}_{\text{eq}}^{\text{coll}}(\epsilon) = \frac{1}{2}\left[f^{\text{charge}}(\epsilon, J_{\text{sd}})\mathbb{1} + f^{\text{spin}}(\epsilon, J_{\text{sd}})\sigma_z\right], \tag{5.50}$$

where we introduced a charge $f^{\text{charge}}(\epsilon, J_{\text{sd}})$ and a spin $f^{\text{spin}}(\epsilon, J_{\text{sd}})$ distribution function that remains to be determined. On the other hand, the underlying Hamiltonian (5.15) is now spatially independent. Its energy spectrum can be directly obtained by a diagonalization and exhibits a spin-splitting in majority and minority electrons with two energy levels that are separated by half the exchange energy splitting J_{sd}

$$\tilde{\mathcal{H}} = \frac{\hbar^2\vec{k}^{\,2}}{2m} + J_{\text{sd}}\sigma_z = \epsilon + J_{\text{sd}}\sigma_z. \tag{5.51}$$

The collision integral vanishes in equilibrium and forces the distribution of free majority and minority electrons to be spin-resolved Fermi-Dirac distributions

$$f(\epsilon, \pm J_{\text{sd}}) = \frac{1}{e^{\beta(\epsilon \pm J_{\text{sd}} - \mu)} + 1}, \tag{5.52}$$

with electrochemical potential μ.
Alternatively, the solution to Eq. (5.49) can also be directly obtained from the ansatz of a matrix-valued Fermi-Dirac distribution

$$\begin{aligned}
\hat{f}_{\text{eq}}^{\text{coll}}(\epsilon) &= \left[\exp(\beta(\epsilon\mathbb{1} + J_{\text{sd}}\sigma_z - \mu\mathbb{1})) + \mathbb{1}\right]^{-1} \\
&= \begin{pmatrix} \left[\exp(\beta(\epsilon + J_{\text{sd}} - \mu)) + 1\right]^{-1} & 0 \\ 0 & \left[\exp(\beta(\epsilon - J_{\text{sd}} - \mu)) + 1\right]^{-1} \end{pmatrix} \\
&= \begin{pmatrix} f(\epsilon, +J_{\text{sd}}) & 0 \\ 0 & f(\epsilon, -J_{\text{sd}}) \end{pmatrix} \\
&= \frac{1}{2}\left[\left(f(\epsilon, +J_{\text{sd}}) + f(\epsilon, -J_{\text{sd}})\right)\mathbb{1} + \left(f(\epsilon, +J_{\text{sd}}) - f(\epsilon, -J_{\text{sd}})\right)\sigma_z\right] \\
&= \frac{1}{2}\left[f^{\text{charge}}(\epsilon, J_{\text{sd}})\mathbb{1} + f^{\text{spin}}(\epsilon, J_{\text{sd}})\sigma_z\right].
\end{aligned} \tag{5.53}$$

The equilibrium solution Eq. (5.53) is the equilibrium solution of the two-current model with the following definition of the minority and majority electron distributions

$$f^{\uparrow}(\epsilon) \equiv \frac{1}{e^{\beta(\epsilon + J_{\text{sd}} - \mu)} + 1} = f(\epsilon, +J_{\text{sd}}), \tag{5.54}$$

$$f^{\downarrow}(\epsilon) \equiv \frac{1}{e^{\beta(\epsilon - J_{\text{sd}} - \mu)} + 1} = f(\epsilon, -J_{\text{sd}}). \tag{5.55}$$

5.2.2 Non-equilibrium solution

In the non-equilibrium case ($\vec{E} \neq 0$, $\mathcal{I}[f_{\vec{k}}^s(\vec{r})] \neq 0$), in linear response to an electric field $\vec{E}$, the spin-generalized version of the Boltzmann equation reads for the two-current model [182]

$$\vec{v}_{\vec{k}}\vec{\nabla}_{\vec{r}}g_{\vec{k}}^s(\vec{r}) - e\vec{v}_{\vec{k}}\vec{E}\partial_\epsilon f_{\text{eq}}^s(\epsilon) = -\frac{g_{\vec{k}}^s(\vec{r})}{\tau^s} - \frac{g_{\vec{k}}^s(\vec{r}) - g_{\vec{k}}^{-s}(\vec{r})}{2\tau_{\text{sf}}}, \tag{5.56}$$

that determines the non-equilibrium distribution $g^s_{\vec{k}}(\vec{r}) = f^s_{\vec{k}}(\vec{r}) - f^s_{\text{eq}}(\epsilon)$. Equation (5.56) is derived by inserting the equilibrium solution (5.53) in the Boltzmann equation (5.47) and linearizing it with respect to the electric field. We choose the simplest non-trivial ansatz for the relaxation times by parameterizing the collisions in terms of two *spin*-conserving relaxation times τ^s that characterize at finite temperature the relaxation of *momentum* to the lattice within each spin channel and one single, *momentum* conserving spin-flip relaxation time τ_{sf} that couples the two spin channels (cf. section 2.4.2.1 for a discussion of the scattering processes in non-magnetic metals). At low temperatures, τ^s depends on the spin-dependent impurity potential and the spin-dependent density of states (cf. Eq. (2.32)). [183] Note that the spin-flip scattering balances the spin distributions of both channels in a rate equation: a loss in the s-channel is compensated by a gain in the $-s$-channel. Thus, spin-flip processes transfer momentum between both channels. Spin-flip events are, e.g., due to spin-orbit coupling at magnetic impurities or the interaction with magnons. Electron-magnon scattering partly conserves the momentum of the electron: $\vec{k}' \rightarrow \vec{k} + \vec{q}$. Here, $\vec{k}$ is the momentum of the incident electron, $\vec{k}'$ is the momentum of the scattered electron and $\vec{q}$ represents the momentum of the magnon. At finite, but relatively low temperatures, the momentum of the magnon is negligible compared to the Fermi momentum k_{F} ($|\vec{q}| \ll k_{\text{F}}$) and the momentum of the scattered majority electrons is almost completely transferred to the minority electron and vice versa. Since spin-flip processes approximately conserve momentum, they cannot directly result in additional dissipation for the charge current. [98] For simplifications we assume an equal probability for a spin flip from up to down and vice versa.
In the bulk ferromagnet the majority, minority distributions are spatially independent ($g^s_{\vec{k}}(\vec{r}) \rightarrow g^s_{\vec{k}}$) and Eq. (5.56) reduces to

$$\frac{g^s_{\vec{k}}}{\tau^s} + \frac{g^s_{\vec{k}} - g^{-s}_{\vec{k}}}{2\tau_{\text{sf}}} = e\vec{v}_{\vec{k}}\vec{E}\partial_\epsilon f^s_{\text{eq}}(\epsilon). \tag{5.57}$$

A decoupling of Eq. (5.57) yields

$$g^s_{\vec{k}} = e\frac{\tau^s\left[2\tau_{\text{sf}}\partial_\epsilon f^s_{\text{eq}}(\epsilon) + \tau^{-s}\left(\partial_\epsilon f^s_{\text{eq}}(\epsilon) + \partial_\epsilon f^{-s}_{\text{eq}}(\epsilon)\right)\right]}{\tau^s + \tau^{-s} + 2\tau_{\text{sf}}}\vec{v}_{\vec{k}}\vec{E}. \tag{5.58}$$

Equation (5.58) marks the result for collinear magnetotransport that allows for the computation of transport coefficients.

But before we discuss the transport coefficients, we first want to rederive the result for the non-equilibrium distributions (5.58) from the matrix form of the kinetic equation (5.45). On the one hand it is a good way to become familiar with the matrix structure of the generalized kinetic equation in non-collinear magnetization textures, on the other hand it is a test to control whether the more general matrix form (5.45) reproduces the right limit in collinear magnetization textures. If we neglect the spatial dependence of the magnetization and insert the equilibrium solution (5.53) into Eq. (5.45), the non-equilibrium kinetic equation reads -with the collision integral specified in section 5.1.3-

$$i\frac{J_{\text{sd}}}{\hbar}[\sigma_z, \hat{g}^{\text{coll}}_{\vec{k}}] - e\vec{v}_{\vec{k}}\vec{E}\partial_\epsilon \hat{f}^{\text{coll}}_{\text{eq}}(\epsilon) = -\frac{1}{2}\{\hat{\tau}^{-1}, \hat{g}^{\text{coll}}_{\vec{k}}\} - \frac{^{\text{sf}}\hat{g}^{\text{coll}}_{\vec{k}}}{\tau_{\text{sf}}}. \tag{5.59}$$

Due to the diagonal spin-structure of the equilibrium solution (5.53), the electric field part on the l.h.s. of Eq. (5.59) is diagonal too. Considering relation (5.48), the momentum relaxation time matrix is

diagonal according to its definition in Eq. (5.44). Taken all this together requires the non-equilibrium distribution matrix to be diagonal

$$\hat{g}_{\vec{k}}^{\text{coll}} = \frac{1}{2}\left[g_{\vec{k}}^{\text{charge}}\mathbb{1} + g_{\vec{k}}^{\text{spin}}\sigma_z\right], \tag{5.60}$$

where we introduced the non-equilibrium distribution $\hat{g}_{\vec{k}}^{\text{coll}}$ analogously to Eq. (5.50). By means of Eq. (5.60), we compute the spin-flip distribution from Eq. (5.35)

$$\begin{aligned} {}^{\text{sf}}\hat{g}_{\vec{k}}^{\text{coll}} &= \left(\hat{g}_{\vec{k}}^{\text{coll}} - \mathbb{1}\frac{\operatorname{Tr}\hat{g}_{\vec{k}}^{\text{coll}}}{2}\right) \\ &= \frac{1}{2}\left[g_{\vec{k}}^{\text{charge}}\mathbb{1} + g_{\vec{k}}^{\text{spin}}\sigma_z - g_{\vec{k}}^{\text{charge}}\mathbb{1}\right] \\ &= \frac{1}{2}g_{\vec{k}}^{\text{spin}}\sigma_z. \end{aligned} \tag{5.61}$$

The generalized definition of the spin-flip scattering in Eq. (5.35) secures that spin-flip processes act only on the spin channel (via $g_{\vec{k}}^{\text{spin}}$) while it causes no momentum dissipation and thus does not contribute to the resistance of the charge channel (via $g_{\vec{k}}^{\text{charge}}$). The role of spin-flip scattering will now be illustrated in more detail. But before we must discuss momentum scattering. Due to relation (5.48) the momentum relaxation time matrix in Eq. (5.44) reduces to

$$\hat{\tau}^{-1} = \frac{1}{2}\left[\tau_c^{-1}\mathbb{1} + \tau_s^{-1}\sigma_z\right]. \tag{5.62}$$

An evaluation of the anticommutator in Eq. (5.59) yields

$$\begin{aligned} \frac{1}{2}\{\hat{\tau}^{-1}, \hat{g}_{\vec{k}}^{\text{coll}}\} &= \frac{1}{8}\{\left[\tau_c^{-1}\mathbb{1} + \tau_s^{-1}\sigma_z\right], \left[g_{\vec{k}}^{\text{charge}}\mathbb{1} + g_{\vec{k}}^{\text{spin}}\sigma_z\right]\} \\ &= \frac{1}{4}\left[\left(\tau_c^{-1}g_{\vec{k}}^{\text{charge}} + \tau_s^{-1}g_{\vec{k}}^{\text{spin}}\right)\mathbb{1} + \left(\tau_c^{-1}g_{\vec{k}}^{\text{spin}} + \tau_s^{-1}g_{\vec{k}}^{\text{charge}}\right)\sigma_z\right]. \end{aligned} \tag{5.63}$$

Due to the spin structure of the Eqns. (5.60), (5.61) and (5.63) the kinetic equation can be decomposed into the charge channel $\propto \mathbb{1}$ and the spin channel $\propto \sigma_z$

$$\frac{1}{2}\left(\tau_c^{-1}g_{\vec{k}}^{\text{charge}} + \tau_s^{-1}g_{\vec{k}}^{\text{spin}}\right) = e\vec{v}_{\vec{k}}\vec{E}\partial_\epsilon f^{\text{charge}}(\epsilon, J_{\text{sd}}), \tag{5.64}$$

$$\frac{1}{2}\left(\tau_c^{-1}g_{\vec{k}}^{\text{spin}} + \tau_s^{-1}g_{\vec{k}}^{\text{charge}}\right) + \frac{1}{\tau_{\text{sf}}}g_{\vec{k}}^{\text{spin}} = e\vec{v}_{\vec{k}}\vec{E}\partial_\epsilon f^{\text{spin}}(\epsilon, J_{\text{sd}}). \tag{5.65}$$

The spin-flip term solely appears in the spin channel (5.65). As a dissipative process for the spin sector it limits the spin current while it does not directly affect the charge transport.
We now link the equilibrium spin distribution to the charge distribution

$$\partial_\epsilon f^{\text{spin}}(\epsilon, J_{\text{sd}}) \equiv P\partial_\epsilon f^{\text{charge}}(\epsilon, J_{\text{sd}}), \tag{5.66}$$

where the polarization P is a constant at the Fermi energy and given by

$$P \equiv \frac{\partial_\epsilon f^{\text{spin}}(\epsilon, J_{\text{sd}})}{\partial_\epsilon f^{\text{charge}}(\epsilon, J_{\text{sd}})} = \frac{\partial_\epsilon\left(f^{\uparrow}(\epsilon) - f^{\downarrow}(\epsilon)\right)}{\partial_\epsilon\left(f^{\uparrow}(\epsilon) + f^{\downarrow}(\epsilon)\right)} = \frac{\left(\frac{n^{\uparrow}}{m^{\uparrow}} - \frac{n^{\downarrow}}{m^{\downarrow}}\right)}{\left(\frac{n^{\uparrow}}{m^{\uparrow}} + \frac{n^{\downarrow}}{m^{\downarrow}}\right)}. \tag{5.67}$$

Equation (5.67) links the polarization P to the majority, minority densities (effective masses) n^s (m^s), where $s = \{1, -1\} = \{\uparrow, \downarrow\}$ denotes the majority, minority case. A proper definition of the polarization is a non-trivial task (cf. Ref. [69] and references therein). We only want to mention here that the definition (5.67) is appropriate in terms of transport as it links the distributions of majority and minority electrons, that are the important quantities in transport.
With the introduction of the polarization P in Eq. (5.66) the solution to Eqns. (5.64) and (5.65) reads

$$g_{\vec{k}}^{\text{charge}} = \frac{2e\tau_c\tau_s\left(2\tau_c\tau_s + (\tau_s - P\tau_c)\,\tau_{\text{sf}}\right)}{2\tau_c\tau_s^2 + \tau_{\text{sf}}\left(\tau_s^2 - \tau_c^2\right)}\vec{v}_{\vec{k}}\vec{E}\partial_\epsilon f^{\text{charge}}(\epsilon, J_{\text{sd}}), \tag{5.68}$$

$$g_{\vec{k}}^{\text{spin}} = -\frac{2e\tau_c\tau_s\tau_{\text{sf}}\left(\tau_c - P\tau_s\right)}{2\tau_c\tau_s^2 + \tau_{\text{sf}}\left(\tau_s^2 - \tau_c^2\right)}\vec{v}_{\vec{k}}\vec{E}\partial_\epsilon f^{\text{charge}}(\epsilon, J_{\text{sd}}). \tag{5.69}$$

The majority, minority distributions follow by inserting the definition of the relaxation times $\tau_c = \left(\frac{1}{\tau^\uparrow} + \frac{1}{\tau^\downarrow}\right)^{-1}$, $\tau_s = \left(\frac{1}{\tau^\uparrow} - \frac{1}{\tau^\downarrow}\right)^{-1}$ and after a decomposition of the charge and spin channel

$$g_{\vec{k}}^{\uparrow} = \frac{1}{2}(g_{\vec{k}}^{\text{charge}} + g_{\vec{k}}^{\text{spin}}) = e\frac{\tau^\uparrow\left[\tau^\downarrow + \tau_{\text{sf}}\left(1 + P\right)\right]}{\tau^\uparrow + \tau^\downarrow + 2\tau_{\text{sf}}}\vec{v}_{\vec{k}}\vec{E}\partial_\epsilon f^{\text{charge}}(\epsilon, J_{\text{sd}}), \tag{5.70}$$

$$g_{\vec{k}}^{\downarrow} = \frac{1}{2}(g_{\vec{k}}^{\text{charge}} - g_{\vec{k}}^{\text{spin}}) = e\frac{\tau^\downarrow\left[\tau^\uparrow + \tau_{\text{sf}}\left(1 - P\right)\right]}{\tau^\uparrow + \tau^\downarrow + 2\tau_{\text{sf}}}\vec{v}_{\vec{k}}\vec{E}\partial_\epsilon f^{\text{charge}}(\epsilon, J_{\text{sd}}). \tag{5.71}$$

We note that Eqns. (5.70) and (5.71) coincide with the result in Eq. (5.58) with the identification

$$2\partial_\epsilon f_{\text{eq}}^s(\epsilon) = (1 + sP)\partial_\epsilon f^{\text{charge}}(\epsilon, J_{\text{sd}}), \tag{5.72}$$

Accordingly, the generalized kinetic equation (5.45) reduces to the two-current model in collinear magnetization textures.
As a closing remark to this chapter, we would like to discuss the conduction coefficients in collinear textures. As we are dealing with single particle distributions the macroscopic current is computed by the momentum average of the charge distribution (cf. Eq. (5.4))

$$\begin{aligned}\vec{j}_{\text{charge}} &= -e\int\frac{d^3k}{(2\pi)^3}\vec{v}_{\vec{k}}g_{\vec{k}}^{\text{charge}} \\ &= \frac{e^2n\left[((1+P)\tau^\uparrow + (1-P)\tau^\downarrow)\tau_{\text{sf}} + 2\tau^\uparrow\tau^\downarrow\right]}{m(\tau^\uparrow + \tau^\downarrow + 2\tau_{\text{sf}})}\vec{E},\end{aligned} \tag{5.73}$$

and the spin current of the spin distribution (cf. Eq. (5.5))

$$\begin{aligned}\vec{j}_{\text{spin}} &= -\mu_{\text{B}}\int\frac{d^3k}{(2\pi)^3}\vec{v}_{\vec{k}}g_{\vec{k}}^{\text{spin}} \\ &= \frac{\mu_{\text{B}}}{e}\frac{e^2n\tau_{\text{sf}}\left[(1+P)\tau^\uparrow - (1-P)\tau^\downarrow\right]}{m(\tau^\uparrow + \tau^\downarrow + 2\tau_{\text{sf}})}\vec{E}.\end{aligned} \tag{5.74}$$

Equations (5.73) and (5.74) are the results that will now be discussed in several limiting cases of interest.
First we turn off spin-flip scattering ($\tau_{\text{sf}} \to \infty$) and obtain the well-known results for the two-current

model

$$\lim_{\tau_{\text{sf}}\to\infty}\vec{j}_{\text{charge}} = \frac{e^2 n}{2m}\left[(1+P)\tau^{\uparrow}+(1-P)\tau^{\downarrow}\right]\vec{E}$$
$$= e^2\left(\frac{n^{\uparrow}\tau^{\uparrow}}{m^{\uparrow}}+\frac{n^{\downarrow}\tau^{\downarrow}}{m^{\downarrow}}\right)\vec{E} \equiv \left(\sigma^{\uparrow}+\sigma^{\downarrow}\right)\vec{E}, \tag{5.75}$$

$$\lim_{\tau_{\text{sf}}\to\infty}\vec{j}_{\text{spin}} = \frac{\mu_{\text{B}}}{e}\frac{e^2 n}{2m}\left[(1+P)\tau^{\uparrow}-(1-P)\tau^{\downarrow}\right]\vec{E}$$
$$= \frac{\mu_{\text{B}}}{e}e^2\left(\frac{n^{\uparrow}\tau^{\uparrow}}{m^{\uparrow}}-\frac{n^{\downarrow}\tau^{\downarrow}}{m^{\downarrow}}\right)\vec{E} \equiv \frac{\mu_{\text{B}}}{e}\left(\sigma^{\uparrow}-\sigma^{\downarrow}\right)\vec{E}, \tag{5.76}$$

where we introduced the spin resolved conductivities $\sigma^{\uparrow}$, $\sigma^{\downarrow}$. In the second step we employ the identifications

$$(1+P)\frac{n}{m} = 2\frac{n^{\uparrow}}{m^{\uparrow}},$$
$$(1-P)\frac{n}{m} = 2\frac{n^{\downarrow}}{m^{\downarrow}}. \tag{5.77}$$

Next we consider the opposite limit of dominating spin-flip scattering ($\tau_{\text{sf}} \to 0$). In this limit the population of both channels is equal to 1/2 and thus the spin current tends to zero

$$\lim_{\tau_{\text{sf}}\to 0}\vec{j}_{\text{charge}} = \frac{2e^2 n}{m}\left[\frac{1}{\tau^{\uparrow}}+\frac{1}{\tau^{\downarrow}}\right]^{-1}\vec{E}, \tag{5.78}$$

$$\lim_{\tau_{\text{sf}}\to 0}\vec{j}_{\text{spin}} = 0. \tag{5.79}$$

As expected, strong spin-flip scattering limits the spin current while it does not affect the charge current. Furthermore, the result for the charge current in Eq. (5.75) does no longer depend on the spin polarization P of the current. In the limit of two equal channels ($\tau^{\uparrow} = \tau^{\downarrow} = \tau$) the charge conductivity reduces to the Drude formula $\sigma = \frac{e\tau n}{m}$.
At last we consider equal scattering rates for both spin channels ($\tau^{\uparrow} = \tau^{\downarrow} = \tau$)

$$\vec{j}_{\text{charge}} = \frac{e^2\tau n}{m}\vec{E} = e^2\tau\left[\frac{n^{\uparrow}}{m^{\uparrow}}+\frac{n^{\downarrow}}{m^{\downarrow}}\right]\vec{E}, \tag{5.80}$$

$$\vec{j}_{\text{spin}} = \frac{\mu_{\text{B}}}{e}\frac{Pe^2 n}{m}\left[\frac{1}{\tau}+\frac{1}{\tau_{\text{sf}}}\right]^{-1}\vec{E} = \frac{\mu_{\text{B}}}{e}e^2\left[\frac{1}{\tau}+\frac{1}{\tau_{\text{sf}}}\right]^{-1}\left[\frac{n^{\uparrow}}{m^{\uparrow}}-\frac{n^{\downarrow}}{m^{\downarrow}}\right]\vec{E}. \tag{5.81}$$

From Eqns. (5.80) and (5.81) we see that in symmetric channels the spin-flip does not affect the charge current while it serves as a source of extra resistance for the spin channel. As expected for equal relaxation times $\tau^{\uparrow} = \tau^{\downarrow}$ the polarization does not influence the charge current but has an impact on the spin current.

As a concluding remark we like to mention that the essence of collinear magnetotransport can be comprised within a two-channel equivalent circuit. This model has been extensively used to interpret the giant magnetoresistance and the tunneling magnetoresistance effect. [34, 169, 182]

5.3 Non-collinear magnetotransport

This section focuses on the general equilibrium solution to the kinetic equation in non-collinear magnetization textures. The general equilibrium solution permits the derivation of a general non-equilibrium linear response kinetic equation that will be solved in the subsequent sections for several different limiting cases.

5.3.1 Equilibrium solution for general non-collinear magnetization textures

In non-collinear magnetization textures the sd-Hamiltonian $\mathcal{H}_{sd} = J_{\text{sd}}\vec{\sigma}\vec{m}(\vec{r})$ is spatially dependent and does no longer commute with the complete Hamiltonian (5.15), $[\mathcal{H}, \mathcal{H}_{sd}] \neq 0$. Consequently, the electron-spin $\vec{\sigma}$ is no longer a constant of motion[3]. Spatial derivatives of the magnetization do not vanish ($\vec{\nabla}_{\vec{r}}(\vec{\sigma}\vec{m}(\vec{r})) \neq 0$) in the generalized kinetic equation (5.45) and two extra terms proportional to the gradient of the magnetization appear in the equilibrium kinetic equation (5.46)

$$\begin{aligned} &\vec{v}_{\vec{k}}\vec{\nabla}_{\vec{r}}\hat{f}_{\text{eq}}^{\text{non-coll}}(\vec{m}(\vec{r}),\epsilon) + i\frac{J_{\text{sd}}}{\hbar}[\vec{\sigma}\vec{m}(\vec{r}), \hat{f}_{\text{eq}}^{\text{non-coll}}(\vec{m}(\vec{r}),\epsilon)] \\ &\quad + \frac{J_{\text{sd}}}{2\hbar}\{\vec{\nabla}_{\vec{r}}(\vec{\sigma}\vec{m}(\vec{r})), \vec{\nabla}_{\vec{k}}\hat{f}_{\text{eq}}^{\text{non-coll}}(\vec{m}(\vec{r}),\epsilon)\} = 0. \end{aligned} \tag{5.82}$$

Equation (5.82) consists of four coupled partial differential equations to determine the equilibrium distribution $\hat{f}_{\text{eq}}^{\text{non-coll}}(\vec{m}(\vec{r}),\epsilon)$ in non-collinear magnetization textures. In general, its solution depends crucially on the imposed boundary conditions. The intention of this chapter is to derive a general analytical solution by employing some physical intuition about the solution. First, no transverse components should appear in an equilibrium solution. Transverse components result in a torque on the local magnetization and cause dynamics in the time-domain that should be absent in equilibrium. Accordingly, our first assumption is that the spin part of the equilibrium solution points parallel to the local magnetization. This secures that majority and minority channels are well defined with respect to a spatially varying quantization axis in non-collinear magnetization textures.
Assertion: The equilibrium distribution in non-collinear magnetization textures is given by

$$\hat{f}_{\text{eq}}^{\text{non-coll}}(\vec{m}(\vec{r}),\epsilon) = \frac{1}{2}\left[f^{\text{charge}}(\epsilon, J_{\text{sd}})\mathbb{1} + J_{\text{sd}}\partial_{J_{\text{sd}}}f^{\text{spin}}(\epsilon, J_{\text{sd}})(\vec{\sigma}\vec{m}(\vec{r}))\right]. \tag{5.83}$$

[3]This must be distinguished from the spatially homogeneous case, where the total angular momentum is still a good quantum number in contrast to the individual orbital and spin quantum numbers. [176]

Proof: For the three terms of Eq. (5.82) the insertion of solution (5.83) in Eq. (5.82) yields individually

$$\vec{v}_{\vec{k}}\vec{\nabla}_{\vec{r}}\hat{f}^{\text{non-coll}}_{\text{eq}}(\vec{m}(\vec{r}),\epsilon) = \frac{1}{2}J_{\text{sd}}\partial_{J_{\text{sd}}}f^{\text{spin}}(\epsilon,J_{\text{sd}})\vec{v}_{\vec{k}}\vec{\nabla}_{\vec{r}}(\vec{\sigma}\vec{m}(\vec{r})), \tag{5.84}$$

$$i\frac{J_{\text{sd}}}{\hbar}[\vec{\sigma}\vec{m}(\vec{r}),\hat{f}^{\text{non-coll}}_{\text{eq}}(\vec{m}(\vec{r}),\epsilon)] = 0, \tag{5.85}$$

$$\begin{aligned}
\frac{J_{\text{sd}}}{2\hbar}\{\vec{\nabla}_{\vec{r}}(\vec{\sigma}\vec{m}(\vec{r})),\vec{\nabla}_{\vec{k}}\hat{f}^{\text{non-coll}}_{\text{eq}}(\vec{m}(\vec{r}),\epsilon)\} &= \frac{J_{\text{sd}}}{4}\partial_\epsilon f^{\text{charge}}(\epsilon,J_{\text{sd}})\vec{v}_{\vec{k}}\vec{\nabla}_{\vec{r}}\{\mathbb{1},(\vec{\sigma}\vec{m}(\vec{r}))\} \\
&\quad - \frac{J_{\text{sd}}^2}{4}\partial_\epsilon\partial_{J_{\text{sd}}}f^{\text{spin}}(\epsilon,J_{\text{sd}})\left\{\vec{v}_{\vec{k}}\vec{\nabla}_{\vec{r}}(\vec{\sigma}\vec{m}(\vec{r})),(\vec{\sigma}\vec{m}(\vec{r}))\right\} \\
&= \frac{J_{\text{sd}}}{2}\partial_\epsilon f^{\text{charge}}(\epsilon,J_{\text{sd}})\vec{v}_{\vec{k}}\vec{\nabla}_{\vec{r}}(\vec{\sigma}\vec{m}(\vec{r})) \\
&\quad - \frac{J_{\text{sd}}^2}{4}\partial_\epsilon\partial_{J_{\text{sd}}}f^{\text{spin}}(\epsilon,J_{\text{sd}})\sum_{\mu,\nu}m^\nu(\vec{r})(\vec{v}_{\vec{k}}\vec{\nabla}_{\vec{r}})m^\mu(\vec{r})\{\sigma^\mu,\sigma^\nu\} \\
&= \frac{J_{\text{sd}}}{2}\partial_\epsilon f^{\text{charge}}(\epsilon,J_{\text{sd}})\vec{v}_{\vec{k}}\vec{\nabla}_{\vec{r}}(\vec{\sigma}\vec{m}(\vec{r})) - \frac{J_{\text{sd}}^2}{2}\partial_\epsilon\partial_{J_{\text{sd}}}f^{\text{spin}}(\epsilon,J_{\text{sd}})\vec{m}(\vec{r})(\vec{v}_{\vec{k}}\vec{\nabla}_{\vec{r}})\vec{m}(\vec{r}) \\
&= \frac{J_{\text{sd}}}{2}\partial_\epsilon f^{\text{charge}}(\epsilon,J_{\text{sd}})\vec{v}_{\vec{k}}\vec{\nabla}_{\vec{r}}(\vec{\sigma}\vec{m}(\vec{r})).
\end{aligned} \tag{5.86}$$

The equilibrium equation (5.82) is solved by Eq. (5.83) for all functions that fulfill the relation

$$\partial_\epsilon f^{\text{charge}}(\epsilon,J_{\text{sd}}) = -\partial_{J_{\text{sd}}}f^{\text{spin}}(\epsilon,J_{\text{sd}}). \tag{5.87}$$

To uniquely determine the general non-equilibrium solution (5.83), one more assumption is necessary. The charge distribution that describes the charge transport should be the same for a spatially homogeneous and a spatially inhomogeneous magnetization texture. More precisely, this has been implicitly assumed by choosing the charge part in the ansatz (5.83) spatially independent. In section 5.2 we deduced that the vanishing of the collision integral in equilibrium demands that the charge distribution function is the sum of the spin-up and spin-down Fermi-Dirac distributions. Thus we will identify the charge component in non-collinear magnetization textures with the collinear one

$$f^{\text{charge}}_{\text{non-coll}}(\epsilon,J_{\text{sd}}) \equiv f^{\text{charge}}_{\text{coll}}(\epsilon,J_{\text{sd}}) = f^{\uparrow}(\epsilon) + f^{\downarrow}(\epsilon), \tag{5.88}$$

where $f^{\uparrow}(\epsilon)$ and $f^{\downarrow}(\epsilon)$ are given in Eqns. (5.54), (5.55). Equations (5.83) and (5.88) determine the general non-collinear equilibrium distribution

$$\begin{aligned}
\hat{f}^{\text{non-coll}}_{\text{eq}}(\vec{m}(\vec{r}),\epsilon) = \frac{1}{2}\Big[&\left((e^{\beta(\epsilon+J_{\text{sd}}-\mu)}+1)^{-1}+(e^{\beta(\epsilon-J_{\text{sd}}-\mu)}+1)^{-1}\right)\mathbb{1} \\
&+\frac{J_{\text{sd}}\beta}{4}\left(\cosh^{-2}(\frac{\beta}{2}(\epsilon+J_{\text{sd}}-\mu))+\cosh^{-2}(\frac{\beta}{2}(\epsilon-J_{\text{sd}}-\mu))\right)(\vec{\sigma}\vec{m}(\vec{r}))\Big].
\end{aligned} \tag{5.89}$$

In summary, the equilibrium distribution function for non-collinear magnetization textures (5.89) is the general unambiguous solution that is derived under two additional assumptions: the spin part of the distribution function points in the direction of the local magnetization and the charge part is the same in the collinear and non-collinear case and therefore spatially independent.
We can express the matrix equilibrium distribution in Eq. (5.89) through global spin-up and spin-down distributions by employing the projector in the local reference frame of the magnetization

$$u^s(\vec{m}(\vec{r})) = \frac{\mathbb{1}+s\,(\vec{\sigma}\vec{m}(\vec{r}))}{2}, \tag{5.90}$$

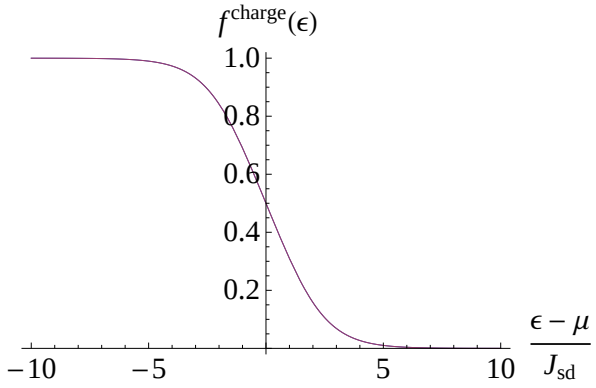

Figure 5.1: (Color online) The global charge equilibrium distribution for collinear and non-collinear magnetization textures for an inverse temperature $\beta^{-1} = J_{\text{sd}}$.

where $s = 1$ ($s = -1$) labels minority (majority) electrons. The spin up (spin down) expectation value is computed as

$$\begin{aligned}\langle f^s \rangle &= \text{Tr}\left[u^s(\vec{m}(\vec{r}))\hat{f}_{\text{eq}}^{\text{non-coll}}(\vec{m}(\vec{r}),\epsilon)\right] \\ &= \frac{1}{2}\left[f^{\text{charge}}(\epsilon, J_{\text{sd}}) + sJ_{\text{sd}}\partial_{J_{\text{sd}}} f^{\text{spin}}(\epsilon, J_{\text{sd}})\right]. \end{aligned} \tag{5.91}$$

The result in Eq. (5.91) reflects that the equilibrium splitting for spin up and down still holds in non-collinear magnetization textures. This provides an essential justification of the ansatz (5.83).
Despite of the different shapes of the global spin-distribution functions in the collinear and non-collinear case, their integrals that determine the macroscopic transport properties by the Eqns. (5.2) to (5.5) are equal.
Figure 5.1 depicts the equilibrium charge distribution $f^{\text{charge}}(\epsilon, J_{\text{sd}})$ that is equal for homogeneous and inhomogeneous magnetization textures. In equilibrium the magnetization pattern does not affect the distribution of charge carriers. Figure 5.2 depicts the spin distribution for homogeneous and inhomogeneous magnetization textures for a thermal energy $1/\beta$ equal to the sd-splitting energy J_{sd}. Temperatures above the sd-splitting only cause small deviations compared with the collinear case (cf. Fig. 5.2). Deviations occur if the temperature sinks below the exchange splitting J_{sd}. Figure 5.3 depicts the spin distribution for non-collinear magnetization patterns for five different inverse temperatures β. For higher temperatures (lower β) the distribution approaches the collinear shape of Fig. 5.2 (blue curve). For temperatures lower than the sd-exchange splitting energy J_{sd} deviations occur and alter the shape of the spin distribution substantially. This is a hint that the gradient expansion is implicitly a high temperature expansion and thus only valid for temperatures above the sd-splitting energy. This conjecture is supported by the shape of the equilibrium spin-distribution function (5.89). It is proportional to $J_{\text{sd}}/k_{\text{B}}T$ and thus resembles a first-order expansion term in the dimensionless parameter $J_{\text{sd}}/k_{\text{B}}T$. Such an expansion requires $J_{\text{sd}}/k_{\text{B}}T < 1$. During the derivation of the general kinetic equation (5.45), we expanded the quantum mechanically commutator of the density matrix and the Hamiltonian systematically in Poisson brackets. We truncate the expansion after the first Poisson bracket. This cut-off corresponds to the classical limit ($\hbar \to 0$) and neglects quantum corrections that

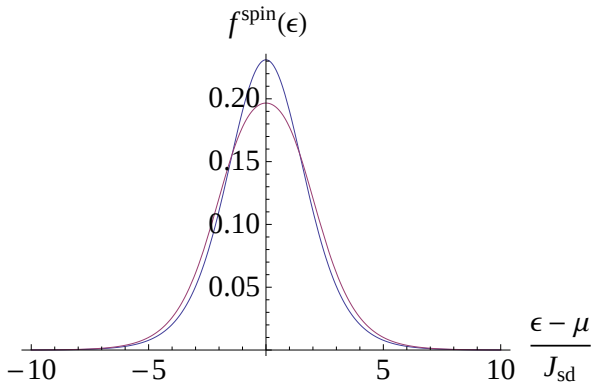

Figure 5.2: (Color online) The global equilibrium spin distribution for collinear (blue) and non-collinear (red) magnetization textures for an inverse temperature $\beta^{-1} = J_{\text{sd}}$.

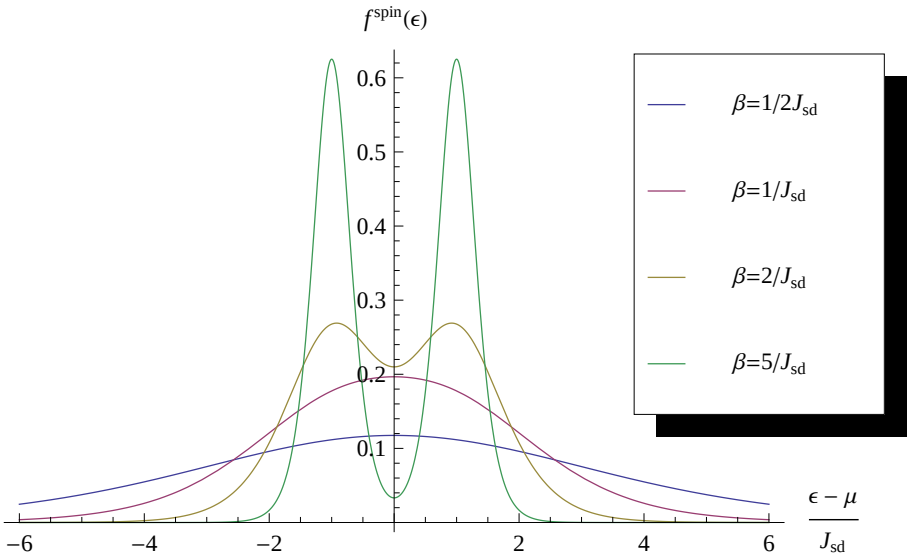

Figure 5.3: (Color online) Temperature dependence of the global equilibrium spin distribution function in non-collinear magnetization textures.

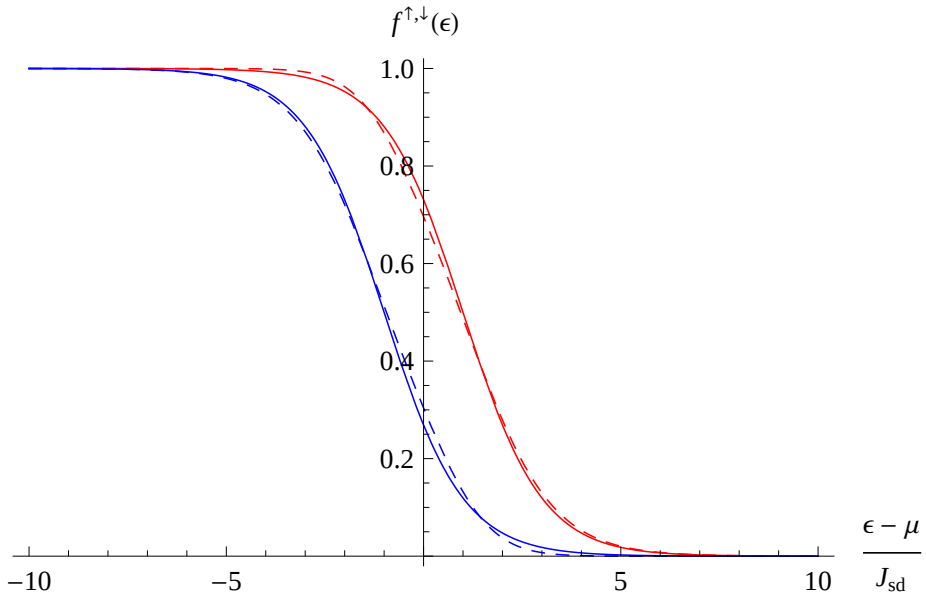

Figure 5.4: (Color online) The global spin-up (blue) and spin-down (red) equilibrium distributions for an inverse temperature $\beta^{-1} = J_{\text{sd}}$. The solid lines represent the collinear situation, while the dashed lines depict the distributions for non-collinear magnetization textures.

arise as higher-order Poisson brackets. Quantum effects become more important at low temperatures while they are negligible for higher temperatures. The expansion that leads to Eq. (5.45) as well as its equilibrium solution in Eq. (5.89) is therefore correct until the temperature approaches the sd-splitting. Figure 5.4 depicts the differences in spin-up and down distributions for homogeneous and inhomogeneous magnetization textures for an inverse temperature equal to the magnetization energy and supports the physical conjecture that the spin-up and spin-down splitting of the collinear situation also holds in the non-collinear case. Deviations appear at lower temperatures due to quantum effects. The equilibrium distribution for inhomogeneous magnetization patterns points locally in the direction of the magnetization. Thus, the second term in the equilibrium kinetic equation (5.82) is automatically zero. The spatial variation (first term of Eq. (5.82)) must be compensated by a change of the spin-distribution in energy space. The space-momentum coupling in the third term of Eq. (5.82) stems from the Wigner transform and is a pure quantum mechanical effect. Its origin is non-commutation of the position and momentum operators and as a result the Hamiltonian contrarily to the homogeneous case is not diagonalized by a local unitary rotation $U(\vec{m}(\vec{r}))$. In non-collinear magnetization textures the rotation no longer commutes with the kinetic energy $[U(\vec{m}(\vec{r})), \hat{p}_i \mathbb{1}] \neq 0, \quad i = x, y, z$. [63] The non-vanishing commutator induces a twist that translates in the semiclassical kinetic equation to a spin-position coupling term that in turn induces a change in the momentum distribution in the presence of a spatial varying magnetization. Consequently, a non-collinear magnetization texture exerts a driving force similar to the electric field on the distribution function.

The transition from a situation in a domain with its collinear background magnetization to a non-collinear magnetization is not continuous. A collinear and a non-collinear magnetization are distinct

cases with respect to spin transport due to the quantum mechanical nature of the conduction electron spin. This becomes manifest in different equilibrium conditions that result in different equilibrium solutions concerning the distributions of conduction electron spins. Though the equilibrium solution for non-collinear magnetization textures (5.82) do not coincide with the equilibrium solution for the collinear case in Eq. (5.53) it provides also a solution for the collinear case. The difference does not affect the calculation of transport properties and can be considered as a quantum mechanical effect that shows up at temperatures in the regime of J_{sd} in slightly different equilibrium spin distributions (cf. Fig. 5.2).

5.3.2 Identification of the polarization

A priori it is not clear how a proper definition of the polarization should look like in a ferromagnet (cf. Ref. [69] and references therein). A definition of the polarization in terms of the difference in the density of states of majority and minority electrons is indeed appropriate in equilibrium, but suffers from the fact that this tells us little about the relation to transport properties. Thus, we are in need of an identification of the polarization in terms of transport properties. However, the equilibrium solution of the generalized kinetic equation (5.89) allows for an identification of the polarization in terms of our model parameters. The polarization is no longer just a parameter to be determined from experiment but is directly related to quantities that are relevant for transport. In the spirit of the identification (5.66), we link the spin distribution to the charge distribution by means of

$$J_{\text{sd}}\partial_\epsilon f^{\text{spin}}(\epsilon, J_{\text{sd}}) = -J_{\text{sd}}\partial_\epsilon^2 f^{\text{charge}}(\epsilon, J_{\text{sd}}) \to P\partial_\epsilon f^{\text{charge}}(\epsilon, J_{\text{sd}}). \tag{5.92}$$

In contrast to collinear magnetotransport, where the polarization P has been introduced as a phenomenological parameter (cf. Eq. (5.66)), the equilibrium solution to the generalized kinetic equation allows for a direct calculation. Integration of Eq. (5.92) over momentum by $\int \frac{d^3k}{(2\pi)^3}$ yields the expression for the macroscopic polarization

$$\begin{aligned} P &= J_{\text{sd}}\frac{N(\epsilon_{\text{F}})}{n} \\ &= \frac{3}{2}\frac{J_{\text{sd}}}{\epsilon_{\text{F}}} \\ &\approx 3\,\frac{k_F^{\uparrow} - k_F^{\downarrow}}{k_F^{\uparrow} + k_F^{\downarrow}}, \end{aligned} \tag{5.93}$$

which is a proper ballistic definition of the spin polarization of the current with respect to transport. [16, 69, 172] We note that the identification in Eq. (5.93) is restricted to linear response and reflects what is expected for an exchange spin-split band for itinerant electrons. [184] Solely quantities at the Fermi surface that constitutes the only relevant energy scale in linear response theory are present. Moreover, the identification (5.93) holds strictly speaking only for a single parabolic band. As a macroscopic observable, an identification of the polarization is only reasonable on the macroscopic level (after the momentum integration) to remove any energy dependence in its definition. Note that the identification of the polarization (5.93) is valid in the semiclassical limit up to first order in $\hbar$. Quantum corrections that correspond to higher-order terms in the semiclassical expansion of the kinetic equation might eventually modify the result in Eq. (5.93).

The polarization in Eq. (5.93) is given by the ration of sd exchange splitting to the kinetic energy (Fermi energy) and thus provides a clear interpretation in the one-particle picture. [53] Moreover, it constitutes a proper definition with respect to the relevant transport quantities in magnetotransport in the sense as discussed above.
As a remark, we would like to mention that the same expression for the polarization (5.93) appears in Eq. (32) of Ref. [185] without a traceable derivation. Thus, in conclusion, our microscopic derivation allows for a calculation of the polarization of the current by relation (5.93), that has been introduced previously phenomenologically in the literature. [5, 185]

5.3.3 Linearized non-equilibrium kinetic equation for general non-collinear magnetization textures

In order to solve the kinetic equation and calculate conduction coefficients, we have to specify the collision integral. In the further derivations we consider weak ferromagnets ($J_{\text{sd}} \ll \epsilon_{\text{F}}$) and we disregard gradient corrections to the collision integral. This corresponds to a local collision integral by neglecting corrections of order $\mathcal{O}(J_{\text{sd}}/\epsilon_{\text{F}})$. Despite this restriction, the formalism should capture the essential physics for transition-metal ferromagnets. [53] The consideration of realistic band structures, spin-orbit coupling, and Coulomb interactions should provide more important corrections compared to gradient corrections to the collision integral as long as ($J_{\text{sd}} \ll \epsilon_{\text{F}}$). Gradient corrections cannot be neglected when the exchange energy is of the order of the Fermi energy. [82]
The collision integral in the relaxation time approximation (cf. section 5.1.3) reads

$$\begin{aligned}\hat{\mathcal{I}}[\hat{f}_{\vec{k}}(\vec{r})] &= \hat{\mathcal{I}}[\hat{f}_{\vec{k}}(\vec{r})] + \hat{\mathcal{I}}_{\text{sf}}[\hat{f}_{\vec{k}}(\vec{r})] \\ &= -\frac{1}{2}\{\hat{\tau}^{-1}(\vec{m}(\vec{r})), (\hat{f}_{\vec{k}}(\vec{r}) - \hat{f}_{\text{eq}}(\vec{m}(\vec{r}), \epsilon))\} - \frac{{}^{\text{sf}}\hat{f}_{\vec{k}}(\vec{r}) - {}^{\text{sf}}\hat{f}_{\text{eq}}(\vec{m}(\vec{r}), \epsilon)}{\tau_{\text{sf}}}. \end{aligned} \tag{5.94}$$

If an external electric field is applied, the electrons as well as the spins are in non-equilibrium and as a consequence a steady current flows. We want to determine the linear response solution to the distribution functions for the non-equilibrium case ($\vec{E} \neq 0$, $\hat{\mathcal{I}}[\hat{f}_{\vec{k}}(\vec{r})] \neq 0$) and consider small electric fields such that the system is still close to equilibrium where it is sufficient to focus on deviations that are linear in the electric field. A linearization of the general kinetic equation (5.45) for small electric fields is achieved by parameterizing the non-equilibrium distribution as a linear deviation from the equilibrium solution

$$\hat{f}_{\vec{k}}(\vec{r}) = \hat{f}_{\text{eq}}(\vec{m}(\vec{r}), \epsilon) + \hat{g}_{\vec{k}}(\vec{r}), \tag{5.95}$$

where $\hat{g}_{\vec{k}}(\vec{r})$ is the non-equilibrium shift proportional to the electric field and the relaxation times. Inserting the ansatz (5.95) into the kinetic equation (5.45) yields, by retaining only terms linear in the electric field,

$$\begin{aligned} &\vec{v}_{\vec{k}}\vec{\nabla}_{\vec{r}}\hat{f}_{\text{eq}}(\vec{m}(\vec{r}), \epsilon) + \vec{v}_{\vec{k}}\vec{\nabla}_{\vec{r}}\hat{g}_{\vec{k}}(\vec{r}) + i\frac{J_{\text{sd}}}{\hbar}[\vec{\sigma}\vec{m}(\vec{r}), \hat{f}_{\text{eq}}(\vec{m}(\vec{r}), \epsilon)] + i\frac{J_{\text{sd}}}{\hbar}[\vec{\sigma}\vec{m}(\vec{r}), \hat{g}_{\vec{k}}(\vec{r})] \\ &\quad -\frac{e}{\hbar}\vec{E}(\vec{r})\vec{\nabla}_{\vec{k}}\hat{f}_{\text{eq}}(\vec{m}(\vec{r}), \epsilon) + \mathcal{O}(\vec{E}\vec{\nabla}_{\vec{k}}\hat{g}_{\vec{k}}(\vec{r})) \\ &\quad +\frac{J_{\text{sd}}}{2\hbar}\{\vec{\nabla}_{\vec{r}}(\vec{\sigma}\vec{m}(\vec{r})), \vec{\nabla}_{\vec{k}}\hat{f}_{\text{eq}}(\vec{m}(\vec{r}), \epsilon)\} + \frac{J_{\text{sd}}}{2\hbar}\{\vec{\nabla}_{\vec{r}}(\vec{\sigma}\vec{m}(\vec{r})), \vec{\nabla}_{\vec{k}}\hat{g}_{\vec{k}}(\vec{r})\} \\ &= -\frac{1}{2}\{\hat{\tau}^{-1}(\vec{m}(\vec{r})), \hat{g}_{\vec{k}}(\vec{r})\} - \frac{{}^{\text{sf}}\hat{g}_{\vec{k}}(\vec{r})}{\tau_{\text{sf}}}. \end{aligned} \tag{5.96}$$

Insertion of the equilibrium solution (5.83) simplifies Eq. (5.96) with the help of Eq. (5.82)

$$\vec{v}_{\vec{k}}\vec{\nabla}_{\vec{r}}\hat{g}_{\vec{k}}(\vec{r}) + \frac{1}{2}\{\hat{\tau}^{-1}(\vec{m}(\vec{r})), \hat{g}_{\vec{k}}(\vec{r})\} + \frac{^{\text{sf}}\hat{g}_{\vec{k}}(\vec{r})}{\tau_{\text{sf}}} + i\frac{J_{\text{sd}}}{\hbar}[\vec{\sigma}\vec{m}(\vec{r}), \hat{g}_{\vec{k}}(\vec{r})]$$
$$+\frac{J_{\text{sd}}}{2\hbar}\{\vec{\nabla}_{\vec{r}}(\vec{\sigma}\vec{m}(\vec{r})), \vec{\nabla}_{\vec{k}}\hat{g}_{\vec{k}}(\vec{r})\} = e\vec{v}_{\vec{k}}\vec{E}(\vec{r})\partial_\epsilon\hat{f}_{\text{eq}}(\vec{m}(\vec{r}), \epsilon). \tag{5.97}$$

Equation (5.97) is the non-equilibrium kinetic equation valid for general magnetization textures. In the next sections we will solve Eq. (5.97) by imposing different limiting conditions on the magnetization texture $\vec{m}(\vec{r})$.

To proceed further on in the derivation, we have to specify the relaxation times of section 5.1.3 that appear in Eq. (5.97). For the spin-conserving relaxation time matrix we find

$$\begin{aligned}
&\frac{1}{2}\{\hat{\tau}^{-1}(\vec{m}(\vec{r})), \hat{g}_{\vec{k}}(\vec{r})\} \\
&= \frac{1}{2}\{\frac{1}{2}\left((\tau^0)^{-1}\mathbb{1} + (\vec{\tau})^{-1}(\vec{m}(\vec{r}))\vec{\sigma}\right), \frac{1}{2}\left(g_{\vec{k}}(\vec{r})\mathbb{1} + \vec{g}_{\vec{k}}(\vec{r})\vec{\sigma}\right)\} \\
&= \frac{1}{8}\Big[(\tau^0)^{-1}g_{\vec{k}}(\vec{r})\{\mathbb{1}, \mathbb{1}\} + (\tau^0)^{-1}\{\mathbb{1}, \vec{g}_{\vec{k}}(\vec{r})\vec{\sigma}\} \\
&\quad + g_{\vec{k}}(\vec{r})\{(\vec{\tau})^{-1}(\vec{m}(\vec{r}))\vec{\sigma}, \mathbb{1}\} + \{(\vec{\tau})^{-1}(\vec{m}(\vec{r}))\vec{\sigma}, \vec{g}_{\vec{k}}(\vec{r})\vec{\sigma}\}\Big] \\
&= \frac{1}{4}\left[(\tau^0)^{-1}g_{\vec{k}}(\vec{r})\mathbb{1} + (\tau^0)^{-1}\vec{g}_{\vec{k}}(\vec{r})\vec{\sigma} + (\vec{\tau})^{-1}(\vec{m}(\vec{r}))g_{\vec{k}}(\vec{r})\vec{\sigma} + (\vec{\tau})^{-1}(\vec{m}(\vec{r}))\vec{g}_{\vec{k}}(\vec{r})\mathbb{1}\right] \\
&= \frac{1}{4}\left[\left((\tau^0)^{-1}g_{\vec{k}}(\vec{r}) + (\vec{\tau})^{-1}(\vec{m}(\vec{r}))\vec{g}_{\vec{k}}(\vec{r})\right)\mathbb{1} + \left((\tau^0)^{-1}\vec{g}_{\vec{k}}(\vec{r}) + (\vec{\tau})^{-1}(\vec{m}(\vec{r}))g_{\vec{k}}(\vec{r})\right)\vec{\sigma}\right].
\end{aligned} \tag{5.98}$$

The spin-flip relaxation term (5.35) yields

$$^{\text{sf}}\hat{g}_{\vec{k}}(\vec{r}) = \frac{1}{2}\vec{g}_{\vec{k}}(\vec{r})\vec{\sigma}. \tag{5.99}$$

The commutator in the kinetic equation (5.97) evaluates as follows

$$\begin{aligned}
i\frac{J_{\text{sd}}}{\hbar}[\vec{\sigma}\vec{m}(\vec{r}), \hat{g}_{\vec{k}}(\vec{r})] &= i\frac{J_{\text{sd}}}{\hbar}\sum_{\mu,\nu} m^\mu(\vec{r})g^\nu_{\vec{k}}(\vec{r})[\sigma_\mu, \sigma_\nu] \\
&= i\frac{J_{\text{sd}}}{\hbar}2i\sum_{\mu,\nu,\rho}\epsilon_{\mu\nu\rho}m^\mu(\vec{r})g^\nu_{\vec{k}}(\vec{r})\sigma_\rho = -\gamma\vec{\sigma}\left(\vec{m}(\vec{r}) \times \vec{g}_{\vec{k}}(\vec{r})\right),
\end{aligned} \tag{5.100}$$

where we introduced the abbreviation $\gamma := 2J_{\text{sd}}/\hbar$.

The expressions for the relaxation times in Eqns. (5.98) and (5.99) allow for the decomposition of the linearized non-equilibrium kinetic equation (5.97) into the charge distribution and the three macroscopic magnetization distributions that govern the magnetization of the conduction electrons. The decomposition is achieved by employing relation (5.8) and results in two coupled kinetic equations with a scalar distribution function $g_{\vec{k}}(\vec{r})$ for the charge non-equilibrium distribution (Eq. (5.101)) and a vector distribution $\vec{g}_{\vec{k}}(\vec{r})$ for the non-equilibrium spin distribution (Eq. (5.102))

$$\begin{aligned}
&\vec{v}_{\vec{k}}\vec{\nabla}_{\vec{r}}g_{\vec{k}}(\vec{r}) + \tau_c^{-1}g_{\vec{k}}(\vec{r}) + (\vec{\tau})^{-1}(\vec{m}(\vec{r}))\vec{g}_{\vec{k}}(\vec{r}) \\
&\quad + \frac{J_{\text{sd}}}{\hbar}(\vec{\nabla}_{\vec{r}}\vec{m}(\vec{r})) \cdot (\vec{\nabla}_{\vec{k}}\vec{g}_{\vec{k}}(\vec{r})) = e\vec{v}_{\vec{k}}\vec{E}(\vec{r})\partial_\epsilon f^{\text{charge}}(\epsilon, J_{\text{sd}}),
\end{aligned} \tag{5.101}$$

$$\begin{aligned}
&\vec{v}_{\vec{k}}\vec{\nabla}_{\vec{r}}\vec{g}_{\vec{k}}(\vec{r}) - \gamma\left(\vec{m}(\vec{r}) \times \vec{g}_{\vec{k}}(\vec{r})\right) + \tau_+^{-1}\vec{g}_{\vec{k}}(\vec{r}) + (\vec{\tau})^{-1}(\vec{m}(\vec{r}))g_{\vec{k}}(\vec{r}) \\
&\quad + \frac{J_{\text{sd}}}{\hbar}(\vec{\nabla}_{\vec{r}}\vec{m}(\vec{r})) \cdot (\vec{\nabla}_{\vec{k}}g_{\vec{k}}(\vec{r})) = -J_{\text{sd}}e(\vec{v}_{\vec{k}}\vec{E}(\vec{r}))\vec{m}(\vec{r})\partial_\epsilon^2 f^{\text{charge}}(\epsilon, J_{\text{sd}}).
\end{aligned} \tag{5.102}$$

In Eq. (5.102) we introduced the abbreviation

$$\tau_+^{-1} \equiv \tau_c^{-1} + \tau_{\text{sf}}^{-1}. \tag{5.103}$$

In section 5.1.3 we gave explicit expressions for the spin-conserving relaxation times

$$\frac{1}{2}(\tau^0)^{-1} = \frac{1}{2}\left(\frac{1}{\tau^\uparrow} + \frac{1}{\tau^\downarrow}\right) \equiv \tau_c^{-1}, \tag{5.104}$$

$$\frac{1}{2}(\vec{\tau})^{-1}(\vec{m}(\vec{r})) = \frac{1}{2}\left(\frac{1}{\tau^\uparrow} - \frac{1}{\tau^\downarrow}\right)\vec{m}(\vec{r}) \equiv \tau_s^{-1}\vec{m}(\vec{r}). \tag{5.105}$$

Inserting Eqns. (5.104) and (5.105) into Eq. (5.101) and Eq. (5.102) yields

$$\begin{aligned} &\vec{v}_{\vec{k}}\vec{\nabla}_{\vec{r}} g_{\vec{k}}(\vec{r}) + \tau_c^{-1} g_{\vec{k}}(\vec{r}) + \tau_s^{-1}\vec{m}(\vec{r})\vec{g}_{\vec{k}}(\vec{r}) \\ &\quad + \frac{J_{\text{sd}}}{\hbar}(\vec{\nabla}_{\vec{r}}\vec{m}(\vec{r})) \cdot (\vec{\nabla}_{\vec{k}}\vec{g}_{\vec{k}}(\vec{r})) = e\vec{v}_{\vec{k}}\vec{E}(\vec{r})\partial_\epsilon f^{\text{charge}}(\epsilon, J_{\text{sd}}), \end{aligned} \tag{5.106}$$

$$\begin{aligned} &\vec{v}_{\vec{k}}\vec{\nabla}_{\vec{r}}\vec{g}_{\vec{k}}(\vec{r}) - \gamma\left(\vec{m}(\vec{r}) \times \vec{g}_{\vec{k}}(\vec{r})\right) + \tau_+^{-1}\vec{g}_{\vec{k}}(\vec{r}) + \tau_s^{-1}\vec{m}(\vec{r})g_{\vec{k}}(\vec{r}) \\ &\quad + \frac{J_{\text{sd}}}{\hbar}(\vec{\nabla}_{\vec{r}}\vec{m}(\vec{r})) \cdot (\vec{\nabla}_{\vec{k}} g_{\vec{k}}(\vec{r})) = -J_{\text{sd}} e(\vec{v}_{\vec{k}}\vec{E}(\vec{r}))\vec{m}(\vec{r})\partial_\epsilon^2 f^{\text{charge}}(\epsilon, J_{\text{sd}}). \end{aligned} \tag{5.107}$$

The two coupled equations (5.101) and (5.102) are the general equations for the non-equilibrium charge and spin distributions in the presence of an external electric field and our phenomenological parametrization of the collision integral in terms of relaxation times. The scope of the next sections is to focus on the solution of the kinetic equation in certain special limiting cases. More precisely, first we will derive local transport coefficients for general spatially slowly varying magnetization textures in section 5.4 (cf. appendix C for the inclusion of spin-orbit interaction). Secondly we solve an one-dimensional version of (5.97) for the case of a domain wall. This grants an insight into the regime of non-adiabatic spatial variations of the magnetization as will be discussed in section 5.5.

5.4 Adiabatic magnetotransport – constant transport coefficients

This section provides the linear response solution of the non-equilibrium kinetic equation for general, spatially slowly varying magnetization textures. A smooth magnetization texture that varies spatially slowly allows for a gradient expansion in the magnetization, such that second or higher spatial derivatives can be neglected, as they are small compared to the magnetization itself or its first derivatives. This condition characterizes the regime of *adiabatic* magnetotransport where the conduction electron spin can follow the local magnetization adiabatically. The transport coefficients turn out to be constant and the spatial dependence of the spin-transfer torque is entirely determined in terms of the local magnetization.

The characterization of the regime of *adiabatic* magnetotransport becomes most evident in the case of a domain wall. If the thickness of the domain wall λ is much larger than any characteristic length scale relevant for magnetotransport ($\lambda \gg k_{\mathrm{F}}^{-1}, v_{\mathrm{F}}\tau_{\mathrm{sd}}, v_{\mathrm{F}}\tau_c$), no spin mistracking occurs when the conduction electron propagates through the domain wall and the spins of the conduction electrons follow the local magnetization adiabatically. In this case the spin resides in either the majority or minority channel and domain walls exhibit an intrinsic Ohmic resistance that is negligible compared with the bulk resistance or magnetoresistive effects, for instance the anisotropic magnetoresistance. The situation changes in narrow domain walls where $\lambda \sim v_{\mathrm{F}}\tau_{\mathrm{sd}}, v_{\mathrm{F}}\tau_c \gg k_{\mathrm{F}}^{-1}$. Here, the conduction electron spin cannot follow the spatially abrupt changing magnetization and spin mistracking due to a mixing of spin channels occurs. The transition from the adiabatic transport regime to the transport regime of narrow domain walls introduces a spatial dependence of the spin-transfer torque on the details of the magnetization texture and involves an intrinsic domain-wall resistivity. Narrow domain walls and non-adiabatic transport are the subject of section 5.5.

In 2004 Zhang and Li derived two contributions of the spin-transfer torque for general, spatially slowly varying magnetization patterns based on a phenomenological diffusion equation, the adiabatic and the non-adiabatic spin-transfer torque. [5] While the adiabatic torque has been already suggested by other authors [47, 49, 51, 97], Zhang and Li were the first to propose the non-adiabatic torque. Since the proposal of the general mathematical form of the spin-transfer torque, numerous researchers attempted with various methods at deriving microscopic expressions for the spin-transfer torque. The aim of these efforts is to shed light on the microscopic origin of the spin-transfer torque. In this context, the degree of non-adiabaticity that parametrizes the strength of the non-adiabatic torque has attracted special interest. As noted exemplarily, Xiao, Zangwill and Stiles reported numerical derivations of the spin-transfer torque within an one-dimensional domain wall. [56] Their results cast doubt on the existence of the non-adiabatic torque at all and consequently they claim $\xi = 0$. [56] However, the magnitude as well as the microscopic origin of the non-adiabatic spin-transfer torque are under debate and its derivation is one of the most urgent issues in current-induced magnetization dynamics. Let us briefly mention the most prominent microscopic derivations that include the non-adiabatic spin-transfer torque. Tserkovnyak, Skadsem, Brataas and Bauer derived a kinetic equation within the local density approximation. [53] They phenomenologically introduced a transverse spin relaxation time as the origin of non-adiabaticity. Tatatara, Kohno et al. employed imaginary time-methods to calculate

the transport coefficients perturbatively. They performed a full quantum mechanical linear response calculation by means of the Kubo formula [54, 57, 58], the Mori formula [59] and a spin continuity equation [60]. Besides the known torques, they also derived a non-local non-adiabatic spin-transfer torque. [59] Duine et al. employed the functional Keldysh method and in contrast to all previous authors an itinerant model of ferromagnetism. [55] The functional Keldysh method enabled them to derive a stochastic version of the Landau-Lifshitz-Gilbert equation for finite temperatures. By adopting the same impurity model as Ref. [59], they obtained the same results for the transport coefficients and the degree of non-adiabaticity. Piéchon and Thiaville employed a kinetic equation similar to ours, but the results of their calculations suffered from an incorrect equilibrium solution. [186]

Section 5.4.1 provides the non-equilibrium solution of the kinetic equation for general, spatially slowly varying magnetization textures. In section 5.4.2 the transport coefficients are calculed from the distribution functions as obtained in the previous section. The main results of this section are summarized in section 5.4.4 before we close with a comparison of our result with the literature in section 5.4.5.

5.4.1 Non-equilibrium solution for adiabatic magnetotransport

In contrast to the equilibrium solution (cf. section 5.3.1) that is valid for general, non-collinear magnetization textures a closed solution to the non-equilibrium kinetic equations (5.101) and (5.102) is not possible. The solution of the coupled partial differential equations depend crucially on the imposed boundary conditions. Moreover, due to the non-trivial commutation relations for the spin non-equilibrium, transverse components of the spin distribution emerge in non-collinear magnetization textures that cannot be neglected in the presence of the electric field and collisions.
However, in the regime of adiabatic magnetotransport bulk solutions that are independent of the details of the magnetization texture are expected for the transport coefficients. In this sense the transport coefficients in adiabatic magnetotransport are material parameter as the factorization of the spatial and the momentum dependence holds for non-equilibrium. In adiabatic magnetotransport the spatial dependence of the distributions functions must entirely be given in terms of the magnetization

$$\hat{f}_{\vec{k}}(\vec{r}) = \hat{f}_{\vec{k}}(\vec{m}(\vec{r})). \tag{5.108}$$

In this case the macroscopic physical quantities are computed from the Eqns. (5.2), (5.3) and (5.4), (5.5) by virtue of the substitution $\hat{f}_{\vec{k}}(\vec{r}) \to \hat{f}_{\vec{k}}(\vec{m}(\vec{r}))$. The aim of this section is the calculation of transport coefficients from the coupled equations (5.106) and (5.107) up to first spatial derivatives of the magnetization. The gradient expansion in the magnetization restricts the validity of the results to spatially slowly varying magnetization textures, but removes the direct spatial dependence of the distribution functions according to (5.108) and enables a closed solution. With the perspective of obtaining constant conduction coefficients, we refrain from an actual computation of the distribution functions themselves, but instead focus on the derivation of the transport coefficients. This procedure fits very well to the adiabatic transport regime, where the details of the magnetization texture do not play a role with regard to the transport coefficients that turn out to be material parameters.

As discussed in section 5.3.2, we relate the spin part of $\hat{f}_{\text{eq}}(\vec{m}(\vec{r}),\epsilon)$ to the charge part by the introduction of the polarization (cf. Eq. (5.92))

$$J_{\text{sd}}\partial_{J_{\text{sd}}} f^{\text{spin}}(\epsilon, J_{\text{sd}}) \to P f^{\text{charge}}(\epsilon, J_{\text{sd}}). \tag{5.109}$$

The link to microscopic parameters is established by means of relation (5.93). With the introduction of the polarization in Eq. (5.109), the equations to solve for the non-equilibrium distributions $\hat{g}_{\vec{k}}(\vec{r}) = \hat{f}_{\vec{k}}(\vec{r}) - \hat{f}_{\text{eq}}(\vec{m}(\vec{r}),\epsilon)$ that is linear in the electric field $\vec{E}(\vec{r})$ now read

$$\begin{aligned}
&\vec{v}_{\vec{k}}\vec{\nabla}_{\vec{r}} g_{\vec{k}}(\vec{r}) + \tau_c^{-1} g_{\vec{k}}(\vec{r}) + \tau_s^{-1}\vec{m}(\vec{r})\vec{g}_{\vec{k}}(\vec{r}) \\
&\quad + \frac{J_{\text{sd}}}{\hbar}(\vec{\nabla}_{\vec{r}}\vec{m}(\vec{r}))\cdot(\vec{\nabla}_{\vec{k}}\vec{g}_{\vec{k}}(\vec{r})) = e\vec{v}_{\vec{k}}\vec{E}(\vec{r})\partial_\epsilon f^{\text{charge}}(\epsilon, J_{\text{sd}}), \qquad (5.110)\\
&\vec{v}_{\vec{k}}\vec{\nabla}_{\vec{r}}\vec{g}_{\vec{k}}(\vec{r}) - \gamma\left(\vec{m}(\vec{r})\times\vec{g}_{\vec{k}}(\vec{r})\right) + \tau_+^{-1}\vec{g}_{\vec{k}}(\vec{r}) + \tau_s^{-1}\vec{m}(\vec{r})g_{\vec{k}}(\vec{r}) \\
&\quad + \frac{J_{\text{sd}}}{\hbar}(\vec{\nabla}_{\vec{r}}\vec{m}(\vec{r}))\cdot(\vec{\nabla}_{\vec{k}} g_{\vec{k}}(\vec{r})) = Pe(\vec{v}_{\vec{k}}\vec{E}(\vec{r}))\vec{m}(\vec{r})\partial_\epsilon f^{\text{charge}}(\epsilon, J_{\text{sd}}). \qquad (5.111)
\end{aligned}$$

For further calculations it is convenient to expand the spin-dependent part of the distribution matrix in the local reference frame of the magnetization. We choose the following ansatz for the distribution functions in order to linearize Eqns. (5.110) and (5.111) with respect to the magnetization

$$g_{\vec{k}}(\vec{r}) = g(\vec{r},\vec{k}), \tag{5.112}$$

$$\vec{g}_{\vec{k}}(\vec{r}) = g_{\vec{m}}(\vec{k})\vec{m}(\vec{r}) + \sum_j g_\perp^{(1)}(\vec{k})(\vec{e}_j\vec{\nabla}_{\vec{r}})\vec{m}(\vec{r}) + \sum_j g_\perp^{(2)}(\vec{k})\vec{m}(\vec{r})\times(\vec{e}_j\vec{\nabla}_{\vec{r}})\vec{m}(\vec{r}), \tag{5.113}$$

where $\vec{e}_j$, $j = x, y, z$ are a complete set of unit vectors in real space that serve as tensorial indices. Note that the vectors $\vec{m}(\vec{r})$, $\sum_j(\vec{e}_j\vec{\nabla}_{\vec{r}})\vec{m}(\vec{r})$ and $\sum_j \vec{m}(\vec{r})\times(\vec{e}_j\vec{\nabla}_{\vec{r}})\vec{m}(\vec{r})$ are linearly independent from each other due to the relation (A.5). They form a basis of $\mathbb{R}^3$ that allows for the expansion of any vector. The ansatz (5.113) corresponds to a gradient expansion in the spatially varying reference frame of the magnetization, where we truncate the expansion after derivatives of first order. This expansion is valid as long as $\vec{\nabla}_{\vec{r}}\vec{m} \gg (\vec{\nabla}_{\vec{r}}\vec{m})^2$. Including higher derivatives of the magnetization in the expansion (5.113) would be redundant as the Ansatz (5.113) constitutes already a basis of $\mathbb{R}^3$. Higher derivative terms could be expanded in the basis (5.113). This would result in spatially dependent expansion coefficients, which transcend the adiabatic approximation.
For brevity we will omit the explicit reference to the spatial dependence of the magnetization and the electric field throughout the rest of this section.

5.4.1.1 Gradient expansion with respect to the magnetization

If we insert the ansatz (5.112) and (5.113) in the kinetic equation for the charge distribution (5.110), we end up in linear order of the magnetization gradient with

$$\begin{aligned}
&\vec{v}_{\vec{k}}\vec{\nabla}_{\vec{r}}g_{\vec{k}}(\vec{r}) + \tau_c^{-1}g_{\vec{k}}(\vec{r}) \\
&+\tau_s^{-1}\left(\vec{m}^2 g_{\vec{m}}(\vec{k}) + \sum_j g_\perp^{(1)}(\vec{k})\underbrace{\vec{m}\cdot(\vec{e}_j\vec{\nabla}_{\vec{r}})\vec{m}}_{=0} + \sum_j g_\perp^{(2)}(\vec{k})\underbrace{\vec{m}\cdot(\vec{m}\times(\vec{e}_j\vec{\nabla}_{\vec{r}})\vec{m})}_{=0}\right) \\
&+\frac{J_{\text{sd}}}{\hbar}\underbrace{\vec{m}\cdot(\vec{\nabla}_{\vec{k}}g_{\vec{m}}(\vec{k})\vec{\nabla}_{\vec{r}})\vec{m}}_{=0} + \mathcal{O}((\vec{\nabla}_{\vec{r}}\vec{m})^2) \\
&= e\vec{v}_{\vec{k}}\vec{E}(\vec{r})\partial_\epsilon f^{\text{charge}}(\epsilon, J_{\text{sd}}).
\end{aligned} \tag{5.114}$$

In Eq. (5.114) we employed the relation (A.5), as any spatial derivative of the magnetization is perpendicular to the magnetization itself. Next we perform the same procedure by inserting the ansatz (5.112) and (5.113) in the vectorial spin part of the kinetic equation (5.111). Up to first derivatives of the magnetization Eq. (5.111) then reads

$$\begin{aligned}
&\vec{v}_{\vec{k}}\vec{\nabla}_{\vec{r}}\vec{m}g_{\vec{m}}(\vec{k}) - \gamma g_{\vec{m}}(\vec{k})\underbrace{\vec{m}\times\vec{m}}_{=0} \\
&-\gamma\sum_j g_\perp^{(1)}(\vec{k})\vec{m}\times(\vec{e}_j\vec{\nabla}_{\vec{r}})\vec{m} - \gamma\vec{m}\times\sum_j g_\perp^{(2)}(\vec{k})\vec{m}\times(\vec{e}_j\vec{\nabla}_{\vec{r}})\vec{m} \\
&+\tau_+^{-1}\left[g_{\vec{m}}(\vec{k})\vec{m} + \sum_j g_\perp^{(1)}(\vec{k})(\vec{e}_j\vec{\nabla}_{\vec{r}})\vec{m} + \sum_j g_\perp^{(2)}(\vec{k})\vec{m}\times(\vec{e}_j\vec{\nabla}_{\vec{r}})\vec{m}\right] \\
&+\tau_s^{-1}\vec{m}g_{\vec{k}}(\vec{r}) + \frac{J_{\text{sd}}}{\hbar}\vec{\nabla}_{\vec{r}}\vec{m}\vec{\nabla}_{\vec{k}}g_{\vec{k}}(\vec{r}) + \mathcal{O}((\vec{\nabla}_{\vec{r}}\vec{m})^2) \\
&= Pe\vec{v}_{\vec{k}}\vec{E}\vec{m}\partial_\epsilon f^{\text{charge}}(\epsilon, J_{\text{sd}}).
\end{aligned} \tag{5.115}$$

A decomposition of Eq. (5.115) into the three linear independent unit vectors $\vec{m}$, $\sum_j(\vec{e}_j\vec{\nabla}_{\vec{r}})\vec{m}$ and $\sum_j \vec{m}\times(\vec{e}_j\vec{\nabla}_{\vec{r}})\vec{m}$ yields with Eq. (5.114) four determining equations for the non-equilibrium distributions $g_{\vec{k}}(\vec{r})$, $g_{\vec{m}}(\vec{k})$, $g_\perp^{(1)}(\vec{k})$ and $g_\perp^{(2)}(\vec{k})$. The determining equations are independent of the magnetization. This can be understood as follows: As we restrict ourselves to spatially slowly varying magnetization textures, we skip all terms that are of the order $\mathcal{O}(\vec{\nabla}_{\vec{r}}^2\vec{m})$. In this order of the expansion, the expansion coefficients $g_{\vec{m}}(\vec{k})$, $g_\perp^{(1)}(\vec{k})$ and $g_\perp^{(2)}(\vec{k})$ are spatially constant and thus cannot depend on the magnetization.

In the adiabatic regime in the presence of a spatially slowly varying magnetization texture the following set of coupled equations remains to be solved in order to calculate transport properties

$$\vec{v}_{\vec{k}}\vec{\nabla}_{\vec{r}}g_{\vec{k}}(\vec{r}) + \tau_c^{-1}g_{\vec{k}}(\vec{r}) + \tau_s^{-1}g_{\vec{m}}(\vec{k}) = e\vec{v}_{\vec{k}}\vec{E}\partial_\epsilon f^{\text{charge}}(\epsilon, J_{\text{sd}}), \tag{5.116}$$

$$\tau_+^{-1}g_{\vec{m}}(\vec{k}) + \tau_s^{-1}g_{\vec{k}}(\vec{r}) = Pe\vec{v}_{\vec{k}}\vec{E}\partial_\epsilon f^{\text{charge}}(\epsilon, J_{\text{sd}}), \tag{5.117}$$

$$\sum_i \delta_{ij}(\vec{e}_i\vec{v}_{\vec{k}})g_{\vec{m}}(\vec{k}) + \gamma g_\perp^{(2)}(\vec{k}) + \tau_+^{-1}g_\perp^{(1)}(\vec{k}) + \frac{J_{\text{sd}}}{\hbar}\sum_i \delta_{ij}(\vec{e}_i\vec{\nabla}_{\vec{k}})g_{\vec{k}}(\vec{r}) = 0, \tag{5.118}$$

$$-\gamma g_\perp^{(1)}(\vec{k}) + \tau_+^{-1}g_\perp^{(2)}(\vec{k}) = 0. \tag{5.119}$$

We are interested in bulk conduction properties in the presence of a homogeneous electric field $\vec{E} = const.$ and neglect the spatial dependence of the charge distribution $g_{\vec{k}}(\vec{r}) = g(\vec{k})$. In this case Eqns. (5.116) to (5.119) reduce to a set of four coupled algebraic equations. This presents a huge simplification in comparison to four coupled partial differential equations that we started with. According to Eq. (5.108), the choice of the product ansatz in Eqns. (5.112) and (5.113) shifts the spatial dependence from the distribution function onto the magnetization. This results in the homogeneous, spatially independent equations (5.116), (5.117), (5.118) and (5.119) for the expansion coefficients, the four distribution functions $g(\vec{k}), g_{\vec{m}}(\vec{k}), g_{\perp}^{(1)}(\vec{k}), g_{\perp}^{(2)}(\vec{k})$ and confirms our physical conjecture that led to the ansatz (5.108). In the adiabatic approximation, the distribution functions exhibit solely the necessary spatial dependence that arise from the expansion in the spatially varying reference frame of the magnetization.
Equations (5.116) and (5.117) determine the charge distribution and the part of the spin distribution that points collinear to the local magnetization. They coincide with the two-current model in collinear magnetization textures (cf. Eq. (5.68) and (5.69)). Equation (5.119) couples both transverse parts of the spin distribution. In turn, Eq. (5.118) establishes the connection between the transverse spin distributions and the charge and the collinear distributions.
A decoupling of Eq. (5.116) and (5.117) yields the non-equilibrium solution for the charge distribution and the longitudinal spin distribution that is collinear with the magnetization

$$g(\vec{k}) = \frac{e\tau_c\tau_s\left(P\tau_+ - \tau_s\right)}{\tau_c\tau_+ - \tau_s^2}\vec{v}_{\vec{k}}\vec{E}\partial_\epsilon f^{\text{charge}}(\epsilon, J_{\text{sd}}), \tag{5.120}$$

$$g_{\vec{m}}(\vec{k}) = -\frac{e\tau_+\tau_s\left(P\tau_s - \tau_c\right)}{\tau_c\tau_+ - \tau_s^2}\vec{v}_{\vec{k}}\vec{E}\partial_\epsilon f^{\text{charge}}(\epsilon, J_{\text{sd}}). \tag{5.121}$$

We note that the distributions in Eqns. (5.120) and (5.121) coincide with the charge and spin distributions of the two-current model (cf. Eqns. (5.68) and (5.69)). This perfectly agrees with the adiabatic approximation. A majority, minority spin resides in its spin state during the traversal of the spatially slowly varying magnetization texture. Except for the weak scattering at spin-flip impurities there is no mixing of channels and both kinds of spins can be treated separately.
To solve for the perpendicular spin distributions, we insert Eqns. (5.120) and (5.121) into Eq. (5.118) under consideration of Eq. (5.119). During the derivation we employed the relation

$$\begin{aligned}&\frac{1}{\hbar}\sum_i \delta_{ij}(\vec{e}_i\vec{\nabla}_{\vec{k}})\vec{v}_{\vec{k}}\vec{E}\partial_\epsilon f^{\text{charge}}(\epsilon, J_{\text{sd}})\\ &= \sum_i \delta_{ij}(\vec{e}_i M_{\vec{k}}^{-1}\vec{E})\partial_\epsilon f^{\text{charge}}(\epsilon, J_{\text{sd}}) + \sum_i \delta_{ij}(\vec{e}_i\vec{v}_{\vec{k}})\vec{v}_{\vec{k}}\vec{E}\partial_\epsilon^2 f^{\text{charge}}(\epsilon, J_{\text{sd}}),\end{aligned} \tag{5.122}$$

where the effective mass tensor $M_{\vec{k}}^{-1}$ is defined in Eq. (2.21). The result for the transverse spin distributions reads

$$\begin{aligned}g_\perp^{(1)}(\vec{k}) = &-\frac{e\tau_+\tau_s}{(1+\gamma^2\tau_+^2)(\tau_c\tau_+ - \tau_s^2)}\\ &\Big[\left(J_{\text{sd}}\sum_i \delta_{ij}(\vec{e}_i M_{\vec{k}}^{-1}\vec{E})\tau_c(P\tau_+ - \tau_s) - \sum_i \delta_{ij}(\vec{e}_i\vec{v}_{\vec{k}})\vec{v}_{\vec{k}}\vec{E}\tau_+(P\tau_s - \tau_c)\right)\partial_\epsilon f^{\text{charge}}(\epsilon, J_{\text{sd}})\\ &+ J_{\text{sd}}\sum_i \delta_{ij}(\vec{e}_i\vec{v}_{\vec{k}})\vec{v}_{\vec{k}}\vec{E}\tau_c(P\tau_+ - \tau_s)\partial_\epsilon^2 f^{\text{charge}}(\epsilon, J_{\text{sd}})\Big].\end{aligned} \tag{5.123}$$

$$
\begin{aligned}
g_{\perp}^{(2)}(\vec{k}) &= \gamma\tau_{+} g_{\perp}^{(1)}(\vec{k}) \\
&= -\frac{e\gamma\tau_{+}^{2}\tau_{s}}{(1+\gamma^{2}\tau_{+}^{2})(\tau_{c}\tau_{+}-\tau_{s}^{2})} \\
&\Big[\left(J_{\text{sd}}\sum_{i}\delta_{ij}(\vec{e}_{i}M_{\vec{k}}^{-1}\vec{E})\tau_{c}(P\tau_{+}-\tau_{s}) - \sum_{i}\delta_{ij}(\vec{e}_{i}\vec{v}_{\vec{k}})\vec{v}_{\vec{k}}\vec{E}\tau_{+}(P\tau_{s}-\tau_{c})\right)\partial_{\epsilon}f^{\text{charge}}(\epsilon, J_{\text{sd}}) \\
&\quad + J_{\text{sd}}\sum_{j}\delta_{ij}(\vec{e}_{i}\vec{v}_{\vec{k}})\vec{v}_{\vec{k}}\vec{E}\tau_{c}(P\tau_{+}-\tau_{s})\partial_{\epsilon}^{2}f^{\text{charge}}(\epsilon, J_{\text{sd}})\Big]. \qquad (5.124)
\end{aligned}
$$

We note from Eq. (5.124) the simple proportionality among the two transverse distribution functions $g_{\perp}^{(1)}(\vec{k})$ and $g_{\perp}^{(2)}(\vec{k})$. Though the factor of proportionality $\gamma\tau_{+}$ depends on the specific form of the collision integral, the proportionality itself is generic on the level of the distribution functions. As we will be shown in section 5.4.2.2, the factor of proportionality corresponds to the degree of non-adiabaticity. In this connection, the degree of non-adiabaticity does not depend on the band-structure and must be regarded as quite general because it constitutes a relation between distribution functions. The four distributions (5.120), (5.121), (5.123) and (5.124) can be rewritten in the form of a distribution matrix

$$
\begin{aligned}
\hat{g}_{\vec{k}}(\vec{r}) = \frac{1}{2}\Big[&g(\vec{k})\mathbb{1} + g_{\vec{m}}(\vec{k})(\vec{\sigma}\vec{m}(\vec{r})) \\
&+ \sum_{j} g_{\perp}^{(1)}(\vec{k})(\vec{e}_{j}\vec{\nabla}_{\vec{r}})(\vec{\sigma}\vec{m}(\vec{r})) + \sum_{j} g_{\perp}^{(2)}(\vec{k})\vec{\sigma}\cdot(\vec{m}(\vec{r})\times(\vec{e}_{j}\vec{\nabla}_{\vec{r}})\vec{m}(\vec{r}))\Big]. \qquad (5.125)
\end{aligned}
$$

Equation (5.125) constitutes the general non-equilibrium distribution matrix valid for small external electric field and spatially slowly varying magnetization patterns. If we project out the spin up (spin down) components of Eq. (5.125) with the help of the projector that is defined according to Eq. (5.90), we obtain

$$
\begin{aligned}
\langle g^{s}\rangle &= \text{Tr}\,\left[u^{s}(\vec{m}(\vec{r}))\hat{g}_{\vec{k}}(\vec{r})\right] \\
&= \frac{1}{4}\text{Tr}\,\Big[g(\vec{k})\mathbb{1} + g_{\vec{m}}(\vec{k})(\vec{\sigma}\vec{m}(\vec{r})) + \sum_{j} g_{\perp}^{(1)}(\vec{k})(\vec{e}_{j}\vec{\nabla}_{\vec{r}})(\vec{\sigma}\vec{m}(\vec{r})) \\
&\quad + \sum_{j} g_{\perp}^{(2)}(\vec{k})\vec{m}(\vec{r})\times(\vec{e}_{j}\vec{\nabla}_{\vec{r}})(\vec{\sigma}\vec{m}(\vec{r})) + sg(\vec{k})(\vec{\sigma}\vec{m}(\vec{r})) + sg_{\vec{m}}(\vec{k})\mathbb{1} \\
&\quad + s(\vec{\sigma}\vec{m}(\vec{r}))\cdot\sum_{j} g_{\perp}^{(1)}(\vec{k})(\vec{e}_{j}\vec{\nabla}_{\vec{r}})(\vec{\sigma}\vec{m}(\vec{r})) + s(\vec{\sigma}\vec{m}(\vec{r}))\cdot\sum_{j} g_{\perp}^{(2)}(\vec{k})\vec{m}(\vec{r})\times(\vec{e}_{j}\vec{\nabla}_{\vec{r}})(\vec{\sigma}\vec{m}(\vec{r}))\Big] \\
&= \frac{1}{2}\Big[g(\vec{k}) + sg_{\vec{m}}(\vec{k})\Big]. \qquad (5.126)
\end{aligned}
$$

During the calculation of Eq. (5.126), we employed relation (A.5) and the property of the Pauli matrices to be traceless. The message of Eq. (5.126) is that even in non-equilibrium a global separation in spin up, spin down channel holds for spatially slowly varying magnetization textures. This is expected from the adiabatic approximation, where the variation in the magnetization happens so slowly that the spin of the conduction electron can follow the local magnetization. In this case the spin resides in either the majority or minority channel that as a consequence must be well defined. Analogously to collinear magnetization textures the charge transport coefficients are entirely determined in terms

of the spin up and spin down distribution functions. Moreover, they are equal to the distributions in collinear magnetotransport. This reflects that adiabatic magnetotransport does not result in an intrinsic resistivity due to the magnetization texture. The global separation in spin up and spin down distribution functions justifies our choice in introducing the polarization as in Eq. (5.92).
In addition to collinear magnetization textures two extra transverse channels emerge. The off-diagonal components in the matrix notation (5.125), the transverse distribution functions $g_\perp^{(1)}(\vec{k})$, $g_\perp^{(2)}(\vec{k})$ are responsible for a *mixing conductance* that constitutes the transverse magnetization of the conduction electrons and the spin-transfer torque (cf. section 2.3).
Compared with collinear magnetotransport, the situation is the following: additionally to the familiar charge and longitudinal components, two components, transverse to the local magnetization, emerge in non-equilibrium. They are due to the twist of the two spin channels in the presence of a spatially varying magnetization. Together with the two channels already familiar from collinear magnetotransport this constitutes the framework of a *four channel model* that describes *adiabatic* non-collinear magnetotransport appropriately.

5.4.2 Global transport coefficients

In this section we derive the transport coefficients for the charge current, the spin current and the spin-transfer torque based on a simple parabolic band-structure from the distribution functions (5.120), (5.121), (5.123) and (5.124).

5.4.2.1 Charge conductivity

The knowledge of the distribution functions in Eqns. (5.120), (5.121), (5.123) and (5.124) enables us to calculate the bulk conduction coefficients in the presence of a spatially homogeneous external electric field. To calculate the ohmic conductivity we focus on the charge, non-equilibrium distribution function

$$g(\vec{k}) = \frac{e\tau_c\tau_s\left(P\tau_+ - \tau_s\right)}{\tau_c\tau_+ - \tau_s^2}\vec{v}_{\vec{k}}\vec{E}\partial_\epsilon f^{\text{charge}}(\epsilon, J_{\text{sd}}). \tag{5.127}$$

As the equilibrium part $f_{\text{eq}}(\epsilon)$ yields no current, the current is computed by tracing out the momentum of the non-equilibrium charge distribution

$$\begin{aligned}\vec{j} &= -e\int \frac{d^3k}{(2\pi)^3}\vec{v}_{\vec{k}}g(\vec{k}) \\ &= \frac{e^2\tau_c\tau_s\left(P\tau_+ - \tau_s\right)}{\tau_c\tau_+ - \tau_s^2}\Big[\int \frac{d^3k}{(2\pi)^3}\vec{v}_{\vec{k}}\otimes\vec{v}_{\vec{k}}(-\partial_\epsilon f^{\text{charge}}(\epsilon, J_{\text{sd}}))\Big]\vec{E}.\end{aligned} \tag{5.128}$$

The transition metals exhibit in general very involved band structures. [187] Nevertheless, transport in metals is dominated by the free-electron-like behavior that stems mostly from the sp bands. [34] Therefore, a free-electron model should provide at least an adequate qualitative description. Throughout this thesis we consider a free-electron picture for the calculation of transport properties. Furthermore, we will not consider asymmetries in the conduction quantities due to crystal anisotropies. Thus, the calculations are conducted for bulk materials without crystalline anisotropy, for instance crystals

of cubic symmetry. Then we can average over $\vec{k}$-space by exploiting the identity

$$\int \frac{d^3k}{(2\pi)^3} v^i_{\vec{k}} v^j_{\vec{k}} = \frac{\delta_{ij}}{3} \int \frac{d^3k}{(2\pi)^3} \vec{v}^2_{\vec{k}}. \tag{5.129}$$

As the $\vec{k}$ integration in Eq. (5.128) only depends on the energy, we can simplify the integration

$$\int \frac{d^3k}{(2\pi)^3} \rightarrow \int d\epsilon\, N(\epsilon), \tag{5.130}$$

by introducing the three-dimensional density of states

$$N(\epsilon) = \frac{m\sqrt{2m\epsilon}}{\pi^2\hbar^3}. \tag{5.131}$$

The integral for the current in Eq. (5.128) reads with the help of Eq. (5.130) and the fact that the energy derivative of the Fermi-Function can be approximated for low temperatures with respect to the Fermi energy by a delta function

$$\begin{aligned} \vec{j} &= \frac{e^2\tau_c\tau_s\left(P\tau_+ - \tau_s\right)}{\tau_c\tau_+ - \tau_s^2} \frac{1}{3} \int d\epsilon N(\epsilon) \vec{v}^2_{\vec{k}} \delta(\epsilon - \epsilon_{\mathrm{F}}) \vec{E} \\ &= \frac{e^2\tau_c\tau_s\left(P\tau_+ - \tau_s\right)}{\tau_c\tau_+ - \tau_s^2} \frac{1}{3} \vec{v}^{\,2}(\epsilon_{\mathrm{F}}) N(\epsilon_{\mathrm{F}}) \vec{E} \\ &= \frac{e^2 n\tau_c\tau_s\left(P\tau_+ - \tau_s\right)}{m\left(\tau_c\tau_+ - \tau_s^2\right)} \vec{E}. \end{aligned} \tag{5.132}$$

The density of the conduction electrons is defined as

$$n = \frac{1}{3} m\, \vec{v}^{\,2}(\epsilon_{\mathrm{F}}) N(\epsilon_{\mathrm{F}}). \tag{5.133}$$

For a homogeneous applied electric field, the current in Eq. (5.132) yields the Ohmic bulk conductivity

$$\sigma = \frac{e^2 n\tau_c\tau_s\left(P\tau_+ - \tau_s\right)}{m\left(\tau_c\tau_+ - \tau_s^2\right)}. \tag{5.134}$$

The corresponding ohmic resistivity is obtained by the inverse of the conductivity in Eq. (5.134)

$$\rho = \frac{1}{\sigma} = \frac{m\left(\tau_c\tau_+ - \tau_s^2\right)}{e^2 n\tau_c\tau_s\left(P\tau_+ - \tau_s\right)}. \tag{5.135}$$

Equation (5.135) reads expressed in terms of τ_c, τ_s and τ_{sf}

$$\rho = \frac{m\left[\tau_c\tau_s^2 + (\tau_s^2 - \tau_c^2)\tau_{\mathrm{sf}}\right]}{e^2 n\tau_c\tau_s\left[\tau_c(\tau_s - P\tau_{\mathrm{sf}}) + \tau_s\tau_{\mathrm{sf}}\right]}, \tag{5.136}$$

or equivalently by the spin up and spin down relaxation times $\tau^\uparrow$, $\tau^\downarrow$

$$\rho = \frac{m\left(\tau^\uparrow + \tau^\downarrow + 2\tau_{\mathrm{sf}}\right)}{e^2 n\left[((1+P)\tau^\uparrow + (1-P)\tau^\downarrow)\tau_{\mathrm{sf}} + 2\tau^\uparrow\tau^\downarrow\right]}. \tag{5.137}$$

Equation (5.137) coincides with the result of the two-current model (cf. Eq. (5.73)). Thus, all limiting cases for the charge conductivity discussed in section 5.2 are still valid in spatially slowly varying magnetization patterns. In the case of vanishing spin-flip scattering the resistivity reduces to

$$\lim_{\tau_{\text{sf}}\to\infty}\rho = \frac{m\left(\tau_c^2-\tau_s^2\right)}{e^2 n\tau_c\tau_s\left(P\tau_c-\tau_s\right)} = \frac{2m}{e^2 n\left[(1+P)\tau^{\uparrow}+(1-P)\tau^{\downarrow}\right]}. \tag{5.138}$$

With the obvious identifications

$$\begin{aligned}(1+P)\frac{n}{m} &= 2\frac{n^{\uparrow}}{m^{\uparrow}},\\ (1-P)\frac{n}{m} &= 2\frac{n^{\downarrow}}{m^{\downarrow}},\end{aligned} \tag{5.139}$$

the result in the absence of spin-flip scattering Eq. (5.138) coincides with the two-channel model, i.e., resistance of the two spin channels running in parallel

$$\lim_{\tau_{\text{sf}}\to\infty}\rho = \left[e^2\left(\frac{n^{\uparrow}\tau^{\uparrow}}{m^{\uparrow}}+\frac{n^{\downarrow}\tau^{\downarrow}}{m^{\downarrow}}\right)\right]^{-1}. \tag{5.140}$$

5.4.2.2 Conduction coefficients for the spin-transfer torque

As introduced in section 2.3, we adopt the current-induced torque picture. [95] The spin-transfer torque is then given by the counteraction of the magnetization of the conduction electrons on the local magnetization. The transfer of spin-angular momentum of the spin-polarized s electrons to the localized d electrons is accomplished via the sd exchange interaction. The torque is a geometric effect that stems from the directional mismatch between the magnetization of the conduction electrons and the local magnetic moments

$$\begin{aligned}\vec{\tau}_{\text{STT}}(\vec{r}) &= -\langle\frac{\delta\mathcal{H}_{\text{sd}}}{\hbar\delta\vec{m}(\vec{r})}\rangle\times\vec{m}(\vec{r})\\ &= -\frac{J_{\text{sd}}}{\hbar}\langle\hat{\vec{\sigma}}(\vec{r})\rangle\times\vec{m}(\vec{r})\\ &= -\frac{1}{\tau_{\text{sd}}}\langle\hat{\vec{\sigma}}(\vec{r})\rangle_{\text{neq}}\times\vec{m}(\vec{r}).\end{aligned} \tag{5.141}$$

In Eq. (5.141), $\vec{m}(\vec{r})$ represents the magnetization of the localized d electrons and $\langle\hat{\vec{\sigma}}(\vec{r})\rangle$ comprises the magnetization of the itinerant s electrons. In Eq. (5.141) we introduced the characteristic time that belongs to the sd exchange interaction

$$\tau_{\text{sd}} \equiv \frac{2}{\gamma} = \frac{\hbar}{J_{\text{sd}}}. \tag{5.142}$$

τ_{sd} is the inverse frequency with which the conduction spins precess around the local magnetization. According to its definition in Eq. (5.141), the calculation of the spin-transfer torque reduces to the task of determining the magnetization of the conduction electrons $\langle\hat{\vec{\sigma}}(\vec{r})\rangle$. The magnetization of the itinerant s electrons splits into two parts

$$\langle\hat{\vec{\sigma}}(\vec{r})\rangle = \langle\hat{\vec{\sigma}}(\vec{r})\rangle_{\text{eq}} + \langle\hat{\vec{\sigma}}(\vec{r})\rangle_{\text{neq}}. \tag{5.143}$$

The first part in Eq. (5.143) stems from the equilibrium distribution and points antiparallel to the local magnetization of the d electrons

$$\langle\hat{\vec{\sigma}}(\vec{r})\rangle_{\text{eq}} = -\mu_{\text{B}}\int\frac{d^3k}{(2\pi)^3}\text{Tr}\,\hat{f}_{\text{eq}}(\vec{m}(\vec{r}),\epsilon)\vec{\sigma} = -P\mu_{\text{B}}n\vec{m}(\vec{r}). \tag{5.144}$$

The second part $\langle\hat{\vec{\sigma}}(\vec{r})\rangle_{\text{neq}}$ is induced by the electric field. The longitudinal component of the non-equilibrium magnetization $g_{\vec{m}}(\vec{k})$ is odd in the velocity (cf. Eq. (5.121)) and consequently vanishes due to the momentum integration[4]

$$\langle\hat{\vec{\sigma}}_{\vec{m}}(\vec{r})\rangle_{\text{neq}} = -\mu_{\text{B}}\int\frac{d^3k}{(2\pi)^3}g_{\vec{m}}(\vec{k})\vec{m}(\vec{r}) = 0. \tag{5.145}$$

Accordingly, the non-equilibrium magnetization of the conduction electrons points perpendicular to the local magnetization. Furthermore, it is obvious from the definition of the spin-transfer torque in Eq. (5.141) that only the transverse part of the magnetization of the conduction electrons contributes to the spin-transfer torque. This is the reason why we substituted $\langle\hat{\vec{\sigma}}(\vec{r})\rangle$ with $\langle\hat{\vec{\sigma}}(\vec{r})\rangle_{\text{neq}}$ in Eq. (5.141). The non-equilibrium parts are according to Eq. (5.145) transverse to the local moments and stem from $g_{\perp}^{(1)}(\vec{k})$ and $g_{\perp}^{(2)}(\vec{k})$. They serve for the computation of the transverse magnetization of the conduction electrons in the following. These are the contributions that act as a counteraction on the local magnetization of the localized d electrons and causes the spin-transfer torque.

Adiabatic spin-transfer torque In this section we derive the transport coefficients responsible for the adiabatic spin-transfer torque in terms of microscopic relaxation times. The terms that constitute the adiabatic spin-transfer torque stem from the non-equilibrium function $g_{\perp}^{(2)}(\vec{k})$. The local magnetization of the conduction electrons is obtained by tracing out the momentum part of the spin distribution

$$\frac{1}{\tau_{\text{sd}}}\langle\hat{\vec{\sigma}}_{\text{ad}}(\vec{r})\rangle_{\text{neq}} = -\frac{\mu_{\text{B}}}{\tau_{\text{sd}}}\int\frac{d^3k}{(2\pi)^3}\sum_j g_{\perp}^{(2)}(\vec{k})\vec{m}(\vec{r})\times(\vec{e}_j\vec{\nabla}_{\vec{r}})\vec{m}(\vec{r}). \tag{5.146}$$

Computation of Eq. (5.146) yields the adiabatic spin-transfer torque according to Eq. (5.141). The adiabatic distribution function $g_{\perp}^{(2)}(\vec{k})$ is given by Eq. (5.124)

$$\begin{aligned}
g_{\perp}^{(2)}(\vec{k}) = &-\frac{e\gamma\tau_+^2\tau_s}{(1+\gamma^2\tau_+^2)(\tau_c\tau_+-\tau_s^2)}\\
&\Big[\left(J_{\text{sd}}\sum_i\delta_{ij}(\vec{e}_iM_{\vec{k}}^{-1}\vec{E})\tau_c(P\tau_+-\tau_s)+\sum_i\delta_{ij}(\vec{e}_i\vec{v}_{\vec{k}})\vec{v}_{\vec{k}}\vec{E}\tau_+(\tau_c-P\tau_s)\right)\partial_\epsilon f^{\text{charge}}(\epsilon,J_{\text{sd}})\\
&\quad+J_{\text{sd}}\sum_j\delta_{ij}(\vec{e}_i\vec{v}_{\vec{k}})\vec{v}_{\vec{k}}\vec{E}\tau_c(P\tau_+-\tau_s)\partial_\epsilon^2 f^{\text{charge}}(\epsilon,J_{\text{sd}})\Big]\\
\equiv\ &c_1\sum_i\delta_{ij}(\vec{e}_iM_{\vec{k}}^{-1}\vec{E})\partial_\epsilon f^{\text{charge}}(\epsilon,J_{\text{sd}})+c_2\sum_i\delta_{ij}(\vec{e}_i\vec{v}_{\vec{k}})\vec{v}_{\vec{k}}\vec{E}\partial_\epsilon f^{\text{charge}}(\epsilon,J_{\text{sd}})\\
&+c_1\sum_i\delta_{ij}(\vec{e}_i\vec{v}_{\vec{k}})\vec{v}_{\vec{k}}\vec{E}\partial_\epsilon^2 f^{\text{charge}}(\epsilon,J_{\text{sd}}).
\end{aligned} \tag{5.147}$$

[4] In contrast, the non-equilibrium component collinear to the local magnetization $g_{\vec{m}}(\vec{k})$ gives rise to a non-vanishing *spin-current tensor* whose modulus coincides with the spin current in the two-current model (cf. section 5.4.2.3).

Inserting the distribution function of Eq. (5.147) into Eq. (5.146) requires to carry out three different integrations. As explained in the previous section, we restrict ourselves in the further calculations to the case of crystal cubic symmetry (cf. Eq. (5.129)) and one parabolic band. In this case the effective mass tensor reduces to a constant effective mass $M_{\vec{k}}$.
Evaluation of the first term in Eq. (5.147) yields

$$\begin{aligned} & c_1 \int \frac{d^3k}{(2\pi)^3} \sum_i \delta_{ij} (\vec{e}_i M_{\vec{k}}^{-1} \vec{E}) \partial_\epsilon f^{\text{charge}}(\epsilon, J_{\text{sd}}) = -\frac{c_1}{m} \sum_i \delta_{ij} (\vec{e}_i \vec{E}) \int \frac{d^3k}{(2\pi)^3} (-\partial_\epsilon f^{\text{charge}}(\epsilon, J_{\text{sd}})) \\ &= -\frac{c_1}{m} \sum_i \delta_{ij} (\vec{e}_i \vec{E}) \int d\epsilon N(\epsilon) \delta(\epsilon - \epsilon_{\text{F}}) \\ &= -\frac{c_1 N(\epsilon_{\text{F}})}{m} \sum_i \delta_{ij} (\vec{e}_i \vec{E}). \end{aligned} \tag{5.148}$$

The second term in Eq. (5.147) is evaluated under consideration of the relation (5.129)

$$\begin{aligned} & c_2 \int \frac{d^3k}{(2\pi)^3} \sum_i \delta_{ij} (\vec{e}_i \vec{v}_{\vec{k}}) \vec{v}_{\vec{k}} \vec{E} \partial_\epsilon f^{\text{charge}}(\epsilon, J_{\text{sd}}) = -\frac{c_2}{3} \sum_j (\vec{e}_j \vec{E}) \int \frac{d^3k}{(2\pi)^3} \vec{v}_{\vec{k}}^2 (-\partial_\epsilon f^{\text{charge}}(\epsilon, J_{\text{sd}})) \\ &= -\frac{c_2}{3} \sum_i \delta_{ij} (\vec{e}_i \vec{E}) \vec{v}^2(\epsilon_{\text{F}}) N(\epsilon_{\text{F}}) \\ &= -\frac{c_2 n}{m} \sum_i \delta_{ij} (\vec{e}_i \vec{E}). \end{aligned} \tag{5.149}$$

We now rewrite the third term in Eq. (5.147) after applying the identity in Eq. (5.122) and a partial integration, where the constant terms vanish due to the periodicity of the integrated functions on the Bravais lattice [76]

$$\begin{aligned} & c_1 \int \frac{d^3k}{(2\pi)^3} \sum_i \delta_{ij} (\vec{e}_i \vec{v}_{\vec{k}}) \vec{v}_{\vec{k}} \vec{E} \partial_\epsilon^2 f^{\text{charge}}(\epsilon, J_{\text{sd}}) = c_1 \sum_{\mu,\nu} \sum_i \delta_{ij} e_i^\mu E^\nu \int \frac{d^3k}{(2\pi)^3} v_{\vec{k}}^\mu v_{\vec{k}}^\nu \partial_\epsilon^2 f^{\text{charge}}(\epsilon, J_{\text{sd}}) \\ &= \frac{c_1}{\hbar} \sum_{\mu,\nu} \sum_i \delta_{ij} e_i^\mu E^\nu \int \frac{d^3k}{(2\pi)^3} v_{\vec{k}}^\mu \nabla_{\vec{k}}^\nu \partial_\epsilon f^{\text{charge}}(\epsilon, J_{\text{sd}}) \\ &= \frac{c_1}{\hbar} \sum_{\mu,\nu} \sum_i \delta_{ij} e_i^\mu E^\nu \int \frac{d^3k}{(2\pi)^3} \Big(\nabla_{\vec{k}}^\nu v_{\vec{k}}^\mu \Big) \Big(-\partial_\epsilon f^{\text{charge}}(\epsilon, J_{\text{sd}}) \Big) \\ &= \frac{c_1}{m} \sum_i \delta_{ij} (\vec{e}_i \vec{E}) \int \frac{d^3k}{(2\pi)^3} \delta(\epsilon - \epsilon_{\text{F}}) \\ &= \frac{c_1 N(\epsilon_{\text{F}})}{m} \sum_i \delta_{ij} (\vec{e}_i \vec{E}). \end{aligned} \tag{5.150}$$

Note that the cancellation of the contributions in Eqns. (5.148) and (5.150) is a peculiarity of the simple parabolic one-band model that does not hold for realistic band structures.

The result for the local magnetization of the itinerant electrons is given by the sum of the Eqns. (5.148), (5.149) and (5.150)

$$\frac{1}{\tau_{\text{sd}}} \langle \hat{\vec{\sigma}}_{\text{ad}}(\vec{r}) \rangle_{\text{neq}} = -\frac{\mu_{\text{B}}}{e} \vec{m}(\vec{r}) \times (\vec{j}_{\text{spin}}^{\text{trans}} \vec{\nabla}_{\vec{r}}) \vec{m}(\vec{r}), \tag{5.151}$$

with the definition of the transverse spin current

$$\vec{j}_{\text{spin}}^{\text{trans}} = \sigma_{\text{spin}}^{\text{trans}} \vec{E}. \tag{5.152}$$

The transverse spin conductivity reads

$$\sigma_{\text{spin}}^{\text{trans}} = \frac{1}{\tau_{\text{sd}}} \frac{e^2 n \gamma \tau_+^3 \tau_s \left(\tau_c - P\tau_s\right)}{m(1+\gamma^2\tau_+^2)(\tau_c\tau_+ - \tau_s^2)}. \tag{5.153}$$

Expressing the transverse spin conductivity in terms of the spin up and spin down relaxation times and the sd exchange time defined in Eq. (5.142) yields the final result

$$\sigma_{\text{spin}}^{\text{trans}} = \frac{8e^2 n (\tau^\uparrow)^2 (\tau^\downarrow)^2 \tau_{\text{sf}}^3 \left[(1+P)\tau^\uparrow - (1-P)\tau^\downarrow\right]}{m(\tau^\uparrow + \tau^\downarrow + 2\tau_{\text{sf}}) \left(\tau_{\text{sd}}^2 \tau_{\text{sf}} \tau^\uparrow (\tau_{\text{sf}}\tau^\uparrow + 2\tau^\downarrow(\tau_{\text{sf}} + 2\tau^\uparrow)) + \tau_{\text{sd}}^2 (\tau^\downarrow)^2 (\tau_{\text{sf}} + 2\tau^\uparrow)^2 + 16(\tau^\uparrow)^2(\tau^\downarrow)^2\tau_{\text{sf}}^2\right)}. \tag{5.154}$$

In contrast to the charge conductivity in Eq. (5.134), the transverse spin conductivity in Eq. (5.154) additionally depends on the sd-exchange time τ_{sd}. We note that the transverse spin conductivity possesses the right limit when turning off the sd-interaction. The transverse spin conductivity and thus the spin-transfer torque vanish with vanishing sd exchange splitting ($J_{\text{sd}} \to 0$)

$$\lim_{\tau_{\text{sd}} \to \infty} \sigma_{\text{spin}}^{\text{trans}} = 0. \tag{5.155}$$

By contrast, in the case of dominating sd-splitting $J_{\text{sd}} \to \infty$, the transverse spin conductivity reduces to 1/2 of the spin-conductivity in the two channel-model (cf. Eq. (5.74))

$$\lim_{\tau_{\text{sd}} \to 0} \sigma_{\text{spin}}^{\text{trans}} = \frac{e^2 n \tau_{\text{sf}} \left[(1+P)\tau^\uparrow - (1-P)\tau^\downarrow\right]}{2m(\tau^\downarrow + \tau^\uparrow + 2\tau_{\text{sf}})}. \tag{5.156}$$

In the absence of spin flip scattering the transverse spin conductivity reduces to

$$\begin{aligned}
\lim_{\tau_{\text{sf}} \to \infty} \sigma_{\text{spin}}^{\text{trans}} &= \frac{4e^2 n (\tau^\uparrow)^2 (\tau^\downarrow)^2 \left[(1+P)\tau^\uparrow - (1-P)\tau^\downarrow\right]}{m\left[\tau_{\text{sd}}^2 (\tau^\uparrow + \tau^\downarrow)^2 + (4\tau^\uparrow\tau^\downarrow)^2\right]} \\
&= \frac{8(\tau^\uparrow)^2(\tau^\downarrow)^2}{\left[\tau_{\text{sd}}^2(\tau^\uparrow + \tau^\downarrow)^2 + (4\tau^\uparrow\tau^\downarrow)^2\right]} e^2 \left[\frac{n^\uparrow \tau^\uparrow}{m^\uparrow} - \frac{n^\downarrow \tau^\downarrow}{m^\downarrow}\right] \\
&= \frac{1}{4} \frac{1}{1 + \left(\frac{\tau_{\text{sd}}(\frac{1}{\tau^\uparrow} + \frac{1}{\tau^\downarrow})}{4}\right)^2} \frac{e^2 n}{m} \left[(1+P)\tau^\uparrow - (1-P)\tau^\downarrow\right] \\
&= \frac{1}{2} f(\xi|_{\text{sf}=0}) \frac{e^2 n}{2m} \left[(1+P)\tau^\uparrow - (1-P)\tau^\downarrow\right].
\end{aligned} \tag{5.157}$$

Apart from a prefactor Eq. (5.157) coincides with the spin current of the two-current model (cf. Eq. (5.74)). The prefactor exhibits a standard Cauchy distribution $f(\xi|_{\text{sf}=0}) = 1/1 + (\xi|_{\text{sf}=0})^2$, a Lorentz distribution with width 1, for the parameter $\xi|_{\text{sf}=0} \equiv \tau_{\text{sd}}(\tau^\uparrow + \tau^\downarrow)/4\tau^\uparrow\tau^\downarrow$ that coincides with the degree of non-adiabaticity (cf. Eq. (5.163)) in the absence of spin-flip scattering. The prefactor resembles the degree of coherence between the majority and minority spin channel. Figure 5.5

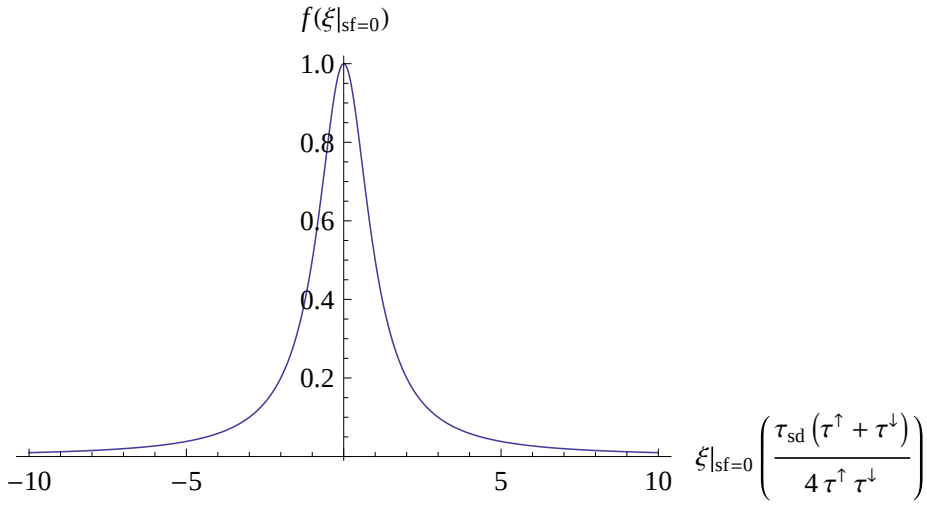

Figure 5.5: (Color online) Spin coherence factor for the transverse spin conductivity in the absence of spin-flip scattering.

depicts the resonant behavior of the coherence factor for the transverse spin conductivity in the absence of spin-flip scattering. The resonance curve reaches its maximum for dominating sd-interaction ($\tau_{\text{sd}} \to 0$) that corresponds to small values of non-adiabaticity ($\xi|_{\text{sf}=0} \to 0$) and reduces in this limit to $1/2$ of the spin current of the two-current model (cf. Eq. (5.74)). In contrast, for higher values of non-adiabaticity ($\xi|_{\text{sf}=0} \to \infty$) the transverse spin conductivity monotonously decreases. In this case the enhanced non-adiabaticity suppresses the efficient transfer of spin-angular momentum and an enhanced spin relaxation reduces the spin-transfer torque.
While the charge transport is entirely diffusive, different values of $\xi|_{\text{sf}=0}$ distinguish different transport regimes for the spin transport. The regime of small values for $f(\xi|_{\text{sf}=0})$ is the regime where the spin transport is diffusive with $\tau_{\text{sd}}/\tau_c > 1$ that corresponds to $\xi|_{\text{sf}=0} > 1/2$. In this case the spin transport is dominated by scattering at (magnetic) impurities. Due to the twist of spin channels, the collisions destroy the coherence in the spin sector and as a result decrease the efficiency in the transfer of spin-angular momentum (cf. Fig. 5.5). The contrary case with $\tau_{\text{sd}}/\tau_c < 1$ or $\xi|_{\text{sf}=0} < 1/2$ constitutes the regime of ballistic spin transport, where the spin has enough time between two collisions to precess around the local magnetization. In this case the deterministic flow part of the kinetic equation (5.45) is predominant for the spin transport and the coherence in the spin sector enhances the spin-transfer torque. In general, the spin coherence factor takes into account that ballistic spin transport enhances the spin-transfer torque while diffusive spin transport results in a decrease of the spin-transfer efficiency. For a more detailed discussion of the contribution of spin mistracking to non-adiabaticity we refer to section 5.5, where we explicitly solve the kinetic equation in the case of a domain wall.

Dominating spin-flip scattering suppresses the transverse spin conductivity

$$\lim_{\tau_{\text{sf}} \to 0} \sigma_{\text{spin}}^{\text{trans}} = 0, \tag{5.158}$$

and thus no spin-transfer torque arises. This is reasonable as in this case the conduction electron spin relaxes instantaneously such that no transfer of angular momentum to the localized d electrons is possible and no spin-transfer torque takes place. The adiabatic spin-transfer torque follows by inserting the result (5.151) into Eq. (5.141)

$$\vec{\tau}_{\text{ad}}(\vec{r}) = -\frac{\mu_{\text{B}}}{eM_s^3}\vec{M}(\vec{r}) \times \vec{M}(\vec{r}) \times (\vec{j}_{\text{spin}}^{\text{trans}}\vec{\nabla}_{\vec{r}})\vec{M}(\vec{r}). \tag{5.159}$$

Non-adiabatic spin-transfer torque In this section we derive the conduction coefficient responsible for the non-adiabatic spin-transfer torque. The terms that contribute to the non-adiabatic spin-transfer torque stem from the non-equilibrium function $g_{\perp}^{(1)}(\vec{k})$. The local magnetization of the conduction electrons evaluates to

$$\frac{1}{\tau_{\text{sd}}}\langle\hat{\vec{\sigma}}_{\text{non-ad}}(\vec{r})\rangle_{\text{neq}} = -\frac{\mu_{\text{B}}}{\tau_{\text{sd}}}\int\frac{d^3k}{(2\pi)^3}\sum_j g_{\perp}^{(1)}(\vec{k})(\vec{e}_j\vec{\nabla}_{\vec{r}})\vec{m}(\vec{r}), \tag{5.160}$$

and serves for computing the spin-transfer torque according to Eq. (5.141). The non-adiabatic distribution function $g_{\perp}^{(1)}(\vec{k})$ is linked to the adiabatic distribution by means of (cf. Eq. (5.123))

$$g_{\perp}^{(1)}(\vec{k}) = \frac{g_{\perp}^{(2)}(\vec{k})}{\gamma\tau_+}, \tag{5.161}$$

and thus the magnetization of the conduction electrons is calculated analogously to the preceding section

$$\frac{1}{\tau_{\text{sd}}}\langle\hat{\vec{\sigma}}_{\text{non-ad}}(\vec{r})\rangle_{\text{neq}} = -\frac{\mu_{\text{B}}\xi}{e}(\vec{j}_{\text{spin}}^{\text{trans}}\vec{\nabla}_{\vec{r}})\vec{m}(\vec{r}), \tag{5.162}$$

where the transverse spin current is defined in Eq. (5.152). The ratio between the non-adiabatic and adiabatic spin-transfer torque determines the parameter ξ of non-adiabaticity

$$\begin{aligned}\xi &= \frac{1}{\gamma\tau_+} = \frac{\hbar}{2J_{\text{sd}}\tau_+} = \frac{\tau_{\text{sd}}}{2\tau_+} \\ &= \frac{\tau_{\text{sd}}}{4}\left(\frac{1}{\tau^{\uparrow}} + \frac{1}{\tau^{\downarrow}} + \frac{2}{\tau_{\text{sf}}}\right).\end{aligned} \tag{5.163}$$

The expression for the degree of non-adiabaticity in Eq. (5.163) is reminiscent of *Matthiessen's Rule* except that the degree of non-adiabaticity ξ is not an ohmic resistance but a measure for spin relaxation. [76, 117, 188] The additivity of single relaxation times that appear in our model reflects the statistical independence of the individual sources of scattering that contribute to the degree of non-adiabaticity. All sources of spin-dependent scattering contribute in an equal manner. The strength of the degree of non-adiabaticity solely depends on the relaxation times and thus on the collisions. It is not affected by the band structure.

For equal up and down relaxation times $\tau^{\uparrow} = \tau^{\downarrow}$, ξ reduces to

$$\xi = \frac{\tau_{\text{sd}}}{2}\left(\frac{1}{\tau} + \frac{1}{\tau_{\text{sf}}}\right). \tag{5.164}$$

For metallic films, usually the relation $\tau_{\text{sf}} \gg \tau^{\uparrow}, \tau^{\downarrow}$ holds and one can neglect the spin-flip contribution to the degree of non-adiabaticity ξ.

The local non-adiabatic torque is obtained by inserting the result (5.162) in Eq. (5.141)

$$\vec{\tau}_{\text{non-ad}}(\vec{r}) = -\frac{\mu_{\text{B}}\xi}{eM_s^2}\vec{M}(\vec{r}) \times (\vec{j}_{\text{spin}}^{\text{trans}}\vec{\nabla}_{\vec{r}})\vec{M}(\vec{r}). \tag{5.165}$$

5.4.2.3 Conduction coefficient for the spin-current tensor

The definition of the spin-current tensor is given in Eq. (5.5). Solely terms that are even in the velocity $\vec{v}_{\vec{k}}$ survive the momentum integration. As a consequence the equilibrium part of the spin current vanishes

$$\hat{J}_{\text{eq}}(\vec{r}) = 0, \tag{5.166}$$

and the spin current is entirely determined by the collinear non-equilibrium component $g_{\vec{m}}(\vec{k})$

$$\begin{aligned}
\hat{J}_{\text{neq}}(\vec{r}) &= -\mu_{\text{B}} \int \frac{d^3k}{(2\pi)^3} \vec{v}_{\vec{k}} \otimes g_{\vec{m}}(\vec{k}) \vec{m}(\vec{r}) \\
&= -\mu_{\text{B}} \int \frac{d^3k}{(2\pi)^3} \vec{v}_{\vec{k}} \otimes \left(-\frac{e\tau_+\tau_s \left(P\tau_s - \tau_c\right)}{\tau_c\tau_+ - \tau_s^2} \partial_\epsilon f^{\text{charge}}(\epsilon, J_{\text{sd}}) \right) (\vec{v}_{\vec{k}} \vec{E}) \vec{m}(\vec{r}) \\
&= \left(-\frac{e\mu_{\text{B}}\tau_+\tau_s \left(P\tau_s - \tau_c\right)}{\tau_c\tau_+ - \tau_s^2} \right) \vec{E} \otimes \vec{m}(\vec{r}) \\
&= \frac{\mu_{\text{B}}}{e} \vec{j}_{\text{spin}} \otimes \vec{m}(\vec{r}).
\end{aligned} \tag{5.167}$$

The spin current is given by

$$\vec{j}_{\text{spin}} = \sigma_{\text{spin}} \vec{E}, \tag{5.168}$$

with the definition of the spin current conductivity

$$\begin{aligned}
\sigma_{\text{spin}} &= -\frac{e^2\tau_+\tau_s \left(P\tau_s - \tau_c\right)}{\tau_c\tau_+ - \tau_s^2} \\
&= \frac{e^2 n \tau_{\text{sf}} \left[(1+P)\tau^{\uparrow} - (1-P)\tau^{\downarrow}\right]}{m(\tau^{\uparrow} + \tau^{\downarrow} + 2\tau_{\text{sf}})}.
\end{aligned} \tag{5.169}$$

In contrast to collinear magnetotransport, the spin current is no longer a vector but a tensor with a direction of flow and a direction of polarization. However, in spatially slowly varying magnetization textures the spin current from collinear magnetotransport coincides with the component parallel to the local magnetization in the spin-current tensor (cf. Eq. (5.74)). All limiting cases for the spin current in the two-current model are thus valid for the spin-current tensor in spatially slowly varying non-collinear magnetization textures.

The spin-current tensor in Eq. (5.167) flows in real space in the direction of the electric field and points in magnetization space in the direction of the local magnetization. This is expected from the adiabatic approximation. [56, 96, 97] Due to the pairwise cancellation between forward and backward moving spins, transverse components are absent in the spin-current tensor. As the cancellation is exact within each band, this result should not be affected by realistic band structures and intraband scattering that we do not consider within this thesis. [56] Our result for the spin-current tensor in Eq. (5.167) thus confirms the conjecture that in the adiabatic approximation the polarization of the spin-current tensor points along the local magnetization. [5, 52] This is an essential justification, as this feature has been introduced by hand in the phenomenological diffusion equation of Ref. [5] that serves as a key ingredient for the computation of the non-adiabatic spin-transfer torque. [65]

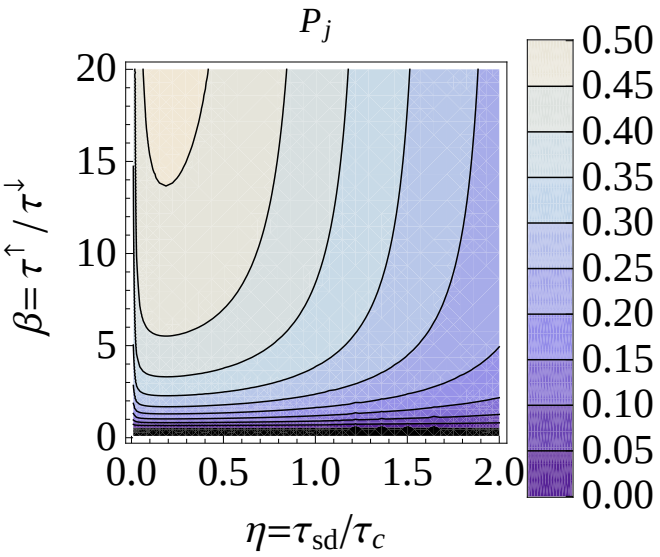

Figure 5.6: (Color online) Diffusive spin polarization of the electric current concerning the spin-transfer torque in dependence of transport regime $\eta = \tau_{\text{sd}}/\tau_c$ and anisotropy of scattering $\beta = \tau^{\uparrow}/\tau^{\downarrow}$ for $\tau_{\text{sf}} = 1 \cdot 10^{-12}$ s and $\tau_{\text{sd}} = 4.136 \cdot 10^{-15}$ s.

5.4.3 Spin polarization of the current

The microscopic expressions for the charge conductivity in Eq. (5.134) and the spin conductivity that determines the transverse spin current in Eq. (5.153) allows the determination of the diffusive spin polarization for the spin-transfer torque according to

$$P_j := \frac{\sigma_{\text{spin}}^{\text{trans}}}{\sigma_{\text{charge}}} \neq \frac{\sigma_{\text{spin}}}{\sigma_{\text{charge}}} = \frac{\sigma^{\uparrow} - \sigma^{\downarrow}}{\sigma^{\uparrow} + \sigma^{\downarrow}} =: P_j^{\text{coll}}. \tag{5.170}$$

The diffusive spin polarization in Eq. (5.170) constitutes the appropriate factor to convert the charge current into the transverse spin current that is responsible for the spin-transfer torque (cf. Eq. (2.10) and (2.15)). We note that the diffusive spin polarization in Eq. (5.170), which serves to convert the charge current into the transverse spin current in the phenomenological theory of Ref. [5], do not coincide with the common definition of the longitudinal spin polarization of the two-current model $P_j^{\text{coll}} = (\sigma^{\uparrow} - \sigma^{\downarrow})/(\sigma^{\uparrow} + \sigma^{\downarrow})$ valid for collinear magnetotransport in monodomain ferromagnets (cf. section 5.2). It is the transverse spin current ($\propto \sigma_{\text{spin}}^{\text{trans}}$) that constitutes the spin-transfer torque in non-collinear magnetization textures and not the longitudinal one ($\propto \sigma_{\text{spin}} = \left(\sigma^{\uparrow} - \sigma^{\downarrow}\right)$) as given by Eq. (5.169). We note that for spatially slowly varying magnetization textures the longitudinal spin polarization $P_j^{\text{coll}} \equiv P_j^{\text{long}}$ coincides with the collinear spin polarization.
Figure 5.6 depicts the diffusive spin polarization in dependence on the parameters $\eta = \tau_{\text{sd}}/\tau_c$ that characterizes the transport regime and the anisotropy of scattering $\beta = \tau^{\uparrow}/\tau^{\downarrow}$. The diffusive spin polarization of the current increases by increasing the anisotropy in the relaxation times β and by decreasing the transport regime η. $\eta \to 0$ corresponds to an enhanced sd splitting $J_{\text{sd}} \to \infty$ and

enhances the polarization of the electric current as it concerns the transverse spin current. The dependence of the diffusive spin polarization on the sd splitting J_{sd} is a new feature that is absent in collinear magnetotransport. At this point we just note that $\eta < 1$ corresponds to ballistic spin transport, while $\eta > 1$ characterizes diffusive spin transport (cf. section 5.5.5.2 for a detailed discussion of this point). Experimental values of β read for Py (=$Ni_{80}Fe_{20}$): $\beta_{\text{Py}} \approx 7.67$. [189] The parameters employed in Fig. 5.6 are chosen such that the spin polarization agrees with recent experimental data $P_j \sim 0.4$ for Py. [190]

5.4.4 Summary

The main result of this section is the consistent derivation of the spin-transfer torque from a microscopic theory that starts with the Hamiltonian as expressed by Eq. (5.15). Our derivation confirms that the non-adiabatic spin-transfer torque is a generic feature in non-collinear magnetotransport. The full spin-transfer torque in spatially slowly varying magnetization textures is the sum of the adiabatic and the non-adiabatic spin-transfer torque and given by

$$\begin{aligned}\vec{\tau}_{\text{STT}} &= \vec{\tau}_{\text{ad}} + \vec{\tau}_{\text{non-ad}} \\ &= -\frac{\mu_{\text{B}}}{eM_s^3}\vec{M}(\vec{r}) \times \vec{M}(\vec{r}) \times (\vec{j}_{\text{spin}}^{\text{trans}}\vec{\nabla}_{\vec{r}})\vec{M}(\vec{r}) - \frac{\mu_{\text{B}}\xi}{eM_s^2}\vec{M}(\vec{r}) \times (\vec{j}_{\text{spin}}^{\text{trans}}\vec{\nabla}_{\vec{r}})\vec{M}(\vec{r}).\end{aligned} \tag{5.171}$$

Their constituting transport coefficient is the transverse spin conductivity that determines the transverse spin current via the relation $\vec{j}_{\text{spin}}^{\text{trans}} = \sigma_{\text{spin}}^{\text{trans}}\vec{E}$

$$\sigma_{\text{spin}}^{\text{trans}} = \frac{8e^2 n(\tau^\uparrow)^2(\tau^\downarrow)^2\tau_{\text{sf}}^3\left[(1+P)\tau^\uparrow - (1-P)\tau^\downarrow\right]}{m(\tau^\uparrow+\tau^\downarrow+2\tau_{\text{sf}})\left(\tau_{\text{sd}}^2\tau_{\text{sf}}\tau^\uparrow(\tau_{\text{sf}}\tau^\uparrow + 2\tau^\downarrow(\tau_{\text{sf}}+2\tau^\uparrow)) + \tau_{\text{sd}}^2(\tau^\downarrow)^2(\tau_{\text{sf}}+2\tau^\uparrow)^2 + 16(\tau^\uparrow)^2(\tau^\downarrow)^2\tau_{\text{sf}}^2\right)}. \tag{5.172}$$

Furthermore, our model allows for a determination of the degree of non-adiabaticity in terms of microscopic scattering times

$$\xi = \frac{\tau_{\text{sd}}}{4}\left(\frac{1}{\tau^\uparrow} + \frac{1}{\tau^\downarrow} + \frac{2}{\tau_{\text{sf}}}\right). \tag{5.173}$$

All sources of scattering contribute to the degree of non-adiabaticity in Eq. (5.173) due to the spatially vayring magnetization that causes a twist of the spin channels. Up to first spatial gradients in the magnetization, the spatial and the energy dependence of the distribution function factorize in spatially slowly varying magnetization textures. The factorization results in four coupled, algebraic equations for globally defined non-equilibrium functions that completely determine *adiabatic* magnetotransport. The separation in a global spin-up and spin-down channel that we have found in the equilibrium case (cf. section 5.3.1) is also present in non-equilibrium. In the presence of an electric field the local magnetization of the conduction electrons acquires two transverse, explicitly non-equilibrium components in addition to the usual equilibrium component. Thus, in addition to the spin up and spin down channels of collinear magnetotransport (cf. section 5.2), two extra, transverse channels emerge in non-collinear magnetotransport. They are global in the sense that their spatial direction is distinct perpendicular to the direction of the local magnetization while their magnitude remains

spatially constant.
In summary, we find that *adiabatic*, non-collinear magnetotransport can be described in terms of a *four channel model*. The physical significance of the individual channels is the following: While the spin up and spin down channels are responsible for the Ohmic conductivity and the spin current, the two transverse channels give rise to the adiabatic and the non-adiabatic spin-transfer torque. In this framework the adiabatic as well as the non-adiabatic channel arise generically from the twist of spin channels in the presence of a spatially varying magnetization texture. We adopt the current-induced torque picture (cf. section 2.3), where the transverse magnetization of the conduction electrons exerts a torque on the local moments and the identification of the transverse channels with the spin-transfer torques stems from directional mismatch. The difference in modulus of the non-adiabatic and the adiabatic channel defines the degree of non-adiabaticity, whose origin and magnitude are currently under hot debate in the magnetic community.

5.4.5 Conclusion and comparison with results of the literature

In this section, we discuss the results concerning the spin-transfer torque in spatially slowly varying magnetization textures as obtained in this section and contrast them with results of the literature. Table 5.1 presents a selection of the most prominent results of the literature that calculated the degree of non-adiabaticity ξ and the methods that were employed for its derivation. The third column of Table 5.1 specifies, whether the authors employed a localized or an itinerant model of ferromagnetism. Zhang and Li [5] employed a phenomenological macroscopic diffusion equation that does not allow for the computation of transport coefficients. By physical intuition, they linked ξ to a phenomenologically introduced spin-flip relaxation time. Tserkovnyak, Skadsem, Brataas, and Bauer [53] linked ξ to a phenomenologically introduced transverse spin-relaxation time. Kohno, Tatara, and Shibata [54] and Duine, Núñez, Sinova, and MacDonald [55] employed the same microscopic impurity model and consequently derived the same expression for ξ. Due to their full microscopic approach they were able to separate the spin-relaxation time τ_s into transverse and longitudinal parts. A symmetric treatment of the scattering rates reduces their result to those of all other authors, with the exception that their relaxation time is a mix of transverse and longitudinal spin relaxation.

As already discussed in section 2.3, Zhang and Li [5] introduced phenomenologically a relaxation time $\tau_{\mathrm{sf}}^{\mathrm{ZL}}$ that served as a mechanism to relax the transverse magnetization of the conduction electrons to the local magnetization. Their phenomenological macroscopic approach did not allow them to specify a microscopic process responsible for the relaxation. Our result in Eq. (5.163) relates their phenomenological spin-flip relaxation time to the spin-conserving, momentum relaxation times $\tau^{\uparrow}$, $\tau^{\downarrow}$ and the momentum conserving, spin-flip relaxation time τ_{sf} familiar from collinear magnetotransport (cf. section 5.2)

$$\frac{1}{\tau_{\mathrm{sf}}^{\mathrm{ZL}}} = \frac{1}{4}\left(\frac{1}{\tau^{\uparrow}} + \frac{1}{\tau^{\downarrow}} + \frac{2}{\tau_{\mathrm{sf}}}\right). \tag{5.174}$$

A central result of our derivation is that either processes that conserve or do not conserve the momentum contribute cumulatively to the total relaxation of the transverse magnetization according to relation (5.174). [190] Expressed in more technical terms, all relaxation processes that reside in the charge subspace contribute in the net result to the relaxation of the transverse magnetization of the

Table 5.1: Comparison of the result for the degree of non-adiabaticity for different approaches.

author	method	model	ξ	comment / microscopic origin
Zhang, Li [5]	phen. spin-continuity eq.	loc.	$\xi = \frac{\tau_{\mathrm{sd}}}{\tau_{\mathrm{sf}}}$	spin-relaxation of conduction electrons due to spin-flip scattering
Tserkovnyak, Skadsem, Brataas, and Bauer [53]	LDA kinetic equation	loc.	$\xi = \frac{\tau_{\mathrm{sd}}}{\tau_\sigma}$	phenomenological spin-dephasing time: transverse spin relaxation τ_σ / $\xi = \alpha_{\mathrm{LDA}}$
Kohno, Tatara, and Shibata [54]	microscopic (imag. time methods)	loc.	$\xi = \frac{\tau_{\mathrm{sd}}}{2\tau_s}$	spin-relaxation modeled by quenched magnetic impurities, fully quantum mechanical calculation / spin-dependent scattering, $\xi \neq \alpha$
Duine, Núñez, Sinova, and MacDonald [55]	microscopic Keldysh	itin.	same as Kohno et. al.	same impurity model as Kohno et. al. / $\xi \neq \alpha$

conduction electrons. In this sense spin-independent as well as spin-dependent impurity scattering contribute to non-adiabaticity due to the non-trivial spin-structure of the distribution matrix. There exists a lot of confusion about this point in the literature. The reason for this stems from the absence of a consistent terminology with respect to scattering in non-collinear magnetization textures. This rests on a subtle reasoning. In collinear ferromagnets there exist two kinds of scattering: spin-conserving and spin non-conserving scattering. On the contrary, in spatially varying magnetization textures the wavefunctions of the itinerant electrons do not belong to a spin eigenstate and therefore the spin channels are generically mixed. [63] Since the spin is not a good quantum number it is meaningless to distinguish between spin-conserving and spin-flip scattering in non-collinear magnetization textures. However, our conclusion must therefore be: As long as the conduction electron does not pass the spatially inhomogeneous magnetization texture ballistically (without scattering), the microscopic origin of non-adiabaticity rests on the intrinsic twist of channels in non-collinear magnetization textures due to the magnetization twist (cf. section 5.5 for a detailed discussion in terms of a gauge field) and does not depend on a special kind of impurity potential. Thus, not scattering at spin-flip impurities alone, but all kinds of scattering contribute in a statistically independent manner to non-adiabaticity due to the twist of spin channels. The intrinsic twist of channels has been overlooked thus far. In this connection, non-adiabaticity appears as a general property of transverse magnetization dynamics that does not rely on the specific nature of the impurities, whereas the strength of the non-adiabaticity is determined by the kind and concentration of the impurities.
In the absence of spin-flip scattering ξ reduces to the expression

$$\lim_{\tau_{\mathrm{sf}}\to\infty} \xi = \frac{\tau_{\mathrm{sd}}(\tau^{\uparrow} + \tau^{\downarrow})}{4\tau^{\uparrow}\tau^{\downarrow}}, \tag{5.175}$$

and is thus still finite. The result in Eq. (5.175) contrasts the conjecture that the parameter ξ is due to spin-flip impurities alone. [5] A fact that becomes in particular apparent at low temperatures. At low temperatures no scattering at spin-flip impurities takes place ($T \to 0, 1/\tau_{\mathrm{sf}} \to 0$) [98], whereas $1/\tau_{\mathrm{sf}}^{\mathrm{ZL}} \neq 0$ stays finite due to the spin-conserving intrachannel scattering $\tau^{\uparrow}$, $\tau^{\downarrow}$ that does not vanish in the limit of low temperatures. The physical reason for a vanishing $1/\tau_{\mathrm{sf}}$ at low temperatures is that the scattering at the weak spin-orbit potentials leads to an almost zero mean value of the scattered wavevector $\vec{k}'$. At finite temperatures, the non-zero value for $1/\tau_{\mathrm{sf}}$ is ascribed to spin-flip scattering at magnons that partly conserves the momentum. [98] Scattering at spin-flip impurities also contributes to non-adiabaticity but was shown in this work not to be the sole ingredient and at least for clean transition metals to be of minor importance.

Vanhaverbeke and Viret pointed out that the existence of a non-adiabatic torque requires that the total spin comprising conduction electrons and local magnetization is not conserved. [22] To fulfill this condition the transverse spin-flip scattering events $\tau_{\mathrm{sf}}^{\mathrm{ZL}}$ must not conserve the total magnetization. The microscopic condition for this is that the total scattering Hamiltonian does not commute with the total spin of the conduction electron. Due to the non-trivial spin structure of the distribution matrix and the collision integral (cf. section 5.1.3) this condition is always fulfilled as soon as the magnetization texture is non-collinear. In this sense, the appearance of the non-adiabatic spin-transfer torque is generic and does not depend on the details of scattering, as long as the spin of the conduction electron is properly taken into account. Our result for the non-adiabatic spin-transfer torque is thus in agreement with the arguments presented in Ref. [22]. Note that the non-adiabatic spin-transfer torque would be absent if we assume conservation of the total spin-angular momentum and compute it from the divergence of the spin current in Eq. (5.167). [51, 95] The necessary ingredient for a finite non-adiabatic component of the spin-transfer torque is impurity scattering, as the conduction electron does not traverse a mesoscopic ferromagnet without collisions.

Tserkovnyak, Skadsem, Brataas, and Bauer [53] claimed that transverse spin relaxation is the microscopic process responsible to relax the transverse magnetization of the conduction electrons. We showed without introducing any additional transverse mechanism to relax the magnetization of the conduction electrons [98], for instance by means of spin-orbit interactions, that longitudinal relaxation alone suffices to explain the appearance of non-adiabaticity due to a twist of the spin channels in non-collinear magnetization textures. We do not consider transverse relaxation, though it would also contribute to ξ in our model. In this sense transverse spin relaxation is not the microscopic origin of non-adiabaticity.

Xiao, Zangwill, and Stiles questioned in general the existence of a non-adiabatic component of the spin-transfer torque due to a relaxation of the non-equilibrium transverse magnetization of the conduction electrons toward an alignment with the local magnetization. [56] However, even though the phenomenological mechanism of Ref. [5] can be doubted, the appearance of the non-adiabatic torque takes place on equal ground with the adiabatic torque and thus is generic in our approach. Throughout their calculation, Ref. [56] employed the spin-resolved Fermi distributions of collinear magnetotransport and thus did not take properly into account the twist of the spin channels in non-collinear

magnetization textures due to the non-trivial commutation relations for the spin.

Finally, we compare our result for the conductivity of the transverse spin current as given in Eq. (5.154) with the different microscopic approaches of Refs. [54, 55]. To this attempt, we focus on our result in the case of vanishing spin-flip scattering as given by Eq. (5.157). In this case our result in Eq. (5.157) reduces to 1/2 of the result of Zhang and Li [5] with the exception that the relaxation mechanism is dominated by spin-conserving and not spin-flip impurities. Accordingly, our degree of non-adiabaticity is then given by Eq. (5.175). A comparison with the expression of Eq. (23) from Ref. [54] identifies their microscopically calculated spin up and spin down relaxation times with ours. Nevertheless, the spin coherence factor that we discussed in detail in section 5.4.2.2 is absent in the results of Refs. [54, 55]. This is not surprising as their calculations employed a perturbative treatment with respect to a gauge field and this approach restricts the validity of their calculations to the regime of ballistic spin transport. [58] For isotropic impurities the result for the degree of non-adiabaticity of Ref. [54] agrees with ours with appropriate modifications of notations. The authors employed a quantum mechanical impurity model that allows for a microscopic calculation of the relaxation times. In the absence of isotropic impurities a striking difference arises between their and our results: While their result for ξ is proportional to the difference in spin up and spin down relaxation times and spin-independent impurity scattering drops out of their expression for ξ, our result is proportional to the sum of spin up and spin down relaxation times (cf. Eq. (5.163)) and in turn depends on spin-independent momentum relaxation. Moreover, in contrast to our result, the outcome of Refs. [54, 55] provides the possibility of negative values for ξ due to spin relaxation dependent on the kind of impurities. In spatially slowly varying magnetization textures negative values of ξ are experimentally not reported up to date. The main concern with the methods as adopted by Refs. [53–55] is that they performed a perturbative expansion around a homogeneous magnetization. The interesting question is, whether they missed some important physics, for instance non-adiabaticity, in comparison with an expansion around an inhomogeneous magnetic equilibrium configuration. [155] We note, however, that a repetition of their calculations in an adiabatic spin frame for the conduction electrons raised some unresolved questions in the case of anisotropic impurities. [57]

At last, we like to make a few comments about the value of the degree of non-adiabaticity itself. The determination of its value is crucial for the experimental understanding of current-induced magnetization dynamics and currently hotly debated. [5, 53–55, 101] For a long period, ξ has been estimated to equal the Gilbert damping (for permalloy $\alpha \approx 0.01$ [72]). Recently, some experimental values for permalloy of $\xi \approx 0.01 - 0.1$ have been reported. [102–109, 191, 192] This differs by one order of magnitude. However, our derivation shows that for general spatially slowly varying magnetization textures ξ depends inversely on the spin-conserving relaxation time that is usually one order of magnitude smaller compared with what is usually assumed for transverse spin-flip relaxation times. [5] This finding is in accordance with the experiments that found ξ to be about one order of magnitude larger than α. [104, 105] In this context, we note in passing that a recent publication proposes to measure the degree of non-adiabaticity for the case of a magnetic vortex. [165] The presented measurement scheme allows the determination of the degree of non-adiabaticity from the static deflection of the vortex core, which facilitates an accurate determination of ξ. However, in section 5.5 we will see that

there are two different contributions to the degree of non-adiabaticity that arise from different origins. On the one hand a finite non-adiabatic component originates from spin relaxation of the transverse magnetization of the conduction electrons and can be regarded as a constant material parameter as it is independent of the actual magnetization texture. This case is dominant in spatially slowly varying magnetization textures and has been discussed in this section. On the other hand, ξ can drastically increase in narrow domain walls due to the non-adiabaticity as introduced by the strongly varying magnetization texture (cf. section 5.5 for a detailed discussion). Keeping this in mind, it is not that astonishing, that the experimental results for ξ vary by one order of magnitude, as it is up to date not clear how to separate both contributions in experiments.

At this point of the discussion, we like to make a statement concerning the relation between ξ and the Gilbert damping α. ξ and α are the dissipative parameters that enter the generalized Landau-Lifshitz Gilbert equation (4.2) and the ratio ξ/α determines the terminal velocity of domain-wall motion. [5] Moreover their relation is of high interest as $\alpha = \xi$ allows for peculiar magnetization dynamics. The equality causes Galilean invariance at a macroscopic level and allows for the drift of static magnetization patterns. [53, 55, 101] Thus some authors claim that $\alpha = \xi$ holds [53, 101], while other found that an equality is not a general property but occurs only accidentally in specific models. [54, 55] Though the here presented formalism is also capable to discuss the relation of the non-adiabatic component of the spin-transfer torque and Gilbert damping we do not pursue this throughout this thesis for the following reason: Transverse magnetization of the conduction electrons and thus the spin-transfer torque is purely a non-equilibrium feature. On the other hand the Gilbert damping is primarily an equilibrium phenomenon ($\vec{j} = 0$), though it will surely experience a renormalization in non-equilibrium. [5, 47, 51] In our opinion, a computation of the renormalization is useless without identifying a microscopic expression for the equilibrium value. Accordingly, we cannot contribute to the controversy about the relation of α and ξ, as we only compute ξ in this thesis. But we want to mention here that our result supports the experiments for permalloy [104, 105] that found $\alpha \neq \xi$ in general. As all kinds of scattering mechanisms contribute to ξ due to the twist of spin channels, an equality of ξ and α seems to be rather unlikely. The potential disorder breaks any relation between α and ξ at the macroscopic level. [155] Recently, experiments in permalloy wires doped with vanadium find that the doping concentration affects the value of ξ but has no effect on α. [190] This experimental finding supports the arguments that argues for $\alpha \neq \xi$.

5.5 Local spin-transfer torque and resistivity within a domain wall

This section is devoted to an analytical solution of the general kinetic equation (5.45) for the particular case of an one-dimensional domain wall. A perturbative expansion in the domain-wall width allows for an analytical solution of the kinetic equation. The individual orders of expansion exhibit a clear interpretation in terms of physical processes. Thus, the perturbative treatment results in an unifying perspective of the complex physical mechanisms that are involved in non-collinear magnetotransport. The zeroth-order solution is the bulk solution of a homogeneous monodomain. The first-order correction yields the transverse magnetization of the conduction electrons that constitutes as a counteraction on the local magnetization the spin-transfer torque. The second-order solution yields a correction to the charge current and gives thus rise to an intrinsic domain-wall resistivity, while the spatial modulations of the longitudinal component of the conduction electron magnetization are responsible for momentum transfer. It turns out that in spatially strongly varying magnetization textures it is spin mistracking, i.e., the inability of the of the conduction electron spin to follow the local magnetization that gives rise to a contribution to the non-adiabatic spin-transfer torque and acts as the source of domain-wall resistivity and momentum transfer.

In mesoscopic ferromagnets, a domain structure consists of regions in which the magnetization points in different spatial directions. A domain structure is energetically more favorable compared with a monodomain. This is due to the long-range demagnetization energy that overcomes in specimens of considerable spatial extensions the short-range exchange energy. The boundaries between individual domains provide a smooth change of the spatial direction of the magnetization. The homogeneous domains are separated by topological defects, domain walls, where the magnetization changes continuously. A domain wall modifies the electron transport due to its spin structure and is thus a prime example of the research field of spintronics, where charge transport is affected by the spin degree of freedom of the electron and vice versa. Even a single domain wall exhibits an intrinsic magnetoresistance and the determination of its strength and sign attracted a lot of interest. [3, 63, 111, 183, 185, 193–216] Up to date, the problem of domain-wall magnetoresistance is not ultimately solved, particularly with regard to the sign of the resistivity correction. [16]
In specimens that are smaller compared with the typical size of a domain (1-10 μm), a magnetic field sweep will result in the nucleation, depinning, motion, and subsequent annihilation of few disjoined domain walls. Providing that domain walls exhibit an intrinsic magnetoresistivity, the incidence of single domain walls results in discrete jumps in the measured resistivity. In bulk samples these tiny jumps are hard to measure, since the contribution of many domain walls will mask the observation of single domain walls where the low field magnetoresistance simply reflects the domain configuration. [207] It is worth noting that recent progress in the processing technology of nanostructures enables the fabrication of samples that contain single narrow domain walls. [10, 217] For instance, the short linear walls for that we analytically calculate the spin-transfer torque in section 5.5.5 are expected to be present in nanometer-sized constrictions [218–220] and experimental investigations of linear domain walls already take place. [221] As addressed by Ref. [220], a geometrically constrained linear wall differs from the usual Bloch or Néel wall and therefore constitutes a new kind of domain wall. However, in ferromagnetic materials with strong (perpendicular) anisotropy, the pre-

dicted domain-wall width is solely a few nm. [222] In this sense, the presence of narrow domain walls in this class of materials is generic. An efficient current-induced displacement in narrow domain walls that cannot be explained with small values of non-adiabaticity has been recently reported. [223] For ferromagnets without strong anisotropy the domain-wall width can be reduced by reinforcing the shape anisotropy [212] or by a trapping of the domain wall in a current-confined-path geometry [224]. Furthermore, narrow domain walls appear in nano contacts. [25, 220, 225, 226] Here, the width of the domain wall can be varied by means of the length of the constriction. However, for atomic scale domain walls where the conductance is quantized precession of the conduction electrons is forbidden due to vanishing transverse spin expectation values. [226]
In narrow domain walls the precession length $v_{\mathrm{F}}\tau_{\mathrm{sd}}$ of the spins of the conduction electrons approaches the domain-wall width λ. Furthermore the spin relaxation length $v_{\mathrm{F}}\tau_c$ is usually of the same order. The interplay of these three length scales promises non-classical features due to the quantum nature of the spin of the conduction electron spin. Accordingly, a comprehension of the interplay between current and domain walls that are of intermediate width is a current issue.

The perception that a domain wall alters the electron transport properties dates back to 1973. [193, 194] The same year also noted the proposal of the influence of spin-polarized currents onto the magnetization dynamics. [35] Since the beginning there are two communities, who either focus on the influence of domain walls on the electronic transport (the phenomenon of conduction modulation) or on the influence of the current on the domain wall (domain-wall motion), although both phenomena are but different aspects of the mutual sd interaction. This separated treatment somehow obscures the intimate relation of both effects, though they can be considered as being inverse to each other. In a preceding section of this thesis, we developed a semiclassical transport framework that treats electron and spin transport on equal footing. The formalism keeps the conduction electron's spin degree of freedom fully quantum mechanically while it treats its spatial and momentum degrees of freedom quasiclassically. In this section, we apply our formalism to a Bloch wall and calculate the spatially resolved spin-transfer torque, domain-wall resistivity and momentum transfer within the same framework. Our perturbative treatment connects both aspects of the sd interaction mentioned above. In particular, they are identified as mutually causing each other. This provides a natural interpretation of the involved physical processes. It turns out that the treatment of coupled charge and spin transport offers startling insight in fascinating physics in an intermediate transport regime that comprises diffusive charge transport and ballistic spin transport at the same time.

This section is organized as follows. First, we give a survey of the literature and review the results for the domain-wall resistivity in section 5.5.1 and the spin-transfer torque in section 5.5.2. In section 5.5.4 we derive a non-equilibrium kinetic equation for general one-dimensional domain wall profiles. Section 5.5.5 is engaged with a perturbative analytical solution for a linear domain wall profile. The perturbative approach provides the calculation of the spin-transfer torque, the domain-wall resistivity and the momentum transfer in the regimes of ballistic and diffusive spin transport and enables us to analytically study the crossover between the regimes.

5.5.1 Domain-wall magnetoresistance

Thus far, the magnetoresistance observed in bulk ferromagnets is well understood in terms of magnetoresistance effects, such as the anisotropic magnetoresistance [147, 148] or the ordinary magnetoresistance [205–207]. In macroscopic bulk samples complex domain configurations occur where the magnetization changes slowly and it is sufficient to consider the influence of the average magnetization on the electron transport. The situation changes in mesoscopic, low-dimensional scenarios, where the magnetization varies spatially more rapidly in narrow, single domain walls. Here, the interaction of the spin of the conduction electron with the spatially varying magnetization alters the electronic transport properties significantly.
In this section we will shortly mention some of the most important results on domain-wall resistivity. A extensive review is given, for instance by Ref. [16]. The first experiments that demonstrated domain walls to be a source of electrical resistance have been performed on iron whiskers in 1968. [227] The first studies of intrinsic domain-wall resistivity date back to 1973, where Cabrera and Falicov studied electron transport through a sharp domain wall in terms of tunneling. [193, 194] They found an exponentially small magnetoresistance due to the backscattering of the electrons at the domain wall. Berger invented a classical model that proposed a domain-wall resistivity due to scattering of the conduction electron with the wall. [3] Based on their investigations, domain walls with widths exceeding the Fermi wave-length $\lambda \gg k_{\mathrm{F}}^{-1}$ have been considered for a long time to be negligible with respect to electron transport in transition metal ferromagnets and this view changed only recently. [211] Owing to the progress in the fabrication of nanostructures, the discovery of the giant magnetoresistance effect [17, 18] stimulated new experiments concerning the intrinsic domain-wall resistivity. The first direct observation of electron scattering at ferromagnetic domain walls and a concomitant enhancement of the resistance in the presence of domain walls dates back to 1996. [201] Reference [201] investigated striped domain walls in thin-films of cobalt with domain-wall width too large to account for quantum mechanical reflections. This investigation has induced an anewed interest of theoreticians in the topic. Tatara and Fukuyama employed a diagrammatic technique to compute the domain-wall resistivity. [111] They predicted a negative domain-wall resistivity due to quantum effects, i.e., the destruction of weak-localization of the electrons by dephasing. The domain wall destroys the interference among the electrons and thus contributes a negative quantum correction to the resistivity that can overcome the classical increase due to reflections of the conduction electrons at sufficiently low temperatures. [228] Levy and Zhang calculated the twist-induced correction of the spin eigenstates in the presence of a domain wall and found a positive domain-wall resistivity due to spin-dependent impurity scattering. [63] Van Hoof et al. computed the domain-wall magnetoresistance in the ballistic limit with various methods. By first-principles calculations they found that realistic band-structures enhance the domain-wall magnetoresistance by orders of magnitude. Hence, a domain wall geometrically trapped in a nanostructured point contact can enhance the magnetoresistance up to 70% due to its small domain-wall width. [195] Brataas, Tatara and Bauer generalized the calculations of Ref. [111] to asymmetric impurity scattering lifetimes and screening of the domain wall potential and obtained qualitatively similar results. [196] Based on a semiclassical treatment van Gorkom, Brataas and Bauer considered diffusive transport and calculated the electron densities in the presence of a domain wall. [183] They found that a modified magnetization by the redistribution of the electrons between the majority and minority channels causes the domain-wall resistivity to be positive or nega-

tive depending on the difference between the spin-dependent scattering lifetimes. Šimánek and Rebei performed a gauge-transformation on the Hamiltonian level and subsequently derived a kinetic equation that served for computing an intrinsic domain-wall resistivity by means of the resulting macroscopic equations. [185, 197] They traced back the origin of domain-wall resistivity to a quenching of the spin accumulation in the presence of the domain wall due to the rapid transverse precession and predicted an oscillation of the resistivity with the domain-wall width. [197] However, objections arose that their kinetic equation contains a term that violates particle number conservation. [198] Dugaev et al. took into account the interaction between the conduction electrons and calculated the modification of the spin and charge distributions due to the domain wall, the relaxation times as well as charge and spin conductivities. [199] Bergeret, Volkov and Efetov derived a kinetic equation and solved it in the diffusion approximation for either small or wide domain walls. [198] A Keldysh approach that does not suffer from a phenomenological introduction of relaxation times has recently been given in Ref. [200]. They obtained similar results as Ref. [196].
It is of experimental evidence that a domain wall contributes either an increase in resistance, that corresponds to a positive intrinsic domain-wall resistivity [201–203, 211, 212, 215, 216] or a decrease in resistance, that corresponds to a negative intrinsic domain-wall resistivity [204–210, 213]. All theoretical attempts that calculated the intrinsic domain-wall resistivity found positive corrections except for Refs. [111, 183, 200]. Reference [111] traced back the origin of negative domain-wall resistivity to the dephasing of the conduction electrons leading to a breakdown of weak localization. This is a low temperature effect and cannot explain the observed negative resistances at ambient temperatures (cf. [205–207]). Thus, Refs. [183, 200] provide the sole explanations of negative intrinsic domain-wall resistivity at ambient temperature. While Ref. [183] claimed that the origin of negative domain-wall resistivity is associated with the kind of impurities and thus links negative domain-wall resistivity to spin-dependent impurity scattering, Ref. [200] pointed out that a realistic band structure can also lead to negative domain-wall resistivity. If the band structure is the dominating effect, first-principle band-structure calculations are needed to clarify whether a material exhibits a positive or a negative domain-wall resistivity.

5.5.2 Spin-transfer torque versus momentum transfer

The first proposal that an electric current exerts a force on a domain wall and causes its motion goes back to the early seventies by Berger. [2, 3, 35] The experimental demonstration of current-induced domain-wall motion dates back to 1985. [229, 230] It lasted almost twenty-five years from Berger's pioneering work [35] to the proposal in 1996 independently by Slonczewski [14] and Berger [15] that the spin-transfer torque is established as an important effect in the magnetic community and thirty years to the first experimental observation of the spin-transfer torque effect [231]. Since then a variety of theoretical attempts aimed at establishing a tractable theory of the spin-transfer torque. The theoretical challenge of computing the interaction of electrical current and the ferromagnetic order parameter is that it constitutes an interesting non-equilibrium transport problem.
Tatara and Kohno presented a self-contained theory of current and magnetization and compared the limiting cases of domain-wall motion due to spin-transfer torque and momentum transfer. [49] Waintal and Viret considered ballistic transport and computed a spatially oscillating non-adiabatic torque due to the Larmor precession of the conduction electrons around the local magnetization. [172] The non-

local oscillatory torque is of quantum origin and arises from the non-adiabaticity that is associated with the finite width of the domain wall. Zhang and Li proposed a general theory of the spin-transfer torque with constant transport coefficients for spatially slowly varying magnetization textures. [5] Xiao, Zangwill and Stiles found by numerical calculations a non-local torque that becomes significant in narrow domain walls. [56] Their results casted doubt on the existence of the non-adiabatic torque as proposed by Ref. [5]. Vanhaverbeke and Viret studied analytically and numerically the evolution of the spin of the conduction electrons when passing a domain wall by means of a purely classical time-dependent Larmor equation. [22] They found the non-adiabatic spin-transfer torque about one order of magnitude larger compared to the general value of Ref. [5] valid for wide domain walls. Moreover, they reported on oscillations in the non-adiabaticity with a concomitant sign change for narrow walls. Taniguchi et al. extended the work of Šimánek and Rebei [185, 197] and calculate the local spin-transfer torque within a domain wall in the diffusive approximation by solving macroscopic transport equations. [232] By considering the macroscopic transport equations of Ref. [185, 197], they restricted themselves to the regime of diffusive transport and do not take into account possible quantum coherence effects in the spin sector. In accordance with Ref. [22], they found that the non-adiabaticity enhances about one order of magnitude in narrow domain walls. Thorwart and Egger derived classical Bloch-Redfield equations by taking into account spin relaxation due to a Caldeira-Leggett bath. [233] This enabled them to calculate higher-order spin-transfer torque terms that they show to be responsible for a shape-deformation of the domain wall.

5.5.2.1 Phenomenological explanation of the spin-transfer torque and the momentum transfer effect

There are basically two mechanisms that cause current-induced domain-wall motion: spin-transfer torque and momentum transfer. Both mechanism dominate in different regimes concerning the width of the domain wall: In the regime of narrow walls, for instance at sharp interfaces such as giant magnetoresistance devices or point contacts, momentum transfer dominates. In this case the domain wall translates due to the reflection of the conduction electrons at the wall. In this process the spin is preserved and no transfer of spin-angular momentum, i.e., no spin-transfer torque occurs. In contrast, in the regime of wide domain walls, the reflection probability for the conduction electron is strongly suppressed and the spin-transfer torque effect is predominant. Here, the domain wall translates due to the transfer of spin-angular momentum between wall and conduction electron. Microscopically the transfer of spin causes spin-flips that take place in discrete units of $\hbar$. Macroscopically the conduction electron magnetization precesses around the local magnetization and causes a torque on the local magnetization. Though momentum transfer and spin-transfer torque are complete disjunct phenomena in their mode of operation, both phenomena occur at the same time in domain walls of intermediate width. Their relative ratio depends crucially on the geometry and on transport parameters.
In domain walls of medium width, spin mistracking of the conduction electron spins is the predominant effect. The strong spatial variation due to the domain wall reduces the ability to track the local moments. This results in an enhancement of the non-adiabatic spin-transfer torque. [22, 232] Moreover, spin mistracking is responsible for a considerable domain-wall resistivity and momentum transfer due to the mixing of spin channels in narrow domain walls. [63]. The spin of the conduction electron cannot follow the local magnetization and gets scattered by the wall.

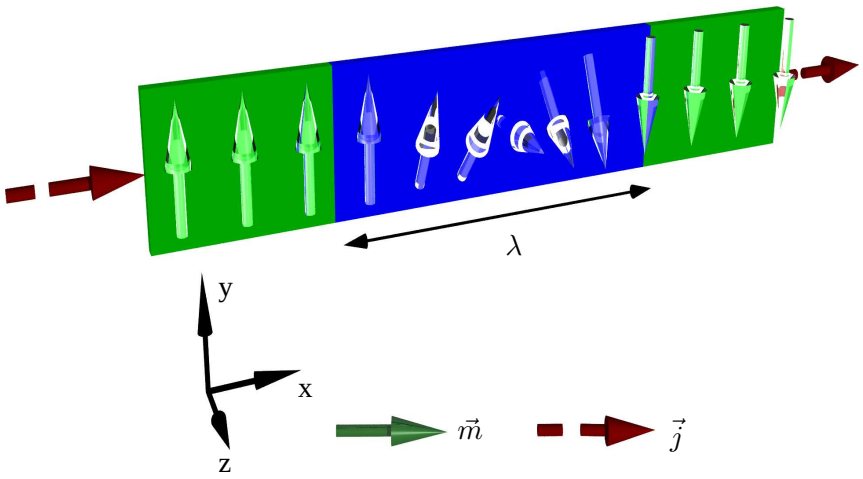

Figure 5.7: (Color online) Sketch of a transverse domain wall (Bloch wall) (blue region) enclosed between two homogeneous adjacent domains (green regions).

We define the degree of spin mistracking by the relevant transport parameters according to

$$\varrho := \frac{v_{\mathrm{F}}\tau_{\mathrm{sd}}}{\lambda} = \frac{\omega_\lambda}{\omega_{\mathrm{sd}}}. \tag{5.176}$$

Here, v_{F} is the Fermi velocity, λ is the domain-wall width and $\tau_{\mathrm{sd}} = \hbar/J_{\mathrm{sd}}$ is the precession time associated with the sd interaction. According to Eq. (5.176) the degree of spin mistracking ϱ is determined by the ratio of the rate of the rotation of the local moments within the domain wall ω_λ and the precession frequency of the spins of the conduction electron around the local moments ω_{sd}. For a given exchange interaction J_{sd}, the degree of spin mistracking is entirely determined by the width of the domain wall. Wide walls ($\lambda \to \infty$) correspond to small values of spin mistracking ($\varrho \ll 1$). This is the adiabatic limit, where the spin of the conduction electron resides in its majority or minority spin state during its traversal of the domain wall and no mixing of spin channels occurs. Narrow walls ($\varrho \approx 1$) constitute a more abrupt transition. Here, the ability of the conduction electron spin to track the local moments decreases until it cannot longer follow the local magnetization. As a consequence, the spin of the conduction electron resides in a coherent superposition of majority and minority spin states due to the strong magnetization twist. This condition characterizes the non-adiabatic transport regime, where spin mistracking dominates the magnetotransport.

To understand the involved magnetotransport within a domain wall and to give a phenomenological explanation of what happens to the spin of the conduction electron when propagating through a domain wall, we follow Ref. [172] and sketch their heuristic explanation of the spin-transfer torque effect. As depicted in Fig. 5.7, the model system of a domain wall can be divided into three regions. Two homogeneous domains are connected by a domain wall of length λ where the magnetization changes continuously. An electron that traverses the domain wall initially has its spin aligned with the magnetization of the adjacent homogeneous domain. Due to the electric field the conduction electron propagates through the wall.

The parameter ϱ separates the adiabatic ($\varrho \ll 1$) from the abrupt case ($\varrho \gg 1$) and characterizes the predominant effect in both limits. In the adiabatic case ($\lambda \to \infty$, $\varrho \to 0$) the conduction electron spin starts and ends with the spin of the respective adjacent domain. When the electron enters the domain wall the local moments change slightly their direction and cause a small angle between the conduction electron spin and the magnetization. As a result of the small angle the spin of the conduction electron starts to precess around the local moments. The precessional motion is superimposed to the drift through the domain wall as induced by the electric field. If the spatial variation of the local moments is slow enough the precession allows the spin of the conduction electron to track the local magnetization. The precession frequency is set by the sd interaction $\omega_{\text{sd}} = 1/\tau_{\text{sd}}$. At the end of every period of precession the electron has traveled a distance of $v_{\text{F}}\tau_{\text{sd}}$ and is again aligned with the local magnetization. The precession stops by reaching the end of the domain wall where the conduction electron spin is aligned with the magnetization of the homogeneous adjacent domain to the right. During its constant precession it covers a rotation of π and looses quantum mechanically an angular momentum of $\hbar$. As a counteraction that relies on conservation of angular momentum, a torque of equal magnitude and opposite sign is exerted on the local magnetization and the domain wall translates by a change of the local moments. The spin-transfer torque is a local phenomenon and the exchange of spin-angular momentum between the wall and the conduction electrons that results in domain-wall motion occurs locally. No momentum scattering with the magnetization texture takes place and no domain-wall resistivity is present in the adiabatic limit as every electron passes the domain wall. A sharp domain wall ($\lambda \to 0$, $\varrho \to \infty$) constitutes an abrupt change in the magnetization texture, for instance the anti-parallel aligned layers within a spin valve. In the abrupt limit, the small width of the domain wall does not allow for a complete rotation of the conduction electron spin. The different band-structures of the anti-parallel aligned homogeneous domains cause an effective potential barrier that causes scattering of the conduction electrons. The spin either passes the domain wall with no change of its spin direction or is reflected by the domain wall. An abrupt wall will act as a source of extra resistance as it causes reflection of the conduction electrons. The reflection results in a transfer of momentum between conduction electron spin and domain wall, which leads to a drift of the whole magnetization configuration. This is the descriptive origin of domain-wall motion due to momentum transfer. [49] Momentum transfer acts comparable to a magnetic field on the domain wall as a whole and in this sense constitutes a non-local effect. [56, 59, 172, 191]

For an infinitely strong sd interaction J_{sd}, no precession occurs and the spin of the conduction electron follows the local moments in perfect adiabaticity, such that no spin mistracking occurs. In this case the transfer of spin-angular momentum between the spin of the conduction electron and the local moments is complete, in the sense that no dissipation occurs. In the perfect adiabatic case dissipation solely takes place in the sector of the local moments by means of Gilbert damping. A finite sd interaction J_{sd} results in precession of the spin of the conduction electron around the local moments. For finite J_{sd} the tracking is not perfect and the transfer of angular momentum between the spins of the conduction electrons and the local magnetization does not have to be complete but some angular momentum may be dissipated in the sector of the conduction electrons. There are two main sources of spin-dissipation in the conduction electron sector: spin relaxation due to impurity scattering and spin mistracking due to a spatially strongly varying magnetization texture. [5, 201, 202] Spin relaxation is always present whether the spin of the conduction electron can follow the local magnetization adia-

batically or not. Spin mistracking is a feature that arises from the strong magnetization twist and is linked with a non-adiabatic traversal of the conduction electron through a narrow domain wall. However, all deviations from perfect adiabaticity (complete transfer of angular momentum) give rise to a non-adiabatic spin-transfer torque and to a non-zero degree of non-adiabaticity ξ. [5] For wide domain walls ($\lambda \to \infty$) spin mistracking does not play a role and the non-adiabatic spin-transfer torque is entirely caused by spin relaxation. In the regime of narrow domain walls, when the domain-wall width approaches the precession length ($\varrho \approx 1$), the fast sd precession of the conduction electron spin around the spatially changing local magnetization does not preserve the angular momentum. The reason is that the spatial variations of the local moments $\vec{m}(\vec{r})$ become so strong that the sd precession frequency does not suffice to track the local moments. This implies a non-adiabatic passage through the domain wall. Here, the spin does not reside in its majority or minority spin state with respect to the adjacent homogeneous domain during its traversal of the domain wall. In this context the non-adiabatic spin-transfer torque acquires an additional contribution due to the spatially strongly varying magnetization texture that arises due to channel mixing caused by spin mistracking. This effect obviously increases with decreasing domain-wall width and provides a second contribution besides spin relaxation to the non-adiabatic spin-transfer torque in narrow domain walls. The contribution from the spatially constant finite delay due to spin relaxation must thus be discriminated from the contribution due to spin mistracking. While the contribution due to spin relaxation is determined by the parameters of the material, the contribution due to spin mistracking depends on the details of the magnetization texture. It is worth noting that the contribution of spin mistracking to the degree non-adiabaticity removes the independence of the spin-transfer torque from the domain-wall width λ that holds in the adiabatic transport regime for wide domain walls. [48]

Besides the increase of the non-adiabaticity, the enhanced inability of the spin of the conduction electron to follow the local moments with decreasing domain-wall width causes a spin accumulation at the wall. The spin accumulation translates into a charge accumulation due to the inherent coupling of charge and spin degree of freedom as provided by the magnetization twist in the presence of the domain wall. The charge accumulation induces a potential barrier, which results in excess resistivity. [182, 215] In narrow walls ($\varrho \approx 1$), the considerable amount of spin accumulation leads to a resistivity-correction due to the presence of the domain wall. [185] Quantum mechanically a conduction electron that resides in a majority spin state obtains due to the magnetization twist an admixture of the minority spin state, which acts in combination with the spin polarization of the electric current in a ferromagnet as the source of spin accumulation in the vicinity of the wall. The excess resistance in narrow walls stems from the mixture of spin channels that removes the possibility of a high-conducting shunt channel as present in homogeneous ferromagnets.[5] [63, 185, 197]

A second analogy to understand the intrinsic domain-wall resistivity rests on its close relation to the giant magnetoresistance effect. A spin valve with anti-parallel magnetized ferromagnetic layers is equivalent to an abrupt domain wall and constitutes a large potential barrier for the spin-polarized electrons that causes scattering and subsequent reflection of the conduction electrons. A domain wall of finite width can be approximated by a multitude of interfaces with successive potential steps. For wide walls the equivalent number of layers tends to infinity and the height of each potential barrier tends to zero. Consequently, no reflection at potential steps or resistance is present. With decreasing

[5] This effect is also responsible for the giant magnetoresistance effect in magnetic multilayer.

domain-wall width the height of the potential steps increases gradually until one sharp interface with an abrupt transition is reached. As the reflection probability is proportional to the barrier height, the intrinsic domain-wall resistivity increases with decreasing domain-wall width.

5.5.3 Transport characteristics for different types of domain walls

The domain-wall width λ constitutes the most important parameter, as it concerns magnetotransport through a domain wall. It governs the coupling between the spin of the conduction electron and the domain wall. The calculation of transport properties requires different theoretical treatments in dependence on the domain-wall width. Concerning ballistic spin transport a characterization of domain-wall magnetotransport in terms of the degree of spin mistracking ϱ as given by Eq. (5.176) is possible. Although there is a smooth transition between them, there are mainly three types of domain walls: wide, narrow and sharp domain walls (cf. first row in Table 5.2). Depending on the type of the domain wall different technical approaches to the problem are more appropriate compared with others. While the adiabatic regime is best suited for a perturbative expansion in the magnetization twist, a perturbative expansion around an uniform magnetic state fails for the sharp wall. A sharp wall defines a quantum-mechanical scattering problem. Accordingly, every domain-wall type yields its own distinct physics. The physics of the three domain wall types has been discussed in the previous section. This situation is illustrated in Table 5.2. For narrow domain walls the mechanisms of spin relaxation and reflection as origins for the non-adiabatic spin-transfer torque and domain-wall resistivity, respectively, are listed for completeness. The mechanisms of spin relaxation and reflection are of minor importance in narrow domain walls and therefore put in parentheses. As long as spin-orbit interactions can be disregarded, there exists no coupling between real space and spin space and the arguments and calculations of this section apply to both kinds of domain walls, Néel and Bloch walls.
As the domain wall constitutes a macroscopic object it can be treated classically, whereas the spin of the conduction electron should be treated quantum mechanically (cf. discussions in section 2.1 and 5.1.1). [58, 100] For a domain-wall width that exceeds the Fermi wavelength $\lambda \gg k_{\mathrm{F}}^{-1}$, magnetotransport through a domain wall is a semiclassical transport problem, rather than a coherent quantum-mechanical wave problem. [22, 100] The spatial coherence of the wavefunction inside the domain wall is broken due to impurity scattering of the conduction electrons. In this case a description of the spin-transfer torque and the domain-wall resistivity in terms of local transport coefficients is justified as long as the domain-wall width exceeds the Fermi wavelength $\lambda \gg k_{\mathrm{F}}^{-1}$.
The focus of this section rests on narrow domain walls. Only recently a few studies have been published that are concerned with domain walls of intermediate width. [22, 232] While Ref. [22] employed a rather phenomenological approach, the calculations of Ref. [232] are restricted to the diffusive approximation. We note here that there exist objections about the kinetic equation as derived by Ref. [232]. [198] However, as the presented analysis will show, the physically most interesting regime comprises ballistic spin transport that is not accessible by the entire diffusive approach of Ref. [232].

5.5.4 General non-equilibrium kinetic equation in the presence of a domain wall

This section sketches the derivation of the general one-dimensional kinetic equation for arbitrary domain-wall profiles. In the following, we consider a domain wall that is embedded in a bulk system.

Table 5.2: Transport characteristics for different types of domain walls.

Domain wall type	sharp ($\varrho \to \infty$)	narrow ($\varrho \approx 1$)	wide ($\varrho \to 0$)
Domain-wall magnetotransport governed by	material	magnetization texture	material
Problem type	scattering	non-adiabatic	adiabatic
Most important property	band structure	spatial variations	nature of impurities
Most appropriate method	qm a priori scattering problem	kinetic approach; takes properly into account spatial variations	qm perturbative expansion around uniform ground state
Features	domain-wall resistivity, momentum transfer	spin-transfer torque, domain-wall resistivity, momentum transfer	spin-transfer torque
Origin of non-adiabatic spin-transfer torque	none	spin mistracking (spin relaxation)	spin relaxation
Origin of domain-wall resistivity	reflection	spin mistracking (reflection)	none
References	[49, 172, 193–196, 198]	[22, 232]	[49, 63, 183, 185, 196, 198]

Since the domain wall is a macroscopic object, we treat it classically. The mean-field description in the sd Hamiltonian (5.15) inherently neglects quantum fluctuations of the local moments. We focus on a quasi one-dimensional wire extended in x direction and on a transverse domain wall. The quasi-translational invariance in the yz plane reduces the problem to one spatial dimension and the distribution function depend solely on the x coordinate ($\hat{f}_{\vec{k}}(\vec{r}) \rightarrow \hat{f}_{\vec{k}}(x)$). A domain wall is parametrized by a constant angle θ and a spatially dependent angle $\phi(x)$, where $\phi(x)$ denotes the angle between the local moments and the z axis (cf. Fig. 5.7). A transverse domain wall or a Bloch wall is parametrized by the angles $\theta = \pi/2$, $\phi = \phi(x)$ according to

$$\vec{m}(x) = \begin{pmatrix} \cos\theta \\ \sin\theta \cdot \sin\phi \\ \sin\theta \cdot \cos\phi \end{pmatrix} = \begin{pmatrix} 0 \\ \sin\phi(x) \\ \cos\phi(x) \end{pmatrix}. \tag{5.177}$$

The domain wall as given in Eq. (5.177) bears the advantage of strictly being perpendicular to the current flow and is thus not subject to extrinsic magnetoresistance effects like the anisotropic magnetoresistance. This allows for a direct determination of the intrinsic domain-wall resistivity. We note that it is experimentally feasible to disentangle the contribution of the intrinsic domain-wall resistivity from the contribution of the anisotropic magnetoresistance or the ordinary magnetoresistance. [202, 207, 211, 234] Since no coupling between spin and real space is provided by our model, for instance by spin-orbit interaction, the calculation for a Néel wall proceeds analogously to that for the Bloch wall in Eq. (5.177) by an interchange of the variables ϕ and θ. Consequently, the results of this section apply to both types of domain walls as long as spin-orbit interaction can be disregarded.
Another quantity of interest is the magnetization twist $\partial_x\phi(x)$ that determines the gradient of the magnetization in x direction

$$\partial_x\vec{m}(x) = \frac{d\phi(x)}{dx}\begin{pmatrix} 0 \\ \cos\phi(x) \\ -\sin\phi(x) \end{pmatrix} = \frac{d\phi(x)}{dx}\begin{pmatrix} 0 \\ m_z(x) \\ -m_y(x) \end{pmatrix}. \tag{5.178}$$

To attain at analytical solutions, it is appropriate to perform a transformation to the local reference frame of the domain wall. This is achieved by a local gauge transformation in spin space arranged by the unitary rotation matrix

$$\mathcal{U}(\phi(x)) = e^{-i\frac{\phi(x)}{2}\sigma_x} = \cos\frac{\phi(x)}{2}\mathbb{1} - i\sin\frac{\phi(x)}{2}\sigma_x. \tag{5.179}$$

Per construction the gauge transformation (5.179) aligns the magnetization within the domain wall with the z axis of the rotating reference frame

$$\mathcal{U}(\phi(x))\,(\vec{\sigma}\vec{m}(x))\,\mathcal{U}^\dagger(\phi(x)) = \sigma_z. \tag{5.180}$$

Applying the gauge transformation (5.179) to the gradient of the magnetization (5.178) yields

$$\mathcal{U}(\phi(x))\partial_x\,(\vec{\sigma}\vec{m}(x))\,\mathcal{U}^\dagger(\phi(x)) = \frac{d\phi(x)}{dx}\sigma_y. \tag{5.181}$$

Let us now investigate the impact of the gauge transformation on the derivative

$$\begin{aligned}\mathcal{U}(\phi(x))\partial_x\mathcal{U}^\dagger(\phi(x)) &= \partial_x\mathbb{1} + \mathcal{U}(\phi(x))\left(\partial_x\mathcal{U}^\dagger(\phi(x))\right) \\ &= \partial_x\mathbb{1} + \frac{i}{2}\frac{d\phi(x)}{dx}\sigma_x.\end{aligned} \tag{5.182}$$

The gauge transformation introduces via Eq. (5.182) a covariant derivative

$$\mathcal{D}_x = \partial_x \mathbb{1} + iA(x), \tag{5.183}$$

along with a respective gauge connection that is given by the local gauge potential $\vec{A}(x)$ determined by the magnetization twist

$$A(x) = -i\mathcal{U}(\phi(x))\partial_x \mathcal{U}^\dagger(\phi(x)) = \vec{A}(x)\vec{\sigma}, \quad \vec{A}(x) = \frac{1}{2}\frac{d\phi(x)}{dx}\vec{e}_x. \tag{5.184}$$

In this sense, the gauge field $\vec{A}(x)$ comprises the spatial dependence of the axis of quantization. In the case of an one-dimensional domain wall, the spatial variation is parametrized by one single angle $\phi(x)$ and the gauge transformation is a special case of the general $SU(2)$ gauge transformation mentioned in the beginning of chapter 5. More precisely, for the case of a domain wall the gauge transformation is a local $U(1)$ that introduces one local transverse gauge field $A(x)$ instead of three independent gauge fields in the general $SU(2)$ case. [101]

After the preliminaries, we now derive the general kinetic equation for a domain wall. An one-dimensional version of the generalized kinetic equation (5.97) reads assuming translational invariance in the yz plane

$$\begin{aligned} v_x\partial_x \hat{g}_{\vec{k}}(x) + \frac{1}{2}\{\hat{\tau}_{\text{sc}}^{-1}(\vec{m}(x)), \hat{g}_{\vec{k}}(x)\} + \frac{^{\text{sf}}\hat{g}_{\vec{k}}(x)}{\tau_{\text{sf}}} - \frac{\gamma}{2i}[\vec{\sigma}\vec{m}(x), \hat{g}_{\vec{k}}(x)] \\ + \frac{J_{\text{sd}}}{2\hbar}\{\partial_x(\vec{\sigma}\vec{m}(x)), \partial_{k_x}\hat{g}_{\vec{k}}(x)\} = ev_x E_x \partial_\epsilon \hat{f}_{\text{eq}}(\vec{m}(x), \epsilon). \end{aligned} \tag{5.185}$$

The next step is to perform the gauge transformation (5.179) on Eq. (5.185)

$$\begin{aligned} \mathcal{U}\left(v_x\partial_x \hat{g}_{\vec{k}}(x)\right)\mathcal{U}^\dagger + \frac{1}{2}\mathcal{U}\{\hat{\tau}_{\text{sc}}^{-1}(\vec{m}(x)), \hat{g}_{\vec{k}}(x)\}\mathcal{U}^\dagger + \mathcal{U}\frac{^{\text{sf}}\hat{g}_{\vec{k}}(x)}{\tau_{\text{sf}}}\mathcal{U}^\dagger - \frac{\gamma}{2i}\mathcal{U}[\vec{\sigma}\vec{m}(x), \hat{g}_{\vec{k}}(x)]\mathcal{U}^\dagger \\ + \frac{J_{\text{sd}}}{2\hbar}\mathcal{U}\{\partial_x(\vec{\sigma}\vec{m}(x)), \partial_{k_x}\hat{g}_{\vec{k}}(x)\}\mathcal{U}^\dagger = ev_x E_x \mathcal{U}\left(\partial_\epsilon \hat{f}_{\text{eq}}(\vec{m}(x), \epsilon)\right)\mathcal{U}^\dagger, \end{aligned} \tag{5.186}$$

where we omitted the argument of $\mathcal{U}(\phi(x))$ for brevity.
Equation (5.186) holds a few terms to evaluate. Let us start with the kinetic term

$$\begin{aligned} \mathcal{U}\left(v_x\partial_x \hat{g}_{\vec{k}}(x)\right)\mathcal{U}^\dagger &= \mathcal{U}v_x\left(\partial_x \hat{g}_{\vec{k}}(x)\mathcal{U}^\dagger\right) - \mathcal{U}v_x\hat{g}_{\vec{k}}(x)\left(\partial_x\mathcal{U}^\dagger\right) \\ &= \mathcal{U}v_x\left(\partial_x\mathcal{U}^\dagger\mathcal{U}\hat{g}_{\vec{k}}(x)\mathcal{U}^\dagger\right) - \mathcal{U}v_x\hat{g}_{\vec{k}}(x)\mathcal{U}^\dagger\mathcal{U}\left(\partial_x\mathcal{U}^\dagger\right) \\ &= \mathcal{U}v_x\left(\partial_x\mathcal{U}^\dagger\tilde{\hat{g}}_{\vec{k}}(x)\right) - v_x\tilde{\hat{g}}_{\vec{k}}(x)\mathcal{U}\left(\partial_x\mathcal{U}^\dagger\right) \\ &= v_x\partial_x\tilde{\hat{g}}_{\vec{k}}(x) + v_x[\mathcal{U}\left(\partial_x\mathcal{U}^\dagger\right), \tilde{\hat{g}}_{\vec{k}}(x)] \\ &= v_x\partial_x\tilde{\hat{g}}_{\vec{k}}(x) + iv_x[\vec{A}\vec{\sigma}, \tilde{\hat{g}}_{\vec{k}}(x)], \end{aligned} \tag{5.187}$$

where we introduced the gauge transformed distribution matrix

$$\tilde{\hat{g}}_{\vec{k}}(x) \equiv \mathcal{U}\hat{g}_{\vec{k}}(x)\mathcal{U}^\dagger = \frac{1}{2}\left[\tilde{g}_{\vec{k}}(x)\mathbb{1} + \tilde{\vec{g}}_{\vec{k}}(x)\vec{\sigma}\right]. \tag{5.188}$$

Equation (5.188) yields the non-equilibrium distribution matrix in the reference frame of the local magnetization that is given by the orthonormal basis $\{-\left(\partial_x\phi(x)\right)^{-1}\vec{m}(x)\times\partial_x\vec{m}(x), \left(\partial_x\phi(x)\right)^{-1}\partial_x\vec{m}(x), \vec{m}(x)\}$.
Thus far, the validity of Eq. (5.187) is general for spatially one-dimensional problems. Next we employ the explicit form of the gauge transformation (5.179) for the case of a domain wall and evaluate the commutator in Eq. (5.187)

$$\begin{aligned}
\mathcal{U}\left(v_x\partial_x\hat{g}_{\vec{k}}(x)\right)\mathcal{U}^\dagger &= v_x\partial_x\tilde{\hat{g}}_{\vec{k}}(x) + \frac{iv_x}{2}\frac{d\phi(x)}{dx}[\sigma_x,\tilde{\hat{g}}_{\vec{k}}(x)] \\
&= v_x\partial_x\tilde{\hat{g}}_{\vec{k}}(x) + \frac{iv_x}{2}\frac{d\phi(x)}{dx}\frac{1}{2}\left([\sigma_x,\mathbb{1}]\tilde{g}_{\vec{k}}(x) + [\sigma_x,\sigma_\mu]\tilde{g}^\mu_{\vec{k}}(x)\right) \\
&= v_x\partial_x\tilde{\hat{g}}_{\vec{k}}(x) + \frac{iv_x}{2}\frac{d\phi(x)}{dx}\frac{1}{2}2i\left(\tilde{g}^y_{\vec{k}}(x)\sigma_z - \tilde{g}^z_{\vec{k}}(x)\sigma_y\right) \\
&= v_x\partial_x\tilde{\hat{g}}_{\vec{k}}(x) - \frac{v_x}{2}\frac{d\phi(x)}{dx}\left(\tilde{g}^y_{\vec{k}}(x)\sigma_z - \tilde{g}^z_{\vec{k}}(x)\sigma_y\right).
\end{aligned} \tag{5.189}$$

The spin-conserving scattering term transforms as follows

$$\begin{aligned}
\frac{1}{2}\mathcal{U}\{\hat{\tau}_{\text{sc}}^{-1}(\vec{m}(x)),\hat{g}_{\vec{k}}(x)\}\mathcal{U}^\dagger &= \frac{1}{2}\{\mathcal{U}\hat{\tau}_{\text{sc}}^{-1}(\vec{m}(x))\mathcal{U}^\dagger, \mathcal{U}\hat{g}_{\vec{k}}(x)\mathcal{U}^\dagger\} \\
&= \frac{1}{4}\{\mathcal{U}\left[\tau_c^{-1}\mathbb{1} + \tau_s^{-1}\vec{m}(x)\vec{\sigma}\right]\mathcal{U}^\dagger, \tilde{\hat{g}}_{\vec{k}}(x)\} \\
&= \frac{1}{4}\{\left[(\tau_c^{-1}\mathbb{1} + \tau_s^{-1}\mathcal{U}(\vec{m}(x)\vec{\sigma})\mathcal{U}^\dagger\right], \tilde{\hat{g}}_{\vec{k}}(x)\} \\
&= \frac{1}{4}\left(\{\tau_c^{-1}\mathbb{1}, \tilde{\hat{g}}_{\vec{k}}(x)\} + \{\tau_s^{-1}\sigma_z, \tilde{\hat{g}}_{\vec{k}}(x)\}\right) \\
&= \frac{1}{8}\Big[\tau_c^{-1}\left(\{\mathbb{1},\mathbb{1}\}\tilde{g}_{\vec{k}}(x) + \{\mathbb{1},\vec{\sigma}\}\tilde{\vec{g}}_{\vec{k}}(x)\right) \\
&\quad + \tau_s^{-1}\left(\{\sigma_z,\mathbb{1}\}\tilde{g}_{\vec{k}}(x) + \{\sigma_z,\vec{\sigma}\}\tilde{\vec{g}}_{\vec{k}}(x)\right)\Big] \\
&= \frac{1}{2}\Big[\tau_c^{-1}\tilde{\hat{g}}_{\vec{k}}(x) + \frac{1}{2}\tau_s^{-1}\left(\sigma_z\tilde{g}_{\vec{k}}(x) + \mathbb{1}\tilde{g}^z_{\vec{k}}(x)\right)\Big],
\end{aligned} \tag{5.190}$$

where we employed the anticommutation relation of the Pauli matrices as given in Eq. (A.3).
The spin-flip term transforms according to

$$\begin{aligned}
\mathcal{U}\frac{^{\text{sf}}\hat{g}_{\vec{k}}(x)}{\tau_{\text{sf}}}\mathcal{U}^\dagger &= \frac{1}{2\tau_{\text{sf}}}\mathcal{U}\vec{g}_{\vec{k}}(x)\vec{\sigma}\mathcal{U}^\dagger \\
&= \frac{1}{2\tau_{\text{sf}}}\tilde{\vec{g}}_{\vec{k}}(x)\vec{\sigma} \\
&= \frac{^{\text{sf}}\tilde{\hat{g}}_{\vec{k}}(x)}{\tau_{\text{sf}}}.
\end{aligned} \tag{5.191}$$

The precession term turns into

$$\begin{aligned}
-\frac{\gamma}{2i}\mathcal{U}[\vec{\sigma}\vec{m}(x),\hat{g}_{\vec{k}}(x)]\mathcal{U}^\dagger &= -\frac{\gamma}{2i}[\mathcal{U}\vec{\sigma}\vec{m}(x)\mathcal{U}^\dagger,\mathcal{U}\hat{g}_{\vec{k}}(x)\mathcal{U}^\dagger] \\
&= -\frac{\gamma}{2i}[\sigma_z,\tilde{\hat{g}}_{\vec{k}}(x)] \\
&= -\frac{\gamma}{4i}\left([\sigma_z,\mathbb{1}]\tilde{g}_{\vec{k}}(x)+[\sigma_z,\vec{\sigma}]\tilde{\vec{g}}_{\vec{k}}(x)\right) \\
&= -\frac{\gamma}{4i}2i\epsilon_{z\mu\nu}\tilde{g}^{\mu}_{\vec{k}}(x)\sigma_\nu \\
&= -\frac{\gamma}{2}\left(\tilde{g}^{x}_{\vec{k}}(x)\sigma_y-\tilde{g}^{y}_{\vec{k}}(x)\sigma_x\right). \qquad (5.192)
\end{aligned}$$

The spatial derivative of the magnetization term transforms as follows

$$\begin{aligned}
\frac{J_{\text{sd}}}{2\hbar}\mathcal{U}\{\partial_x(\vec{\sigma}\vec{m}(x)),\partial_{k_x}\hat{g}_{\vec{k}}(x)\}\mathcal{U}^\dagger &= \frac{J_{\text{sd}}}{2\hbar}\{\mathcal{U}\partial_x(\vec{\sigma}\vec{m}(x))\mathcal{U}^\dagger,\mathcal{U}\partial_{k_x}\hat{g}_{\vec{k}}(x)\mathcal{U}^\dagger\} \\
&= \frac{J_{\text{sd}}}{2\hbar}\{\mathcal{U}\partial_x(\vec{\sigma}\vec{m}(x))\mathcal{U}^\dagger,\partial_{k_x}\mathcal{U}\hat{g}_{\vec{k}}(x)\mathcal{U}^\dagger\} \\
&= \frac{J_{\text{sd}}}{2\hbar}\{\frac{d\phi(x)}{dx}\sigma_y,\partial_{k_x}\tilde{\hat{g}}_{\vec{k}}(x)\} \\
&= \frac{J_{\text{sd}}}{4\hbar}\frac{d\phi(x)}{dx}\left(\{\sigma_y,\mathbb{1}\}\partial_{k_x}\tilde{g}_{\vec{k}}(x)+\{\sigma_y,\vec{\sigma}\}\partial_{k_x}\tilde{\vec{g}}_{\vec{k}}(x)\right) \\
&= \frac{J_{\text{sd}}}{2\hbar}\frac{d\phi(x)}{dx}\left(\sigma_y\partial_{k_x}\tilde{g}_{\vec{k}}(x)+\mathbb{1}\partial_{k_x}\tilde{g}^{y}_{\vec{k}}(x)\right) \\
&= \frac{1}{2\tau_{\text{sd}}}\frac{d\phi(x)}{dx}\left(\sigma_y\partial_{k_x}\tilde{g}_{\vec{k}}(x)+\mathbb{1}\partial_{k_x}\tilde{g}^{y}_{\vec{k}}(x)\right), \qquad (5.193)
\end{aligned}$$

where we employed relation (5.181) and that the gauge transformation is independent of $\vec{k}$ (cf. definition of $\mathcal{U}$ in Eq. (5.179)). Finally the electric field term remains to be transformed

$$\begin{aligned}
ev_xE_x\mathcal{U}\left(\partial_\epsilon\hat{f}_{\text{eq}}(\vec{m}(x),\epsilon)\right)\mathcal{U}^\dagger &= \frac{e}{2}v_xE_x\partial_\epsilon\Big(f^{\text{charge}}(\epsilon,J_{\text{sd}})\mathcal{U}\mathbb{1}\mathcal{U}^\dagger \\
&\quad + J_{\text{sd}}\partial_{J_{\text{sd}}}f^{\text{spin}}(\epsilon,J_{\text{sd}})\mathcal{U}\vec{m}(x)\vec{\sigma}\mathcal{U}^\dagger\Big) \\
&= \frac{e}{2}v_xE_x\Big(\partial_\epsilon f^{\text{charge}}(\epsilon,J_{\text{sd}})\mathbb{1}-J_{\text{sd}}\partial^2_\epsilon f^{\text{charge}}(\epsilon,J_{\text{sd}})\sigma_z\Big) \\
&= \frac{e}{2}v_xE_x\Big(\partial_\epsilon f^{\text{charge}}(\epsilon,J_{\text{sd}})\mathbb{1}-\frac{\hbar}{\tau_{\text{sd}}}\partial^2_\epsilon f^{\text{charge}}(\epsilon,J_{\text{sd}})\sigma_z\Big). \qquad (5.194)
\end{aligned}$$

Collecting the individual results from Eqns. (5.189) to (5.194) yields the general gauge transformed kinetic equation

$$\begin{aligned}
&\left(v_x\partial_x\tilde{g}_{\vec{k}}(x)+\frac{1}{2\tau_c}\tilde{g}_{\vec{k}}(x)+\frac{1}{\tau_{\text{sd}}}\frac{d\phi(x)}{dx}\partial_{k_x}\tilde{g}^y_{\vec{k}}(x)+\frac{1}{2\tau_s}\tilde{g}^z_{\vec{k}}(x)\right)\mathbb{1}\\
&\quad+\left(v_x\partial_x\tilde{g}^x_{\vec{k}}(x)+\frac{1}{\tilde{\tau}}\tilde{g}^x_{\vec{k}}(x)+\gamma\tilde{g}^y_{\vec{k}}(x)\right)\sigma_x\\
&\quad+\left(v_x\partial_x\tilde{g}^y_{\vec{k}}(x)+\frac{1}{\tau_{\text{sd}}}\frac{d\phi(x)}{dx}\partial_{k_x}\tilde{g}_{\vec{k}}(x)-\gamma\tilde{g}^x_{\vec{k}}(x)+\frac{1}{\tilde{\tau}}\tilde{g}^y_{\vec{k}}(x)+v_x\frac{d\phi(x)}{dx}\tilde{g}^z_{\vec{k}}(x)\right)\sigma_y\\
&\quad+\left(v_x\partial_x\tilde{g}^z_{\vec{k}}(x)+\frac{1}{2\tau_s}\tilde{g}_{\vec{k}}(x)-v_x\frac{d\phi(x)}{dx}\tilde{g}^y_{\vec{k}}(x)+\frac{1}{\tilde{\tau}}\tilde{g}^z_{\vec{k}}(x)\right)\sigma_z\\
&=ev_xE_x\Big(\partial_\epsilon f^{\text{charge}}(\epsilon,J_{\text{sd}})\mathbb{1}-\frac{\hbar}{\tau_{\text{sd}}}\partial^2_\epsilon f^{\text{charge}}(\epsilon,J_{\text{sd}})\sigma_z\Big),
\end{aligned}\tag{5.195}$$

where we introduced the abbreviation $\frac{1}{\tilde{\tau}}\equiv\frac{1}{2\tau_c}+\frac{1}{\tau_{\text{sf}}}$.
Now we want to employ the vector notation of the charge and the three components of the macroscopic spin distribution function $\vec{\tilde{g}}_{\vec{k}}(x)=\{\tilde{g}_{\vec{k}}(x),\tilde{\vec{g}}_{\vec{k}}(x)\}^T=\{\tilde{g}_{\vec{k}}(x),\tilde{g}^x_{\vec{k}}(x),\tilde{g}^y_{\vec{k}}(x),\tilde{g}^z_{\vec{k}}(x)\}^T$. They are obtained by taking the expectation value in Pauli spin space by means of the relation (5.8). Then Eq. (5.195) can be written in a compact matrix notation as follows

$$\begin{aligned}
&v_x\partial_x\begin{pmatrix}\tilde{g}_{\vec{k}}(x)\\ \tilde{g}^x_{\vec{k}}(x)\\ \tilde{g}^y_{\vec{k}}(x)\\ \tilde{g}^z_{\vec{k}}(x)\end{pmatrix}+\begin{pmatrix}\frac{1}{2\tau_c} & 0 & \frac{1}{\tau_{\text{sd}}}\frac{d\phi(x)}{dx}\partial_{k_x} & \frac{1}{2\tau_s}\\ 0 & \frac{1}{\tilde{\tau}} & \gamma & 0\\ \frac{1}{\tau_{\text{sd}}}\frac{d\phi(x)}{dx}\partial_{k_x} & -\gamma & \frac{1}{\tilde{\tau}} & v_x\frac{d\phi(x)}{dx}\\ \frac{1}{2\tau_s} & 0 & -v_x\frac{d\phi(x)}{dx} & \frac{1}{\tilde{\tau}}\end{pmatrix}\begin{pmatrix}\tilde{g}_{\vec{k}}(x)\\ \tilde{g}^x_{\vec{k}}(x)\\ \tilde{g}^y_{\vec{k}}(x)\\ \tilde{g}^z_{\vec{k}}(x)\end{pmatrix}\\
&=ev_xE_x\begin{pmatrix}\partial_\epsilon f^{\text{charge}}(\epsilon,J_{\text{sd}})\\ 0\\ 0\\ -\frac{\hbar}{\tau_{\text{sd}}}\partial^2_\epsilon f^{\text{charge}}(\epsilon,J_{\text{sd}})\end{pmatrix}.
\end{aligned}\tag{5.196}$$

With the help of the relation $\gamma=\frac{2J_{\text{sd}}}{\hbar}=\frac{2}{\tau_{\text{sd}}}$ Eq. (5.196) turns into

$$\begin{aligned}
&v_x\partial_x\vec{\tilde{g}}_{\vec{k}}(x)+\begin{pmatrix}\frac{1}{2\tau_c} & 0 & 0 & \frac{1}{2\tau_s}\\ 0 & \frac{1}{\tilde{\tau}} & \frac{2}{\tau_{\text{sd}}} & 0\\ 0 & -\frac{2}{\tau_{\text{sd}}} & \frac{1}{\tilde{\tau}} & 0\\ \frac{1}{2\tau_s} & 0 & 0 & \frac{1}{\tilde{\tau}}\end{pmatrix}\vec{\tilde{g}}_{\vec{k}}(x)\\
&\quad+v_x\frac{d\phi(x)}{dx}\begin{pmatrix}0&0&0&0\\0&0&0&0\\0&0&0&1\\0&0&-1&0\end{pmatrix}\vec{\tilde{g}}_{\vec{k}}(x)+\frac{\hbar v_x}{\tau_{\text{sd}}}\frac{d\phi(x)}{dx}\begin{pmatrix}0&0&1&0\\0&0&0&0\\1&0&0&0\\0&0&0&0\end{pmatrix}\partial_\epsilon\vec{\tilde{g}}_{\vec{k}}(x)\\
&=ev_xE_x\begin{pmatrix}\partial_\epsilon f^{\text{charge}}(\epsilon,J_{\text{sd}})\\ 0\\ 0\\ -\frac{\hbar}{\tau_{\text{sd}}}\partial^2_\epsilon f^{\text{charge}}(\epsilon,J_{\text{sd}})\end{pmatrix}.
\end{aligned}\tag{5.197}$$

In Eq. (5.197) we employ the vector notation of the charge and the three components of the macroscopic spin distribution function $\vec{\tilde{g}}_{\vec{k}}(x) = \{\tilde{g}_{\vec{k}}(x), \tilde{g}^x_{\vec{k}}(x), \tilde{g}^y_{\vec{k}}(x), \tilde{g}^z_{\vec{k}}(x)\}^T$. Equation (5.197) is the non-equilibrium kinetic equation that is valid for general one-dimensional domain-wall profiles. Besides the drift, diffusion and relaxation terms, two terms proportional to the magnetization twist $\partial_x\phi(x)$ arise as a consequence of the gauge-transformation. The second of these terms contains an energy derivative and thus characterizes the influence of the band-structure due to non-adiabaticity. In the extreme adiabatic limit ($\partial_x\phi(x) \to 0$) these contributions vanish.
Equation (5.197) is still a very involved equation due to the simultaneous spatial and energy derivative. In dependence of the complexity of the wall type, Eq. (5.197) has to be solved numerically. In this case, Eq. (5.197) is the starting point for a numerical implementation. However, in the next chapter we want to pursue a different approach and focus on the simplest domain wall type that allows for an analytical treatment.

5.5.5 Perturbative solution of the kinetic equation for a domain wall

To obtain analytical results, we now solve the kinetic equation (5.196) for the simplest domain-wall profile: a 180° linear domain wall. We believe that even this simplest wall type comprises the essential physics. A linear wall is parametrized by

$$\begin{aligned} \phi(x) &= \frac{\pi}{\lambda}x, \quad 0 \leq x \leq \lambda, \\ \theta &= \frac{\pi}{2} = const., \end{aligned} \tag{5.198}$$

where λ constitutes the domain-wall width, usually a compromise between exchange energy A and the shape-anisotropy energy K: $\lambda = \sqrt{A/K}$. The linear wall specified in Eq. (5.198) is a finite part of an one-dimensional spin spiral with constant magnetization twist [63]

$$\partial_x\phi(x) = \frac{\pi}{\lambda} = const.. \tag{5.199}$$

Note that the local gauge potential becomes constant in this case and the gauge transformation (5.179) corresponds to a global $U(1)$ gauge transformation. The constant gradient in Eq. (5.199) removes the explicit spatial dependence from the kinetic equation (5.196). This yields an enormous simplification of the calculations and provides the possibility to obtain analytical results. In view of the huge parameter space, analytical solutions are eligible as they provide the possibility to study the transition between different transport regimes.

In the case of a linear wall the kinetic equation (5.197) reads

$$
\begin{aligned}
&v_x\partial_x \begin{pmatrix} \tilde{g}_{\vec{k}}(x) \\ \tilde{g}^x_{\vec{k}}(x) \\ \tilde{g}^y_{\vec{k}}(x) \\ \tilde{g}^z_{\vec{k}}(x) \end{pmatrix} + \begin{pmatrix} \frac{1}{2\tau_c} & 0 & 0 & \frac{1}{2\tau_s} \\ 0 & \frac{1}{\tilde{\tau}} & \frac{2}{\tau_{\text{sd}}} & 0 \\ 0 & -\frac{2}{\tau_{\text{sd}}} & \frac{1}{\tilde{\tau}} & 0 \\ \frac{1}{2\tau_s} & 0 & 0 & \frac{1}{\tilde{\tau}} \end{pmatrix} \begin{pmatrix} \tilde{g}_{\vec{k}}(x) \\ \tilde{g}^x_{\vec{k}}(x) \\ \tilde{g}^y_{\vec{k}}(x) \\ \tilde{g}^z_{\vec{k}}(x) \end{pmatrix} \\
&\quad + \frac{1}{\lambda}\left[\pi v_x \begin{pmatrix} 0 & 0 & 0 & 0 \\ 0 & 0 & 0 & 0 \\ 0 & 0 & 0 & 1 \\ 0 & 0 & -1 & 0 \end{pmatrix} \begin{pmatrix} \tilde{g}_{\vec{k}}(x) \\ \tilde{g}^x_{\vec{k}}(x) \\ \tilde{g}^y_{\vec{k}}(x) \\ \tilde{g}^z_{\vec{k}}(x) \end{pmatrix} + \frac{\pi}{\tau_{\text{sd}}} \begin{pmatrix} 0 & 0 & 1 & 0 \\ 0 & 0 & 0 & 0 \\ 1 & 0 & 0 & 0 \\ 0 & 0 & 0 & 0 \end{pmatrix} \partial_{k_x} \begin{pmatrix} \tilde{g}_{\vec{k}}(x) \\ \tilde{g}^x_{\vec{k}}(x) \\ \tilde{g}^y_{\vec{k}}(x) \\ \tilde{g}^z_{\vec{k}}(x) \end{pmatrix} \right] \\
&= ev_xE_x \begin{pmatrix} \partial_\epsilon f^{\text{charge}}(\epsilon, J_{\text{sd}}) \\ 0 \\ 0 \\ -\frac{\hbar}{\tau_{\text{sd}}}\partial^2_\epsilon f^{\text{charge}}(\epsilon, J_{\text{sd}}) \end{pmatrix}.
\end{aligned}
\tag{5.200}
$$

The thickness of the wall λ is an important parameter, as it governs the coupling between the domain wall and the conduction electrons. From Eq. (5.200) different regimes naturally emerge that depend on the domain-wall width λ. For wide walls ($\lambda \to \infty$) the spin of the conduction electron follows the magnetization of the domain wall adiabatically and the change in momentum is negligibly small. For smaller wall widths, we perturbatively approach the regime of narrow domain walls. The spatial variations become important and the spin of the conduction electron cannot longer follow the magnetization adiabatically. The consequence is a finite change in momentum that causes an intrinsic domain-wall resistivity and a momentum transfer. For sharp walls ($\lambda \to 0$), the spatial variations are unimportant as the change in momentum due to scattering at the domain wall entirely determines the magnetotransport. This regime is entirely dominated by the band structure. The main points are summarized in Table 5.2.

Even in one spatial dimension the general non-equilibrium kinetic equation (5.200) is a complicated partial differential equation in space and momentum and domain-wall magnetotransport constitutes an involved problem. To solve this, we will perform a series expansion of the non-equilibrium distribution matrix in inverse powers of the wall width. The physical idea behind this perturbative expansion is to perform a perturbation expansion around the perfect adiabatic limit with infinitively small slope ($\lambda \to \infty$). The expansion takes place in the magnetization twist that characterizes the twist of the magnetization texture in terms of inverse powers of the domain-wall width (cf. Eq. (5.199)). To check the regime of validity concerning such a perturbative expansion in λ^{-1}, a dimensional analysis is required. The necessary condition for the perturbative expansion follows from the kinetic equa-

tion (5.200)

$$\begin{aligned}\frac{1}{\lambda}\left(v_x + v_x J_{\text{sd}}\partial_\epsilon\right) &\ll \left(v_x\partial_x + \frac{1}{\tau}\right)\\ \frac{v_x\tau}{\lambda} &\ll \frac{1+v_x\tau\partial_x}{1+J_{\text{sd}}\partial_\epsilon}\\ \frac{v_x\tau}{\lambda} &\ll \frac{1+\frac{v_x\tau}{v_x\tau}}{1+\frac{J_{\text{sd}}}{\epsilon_{\text{F}}}}\\ \frac{v_x\tau}{\lambda} &\ll 2+\mathcal{O}(\frac{J_{\text{sd}}}{\epsilon_{\text{F}}}),\end{aligned} \tag{5.201}$$

where τ stands for the characteristic time scale of the system associated with the the mean free path or the coherence length. The spatial variations are set by $\partial_x \sim (v_x\tau)^{-1}$. To perform a dimensionless perturbative expansion, we will pursue an expansion in the parameter

$$\kappa = \frac{l_{\text{mfp}}}{\lambda}, \tag{5.202}$$

where l_{mfp} is the mean free path set either by the collisions $v_{\text{F}}\tau_c$ or the sd precession $v_{\text{F}}\tau_{\text{sd}}$. The considerations in Eq. (5.201) confirm the conjecture that a perturbative solution of the kinetic equation in inverse powers of the wall width is appropriate for $\kappa \ll 1$, i.e., as long as the domain-wall width does not exceed the mean free path. This restricts the validity of our approach to diffusive charge transport. Note that an expansion in κ corresponds to a perturbative expansion in the gauge field $A(x) \propto \partial_x\phi(x) \propto 1/\lambda$ (cf. Eqns. (5.184) and (5.199)) that comprises the twist of the magnetization texture due to the domain wall. [58] The final results will be independent of l_{mfp} and the identification of l_{mfp} will take place in the retrospective when examining the macroscopic variables.
In perspective of a perturbative treatment, we rearrange the kinetic equation for a linear domain wall (5.200) as follows

$$l_{\text{mfp}}\left(v_x\partial_x + \mathcal{A}\right)\vec{\tilde{g}}_{\vec{k}}(x) + \kappa\left(v_x\mathcal{B} + \mathcal{C}\partial_{k_x}\right)\vec{\tilde{g}}_{\vec{k}}(x) = l_{\text{mfp}}v_xE_x\vec{\mathcal{D}}(\epsilon), \tag{5.203}$$

where we employ the definitions

$$\mathcal{A} = \begin{pmatrix} \frac{1}{2\tau_c} & 0 & 0 & \frac{1}{2\tau_s}\\ 0 & \frac{1}{\tilde{\tau}} & \frac{2}{\tau_{\text{sd}}} & 0\\ 0 & -\frac{2}{\tau_{\text{sd}}} & \frac{1}{\tilde{\tau}} & 0\\ \frac{1}{2\tau_s} & 0 & 0 & \frac{1}{\tilde{\tau}}\end{pmatrix}, \tag{5.204}$$

$$\mathcal{B} = \pi\begin{pmatrix} 0 & 0 & 0 & 0\\ 0 & 0 & 0 & 0\\ 0 & 0 & 0 & 1\\ 0 & 0 & -1 & 0\end{pmatrix}, \tag{5.205}$$

$$\mathcal{C} = \frac{\pi}{\tau_{\text{sd}}}\begin{pmatrix} 0 & 0 & 1 & 0\\ 0 & 0 & 0 & 0\\ 1 & 0 & 0 & 0\\ 0 & 0 & 0 & 0\end{pmatrix}, \tag{5.206}$$

$$\vec{\mathcal{D}}(\epsilon) = e \begin{pmatrix} \partial_\epsilon f^{\text{charge}}(\epsilon, J_{\text{sd}}) \\ 0 \\ 0 \\ -\frac{\hbar}{\tau_{\text{sd}}} \partial_\epsilon^2 f^{\text{charge}}(\epsilon, J_{\text{sd}}) \end{pmatrix}. \tag{5.207}$$

The matrix $\mathcal{A}$ in Eq. (5.204) determines the homogeneous solution of the kinetic equation and exhibits a block-diagonal form if we exchange the last with the central lines. The transverse channels $\tilde{g}^x_{\vec{k}}(x), \tilde{g}^y_{\vec{k}}(x)$ that are given by the second and third columns in the matrix notation decouple from the charge $\tilde{g}_{\vec{k}}(x)$ (first column) and longitudinal $\tilde{g}^z_{\vec{k}}(x)$ (fourth column) channels. The matrices $\mathcal{B}$ (5.205) and $\mathcal{C}$ (5.206) originate from the gauge transformation and are thus associated with the magnetization twist that comprises the spatial variations and couples the otherwise block-diagonal channels.
A perturbative expansion in κ fulfills the ansatz

$$\vec{\tilde{g}}_{\vec{k}}(x) = \sum_{i=0}^{\infty} \kappa^i \vec{\tilde{g}}^{(i)}_{\vec{k}}(x) = \vec{\tilde{g}}^{(0)}_{\vec{k}}(x) + \kappa \vec{\tilde{g}}^{(1)}_{\vec{k}}(x) + \kappa^2 \vec{\tilde{g}}^{(2)}_{\vec{k}}(x) + \dots, \tag{5.208}$$

where we truncate the expansion after the second order. Inserting the ansatz (5.208) into the kinetic equation (5.203) yields the result up to $\mathcal{O}(\kappa^3)$

$$\begin{aligned} &\left(l_{\text{mfp}} v_x \partial_x \vec{\tilde{g}}^{(0)}_{\vec{k}}(x) + l_{\text{mfp}} \mathcal{A} \vec{\tilde{g}}^{(0)}_{\vec{k}}(x) - l_{\text{mfp}} v_x E_x \vec{\mathcal{D}}(\epsilon) \right) \\ &+ \kappa \left(l_{\text{mfp}} v_x \partial_x \vec{\tilde{g}}^{(1)}_{\vec{k}}(x) + l_{\text{mfp}} \mathcal{A} \vec{\tilde{g}}^{(1)}_{\vec{k}}(x) + v_x \mathcal{B} \vec{\tilde{g}}^{(0)}_{\vec{k}}(x) + \mathcal{C} \partial_{k_x} \vec{\tilde{g}}^{(0)}_{\vec{k}}(x) \right) \\ &+ \kappa^2 \left(l_{\text{mfp}} v_x \partial_x \vec{\tilde{g}}^{(2)}_{\vec{k}}(x) + l_{\text{mfp}} \mathcal{A} \vec{\tilde{g}}^{(2)}_{\vec{k}}(x) + v_x \mathcal{B} \vec{\tilde{g}}^{(1)}_{\vec{k}}(x) + \mathcal{C} \partial_{k_x} \vec{\tilde{g}}^{(1)}_{\vec{k}}(x) \right) \\ &+ \mathcal{O}(\kappa^3) = 0. \end{aligned} \tag{5.209}$$

As will be shown in the following, the particularity of the perturbative approach is that every order of the expansion in Eq. (5.209) can be associated with a physical process. Thus instead of solving the kinetic equation numerically in a brute force manner, every order of the expansion supplies us with a clear semiclassical interpretation of the involved physical processes.

5.5.5.1 Zeroth-order solution – the perfect adiabatic limit

In the zeroth-order approximation, i.e., the perfect adiabatic limit, we expect to reproduce the monodomain result without transverse magnetization of the conduction electrons. Transverse components $\{\partial_x \vec{m}(x), \vec{m}(x) \times \partial_x \vec{m}(x)\}$ vanish in the limit of an infinite domain wall due to its vanishing slope ($\lambda \to \infty$, $\kappa \to 0$). Here, the zeroth-order approximation is exact. The spin of the conduction electron is able to follow the local magnetization in perfect adiabaticity and no mixing of the majority, minority spin channels occurs.
Gathering all terms $\propto \kappa^0$ from Eq. (5.209) yields

$$v_x \partial_x \vec{\tilde{g}}^{(0)}_{\vec{k}}(x) + \mathcal{A} \vec{\tilde{g}}^{(0)}_{\vec{k}}(x) = v_x E_x \vec{\mathcal{D}}(\epsilon). \tag{5.210}$$

Equation (5.210) reads in components

$$v_x\partial_x \begin{pmatrix} {}^{(0)}\tilde{g}_{\vec{k}}(x) \\ {}^{(0)}\tilde{g}^x_{\vec{k}}(x) \\ {}^{(0)}\tilde{g}^y_{\vec{k}}(x) \\ {}^{(0)}\tilde{g}^z_{\vec{k}}(x) \end{pmatrix} + \begin{pmatrix} \frac{1}{2\tau_c} & 0 & 0 & \frac{1}{2\tau_s} \\ 0 & \frac{1}{\tilde{\tau}} & \frac{2}{\tau_{\text{sd}}} & 0 \\ 0 & -\frac{2}{\tau_{\text{sd}}} & \frac{1}{\tilde{\tau}} & 0 \\ \frac{1}{2\tau_s} & 0 & 0 & \frac{1}{\tilde{\tau}} \end{pmatrix} \begin{pmatrix} {}^{(0)}\tilde{g}_{\vec{k}}(x) \\ {}^{(0)}\tilde{g}^x_{\vec{k}}(x) \\ {}^{(0)}\tilde{g}^y_{\vec{k}}(x) \\ {}^{(0)}\tilde{g}^z_{\vec{k}}(x) \end{pmatrix} = ev_xE_x \begin{pmatrix} \partial_\epsilon f^{\text{charge}}(\epsilon, J_{\text{sd}}) \\ 0 \\ 0 \\ -\frac{\hbar}{\tau_{\text{sd}}}\partial^2_\epsilon f^{\text{charge}}(\epsilon, J_{\text{sd}}) \end{pmatrix}. \tag{5.211}$$

A reordering of Eq. (5.211) yields

$$v_x\partial_x \begin{pmatrix} {}^{(0)}\tilde{g}_{\vec{k}}(x) \\ {}^{(0)}\tilde{g}^z_{\vec{k}}(x) \\ {}^{(0)}\tilde{g}^x_{\vec{k}}(x) \\ {}^{(0)}\tilde{g}^y_{\vec{k}}(x) \end{pmatrix} + \begin{pmatrix} \frac{1}{2\tau_c} & \frac{1}{2\tau_s} & 0 & 0 \\ \frac{1}{2\tau_s} & \frac{1}{\tilde{\tau}} & 0 & 0 \\ 0 & 0 & \frac{1}{\tilde{\tau}} & \frac{2}{\tau_{\text{sd}}} \\ 0 & 0 & -\frac{2}{\tau_{\text{sd}}} & \frac{1}{\tilde{\tau}} \end{pmatrix} \begin{pmatrix} {}^{(0)}\tilde{g}_{\vec{k}}(x) \\ {}^{(0)}\tilde{g}^z_{\vec{k}}(x) \\ {}^{(0)}\tilde{g}^x_{\vec{k}}(x) \\ {}^{(0)}\tilde{g}^y_{\vec{k}}(x) \end{pmatrix} = ev_xE_x \begin{pmatrix} \partial_\epsilon f^{\text{charge}}(\epsilon, J_{\text{sd}}) \\ -\frac{\hbar}{\tau_{\text{sd}}}\partial^2_\epsilon f^{\text{charge}}(\epsilon, J_{\text{sd}}) \\ 0 \\ 0 \end{pmatrix}, \tag{5.212}$$

and exhibits explicitly the block diagonal structure of the zeroth order. As expected the transverse magnetization dynamics decouples from the charge and longitudinal dynamics. Equation (5.212) can be simplified by means of a complexification of the transverse components

$$\tilde{g}^{\text{trans}}_{\vec{k}}(x) := \tilde{g}^x_{\vec{k}}(x) + i\tilde{g}^y_{\vec{k}}(x). \tag{5.213}$$

This leads to

$$\begin{aligned} v_x\partial_x \begin{pmatrix} {}^{(0)}\tilde{g}_{\vec{k}}(x) \\ {}^{(0)}\tilde{g}^z_{\vec{k}}(x) \\ {}^{(0)}\tilde{g}^{\text{trans}}_{\vec{k}}(x) \end{pmatrix} + \begin{pmatrix} \frac{1}{2\tau_c} & \frac{1}{2\tau_s} & 0 \\ \frac{1}{2\tau_s} & \frac{1}{\tilde{\tau}} & 0 \\ 0 & 0 & \left(\frac{1}{\tilde{\tau}} - i\frac{2}{\tau_{\text{sd}}}\right) \end{pmatrix} \begin{pmatrix} {}^{(0)}\tilde{g}_{\vec{k}}(x) \\ {}^{(0)}\tilde{g}^z_{\vec{k}}(x) \\ {}^{(0)}\tilde{g}^{\text{trans}}_{\vec{k}}(x) \end{pmatrix} \\ = ev_xE_x \begin{pmatrix} \partial_\epsilon f^{\text{charge}}(\epsilon, J_{\text{sd}}) \\ -\frac{\hbar}{\tau_{\text{sd}}}\partial^2_\epsilon f^{\text{charge}}(\epsilon, J_{\text{sd}}) \\ 0 \end{pmatrix}. \end{aligned} \tag{5.214}$$

As the transverse components decouple from the charge and longitudinal components, it can be solved according to

$${}^{(0)}\tilde{g}^{\text{trans}}_{\vec{k}}(x) = const. \cdot e^{-\frac{\left(\frac{1}{\tilde{\tau}} - i\frac{2}{\tau_{\text{sd}}}\right)x}{v_x}}. \tag{5.215}$$

From the boundary condition $\tilde{g}^{\text{trans}}_{\vec{k}}(0) = 0$, it immediately follows

$${}^{(0)}\tilde{g}^{\text{trans}}_{\vec{k}}(x) = 0. \tag{5.216}$$

As expected, there is no transverse magnetization in $\mathcal{O}(\kappa^0)$. The result (5.216) agrees with symmetry considerations: The spin-transfer torque is sensitive to the sense of rotation of the local moments within the domain wall and thus of $\mathcal{O}(\kappa^1)$. In absence of the magnetization twist, no transverse magnetization dynamics and therefore no spin-transfer torque takes place (cf. section 5.2).

With the elimination of the transverse components, we end up with two coupled equations for the zeroth-order charge and collinear spin distributions

$$v_x\partial_x\begin{pmatrix}{}^{(0)}\tilde{g}_{\vec{k}}(x)\\ {}^{(0)}\tilde{g}^z_{\vec{k}}(x)\end{pmatrix}+\begin{pmatrix}\frac{1}{2\tau_c} & \frac{1}{2\tau_s}\\ \frac{1}{2\tau_s} & \frac{1}{\tilde{\tau}}\end{pmatrix}\begin{pmatrix}{}^{(0)}\tilde{g}_{\vec{k}}(x)\\ {}^{(0)}\tilde{g}^z_{\vec{k}}(x)\end{pmatrix}=ev_xE_x\begin{pmatrix}\partial_\epsilon f^{\text{charge}}\\ -\frac{\hbar}{\tau_{\text{sd}}}\partial^2_\epsilon f^{\text{charge}}(\epsilon,J_{\text{sd}})\end{pmatrix}. \quad (5.217)$$

Equation (5.217) recovers exactly the equations that constitute the two-current model for a homogeneous monodomain (cf. Eq. (5.56)). Accordingly, the spatially homogeneous zeroth-order solutions reads after a decoupling of Eq. (5.217)

$${}^{(0)}\tilde{g}_{\vec{k}}=\frac{2e\tau_c\tau_s\left[\hbar\tau_c\tau_{\text{sf}}\partial^2_\epsilon f^{\text{charge}}(\epsilon,J_{\text{sd}})+\tau_s\tau_{\text{sd}}(2\tau_c+\tau_{\text{sf}})\partial_\epsilon f^{\text{charge}}(\epsilon,J_{\text{sd}})\right]}{\tau_{\text{sd}}\left[2\tau_c\tau_s^2+\tau_{\text{sf}}\left(\tau_s^2-\tau_c^2\right)\right]}v_xE_x, \quad (5.218)$$

$${}^{(0)}\tilde{g}^z_{\vec{k}}=-\frac{2e\tau_c\tau_s\tau_{\text{sf}}\left[\hbar\tau_s\partial^2_\epsilon f^{\text{charge}}(\epsilon,J_{\text{sd}})+\tau_c\tau_{\text{sd}}\partial_\epsilon f^{\text{charge}}(\epsilon,J_{\text{sd}})\right]}{\tau_{\text{sd}}\left[2\tau_c\tau_s^2+\tau_{\text{sf}}\left(\tau_s^2-\tau_c^2\right)\right]}v_xE_x. \quad (5.219)$$

Equations (5.218) and (5.219) coincide with the spatially independent non-equilibrium distributions of the two-current model (5.68) and (5.69). With the help of the polarization given in Eq. (5.92), the electric current and the spin current read

$$\begin{aligned}j^{(0)}_{\text{charge}}&=-e\int\frac{d^3k}{(2\pi)^3}v_x^{(0)}\tilde{g}_{\vec{k}}\\&=\frac{e^2\left[\hbar N(\epsilon_{\text{F}})\tau_{\text{sf}}(\tau^\uparrow-\tau^\downarrow)+n\tau_{\text{sd}}(\tau_{\text{sf}}\tau^\uparrow+\tau^\downarrow(\tau_{\text{sf}}+2\tau^\uparrow))\right]}{m\tau_{\text{sd}}(\tau^\uparrow+\tau^\downarrow+2\tau_{\text{sf}})}E_x\\&=\frac{e^2n\left[((1+P)\tau^\uparrow+(1-P)\tau^\downarrow)\tau_{\text{sf}}+2\tau^\uparrow\tau^\downarrow\right]}{m(\tau^\uparrow+\tau^\downarrow+2\tau_{\text{sf}})}E_x, \quad (5.220)\\ j^{(0)}_{\text{spin}}&=-\mu_{\text{B}}\int\frac{d^3k}{(2\pi)^3}v_x^{(0)}\tilde{g}^z_{\vec{k}}\\&=\frac{\mu_{\text{B}}}{e}\frac{e^2\tau_{\text{sf}}\left[n\tau_{\text{sd}}(\tau^\uparrow-\tau^\downarrow)+\hbar N(\epsilon_{\text{F}})(\tau^\uparrow+\tau^\downarrow)\right]}{m\tau_{\text{sd}}(\tau^\uparrow+\tau^\downarrow+2\tau_{\text{sf}})}E_x\\&=\frac{\mu_{\text{B}}}{e}\frac{e^2n\tau_{\text{sf}}\left[(1+P)\tau^\uparrow-(1-P)\tau^\downarrow\right]}{m(\tau^\uparrow+\tau^\downarrow+2\tau_{\text{sf}})}E_x. \quad (5.221)\end{aligned}$$

For an infinite domain wall the quantization axis varies spatially infinitely slowly, the spin of the conduction electron follows the local magnetization in perfect adiabaticity and the zeroth-order solutions in Eqns. (5.220) and (5.221) are spatially independent. This is in accordance with that result for the zeroth-order in Eqns. (5.220) and (5.221) coincides with the monodomain solution as given in Eqns. (5.73) and (5.74).
These considerations illustrate that the perturbative approach corresponds to an expansion around a spatially homogeneous groundstate as provided by the perfect adiabatic limit.

5.5.5.2 First-order solution – spin-transfer torque

In the preceding section, we calculated the zeroth-order solution that coincides with the spatially independent homogeneous solution

$$
{}^{(0)}\vec{\tilde{g}}_{\vec{k}} = \frac{2e\tau_c\tau_s}{\tau_{\mathrm{sd}}\left[2\tau_c\tau_s^2+\tau_{\mathrm{sf}}\left(\tau_s^2-\tau_c^2\right)\right]}v_xE_x \begin{pmatrix} \hbar\tau_c\tau_{\mathrm{sf}}\partial_\epsilon^2 f^{\mathrm{charge}}(\epsilon,J_{\mathrm{sd}})+\tau_s\tau_{\mathrm{sd}}(2\tau_c+\tau_{\mathrm{sf}})\partial_\epsilon f^{\mathrm{charge}}(\epsilon,J_{\mathrm{sd}}) \\ 0 \\ 0 \\ -\tau_{\mathrm{sf}}\left[\hbar\tau_s\partial_\epsilon^2 f^{\mathrm{charge}}(\epsilon,J_{\mathrm{sd}})+\tau_c\tau_{\mathrm{sd}}\partial_\epsilon f^{\mathrm{charge}}(\epsilon,J_{\mathrm{sd}})\right] \end{pmatrix}. \tag{5.222}
$$

The determining equation for the first-order solution follows from Eq. (5.209) by a comparison of the coefficients proportional to κ

$$
v_x\partial_x\vec{\tilde{g}}^{(1)}_{\vec{k}}(x)+\mathcal{A}\vec{\tilde{g}}^{(1)}_{\vec{k}}(x) = -l_{\mathrm{mfp}}^{-1}\left(v_x\mathcal{B}\vec{\tilde{g}}^{(0)}_{\vec{k}}+\mathcal{C}\partial_{k_x}\vec{\tilde{g}}^{(0)}_{\vec{k}}\right). \tag{5.223}
$$

The zeroth-order solution in Eq. (5.222) provides the solution of Eq. (5.223), which yields the transverse first-order components of the distribution matrix up to $\mathcal{O}(\kappa^3)$. This is a general feature of the perturbative approach: Corrections to the charge and longitudinal component emerge in even orders of κ, while transverse components are present in odd orders of κ. This perturbative feature is in accordance with physical considerations. The perturbative parameter κ is proportional to the magnetization twist (cf. Eq. (5.199)). The spin-transfer torque depends on the sense of rotation and is thus associated with odd orders of the magnetization twist. In contrast, domain-wall resistivity and momentum transfer are associated with the energy of the domain wall and cannot depend on the sign of the rotation. Thus, domain-wall resistivity and momentum transfer are associated with even orders of κ.
In the limit of wide walls ($\kappa \ll 1$), the zeroth and the first order of the κ expansion constitute the adiabatic solution in consistence with the adiabatic approximation (cf. section 5.4), where the spin of the conduction electron follows the local magnetization adiabatically and no intrinsic domain-wall resistivity or momentum transfer of the conduction electrons to the domain wall occurs. Domain-wall motion in this order of κ is possible solely due to the spin-transfer torque.
The l.h.s. of the spatial differential equation in Eq. (5.223) possesses the same structure as the l.h.s. of the zeroth-order differential equation (5.223). Thus the decomposition in transverse and longitudinal degrees of freedom that we found for the zeroth order also holds for the homogeneous first-order equation (5.214). The coupling of the majority and minority channels to the transverse distributions is provided by the magnetization twist. Note that the matrices $\mathcal{B}, \mathcal{C}$ on the r.h.s. of Eq. (5.223) originate from the gauge transformation, i.e., the magnetization twist. Accordingly, it is the spatial variations due to the presence of the domain wall that cause non-vanishing transverse distributions.
The perturbative approach offers two distinct advantages. First, the coupled partial differential equations in space and momentum reduce in every order to coupled first-order spatial differential equations and for the one-dimensional case an ordinary differential equation remains to be solved. Secondly, the transverse channels decouple in every order from the charge and longitudinal components. Thus, at least in principle the problem becomes integrable. The recursive solution procedure satisfies automatically the appropriate boundary conditions for k_x.

To proceed further on and to solve Eq. (5.223), we have to calculate $\partial_{k_x}\vec{\tilde{g}}^{(0)}_{\vec{k}}$

$$\partial_{k_x}\vec{\tilde{g}}^{(0)}_{\vec{k}} = \frac{2e\tau_c\tau_s}{\tau_{\text{sd}}\left[2\tau_c\tau_s^2+\tau_{\text{sf}}\left(\tau_s^2-\tau_c^2\right)\right]}E_x \begin{pmatrix} \hbar\Big[\frac{1}{m}\tau_s\tau_{\text{sd}}(2\tau_c+\tau_{\text{sf}})\partial_\epsilon f^{\text{charge}}(\epsilon,J_{\text{sd}}) \\ 0 \\ 0 \\ -\hbar\tau_{\text{sf}}\Big[\frac{1}{m}\tau_c\tau_{\text{sd}}\partial_\epsilon f^{\text{charge}}(\epsilon,J_{\text{sd}}) \\ +\left(\frac{\hbar}{m}\tau_c\tau_{\text{sf}}+\tau_s\tau_{\text{sd}}\left(2\tau_c+\tau_{\text{sf}}\right)v_x^2\right)\partial_\epsilon^2 f^{\text{charge}}(\epsilon,J_{\text{sd}})+\hbar\tau_c\tau_{\text{sf}}v_x^2\partial_\epsilon^3 f^{\text{charge}}(\epsilon,J_{\text{sd}})\Big] \\ 0 \\ 0 \\ +\left(\frac{\hbar}{m}\tau_s+\tau_c\tau_{\text{sd}}v_x^2\right)\partial_\epsilon^2 f^{\text{charge}}(\epsilon,J_{\text{sd}})+\hbar\tau_s v_x^2\partial_\epsilon^3 f^{\text{charge}}(\epsilon,J_{\text{sd}})\Big] \end{pmatrix}, \tag{5.224}$$

where we employed the relation

$$\frac{1}{\hbar}\partial_{k_x}\partial_\epsilon f^{\text{charge}}(\epsilon,J_{\text{sd}}) = \frac{1}{\hbar}\frac{\partial\epsilon}{\partial k_x}\partial_\epsilon^2 f^{\text{charge}}(\epsilon,J_{\text{sd}}) = v_x\partial_\epsilon^2 f^{\text{charge}}(\epsilon,J_{\text{sd}}). \tag{5.225}$$

The boundary conditions of the adjacent homogeneous domains for the charge and longitudinal components as given by Eq. (5.57) are already implemented in the zeroth-order solution. Thus in all higher orders the corresponding spatial differential equations remain to be solved with vanishing boundary conditions. A solution of Eq. (5.223) with vanishing boundary condition ($\vec{\tilde{g}}^{(1)}_{\vec{k}}(0,\lambda)=0$) at the beginning and the end of the domain wall, yields the first-order results

$$^{(1)}\tilde{g}_{\vec{k}}(x) = 0, \tag{5.226}$$

$$^{(1)}\tilde{g}^z_{\vec{k}}(x) = 0. \tag{5.227}$$

The first-order in κ does not yield a correction of the majority, minority distributions. This is in accordance with the perfect adiabatic limit. Wide walls ($\lambda\to\infty$) correspond to small values of spin mistracking ($\kappa\to 0$). In the adiabatic approximation the conduction electron spin can follow the local magnetization and no intrinsic domain-wall resistivity due to spin mistracking occurs.
A complexification of the transverse first-order distributions $^{(1)}\tilde{g}^{\text{trans}}_{\vec{k}}(x) = {}^{(1)}\tilde{g}^x_{\vec{k}}(x) + i\,{}^{(1)}\tilde{g}^y_{\vec{k}}(x)$ results in the following differential equation for the first-order transverse components

$$v_x\partial_x\,{}^{(1)}\tilde{g}^{\text{trans}}_{\vec{k}}(x) + \left(\frac{1}{\tilde{\tau}}-i\frac{2}{\tau_{\text{sd}}}\right){}^{(1)}\tilde{g}^{\text{trans}}_{\vec{k}}(x) = i\mathcal{D}(\epsilon), \tag{5.228}$$

where we employed the abbreviation

$$\mathcal{D}(\epsilon) = -\frac{2\pi e\tau_c\tau_s E_x}{l_{\text{mfp}}m\tau_{\text{sd}}^2\left(2\tau_c\tau_s^2+\tau_{\text{sf}}(\tau_s^2-\tau_c^2)\right)} \Big[\partial_\epsilon f^{\text{charge}}(\epsilon,J_{\text{sd}})\tau_{\text{sd}}(\hbar\tau_s(2\tau_c+\tau_{\text{sf}})-mv_x^2\tau_c\tau_{\text{sd}}\tau_{\text{sf}}) + \partial_\epsilon^2 f^{\text{charge}}(\epsilon,J_{\text{sd}})\hbar\left(\hbar\tau_c\tau_{\text{sf}}+2mv_x^2\tau_s\tau_{\text{sd}}\tau_c\right) + \partial_\epsilon^3 f^{\text{charge}}(\epsilon,J_{\text{sd}})\hbar^2 mv_x^2\tau_c\tau_{\text{sf}}\Big]. \tag{5.229}$$

The general solution to Eq. (5.228) reads

$$\tilde{g}^{\text{trans}}_{\vec{k}}(x) = i\frac{\mathcal{D}(\epsilon)}{\left(\frac{1}{\tilde{\tau}} - i\frac{2}{\tau_{\text{sd}}}\right)}\left(1 + F(\vec{v}_{\vec{k}})e^{-\frac{\left(\frac{1}{\tilde{\tau}} - i\frac{2}{\tau_{\text{sd}}}\right)}{v_x}x}\right). \tag{5.230}$$

The thus far arbitrary function $F(\vec{v}_{\vec{k}})$ in Eq. (5.230) is determined by the boundary conditions at the beginning ($x = 0$) and end ($x = \lambda$) of the domain wall. [235] Let us choose $\tilde{g}^{\text{trans}}_{\vec{k}}(0) = 0$ for all rightmoving transverse spins with $v_x > 0$ and accordingly $\tilde{g}^{\text{trans}}_{\vec{k}}(\lambda) = 0$ for all leftmoving transverse spins with $v_x < 0$. Then the solutions for the transverse distributions read

$$\overset{(1)}{+}\tilde{g}^{\text{trans}}_{\vec{k}}(x) = i\frac{\mathcal{D}(\epsilon)}{\left(\frac{1}{\tilde{\tau}} - i\frac{2}{\tau_{\text{sd}}}\right)}\left(1 - e^{-\frac{\left(\frac{1}{\tilde{\tau}} - i\frac{2}{\tau_{\text{sd}}}\right)}{v_x}x}\right), \qquad (v_x > 0), \tag{5.231}$$

$$\overset{(1)}{-}\tilde{g}^{\text{trans}}_{\vec{k}}(x) = i\frac{\mathcal{D}(\epsilon)}{\left(\frac{1}{\tilde{\tau}} - i\frac{2}{\tau_{\text{sd}}}\right)}\left(1 - e^{\frac{\left(\frac{1}{\tilde{\tau}} - i\frac{2}{\tau_{\text{sd}}}\right)}{v_x}(\lambda - x)}\right), \qquad (v_x < 0). \tag{5.232}$$

By employing of the Θ-function the solutions Eqns. (5.231) and (5.232) can be combined and written in a compact manner

$$\begin{aligned}
\overset{(1)}{}\tilde{g}^{\text{trans}}_{\vec{k}}(x) &= i\frac{\mathcal{D}(\epsilon)}{\left(\frac{1}{\tilde{\tau}} - i\frac{2}{\tau_{\text{sd}}}\right)}\left[\Theta(v_x)\left(1 - e^{-\frac{\left(\frac{1}{\tilde{\tau}} - i\frac{2}{\tau_{\text{sd}}}\right)}{v_x}x}\right) + \Theta(-v_x)\left(1 - e^{\frac{\left(\frac{1}{\tilde{\tau}} - i\frac{2}{\tau_{\text{sd}}}\right)}{v_x}(\lambda - x)}\right)\right] \\
&= -4\pi i\left[\Theta(v_x)\left(1 - e^{-\frac{\left(\frac{1}{\tilde{\tau}} - i\frac{2}{\tau_{\text{sd}}}\right)}{v_x}x}\right) + \Theta(-v_x)\left(1 - e^{\frac{\left(\frac{1}{\tilde{\tau}} - i\frac{2}{\tau_{\text{sd}}}\right)}{v_x}(\lambda - x)}\right)\right] \\
&\quad \frac{eE_x\tau_c^2\tau_s\tau_{\text{sf}}}{l_{\text{mfp}}m\tau_{\text{sd}}\left(2\tau_c\tau_s^2 + \tau_{\text{sf}}\left(\tau_s^2 - \tau_c^2\right)\right)\left(2\tau_c(\tau_{\text{sd}} - 2i\tau_{\text{sf}}) + \tau_{\text{sf}}\tau_{\text{sd}}\right)} \\
&\quad \Big[\partial_\epsilon f^{\text{charge}}(\epsilon, J_{\text{sd}})\tau_{\text{sd}}(\hbar\tau_s(2\tau_c + \tau_{\text{sf}}) - mv_x^2\tau_c\tau_{\text{sd}}\tau_{\text{sf}}) \\
&\quad\quad + \partial_\epsilon^2 f^{\text{charge}}(\epsilon, J_{\text{sd}})\hbar\left(\hbar\tau_c\tau_{\text{sf}} + 2mv_x^2\tau_s\tau_{\text{sd}}\tau_c\right) \\
&\quad\quad + \partial_\epsilon^3 f^{\text{charge}}(\epsilon, J_{\text{sd}})\hbar^2 mv_x^2\tau_c\tau_{\text{sf}}\Big].
\end{aligned} \tag{5.233}$$

The factorization of the spatial and the momentum dependence of the non-equilibrium distribution functions that we found for the adiabatic case in section 5.4 does not hold for Eq. (5.233) except for the limit ($\lambda \to \infty$). The intertwinement marks the departure from adiabaticity by introducing non-adiabatic corrections due to a finite domain-wall width. In the adiabatic approximation the spin resides in its majority, minority spin state during the traversal of the domain wall and the magnetotransport can be viewed to be composed of two separate electron gases for the majority and minority electrons, respectively. [236] Additionally, the majority and minority spins are subject to additional gauge potentials induced by the spatial variations in the magnetization texture. This resulted in section 5.4 in the transverse magnetization of the conduction electrons with a spatially constant angle between the spin of the conduction electron and the local moments. By decreasing the domain-wall width λ, more precisely when approaching ($\kappa \to 1$), the spin can no longer follow the local moments and does no longer reside in its initial spin state during the traversal of the domain wall. The spin channels mix and

a majority, minority spin of the adjacent homogeneous domain acquires a portion of the opposite spin component. As a consequence, the spin of the conduction electrons does not perform an adiabatic passage through the domain wall. The emergence of an opposite spin component serves as a definition of a non-adiabatic traversal through the domain wall and constitutes the reason for spin mistracking and spatial precession. [236, 237] A superposition of majority and minority spin eigenstates causes spatial oscillations. [173, 197] A non-adiabatic traversal of the domain wall introduces a spatial dependence to the transverse distribution functions according to Eq. (5.233) and thus the spin-transfer torque that is absent in the adiabatic limit (cf. section 5.4). Non-adiabatic corrections due to a finite width of the domain wall are thus comprised inherently by the presented formalism.

According to Eq. (5.3) the macroscopic magnetization of the conduction electrons follows from Eq. (5.233) by taking the expectation value with respect to momentum. The calculation is sketched in appendix E. The entire linear response, complex first-order magnetization reads in short hand notation

$$\langle {}^{(1)}\hat{\sigma}^{\text{trans}}(x)\rangle = -\frac{\mu_{\text{B}}}{e\lambda} i\pi \frac{e^2 n \tau_c^2 \tau_s \tau_{\text{sf}}}{2m\tau_{\text{sd}}\left(2\tau_c\tau_s^2 + \tau_{\text{sf}}\left(\tau_s^2 - \tau_c^2\right)\right)\Lambda}\left[\Delta(x) + \Delta\left(\lambda - x\right)\right] E_x, \quad (5.234)$$

where we employed the definition of the functions

$$\begin{aligned}\Delta(x) = {} & 2\tau_{\text{sd}}\tau_{\text{sf}}\left(\frac{3\hbar\tau_s}{m v_{\text{F}}^2} - \tau_c\tau_{\text{sd}}\right) \\ & + e^{-\frac{\left(\frac{1}{2\tau_c} + \frac{1}{\tau_{\text{sf}}} - i\frac{2}{\tau_{\text{sd}}}\right)x}{v_{\text{F}}}}\left[2\tau_{\text{sd}}\tau_{\text{sf}}\left(\tau_c\tau_{\text{sd}} - \frac{3\hbar\tau_s}{m v_{\text{F}}^2}\right) - x\Lambda\left(\frac{3\hbar^2}{m^2 v_{\text{F}}^5 \tau_{\text{sd}}} + \frac{\tau_{\text{sd}}}{2v_{\text{F}}}\right) + x^2\Lambda^2\frac{1}{4v_{\text{F}}^2\tau_c\tau_{\text{sf}}}\right] \\ & + \text{Ei}\left(\left(\frac{1}{2\tau_c} + \frac{1}{\tau_{\text{sf}}} - i\frac{2}{\tau_{\text{sd}}}\right)\frac{x}{v_{\text{F}}}\right)\left[x\Lambda\frac{3\hbar\tau_s\left(2\tau_c + \tau_{\text{sf}}\right)}{m v_{\text{F}}^3\tau_c\tau_{\text{sf}}} - x^3\Lambda^3\frac{1}{8v_{\text{F}}^3\tau_c^2\tau_{\text{sd}}\tau_{\text{sf}}^2}\right], \quad (5.235)\end{aligned}$$

$$\Lambda = 2\tau_c(\tau_{\text{sd}} - 2i\tau_{\text{sf}}) + \tau_{\text{sf}}\tau_{\text{sd}}, \quad (5.236)$$

and the integral exponential function is defined in Eq. (E.12). The result (5.234) yields the transverse conduction electron magnetization up to order $\mathcal{O}(\kappa^3)$.
The cartesian x and y components of the transverse magnetization of the conduction electrons are given by the real and imaginary part of Eq. (5.234) according to

$$\langle\hat{\sigma}_{\text{trans}}(x)\rangle = \langle\hat{\sigma}_x(x)\rangle + i\langle\hat{\sigma}_y(x)\rangle. \quad (5.237)$$

In the current-induced torque picture the transverse components $\langle\hat{\sigma}_x(x)\rangle$, $\langle\hat{\sigma}_y(x)\rangle$ constitute the spin-transfer torque according to Eq. (5.141) as a counteraction on the local magnetization. [5] While the real part corresponds to the adiabatic spin-transfer torque

$$\tau_{\text{STT}}^{\text{adiabatic}}(x) = \frac{1}{\tau_{\text{sd}}}\Re(\langle\hat{\sigma}_{\text{trans}}(x)\rangle) = \frac{1}{\tau_{\text{sd}}}\langle\hat{\sigma}_x(x)\rangle, \quad (5.238)$$

$$\tau_{\text{STT}}^{\text{non-adiabatic}}(x) = -\frac{1}{\tau_{\text{sd}}}\Im(\langle\hat{\sigma}_{\text{trans}}(x)\rangle) = -\frac{1}{\tau_{\text{sd}}}\langle\hat{\sigma}_y(x)\rangle, \quad (5.239)$$

the imaginary part yields the non-adiabatic spin-transfer torque. The spin-transfer torque in the Eqns. (5.238) and (5.239) consists of a spatially dependent oscillating and a spatially independent part. The spatially varying part is caused by the magnetization texture and its net effect is small for

wide domain walls. In the limit of wide domain walls the spatially dependent, oscillating part will average to zero and the spin-transfer torque will become constant in accordance to what is found in section 5.4.
The spatially independent part of Eq. (5.234) holds the following constant contributions to the spin-transfer torque

$$\begin{aligned} {}^{(1)}\tau_{\text{STT}}^{\text{ad}} &= \frac{1}{\tau_{\text{sd}}}\Re(\langle {}^{(1)}\hat{\sigma}_{\text{trans}}\rangle) \\ &= \frac{\pi\mu_{\text{B}}}{2e\lambda}\sigma_{\text{spin}}^{\text{trans}}E_x, \end{aligned} \tag{5.240}$$

$$\begin{aligned} {}^{(1)}\tau_{\text{STT}}^{\text{non-ad}} &= -\frac{1}{\tau_{\text{sd}}}\Im(\langle {}^{(1)}\hat{\sigma}_{\text{trans}}\rangle) \\ &= \frac{\pi\mu_{\text{B}}\xi}{2e\lambda}\sigma_{\text{spin}}^{\text{trans}}E_x. \end{aligned} \tag{5.241}$$

By considering the magnetization twist in Eq. (5.199), except for a factor of 1/2 the results (5.240) and (5.241) agree with the spin-conductivity of transverse magnetization dynamics that has been derived for general, spatially slowly varying magnetization textures in section 5.4.2.2 (cf. Eqns. (5.151), (5.152) and (5.154)). The different numerical factor stems from the momentum integration. In section 5.4 we focus on bulk properties and employed the velocity average in Eq. (5.129). More realistic domain-wall profiles would alter the geometric prefactor in Eqns. (5.240) and (5.241), but would not affect the result in a qualitative manner, i.e., in terms of its dependence on relaxation times.
The degree of non-adiabaticity is defined as the ratio of the non-adiabatic and the adiabatic spin-transfer torque. In the model of an one-dimensional domain wall the degree of non-adiabaticity is given as

$$\begin{aligned} \xi &\equiv -\frac{\Im\langle {}^{(1)}\hat{\sigma}^{\text{trans}}\rangle}{\Re\langle {}^{(1)}\hat{\sigma}^{\text{trans}}\rangle} \\ &= -\tan\arg\langle {}^{(1)}\hat{\sigma}_{\text{trans}}\rangle \\ &= \frac{\tau_{\text{sd}}}{4}\left(\frac{1}{\tau^{\uparrow}}+\frac{1}{\tau^{\downarrow}}+\frac{2}{\tau_{\text{sf}}}\right), \end{aligned} \tag{5.242}$$

that agrees with the result for general, spatially slowly varying magnetization textures as given in Eq. (5.163) and underlines its generic meaning for adiabatic magnetotransport.

Let us now focus on the full spatial dependence of the general solution (5.234). The definition in Eq. (5.242) serves for a generalization of the degree of non-adiabaticity for finite domain-wall widths. For a domain wall the degree of non-adiabaticity ξ varies spatially according to

$$\xi(x,\lambda) = -\tan\arg\langle\hat{\sigma}_{\text{trans}}(x)\rangle. \tag{5.243}$$

The generalized degree of non-adiabaticity (5.243) is composed of a constant part due spin relaxation given by Eq. (5.242) and a spatially varying part, which is caused by spin mistracking due to the magnetization texture. [172] Both parts stem from entirely different origins and are often confused in the literature. The spatially independent part in Eq. (5.242) has already been derived in section 5.4 and attributes a finite degree of non-adiabaticity ($\xi \neq 0$) due to spin relaxation. We explicitly note at this

point that the common terminology to refer to the contribution due to spin relaxation as non-adiabatic is accidental (cf. comments in section 2.3). However, in order to avoid confusion we will stay with this widely established terminology. In section 5.4 we have explicitly shown that the presence of the contribution due to spin relaxation is generic in the adiabatic case as long as the spin transfer between the conduction electrons and the local magnetization does not completely conserve the spin. The thereby introduced non-adiabaticity due to spin relaxation results in a constant finite delay of the magnetization of the conduction electrons, even in the extreme limit of infinitely wide walls. Due to the independence with respect to the magnetization texture, the contribution of spin relaxation to the degree of non-adiabaticity must be viewed as a constant material parameter that depends solely on the microscopic parameters of relaxation times and exchange splitting. In contrast, the spatially dependent part that is given by $(\xi(x,\lambda)-\xi)$ takes into account the non-adiabatic passage of the spin of the conduction electron through the wall, i.e., spin mistracking due to the enhanced coupling between the spins of the conduction electrons and the local moments in narrow domain walls. In this connection the contribution due to spin-mistracking constitutes a truely non-adiabatic contribution (cf. footnote in section 2.3) in addition to the constant contribution due to spin relaxation in Eq. (5.242). The contribution due to spin mistracking averages out for wide domain walls ($\xi(x,\lambda)\to\xi$, for $\lambda\to\infty$) and is not a property of the material but depends crucially on the details of the magnetization texture. In order to separate both contributions, we focus in the following sections the exclusive contribution to non-adiabaticity caused by the magnetization texture by means of dividing the entire degree of non-adiabaticity by the degree of non-adiabaticity that stems from spin relaxation ($\xi(x,\lambda)/\xi$).
It is really interesting that the contribution due to spin mistracking simply renormalizes the constant part due to spin relaxation and can thus still be incorporated in the classical Landau-Lifshitz-Gilbert phenomenology. This fact owes to our semiclassical approach. In entire quantum mechanical approaches true non-adiabatic contributions are per definition non-local and cannot be comprised within local spin-transfer torque terms. [56, 58, 71, 172] However, for the description of domain-wall dynamics in terms of collective coordinates it is found to be of general validity that non-local contributions can always be summed up to renormalize the degree of non-adiabaticity in the effective equation of motions for a domain wall (cf. discussion in section 5.5.5.3). [58, 71]
In the regime of wide domain walls the terminal domain-wall velocity is proportional to ξ/α and thus independent of the shape and the width of the domain wall. [5, 48] This stems from the factorization of spatial and momentum dependence of the distribution functions in adiabatic magnetotransport and has been extensively discussed in section 5.4. This curiosity is lifted in narrow domain walls, where the width and the shape of the domain wall determines the degree of non-adiabaticity via Eq. (5.243) and thus the domain-wall velocity. In this context, the case of $\xi=\alpha$ that corresponds to Galilean invariance and the drift of the whole magnetization pattern with the current cannot be deduced from general principles but our microscopic derivation shows that the equality $\xi=\alpha$ takes place only accidentally. [155]

The total torque is obtained by summing up the local magnetization of the conduction electrons (5.234) within the domain wall. Instead of directly integrating Eq. (5.234), it is more appropriate to inter-

change the order of the spatial and the momentum integrations. We obtain

$$
\begin{aligned}
\langle {}^{(1)}\hat{\sigma}_{\text{tot}}^{\text{trans}} \rangle &= \int_0^\lambda dx \, \langle {}^{(1)}\hat{\sigma}_{\text{tot}}^{\text{trans}}(x) \rangle \\
&= -\kappa\mu_{\text{B}} \int \frac{d^3k}{(2\pi)^3} \int_0^\lambda dx \, \tilde{g}_{\vec{k}}^{\text{trans}}(x) \\
&= \frac{\mu_{\text{B}}}{e\lambda} i\pi \frac{e^2 n \tau_c^2 \tau_s \tau_{\text{sf}}}{4m\tau_{\text{sd}} \left(2\tau_c\tau_s^2 + \tau_{\text{sf}}\left(\tau_s^2 - \tau_c^2\right)\right)\Lambda} E_x \\
&\quad \Bigg(\Big[-\frac{12}{m^2 v_{\text{F}}^3 \Lambda} \tau_c \tau_{\text{sd}} \tau_{\text{sf}} (1 - e^{-\frac{\left(\frac{1}{2\tau_c} + \frac{1}{\tau_{\text{sf}}} - i\frac{2}{\tau_{\text{sd}}}\right)\lambda}{v_{\text{F}}}}) \\
&\qquad \left(-4\hbar^2 \tau_c \tau_{\text{sf}} + m^2 v_{\text{F}}^4 \tau_c \tau_{\text{sd}}^2 \tau_{\text{sf}} + 2\hbar m v_{\text{F}}^2 \tau_s \tau_{\text{sd}} \left(2\tau_c - \tau_{\text{sf}}\right)\right) \Big] \\
&\quad + \lambda \Big[\frac{2}{m^2 v_{\text{F}}^4} \Big(4m v_{\text{F}}^2 \tau_{\text{sd}} \tau_{\text{sf}} \left(-3\hbar\tau_s + m v_{\text{F}}^2 \tau_c \tau_{\text{sd}}\right) \\
&\qquad + e^{-\frac{\left(\frac{1}{2\tau_c} + \frac{1}{\tau_{\text{sf}}} - i\frac{2}{\tau_{\text{sd}}}\right)\lambda}{v_{\text{F}}}} \left(-12\hbar^2 \tau_c \tau_{\text{sf}} - m^2 v_{\text{F}}^4 \tau_c \tau_{\text{sd}}^2 \tau_{\text{sf}} + 6\hbar m v_{\text{F}}^2 \tau_s \tau_{\text{sd}} \left(2\tau_c + \tau_{\text{sf}}\right)\right) \Big) \Big] \\
&\quad + \lambda^2 \Big[\frac{\Lambda}{2m v_{\text{F}}^3 \tau_c \tau_{\text{sf}}} e^{-\frac{\left(\frac{1}{2\tau_c} + \frac{1}{\tau_{\text{sf}}} - i\frac{2}{\tau_{\text{sd}}}\right)\lambda}{v_{\text{F}}}} \\
&\qquad \left(m v_{\text{F}}^2 \tau_c \tau_{\text{sd}} \tau_{\text{sf}} - 12 e^{\frac{\left(\frac{1}{2\tau_c} + \frac{1}{\tau_{\text{sf}}} - i\frac{2}{\tau_{\text{sd}}}\right)\lambda}{v_{\text{F}}}} \hbar\tau_s \left(2\tau_c + \tau_{\text{sf}}\right) \Gamma\left(0, \frac{\left(\frac{1}{2\tau_c} + \frac{1}{\tau_{\text{sf}}} - i\frac{2}{\tau_{\text{sd}}}\right)\lambda}{v_{\text{F}}}\right)\right) \Big] \\
&\quad - \lambda^3 \Big[\frac{\Lambda^2}{4 v_{\text{F}}^2 \tau_c \tau_{\text{sf}}} e^{-\frac{\left(\frac{1}{2\tau_c} + \frac{1}{\tau_{\text{sf}}} - i\frac{2}{\tau_{\text{sd}}}\right)\lambda}{v_{\text{F}}}} \Big] \\
&\quad + \lambda^4 \Big[\frac{\Lambda^3}{8 v_{\text{F}}^3 \tau_c^2 \tau_{\text{sd}} \tau_{\text{sf}}^2} \Gamma\left(0, \frac{\left(\frac{1}{2\tau_c} + \frac{1}{\tau_{\text{sf}}} - i\frac{2}{\tau_{\text{sd}}}\right)\lambda}{v_{\text{F}}}\right) \Big] \Bigg),
\end{aligned}
\tag{5.244}
$$

where the incomplete Γ-function is defined in Eq. (E.13). Note that the $1/\lambda$ dependence of Eq. (5.244) secures that the spin-transfer torque remains finite, even in the limit of wide walls ($\lambda \to \infty$). Here, the oscillations wash out, the influence of the non-adiabaticity due to spin mistracking vanishes and the spin-transfer torque approaches its constant value corresponding to an adiabatic traversal of the domain wall. In contrast, higher-order corrections in κ such as the domain-wall resistivity vanish in the adiabatic limit ($\lambda \to \infty$).

The results for the transverse magnetization of the conduction electrons (5.234) and (5.244) announce that the exponential decay of the oscillations in the spin-transfer torque is given by the mean free path that is set by the collisions $v_{\text{F}}\tau_c$. In contrast, the imaginary parts in the exponential and related functions exhibit a periodicity that can roughly be estimated as

$$
\lambda_{\text{F}} = \pi v_{\text{F}} \tau_{\text{sd}}. \tag{5.245}
$$

The wavelength as defined in Eq. (5.245) should not to be confused with the domain wall length λ. Interestingly, the spatial modulations of the precession angle takes place with the same period that sets

the frequency for the precession of the conduction electrons around the local moments. Both originate from the sd interaction. The wavelength as defined in Eq. (5.245) coincides with the difference in momentum between spin up and spin down electrons $\lambda_{\mathrm{F}} = \pi/|k_{\mathrm{F}}^{\uparrow} - k_{\mathrm{F}}^{\downarrow}|$ that arises within a ferromagnet due to the exchange splitting. [172, 173, 197] When injecting a polarized electron beam into a collinear ferromagnet with spin polarization and magnetization being non-collinear to each other the electrons precess around the local moments with the same wavelength as given by Eq. (5.245) until their spins relax due to spin-dependent scattering or the damping caused by the local moments. It follows from quantum mechanical considerations that spatial precession occurs when a coherent superposition of majority and minority states possesses the same Fermi energy but different wavevectors. [173]

Before proceeding to discuss the results as given in Eqns. (5.234) and (5.244) in more detail, let us compare the presented results with the work of Tatara et al. [49, 58, 59, 71]. They performed a perturbative expansion in a gauge field that comprises the magnetization texture and found non-local contributions showing up at $\mathcal{O}((k_{\mathrm{F}}\lambda)^{-2})$. [59] Descriptively non-adiabatic corrections are associated with scattering of the conduction electrons at the domain wall that becomes important in abrupt walls, when the domain-wall width approaches the Fermi wavelength $\lambda \sim k_{\mathrm{F}}^{-1}$ of the conduction electrons. The domain-wall width approaching the Fermi wavelength $\lambda \sim k_{\mathrm{F}}^{-1}$ marks the breakdown of a semiclassical description of magnetotransport. As it concerns the degree of non-adiabaticity the contribution to reflection must be discriminated from the contribution due to spin mistracking as computed in this thesis. Spin mistracking becomes already important at $v_{\mathrm{F}}\tau_{\mathrm{sd}} \sim \lambda$. The relation $J_{\mathrm{sd}}/\epsilon_{\mathrm{F}} = v_{\mathrm{F}}\tau_{\mathrm{sd}}k_{\mathrm{F}}$ determines the dominant correction in narrow domain walls. As long as the condition $\lambda > k_{\mathrm{F}}^{-1}$ holds, spin mistracking sets in earlier compared with non-local quantum mechanical corrections due to reflection. This is the case for weak ferromagnets ($J_{\mathrm{sd}}/\epsilon_{\mathrm{F}} \ll 1$), whereas for strong ferromagnets $J_{\mathrm{sd}}/\epsilon_{\mathrm{F}} \sim \mathcal{O}(0.1 - 1)$ it would be really interesting to determine the dominant correction. [238]

Definition of spin transport regimes As discussed in section 5.1.2, charge transport in mesoscopic magnetotransport is entirely diffusive for typical domain-wall widths in ferromagnetic transition metals, while spin transport is diffusive or ballistic. As it concerns the spin transport, the result for the spatially resolved transverse magnetization of the conduction electrons (5.234) as well as the integrated spin-transfer torque (5.244) is not restricted to one transport regime or the other and is in general valid as long as the perturbative condition $l_{\mathrm{mfp}} < \lambda$ is fulfilled. The mean free path is determined either by the precession $v_{\mathrm{F}}\tau_{\mathrm{sd}}$ or spin relaxation $v_{\mathrm{F}}\tau_c$.
It is appropriate to introduce the parameter

$$\eta = \frac{\tau_{\mathrm{sd}}}{\tau_c}, \tag{5.246}$$

to characterize the spin transport regime. $\eta < 1$ defines the regime of ballistic spin transport valid in strong ferromagnets, where, between two collisions, the spin has enough time to precess around the local magnetization. In contrary, $\eta > 1$ distinguishes the diffusive transport regime in relatively dirty systems where the precession of the transverse magnetization is damped out due to relaxation. As it concerns experiments, ferromagnetic transition metals are supposed to be in the ballistic spin transport regime with $\eta < 1$.

Both transport regimes will be discussed individually in the following. For this purpose we visualize the results of Eqns. (5.234) and (5.244) with the following set of parameters throughout all plots: $\tau_{\text{sf}} = 10^{-12}$ s, $\tau_{\text{sd}} = 4.136 \cdot 10^{-15}$ s, $v_{\text{F}} = 1.33 \cdot 10^{6}$ m/s.
Moreover, we introduce the parameter

$$\beta = \frac{\tau^{\uparrow}}{\tau^{\downarrow}}, \tag{5.247}$$

which characterizes the anisotropy of scattering and yields the ratio between the averaged electron momentum lifetimes for majority and minority spins. The ratio β determines whether the electric current is carried by majority or minority electrons. $\beta > 1$ translates to $\tau^{\uparrow} > \tau^{\downarrow}$ and the majority electrons dominate the transport, while $\beta < 1$ corresponds to $\tau^{\uparrow} < \tau^{\downarrow}$ and the current is carried mainly by the minority electrons due to a higher resistivity for the majority electrons.

Ballistic spin transport This section is concerned with the physically most interesting transport regime ($\eta < 1$), where the shortest time is set by the coherence time τ_{sd}, the inverse frequency with which the conduction spins precess around the local magnetization. Though the conduction electron is scattered many times during its traversal of the domain wall and the charge transport is far away from being in the ballistic regime, the spin transport is ballistic with respect to the fast sd precession. There are two possible cases: $\beta \gtrless 1$.
First, we focus on the regime $\beta < 1$. Figure 5.8 depicts the result (5.234) for the spatially varying components $\langle \sigma_x(x) \rangle$ and $\langle \sigma_y(x) \rangle$ of the magnetization of the conduction electrons that correspond to the adiabatic and the non-adiabatic spin-transfer torque for $\beta = 0.57$ and three domain-wall widths. Both components oscillate within the domain wall due to the sd exchange interaction that causes a precession around the local moments. [22, 172] When the electron approaches the domain wall the quantization axis changes and the electric field assembles transverse magnetization of the conduction electrons. The oscillations are damped due to spin decoherence caused by impurity scattering rather than due to an averaging process and the sign change in the average non-adiabatic spin-transfer torque (cf. Fig. 5.8 (c)) must be unambiguously attributed to spin-dependent scattering. [22] A particular feature of the domain-wall profile with constant gradient is that for longer domain-wall widths the oscillations are almost completely damped out such that the transverse magnetization aligns at a constant angle with the local magnetization. This is due to the spin decoherence caused by impurity scattering. The spatial oscillations of the torques are generic and thus also present in smooth wall profiles. The pronounced behavior at the boundaries of the domain wall traces back to the non-differentiable transition between the homogeneous domain and the linear wall. The linear wall profile with constant magnetization gradient is also responsible for the alignment in the middle of wide domain walls as depicted in Fig. 5.8 (a). The constant angle characterizes an adiabatic passage of the domain wall. More realistic, smooth domain-wall profiles will exhibit an intermediate behavior. Here, oscillations at the boundaries will be less pronounced due to a smooth transition but in turn will persists throughout the entire domain wall due to a non-constant magnetization gradient. It can be expected that both influences counterbalance each other for reasonable domain-wall width and that the precise domain-wall profile is therefore not crucial for the qualitative behavior. However, a quantitative analysis requires the numerical solution of the kinetic equation for different wall profiles. These will clarify the influence of specific domain-wall profiles on the spatial variation of the magnetization of the conduction electrons. The end of the domain wall represents again a change of the quantization axis with con-

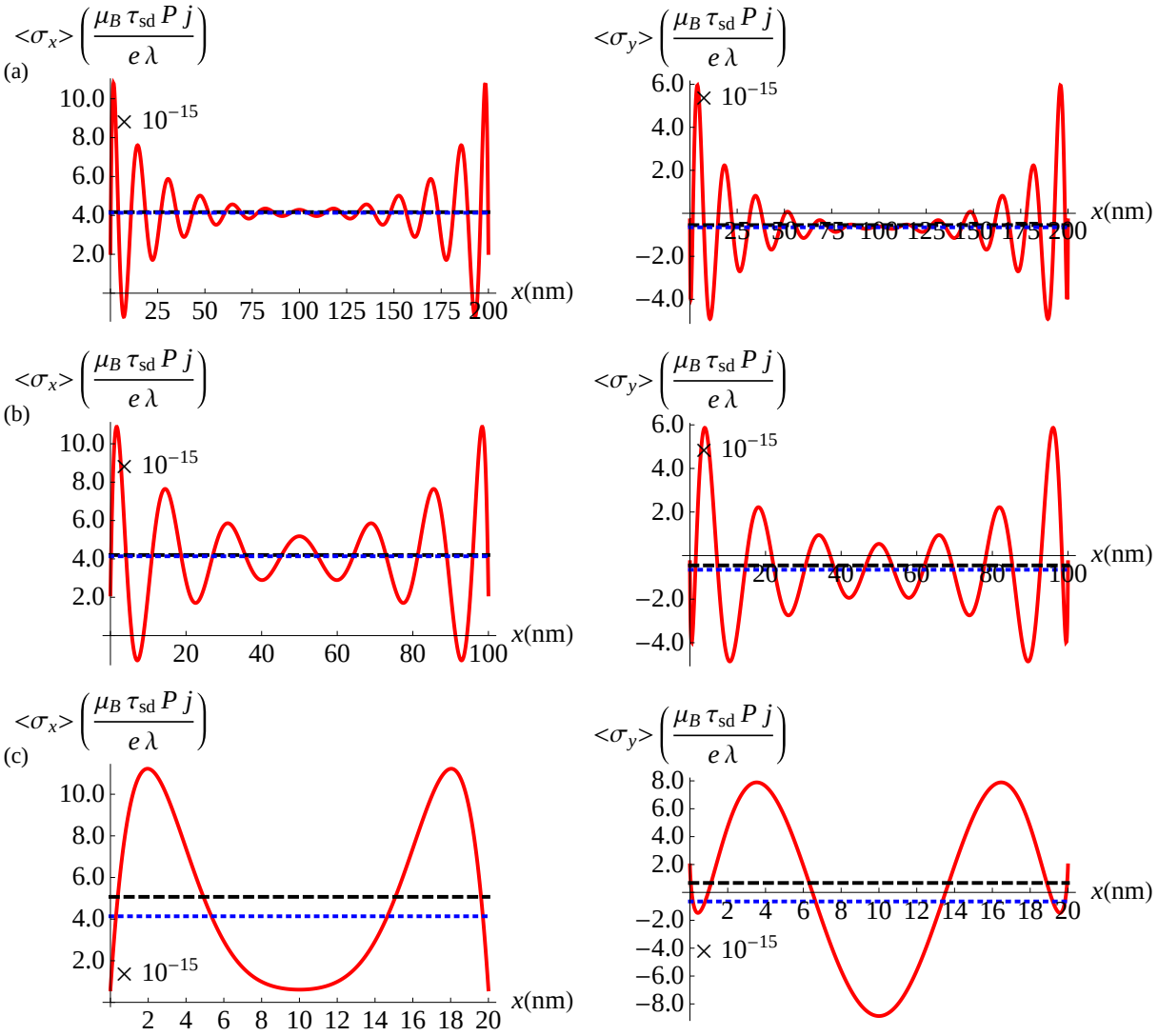

Figure 5.8: (Color online) Cartesian components of the magnetization of the conduction electrons within domain walls of different width λ for $l_{\mathrm{mfp}} = 5.49$ nm. (a) λ = 200 nm, (b) λ = 100 nm and (c) λ = 20 nm. The transport regime is ballistic ($\eta = 0.62$) with a ratio of relaxation times smaller than one ($\beta = 0.57$). The dashed black line represents the average magnetization while the blue dotted line depicts its spatially independent part. The frequency of the oscillations is determined by the sd interaction.

comitant oscillations.
For finite wall widths, the spatial averaged spin-transfer torque deviates from the constant value as proposed by the adiabatic theory of the spin-transfer torque. [5] The spatial oscillations of the spin-transfer torque cause a different spatial average and are thus the reasons for the deviations that becomes negligible for wide walls. For infinite wide walls ($\lambda \rightarrow \infty$) the oscillations average out and the constant value as proposed by the adiabatic theory of the spin-transfer torque is recovered. Notice how close the spatially averaged quantities as indicated by the dashed black lines in Fig. 5.8 (a), (b) remain to the spatially constant value of infinitely wide walls marked by the dotted blue lines. This states impressively why the assumption of a constant spin-transfer torque turns out to be a reasonable approximation for wide domain walls in the adiabatic regime, though the spatial substructure is quite inhomogeneous. In contrast, for narrow walls as depicted in Fig. 5.8 (c) severe deviations comprising a sign change occur.
A spatially varying magnetization of the conduction electrons that constitutes the spin-transfer torque implies a spatially varying coupling between current and magnetization. This stands in sharp contrast to the adiabatic case that predicts a constant coupling. [5, 48] Micromagnetic simulations should be conducted to properly estimate the consequences of the spatial oscillations that can result in domain-wall distortion and even in transformation. A current-induced deformation of the domain-wall structure has been experimentally observed. [233, 239]
As addressed by Ref. [172], a spatially oscillating spin-transfer torque may enhance the depinning of domain walls. An enhancement in the depinning probability corresponds to a decrease of the threshold current needed to induce domain-wall motion and is of particular technological interest. [19, 22, 29] However, these conjectures should be confirmed with detailed micromagnetic simulations.

Figure 5.9 depicts the total adiabatic and non-adiabatic spin-transfer torque (5.244) and the non-adiabaticity exclusively caused by spin mistracking due to the spatially strongly varying magnetization texture. In the case of narrow domain walls the degree of non-adiabaticity ξ depicted in Fig. 5.9 (c) increases drastically. This is a direct consequence of the strong spatial oscillations in narrow domain walls that cause considerable deviations of the average from the spatially constant spin-transfer torque. For finite wall widths it is spin-dependent scattering that results in an average spin-transfer torque that deviates from the constant value expected from the adiabatic approximation. [172] In this sense scattering is responsible for a considerable change in the total spin-transfer torque that acts on the domain wall. This is somewhat reminiscent to the adiabatic case: Here, scattering causes a finite degree of non-adiabaticity due to spin relaxation. Without the presence of spin relaxation the spatial oscillations due to spin mistracking would be symmetric and yield a zero average. [172] The zero average would not alter the constant value and the total spin-transfer torque on the domain-wall would be the same for narrow and wide domain walls, though its spatial substructure is entirely different. This is the result of the ballistic quantum mechanical calculation by Ref. [172]. This impressively states the influence of scattering on the spin-transfer torque. The enhanced degree of non-adiabaticity underlines the need for micromagnetic simulations to properly estimate the consequences of the drastic increase that can result from domain-wall distortion to even transformations in the wall structure.
A very exciting feature for $\beta < 1$ is, that the non-adiabaticity changes its sign with the domain-wall width λ in narrow domain walls. As the final domain-wall velocity is set by the ratio ξ/α [5], a vari-

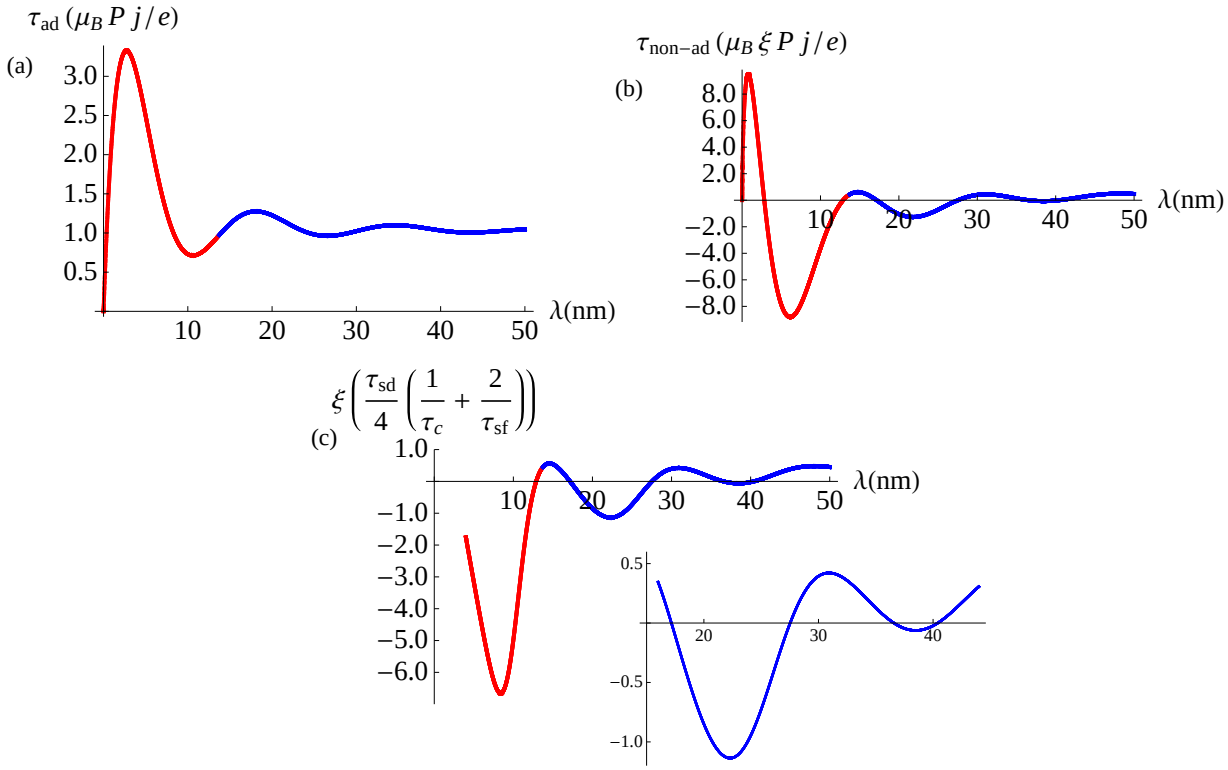

Figure 5.9: (Color online) Integrated torques for different domain-wall widths λ. (a) The adiabatic τ_{ad} and (b) non-adiabatic spin-transfer torque $\tau_{\text{non-ad}}$. (c) The degree of non-adiabaticity ξ. The solid red line indicates the regime where the perturbation theory starts to be unreliable.

ation of ξ with the domain-wall width allows tuning domain-wall motion by means of λ, for instance via the (shape) anisotropy (cross section of the wire). Provided that the domain wall keeps its rigid shape, a sign change in ξ would result in a reversed motion of the domain wall. As addressed by Ref. [183], $\beta < 1$ corresponds to an impurity-specific negative correction to the resistivity as caused by the domain wall (cf. section 5.5.5.3). Moreover, at certain widths that correspond to $\xi = 0$, the conduction electron spin is able to follow the magnetization in perfect adiabaticity and additional dissipation by the magnetization texture is absent. Likewise, $\xi = 0$ implies intrinsic pinning [49] and a vanishing terminal velocity of the domain wall. This provides a geometric trapping of the domain wall that does not rely on pinning centers. Furthermore, the equality of $\xi = \alpha$ is possible. For the special case of $\xi = \alpha$ solutions of the Landau-Lifshitz-Gilbert equation exist that possess the form $\vec{m}(\vec{r} - \vec{v}t)$ in accordance with Galilean invariance. [55, 101] This means that an arbitrary static solution $\vec{m}(\vec{r})$ of the Landau-Lifshitz-Gilbert equation moves at a constant velocity $\vec{v}$ without deformations. Thus, $\xi = \alpha$ causes Galilean invariance at a macroscopic level and allows for the drift of static magnetization patterns as a whole. Moreover, $\xi = \alpha$ implies the absence of a current-induced ferromagnetic instability [53, 155]. The oscillations in the non-adiabaticity in Figs. 5.9 (b), (c) are of quantum origin and emphasize the particular relevance and the corresponding special treatment of the spin degree of freedom with respect to non-adiabatic magnetotransport in narrow domain walls where the coupling of conduction electron spin and local moment is enhanced.
Next, we focus on the regime with $\beta > 1$. Figure 5.10 depicts the $\langle \sigma_x \rangle$ and $\langle \sigma_y \rangle$ components of the magnetization of the conduction electrons according to Eq. (5.234) for three different domain-wall widths and $\beta = 1.2$. Compared to the case of $\beta < 1$ depicted in Fig. 5.8 the spatial oscillations are less pronounced and the idea of a spatially constant spin-transfer torque can be more reliably sustained. As a consequence the average torque indicated by the black dashed line keeps quite close to the spatially independent part (blue dotted line). Though the deviation in narrow domain walls is measurable as indicated in Fig. 5.10 (c), the most important point is that for $\beta > 1$ no sign change of the spatially averaged non-adiabatic spin-transfer torque occurs. A direct consequence of the less pronounced spatial oscillations for $\beta > 1$ is a smoother dependence of the spatially integrated spin-transfer torque on the domain-wall width as depicted in Fig. 5.11. In particular, no sign change in the non-adiabatic spin-transfer torque occurs (cf. Fig. 5.11 (b), (c)). The obvious conclusion is therefore that constant transport coefficients, in particular a constant ξ, are much better justified for the case of $\beta > 1$. Nevertheless, the increase in magnitude of the non-adiabaticity by decreasing domain-wall width is generic (cf. Fig 5.11 (c)).

Diffusive spin transport In the diffusive transport regime the mean free path is given by $v_{\mathrm{F}}\tau_c$ that constitutes the shortest length scale besides the Fermi wavelength in domain-wall magnetotransport. Spin relaxation dominates the spin transport and suppresses the precession of the conduction electrons around the local magnetization. In this sense the absence of spin mistracking is simply a consequence of the absence of precession. The magnetotransport is dominated by impurity scattering. Again, the two alternative cases, $\beta \gtrless 1$, have to be distinguished.
Figure 5.12 depicts the result (5.234) of the $\langle \sigma_x \rangle$ and $\langle \sigma_y \rangle$ components of the magnetization of the conduction electrons for three different domain-wall widths and a value of $\beta = 0.57$. Although clearly present, the spatial oscillations are much less pronounced in the diffusive transport regime compared

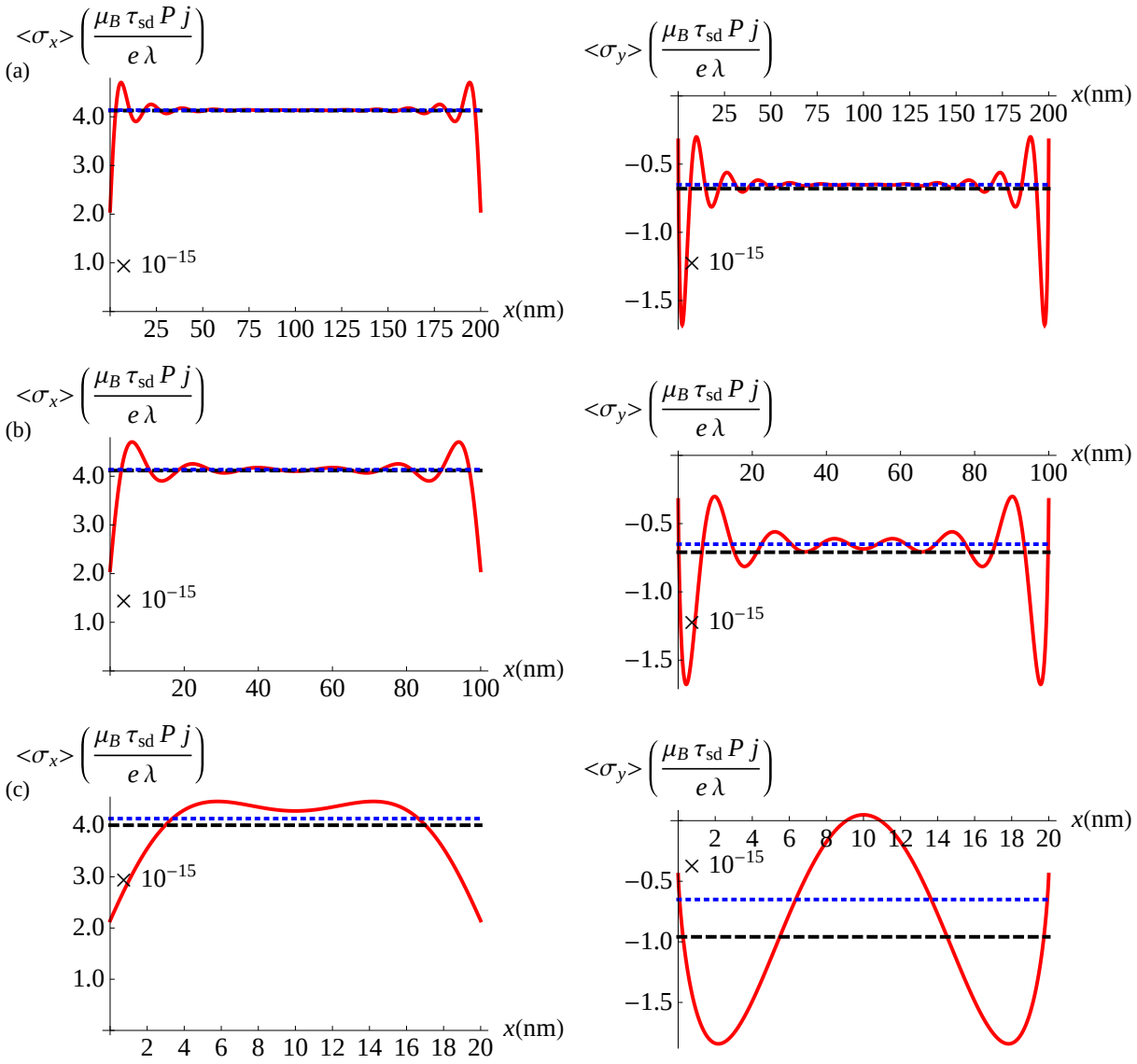

Figure 5.10: (Color online) Cartesian components of the magnetization of the conduction electrons within three domain walls of different width λ. (a) λ = 200 nm, (b) λ = 100 nm and (c) λ = 20 nm. The transport regime is ballistic ($\eta = 0.62$) with a ratio of relaxation times larger than one ($\beta = 1.2$). The dashed black line represents the average magnetization while the blue dotted line depicts its spatially independent part.

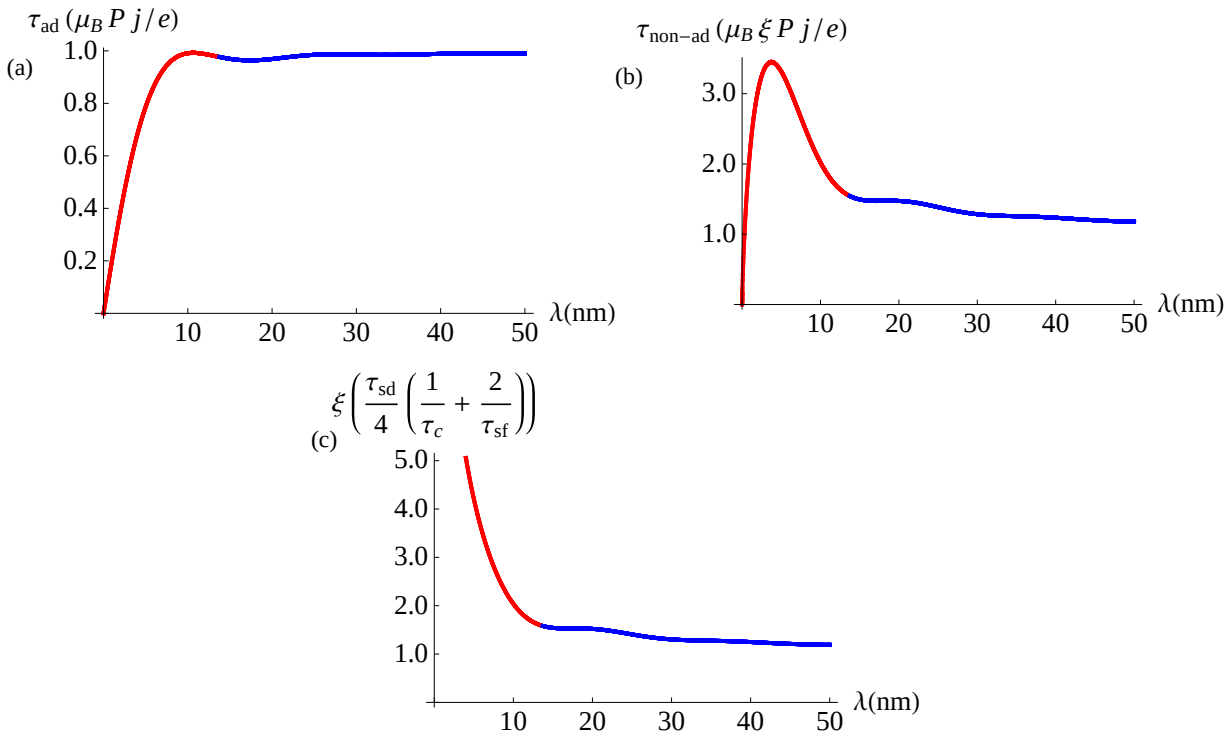

Figure 5.11: (Color online) Integrated torques for different domain-wall widths λ. (a) The adiabatic τ_{ad} and (b) non-adiabatic spin-transfer torque $\tau_{\text{non-ad}}$. (c) The degree of non-adiabaticity ξ. The solid red line indicates the regime where the perturbation theory starts to be unreliable.

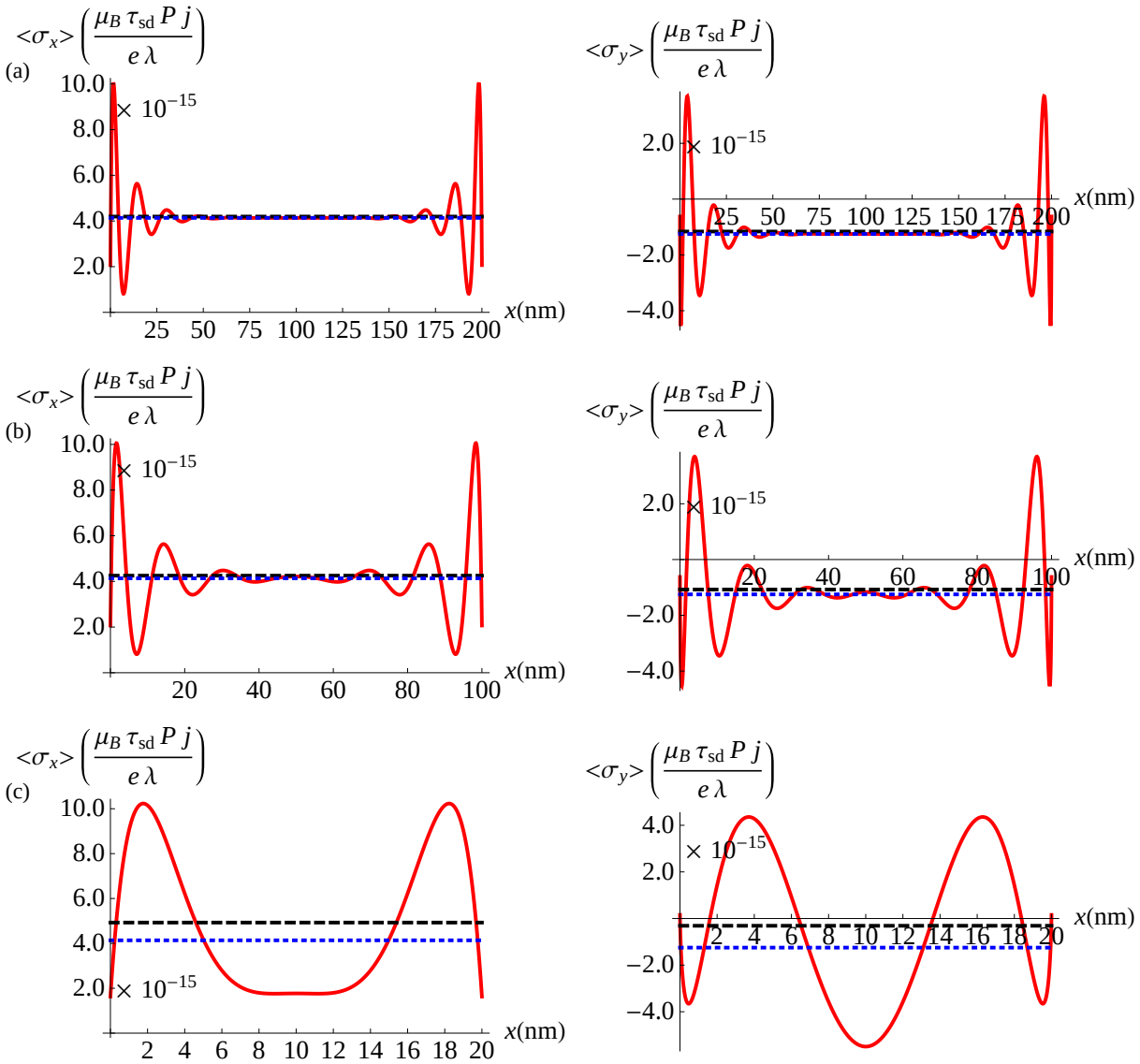

Figure 5.12: (Color online) Cartesian components of the magnetization of the conduction electrons within three domain walls of different width λ. (a) λ = 200 nm, (b) λ = 100 nm and (c) λ = 20 nm. The transport regime is diffusive ($\eta = 1.2$) with a ratio of relaxation times smaller than one ($\beta = 0.57$). The dashed black line represents the average magnetization while the blue dotted line depicts its spatially independent part.

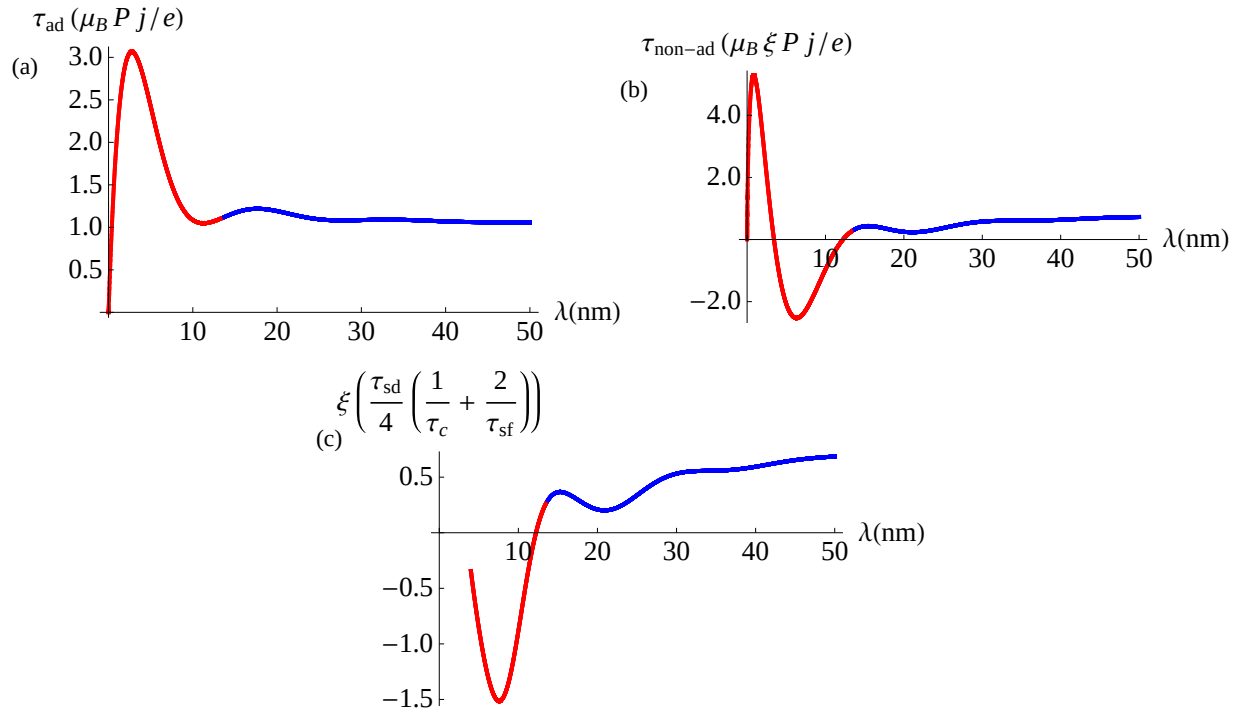

Figure 5.13: (Color online) Integrated torques for different domain-wall widths λ. (a) The adiabatic τ_{ad} and (b) non-adiabatic spin-transfer torque $\tau_{\text{non-ad}}$. (c) The degree of non-adiabaticity ξ. The solid red line indicates the regime where the perturbation theory starts to be unreliable.

to the ballistic transport regime depicted in Fig. 5.8. A direct consequence is that the spatially averaged part (black dashed line) remains much closer to the spatially independent value as indicated by the blue dotted line. While the adiabatic torque stays quite constant with the domain-wall width as depicted by Fig. 5.13 (a), the strength of the non-adiabatic torque decreases with decreasing domain-wall width but no recurring sign change occurs (cf. Fig. 5.13 (b), (c)).
Next, we investigate the regime with $\beta > 1$. Figure 5.14 depicts the $\langle\sigma_x\rangle$ and $\langle\sigma_y\rangle$ components of the magnetization of the conduction electrons for three different domain-wall widths and a value of $\beta = 1.2$. As expected the regime of diffusive spin transport shows in general less pronounced behavior. In particular no sign change occurs. Both components of the total spin-transfer torque as depicted in Fig. 5.14 coincide to a good extend with the spatially constant values. The same holds for the integrated quantities as depicted in Fig. 5.15. This clearly states that the non-adiabatic torque is determined by spin relaxation in the diffusive regime of spin transport. In conclusion, the regime of diffusive spin transport with $\beta > 1$ comes closest to the assumption of constant coupling parameters for the spin-transfer torque, that are independent of the width of the domain wall.

Crossover from the ballistic to the diffusive regime of spin transport The analytical solution in Eq. (5.244) facilitates the analytical study of the crossover from the ballistic to the diffusive regime of spin transport. For this purpose, we focus on the integrated spin-transfer torque given by Eq. (5.244) and compare it with the domain-wall width λ along with

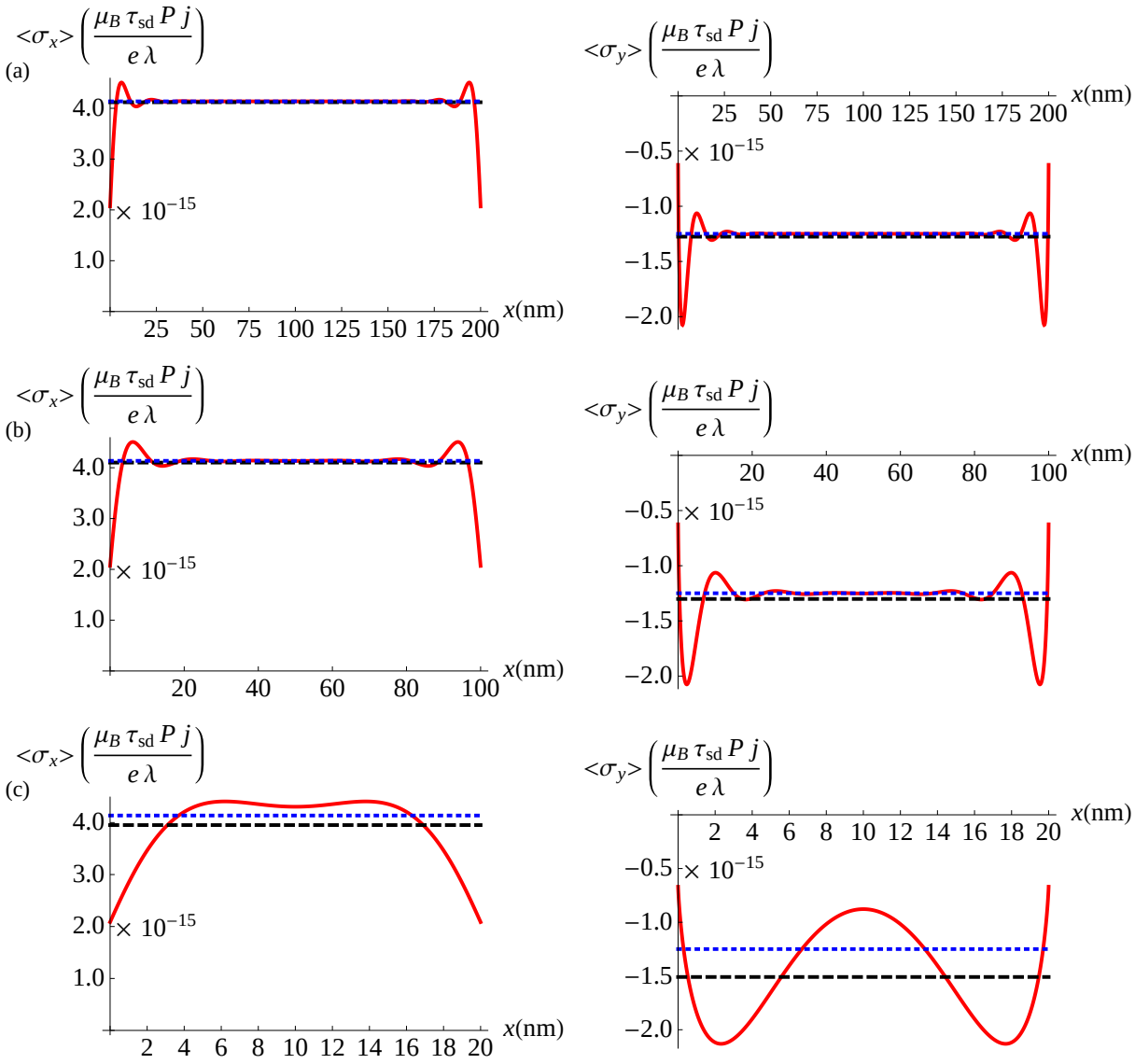

Figure 5.14: (Color online) Cartesian components of the magnetization of the conduction electrons within three domain walls of different width λ. (a) λ = 200 nm, (b) λ = 100 nm and (c) λ = 20 nm. The transport regime is diffusive ($\eta = 1.2$) with a ratio of relaxation times larger than one ($\beta = 1.2$). The dashed black line represents the average magnetization while the blue dotted line depicts its spatially independent part.

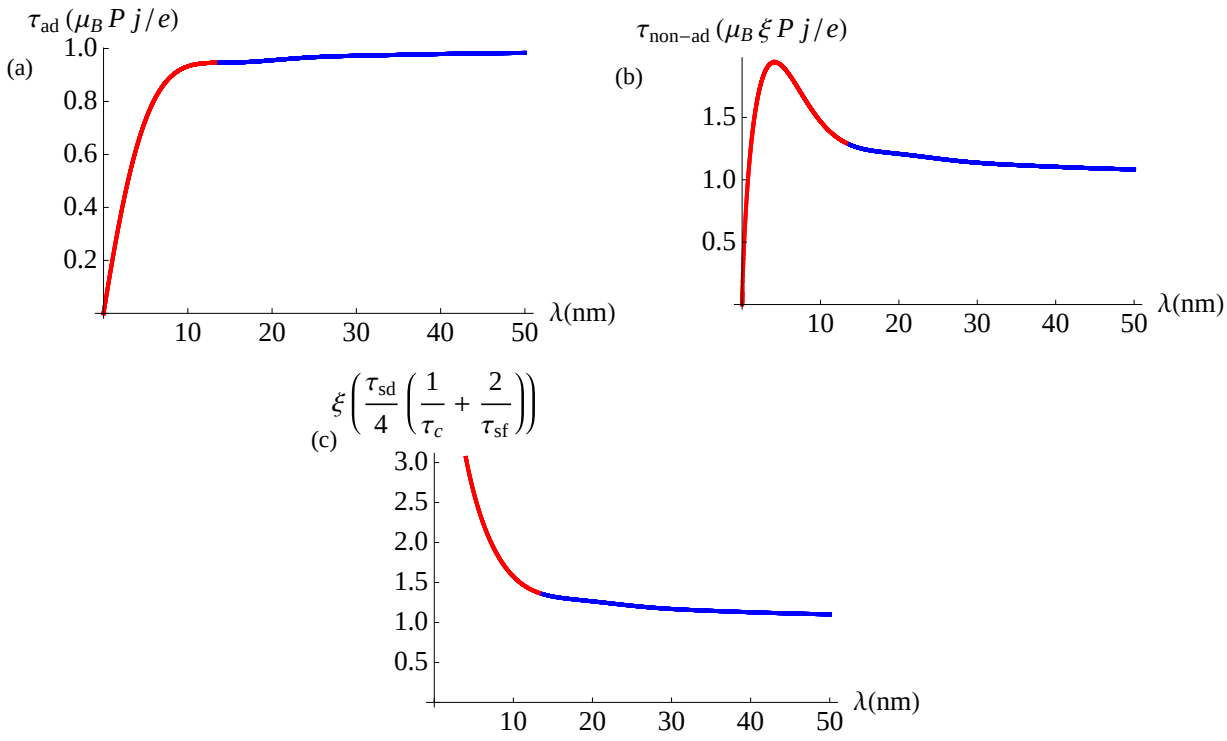

Figure 5.15: (Color online) Integrated torques for different domain-wall widths λ. (a) The adiabatic τ_{ad} and (b) non-adiabatic spin-transfer torque $\tau_{\text{non-ad}}$. (c) The degree of non-adiabaticity ξ. The solid red line indicates the regime where the perturbation theory starts to be unreliable.

- the parameter that indicates the predominant spin transport regime: $\eta = \tau_{\mathrm{sd}}/\tau_c$,
- the ratio of relaxation times: $\beta = \tau^{\uparrow}/\tau^{\downarrow}$.

Figure 5.16 and 5.17 depict the integrated adiabatic and non-adiabatic components of the spin-transfer torque and the degree of non-adiabaticity in dependence of the domain-wall width λ and the transport regime $\eta = \tau_{\mathrm{sd}}/\tau_c$ for $\beta < 1$ and $\beta > 1$, respectively. While the diffusive regime ($\eta > 1$) yields mainly a monotonous behavior of the torques, oscillations occur in the ballistic regime ($\eta < 1$). In general, the oscillations wash out when approaching the diffusive transport regime ($\eta > 1$) and become less pronounced with larger domain-wall width λ. The overall periodicity of the oscillations is given by the wavelength λ_{F} as indicated in the plots ($\lambda_{\mathrm{F}} = 17.23$ nm for the employed parameters). For $\beta < 1$ as depicted in Fig. 5.16 the oscillations are more pronounced compared with the opposite case ($\beta > 1$) shown in Fig. 5.17. In particular, the strong spatial oscillations for $\beta < 1$ in narrow domain walls (cf. Fig. 5.8) cause negative values for the non-adiabatic spin-transfer torque and the degree of non-adiabaticity (cf. Fig. (5.16) (b), (c)). The degree of non-adiabaticity oscillates with the domain-wall width λ and yields as a consequence a recurring sign change. In contrast, for $\beta > 1$ (cf. Fig. 5.17 (b), (c)) the non-adiabatic spin-transfer torque and the degree of non-adiabaticity remain strictly positive. They always exceed a value of one that characterizes pure spin relaxation. In the diffusive regime ($\eta > 1$) spin transport is dominated by impurity scattering and the spatially averaged quantities remain close to the contribution due to spin relaxation for all values of β. As indicated by the spatially resolved solutions of the preceding section, spatial oscillations become negligible in the regime of diffusive spin transport. Due to the absence of precession, spin mistracking plays no role and the degree of non-adiabaticity tends to the value for pure spin relaxation (cf. Fig. 5.16 and 5.17 (c)). By decreasing the impurity scattering ($\tau_c \to \infty, \eta \to 0$) the ballistic regime ($\eta < 1$) is approached and spin mistracking increases. Note that though for $\eta \to 0$ the contribution due to spin mistracking enhances, the overall degree of non-adiabaticity (5.242) tends likewise to zero ($\eta \to 0$, $\xi \to 0$). The limit $\eta \to 0$ corresponds to $J_{\mathrm{sd}} \to \infty$ and as discussed in section 5.5.2.1, an infinite sd exchange interaction permits perfect spin transfer due to the complete conservation of spin-angular momentum. Consequently, in the limit of infinite exchange interaction ($\eta \to 0$), no non-adiabatic spin-transfer torque is present at all.

Figure 5.18 and 5.19 depict the integrated spin-transfer torque and the degree of non-adiabaticity in dependence of the domain-wall width λ and the ratio of relaxation times $\beta = \tau^{\uparrow}/\tau^{\downarrow}$ for either ballistic ($\eta < 1$) or diffusive ($\eta > 1$) spin transport. In the regime of ballistic spin transport ($\eta < 1$) strong oscillations in the non-adiabatic torque and the degree of non-adiabaticity occur as depicted in Fig. 5.18 (b), (c). The oscillations are absent in the regime of diffusive spin transport (cf. Fig. 5.19 (b), (c)). A comparison of the ballistic (cf. Fig. 5.18) with the diffusive case (cf. Fig. 5.19) shows for $\beta, \eta < 1$ a complex behavior including sign changes of the degree of non-adiabaticity ξ (cf. Fig. 5.16 (c)). In particular, it can be deduced from Fig. 5.18 (c) that ξ changes sign at approximately a value of $\beta \approx 0.6$ for the given parameters.

From the Figs. 5.16 and 5.18 we conclude that there exist a quite broad regime of ballistic spin transport with a ratio of the relaxation times smaller than one ($\beta, \eta < 1$) that provides the possibility to tune the degree of non-adiabaticity ξ by means of the domain-wall width λ. As addressed by Ref. [183], the physical significance for β rests on its relation to the intrinsic domain-wall resistivity. $\beta > 1$ corresponds to a positive intrinsic domain-wall resistivity, while $\beta < 1$ results in a negative intrinsic

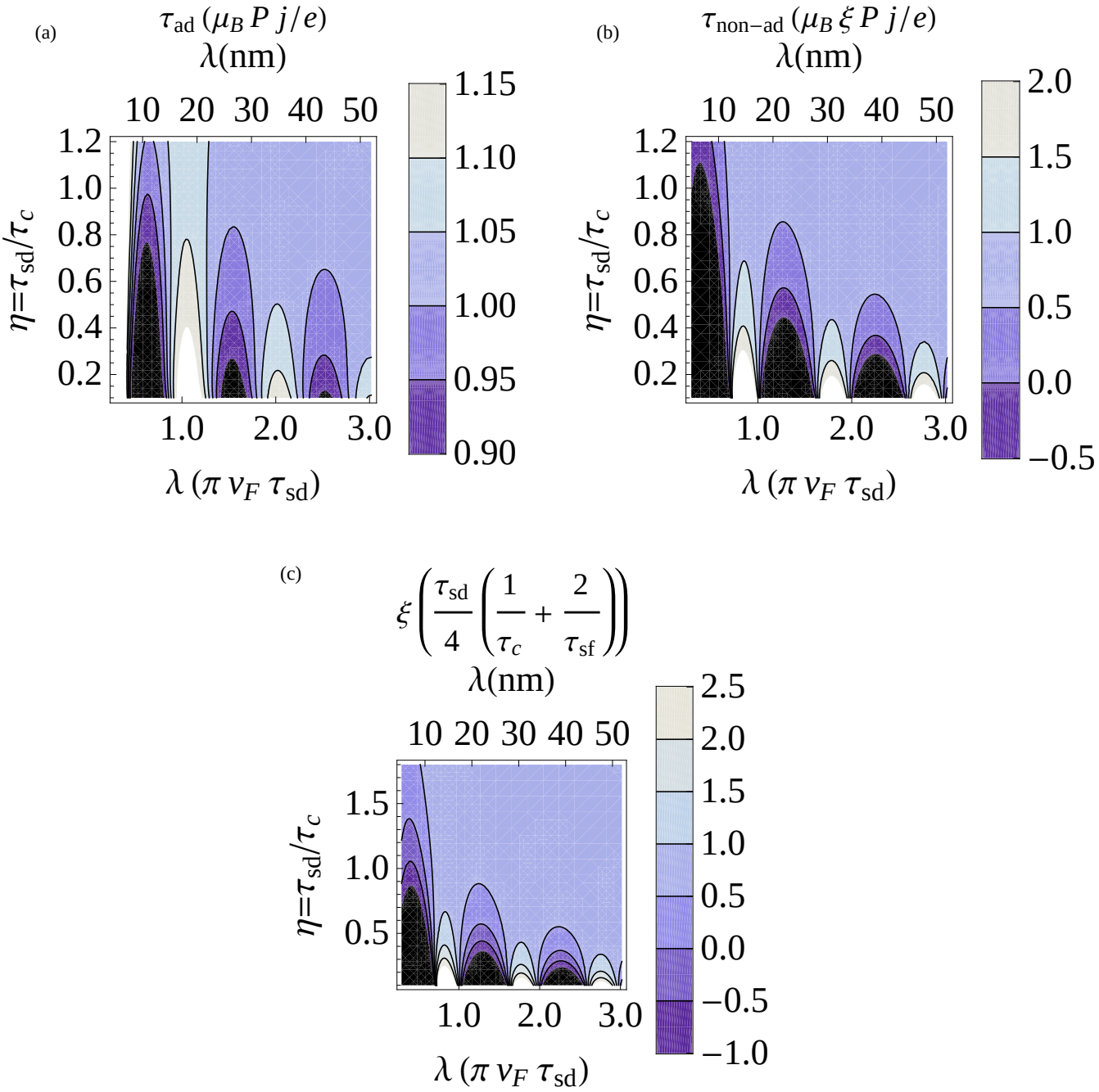

Figure 5.16: (Color online) (a) Adiabatic spin-transfer torque τ_{ad}, (b) non-adiabatic spin-transfer torque $\tau_{\text{non-ad}}$ and (c) degree of non-adiabaticity ξ for various domain-wall widths λ and transport regimes $\eta = \tau_{\mathrm{sd}}/\tau_c$ for a negative intrinsic domain-wall resistivity ($\beta = 0.6$).

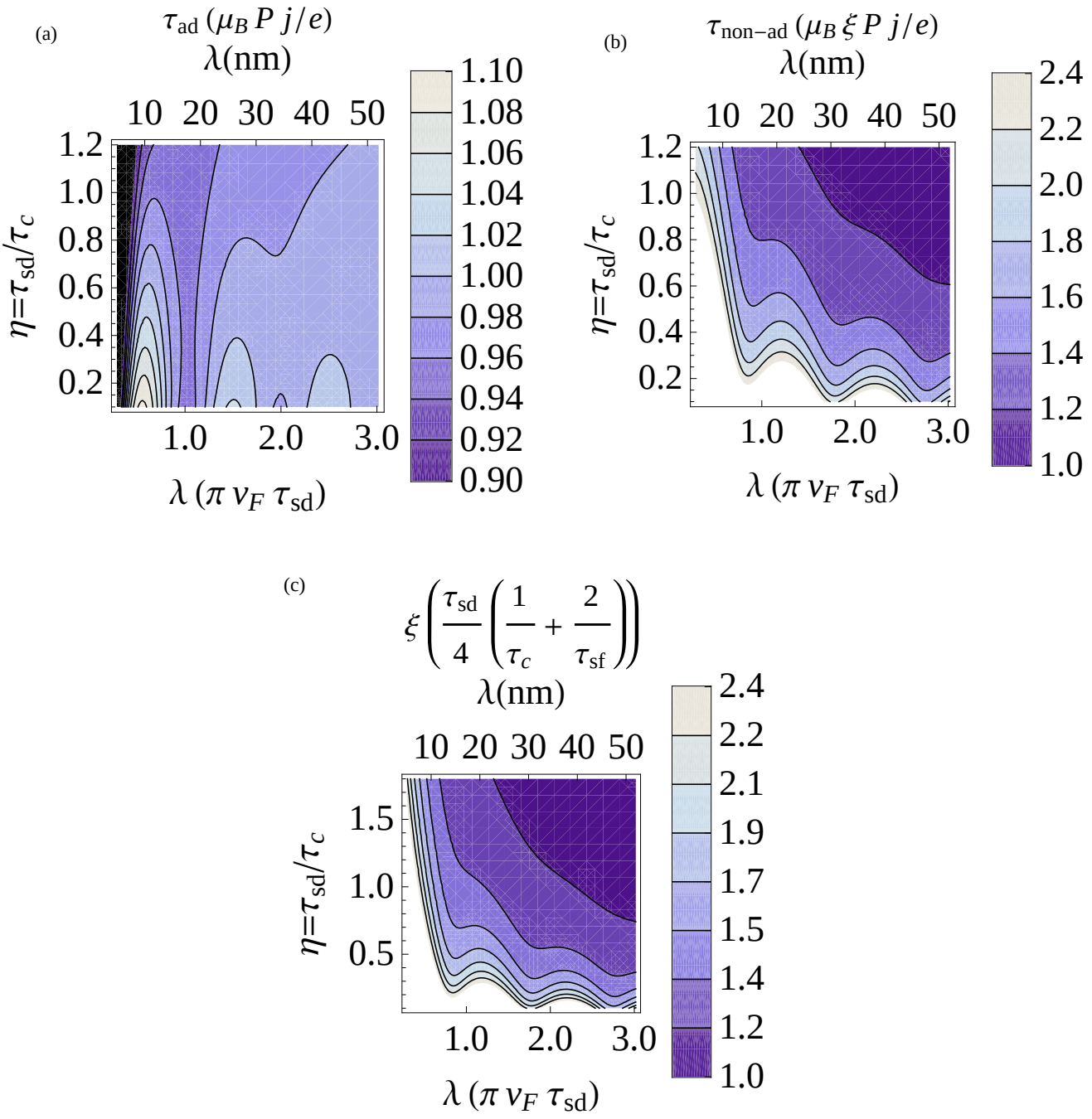

Figure 5.17: (Color online) (a) Adiabatic spin-transfer torque τ_{ad}, (b) non-adiabatic spin-transfer torque $\tau_{non\text{-}ad}$ and (c) degree of non-adiabaticity ξ for various domain-wall widths λ and transport regimes $\eta = \tau_{sd}/\tau_c$ for a positive intrinsic domain-wall resistivity ($\beta = 2$).

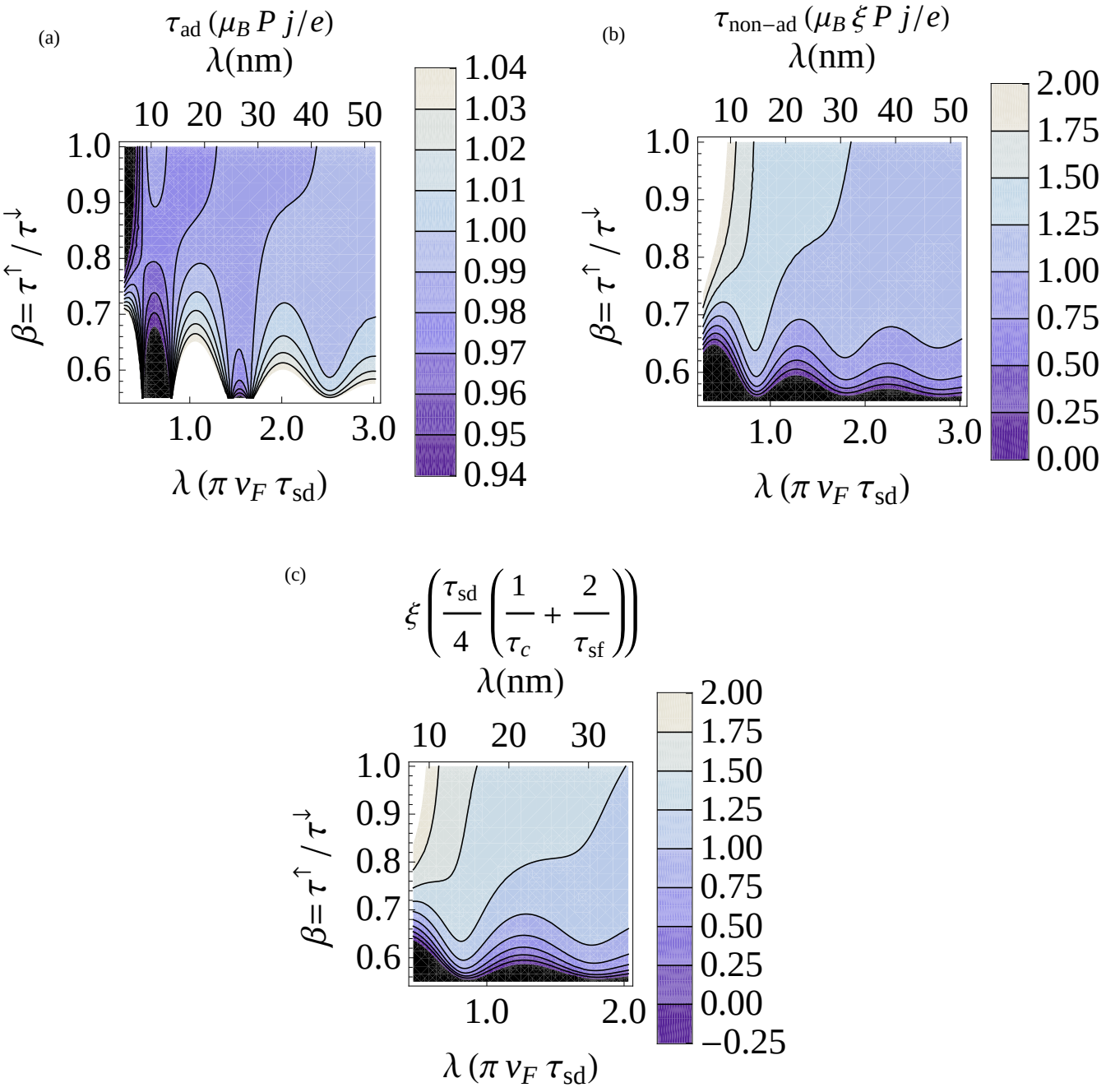

Figure 5.18: (Color online) (a) Adiabatic spin-transfer torque τ_{ad}, (b),(c) non-adiabatic spin-transfer torque and (d) degree of non-adiabaticity ξ for various domain-wall widths λ and anisotropy of scattering $\beta = \tau^{\uparrow}/\tau^{\downarrow}$ in the regime of ballistic spin transport ($\eta = 0.62$).

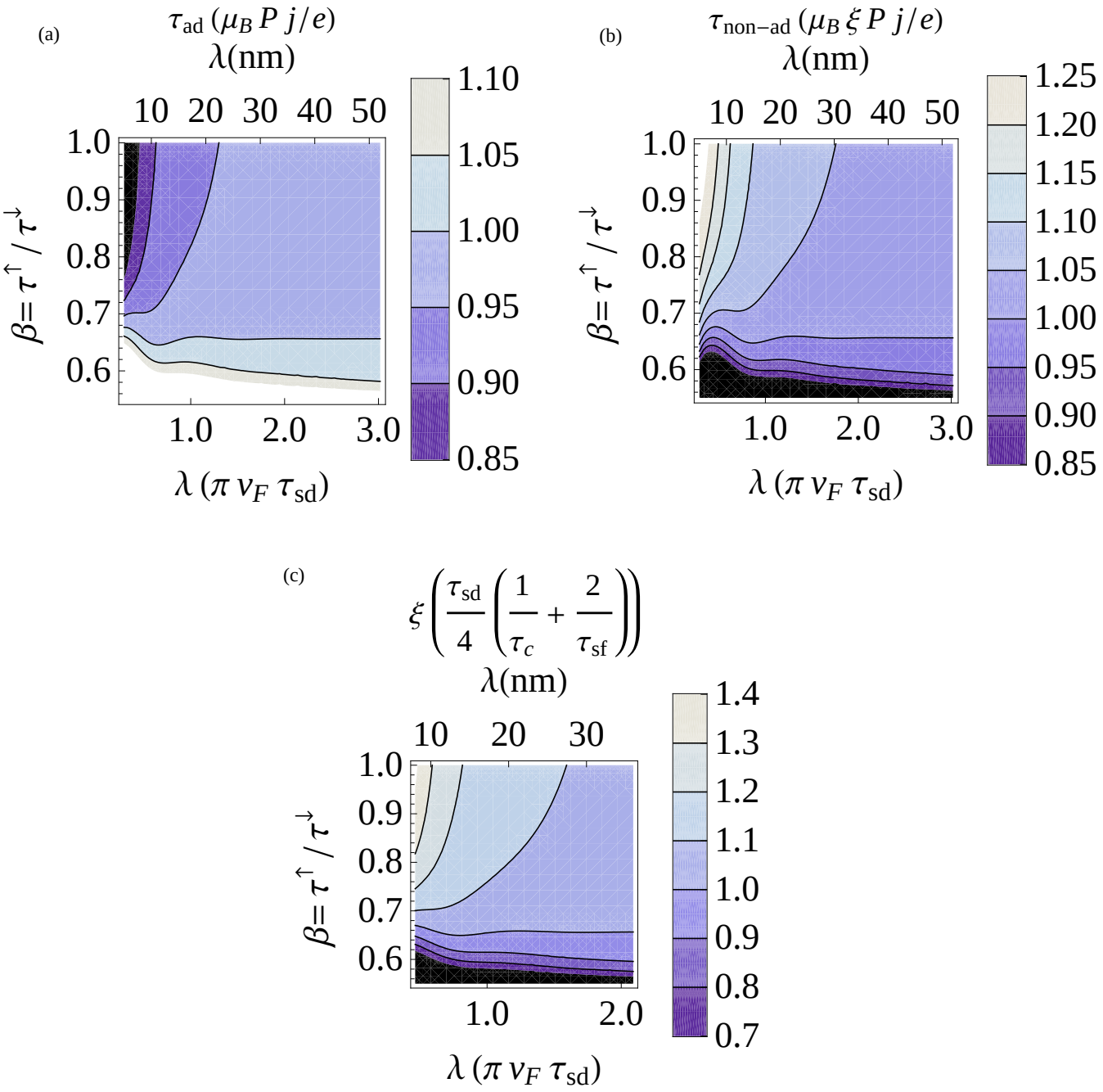

Figure 5.19: (Color online) (a) Adiabatic spin-transfer torque τ_{ad}, (b) non-adiabatic spin-transfer torque $\tau_{\text{non-ad}}$ and (c) degree of non-adiabaticity ξ for various domain-wall widths λ and anisotropy of scattering $\beta = \tau^{\uparrow}/\tau^{\downarrow}$ in the regime of diffusive spin transport ($\eta = 2$).

domain-wall resistivity (cf. discussion in section 5.5.5.3). Spin relaxation in metals is determined by the topology of the Fermi surface and dominated by hot spots on the Fermi surface. [240] Thus, relaxation times in metals and semiconductors can be tailored by modifications of the band structure, such as doping or alloying. Consequently, the ratio of relaxation times β defined in Eq. (5.247) is mainly determined by the kind of impurities. [183] There exist model calculations that predict that the ratio of relaxation times varies from $\beta = 0.2 - 30$ for Ni. [241, 242] As pointed out by Ref. [183], though β is experimentally not available, the experimental ratio of resistivities as given by Refs. [11, 169] is in a reasonable agreement with the calculated values for β. However, spin valve experiments allow the determination of the majority relaxation time and the calculation of the minority relaxation time can be accomplished by means of the two-current model in terms of the Boltzmann equation. [189] The determined values of β read for Py (=$Ni_{80}Fe_{20}$) and Fe, respectively: $\beta_{\text{Py}} \approx 7.7$, $\beta_{\text{Fe}} \approx 0.7$. [189] Accordingly, the dependence on β provides the possibility to experimentally test the sign dependence of the degree of non-adiabaticity by doping samples with impurities of different type and concentration. In this context systematic, experimental studies of the degree of non-adiabaticity in dependence of concentration and nature of impurities as well as the domain-wall width are required. [190]

Finally, we like to comment about experimental results concerning the non-adiabatic spin-transfer torque. First of all, an experimental discrimination of the degree of non-adiabaticity is problematic, since it is usually extracted from dynamical observations of domain-wall motion by fitting the measured data to numerical simulations. [102–109, 190–192] This method is equipped with a high degree of uncertainty, as the analysis is highly susceptible to sample inhomogeneities, Oersted fields or uncertain material parameters, for instance Gilbert damping α or shape anisotropy K. Consequently, the results for the value of ξ reported in the literature [102–109, 191, 192] differ by one order of magnitude. However, a quantitative analysis suffers up to date from the poor knowledge of the input parameters. As discussed in section 5.4.5, one order of magnitude difference in the degree of non-adiabaticity ξ can be already explained by the uncertainty in sd splitting J_{sd} and relaxation time τ_c. However, if non-adiabatic corrections are present, one order of magnitude difference for the same material can be readily explained by the impact of the magnetization texture on ξ. As it concerns the dynamical determination of ξ as extracted from domain-wall motion, a further problem is that the contributions of spin mistracking or other non-adiabatic sources cannot be distinguished from each other, which already led to confusion about interpreting experimental data. [243] This substantiates the need for systematic experimental studies of the degree of non-adiabaticity that circumvents its extraction from dynamical data. [244]
As it concerns narrow domain walls, much less experimental data is available. Recently, Feigenson et al. [223] reported the observation of a remarkably high value of $\xi \approx 0.5$ in $SrRuO_3$, an itinerant ferromagnet with perovskite structure. [58, 71, 215] Here, the domain walls are very narrow with approximately a width of 3 nm due to a very strong uniaxial anisotropy of about 10 T. Furthermore, it is reported that the domain wall moves with the current (against the electron flow), which disagrees with the present theories of spin-transfer torque and momentum transfer. [223] The possibility of a sign change of the non-adiabatic spin-transfer torque in dependence of the domain-wall width as outlined by the presented results serves for an explanation of this experimental finding. Furthermore, the large value of $\xi \approx 0.5$ is too high to originate from spin relaxation. However, following the presented

analysis it can be attributed to spin mistracking caused by the spatially strongly varying magnetization texture.
Recently, an experimental investigation of the degree of non-adiabaticity in narrow domain walls (1-10 nm) for CoNi and FePt wires reported that ξ stays small and quite insensitive with respect to the domain-wall width λ. [110] From the presented analysis such a behavior exists for a parameter regime of $\eta \approx 0.6$ and $\beta \approx 0.7$ (cf. Fig. 5.18 (c)). We note that a value of $\beta \approx 0.7$ is in agreement with experimental results on Fe impurities. [189]

Conclusion and comparison with results of the literature Vanhaverbeke and Viret employed a phenomenological, macroscopic Landau-Lifshitz equation that does not take into account the charge transport, the quantum nature of the spin of the conduction electron or spin-dependent scattering. [22] In particular, Vanhaverbeke and Viret presented numerical results that does not provide explanations. In contrast, our analytical calculation for narrow domain walls reveals the explicit dependence of the spin-transfer torque on the material parameters (foremost on the spin-dependent scattering times $\tau^{\uparrow}$, $\tau^{\downarrow}$). The crucial point in narrow domain walls is the damping of the precession of the conduction electrons due to decoherence. While Vanhaverbeke and Viret numerically took into account the damping of the oscillations in the spin-transfer torque by averaging "on the different directions the Fermi velocity can take on the Fermi sphere" (page 3 in Ref. [22]), our method relates the damping to the spin-dependent scattering times. In particular, $\tau^{\uparrow} < \tau^{\downarrow}$ turned out to be the essential requirement for a sign change in the degree of non-adiabaticity. Our conclusion that thus contrasts with Vanhaverbeke and Viret reads: The averaging process over the Fermi sphere does not cause a sign change, instead the sign change stems from the fact that the current is dominated by the minority electrons ($\tau^{\uparrow} < \tau^{\downarrow}$). Thorwart and Egger derived classical Bloch-Redfield equations and obtained detailed results for non-adiabatic higher-order terms in the spin-transfer torque. [233] They employed purely classical equations of motions that are generally limited to one spatial dimension and derived global coefficients for the higher-order terms. However, no discussion of the dependence of the non-adiabatic spin-transfer torque on the width of the domain wall is provided. Their corrections should be therefore interpreted as corrections to the first-order material parameters, independent of the magnetization texture, but do not indicate a non-trivial dependence of the spin-transfer torque on the width of the domain wall for narrow domain walls. In contrast, in this thesis the spin-transfer torque in narrow domain walls is computed by means of local distribution matrices. This allows to trace back the origin of the increase in the degree of non-adiabaticity and its dependence on the domain-wall width. Consequently, our expressions explicitly take into account the magnetization texture. This is of great importance, since with the perspective of future micromagnetic simulations the locality of our derived spin-transfer torque promises rich current-induced magnetization dynamics that is not accessible by the average, global description as it is provided by Thorwart and Egger. Our critique of the work of Thorwart and Egger bases on the following argument: In our manuscript we demonstrate the need to consider coupled charge and spin transport in narrow domain walls. In particular, due to the magnetization twist the charge along with the longitudinal channel constitute the origin of the spin-transfer torque that result for narrow domain walls in the local, spatially dependent non-adiabatic corrections. Thorwart and Egger do not consider the charge current that in their model decouples from the spin sector and a contribution of the charge transport to the spin-transfer torque is not included in their concept. This

point we put in question as it concerns the correct description of narrow domain walls.
Taniguchi, Sato, and Imamura considered the macroscopic transport equations of Refs. [185, 197] by applying the diffusive approximation to the Boltzmann equation. [232] Accordingly, they restricted themselves to the regime of diffusive transport and did not take into account possible coherence effects in the regime of ballistic spin transport. In the diffusive regime, the spin transport is dominated by spin relaxation and the influence of spin mistracking due to the magnetization texture is negligible. Furthermore, they did not consider spin-dependent scattering. Accordingly, they did not observe a sign change in the non-adiabatic spin-transfer torque with the domain-wall width.

In summary, with the onset of spin mistracking in narrow domain walls, the degree of non-adiabaticity ξ ceases to be a material parameter but depends crucially on the set of parameters: λ, J_{sd}, $\tau^{\uparrow}$, $\tau^{\downarrow}$. This yields a huge parameter space for tailoring nanowires with desired functionality for technological applications. [19, 20]

5.5.5.3 Second-order solution – domain-wall resistivity

In the preceding sections the zeroth and first-order solutions have been calculated that yield the spatially independent bulk solution and the transverse magnetization of the conduction electrons, respectively. In this section we compute the second-order of the non-equilibrium distribution functions that introduces a non-adiabatic, spatially-dependent correction to the majority and minority spin channels as a consequence of the strong magnetization twist in narrow domain walls. The correction to the charge channel leads to an intrinsic domain-wall resistivity and to a spatially inhomogeneous electron density. The correction to the longitudinal component of the magnetization of the conduction electrons is responsible for momentum transfer between the conduction electrons and the domain wall and a spatial dependence in the longitudinal spin current.

For every order of the κ expansion, the spatial differential equation on the left hand side of Eq. (5.249) exhibits the same shape as the zeroth-order differential equation in Eq. (5.210). In this sense, the decomposition in transverse and longitudinal degrees of freedom is perturbatively exact. We proceed with the complexified kinetic equation as given by Eq. (5.214). The first-order solution reads

$$
\begin{aligned}
{}^{(1)}\vec{\tilde{g}}_{\vec{k}}(x) = -4\pi i \Bigg[& \Theta(v_x) \left(1 - e^{-\frac{\left(\frac{1}{2\tau_c} + \frac{1}{\tau_{\mathrm{sf}}} - i\frac{2}{\tau_{\mathrm{sd}}}\right)}{v_x} x} \right) + \Theta(-v_x) \left(1 - e^{\frac{\left(\frac{1}{2\tau_c} + \frac{1}{\tau_{\mathrm{sf}}} - i\frac{2}{\tau_{\mathrm{sd}}}\right)}{v_x} (\lambda - x)} \right) \Bigg] \\
& \frac{eE_x \tau_c^2 \tau_s \tau_{\mathrm{sf}}}{l_{\mathrm{mfp}} m \tau_{\mathrm{sd}} \left(2\tau_c \tau_s^2 + \tau_{\mathrm{sf}} \left(\tau_s^2 - \tau_c^2\right)\right) \left(2\tau_c(\tau_{\mathrm{sd}} - 2i\tau_{\mathrm{sf}}) + \tau_{\mathrm{sf}}\tau_{\mathrm{sd}}\right)} \\
& \Big[\partial_\epsilon f^{\mathrm{charge}}(\epsilon, J_{\mathrm{sd}}) \tau_{\mathrm{sd}} (\hbar\tau_s(2\tau_c + \tau_{\mathrm{sf}}) - m v_x^2 \tau_c \tau_{\mathrm{sd}} \tau_{\mathrm{sf}}) \\
& \quad + \partial_\epsilon^2 f^{\mathrm{charge}}(\epsilon, J_{\mathrm{sd}}) \hbar \left(\hbar\tau_c\tau_{\mathrm{sf}} + 2 m v_x^2 \tau_s \tau_{\mathrm{sd}} \tau_c\right) \\
& \quad + \partial_\epsilon^3 f^{\mathrm{charge}}(\epsilon, J_{\mathrm{sd}}) \hbar^2 m v_x^2 \tau_c \tau_{\mathrm{sf}} \Big] \begin{pmatrix} 0 \\ 0 \\ 1 \end{pmatrix} .
\end{aligned}
\tag{5.248}
$$

The determing equation for the second-order solution follows from Eq. (5.209) by a comparison of the coefficients $\propto \kappa^2$

$$v_x \partial_x \vec{\tilde{g}}^{(2)}_{\vec{k}}(x) + \mathcal{A} \vec{\tilde{g}}^{(2)}_{\vec{k}}(x) = -l_{\text{mfp}}^{-1} \left(v_x \mathcal{B} \vec{\tilde{g}}^{(1)}_{\vec{k}}(x) + \mathcal{C} \partial_{k_x} \vec{\tilde{g}}^{(1)}_{\vec{k}}(x) \right). \tag{5.249}$$

The derivative with respect to k_x of the first-order solution (5.248) reads

$$\begin{aligned}
&\partial_{k_x} \vec{\tilde{g}}^{(1)}_{\vec{k}}(x) \\
&= 2\pi i z_3 \Big[\Theta(v_x) \Big(\partial_\epsilon f^{\text{charge}}(\epsilon, J_{\text{sd}}) \left(d_1 e^{-\frac{z_1}{v_x} x} v_x^{-2} + d_2 e^{-\frac{z_1}{v_x} x} + d_3 \left(1 - e^{-\frac{z_1}{v_x} x} \right) v_x \right) \\
&\quad + \partial_\epsilon^2 f^{\text{charge}}(\epsilon, J_{\text{sd}}) \left(d_4 e^{-\frac{z_1}{v_x} x} v_x^{-2} + d_5 e^{-\frac{z_1}{v_x} x} + d_6 \left(1 - e^{-\frac{z_1}{v_x} x} \right) v_x + d_7 \left(1 - e^{-\frac{z_1}{v_x} x} \right) v_x^3 \right) \\
&\quad + \partial_\epsilon^3 f^{\text{charge}}(\epsilon, J_{\text{sd}}) \left(d_8 e^{-\frac{z_1}{v_x} x} + d_9 \left(1 - e^{-\frac{z_1}{v_x} x} \right) v_x + d_{10} \left(1 - e^{-\frac{z_1}{v_x} x} \right) v_x^3 \right) \\
&\quad + \partial_\epsilon^4 f^{\text{charge}}(\epsilon, J_{\text{sd}}) d_{11} \left(1 - e^{-\frac{z_1}{v_x} x} \right) v_x^3 \Big) + \Theta(-v_x) \left(x \to (x - \lambda) \right) \Big] \begin{pmatrix} 0 \\ 0 \\ 1 \end{pmatrix},
\end{aligned} \tag{5.250}$$

with the abbreviations are given in appendix F. For the determination of the second-order solution, we neglect in the following the contribution due to spin-flip scattering by taking the limit ($\tau_{\text{sf}} \to \infty$) of Eq. (5.249). This means, the spin-dependent momentum relaxation times $\tau^\uparrow$, $\tau^\downarrow$ are from now on the sole remaining scattering times. With this simplification the second-order equation (5.249) reduces to

$$v_x \partial_x \begin{pmatrix} {}^{(2)}\tilde{g}_{\vec{k}}(x) \\ {}^{(2)}\tilde{g}^z_{\vec{k}}(x) \\ {}^{(2)}\tilde{g}^{\text{trans}}_{\vec{k}}(x) \end{pmatrix} + \begin{pmatrix} \frac{1}{2\tau_c} & \frac{1}{2\tau_s} & 0 \\ \frac{1}{2\tau_s} & \frac{1}{2\tau_c} & 0 \\ 0 & 0 & \left(\frac{1}{2\tau_c} - i \frac{2}{\tau_{\text{sd}}} \right) \end{pmatrix} \begin{pmatrix} {}^{(2)}\tilde{g}_{\vec{k}}(x) \\ {}^{(2)}\tilde{g}^z_{\vec{k}}(x) \\ {}^{(2)}\tilde{g}^{\text{trans}}_{\vec{k}}(x) \end{pmatrix} = \frac{\pi}{l_{\text{mfp}}} \begin{pmatrix} \frac{1}{\tau_{\text{sd}}} \Delta_1 \\ v_x \Delta_2 \\ 0 \end{pmatrix}, \tag{5.251}$$

where we introduced the abbreviations

$$\Delta_1 = \Im \left(\lim_{\tau_{\text{sf}} \to \infty} \partial_{k_x} {}^{(1)}\tilde{g}^{\text{trans}}_{\vec{k}}(x) \right), \tag{5.252}$$

$$\Delta_2 = \Im \left(\lim_{\tau_{\text{sf}} \to \infty} {}^{(1)}\tilde{g}^{\text{trans}}_{\vec{k}}(x) \right). \tag{5.253}$$

The explicit expressions for the Eqns. (5.252) and (5.253) can be found in appendix F.
From Eq. (5.251) the influence of the imaginary part of the transverse spin distribution on the majority and minority channel can be recognized. According to Eq. (5.251) the imaginary part of the transverse first-order distribution acts on the r.h.s. of Eq. (5.251) as an inhomogeneity for the second order Eq. (5.251). The channel mixing stems from the gauge transformation as caused by the magnetization twist. According to Eq. (5.239) the imaginary part of the transverse distribution constitutes the non-adiabatic spin-transfer torque. In this sense, the non-adiabatic spin-transfer torque accounts for a non-vanishing second-order result. The magnetization twist couples the majority and minority channels with the non-adiabatic transverse spin channel that is responsible for a correction of the charge and longitudinal channels. In this sense, transverse spin accumulation as provided by the non-adiabatic channel is the origin of domain-wall resistivity and momentum transfer.

As discussed in section 5.2, in the absence of spin-flip scattering the kinetic equation in a homogeneous domain without magnetization twist ($\partial_x \phi(x) = 0$) is diagonal in the majority, minority basis. The majority and minority channels completely decouple and can be treated separately. Accordingly, without the presence of spin-flip scattering the majority, minority basis constitutes a more appropriate basis for the solution of Eq. (5.251). A diagonalization of Eq. (5.251) corresponds to a transformation to the majority, minority spin basis $\{{}^{(2)}\tilde{g}^{\uparrow}_{\vec{k}}(x), {}^{(2)}\tilde{g}\downarrow^{z}_{\vec{k}}(x), {}^{(2)}\tilde{g}^{\text{trans}}_{\vec{k}}(x)\}^T$. In this new basis, Eq. (5.251) reads

$$\begin{pmatrix} v_x\partial_x + \frac{1}{\tau^{\uparrow}} & 0 & 0 \\ 0 & v_x\partial_x + \frac{1}{\tau^{\downarrow}} & 0 \\ 0 & 0 & v_x\partial_x + \left(\frac{1}{2\tau_c} - i\frac{2}{\tau_{\text{sd}}}\right) \end{pmatrix} \begin{pmatrix} {}^{(2)}\tilde{g}^{\uparrow}_{\vec{k}}(x) \\ {}^{(2)}\tilde{g}^{\downarrow}_{\vec{k}}(x) \\ {}^{(2)}\tilde{g}^{\text{trans}}_{\vec{k}}(x) \end{pmatrix} = \frac{\pi}{l_{\text{mfp}}\tau_{\text{sd}}} \begin{pmatrix} \Delta_1 + v_x\tau_{\text{sd}}\Delta_2 \\ \Delta_1 - v_x\tau_{\text{sd}}\Delta_2 \\ 0 \end{pmatrix}. \tag{5.254}$$

In the diagonal basis the three independent Eqns. (5.254) are now easily solved and yield as general solutions

$${}^{(2)}\tilde{g}^{\uparrow}_{\vec{k}}(x) = \left(1 + F(\vec{v}_{\vec{k}})e^{-\frac{x}{v_x\tau^{\uparrow}}}\right)\frac{\pi\tau^{\uparrow}}{l_{\text{mfp}}\tau_{\text{sd}}}\left[\Delta_1 + v_x\tau_{\text{sd}}\Delta_2\right], \tag{5.255}$$

$${}^{(2)}\tilde{g}^{\downarrow}_{\vec{k}}(x) = \left(1 + F(\vec{v}_{\vec{k}})e^{-\frac{x}{v_x\tau^{\downarrow}}}\right)\frac{\pi\tau^{\downarrow}}{l_{\text{mfp}}\tau_{\text{sd}}}\left[\Delta_1 - v_x\tau_{\text{sd}}\Delta_2\right], \tag{5.256}$$

$${}^{(2)}\tilde{g}^{\text{trans}}_{\vec{k}}(x) = F(\vec{v}_{\vec{k}})e^{-\frac{\left(\frac{1}{2\tau_c} - i\frac{2}{\tau_{\text{sd}}}\right)}{v_x}x}. \tag{5.257}$$

Analogously to the first-order solution, the arbitrary functions $F(\vec{v}_{\vec{k}})$ are determined by vanishing boundary conditions at the beginning and the end of the domain wall for each of the Eqns. (5.255) to (5.257) individually. This results immediately in a vanishing second-order transverse distribution

$${}^{(2)}\tilde{g}^{\text{trans}}_{\vec{k}}(x) = 0. \tag{5.258}$$

As discussed in the previous chapters corrections to the transverse magnetization of the conduction electrons solely emerge in odd orders of κ. The reason for this is that transverse corrections are sensitive to the sense of rotation of the local moments within the domain wall.

The necessary boundary conditions for the homogeneous domain are already implemented in the zeroth-order majority and minority distribution functions. Thus all higher orders of the perturbative expansion must be solved with vanishing boundary conditions. As in the case of the first-order solution this determines the function $F(\vec{v}_{\vec{k}})$ and yields for the sum of all rightmoving ($v_x > 0$) and leftmoving ($v_x < 0$) majority, minority distribution functions

$$\begin{aligned} {}^{(2)}\tilde{g}^{s}_{\vec{k}}(x) = \frac{\pi\tau^s}{l_{\text{mfp}}\tau_{\text{sd}}}\Theta(v_x)\Big[&2\Delta_1\left(1 - e^{-\frac{\lambda}{2v_x\tau^s}}\cosh\frac{2(x-\lambda)}{2v_x\tau^s}\right) \\ &+ sv_x\tau_{\text{sd}}\Delta_2\left(2e^{-\frac{\lambda}{2v_x\tau^s}}\sinh\frac{2(x-\lambda)}{2v_x\tau^s}\right)\Big], \end{aligned} \tag{5.259}$$

where $s \pm 1$ stands for $s = \{\uparrow, \downarrow\}$ and denotes the majority, minority character.
We note from Eq. (5.259) that the solutions ${}^{(2)}\tilde{g}^{\uparrow}_{\vec{k}}(x)$ and ${}^{(2)}\tilde{g}^{\downarrow}_{\vec{k}}(x)$ are symmetric with respect to the transformations

$$\begin{aligned} {}^{(2)}\tilde{g}^{\uparrow}_{\vec{k}}(x) &\iff {}^{(2)}\tilde{g}^{\downarrow}_{\vec{k}}(x), \\ \tau^{\uparrow} &\Leftrightarrow \tau^{\downarrow}, \\ \Delta_2 &\Leftrightarrow -\Delta_2. \end{aligned} \tag{5.260}$$

The final result for the spin-dependent second-order non-equilibrium distributions reads

$$\begin{aligned} {}^{(2)}\tilde{g}^{s}_{\vec{k}}(x) = \frac{2\pi\tau^s}{l_{\text{mfp}}\tau_{\text{sd}}}\tilde{z}_2 e^{-\frac{x+\lambda}{2v_x\tau_c}}\Theta(v_x) \\ \Big[\partial_\epsilon f^{\text{charge}}(\epsilon, J_{\text{sd}})A(x,\lambda,v_x) + \partial^2_\epsilon f^{\text{charge}}(\epsilon, J_{\text{sd}})B(x,\lambda,v_x) \\ + \partial^3_\epsilon f^{\text{charge}}(\epsilon, J_{\text{sd}})C(x,\lambda,v_x) + \partial^4_\epsilon f^{\text{charge}}(\epsilon, J_{\text{sd}})D(x,\lambda,v_x)\Big]. \end{aligned} \tag{5.261}$$

with the following abbreviations

$$\begin{aligned} A(x,\lambda,v_x) &= \left(v_x^{-2}\tilde{d}_1 + \tilde{d}_2\right)\mathcal{H}(x,\lambda,v_x)\left(1 - e^{-\frac{\lambda}{2v_x\tau^s}}\cosh\frac{\lambda-2x}{2v_x\tau^s}\right) \\ &\quad + s\tau_{\text{sd}}v_x^3\tilde{c}_2 e^{-\frac{\lambda}{2v_x\tau^s}}\mathcal{G}(x,\lambda,v_x)\sinh\frac{2x-\lambda}{2v_x\tau^s} + v_x\Big[\tilde{d}_3\mathcal{I}(x,\lambda,v_x) \\ &\quad + e^{-\frac{\lambda}{2v_x\tau^s}}\left(-\tilde{d}_3\mathcal{I}(x,\lambda,v_x)\cosh\frac{\lambda-2x}{2v_x\tau^s} + s\tau_{\text{sd}}\tilde{c}_1\mathcal{G}(x,\lambda,v_x)\sinh\frac{2x-\lambda}{2v_x\tau^s}\right)\Big], \\ B(x,\lambda,v_x) &= \left(v_x^{-2}\tilde{d}_4\mathcal{H}(x,\lambda,v_x) + v_x^3\tilde{d}_6\mathcal{I}(x,\lambda,v_x)\right)\left(1 - e^{-\frac{\lambda}{2v_x\tau^s}}\cosh\frac{\lambda-2x}{2v_x\tau^s}\right) \\ &\quad + v_x\Big[\tilde{d}_5\mathcal{I}(x,\lambda,v_x) + e^{-\frac{\lambda}{2v_x\tau^s}}\Big(-\tilde{d}_5\mathcal{I}(x,\lambda,v_x)\cosh\frac{\lambda-2x}{2v_x\tau^s} \\ &\quad + s\tau_{\text{sd}}\tilde{c}_3\mathcal{G}(x,\lambda,v_x)\sinh\frac{2x-\lambda}{2v_x\tau^s}\Big)\Big], \\ C(x,\lambda,v_x) &= \left(\tilde{d}_7\mathcal{H}(x,\lambda,v_x) + v_x\tilde{d}_8\mathcal{I}(x,\lambda,v_x)\right)\left(1 - e^{-\frac{\lambda}{2v_x\tau^s}}\cosh\frac{\lambda-2x}{2v_x\tau^s}\right) \\ &\quad + s\tau_{\text{sd}}v_x^3\tilde{c}_5 e^{-\frac{\lambda}{2v_x\tau^s}}\mathcal{G}(x,\lambda,v_x)\sinh\frac{2x-\lambda}{2v_x\tau^s}, \\ D(x,\lambda,v_x) &= v_x^3\tilde{d}_9\mathcal{I}(x,\lambda,v_x)\left(1 - e^{-\frac{\lambda}{2v_x\tau^s}}\cosh\frac{\lambda-2x}{2v_x\tau^s}\right). \end{aligned} \tag{5.262}$$

To determine the macroscopic quantities according to Eqns. (5.2) to (5.5), we have to carry out the momentum integration of Eq. (5.261). The currents are obtained the same way by an inclusion of a

factor v_x that we add in brackets in the following

$$\begin{aligned}
{}^{(2)}n^s(x)\langle\,{}^{(2)}j^s(x)\rangle &= -\kappa^2\int\frac{d^3k}{(2\pi)^3}\langle v_x\rangle\,{}^{(2)}\tilde{g}^s_{\vec{k}}(x)\,\Theta(v_x)\\
&= -\kappa^2\frac{2\pi\tau^s m^3}{l_{\text{mfp}}\tau_{\text{sd}}}\tilde{z}_2\int\frac{d^3v}{(2\pi\hbar)^3}\,\Theta(v_x)\\
&\quad\langle v_x\rangle e^{-\frac{x+\lambda}{2v_x\tau_c}}\Big[\partial_\epsilon f^{\text{charge}}(\epsilon,J_{\text{sd}})A(x,\lambda,v_x)+\partial_\epsilon^2 f^{\text{charge}}(\epsilon,J_{\text{sd}})B(x,\lambda,v_x)\\
&\quad+\partial_\epsilon^3 f^{\text{charge}}(\epsilon,J_{\text{sd}})C(x,\lambda,v_x)+\partial_\epsilon^4 f^{\text{charge}}(\epsilon,J_{\text{sd}})D(x,\lambda,v_x)\Big],
\end{aligned}\tag{5.263}$$

The ϕ integration is trivial and the Θ-function restricts the $\cos\theta$ integration. The higher derivatives of the Fermi function in Eq. (5.263) are shifted by means of partial integrations

$$\begin{aligned}
{}^{(2)}n^s(x)\langle\,{}^{(2)}j^s(x)\rangle &= \kappa^2\frac{\sqrt{2}\tau^s m^2}{2\pi\hbar^3\sqrt{m}l_{\text{mfp}}\tau_{\text{sd}}}\tilde{z}_2\int_0^\infty d\epsilon\int_0^1 d(\cos\theta)\left(-\partial_\epsilon f^{\text{charge}}(\epsilon,J_{\text{sd}})\right)\\
&\quad\Big[A(x,\lambda,v_x)\sqrt{\epsilon}\langle v_x\rangle e^{-\frac{x+\lambda}{2v_x\tau_c}}-\partial_\epsilon\left(\sqrt{\epsilon}\langle v_x\rangle e^{-\frac{x+\lambda}{2v_x\tau_c}}B(x,\lambda,v_x)\right)\\
&\quad+\partial_\epsilon^2\left(\sqrt{\epsilon}\langle v_x\rangle e^{-\frac{x+\lambda}{2v_x\tau_c}}C(x,\lambda,v_x)\right)-\partial_\epsilon^3\left(\sqrt{\epsilon}\langle v_x\rangle e^{-\frac{x+\lambda}{2v_x\tau_c}}D(x,\lambda,v_x)\right)\Big].
\end{aligned}\tag{5.264}$$

The calculation of the energy derivatives provides the analytical integration of Eq. (5.264). The calculation is too extensive to be presented here and we refrain from giving analytical results at this point. However, the second-order solution holds a few interesting quantities, like a correction to the charge current that gives rise to an intrinsic domain-wall resistivity

$$j^{(2)}_{\text{charge}}(x) = e\left({}^{(2)}j^{\uparrow}(x)+{}^{(2)}j^{\downarrow}(x)\right),\tag{5.265}$$

a spatially varying electron density

$$n^{(2)}(x) = e\left({}^{(2)}n^{\uparrow}(x)+{}^{(2)}n^{\downarrow}(x)\right),\tag{5.266}$$

a spatially varying z component of the magnetization of the conduction electrons

$$\langle{}^{(2)}\hat{\sigma}_z(x)\rangle = \mu_{\text{B}}\left({}^{(2)}n^{\uparrow}(x)-{}^{(2)}n^{\downarrow}(x)\right),\tag{5.267}$$

and a spatially varying longitudinal spin current

$$j^{(2)}_{\text{spin}}(x) = \mu_{\text{B}}\left({}^{(2)}j^{\uparrow}(x)-{}^{(2)}j^{\downarrow}(x)\right).\tag{5.268}$$

Domain-wall resistivity In this section the intrinsic domain-wall resistivity is derived. It follows from symmetry considerations that resistivity corrections appear in the second order of the magnetization twist $\kappa\propto\partial_x\phi(x)$. The intrinsic resistivity of a domain wall is degenerate with respect to the sense of rotation of the local moments within the domain wall. The domain-wall resistivity is thus associated with the energy of the domain wall and is of even order in the magnetization twist. In contrast, the spin-transfer torque as calculated in the previous section depends on the sense of rotation

and is therefore present in odd orders of the magnetization twist.
The total charge conductivity in the presence of a domain wall reads up to fourth order in κ

$$\begin{aligned}\sigma_{\text{tot}} &= \sigma_0 + \sigma_{\text{dw}} + \mathcal{O}(\kappa^4) \\ &= \sigma_0 \left(1 - Z\right), \end{aligned} \tag{5.269}$$

where σ_0 is the bulk conductivity in Eq. (5.220) and

$$Z = -\frac{\sigma_{\text{dw}}}{\sigma_0}, \tag{5.270}$$

symbolizes the correction due to the presence of the domain wall. The conductivity correction translates into a resistivity correction

$$\begin{aligned}\rho_{\text{dw}} &= \rho_{\text{tot}} - \rho_0 \\ &= \rho_0 \left[(1 - Z)^{-1} - 1\right] \\ &\simeq Z\rho_0 \\ &= -\frac{\sigma_{\text{dw}}}{\sigma_0^2}, \end{aligned} \tag{5.271}$$

where we employed that $|Z| \ll 1$.

Figure 5.20 depicts the spatial dependence of the intrinsic domain-wall resistivity within the region of the domain wall for two domain walls of different width λ. The resistivity correction gets more important by decreasing the width of the domain wall. The local resistivity correction changes sign within the domain wall, starting from a negative correction at the beginning to a positive correction at the end. In the regime of ballistic spin transport depicted in Fig. 5.20 (a), (b) the oscillations are more pronounced compared with the diffusive regime as illustrated in Fig. 5.20 (c), (d).
Figure 5.21 depicts the spatially varying correction to the homogeneous electron density due to the presence of a domain wall for two different domain-wall widths. The correction to the electron density becomes more important with decreasing domain-wall width λ. In all cases the correction to the electron density changes sign within the domain wall, starting from a positive correction at the beginning and ending with a negative correction. In the regime of ballistic spin transport depicted in Fig. 5.21 (a), (b) the oscillations are more pronounced compared with the diffusive regime in Fig. 5.21 (c), (d). The pronounced corrections to the resistivity and electron density at the beginning and the end must be attributed to the linear domain-wall profile (cf. discussion in section 5.5.5.2). Accordingly, the corrections become less pronounced in the middle of the domain wall according to the constant gradient in magnetization. The oscillations are damped out due to impurity scattering. The presence of the strong magnetization twist at the beginning of the domain wall causes an accumulation of conduction electrons. A higher local electron density results in a reduced local resistivity. If we compare the resistivity correction in Fig. 5.20 with the local electron density in Fig. 5.21 we find an affirmation of this classical conjecture. Note, however, that a relation between the charge accumulation and the electric current is in general established by the non-local macroscopic transport equations. A spatially varying density of the conduction electrons due to the presence of a domain wall could be experimentally observed by scanning tunneling microscopy (STM).

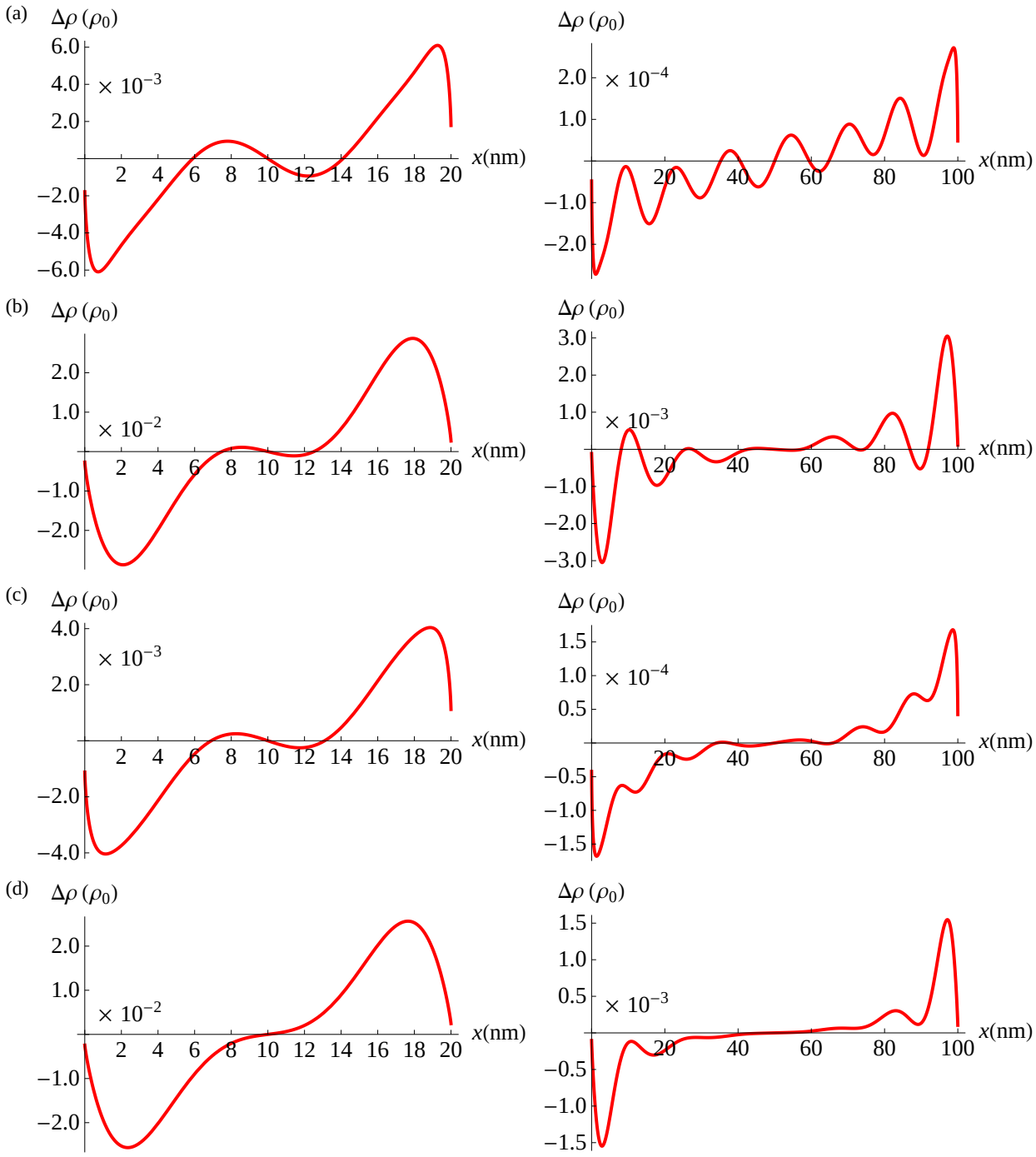

Figure 5.20: (Color online) Spatially resolved resistivity correction within two domain walls of different width λ. Left: λ = 20 nm. Right: λ = 100 nm. (a) The transport regime is ballistic ($\eta = 0.62$) with a ratio of relaxation times smaller than one ($\beta = 0.57$). (b) The transport regime is ballistic ($\eta = 0.62$) with a ratio of relaxation times larger than one ($\beta = 2$). (c) The transport regime is diffusive ($\eta = 1.2$) with a ratio of relaxation times smaller than one ($\beta = 0.57$). (d) The transport regime is diffusive ($\eta = 1.2$) with a ratio of relaxation times larger than one ($\beta = 2$).

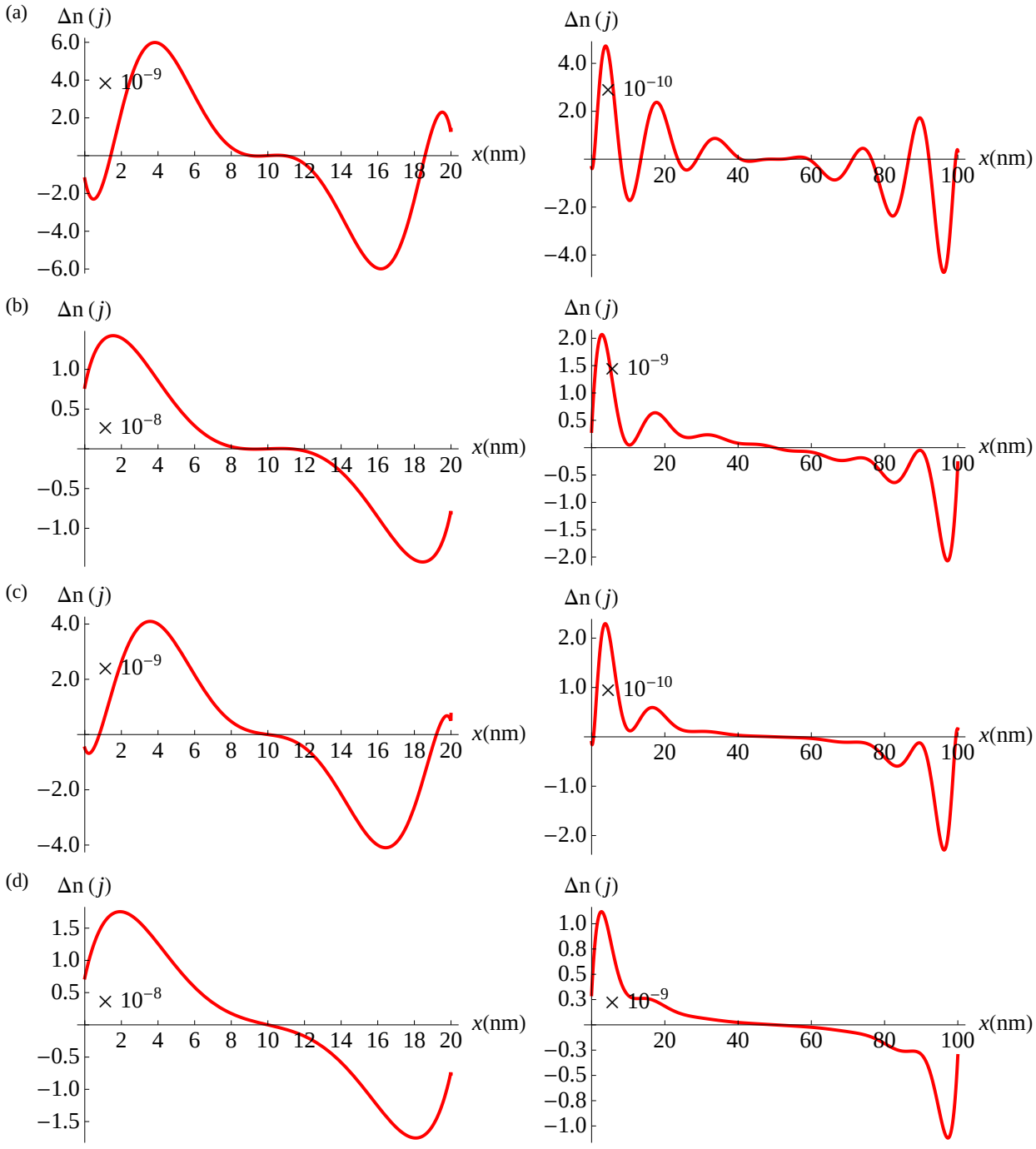

Figure 5.21: (Color online) Spatially resolved correction to the electron density within two domain walls of different width λ. Left: λ = 20 nm. Right: λ = 100 nm. (a) The transport regime is ballistic ($\eta = 0.62$) with a ratio of relaxation times smaller than one ($\beta = 0.57$). (b) The transport regime is ballistic ($\eta = 0.62$) with a ratio of relaxation times larger than one ($\beta = 2$). (c) The transport regime is diffusive ($\eta = 1.2$) with a ratio of relaxation times smaller than one ($\beta = 0.57$). (d) The transport regime is diffusive ($\eta = 1.2$) with a ratio of relaxation times larger than one ($\beta = 2$).

Let us turn the attention to the experimentally most relevant quantity of the total intrinsic domain-wall resistivity that is obtained by summing up the local conductivity correction within the domain wall and calculating the total intrinsic domain-wall resistivity according to Eq. (5.271). Figure 5.22 depicts the total intrinsic domain-wall resistivity in dependence on the domain-wall width λ and the parameter η that indicates the transport regime or β that characterizes the ratio of the relaxation times, respectively. In general, oscillations in the resistivity occur in the limit of ballistic spin transport ($\eta < 1$) and are washed out when approaching the diffusive regime ($\eta > 1$). The sign of the domain-wall resistivity depends for $\beta < 1$ in a non-trivial manner on the set of all parameters, foremost on the width λ of the domain wall. In the case of $\beta < 1$ an enhancement or a suppression of the electron transport depends on the ratio of the domain-wall width λ in comparison with the wavelength λ_F of the conduction electrons as defined in Eq. (5.245). The oscillations of $\Delta\rho$ with λ coincide with the oscillations in the non-adiabatic spin-transfer torque found in narrow domain walls for ballistic spin transport ($\eta < 1$) (cf. Fig. 5.16 (b)). The sign of the resistivity correction depends on the ability of the precessing conduction electron spins to track the local moments: A positive domain-wall resistivity corresponds to a lag of the spin of the conduction electron compared to the local moments, while a negative resistivity relates to itinerant spins that are running ahead. Accordingly, $\Delta\rho$ is positive for $(n + 3/4)\lambda_\mathrm{F}$, negative for $(n + 1/4)\lambda_\mathrm{F}$ and tends to zero for $(n + 1)/2\lambda_\mathrm{F}$, $n \in \mathbb{N}_0$. In analogy to other spin-controlled architectures [245], the precessing conduction-electron spin is found to determine the electrical transport properties in narrow domain walls. Due to the strong magnetization twist in narrow domain walls the majority, minority channels get mixed. A majority electron incident on the domain wall attains a minority contribution and vice versa. The coupling of the non-adiabatic channel to the majority and minority channels causes a redistribution within the majority and minority channels. According to Eq. (5.251) transverse spin accumulation causes the domain-wall resistivity and the oscillations in the transverse spin accumulation directly translate to the domain-wall resistivity. Hence, the oscillations with the domain-wall width λ originate from the precession of the transverse spin accumulation around the local magnetization. [197]

For $\beta > 1$ as depicted in Fig. 5.22 (a) the current is mainly carried by the majority electrons and the domain wall constitutes an entirely positive resistivity correction. This can be attributed to enhanced scattering as caused by the spatially strongly varying magnetization texture. By mixing the majority and minority channels the presence of the domain wall removes the high conducting shunt channel present in a homogeneous ferromagnet. [63] In this case domain-wall resistivity can be regarded as the continuous analogue of the giant magnetoresistance effect in multilayer structures. The resistance is higher for the antiparallel alignment between free and fixed layer – the wire contains a domain wall – and lowered in a parallel reorientation of the free and fixed layer by applying an external magnetic field – by saturating the sample –. For very narrow domain walls the resistivity correction approaches the percent regime. This is in accordance with experimental findings about positive domain-wall resistivities. [215]

In the opposite case ($\beta < 1$) as depicted in Fig. 5.22 (b) the current is mainly carried by the minority electrons. Interestingly, the case of $\beta < 1$ provides the possibility that the presence of a domain wall lowers the resistivity of a nanowire. This can be understood in terms of virtual transport as provided by the minority electrons. [16] The origin of negative domain-wall resistivity rests on the different

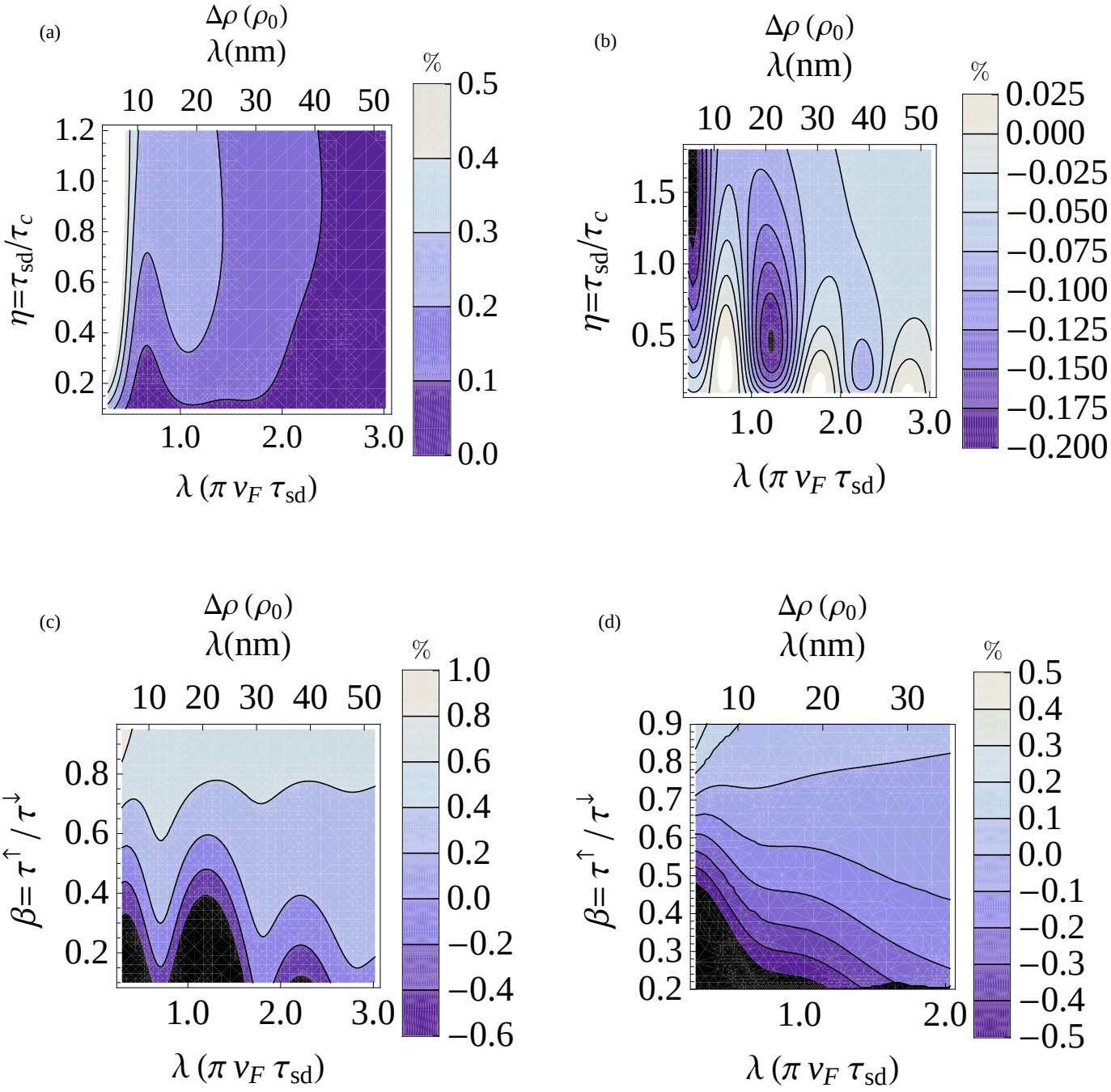

Figure 5.22: (Color online) Color-coded intrinsic domain-wall resistivity in percent versus domain-wall width λ and the parameter that characterizes the transport regime $\eta = \tau_{sd}/\tau_c$ (a) with $\beta = 2$ and (b) $\beta = 0.6$. The spin transport is (c) ballistic $\eta = 0.62$ and (d) diffusive $\eta = 2.07$.

relaxation times of the two spin channels that get mixed due to the spatially strongly varying magnetization. The magnetization twist leads to a redistribution between majority and minority electrons that is also responsible for the spatially inhomogeneous electron density as depicted in Fig. 5.21. [183] As can be understood from the spin-dependent Drude formula of conductivity $\sigma^s = e^2 n^s \tau^s / m$, a change in the spin-resolved number density n^s causes a different spin-resolved conductivity σ^s. [183] A possible outcome of the redistribution is a higher conductivity compared with the homogeneous case with no domain wall. In this case, it would be interesting to observe the redistribution of the spin-resolved electron density n^s within a domain-wall by spin-polarized scanning tunneling microscopy (SP-STM). We note that local changes in the spin-dependent band structure due to the presence of a domain wall have already been observed. [246]
Negative domain-wall resistivity is a pure quantum mechanical effect that originates from the continuous spatial variation of the magnetization within the domain wall. Accordingly, negative domain-wall resistivity does not possess a giant magnetoresistance analogue. Spin transport in transition metal ferromagnets takes place in the ballistic regime ($\eta < 1$). As discussed in the previous section, the non-adiabatic spin-transfer torque is composed of a contribution due to spin relaxation and a contribution due to spin mistracking. For ballistic spin transport in narrow domain walls spin mistracking has been found to constitute the predominant contribution to the non-adiabatic spin-transfer torque (cf. Fig. 5.16). Consequently, the presented analysis confirms spin mistracking as the microscopic origin of domain-wall resistivity in the regime of ballistic spin transport, whereas spin relaxation dominates in the diffusive regime of spin transport. In the diffusive regime of spin transport the spin-dependent scattering mechanism prevails over the spin mistracking as the coherent precession of the conduction electrons is suppressed due to impurity scattering. [197] The result depicted in Fig. 5.22 (b) sheds light on the long-standing controversy about the sign of the domain-wall resistivity. The sign change that has been found in the non-adiabatic spin-transfer torque for spatially strongly varying magnetization textures directly translates to the intrinsic domain-wall resistivity. This serves as an explanation for the seemingly contradictory experimental findings concerning the sign of the domain-wall resistivity. [201–211] For instance, Rüdiger et al. [207] reported a negative intrinsic domain-wall resistivity on Fe wires. As already discussed in the context of the degree of non-adiabaticity, the experimental results corroborate the presented explanation as it holds for Fe $\beta_{\mathrm{Fe}} \approx 0.7$. [189]

Conclusion and comparison with results of the literature While it is a generally accepted consensus that intrinsic domain-wall resistivity is proportional to the inverse squared of the domain-wall width ($\propto \lambda^{-2}$), the sign of the correction is still an open question. [16, 63, 196, 200–202] The here presented results outline the possibility of a negative domain-wall resistivity and thus contrast with the results of Refs. [63, 196] that obtained an entirely positive intrinsic domain-wall resistivity.
Levy and Zhang [63] developed the idea of a continuous version of the giant magnetoresistance effect and calculated the domain-wall resistivity due to spin-dependent scattering. The presence of the domain-wall mixes the majority, minority channels and the presence of a domain wall closes the high conducting shunt channel present in a homogeneous magnetization texture. They concluded that the presence of a domain wall enhances the resistivity and that the intrinsic domain-wall resistivity vanishes for equal scattering times ($\beta = 1$). As depicted in Fig. 5.22 (c), (d) this prediction is not affirmed by the presented results. The reason for this is that they only took into account the twist-

induced correction of the spin eigenstates due to spin-dependent impurity scattering and neglected the influence of spin mistracking due to the magnetization twist. Their results suffer from the usage of an oversimplified Boltzmann equation that does not properly take into account the transverse degrees of freedom. [196] The here presented results refute their statement that spin mistracking by itself does not produce excess resistance. [63]
Šimánek [185] calculated the excess resistance of a domain-wall due to transverse spin accumulation caused by the magnetization twist. He did not take into account the effect of the magnetization twist on the relaxation times and his calculation thus constitutes a somehow complementary approach to Levy and Zhang [63]. By neglecting the impact of the spin degree of freedom on the impurity scattering, he obtained an entirely positive correction for the domain-wall resistivity.
To draw a conclusion, the here presented results confirm the conjecture of Refs. [201, 202] that intrinsic domain-wall resistivity in narrow domain walls must be attributed to a combination of spin mistracking and spin-dependent scattering. Spin-dependent scattering ($\beta \neq 1$) is ascribed to be the origin of the giant magnetoresistance effect and dominates in the regime of diffusive spin transport ($\eta > 1$). Spin mistracking is predominant in the regime of ballistic spin transport ($\eta < 1$) and constitutes in this context an additional feature taking into account the continuous variation of the magnetization texture within the domain wall. Accordingly, domain-wall resistivity can be positive or negative and can be anticipated to be present in materials with $\beta = 1$ that exhibit no giant magnetoresistance effect. Levy and Zhang [63] showed in their calculations that spin-dependent scattering contributes always a positive intrinsic domain-wall resistivity without considering spin mistracking. Šimánek and Rebei calculated the domain-wall resistivity exclusively due to spin mistracking and also found an entirely positive contribution. [185, 197] The obvious conclusion is therefore that the interplay of spin mistracking and spin-dependent impurity scattering in the regime of ballistic spin transport is responsible for negative values of the intrinsic domain-wall resistivity. A negative domain-wall resistivity must thus be attributed to the quantum mechanical nature of the spin degree of freedom and arises in narrow domain walls if the current is mainly carried by minority charge carriers.
In the diffusive regime the spin transport is dominated by spin relaxation and the influence of spin mistracking due to the magnetization texture is negligible. Accordingly, the main result of this section – oscillations of the resistivity with the domain-wall width including a sign change as caused by spin mistracking – are not present in the results of Ref. [183].

In summary, our investigations illuminate the possibility of a positive or a negative intrinsic domain-wall resistivity in dependence of the width of the domain wall. The dependence of the sign of the resistivity correction on β can be tested experimentally by intentionally doping wires with different kinds of impurities. The predicted oscillations should become observable by a variation of the domain-wall width λ. This can be achieved by either a variation of the cross section of the wire via the change in the shape anisotropy or in a nanocontact by a variation of the length of the constriction. [220] The local variation of the resistivity may result in interesting effects, for instance thermoelectric effects like the Peltier effect. To draw an analogy, a narrow domain wall is here evocative of a junction of two metals with different conductivities.

Momentum transfer As previously mentioned there are two different physical mechanism that result in domain-wall motion, spin-transfer torque and momentum transfer. In the presented formalism domain-wall resistivity and momentum transfer occur as corrections of second order of the expansion of the non-equilibrium distribution in the inverse wall width. Momentum transfer can be associated with the reflection of conduction electrons due to the strongly varying magnetization texture and is thus intrinsically related with domain-wall resistivity. [59] In the equations of motion for the domain wall, momentum transfer acts analogously to the non-adiabatic spin-transfer torque as force on the center of mass of the domain wall and results in its translation. Momentum transfer thus determines the dynamics of narrow domain walls, in particular the terminal velocity. [49, 59] As a consequence, momentum transfer and non-adiabatic spin-transfer torque are experimentally not distinguishable by observing domain-wall motion, which led to confusion in interpreting experimental data. [243] The main controversy about momentum transfer centers around its origin. Some authors claim that momentum transfer is of quantum mechanical origin and therefore essentially non-local. [56, 59, 156, 172, 191] We note that Tatara et al. interpret the appearance of a non-local torque as the end of the classical Landau-Lifshitz-Gilbert phenomenology comprising local spin-transfer torque terms. [59] However, at the level of the description of domain-wall motion in terms of collective coordinates the non-local momentum transfer renormalizes the total degree of non-adiabaticity

$$\xi_{\text{tot}} = \xi(\lambda) + \xi_{\text{MT}} = \xi + (\xi(\lambda) - \xi) + \xi_{\text{MT}}, \tag{5.272}$$

where the total degree of non-adiabaticity ξ_{tot} is composed of a part due spin relaxation ξ – this contribution is already present in adiabatic magnetotransport –, a part due to spin mistracking $(\xi(\lambda) - \xi)$ – this part takes into account the finite domain-wall width in narrow domain walls – and a part due to the reflection force ξ_{MT} – the conduction electrons maintain their spin but transfer momentum to the domain wall –.
In our semiclassical framework momentum transfer is necessarily a local quantity. However, it is important to note that solely the momentum transfer averaged over the whole domain wall enters the equation of motion for the domain-wall quasiparticle and there is no way to include momentum transfer as a local term within the spatially resolved Landau-Lifshitz-Gilbert equation.

The origin of momentum transfer rests on the spatial variation of the longitudinal component of the out-of-equilibrium magnetization of the conduction electrons. The physical process behind momentum transfer is that a spatial gradient in energy causes a force. This is distinct different from the spin-transfer torque as defined in Eq. (5.141). The energy of interest stems from the sd exchange interaction between the magnetization of the conduction electrons and the local magnetic moments

$$\begin{aligned} E_{\text{MT}}(\vec{r}) &= \langle \frac{\delta \mathcal{H}_{\text{sd}}}{\delta \vec{m}(\vec{r})} \rangle \cdot \vec{m}(\vec{r}) \\ &= J_{\text{sd}} \langle \hat{\vec{\sigma}}(\vec{r}) \rangle \cdot \vec{m}(\vec{r}). \end{aligned} \tag{5.273}$$

Momentum transfer is the force that stems from the spatial gradient of the sd exchange interaction energy (5.273) [49, 58]

$$\begin{aligned}\vec{F}_{\mathrm{MT}}(\vec{r}) &= -\vec{\nabla}_{\vec{r}} E_{\mathrm{MT}}(\vec{r}) \\ &= -J_{\mathrm{sd}} \vec{\nabla}_{\vec{r}} \left(\langle \hat{\vec{\sigma}}(\vec{r}) \rangle \cdot \vec{m}(\vec{r}) \right) \\ &= -J_{\mathrm{sd}} \vec{\nabla}_{\vec{r}} \left(\langle \hat{\vec{\sigma}}(\vec{r}) \rangle_{\mathrm{neq}} \cdot \vec{m}(\vec{r}) \right). \end{aligned} \tag{5.274}$$

The equilibrium component of the magnetization of the conduction electrons in Eq. (5.144) is always collinear with the local magnetization with a fixed length. Consequently, the term proportional to the equilibrium magnetization of the conduction electrons yields a constant energy that is negligible for the force. This reflects that momentum transfer is a non-equilibrium phenomenon.
For our purpose of the case of an one-dimensional domain wall, momentum transfer can be expressed in terms of the gauge transformed quantities in the reference frame of the wall ($\vec{m}(\vec{r}) \to \vec{e}_z$)

$$\begin{aligned}\vec{F}_{\mathrm{MT}}(\vec{r}) &= -J_{\mathrm{sd}} \vec{\nabla}_{\vec{r}} \left(\langle \hat{\vec{\sigma}}(\vec{r}) \rangle \cdot \vec{e}_z \right) \\ &= -J_{\mathrm{sd}} \vec{\nabla}_{\vec{r}} \langle \hat{\sigma}_z(x) \rangle. \end{aligned} \tag{5.275}$$

We derive Eq. (5.275) by noting that the energy in Eq. (5.273) is a scalar and therefore invariant with respect to rotations. Transverse parts proportional to the derivative of the magnetization point perpendicular to the magnetization and therefore do not play a role for the force (5.275). For the domain wall the sole non-vanishing gradient points in x direction and the momentum transfer reads

$$F_{\mathrm{MT}}(x) = -J_{\mathrm{sd}} \frac{d}{dx} \langle^{(2)} \hat{\sigma}_z(x) \rangle, \tag{5.276}$$

up to $\mathcal{O}(\kappa^4)$. In the quasiparticle picture an inertia mass can be associated with the domain wall. [122] Hence, momentum transfer constitutes a real force on the domain wall. [58, 71] The total force that acts on the center of mass of the domain wall follows from averaging the momentum transfer over the width of the domain-wall

$$\begin{aligned} F_{\mathrm{MT}} &= \frac{1}{\lambda} \int_0^{\lambda} dx F_{\mathrm{MT}}(x) \\ &= -\frac{J_{\mathrm{sd}}}{\lambda} \left[\langle^{(2)} \hat{\sigma}_z(\lambda) \rangle - \langle^{(2)} \hat{\sigma}_z(0) \rangle \right]. \end{aligned} \tag{5.277}$$

Momentum transfer and non-adiabatic spin-transfer torque take the same role in the equation of motion for a domain wall. [59, 191, 247] Therefore, it is suggestive to compare both. Though non-adiabatic spin-transfer torque and momentum transfer are processes of different order in the mistracking parameter as defined in Eq. (5.202), they have comparable magnitude in narrow domain walls due to the smallness of the non-adiabatic spin-transfer torque. A comparison of both allows distinguishing the dominant contribution for domain-wall motion: either the direct influence of the charge current by means of momentum transfer or its indirect influence in terms of the spin current due to the non-adiabatic spin-transfer torque.
Figure 5.23 depicts the interpolated ratio between momentum transfer and non-adiabatic spin-transfer

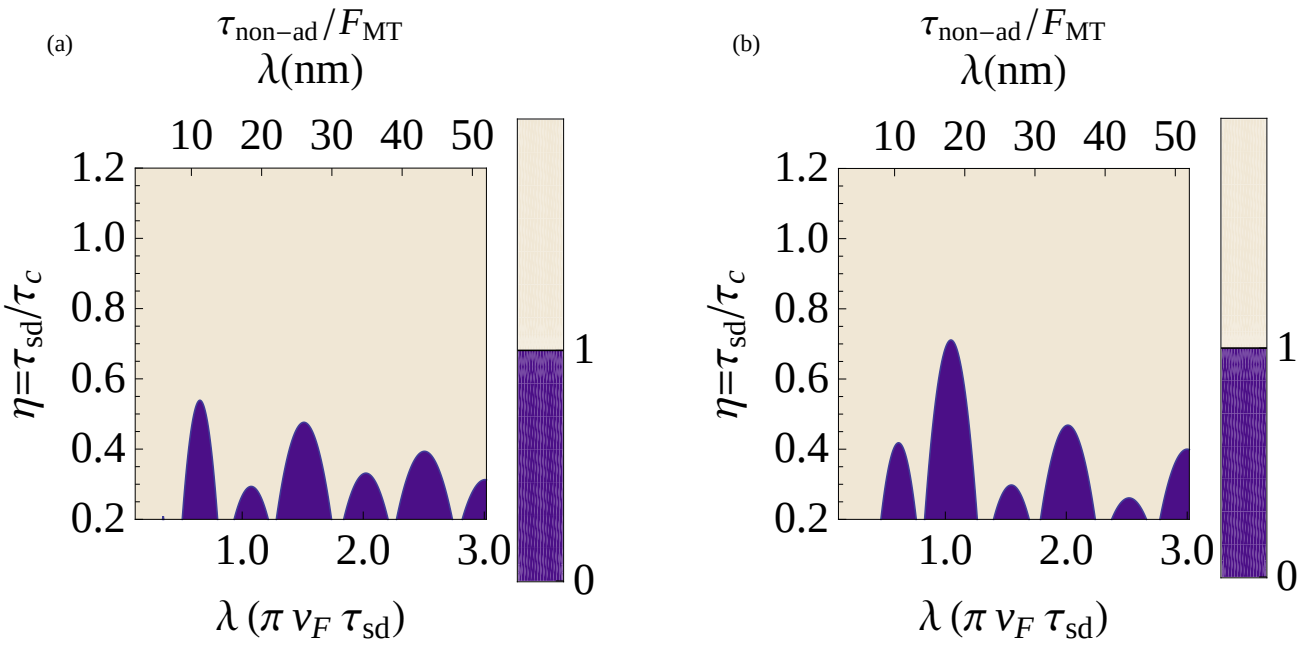

Figure 5.23: (Color online) Interpolated ratio between non-adiabatic spin-transfer torque and momentum transfer for various domain-wall widths λ. For the transport regimes $\eta = \tau_{\text{sd}}/\tau_c$ (a) with $\beta = 0.75$ and (b) $\beta = 2$.

torque that is given by

$$\frac{\xi(\lambda)}{\xi_{\text{MT}}} = \frac{\tau_{\text{non-ad}}}{F_{\text{MT}}} = \frac{-\int_0^\lambda dx \left(\vec{m}(x) \times \frac{d\vec{m}(x)}{dx}\right) \cdot \left(\langle \frac{\delta \mathcal{H}_{\text{sd}}}{\delta \vec{m}(x)} \rangle \times \vec{m}(x)\right)}{-\frac{1}{\lambda}\int_0^\lambda dx \, \frac{d}{dx}\left(\langle \frac{\delta \mathcal{H}_{\text{sd}}}{\delta \vec{m}(\vec{r})} \rangle \cdot \vec{m}(\vec{r})\right)}$$
$$= \frac{\pi}{\lambda} \frac{\Im\left(\langle {}^{(1)}\hat{\sigma}_{\text{tot}}^{\text{trans}} \rangle\right)}{\langle {}^{(2)}\hat{\sigma}_z(\lambda)\rangle - \langle {}^{(2)}\hat{\sigma}_z(0)\rangle}. \tag{5.278}$$

The blue region denotes the parameter subspace where the momentum transfer is dominant, while the white area designates the realm of the non-adiabatic spin-transfer torque. In the diffusive regime ($\eta > 1$) the spin-transfer torque always dominates the domain-wall motion, whereas in the ballistic regime ($\eta < 1$) the dominant driving mechanism depends crucially on the set of parameters. Here, due to the vanishing of the non-adiabatic spin-transfer torque (cf. Fig. 5.16) momentum transfer constitutes the dominant driving mechanism for half-integer or integer wavelength as defined in Eq. (5.245). To conclude, in the regime of ballistic spin transport no general answer can be given.

Chapter 6

Conclusion

THIS THESIS IS DEVOTED to the interplay of inhomogeneous currents and magnetization textures. The methods employed throughout this thesis range from analytical calculation to numerical simulation and cover aspects from macroscopic current-induced magnetization dynamics to the semiclassical description of non-collinear magnetotransport.

As an application of the spin-transfer-torque phenomenon within a novel spintronic device, a magnetic Vortex Random-Access Memory (VRAM) is proposed. It is found that the vortex handedness defined as the product of its topological quantities core polarization and chirality controls the dynamic behavior of the magnetic vortex in a collinear current and magnetic field arrangement. An one-to-one correspondence of the vortex handedness to the binary values "zero" and "one" is established, which serves as a representation of the logical states in an unambiguous manner. The writing mechanism bases on current-induced field assisted vortex-core switching, while the read out mechanism employs a variation of the vortex' gyration amplitude. The VRAM needs not be read or erased preceding the writing and, in general, allows an infinite number of read and write operations. This is an advantage compared with existing memory technologies, such as the FLASH memory, which requires a slow erasing procedure of the present memory state. The VRAM concept is non-volatile and fulfills the stability requirements for a memory device, since the vortex state is stable against temperature and magnetic fields as long as they remain in the millitesla regime. The VRAM shows a good scaling behavior, in general no material fatigue, and is foremost a fast memory concept.

By self-consistently considering the mutual interdependence of spin-polarized electric current and magnetization dynamics, the non-linear response of a magnetic vortex on the applied current density in the presence of the anisotropic magnetoresistance is investigated. Hitherto, theoretical studies of current-induced magnetization dynamics disregarded the counteraction of the magnetization onto the current flow. The effect of the anisotropic magnetoresistance on the vortex gyration is taken into account by self-consistently solving the extended Landau-Lifshitz-Gilbert equation and Poisson's equation. This provides a realistic treatment of electron transport on the macroscopic level. Incorporating the counteraction of the magnetization onto the current flow provides a non-linear coupling of mutual current and magnetization dynamics. The counteraction of the magnetization by means of the anisotropic magnetoresistivity results for the current-driven magnetic vortex in a geometry-dependent

renormalization of the spin-transfer torque coupling parameter and can be interpreted as a correction to the entirely topological motion of vortices in the presence of a homogeneous current flow. In the non-linear regime of vortex motion the change in the shape of the vortex core explicitly introduces a non-linear dependence of the renormalized spin-transfer coupling parameter on the current density. For experimental and technical implications the anisotropic magnetoresistance is identified as a mechanism to reduce the time until the critical velocity for vortex-core switching is reached. The results are obtained by micromagnetic simulations taken the spin-transfer torque as well as the inhomogeneity of the current flow into account.

The construction of a semiclassical transport framework is reported that fully accounts for the quantum mechanical nature of the spin of the conduction electron. The framework provides the local description of coupled charge and spin transport for general, non-collinear magnetization textures and establishes a natural link between the phenomena of spin-transfer torque and domain-wall resistivity. An equilibrium solution for the kinetic equation in non-collinear magnetization textures is derived. The equilibrium solution takes into account the fully spatially inhomogeneous magnetization texture and serves as a starting point for the derivation of a general linear response kinetic equation. The equilibrium solution provides a ballistic, microscopic expression for the spin polarization of the electric current.
For general, spatially slowly varying magnetization textures the solution of the non-equilibrium kinetic equation provides transport coefficients for the charge current, the spin current and the spin-transfer torque in terms of microscopic material parameters. An expression for the *degree of non-adiabaticity* in terms of microscopic scattering times is given that is not affected by a specific band structure. The diffusive, transverse spin polarization is found to constitute the appropriate factor between the electric current and the transverse spin current that determines the spin-transfer torque. It differs from the longitudinal spin polarization of collinear magnetotransport and exhibits additionally a dependence on the exchange splitting. The transport coefficient for the spin-current tensor confirms the wide-spread conjecture that in the adiabatic approximation the polarization of the spin current tensor is aligned with the local magnetization. This provides an essential justification, as this feature has been introduced by hand as a key ingredient in seminal works concerning the spin-transfer torque. The universality of the non-equilibrium solution for spatially slowly varying magnetization textures suggests the description of *adiabatic* magnetotransport in terms of a *four channel model*. In addition to the majority and minority channels familiar from collinear magnetotransport two transverse channels, associated with the spin-transfer torque, arise due to the non-trivial coupling of current and magnetization. The presence of both transverse channels is generic and identifies the adiabatic as well as the non-adiabatic spin-transfer torque on equal grounds. The results highlight the importance of the quantum nature of the spin degree of freedom for a consistent treatment of non-collinear magnetotransport. The twist of spin channels in non-collinear magnetization textures is identified as the microscopic origin of a non-adiabatic spin-transfer torque whose existence is shown not to rely on a specific microscopic impurity model.
For the case of an one-dimensional domain wall a perturbative, analytic solution of the kinetic equation is presented that allows the spatially resolved computation of the spin-transfer torque, the domain-wall resistivity and the momentum transfer. Though strict quantum mechanical techniques possess

their advantages in the extreme cases of either wide or sharp domain walls, the kinetic approach is best suited to take into account the spatial variations that dominate the magnetotransport in narrow domain walls. By narrowing the domain wall, the spin channels get mixed, the coupling of conduction electron spin and local moment is drastically enhanced and the spin of the conduction electron cannot follow the local moments adiabatically. During the traversal of a narrow domain wall the spin of the conduction electron resides in a coherent superposition of majority and minority spin states. With the enhanced coupling between the spin of the conduction electrons and the local moments in narrow domain walls, non-adiabatic corrections introduce a spatial dependence to the transport coefficients that transcend the adiabatic approximation of a spin-transfer torque with constant coupling coefficients. Accordingly, a reduction of the domain-wall width enhances the impact of the spin degree of freedom onto transport characteristics. The spin of the conduction electron determines the magnetotransport in narrow domain walls and the transport coefficients are found to depend on details of the magnetization texture. In the case of ballistic spin and diffusive charge transport the spin-transfer torque as well as the local *degree of non-adiabaticity* oscillate within the domain wall due to the precession of the spin of the conduction electron in the exchange field created by the non-collinear, local moments. In narrow domain walls the spatially strongly inhomogeneous torque caused by the combination of spin mistracking due to the strong magnetization twist and impurity scattering leads to a severe increase in the *degree of non-adiabaticity*. Spin mistracking in combination with impurity scattering cause a strong deviation of the average spin-transfer torque from the spatially independent, adiabatic value for wide walls. In narrow domain walls the *degree of non-adiabaticity* ceases to be a constant material parameter and its dependence on the characteristics of the magnetization texture removes the independence of the domain-wall velocity from its width. The oscillations with the width of the domain wall including a sign change in the total *degree of non-adiabaticity* suggest a geometrical control of domain-wall motion by manipulating the width of the domain wall and open new perspectives for memory applications and domain-wall logic.

The perturbative solution of the non-equilibrium kinetic equation in inverse powers of the domain-wall width unambiguously identifies the transverse spin accumulation that is responsible for the non-adiabatic spin-transfer torque as the origin of intrinsic domain-wall resistivity and momentum transfer. This impressively states the intimate connection of converse aspects of the exchange interaction between itinerant and localized moments and provides a natural explanation of domain-wall resistivity in terms of the non-adiabatic spin-transfer torque by relating the dissipative component of the spin-transfer torque to the charge resistivity. For ballistic spin transport in narrow domain walls a combination of spin mistracking and spin-dependent scattering is responsible for a considerable domain-wall resistivity. The redistribution of the conduction electrons between majority and minority bands due to the presence of the domain wall results in an oscillation of the domain-wall resistivity with the width of the domain wall including a sign change. The sign change in the non-adiabatic spin-transfer torque directly translates to the domain-wall resistivity and in this sense constitutes its origin. The sign of the intrinsic domain-wall resistivity depends on the width of the domain wall, which elucidates the long-standing experimental controversy about the sign of the domain-wall resistivity. Furthermore, non-adiabatic spin-transfer torque and momentum transfer are found to compete for the dominant non-adiabatic driving mechanism in narrow domain walls.

The oscillations in the non-adiabatic spin-transfer torque and the domain-wall resistivity are of quan-

tum origin and highlight the particular relevance of the spin degree of freedom with respect to magnetotransport in narrow domain walls. A sign change in the non-adiabaticity and the domain-wall resistivity is a pure quantum mechanical effect, enabled by coherence in the spin sector and originating from the continuous spatial variation within the domain wall. Necessary requirements are (1) ballistic spin transport that causes mistracking between the spin of the conduction electron and the spatially varying local moments in narrow domain walls and (2) spin-dependent impurity scattering such that the current is mainly carried by the minority electrons. If these ingredients are present, the laws of classical electrodynamics and thermoelectrics acquire subtle corrections due to macroscopic quantum effects in strongly inhomogeneous ferromagnetic order parameters.

Chapter 7

Outlook

PARTS OF THIS THESIS have been spent on the development of a semiclassical transport framework of coupled charge and spin transport. The framework allows for the study of magnetotransport in spatially strongly varying magnetization textures that transcends the adiabatic regime. The presented transport framework provides the appropriate munition to deal with the more and more involved questions concomitant to the current experimental progress. In particular, the investigations as presented in section 5.5 underline the growing importance of the spin degree of freedom for current-induced magnetization dynamics in narrow domain walls. Here, the involved coupling due to the sd exchange interaction provides the perspective for a rich phenomenology of current-induced magnetization dynamics and transport anomalies. Accordingly, all physical laws comprised by classical electrodynamics and thermodynamics deserve a detailed reexamination to discover deviations as caused by the quantum mechanical nature of the spin degree of freedom and its impact with respect to transport in narrow domain walls.

In this connection future questions and tasks appear:

- The results of this thesis substantiate the need for self-consistent micromagnetic simulations comprising a spatially resolved spin-transfer torque as computed by the kinetic equation. This requires the development of a new simulation tool that takes into account the mutual current and magnetization dynamics based on a self-consistent solution of the Landau-Lifshitz-Gilbert equation and the kinetic equation. Within this framework, dynamical processes concerning current-induced magnetization dynamics can be studied. In the regime of ballistic spin transport the strong spatial dependence of the spin-transfer torque should be taken into account in micromagnetic simulations to study its influence on the domain-wall profile and investigate deviations from the quasiparticle approximation. Highly non-linear effects can be expected in spatially strongly varying magnetization textures. In particular, it would be interesting to investigate the consequences of the spatially oscillating spin-transfer torque on the depinning characteristics of domain walls. Here, the strong spatial inhomogeneity of the spin-transfer torque can be expected to result in an increase of the depinning probability.
  Besides an one-dimensional domain wall, the magnetic vortex constitutes a second, predestined model system to study the consequences of the spin degree of freedom on current-induced magnetization dynamics. The vortex core is usually of the order of ten nanometers and thus very

small. This along with its highly non-collinear magnetization pattern distinguishes the magnetic vortex as a model system to prospect for macroscopic quantum effects and coupled non-linear current and magnetization dynamics. It would be important to determine the electrical resistivity of the vortex pattern.

- The kinetic equation for arbitrary, smooth domain-wall profiles requires a numerical solution. In this context, it would be interesting to study the influence of the domain wall characteristics on the spatial structure of the spin-transfer torque. This is in particular interesting with respect to the spatially averaged spin-transfer torque and the degree of non-adiabaticity.

- Detailed studies will serve to discriminate the leading driving mechanism in the dynamics of narrow domain walls, either spin-transfer torque or momentum transfer.

- Thus far, only the transverse magnetization within the region of the domain wall has been considered. In both directions away from the wall, the transverse magnetization of the conduction electrons will decay exponentially. The decay of transverse magnetization outside the domain wall will leave some spin-angular momentum behind in the adjacent homogeneous ferromagnetic domain and cause there some spin-transfer torque. As addressed by Ref. [22], the excess angular momentum may result in spin waves, i.e., large magnon emission in the domains. For larger spin currents, it is conceivable that the magnetization beyond the domain wall will be destabilized with subsequent domain wall nucleation in the adjacent homogeneous domain. [248] This is referred to as the *spin-wave instability*, where above a critical spin current the groundstate of a ferromagnet is a multidomain state instead of a homogeneous domain. Micromagnetic simulations should be conducted to study the possibilities as outlined above.

- At finite temperatures thermal excitations cause stochastic fluctuations of the local magnetization. In non-equilibrium additionally fluctuations in the current are present. The description of current-induced magnetization dynamics at finite temperature takes place in terms of stochastic Langevin equations. It is common practice to capture temperature effects by introducing stochastic fields to the equations of motions. Invoking the fluctuation-dissipation theorem the noise correlators of the stochastic fields are related to the dissipative coefficients of the theory. This closes the gap to the results of this thesis. The dependence of the degree of non-adiabaticity on the domain-wall width appears in the auto-correlator for the stochastic electric current and indicates, at least for narrow domain walls, non-linear domain-wall dynamics at finite temperatures. However, it is not from a priori clear that the fluctuation-dissipation theorem holds in a non-equilibrium situation. We note that the functional Keldysh method enables the derivation of a stochastic version of the Landau-Lifshitz-Gilbert equation for finite temperatures, which contains exactly the noise correlator as expected from the fluctuation-dissipation theorem without resorting to it. [55]

- The extension of the presented transport formalism to the time-domain is straight forward. Here, numerical investigations of time-dependent spin transport becomes important in the context of ultrafast magnetization processes.

- Time-dependent ferromagnetic order parameters give rise to a spin contribution to the electromotive force via Faraday's law. [249] The non-conservative spin forces convert stored magnetic

into electric energy. For instance, a moving domain wall in a nanowire is found to induce a measurable electromotive force. [250] Electromotive forces can be studied within the presented framework by means of time-dependent unitary rotations that introduce time-dependent gauge fields in the non-steady state. As addressed by Refs. [247, 251–253], in narrow domain walls non-adiabatic corrections to the adiabatic Berry-phase electromotive force become important. The non-adiabatic corrections are characterized by means of the degree of non-adiabaticity and the domain-wall resistivity as computed in this thesis. They contribute on top of the adiabatic electromotive force in narrow domain walls.

- The distribution functions that constitute the *four channel model* may serve as the starting point for numerical studies of the influence of real band-structures on *adiabatic*, non-collinear magnetotransport.

- In appendix D of this thesis the influence of spin-orbit coupling has been taken into account via the anisotropic magnetoresistance effect and a computation of the spatially inhomogeneous electric field within the sample. This electric field (cf. appendix D for the case of a Néel wall) can be employed for the numerical derivation of the spin-transfer torque by incorporating it within the kinetic equation. A combination of both tools, the Poisson solver and the kinetic equation solver will serve as a first approach to consider spin-orbit interaction in the kinetic equation. To capture the impact on magnetization dynamics, this can be done self-consistently in combination with the Landau-Lifshitz-Gilbert equation.

- The kinetic framework can be extended to include correlation effects, for instance Coulomb interaction due to electron-electron interaction.

- The collision integral has been introduced on phenomenological grounds in this thesis. Therefore, a microscopic derivation of the collision integral is required, for instance via a Keldysh approach. A systematic computation of gradient corrections will facilitate the introduction of transverse spin relaxation to the collision integral. Gradient corrections should become important in strong ferromagnets, where the exchange splitting approaches the Fermi energy. [53, 82] The investigation of transverse spin relaxation processes from microscopic origins is needed to further clarify the microscopic origin of the degree of non-adiabaticity. Moreover, gradient corrections to the collision integral are expected to be at the origin of the spin Hall effect.

- Thermal gradients induce a non-equilibrium situation similar to that created by an electric field. The combination of thermal gradients and spin-dependent transport gives rise to a novel domain of physics in inhomogeneous ferromagnets: *magnetocaloritronic* or *spin caloritronics*. Already at this stage, a huge class of novel phenomena can be anticipated in narrow domain walls, for instance a spin Seebeck effect, a Peltier effect as already discussed in the context of domain-wall resistance or an anomalous Nernst effect. Within ferromagnetic metals the spin Seebeck effect is generically present in the presence of temperature gradients. [254] The spin Seebeck effect constitutes a method to generate a pure spin current without electric currents. This provides the possibility for thermally induced domain-wall motion. [255] The reverse effect to thermally induced domain-wall motion is the magnetocaloritronic cooling or power generation as induced

by field-induced domain-wall motion. The kinetic description of transport as used throughout this thesis allows for a natural incorporation of thermal effects and constitutes the ideal framework for the derivation of spin-dependent thermal response coefficients and the study of spin-dependent temperature effects.

- The investigation of the spin-transfer torque effect in ferromagnetic semiconductors promises interesting new physics. [27, 256–258] Large non-adiabatic corrections enable domain-wall motion at much lower current densities. In ferromagnetic semiconductors the experimentally determined critical current density for moving domain walls is 2 to 3 orders of magnitude smaller compared with ferromagnetic metals. [27, 256, 257] One possible explanation for this finding is the strong intrinsic spin-orbit interaction that causes an enhanced hole reflection at the domain wall and serves for an enhanced non-adiabatic torque and thus a larger mobility in hole current-driven domain-wall dynamics. [258] Recently, it has been shown that Rashba spin-orbit interaction can drastically enhance the degree of non-adiabaticity ξ. [259]
  In magnetic semiconductors, for instance GaMnAs, the non-adiabaticity and the efficiency of the spin-transfer torque on domain-wall motion is enhanced due to an enhanced sd precession time compared with ferromagnetic metals. [22] Furthermore, the typical domain-wall width in semiconductors is usually very small due to a large anisotropy. Both facts lead to an enhancement of the spin mistracking and provide an earlier access to the non-adiabatic regime.

  An appropriate description of magnetotransport in semiconductors requires the full consideration of spin-orbit interactions within the kinetic equation. A combination of exchange and spin-orbit interaction promise various novel phenomena for current-induced magnetization dynamics in magnetic semiconductors. Accordingly, the spin transfer in magnetic semiconductors deviates from the spin-transfer torque as considered in this thesis in many important aspects. It has been proposed by Ref. [260] that an electric current can induce a torque on the magnetization in a homogeneous domain without the key ingredient of a non-collinear magnetization texture. This spin transfer effect can be viewed as the reciprocal effect of magnetoresistance and thus a system that exhibits the anisotropic magnetoresistance is predicted to exhibit spin-orbit induced spin transfer. Moreover, the large spin-orbit coupling in the conduction band may result in drastically enhanced values for the degree of non-adiabaticity.
  The task is to extend the transport formalism and apply it to low-dimensional semiconductor systems. Therefore, Rashba and Dresselhaus spin-orbit interaction must be taken into account along with an appropriate periodic spin-orbit potential $V(\vec{r}, \vec{k}, \vec{\sigma})$ in the Hamiltonian that gives rise to new terms in the kinetic equation. This requires the knowledge of the effective spin-orbit potential that can be due to impurities, host atoms or structural confinement. For the case of hole mediated transport in magnetic semiconductors, like GaMnAs, the derivation of the kinetic equation must start from the Kohn-Luttinger Hamiltonian. [261]

Appendix A

Properties of Pauli spin space

Throughout this thesis we employ the following representation of the Pauli matrices

$$\sigma_x = \begin{pmatrix} 0 & 1 \\ 1 & 0 \end{pmatrix}, \quad \sigma_y = \begin{pmatrix} 0 & -i \\ i & 0 \end{pmatrix}, \quad \sigma_z = \begin{pmatrix} 1 & 0 \\ 0 & -1 \end{pmatrix}. \tag{A.1}$$

The Pauli matrices σ_i, $i = x, y, z$, are the generators of the $SU(2)$ algebra and satisfy the commutation relations

$$[\sigma_i, \sigma_j] = 2i \sum_k \epsilon_{ijk} \sigma_k \qquad i, j, k = x, y, z. \tag{A.2}$$

Due to their anticommutation relations the Pauli matrices obey a Clifford algebra

$$\{\sigma_i, \sigma_j\} = 2\delta_{ij} \mathbb{1} \qquad i, j = x, y, z. \tag{A.3}$$

According to Eqns. (A.2) and (A.3) it holds for the product of two Pauli matrices

$$\sigma_i \cdot \sigma_j = \delta_{ij} \mathbb{1} + i \sum_k \epsilon_{ijk} \sigma_k \qquad i, j = x, y, z. \tag{A.4}$$

The magnetization is described by a vector field $\vec{m}(\vec{r}) = (m_x, m_y, m_z)^T$ of constant length $||\vec{m}(\vec{r})|| = 1$. Owing to the fact that the magnetization is an unimodular vector field, any derivative is perpendicular to the magnetization itself

$$0 = \partial_i 1 = \partial_i (\vec{m}\vec{m}) = 2\vec{m}(\partial_i \vec{m}), \quad i = t, x, y, z. \tag{A.5}$$

Furthermore, the magnetization can be parametrized in spherical coordinates by the two angles θ and ϕ. They obey the following relations

$$1 = \sqrt{m_x^2 + m_y^2 + m_z^2}, \tag{A.6}$$

$$\theta = \arctan \frac{\sqrt{m_x^2 + m_y^2}}{m_z}, \tag{A.7}$$

$$\phi = \arctan \frac{m_y}{m_x}. \tag{A.8}$$

The most general, local $SU(2)$ gauge transformation is given by a Wigner rotation according to [262]

$$\begin{aligned}\hat{U}(\theta(\vec{r}),\phi(\vec{r})) &= e^{-i\frac{\phi(\vec{r})}{2}\sigma_z}e^{-i\frac{\theta(\vec{r})}{2}\sigma_y} \\ &= \begin{pmatrix} \cos\frac{\theta(\vec{r})}{2}e^{-i\frac{\phi(\vec{r})}{2}} & -\sin\frac{\theta(\vec{r})}{2}e^{-i\frac{\phi(\vec{r})}{2}} \\ \sin\frac{\theta(\vec{r})}{2}e^{i\frac{\phi(\vec{r})}{2}} & \cos\frac{\theta(\vec{r})}{2}e^{i\frac{\phi(\vec{r})}{2}} \end{pmatrix}. \end{aligned} \tag{A.9}$$

θ and ϕ are given by Eqns. (A.7) and (A.8) and define the spatially varying reference frame of the local magnetization. The matrix $\hat{U}$ in Eq. (A.9) provides the transformation between the global spin-coordinate system and the reference frame of the local magnetization.

Appendix B

The Wigner transformation

The non-commutativity of position and momentum precludes the specification of a point in phase space due to Heisenberg's uncertainty principle. Accordingly, the concept of a Liouville distribution function that operates on classical phase space is problematic with respect to a quantum mechanical formulation of transport. The most prominent solution to this problem dates back to Eugene Wigner and Hermann Weyl: They proposed the definition of a quasi-probability distribution. For the above stated reasons the quasi-probability distribution must not exhibit all the essential properties of an ordinary probability distribution. More precisely the Wigner distribution may adopt negative values for non-classical states. This property can in turn be employed to identify non-classical states (cf. section 5.3.1).
According to Wigner the connection of an arbitrary operator $\hat{O}(\vec{r}_1, \vec{r}_2)$ on a Hilbert space with a smooth function $O(\vec{r}, \vec{k})$ on phase space is established by means of a Fourier transform with respect to the fast varying relative coordinate $\vec{r}\,' = \vec{r}_1 - \vec{r}_2$

$$O(\vec{r}, \vec{k}) = \int d^3r'\, \hat{O}(\vec{r} + \frac{\vec{r}\,'}{2}, \vec{r} - \frac{\vec{r}\,'}{2}) e^{i\vec{k}\vec{r}\,'}, \tag{B.1}$$

where $\vec{r} = (\vec{r}_1 + \vec{r}_2)/2$ denotes the center of mass coordinate.
The composition of two operators $\hat{C} = \hat{A} \circ \hat{B}$ is given by

$$\hat{C}(\vec{r}_1, \vec{r}_2) = \int d^3r'\, \hat{A}(\vec{r}_1, \vec{r}\,') \hat{B}(\vec{r}\,', \vec{r}_2). \tag{B.2}$$

Accordingly, the Wigner transform of a product of two operators $\hat{A}$ and $\hat{B}$ yields with the definitions Eqns. (B.1) and (B.2)

$$\begin{aligned} C(\vec{r}, \vec{k}) &= \int d^3r'd^3\rho\, \hat{A}(\vec{r} + \frac{\vec{\rho}}{2}, \vec{r}\,') \hat{B}(\vec{r}\,', \vec{r} - \frac{\vec{\rho}}{2}) e^{i\vec{k}\vec{\rho}} \\ &= \int d^3r'd^3\rho \int \frac{d^3k_1' d^3k_1''}{(2\pi)^6} \\ &\qquad A(\frac{\vec{r} + \frac{\vec{\rho}}{2} + \vec{r}\,'}{2}, \vec{k}_1') B(\frac{\vec{r}\,' + \vec{r} - \frac{\vec{\rho}}{2}}{2}, \vec{k}_1'') e^{i\vec{k}\vec{\rho}} e^{-i\vec{k}_1'(\vec{r} + \frac{\vec{\rho}}{2} - \vec{r}\,')} e^{-i\vec{k}_1''(\vec{r}\,' - \vec{r} + \frac{\vec{\rho}}{2})} \end{aligned}$$

$$C(\vec{r},\vec{k}) = \int d^3r\,'d^3\rho \int \frac{d^3k_1'd^3k_1''}{(2\pi)^6} A(\vec{r}+\frac{\vec{r}\,'-\vec{r}+\frac{\vec{\rho}}{2}}{2},\vec{k}_1')B(\vec{r}+\frac{\vec{r}\,'-\vec{r}-\frac{\vec{\rho}}{2}}{2},\vec{k}_1'')e^{i\vec{k}\vec{\rho}}e^{-i\vec{k}_1'(\vec{r}+\frac{\vec{\rho}}{2}-\vec{r}\,')}e^{-i\vec{k}_1''(\vec{r}\,'-\vec{r}+\frac{\vec{\rho}}{2})}. \tag{B.3}$$

The next step is to introduce new coordinates

$$\begin{aligned}\tilde{\vec{r}}\,' &= \vec{r}\,'-\vec{r}+\frac{\vec{\rho}}{2},\\ \tilde{\vec{\rho}}\,' &= \vec{r}\,'-\vec{r}-\frac{\vec{\rho}}{2},\end{aligned} \tag{B.4}$$

whereas the coordinate transform (B.4) does not change the integral measures

$$|\det\begin{pmatrix}\frac{\partial\tilde{\vec{r}}\,'}{\partial\vec{r}\,'} & \frac{\partial\tilde{\vec{r}}\,'}{\partial\vec{\rho}}\\ \frac{\partial\tilde{\vec{\rho}}\,'}{\partial\vec{r}\,'} & \frac{\partial\tilde{\vec{\rho}}\,'}{\partial\vec{\rho}}\end{pmatrix}| = |\det\begin{pmatrix}1 & \frac{1}{2}\\ 1 & -\frac{1}{2}\end{pmatrix}| = |-1|. \tag{B.5}$$

Equation (B.3) transforms under the coordinate transformation (B.4) according to

$$C(\vec{r},\vec{k}) = \int d^3\tilde{r}\,'d^3\tilde{\rho} \int \frac{d^3k_1'd^3k_1''}{(2\pi)^6} A(\vec{r}+\frac{\tilde{\vec{r}}\,'}{2},\vec{k}_1')B(\vec{r}+\frac{\tilde{\vec{\rho}}}{2},\vec{k}_1'')e^{i\vec{k}(\tilde{\vec{r}}\,'-\tilde{\vec{\rho}})}e^{-i\vec{k}_1'(-\tilde{\vec{\rho}})}e^{-i\vec{k}_1''(\tilde{\vec{r}}\,')}. \tag{B.6}$$

Renaming the variables of integration $\tilde{\vec{r}}\,' \to \vec{r}\,'$, $\tilde{\vec{\rho}}\,' \to \vec{\rho}\,'$ yields

$$C(\vec{r},\vec{k}) = \int d^3r\,'d^3\rho \int \frac{d^3k_1'd^3k_1''}{(2\pi)^6} A(\vec{r}+\frac{\vec{r}\,'}{2},\vec{k}_1')B(\vec{r}+\frac{\vec{\rho}}{2},\vec{k}_1'')e^{i\left[\vec{r}\,'(\vec{k}-\vec{k}_1'')+\vec{\rho}(\vec{k}_1'-\vec{k})\right]}. \tag{B.7}$$

Introducing again new coordinates $\vec{k}-\vec{k}_1'' \to -\vec{k}_2$, $\vec{k}_1'-\vec{k} \to \vec{k}_1$ yields as the final result

$$C(\vec{r},\vec{k}) = \int d^3r\,'d^3\rho \int \frac{d^3k_1d^3k_2}{(2\pi)^6} A(\vec{r}+\frac{\vec{r}\,'}{2},\vec{k}+\vec{k}_1)B(\vec{r}+\frac{\vec{\rho}}{2},\vec{k}+\vec{k}_2)e^{i(\vec{\rho}\vec{k}_1-\vec{r}\,'\vec{k}_2)}. \tag{B.8}$$

The next step is to perform a series expansion of the functions $A(\vec{r}+\frac{\vec{r}\,'}{2},\vec{k}+\vec{k}_1)$, $B(\vec{r}+\frac{\vec{\rho}}{2},\vec{k}+\vec{k}_2)$ under the integral with respect to the small relative coordinates $\vec{r}\,'$, $\vec{\rho}$ and momenta $\vec{k}_1$, $\vec{k}_2$

$$\begin{aligned}A(\vec{r}+\frac{\vec{r}\,'}{2},\vec{k}+\vec{k}_1) &= e^{\left[(\frac{\vec{r}\,'}{2}\vec{\nabla}_{\vec{r}})+(\vec{k}_1\vec{\nabla}_{\vec{k}})\right]}A(\vec{r},\vec{k})\\ &= A(\vec{r},\vec{k})\\ &\quad+\left[(\frac{\vec{r}\,'}{2}\vec{\nabla}_{\vec{r}})+(\vec{k}_1\vec{\nabla}_{\vec{k}})\right]A(\vec{r},\vec{k})\\ &\quad+\frac{1}{2}\left[(\frac{\vec{r}\,'}{2}\vec{\nabla}_{\vec{r}})^2+2(\frac{\vec{r}\,'}{2}\vec{\nabla}_{\vec{r}})(\vec{k}_1\vec{\nabla}_{\vec{k}})+(\vec{k}_1\vec{\nabla}_{\vec{k}})^2\right]A(\vec{r},\vec{k})+\dots,\end{aligned} \tag{B.9}$$

and

$$\begin{aligned}B(\vec{r}+\frac{\vec{\rho}}{2},\vec{k}+\vec{k}_2) &= e^{\left[(\frac{\rho}{2}\vec{\nabla}_{\vec{r}})+(\vec{k}_2\vec{\nabla}_{\vec{k}})\right]}B(\vec{r},\vec{k})\\ &= B(\vec{r},\vec{k})\\ &\quad+\left[(\frac{\rho}{2}\vec{\nabla}_{\vec{r}})+(\vec{k}_2\vec{\nabla}_{\vec{k}})\right]B(\vec{r},\vec{k})\\ &\quad+\frac{1}{2}\left[(\frac{\rho}{2}\vec{\nabla}_{\vec{r}})^2+2(\frac{\rho}{2}\vec{\nabla}_{\vec{r}})(\vec{k}_2\vec{\nabla}_{\vec{k}})+(\vec{k}_2\vec{\nabla}_{\vec{k}})^2\right]B(\vec{r},\vec{k})+\dots.\end{aligned} \tag{B.10}$$

Inserting the expansions (B.9) and (B.10) into Eq. (B.8) yields for the zeroth order the result

$$\begin{aligned}
&A(\vec{r},\vec{k})B(\vec{r},\vec{k})\int d^3r'd^3\rho\int\frac{d^3k_1d^3k_2}{(2\pi)^6}e^{i(\vec{\rho}\vec{k}_1-\vec{r}'\vec{k}_2)}\\
&=A(\vec{r},\vec{k})B(\vec{r},\vec{k})\int d^3r'd^3\rho\,\delta^{(3)}(\vec{\rho})\delta^{(3)}(-\vec{r}')\\
&=A(\vec{r},\vec{k})B(\vec{r},\vec{k}).
\end{aligned}\tag{B.11}$$

The first-order terms of the expansion are set to zero by means of the delta function, for instance

$$\begin{aligned}
&\int d^3r'd^3\rho\int\frac{d^3k_1d^3k_2}{(2\pi)^6}(\frac{\vec{r}'}{2}\vec{\nabla}_{\vec{r}})A(\vec{r},\vec{k})B(\vec{r},\vec{k})e^{i(\vec{\rho}\vec{k}_1-\vec{r}'\vec{k}_2)}\\
&=B(\vec{r},\vec{k})\int d^3r'd^3\rho\,(\frac{\vec{r}'}{2}\vec{\nabla}_{\vec{r}})A(\vec{r},\vec{k})\delta^{(3)}(\vec{\rho})\delta^{(3)}(-\vec{r}')\\
&=0.
\end{aligned}\tag{B.12}$$

The same result as in Eq. (B.12) holds for all other first-order terms and the first order vanishes exactly. In the second order all asymmetric terms vanish for the same reason as the first-order terms. Only the mixed first-order terms yield a non-vanishing result, for instance

$$\begin{aligned}
&\int d^3r'd^3\rho\int\frac{d^3k_1d^3k_2}{(2\pi)^6}(\frac{\vec{r}'}{2}\vec{\nabla}_{\vec{r}})A(\vec{r},\vec{k})(\vec{k}_2\vec{\nabla}_{\vec{k}})B(\vec{r},\vec{k})e^{i(\vec{\rho}\vec{k}_1-\vec{r}'\vec{k}_2)}\\
&=\int d^3r'\int\frac{d^3k_2}{(2\pi)^3}(\frac{\vec{r}'}{2}\vec{\nabla}_{\vec{r}})A(\vec{r},\vec{k})(\vec{k}_2\vec{\nabla}_{\vec{k}})B(\vec{r},\vec{k})e^{-i\vec{r}'\vec{k}_2}.
\end{aligned}\tag{B.13}$$

It is appropriate to proceed further on in components, whereas all terms $i\neq j$ vanish due to the integration over the delta-functions. After the integration over the remaining delta functions is carried out the remaining terms $i=j$ read

$$\begin{aligned}
&\int d^3r'\int\frac{d^3k_2}{(2\pi)^3}(\frac{\vec{r}'}{2}\vec{\nabla}_{\vec{r}})A(\vec{r},\vec{k})(\vec{k}_2\vec{\nabla}_{\vec{k}})B(\vec{r},\vec{k})e^{-i\vec{r}'\vec{k}_2}\\
&=\sum_i\int d^ir'\int\frac{d^ik_2}{2\pi}(\frac{r'^i}{2}\nabla^i_{\vec{r}})A(\vec{r},\vec{k})(k_2^i\nabla^i_{\vec{k}})B(\vec{r},\vec{k})e^{-ir'^ik_2^i}\\
&=\frac{1}{2}\sum_i\int\frac{d^ir'}{2\pi}r'^ie^{-ir'^ik_2^i}\nabla^i_{\vec{r}}A(\vec{r},\vec{k})\int d^ik_2(k_2^i\nabla^i_{\vec{k}})B(\vec{r},\vec{k})\\
&=\frac{i}{2}\sum_i\int d^ik_2\nabla^i_{\vec{k}_2}\left(\delta(-k_2^i)\nabla^i_{\vec{r}}A(\vec{r},\vec{k})\right)(k_2^i\nabla^i_{\vec{k}})B(\vec{r},\vec{k})\\
&=-\frac{i}{2}\sum_i\int d^ik_2\delta(-k_2^i)\nabla^i_{\vec{r}}A(\vec{r},\vec{k})\nabla^i_{\vec{k}}B(\vec{r},\vec{k})\\
&=\frac{1}{2i}\vec{\nabla}_{\vec{r}}A(\vec{r},\vec{k})\vec{\nabla}_{\vec{k}}B(\vec{r},\vec{k}),
\end{aligned}\tag{B.14}$$

where we employed the following identity in the second line of Eq. (B.14)

$$\begin{aligned}\sum_i \int \frac{d^i r'}{(2\pi)^3} r'^i e^{-ir'^i k_2^i} &= \sum_i \int \frac{d^i r'}{(2\pi)^3} i\nabla_{k_2}^i e^{-ir'^i k_2^i} \\ &= i\nabla_{k_2}^i \int \frac{d^3 r'}{(2\pi)^3} e^{-ir'^i k_2^i} \\ &= i\nabla_{k_2}^i \delta(-k_2^i). \end{aligned} \tag{B.15}$$

An interchange of $\vec{\nabla}_{\vec{r}}$, $\vec{\nabla}_{\vec{k}}$ introduces a sign. Thus, up to the fourth order the Wigner transform of a product of two operators reads according to Eq. (B.3)

$$\begin{aligned} C(\vec{r},\vec{k}) = & A(\vec{r},\vec{k})B(\vec{r},\vec{k}) \\ & + \frac{1}{2i}\left(\vec{\nabla}_{\vec{r}} A(\vec{r},\vec{k})\vec{\nabla}_{\vec{k}} B(\vec{r},\vec{k}) - \vec{\nabla}_{\vec{k}} A(\vec{r},\vec{k})\vec{\nabla}_{\vec{r}} B(\vec{r},\vec{k})\right) + \dots , \end{aligned} \tag{B.16}$$

which is the sought result as employed in Eq. (5.18).

Appendix C

Incorporation of spin-orbit interaction into adiabatic magnetotransport

This appendix considers the inclusion of intrinsic spin-orbit interactions within the semiclassical transport framework. This results in tensorial transport coefficients that comprise the anisotropic magnetoresistance as well as the anomalous Hall effect. As a non-equilibrium phenomenon the spin-transfer torque exhibits the anisotropic magnetoresistance but not the anomalous Hall effect. This provides a microscopic justification for the phenomenological resistivity tensor that serves in the macroscopic approach to transport in chapter 4 for the investigation of current-induced magnetization dynamics via the calculation of realistic current paths. Furthermore the degree of non-adiabaticity is not affected by intrinsic spin-orbit interactions.

C.1 Introduction to electron transport in the presence of spin-orbit interactions

In the preceding section we derived global magnetotransport coefficients in the presence of general, spatially slowly varying magnetization textures. Hitherto, we have neglected spin-orbit interactions though they are ubiquitous in realistic materials. In this section, we adjust this point and rederive the transport coefficients of the previous section in the presence of spin-orbit interactions. The incorporation of spin-orbit interactions turns the conductivities of the charge current, the spin-transfer torque and the spin current into tensorial quantities.
Magnetoresistive effects, such as the anisotropic magnetoresistance (AMR) [1] or the anomalous Hall effect (AHE) [263, 264] are ascribed to originate from the interplay of the spin-orbit interaction and the magnetization. [147, 148, 265, 266] In the macroscopic transport equation, Ohm's law, magnetoresistive effects due to spin-orbit interactions are comprised within a global conductivity tensor (cf. chapter 4). In the regime of spatially slowly varying magnetization textures we incorporate spin-orbit interactions by comprising their effects on the band structure due to a modification of the Bloch velocity of the conduction electrons within the anomalous velocity. We exploit that the semiclassical theory of electron transport induced by the Berry curvature in Bloch bands explains the occurrence of the anomalous Hall effect and the anisotropic magnetoresistance in magnetotransport. While the

anomalous velocity modifies the non-equilibrium components by introducing the anisotropic magnetoresistance effect, it introduces an anomalous Hall effect via the equilibrium part of the distribution function. Thus, for the charge and spin current we find an anomalous Hall effect besides the anisotropic magnetoresistance. In this case the conductivity is a tensor with off-diagonal elements. In contrary, the spin-transfer torque that arises due to the non-equilibrium transverse magnetization of the conduction electrons does not exhibit an anomalous Hall effect, though it features the anisotropic magnetoresistance. The physical reason for this is simple to comprehend: The transverse magnetization of the conduction electrons is explicitly a non-equilibrium feature that requires the presence of a finite external electric field (cf. section 5.4). On the other hand in linear response the anomalous Hall effect is related to the equilibrium distribution and is thus not present in the spin-transfer torque.

The anomalous Hall effect has been a puzzle for over fifty years. An extensive coming to terms with the past is beyond the scope of this thesis. For a review however, we refer to Ref. [267]. Recently, a semiclassical theory induced by the Berry curvature in Bloch bands has emerged. [268] Compared to non-transparent quantum mechanical calculations, a semiclassical theory offers the advantage that it deals with gauge invariant quantities that possess a clear semiclassical interpretation. This allows for the development of a physical intuition about the underlying microscopic processes. In ferromagnetic metals the anomalous velocity in terms of the Berry phase was predicted to give rise to the spontaneous Hall conductivity. [268] The Berry phase approach is applicable for slowly varying perturbations and is a geometric phase that a wave function acquires when a quantum system is subject to an adiabatic evolution. Aharonov and Bohm were the first to realize that the impact of a magnetic field on quantum mechanics is twofold. On one hand it determines the classical trajectory due to the Lorentz force and on the other hand it contributes to the phase accumulated along the trajectory. The second effect is a pure quantum mechanical effect that possesses no classical analogon. If the evolution of the particle or wave packet takes place in an adiabatic manner, the contribution to the action depends solely on the phase-space trajectory and not on the rate of motion along the trajectory. [269] The spin-orbit interaction can be associated with a Berry phase that causes a non-classical anomalous velocity due to the non-commutativity of the position operator and the spin-orbit Hamiltonian. [270, 271]
The Hall current is anomalous in the sense that it is dissipationless as it does not depend on scattering times. This expresses the fact that the Hall current is linked to the equilibrium distribution and not to the non-equilibrium one. In Ref. [265, 272] the Hall current is calculated in a full quantum mechanical manner. They traced back the origin of the anomalous Hall effect to spin-orbit interactions of the spin-polarized conduction electrons that leads to a population imbalance as the time-reversal symmetry is spontaneously broken due to the magnetization. This leads in turn to a Hall current proportional to the magnetization.[265] In the theory to the anomalous Hall effect two different microscopic origins were proposed and are controversially discussed in the literature up to date: The extrinsic contribution due to asymmetric scattering [266, 273–275] and an intrinsic, scattering free contribution that stems from the equilibrium distribution induced by the Berry curvature that causes a distortion of the Bloch bands in the presence of an external electric field. [265, 271] The extrinsic contribution yields dissipative transport coefficients that are expressed in terms of states at the Fermi level and are determined by scattering mechanisms due to the non-equilibrium distribution function. The intrinsic or topological contribution is non-dissipative as it does not depend on scattering times. It is expressed in terms of

equilibrium response of all states below the Fermi level. [276] The particularity about the intrinsic contribution is that it occurs due to a change in wave packet group velocity in the presence of an external electric field that is applied to the ferromagnet. In contrast to the extrinsic contribution, the intrinsic contribution is carried by the entire spin-orbit coupled Fermi sea. As a consequence, transport length scales such as the mean free path or, in terms of the spin, the spin diffusion length are absent in the intrinsic contribution.
The anisotropic magnetoresistance effect states that the resistivity is different for a parallel alignment of electrical current and magnetization compared to a perpendicular alignment (cf. chapter 4). The microscopic origin of the anisotropic magnetoresistance is traced back to spin-orbit interactions of the polarized conduction electrons. [147, 148] The connection with the magnetization stems from the fact that the net effect of the spin-orbit interaction is proportional to the extent to which the spins are aligned and thus points in the direction of the spin-orbit force. [265]

In metallic systems spin-orbit interactions are subject to the same impurities that cause the direct potential scattering. However, first-principle calculations of the anomalous Hall effect show that the origin of the anomalous Hall effect is primarily intrinsic for transition metal ferromagnets. [277]. However, in this appendix we focus on intrinsic spin-orbit interactions and neglect scattering contributions in the presence of spin-orbit interaction.[1]
Recently it was proposed [268, 278] that the semiclassical equations of motion for electron transport (2.22), (2.23) acquire a modification for a magnetic Bloch band (MBB). A MBB arises when an electron is simultaneously subject to a periodic potential and a magnetic field. However, the following semiclassical equations were proposed to account for the semiclassical dynamics of electrons in magnetic Bloch bands [268, 278]

$$\vec{v}_{\vec{k}} = \vec{\nabla}_{\vec{k}} \frac{\epsilon_{\vec{k}}}{\hbar} - \dot{\vec{k}} \times \vec{\Omega}, \tag{C.1}$$

$$\hbar \dot{\vec{k}} = -e\vec{E}(\vec{r}) - e\vec{v}_{\vec{k}} \times \vec{B}(\vec{r}), \tag{C.2}$$

where $\vec{\Omega}$ is the curvature of the Berry phase that accounts for the anomalous velocity. The equations can be derived by using a time-dependent variational principle in a Lagrangian formulation [268, 278] or a Hamiltonian approach by formally diagonalizing the Hamiltonian of electrons in a crystal subject to electromagnetic perturbations with accuracy $\hbar$ [279]. The Berry curvature represents a topological term and can be considered as an effective momentum dependent magnetic field. The effective spin-orbit field causes a gauge connection to the coordinate operator and renders the coordinates to become non-commutative. Analogously to the Peierls substitution that introduces a magnetic field to Eq. (C.2), the equation of motion for the coordinate (C.1) obtains a new term proportional to the curvature of its respective gauge connection, the Berry curvature.
The semiclassical description of transport provides the possibility to introduce spin-orbit interactions in the kinetic equation in a clear and simple manner. It takes into account real band structure effects of the ferromagnet in terms of a gauge field in reciprocal space, the Berry phase. [269] A combination of Eqns. (C.1) and (C.2) tells us that the Fermi velocity is not simply given by the slope of the band

[1] We like to mention at this point that a quantitative modeling of impurity scattering in realistic ferromagnets with extreme complicated band-structures has not succeeded to date. [277]

dispersion $\epsilon_{\vec{k}}$ (cf. Eq. (2.20)) but additionally by an electric field dependent term that comprises the Berry curvature $\vec{\Omega}$ of the Bloch state. [271] Due to the modified Bloch velocity the effect of the electric field attains a second meaning. First, it drives the electrons in the drift-term of the Boltzmann equation (2.27) and secondly it gives rise to a correction to the Fermi velocity that mixes the bands at each value of $\vec{k}$. [280]

C.2 Modification of the semiclassical theory of electron transport in the presence of spin-orbit interactions

In this section we derive a modified Bloch velocity to capture the influence of spin-orbit interactions on magnetotransport. The modified or anomalous velocity comprises the effect of a geometric Berry phase that captures the influence of spin-orbit interactions on the band structure. Two ingredients are indispensable for the existence of anomalous velocities. There must be a finite magnetization to destroy the time-reversal symmetry of the basic lattice and the spin-orbit interaction that communicates the lack of time symmetry to the periodic potential of the conduction electrons must be present. [270] In combination with the kinetic equation, the anomalous velocity allows for the derivation of transport coefficients. The kinetic description of electron transport assumes non-interacting particles that are occasionally scattered by phonons, imperfections and impurities. Between the individual collision the conduction electrons are not affected by interactions and can be treated as free particles. However, an interaction with an additional potential, e.g., a Coulomb or an effective spin-orbit interaction potential, will subsequently alter the energy $\epsilon_{\vec{k}}$ of the particles and consequently their velocity according to Eq. (2.20).
In absence of an external magnetic field but in the presence of a finite magnetization $\vec{M}(\vec{r}) = M_s\vec{m}(\vec{r})$ the semiclassical equations of motion (C.1) and (C.2) read [268, 271, 278]

$$\vec{v}_{\vec{k}}^{\,\text{so}} = \vec{v}_{\vec{k}} + \vec{\Omega}(\vec{k}) \times \dot{\vec{k}}, \tag{C.3}$$

$$\hbar\dot{\vec{k}} = -e\vec{E}(\vec{r}) - e\mu_0 M_s \vec{v}_{\vec{k}} \times \vec{m}(\vec{r}). \tag{C.4}$$

As already mentioned in the beginning of this section, the additional term in the semiclassical velocity (C.3) comprises the effect of the spin-orbit interaction on the conduction electrons in terms of the Berry curvature term $\vec{\Omega}(\vec{k})$. [269] A combination of Eqns. (C.3) and (C.4) yields the modified or anomalous Bloch velocity

$$\vec{v}_{\vec{k}}^{\,\text{so}} = \vec{v}_{\vec{k}} + \frac{e}{\hbar}\vec{E}(\vec{r}) \times \vec{\Omega}(\vec{k}) - \frac{e\mu_0 M_s}{\hbar}\vec{\Omega}(\vec{k}) \times \vec{v}_{\vec{k}} \times \vec{m}(\vec{r}). \tag{C.5}$$

The Berry curvature correction to the group velocity of the Block wave packet renders the velocity non-collinear to its momentum. This is the reason for the denotation *anomalous* velocity.
To proceed further on in the derivation we have to make an assumption about the Berry curvature $\vec{\Omega}(\vec{k})$. First, the Berry curvature points in the direction of the magnetization of the conduction electrons. This circumstance is a well known fact from the theory of the anomalous Hall effect. [265, 271] Secondly, we parametrize its strength by the spin-orbit interaction constant $\lambda_{\text{so}}(\vec{k})$. These two assumptions completely determine the Berry curvature for our simplified one-band model

$$\vec{\Omega}(\vec{r}, \vec{k}) = \lambda_{\text{so}}(\vec{k})\langle\hat{\vec{\sigma}}(\vec{r})\rangle. \tag{C.6}$$

The factorization of the spatial and the momentum dependence in Eq. (C.6) is a typical feature of adiabatic transport (cf. section 5.4). The transport fields are spatially slowly varying and the Berry curvature and the magnetization can be treated in the spirit of mean field theory.
According to Eq. (5.143) the magnetization of the conduction electrons splits in an equilibrium part antiparallel to the magnetization (5.144) and two non-equilibrium parts (5.146) and (5.160) transverse to the magnetization. The non-equilibrium components and the current couple via an integral relation. As the non-equilibrium components result in higher-order terms in the electric field we can neglect them in our linear response approach. Inserting the magnetization of the conduction electrons (5.144) into Eq. (C.5) yields the final result for the anomalous velocity by means of Eq. (C.6)

$$\begin{aligned}\vec{v}_{\vec{k}}^{\,\mathrm{so}} &= \vec{v}_{\vec{k}} - \frac{\mu_\mathrm{B} e P n \lambda_\mathrm{so}(\vec{k})}{\hbar}\vec{E}(\vec{r}) \times \vec{m}(\vec{r}) + \frac{\mu_\mathrm{B} e \mu_0 M_s P n \lambda_\mathrm{so}(\vec{k})}{\hbar}\vec{m}(\vec{r}) \times \vec{v}_{\vec{k}} \times \vec{m}(\vec{r}) + \mathcal{O}(\vec{E}^2) \\ &= \left(1 + \frac{\mu_\mathrm{B} e \mu_0 M_s P n \lambda_\mathrm{so}(\vec{k})}{\hbar}\right)\vec{v}_{\vec{k}} - \frac{\mu_\mathrm{B} e P n \lambda_\mathrm{so}(\vec{k})}{\hbar}\vec{E}(\vec{r}) \times \vec{m}(\vec{r}) \\ &\quad - \frac{\mu_\mathrm{B} e \mu_0 M_s P n \lambda_\mathrm{so}(\vec{k})}{\hbar}(\vec{m}(\vec{r})\vec{v}_{\vec{k}})\vec{m}(\vec{r}). \end{aligned} \tag{C.7}$$

The modified Bloch velocity (C.7) is the starting point for the calculation of global transport coefficients in the presence of spin-orbit interactions.

C.3 Global transport coefficients in the presence of spin-orbit interactions

In this section we compute the global conduction coefficients in slowly varying magnetization textures in the presence of spin-orbit interactions. Adequate for the description of mesoscopic systems is a semiclassical formulation of transport that explicitly exploits the smooth variation of transport fields on atomic length scales. The idea is to combine the semiclassical equations for the anomalous velocity (C.7) and the generalized kinetic equation (5.45). The influence of the anomalous velocity on the transport theory is twofold. First, it enters in the macroscopic expression for the currents in Eq. (5.4) and (5.5). Secondly, it modifies the kinetic equation (5.45) that governs the distribution function.
To derive explicit expressions for the entries of the conductivity tensor, we focus on a band structure that consists of one parabolic band throughout the rest of this section. We already employed this oversimplified band structure in section 5.4, where we neglected the $\vec{k}$-dependence of the relaxation times. In this approximation it is consistent to also neglect the $\vec{k}$-dependence in the spin-orbit coupling parameter $\lambda_\mathrm{so}(\vec{k})$ and we set $\lambda_\mathrm{so}(\vec{k}) \equiv \lambda_\mathrm{so}(\epsilon_\mathrm{F})$ throughout the rest of this section.
The appearance of the electric field in the second term of Eq. (C.7) gives rise to a Hall current perpen-

dicular to the magnetization and the electric field

$$\begin{aligned}\vec{j}_{\text{Hall}} &= -e\int \frac{d^3k}{(2\pi)^3}\vec{v}_{\vec{k}}^{\,\text{so}} f^{\text{charge}}(\epsilon, J_{\text{sd}}) \\ &= -e\vec{E}\times\int \frac{d^3k}{(2\pi)^3}\vec{\Omega} f^{\text{charge}}(\epsilon, J_{\text{sd}}) \\ &= \frac{\mu_{\text{B}}e^2Pn}{\hbar}\vec{E}\times\vec{m}(\vec{r})\int \frac{d^3k}{(2\pi)^3}\lambda_{\text{so}}(\vec{k}) f^{\text{charge}}(\epsilon, J_{\text{sd}}) \\ &= \sigma_{\text{AHE}}\vec{E}\times\vec{m}(\vec{r}).\end{aligned} \tag{C.8}$$

The anomalous Hall conductivity is thus related to the equilibrium distribution

$$\begin{aligned}\sigma_{\text{AHE}} &= \frac{\mu_{\text{B}}e^2Pn}{\hbar}\int \frac{d^3k}{(2\pi)^3}\lambda_{\text{so}}(\vec{k}) f^{\text{charge}}(\epsilon, J_{\text{sd}}) \\ &= \frac{\mu_{\text{B}}e^2Pn}{\hbar}\lambda_{\text{so}}(\epsilon_{\text{F}})\int \frac{d^3k}{(2\pi)^3} f^{\text{charge}}(\epsilon, J_{\text{sd}}) \\ &= \frac{\mu_{\text{B}}e^2Pn^2\lambda_{\text{so}}(\epsilon_{\text{F}})}{\hbar}.\end{aligned} \tag{C.9}$$

The result for the anomalous Hall conductivity in Eq. (C.9) states that the anomalous contribution to the Hall effect is entirely of topological nature such that all states below the Fermi energy participate to the Hall current as it is associated with the equilibrium distribution. Furthermore, the anomalous Hall current does not depend on scattering times and is thus dissipationless.

C.3.1 Conductivity tensor for the charge current

The non-equilibrium charge distribution function is derived in Eq. (5.120) and can be abbreviated to

$$\begin{aligned}g(\vec{k}) &= \frac{e\tau_c\tau_s\left(P\tau_+ - \tau_s\right)}{\tau_c\tau_+ - \tau_s^2}\vec{v}_{\vec{k}}\vec{E}\partial_\epsilon f^{\text{charge}}(\epsilon, J_{\text{sd}}) \\ &\equiv \Xi\left(\vec{v}_{\vec{k}}\vec{E}\right)\partial_\epsilon f^{\text{charge}}(\epsilon, J_{\text{sd}}).\end{aligned} \tag{C.10}$$

In the presence of spin-orbit interaction ($\lambda_{\text{so}}(\vec{k}) \neq 0$), the non-equilibrium charge distribution follows from a substitution of the velocity ($\vec{v}_{\vec{k}} \to \vec{v}_{\vec{k}}^{\,\text{so}}$)

$$\begin{aligned}{}^{\text{so}}g(\vec{k}) &= \Xi\left(\vec{v}_{\vec{k}}^{\,\text{so}}\vec{E}\right)\partial_\epsilon f^{\text{charge}}(\epsilon, J_{\text{sd}}) \\ &= \Xi\left(1 + \frac{\mu_{\text{B}}e\mu_0M_sPn\lambda_{\text{so}}(\vec{k})}{\hbar}\right)\left(\vec{v}_{\vec{k}}\vec{E}\right)\partial_\epsilon f^{\text{charge}}(\epsilon, J_{\text{sd}}) \\ &\quad - \Xi\frac{\mu_{\text{B}}e\mu_0M_sPn\lambda_{\text{so}}(\vec{k})}{\hbar}(\vec{m}(\vec{r})\vec{v}_{\vec{k}})(\vec{m}(\vec{r})\vec{E})\partial_\epsilon f^{\text{charge}}(\epsilon, J_{\text{sd}}) + \mathcal{O}(\vec{E}^2).\end{aligned} \tag{C.11}$$

The new charge distribution function (C.11) now drifts in the presence of spin-orbit interactions according to the semiclassical equations of motions (C.3) and (C.4). The validity of the non-equilibrium distribution (C.10) is limited to linear response, as we neglect terms that are of higher order in the

electric field. The current is computed by integrating out the momentum weighted with the spin-orbit modified velocity

$$\begin{aligned}
{}^{\text{so}}\vec{j}(\vec{r}) &= -e\int \frac{d^3k}{(2\pi)^3}\vec{v}_{\vec{k}}^{\,\text{so}}\,{}^{\text{so}}g(\vec{k}) \\
&= -e\,\Xi\int \frac{d^3k}{(2\pi)^3}\partial_\epsilon f^{\text{charge}}(\epsilon, J_{\text{sd}})\Big[\left(1+\frac{\mu_{\text{B}}e\mu_0 M_s P n\lambda_{\text{so}}(\vec{k})}{\hbar}\right)^2\vec{v}_{\vec{k}}(\vec{v}_{\vec{k}}\vec{E}) \\
&\quad -\frac{\mu_{\text{B}}e\mu_0 M_s P n\lambda_{\text{so}}(\vec{k})}{\hbar}\left(1+\frac{\mu_{\text{B}}e\mu_0 M_s P n\lambda_{\text{so}}(\vec{k})}{\hbar}\right)\vec{v}_{\vec{k}}(\vec{m}(\vec{r})\vec{v}_{\vec{k}})(\vec{m}(\vec{r})\vec{E}) \\
&\quad -\frac{\mu_{\text{B}}e\mu_0 M_s P n\lambda_{\text{so}}(\vec{k})}{\hbar}\left(1+\frac{\mu_{\text{B}}e\mu_0 M_s P n\lambda_{\text{so}}(\vec{k})}{\hbar}\right)\vec{m}(\vec{r})(\vec{m}(\vec{r})\vec{v}_{\vec{k}})(\vec{v}_{\vec{k}}\vec{E}) \\
&\quad +\left(\frac{\mu_{\text{B}}e\mu_0 M_s P n\lambda_{\text{so}}(\vec{k})}{\hbar}\right)^2\vec{m}(\vec{r})(\vec{m}(\vec{r})\vec{v}_{\vec{k}})(\vec{m}(\vec{r})\vec{v}_{\vec{k}})(\vec{m}(\vec{r})\vec{E})\Big].
\end{aligned} \tag{C.12}$$

The expression (C.12) reflects the twofold impact of the anomalous velocity. In addition to the direct contribution in the expression for the current (C.12), the anomalous velocity contributes in an indirect manner to the solution of the kinetic equation that is the distribution function (C.11). Carrying out a similar calculation as in section 5.4.2.1 and in particular exploiting the relation (5.129) yields for the current

$$\begin{aligned}
{}^{\text{so}}\vec{j}(\vec{r}) &= \left[\frac{e\Xi}{3}\int d\epsilon N(\epsilon)\left(1+\frac{\mu_{\text{B}}e\mu_0 M_s P n\lambda_{\text{so}}(\vec{k})}{\hbar}\right)^2\vec{v}_{\vec{k}}^{\,2}\delta(\epsilon-\epsilon_{\text{F}})\right]\vec{E} \\
&\quad -\left[\frac{e\Xi}{3}\int d\epsilon N(\epsilon)\frac{\mu_{\text{B}}e\mu_0 M_s P n\lambda_{\text{so}}(\vec{k})}{\hbar}\left(2+\frac{\mu_{\text{B}}e\mu_0 M_s P n\lambda_{\text{so}}(\vec{k})}{\hbar}\right)\vec{v}_{\vec{k}}^{\,2}\delta(\epsilon-\epsilon_{\text{F}})\right] \\
&\quad (\vec{m}(\vec{r})\vec{E})\vec{m}(\vec{r}) \\
&= \frac{e^2 n\tau_c\tau_s\left(P\tau_+-\tau_s\right)}{m\left(\tau_c\tau_+-\tau_s^2\right)}\left(1+\frac{\mu_{\text{B}}e\mu_0 M_s P n\lambda_{\text{so}}(\epsilon_{\text{F}})}{\hbar}\right)^2\vec{E} \\
&\quad -\frac{e^2 n\tau_c\tau_s\left(P\tau_+-\tau_s\right)}{m\left(\tau_c\tau_+-\tau_s^2\right)}\frac{\mu_{\text{B}}e\mu_0 M_s P n\lambda_{\text{so}}(\epsilon_{\text{F}})}{\hbar}\left(2+\frac{\mu_{\text{B}}e\mu_0 M_s P n\lambda_{\text{so}}(\epsilon_{\text{F}})}{\hbar}\right)(\vec{m}(\vec{r})\vec{E})\vec{m}(\vec{r}).
\end{aligned} \tag{C.13}$$

The result (C.13) determines the global bulk conductivities parallel $\sigma_{||}$ and perpendicular $\sigma_\perp$ to the magnetization as well as the Hall conductivity σ_{Hall} for the charge current. The individual contributions can be decomposed according to their vector structure

$$\begin{aligned}
{}^{\text{so}}\vec{j}(\vec{r}) &= \vec{j}_\perp(\vec{r})+\vec{j}_{||}(\vec{r})+\vec{j}_{\text{Hall}}(\vec{r}) \\
&= \sigma_\perp\left(\vec{E}-(\vec{m}(\vec{r})\vec{E})\vec{m}(\vec{r})\right)-\sigma_{\text{Hall}}\vec{m}(\vec{r})\times\vec{E}+\sigma_{||}(\vec{m}(\vec{r})\vec{E})\vec{m}(\vec{r}), \\
&= \sigma_\perp\vec{E}-\sigma_{\text{Hall}}\vec{m}(\vec{r})\times\vec{E}+(\sigma_{||}-\sigma_\perp)(\vec{m}(\vec{r})\vec{E})\vec{m}(\vec{r}).
\end{aligned} \tag{C.14}$$

A comparison of Eqns. (C.13) and (C.14) identifies the individual entries of the conductivity tensor

$$\sigma_\perp = \frac{e^2 n \tau_c \tau_s \left(P\tau_+ - \tau_s\right)}{m\left(\tau_c\tau_+ - \tau_s^2\right)} \left(1 + \frac{\mu_\mathrm{B} e \mu_0 M_s P n \lambda_\mathrm{so}(\epsilon_\mathrm{F})}{\hbar}\right)^2, \tag{C.15}$$

$$\sigma_\mathrm{Hall} = \frac{\mu_\mathrm{B} e^2 P n^2 \lambda_\mathrm{so}(\epsilon_\mathrm{F})}{\hbar}, \tag{C.16}$$

$$\sigma_{||} = \frac{e^2 n \tau_c \tau_s \left(P\tau_+ - \tau_s\right)}{m\left(\tau_c\tau_+ - \tau_s^2\right)}. \tag{C.17}$$

The three conductivities given in Eqns. (C.15) to (C.17) define a conductivity tensor

$${}^{\mathrm{so}}\sigma = \begin{pmatrix} \sigma_\perp & \sigma_\mathrm{Hall} & 0 \\ -\sigma_\mathrm{Hall} & \sigma_\perp & 0 \\ 0 & 0 & \sigma_{||} \end{pmatrix}, \tag{C.18}$$

where we assumed w.l.o.g. that the magnetization $\vec{m}$ points in z direction. The corresponding resistivities are obtained by inverting the conductivity tensor (C.18)

$$\begin{aligned} \rho_\perp &= \frac{\sigma_\perp}{\sigma_\perp^2 + \sigma_\mathrm{Hall}^2} \\ &= \frac{\tau_c\tau_s\left(P\tau_+ - \tau_s\right)\left(\hbar + \mu_\mathrm{B} e\mu_0 M_s P n \lambda_\mathrm{so}(\epsilon_\mathrm{F})\right)^2}{e^2\hbar^2 m n \left(\tau_c\tau_+ - \tau_s^2\right)\left[\left(\frac{\mu_\mathrm{B} P n \lambda_\mathrm{so}(\epsilon_\mathrm{F})}{\hbar}\right)^2 + \left(\frac{\tau_c\tau_s(\tau_s - P\tau_+)\left(\hbar + \mu_\mathrm{B} e\mu_0 M_s P n \lambda_\mathrm{so}(\epsilon_\mathrm{F})\right)^2}{\hbar^2 m(\tau_s^2 - \tau_c\tau_+)}\right)^2\right]}, \end{aligned} \tag{C.19}$$

$$\begin{aligned} \rho_\mathrm{Hall} &= \frac{\sigma_\mathrm{Hall}}{\sigma_\perp^2 + \sigma_\mathrm{Hall}^2} \\ &= \frac{P\mu_\mathrm{B}\lambda_\mathrm{so}(\epsilon_\mathrm{F})}{e^2\hbar\left[\left(\frac{\mu_\mathrm{B} P n \lambda_\mathrm{so}(\epsilon_\mathrm{F})}{\hbar}\right)^2 + \left(\frac{\tau_c\tau_s(\tau_s - P\tau_+)\left(\hbar + \mu_\mathrm{B} e\mu_0 M_s P n \lambda_\mathrm{so}(\epsilon_\mathrm{F})\right)^2}{\hbar^2 m(\tau_s^2 - \tau_c\tau_+)}\right)^2\right]}, \end{aligned} \tag{C.20}$$

$$\rho_{||} = \frac{1}{\sigma_{||}} = \frac{m\left(\tau_c\tau_+ - \tau_s^2\right)}{e^2 n \tau_c \tau_s \left(P\tau_+ - \tau_s\right)}. \tag{C.21}$$

The parallel resistivity coincides with the conductivity in absence of spin-orbit interactions (cf. Eq. (5.135)).
In conclusion, we derived an AMR like behavior for the charge current with the anisotropic magnetoresistivity given by

$$\begin{aligned} \Delta\rho &= \rho_{||} - \rho_\perp \\ &= \frac{m\left(\tau_c\tau_+ - \tau_s^2\right)}{e^2 n \tau_c \tau_s \left(P\tau_+ - \tau_s\right)} \\ &\quad - \frac{\tau_c\tau_s\left(P\tau_+ - \tau_s\right)\left(\hbar + \mu_\mathrm{B} e\mu_0 M_s P n \lambda_\mathrm{so}(\epsilon_\mathrm{F})\right)^2}{e^2\hbar^2 m n \left(\tau_c\tau_+ - \tau_s^2\right)\left[\left(\frac{\mu_\mathrm{B} P n \lambda_\mathrm{so}(\epsilon_\mathrm{F})}{\hbar}\right)^2 + \left(\frac{\tau_c\tau_s(\tau_s - P\tau_+)\left(\hbar + \mu_\mathrm{B} e\mu_0 M_s P n \lambda_\mathrm{so}(\epsilon_\mathrm{F})\right)^2}{\hbar^2 m(\tau_s^2 - \tau_c\tau_+)}\right)^2\right]} \end{aligned}$$

$$\Delta\rho = \left(e^2 mn\right)^{-1} \left(\frac{1}{\tau^\uparrow} + \frac{1}{\tau^\downarrow}\right)\left(\frac{1}{\tau^\uparrow} - \frac{1}{\tau^\downarrow}\right)$$
$$\Big[\frac{m^2(\tau^\uparrow)^2(\tau^\downarrow)^2(\tau^\uparrow+\tau^\downarrow+2\tau_{\text{sf}})}{(\tau^\uparrow+\tau^\downarrow)(\tau^\downarrow-\tau^\uparrow)\left[((1+P)\tau^\uparrow+(1-P)\tau^\downarrow)\tau_{\text{sf}}+2\tau^\uparrow\tau^\downarrow\right]}$$
$$-\frac{\left(\hbar+\mu_{\text{B}}e\mu_0 M_s P n\lambda_{\text{so}}(\epsilon_{\text{F}})\right)^2(\tau^\uparrow+\tau^\downarrow)(\tau^\downarrow-\tau^\uparrow)}{\hbar^2(\tau^\uparrow)^2(\tau^\downarrow)^2(\tau^\uparrow+\tau^\downarrow+2\tau_{\text{sf}})\left(\frac{1}{(\tau^\uparrow)^2}-\frac{1}{(\tau^\downarrow)^2}\right)^2}$$
$$\frac{\left[((1+P)\tau^\uparrow+(1-P)\tau^\downarrow)\tau_{\text{sf}}+2\tau^\uparrow\tau^\downarrow\right]}{\left[\left(\frac{\mu_{\text{B}}Pn\lambda_{\text{so}}(\epsilon_{\text{F}})}{\hbar}\right)^2+\left(\frac{\left(\hbar+\mu_{\text{B}}e\mu_0 M_s Pn\lambda_{\text{so}}(\epsilon_{\text{F}})\right)^2\left(((1+P)\tau^\uparrow+(1-P)\tau^\downarrow)\tau_{\text{sf}}+2\tau^\uparrow\tau^\downarrow\right)}{\hbar^2 m(\tau^\uparrow+\tau^\downarrow+2\tau_{\text{sf}})}\right)^2\right]}\Big]. \tag{C.22}$$

Figure (C.1) depicts the behavior of the anisotropic magnetoresistivity for the charge current

$$\rho_{\text{AMR}} = \frac{\Delta\rho}{\rho_{||}+\rho_\perp} = \frac{\rho_{||}-\rho_\perp}{\rho_{||}+\rho_\perp}, \tag{C.23}$$

in dependence of the effective parameter that parametrizes the strength of the spin-orbit interaction

$$\zeta := \mu_{\text{B}}e\mu_0 M_s P n\lambda_{\text{so}}(\epsilon_{\text{F}}), \tag{C.24}$$

and for different ratios of the relaxation times $\beta = \tau^\uparrow/\tau^\downarrow$. Experimental values for the ratio of relaxation times are in between $\beta = 0.2 - 30$. [183] The charge anisotropic magnetoresistivity is mainly positive but can obtain also negative values for large values of β as depicted in Fig. (C.1) (b). The window of negative values for the anisotropic magnetoresistance decreases as β decreases. Due to the indirect coupling via the macroscopic magnetization in Eq. (C.2) the intrinsic AMR is too weak to constitute the dominant contribution. Accordingly, the dominant part to the AMR must be attributed to the extrinsic mechanism via scattering.
However, it is instructive to examine the AMR ratio (C.22) in certain limiting cases. For a better survey they are listed in Table C.1. The limit of dominating spin-orbit interaction reduces the perpendicular resistivity to zero and should therefore not be taken too literally. In Table C.1 we employed the abbreviation

$$\varphi := \left((1+P)\tau^\uparrow + (1-P)\tau^\downarrow\right), \tag{C.25}$$

in the expression for vanishing spin-flip scattering. Figure (C.2) depicts the behavior of the anomalous Hall magnetoresistivity

$$\rho_{\text{AHE}} = \frac{\rho_{\text{Hall}}}{\rho_{||}+\rho_\perp}, \tag{C.26}$$

for the charge current in dependence of the effective spin-orbit interaction parameter ζ as defined in Eq. (C.24) for various ratios of the relaxation times β. The anomalous Hall magnetoresistivity turns to zero for $|\zeta| \to \infty$.

C.3.2 Conductivity tensor for the spin-transfer torque

The transport coefficients for the spin-transfer torque in the presence of spin-orbit interaction are associated with the transverse non-equilibrium distributions (5.123) and (5.124). The adiabatic non-

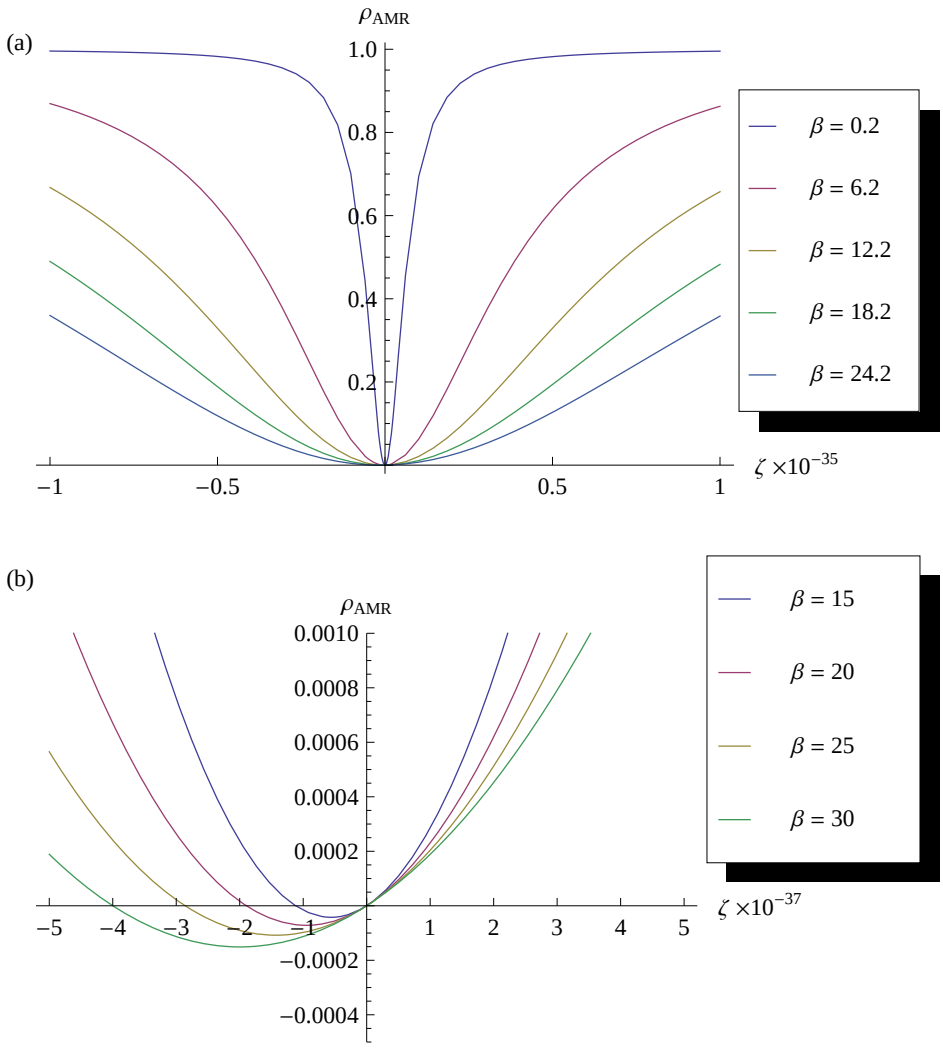

Figure C.1: (Color online) (a) The anisotropic magnetoresistivity for the charge current in dependence of the effective spin-orbit interaction parameter ζ for various values of the ratios of relaxation times $\beta = \tau^{\uparrow}/\tau^{\downarrow}$ for a fully polarized current ($P = 1$). (b) The same as (a) for small values of ζ and high ratios of the relaxation times β.

Table C.1: Several limiting cases for the anisotropic magnetoresistivity for the charge current.

limit	$\Delta\rho$
$\tau^{\uparrow} = \tau^{\downarrow} = \tau$	$\frac{m\zeta(\hbar^2 m^2\zeta + e^2 M_s^2(\hbar+\zeta)^2(2\hbar+\zeta)\mu_0^2\tau^2)}{e^2\hbar^2 m^2 n\zeta^2\tau + e^4 M_s^2 n(\hbar+\zeta)^4\mu_0^2\tau^3}$ equal spin conserving scattering times
$\tau_{\mathrm{sf}} \to \infty$	$\frac{2m\zeta(2e^2\hbar^3 M_s^2\mu_0^2\varphi^2 + 4e^2\hbar M_s^2\zeta^2\mu_0^2\varphi^2 + e^2 M_s^2\zeta^3\mu_0^2\varphi^2 + \hbar^2\zeta(4m^2+5e^2M_s^2\mu_0^2\varphi^2))}{e^2 n\varphi(e^2\hbar^4 M_s^2\mu_0^2\varphi^2 + 4e^2\hbar^3 M_s^2\zeta\mu_0^2\varphi^2 + 4e^2\hbar M_s^2\zeta^3\mu_0^2\varphi^2 + e^2 M_s^2\zeta^4\mu_0^2\varphi^2 + 2\hbar^2\zeta^2(2m^2+3e^2M_s^2\mu_0^2\varphi^2))}$ spin-flip scattering off
$\tau_{\mathrm{sf}} \to 0$	$\frac{m\zeta(\tau^{\downarrow}+\tau^{\uparrow})(\hbar^2 m^2\zeta(\tau^{\downarrow})^2 + 2\hbar^2 m^2\zeta\tau^{\downarrow}\tau^{\uparrow} + (\hbar^2 m^2\zeta + 4e^2 M_s^2(\hbar+\zeta)^2(2\hbar+\zeta)\mu_0^2(\tau^{\downarrow})^2)(\tau^{\uparrow})^2)}{2e^2 n\tau^{\downarrow}\tau^{\uparrow}(\hbar^2 m^2\zeta^2(\tau^{\downarrow})^2 + 2\hbar^2 m^2\zeta^2\tau^{\downarrow}\tau^{\uparrow} + (\hbar^2 m^2\zeta^2 + 4e^2 M_s^2(\hbar+\zeta)^4\mu_0^2(\tau^{\downarrow})^2)(\tau^{\uparrow})^2)}$ dominating spin-flip scattering
$\lambda_{\mathrm{so}}(\epsilon_{\mathrm{F}}) \to 0$	no AMR when spin-orbit interaction is turned off
$\lambda_{\mathrm{so}}(\epsilon_{\mathrm{F}}) \to \infty$ ($\hbar \to 0$) (problematic limit cf. text)	$\frac{m(\tau^{\uparrow}+\tau^{\downarrow}+2\tau_{\mathrm{sf}})}{e^2 n[((1+P)\tau^{\uparrow}+(1-P)\tau^{\downarrow})\tau_{\mathrm{sf}}+2\tau^{\uparrow}\tau^{\downarrow}]}$ dominating SOI charge resistivity (cf. Eq. (5.137))
$P \to 0$	no AMR when polarization is turned off

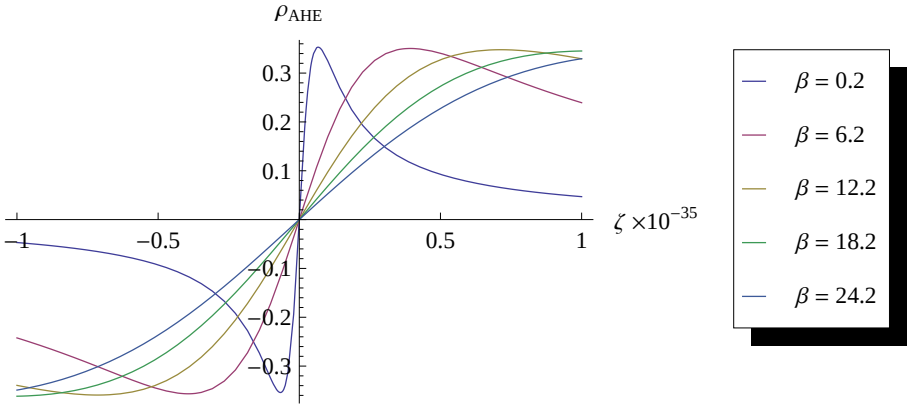

Figure C.2: (Color online) The anomalous Hall magnetoresistivity for the charge current in dependence of the effective spin-orbit interaction parameter ζ.

equilibrium contribution (5.124) reads

$$
\begin{aligned}
g_{\perp}^{(2)}(\vec{k}) = &-\frac{e\gamma\tau_+^2\tau_s}{(1+\gamma^2\tau_+^2)(\tau_c\tau_+ - \tau_s^2)} \\
&\Big[\frac{J_{\text{sd}}\tau_c(P\tau_+ - \tau_s)}{\hbar}\sum_i \delta_{ij}(\vec{e}_i\vec{\nabla}_{\vec{k}})(\vec{v}_{\vec{k}}\vec{E}) + \sum_i \delta_{ij}(\vec{e}_i\vec{v}_{\vec{k}})\vec{v}_{\vec{k}}\vec{E}\tau_+(\tau_c - P\tau_s)\Big]\partial_\epsilon f^{\text{charge}}(\epsilon, J_{\text{sd}}) \\
\equiv\ &\Psi\sum_i \delta_{ij}\Big[\frac{J_{\text{sd}}\tau_c(P\tau_+ - \tau_s)}{\hbar}(\vec{e}_i\vec{\nabla}_{\vec{k}})(\vec{v}_{\vec{k}}\vec{E}) + \tau_+(\tau_c - P\tau_s)(\vec{e}_i\vec{v}_{\vec{k}})\vec{v}_{\vec{k}}\vec{E}\Big]\partial_\epsilon f^{\text{charge}}(\epsilon, J_{\text{sd}}).
\end{aligned}
\tag{C.27}
$$

Analogously to section 5.4.2.2 the first term exactly cancels for the simple one band model due to the momentum integration by an integration of parts. Thus, we focus on the latter and obtain the spin-orbit corrected non-equilibrium transverse spin distribution to the first order in the electric field by virtue of the substitution ($\vec{v}_{\vec{k}} \to \vec{v}_{\vec{k}}^{\,\text{so}}$)

$$
\begin{aligned}
{}^{\text{so}}g_{\perp}^2(\vec{k}) &= \Psi\sum_i \delta_{ij}(\vec{e}_i\vec{v}_{\vec{k}}^{\,\text{so}})(\vec{v}_{\vec{k}}^{\,\text{so}}\vec{E})\partial_\epsilon f^{\text{charge}}(\epsilon, J_{\text{sd}}) \\
&= \Psi\partial_\epsilon f^{\text{charge}}(\epsilon, J_{\text{sd}})\sum_i \delta_{ij}\Big[\left(1 + \frac{\mu_{\text{B}}e\mu_0 M_s P n\lambda_{\text{so}}(\vec{k})}{\hbar}\right)^2 (\vec{e}_i\vec{v}_{\vec{k}})(\vec{v}_{\vec{k}}\vec{E}) \\
&\quad - \frac{\mu_{\text{B}}e\mu_0 M_s P n\lambda_{\text{so}}(\vec{k})}{\hbar}\left(1 + \frac{\mu_{\text{B}}e\mu_0 M_s P n\lambda_{\text{so}}(\vec{k})}{\hbar}\right)(\vec{e}_i\vec{v}_{\vec{k}})(\vec{m}(\vec{r})\vec{v}_{\vec{k}})(\vec{m}(\vec{r})\vec{E}) \\
&\quad - \frac{\mu_{\text{B}}e\mu_0 M_s P n\lambda_{\text{so}}(\vec{k})}{\hbar}\left(1 + \frac{\mu_{\text{B}}e\mu_0 M_s P n\lambda_{\text{so}}(\vec{k})}{\hbar}\right)(\vec{e}_i\vec{m}(\vec{r}))(\vec{m}(\vec{r})\vec{v}_{\vec{k}})(\vec{v}_{\vec{k}}\vec{E}) \\
&\quad + \left(\frac{\mu_{\text{B}}e\mu_0 M_s P n\lambda_{\text{so}}(\vec{k})}{\hbar}\right)^2 (\vec{e}_i\vec{m}(\vec{r}))(\vec{m}(\vec{r})\vec{v}_{\vec{k}})(\vec{m}(\vec{r})\vec{v}_{\vec{k}})(\vec{m}(\vec{r})\vec{E})\Big] + \mathcal{O}(\vec{E}^2),
\end{aligned}
\tag{C.28}
$$

The magnetization of the conduction electrons follows from the momentum integration under consideration of the relation (5.129)

$$
\begin{aligned}
\frac{1}{\tau_{\text{sd}}}\langle {}^{\text{so}}\hat{\vec{\sigma}}_{\text{ad}}(\vec{r})\rangle_{\text{neq}} &= -\frac{\mu_{\text{B}}}{\tau_{\text{sd}}}\int \frac{d^3k}{(2\pi)^3}\,{}^{\text{so}}g_{\perp}^2(\vec{k})\sum_j \vec{m}(\vec{r}) \times (\vec{e}_j\vec{\nabla}_{\vec{r}})\vec{m}(\vec{r}) \\
&= -\frac{\mu_{\text{B}}\Psi}{3}\int d\epsilon N(\epsilon)\left(1 + \frac{\mu_{\text{B}}e\mu_0 M_s P n\lambda_{\text{so}}(\vec{k})}{\hbar}\right)^2 \vec{v}_{\vec{k}}^{\,2}\delta(\epsilon - \epsilon_{\text{F}}) \\
&\quad \vec{m}(\vec{r}) \times (\vec{E}\vec{\nabla}_{\vec{r}})\vec{m}(\vec{r}) \\
&\quad - \frac{e\Xi}{3}\int d\epsilon N(\epsilon)\frac{\mu_{\text{B}}e\mu_0 M_s P n\lambda_{\text{so}}(\vec{k})}{\hbar}\left(2 + \frac{\mu_{\text{B}}e\mu_0 M_s P n\lambda_{\text{so}}(\vec{k})}{\hbar}\right)\vec{v}_{\vec{k}}^{\,2}\delta(\epsilon - \epsilon_{\text{F}}) \\
&\quad \vec{m}(\vec{r}) \times ((\vec{m}(\vec{r})\vec{E})(\vec{m}(\vec{r})\vec{\nabla}_{\vec{r}}))\vec{m}(\vec{r}) \\
&= -\frac{\mu_{\text{B}}}{e}\vec{m}(\vec{r}) \times ({}^{\text{so}}\vec{j}_{\text{spin}}^{\,\text{trans}}\vec{\nabla}_{\vec{r}})\vec{m}(\vec{r}).
\end{aligned}
\tag{C.29}
$$

The same calculation applies to $\langle {}^{\text{so}}\hat{\vec{\sigma}}_{\text{non-ad}}(\vec{r})\rangle_{\text{neq}}$ and the full spin-transfer torque including spin-orbit interaction reads

$$\begin{aligned}\vec{\tau}_{\text{STT}}^{\text{so}} &= \vec{\tau}_{\text{ad}}^{\text{so}} + \vec{\tau}_{\text{non-ad}}^{\text{so}} \\ &= -\frac{\mu_{\text{B}}}{eM_s^3}\vec{M}(\vec{r})\times\vec{M}(\vec{r})\times({}^{\text{so}}\vec{j}_{\text{spin}}^{\text{trans}}\vec{\nabla}_{\vec{r}})\vec{M}(\vec{r}) - \frac{\mu_{\text{B}}\xi}{eM_s^2}\vec{M}(\vec{r})\times({}^{\text{so}}\vec{j}_{\text{spin}}^{\text{trans}}\vec{\nabla}_{\vec{r}})\vec{M}(\vec{r}).\end{aligned} \tag{C.30}$$

with the transverse spin-orbit spin current defined as

$$\begin{aligned}{}^{\text{so}}\vec{j}_{\text{spin}}^{\text{trans}} &= \sigma_{\text{spin}}^{\text{trans}}\left(1+\frac{\mu_{\text{B}}e\mu_0 M_s P n\lambda_{\text{so}}(\vec{k})}{\hbar}\right)^2\vec{E} \\ &\quad - \sigma_{\text{spin}}^{\text{trans}}\frac{\mu_{\text{B}}e\mu_0 M_s P n\lambda_{\text{so}}(\vec{k})}{\hbar}\left(2+\frac{\mu_{\text{B}}e\mu_0 M_s P n\lambda_{\text{so}}(\vec{k})}{\hbar}\right)(\vec{m}(\vec{r})\vec{E})\vec{m}(\vec{r}).\end{aligned} \tag{C.31}$$

In contrast to the charge current (C.13) no transverse Hall current appears in the conductivity tensor of the transverse spin current. The global bulk conductivities parallel $\sigma_{||}^{\text{trans}}$ and perpendicular $\sigma_{\perp}^{\text{trans}}$ to the magnetization read

$$\sigma_{\perp}^{\text{trans}} = \sigma_{\text{spin}}^{\text{trans}}\left(1+\frac{\mu_{\text{B}}e\mu_0 M_s P n\lambda_{\text{so}}(\epsilon_{\text{F}})}{\hbar}\right)^2, \tag{C.32}$$

$$\sigma_{\text{Hall}}^{\text{trans}} = 0, \tag{C.33}$$

$$\sigma_{||}^{\text{trans}} = \sigma_{\text{spin}}^{\text{trans}}. \tag{C.34}$$

The reason for the vanishing Hall conductivity is that the transverse magnetization of the conduction electrons is a pure non-equilibrium phenomenon. We recall from section 5.4.2.2 that in equilibrium the magnetization of the conduction electrons is aligned antiparallel to the local magnetization. Thus, the absence of a transverse equilibrium component is responsible for the missing of an anomalous Hall effect in the transverse spin current. Noting that the intrinsic contribution to the anomalous Hall effect dominates over an extrinsic contribution this result provides an essential justification for the shape of the resistivity tensor as employed in section 4. [277] Similar to the charge current the parallel resistivity in the transverse spin current coincides with the conductivity in absence of the anisotropic magnetoresistance (cf. Eq. (5.172)).
The corresponding resistivities for the transverse spin current read

$$\rho_{\perp}^{\text{trans}} = \frac{1}{\sigma_{\perp}^{\text{trans}}} = \left(\sigma_{\text{spin}}^{\text{trans}}\right)^{-1}\left(1+\frac{\mu_{\text{B}}e\mu_0 M_s P n\lambda_{\text{so}}(\epsilon_{\text{F}})}{\hbar}\right)^{-2}, \tag{C.35}$$

$$\rho_{\text{Hall}}^{\text{trans}} = 0, \tag{C.36}$$

$$\rho_{||}^{\text{trans}} = \frac{1}{\sigma_{||}^{\text{trans}}} = \left(\sigma_{\text{spin}}^{\text{trans}}\right)^{-1}. \tag{C.37}$$

In conclusion, for the transverse spin current that constitutes the spin-transfer torque we find no anomalous Hall effect but an anisotropic magnetoresistance with an anisotropic magnetoresistivity

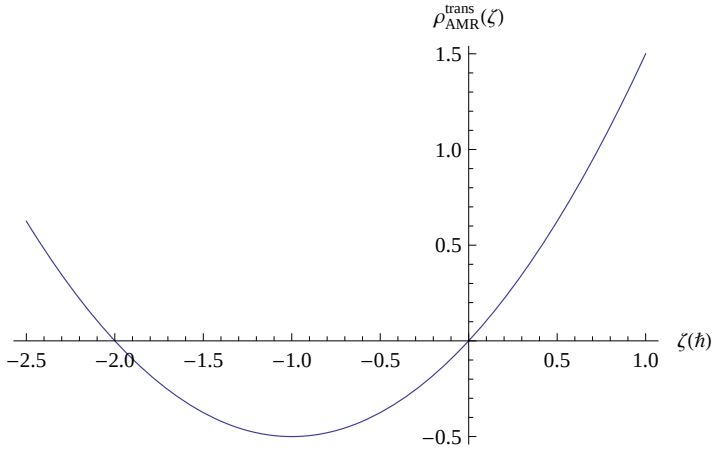

Figure C.3: (Color online) The anisotropic magnetoresistivity for the transverse spin current that constitutes the spin-transfer torque in dependence of the effective spin-orbit interaction parameter ζ.

that reads

$$\begin{aligned}
\Delta\rho_{\mathrm{spin}}^{\mathrm{trans}} &= \rho_{||}^{\mathrm{trans}} - \rho_{\perp}^{\mathrm{trans}} \\
&= \left(\sigma_{\mathrm{spin}}^{\mathrm{trans}}\right)^{-1}\left[1-\left(1+\frac{\mu_{\mathrm{B}}e\mu_0 M_s P n\lambda_{\mathrm{so}}(\epsilon_{\mathrm{F}})}{\hbar}\right)^{-2}\right] \\
&= \frac{\mu_{\mathrm{B}}\mu_0 M_s P m\lambda_{\mathrm{so}}(\epsilon_{\mathrm{F}})\left(2\hbar+\mu_{\mathrm{B}}e\mu_0 M_s P n\lambda_{\mathrm{so}}(\epsilon_{\mathrm{F}})\right)\left(\tau^{\uparrow}+\tau^{\downarrow}+2\tau_{\mathrm{sf}}\right)}{8e^2\left(\hbar+\mu_{\mathrm{B}}e\mu_0 M_s P n\lambda_{\mathrm{so}}(\epsilon_{\mathrm{F}})\right)^2(\tau^{\uparrow})^2(\tau^{\downarrow})^2\tau_{\mathrm{sf}}^3\left[(1+P)\tau^{\uparrow}-(1-P)\tau^{\downarrow}\right]} \\
&\quad\left(\tau_{\mathrm{sd}}^2\tau_{\mathrm{sf}}\tau^{\uparrow}(\tau_{\mathrm{sf}}\tau^{\uparrow}+2\tau^{\downarrow}(\tau_{\mathrm{sf}}+2\tau^{\uparrow}))+\tau_{\mathrm{sd}}^2(\tau^{\downarrow})^2(\tau_{\mathrm{sf}}+2\tau^{\uparrow})^2+16(\tau^{\uparrow})^2(\tau^{\downarrow})^2\tau_{\mathrm{sf}}^2\right).
\end{aligned} \tag{C.38}$$

The anisotropic magnetoresistance for the spin-transfer is given by

$$\begin{aligned}
\rho_{\mathrm{AMR}}^{\mathrm{trans}} &= \frac{\rho_{||}^{\mathrm{trans}} - \rho_{\perp}^{\mathrm{trans}}}{\rho_{||}^{\mathrm{trans}} + \rho_{\perp}^{\mathrm{trans}}} \\
&= \frac{\zeta(2\hbar+\zeta)}{2\hbar^2},
\end{aligned} \tag{C.39}$$

where we employed the definition of the effective spin-orbit interaction parameter ζ in Eq. (C.24). From Eq. (C.39) we conclude that the anisotropic magnetoresistance is entirely determined by the spin-orbit interaction parameter λ_{so} and the conduction electron density n.
Figure (C.3) depicts the behavior of the anisotropic magnetoresistivity for the transverse spin current that constitutes the spin-transfer torque in dependence of the effective spin-orbit interaction parameter ζ as defined in Eq. (C.24). In contrast to the charge current, the anisotropic magnetoresistance for the spin-transfer torque is entirely of topological nature, i.e., it does not depend on scattering times. This allows for large values of the anisotropic magnetoresistance that are unexpected for the charge current from Eq. (C.23) but restricts somehow the parameter range for $\lambda_{\mathrm{so}}(\epsilon_{\mathrm{F}})$. As depicted in Fig. (C.3) the anisotropic magnetoresistance is strictly positive definite for positive $\lambda_{\mathrm{so}}(\epsilon_{\mathrm{F}})$, while for small negative

Table C.2: Several limiting cases for the anisotropic magnetoresistivity for the transverse spin current that constitutes the spin-transfer torque.

limit	$\Delta\rho^{\text{trans}}_{\text{spin}}$
$\tau^{\uparrow}=\tau^{\downarrow}=\tau$	$\frac{m\zeta(2\hbar+\zeta)(\tau+\tau_{\text{sf}})(2\tau\tau_{\text{sd}}^2\tau_{\text{sf}}+\tau_{\text{sd}}^2\tau_{\text{sf}}^2+\tau^2(\tau_{\text{sd}}^2+4\tau_{\text{sf}}^2))}{2e^2nP(\hbar+\zeta)^2\tau^3\tau_{\text{sf}}^3}$ equal scattering rates
$\tau_{\text{sf}}\to\infty$	$\frac{m\zeta(2\hbar+\zeta)\left(\tau_{\text{sd}}^2(\tau^{\uparrow}+\tau^{\downarrow})^2+(4\tau^{\uparrow}\tau^{\downarrow})^2\right)}{4e^2n(\hbar+\zeta)^2(\tau^{\uparrow})^2(\tau^{\downarrow})^2\left[(1+P)\tau^{\uparrow}-(1-P)\tau^{\downarrow}\right]}$ spin-flip scattering off
$\tau_{\text{sf}}\to 0$	no spin-transfer torque in dominating spin-flip scattering
$\tau_{\text{sd}}\to\infty$	no spin-transfer torque in vanishing sd exchange
$\tau_{\text{sd}}\to 0$	$\frac{2m\zeta(2\hbar+\zeta)\left(\tau^{\uparrow}+\tau^{\downarrow}+2\tau_{\text{sf}}\right)}{e^2n(\hbar+\zeta)^2\tau_{\text{sf}}\left[(1+P)\tau^{\uparrow}-(1-P)\tau^{\downarrow}\right]}$ dominating sd exchange
$\lambda_{\text{so}}(\epsilon_{\text{F}})\to 0$	no AMR if spin-orbit interaction is turned off
$\lambda_{\text{so}}(\epsilon_{\text{F}})\to\infty$ ($\hbar\to 0$) (problematic limit cf. text)	$\frac{m(\tau^{\uparrow}+\tau^{\downarrow}+2\tau_{\text{sf}})\left(\tau_{\text{sd}}^2\tau_{\text{sf}}\tau^{\uparrow}(\tau_{\text{sf}}\tau^{\uparrow}+2\tau^{\downarrow}(\tau_{\text{sf}}+2\tau^{\uparrow}))+\tau_{\text{sd}}^2(\tau^{\downarrow})^2(\tau_{\text{sf}}+2\tau^{\uparrow})^2+16(\tau^{\uparrow})^2(\tau^{\downarrow})^2\tau_{\text{sf}}^2\right)}{8e^2n(\tau^{\uparrow})^2(\tau^{\downarrow})^2\tau_{\text{sf}}^3\left[(1+P)\tau^{\uparrow}-(1-P)\tau^{\downarrow}\right]}$ dominating SOI transverse spin resistivity (cf. Eq. (5.172))
$P\to 0$	no AMR when polarization is turned off
$M_s\to 0$	no AMR if magnetization is turned off

values of $\lambda_{\text{so}}(\epsilon_{\text{F}})$ a small window for negative AMR ratios occurs.
Several limits of interest for the anisotropic magnetoresistivity in Eq. (C.38) of the transverse spin current are listed in Table C.2. As in the case of the anisotropic magnetoresistance for the charge current the limit of dominating spin-orbit interaction reduces the perpendicular resistivity in the transverse spin current to zero and should therefore not be taken too literally.
The degree of non-adiabaticity ξ is not affected by intrinsic spin-orbit interactions and remains the same as in Eq. (5.163) without spin-orbit interactions. This is due to the fact that the degree of non-adiabaticity in our model occurs due to scattering and not affected by the band structure. However, spin-flip scattering is caused by extrinsic spin-orbit interactions due to collisions at magnetic impurities and spin-orbit interactions contribute in this sense in an extrinsic manner to ξ.

C.3.3 Conductivity tensor for the spin current

In the presence of spin-orbit interaction the spin-current tensor is calculated according to

$$^{\mathrm{so}}\hat{J}(\vec{r}) = -\mu_{\mathrm{B}} \int \frac{d^3k}{(2\pi)^3}\, ^{\mathrm{so}}\vec{v}_{\vec{k}} \otimes \mathrm{Tr}\ ^{\mathrm{so}}\hat{f}_{\vec{k}}(\vec{r})\vec{\sigma}. \tag{C.40}$$

The surviving terms of the momentum integration yield the result for the spin-current tensor in the presence of spin-orbit interaction

$$\begin{aligned} ^{\mathrm{so}}\hat{J}(\vec{r}) &= -\mu_{\mathrm{B}} \int \frac{d^3k}{(2\pi)^3} \vec{v}_{\vec{k}} \otimes \left(Pf^{\mathrm{charge}}(\epsilon, J_{\mathrm{sd}})\vec{m}(\vec{r}) + \, ^{\mathrm{so}}g_{\vec{m}}(\vec{k})\vec{m}(\vec{r}) \right) \\ &= \frac{\mu_{\mathrm{B}}}{e}\, ^{\mathrm{so}}\vec{j}_{\mathrm{spin}} \otimes \vec{m}(\vec{r}). \end{aligned} \tag{C.41}$$

The spin current constitutes the spatial part of the spin-current tensor that distinguishes its direction of flow

$$\begin{aligned} ^{\mathrm{so}}\vec{j}_{\mathrm{spin}} = {} & \frac{e^2 n \tau_{\mathrm{sf}} \left[(1+P)\tau^{\uparrow} - (1-P)\tau^{\downarrow} \right]}{m(\tau^{\uparrow} + \tau^{\downarrow} + 2\tau_{\mathrm{sf}})} \left(1 + \frac{\mu_{\mathrm{B}} e \mu_0 M_s P n \lambda_{\mathrm{so}}(\epsilon_{\mathrm{F}})}{\hbar} \right)^2 \vec{E} \\ & + \frac{\mu_{\mathrm{B}} e^2 P^2 n^2 \lambda_{\mathrm{so}}(\epsilon_{\mathrm{F}})}{\hbar} \vec{E} \times \vec{m}(\vec{r}) \\ & - \frac{e^2 n \tau_{\mathrm{sf}} \left[(1+P)\tau^{\uparrow} - (1-P)\tau^{\downarrow} \right]}{m(\tau^{\uparrow} + \tau^{\downarrow} + 2\tau_{\mathrm{sf}})} \frac{\mu_{\mathrm{B}} e \mu_0 M_s P n \lambda_{\mathrm{so}}(\epsilon_{\mathrm{F}})}{\hbar} \\ & \left(2 + \frac{\mu_{\mathrm{B}} e \mu_0 M_s P n \lambda_{\mathrm{so}}(\epsilon_{\mathrm{F}})}{\hbar} \right) (\vec{m}(\vec{r})\vec{E})\vec{m}(\vec{r}). \end{aligned} \tag{C.42}$$

The spin part of the spin-current tensor always points in the direction of the local magnetization. In the adiabatic approximation the spin-current tensor does not obtain transverse components (cf. section 5.4.2.3). This also holds in the case of spin-orbit interactions. The conduction coefficients read

$$\sigma_{\perp}^{\mathrm{spin}} = \frac{e^2 n \tau_{\mathrm{sf}} \left[(1+P)\tau^{\uparrow} - (1-P)\tau^{\downarrow} \right]}{m(\tau^{\uparrow} + \tau^{\downarrow} + 2\tau_{\mathrm{sf}})} \left(1 + \frac{\mu_{\mathrm{B}} e \mu_0 M_s P n \lambda_{\mathrm{so}}(\epsilon_{\mathrm{F}})}{\hbar} \right)^2, \tag{C.43}$$

$$\sigma_{\mathrm{Hall}}^{\mathrm{spin}} = \frac{\mu_{\mathrm{B}} e^2 P^2 n^2 \lambda_{\mathrm{so}}(\epsilon_{\mathrm{F}})}{\hbar}, \tag{C.44}$$

$$\sigma_{||}^{\mathrm{spin}} = \frac{e^2 n \tau_{\mathrm{sf}} \left[(1+P)\tau^{\uparrow} - (1-P)\tau^{\downarrow} \right]}{m(\tau^{\uparrow} + \tau^{\downarrow} + 2\tau_{\mathrm{sf}})}. \tag{C.45}$$

The corresponding resistivities for the spin current are obtained by inverting the conductivity tensor

$$\begin{aligned}\rho_{\perp}^{\text{spin}} &= \frac{\sigma_{\perp}^{\text{spin}}}{(\sigma_{\perp}^{\text{spin}})^2 + (\sigma_{\text{Hall}}^{\text{spin}})^2} \\ &= \left[\left(\frac{\mu_{\text{B}} P^2 n \lambda_{\text{so}}(\epsilon_{\text{F}})}{\hbar}\right)^2 + \left(\frac{\tau_{\text{sf}}\left[(1+P)\tau^{\uparrow} - (1-P)\tau^{\downarrow}\right]\left(\hbar + \mu_{\text{B}} e \mu_0 M_s P n \lambda_{\text{so}}(\epsilon_{\text{F}})\right)^2}{\hbar^2 m\left(\tau^{\uparrow} + \tau^{\downarrow} + 2\tau_{\text{sf}}\right)}\right)^2\right]^{-1} \\ &\quad \frac{\tau_{\text{sf}}\left[(1+P)\tau^{\uparrow} - (1-P)\tau^{\downarrow}\right]\left(\hbar + \mu_{\text{B}} e \mu_0 M_s P n \lambda_{\text{so}}(\epsilon_{\text{F}})\right)^2}{e^2 \hbar^2 m n\left(\tau^{\uparrow} + \tau^{\downarrow} + 2\tau_{\text{sf}}\right)}, \end{aligned} \tag{C.46}$$

$$\begin{aligned}\rho_{\text{Hall}}^{\text{spin}} &= \frac{\sigma_{\text{Hall}}^{\text{spin}}}{(\sigma_{\perp}^{\text{spin}})^2 + (\sigma_{\text{Hall}}^{\text{spin}})^2} \\ &= \frac{P^2 \mu_{\text{B}} \lambda_{\text{so}}(\epsilon_{\text{F}})}{e^2 \hbar \left[\left(\frac{\mu_{\text{B}} P^2 n \lambda_{\text{so}}(\epsilon_{\text{F}})}{\hbar}\right)^2 + \left(\frac{\tau_{\text{sf}}\left[(1+P)\tau^{\uparrow} - (1-P)\tau^{\downarrow}\right]\left(\hbar + \mu_{\text{B}} e \mu_0 M_s P n \lambda_{\text{so}}(\epsilon_{\text{F}})\right)^2}{\hbar^2 m\left(\tau^{\uparrow} + \tau^{\downarrow} + 2\tau_{\text{sf}}\right)}\right)^2\right]}, \end{aligned} \tag{C.47}$$

$$\rho_{||}^{\text{spin}} = \frac{1}{\sigma_{||}^{\text{spin}}} = \frac{m(\tau^{\uparrow} + \tau^{\downarrow} + 2\tau_{\text{sf}})}{e^2 n \tau_{\text{sf}}\left[(1+P)\tau^{\uparrow} - (1-P)\tau^{\downarrow}\right]}. \tag{C.48}$$

The parallel resistivity coincides with the spin current resistivity in the absence of spin-orbit interactions and equals the spin current in the two-current model (5.74).
In conclusion, we find an AMR like behavior for the spin current with the anisotropic magnetoresistivity given by

$$\begin{aligned}\Delta\rho^{\text{spin}} &= \rho_{||}^{\text{spin}} - \rho_{\perp}^{\text{spin}} \\ &= \frac{m(\tau^{\uparrow} + \tau^{\downarrow} + 2\tau_{\text{sf}})}{e^2 n \tau_{\text{sf}}\left[(1+P)\tau^{\uparrow} - (1-P)\tau^{\downarrow}\right]} \\ &\quad - \left[\left(\frac{\mu_{\text{B}} P^2 n \lambda_{\text{so}}(\epsilon_{\text{F}})}{\hbar}\right)^2 + \left(\frac{\tau_{\text{sf}}\left[(1+P)\tau^{\uparrow} - (1-P)\tau^{\downarrow}\right]\left(\hbar + \mu_{\text{B}} e \mu_0 M_s P n \lambda_{\text{so}}(\epsilon_{\text{F}})\right)^2}{\hbar^2 m\left(\tau^{\uparrow} + \tau^{\downarrow} + 2\tau_{\text{sf}}\right)}\right)^2\right]^{-1} \\ &\quad \frac{\tau_{\text{sf}}\left[(1+P)\tau^{\uparrow} - (1-P)\tau^{\downarrow}\right]\left(\hbar + \mu_{\text{B}} e \mu_0 M_s P n \lambda_{\text{so}}(\epsilon_{\text{F}})\right)^2}{e^2 \hbar^2 m n\left(\tau^{\uparrow} + \tau^{\downarrow} + 2\tau_{\text{sf}}\right)}. \end{aligned} \tag{C.49}$$

Appendix D

Calculation of the local electric field due to the anisotropic magnetoresistance within a Néel wall

In this appendix we analytically calculate the spatially inhomogeneous electric field due to the anisotropic magnetoresistance within a Néel wall. A Néel wall occurs in ferromagnetic wires with small cross sections. The analytical result may serve in combination with a numerical solution of the non-equilibrium kinetic equation for a domain wall (5.197) for the computation of the spin-transfer torque or the domain-wall resistivity in the presence of spin-orbit interactions.

A domain wall is parametrized by a constant angle θ and a spatially varying angle $\phi(x)$. A typical domain-wall profile is parametrized by

$$\phi(x) = \pi - 2\arctan\left(\exp\frac{x-x_0}{\lambda}\right), \quad 0 \leq x \leq \lambda, \tag{D.1}$$

$$\theta = \frac{\pi}{2} = const., \tag{D.2}$$

where λ is the domain-wall width and x_0 is the center of the domain wall. The domain-wall profile (D.2) is a soliton solution that minimizes an energy functional in one infinite spatial dimension. The width of the domain wall is a compromise between exchange and anisotropy energy

$$\lambda = \sqrt{\frac{A}{K}}, \tag{D.3}$$

where A is the exchange stiffness and K is the shape anisotropy constant due to the demagnetization field.
A one-dimensional Néel wall is parametrized by

$$\vec{m}(x) = \begin{pmatrix} \sin\theta\cdot\cos\phi \\ \sin\theta\cdot\sin\phi \\ \cos\theta \end{pmatrix} = \begin{pmatrix} \tanh(\frac{x-x_0}{\lambda}) \\ \cosh^{-1}(\frac{x-x_0}{\lambda}) \\ 0 \end{pmatrix}. \tag{D.4}$$

The x and y component of the magnetization within the wall are shown in Figs. D.1 and D.2. The

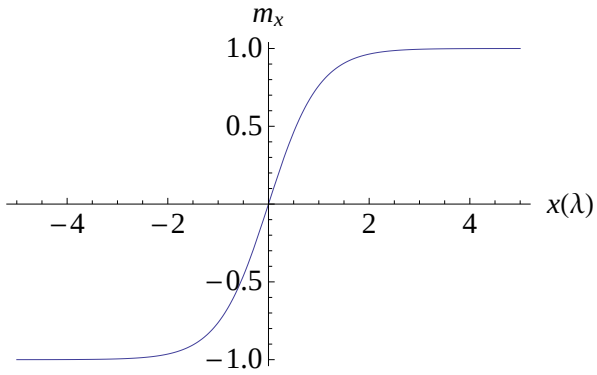

Figure D.1: (Color online) x component of the magnetization within a Néel wall.

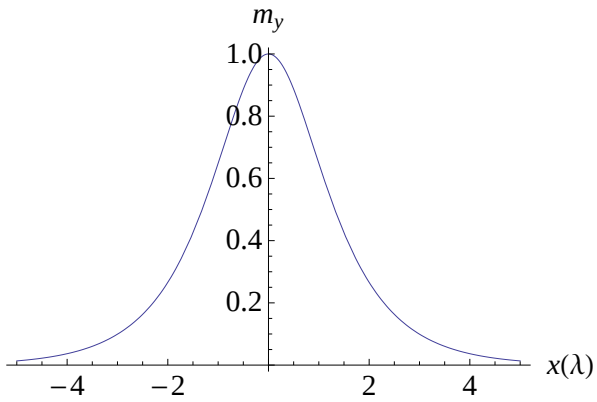

Figure D.2: (Color online) y component of the magnetization within a Néel wall.

magnetization turns by 180° over the domain wall. At the wall's center that is located at the origin of the coordinate system the magnetization points perpendicular to the wire axis that is the x axis.

The calculation of the local electric current proceeds by solving Poisson's equation (4.4) for the electric Potential $\Phi(\vec{r})$ (cf. section 4.2.2)

$$\vec{\nabla}_{\vec{r}}\left[\sigma(\vec{m}(\vec{r}))\vec{\nabla}_{\vec{r}}\,\Phi(\vec{r})\right] = 0. \tag{D.5}$$

In one spatial dimension Eq. (D.5) reads

$$\partial_x\left[\sigma_{xx}(\vec{m}(x))\partial_x\Phi(x)\right] = 0, \tag{D.6}$$

where the conductivity follows from the inverse of the resistivity

$$\sigma_{xx}(\vec{m}(x)) = \rho_{xx}^{-1}(\vec{m}(x)). \tag{D.7}$$

In the one-dimensional case the resistivity reads

$$\rho_{xx}(x) = \rho_\perp + \Delta\rho\cos^2\phi = \rho_{||}\tanh^2(\frac{x-x_0}{\lambda}) + \rho_\perp\cosh^{-2}(\frac{x-x_0}{\lambda}), \tag{D.8}$$

with the abbreviation $\Delta\rho = \rho_{||} - \rho_\perp$. Equation (D.7) yields the conductivity

$$\begin{aligned}\sigma_{xx}(x) \equiv \rho_{xx}^{-1}(x) &= \frac{1}{\rho_{||}\tanh^2(\frac{x-x_0}{\lambda}) + \rho_\perp\cosh^{-2}(\frac{x-x_0}{\lambda})} \\ &= \frac{1}{\rho_{||} - \Delta\rho\cosh^{-2}(\frac{x-x_0}{\lambda})}.\end{aligned} \tag{D.9}$$

The derivative of the conductivity in Eq. (D.9) is given by

$$\partial_x\sigma_{xx}(x) = \frac{2 - \Delta\rho\frac{\tanh(\frac{x-x_0}{\lambda})}{\cosh^2(\frac{x-x_0}{\lambda})}}{\lambda(\rho_{||} - \Delta\rho\cosh^{-2}(\frac{x-x_0}{\lambda}))^2}. \tag{D.10}$$

With the result of Eq. (D.10) Poisson's equation (D.6) reads

$$(\frac{1}{\rho_{||} - \Delta\rho\cosh^{-2}(\frac{x-x_0}{\lambda})})\Phi''(x) + (\frac{2 - \Delta\rho\frac{\tanh(\frac{x-x_0}{\lambda})}{\cosh^2(\frac{x-x_0}{\lambda})}}{\lambda(\rho_{||} - \Delta\rho\cosh^{-2}(\frac{x-x_0}{\lambda}))^2})\Phi'(x) = 0. \tag{D.11}$$

A solution for Eq. (D.11) is provided by

$$\Phi(x) = [2(x-x_0)\rho_{||} - 2\lambda\Delta\rho\tanh(\frac{x-x_0}{\lambda})]c_1 + c_2. \tag{D.12}$$

The constants c_1, c_2 are determined by the boundary conditions

$$\Phi(x)|_{x=x_0} = \Phi_0, \tag{D.13}$$

$$\Phi'(x)|_{x=x_0} = -E_0. \tag{D.14}$$

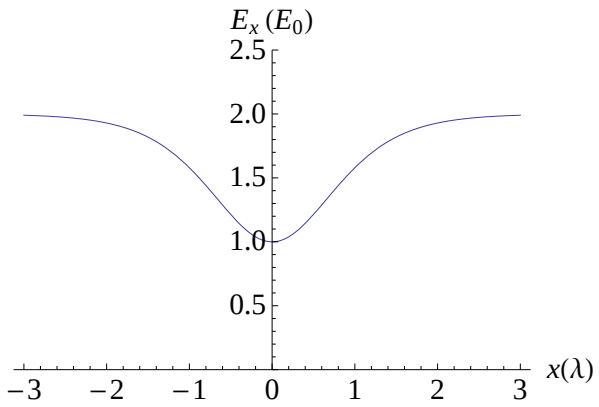

Figure D.3: (Color online) Spatially inhomogeneous distribution of the electric field within a Néel wall due to the anisotropic magnetoresistance for $\rho_\perp = 0.2$, $\rho_{||} = 0.1$, and $x_0 = 0$.

The boundary condition (D.13) fixes the potential and yields $c_2 = \phi_0$ and (D.14) relates c_1 to the external applied electric field by

$$c_1 = -\frac{E_0}{2\rho_\perp}. \tag{D.15}$$

Thus the electric potential in a Néel wall is found to be

$$\Phi(x) = \Phi_0 - [(x - x_0)\frac{\rho_{||}}{\rho_\perp} - \lambda\frac{\Delta\rho}{\rho_\perp}\tanh(\frac{x - x_0}{\lambda})]E_0. \tag{D.16}$$

The electric potential (D.16) gives rise to an electric field

$$E(x) = -\Phi'(x) = \frac{E_0}{\rho_\perp}(\rho_{||} - \Delta\rho\cosh^{-2}(\frac{x - x_0}{\lambda})). \tag{D.17}$$

The electric current is calculated via Ohm's law

$$j(x) = \sigma_{xx}(x)E(x) = \frac{E_0}{\rho_\perp} = const.. \tag{D.18}$$

From Eq. (D.18) it immediately follows that the electric current is conserved $j'(x) = 0$. The calculation is consitent as can be seen by calculating the resistivity

$$\rho(x) = \frac{E(x)}{j(x)} = \rho_{||} - \Delta\rho\cosh^{-2}(\frac{x - x_0}{\lambda}), \tag{D.19}$$

which is the inverse of the conductivity (D.9). Due to the anisotropic magnetoresistance the resistivity is lowest at the center of the Néel wall. The driving electric field has to decrease when approaching the wall's center to obtain a steady current flow due to an increase in the conductivity by means of the perpendicular alignment of current and magnetization. At a large distance from the wall's center the local resistance as well as the electric field attain their maximum values.

Appendix E

Momentum integration of the first-order transverse distribution

To determine the magnetization of the conduction electrons via Eq. (5.3), we have to trace out the momentum in Eq. (5.233). With some abbreviations Eq. (5.233) reads

$$\begin{aligned}{}^{(1)}\tilde{g}_{\vec{k}}^{\text{trans}}(x) = -4\pi i z_2 \Big[\Theta(v_x)\left(1-e^{-\frac{z_1}{v_x}x}\right) + \Theta(-v_x)\left(1-e^{\frac{z_1}{v_x}(\lambda-x)}\right)\Big] \\ \Big[\partial_\epsilon f^{\text{charge}}(\epsilon, J_{\text{sd}})(c_1 + c_2 v_x^2) \\ + \partial_\epsilon^2 f^{\text{charge}}(\epsilon, J_{\text{sd}})(c_3 + c_4 v_x^2) \\ + \partial_\epsilon^3 f^{\text{charge}}(\epsilon, J_{\text{sd}}) c_5 v_x^2\Big]. \end{aligned} \tag{E.1}$$

The constants are defined as follows

$$\begin{aligned} z_1 &= \frac{1}{\tilde{\tau}} - i\frac{2}{\tau_{\text{sd}}}, \\ z_2 &= \frac{eE_x\tau_c^2\tau_s\tau_{\text{sf}}}{l_{\text{mfp}} m\tau_{\text{sd}}\left(2\tau_c\tau_s^2 + \tau_{\text{sf}}\left(\tau_s^2-\tau_c^2\right)\right)\left(2\tau_c(\tau_{\text{sd}} - 2i\tau_{\text{sf}}) + \tau_{\text{sf}}\tau_{\text{sd}}\right)}, \\ c_1 &= \hbar\tau_s\tau_{\text{sd}}(2\tau_c + \tau_{\text{sf}}), \\ c_2 &= -m\tau_c\tau_{\text{sd}}^2\tau_{\text{sf}}, \\ c_3 &= \hbar^2\tau_c\tau_{\text{sf}}, \\ c_4 &= 2\hbar m\tau_s\tau_{\text{sd}}\tau_c, \\ c_5 &= \hbar^2 m\tau_c\tau_{\text{sf}}. \end{aligned} \tag{E.2}$$

The momentum integration is most easily carried out in spherical coordinates (v, θ, ϕ) of velocity space, where we parametrize the velocity space such that $v_x = v\cos\theta$

$$
\begin{aligned}
-\kappa\mu_{\mathrm{B}} \int \frac{d^3k}{(2\pi)^3}\, {}^{(1)}\tilde{g}^{\mathrm{trans}}_{\vec{k}}(x) = 4\pi i\kappa\mu_{\mathrm{B}} z_2 m^3 \\
\int \frac{d^3v}{(2\pi\hbar)^3} \left[\Theta(v_x)\left(1 - e^{-\frac{z_1}{v_x}x}\right) + \Theta(-v_x)\left(1 - e^{\frac{z_1}{v_x}(\lambda - x)}\right)\right] \\
\Big[(c_1 + c_2 v_x^2)\partial_\epsilon f^{\mathrm{charge}}(\epsilon, J_{\mathrm{sd}}) \\
+ c_3\partial_\epsilon^2 f^{\mathrm{charge}}(\epsilon, J_{\mathrm{sd}}) + c_4 v_x^2 \partial_\epsilon^2 f^{\mathrm{charge}}(\epsilon, J_{\mathrm{sd}}) \\
+ c_5 v_x^2 \partial_\epsilon^3 f^{\mathrm{charge}}(\epsilon, J_{\mathrm{sd}})\Big]. \qquad \text{(E.3)}
\end{aligned}
$$

A conversion of the velocity integration into an energy integration yields as a result

$$
\begin{aligned}
-\kappa\mu_{\mathrm{B}} \int \frac{d^3k}{(2\pi)^3}\, {}^{(1)}\tilde{g}^{\mathrm{trans}}_{\vec{k}}(x) = \\
\frac{i\kappa\mu_{\mathrm{B}} z_2\sqrt{2}m^2}{2\pi^2\hbar^3\sqrt{m}} \int_0^\infty d\epsilon \int_{-1}^1 d(\cos\theta) \int_0^{2\pi} d\phi\ \Theta(\cos\theta)\sqrt{\epsilon} \\
\Big[\left(1 - e^{-\frac{z_1}{v_x}x}\right)(c_1 + c_2 v_x^2)\partial_\epsilon f^{\mathrm{charge}}(\epsilon, J_{\mathrm{sd}}) \\
+ \left(1 - e^{-\frac{z_1}{v_x}x}\right) c_3\partial_\epsilon^2 f^{\mathrm{charge}}(\epsilon, J_{\mathrm{sd}}) + \left(1 - e^{-\frac{z_1}{v_x}x}\right) c_4 v_x^2 \partial_\epsilon^2 f^{\mathrm{charge}}(\epsilon, J_{\mathrm{sd}}) \\
+ \left(1 - e^{-\frac{z_1}{v_x}x}\right) c_5 v_x^2 \partial_\epsilon^3 f^{\mathrm{charge}}(\epsilon, J_{\mathrm{sd}})\Big] \\
- \frac{i\kappa\mu_{\mathrm{B}} z_2\sqrt{2}m^2}{2\pi^2\hbar^3\sqrt{m}} \int_0^\infty d\epsilon \int_{-1}^1 d(\cos\theta) \int_0^{2\pi} d\phi\ \Theta(-\cos\theta)\sqrt{\epsilon} \\
\Big[\left(1 - e^{\frac{z_1}{v_x}(\lambda - x)}\right)(c_1 + c_2 v_x^2)\partial_\epsilon f^{\mathrm{charge}}(\epsilon, J_{\mathrm{sd}}) \\
+ \left(1 - e^{\frac{z_1}{v_x}(\lambda - x)}\right) c_3\partial_\epsilon^2 f^{\mathrm{charge}}(\epsilon, J_{\mathrm{sd}}) + \left(1 - e^{\frac{z_1}{v_x}(\lambda - x)}\right) c_4 v_x^2 \partial_\epsilon^2 f^{\mathrm{charge}}(\epsilon, J_{\mathrm{sd}}) \\
+ \left(1 - e^{\frac{z_1}{v_x}(\lambda - x)}\right) c_5 v_x^2 \partial_\epsilon^3 f^{\mathrm{charge}}(\epsilon, J_{\mathrm{sd}})\Big]. \qquad \text{(E.4)}
\end{aligned}
$$

The Θ-function restricts the $\cos\theta$ integration. Let us now get rid of higher derivatives of the Fermi function in Eq. (E.4) by means of partial integrations

$$
\begin{aligned}
-\kappa\mu_{\rm B}\int\frac{d^3k}{(2\pi)^3}\,{}^{(1)}\tilde{g}^{\rm trans}_{\vec{k}}(x) = \\
&\frac{i\kappa\mu_{\rm B}z_2\sqrt{2}m^2}{2\pi^2\hbar^3\sqrt{m}}\int_0^\infty d\epsilon\int_0^1 d(\cos\theta)\int_0^{2\pi}d\phi\,\partial_\epsilon f^{\rm charge}(\epsilon,J_{\rm sd})\\
&\Big[\sqrt{\epsilon}(c_1+c_2v^2\cos^2\theta)\left(1-e^{-\frac{z_1}{v\cos\theta}x}\right)\\
&\quad-c_3\partial_\epsilon\left[\sqrt{\epsilon}\left(1-e^{-\frac{z_1}{v\cos\theta}x}\right)\right]\\
&\quad-c_4\cos^2\theta\partial_\epsilon\left[\sqrt{\epsilon}v^2\left(1-e^{-\frac{z_1}{v\cos\theta}x}\right)\right]\\
&\quad+c_5\cos^2\theta\partial_\epsilon^2\left[\sqrt{\epsilon}v^2\left(1-e^{-\frac{z_1}{v\cos\theta}x}\right)\right]\Big]\\
&+\frac{i\kappa\mu_{\rm B}z_2\sqrt{2}m^2}{2\pi^2\hbar^3\sqrt{m}}\int_0^\infty d\epsilon\int_{-1}^0 d(\cos\theta)\int_0^{2\pi}d\phi\,\partial_\epsilon f^{\rm charge}(\epsilon,J_{\rm sd})\\
&\Big[\sqrt{\epsilon}(c_1+c_2v^2\cos^2\theta)\left(1-e^{\frac{z_1}{v\cos\theta}(\lambda-x)}\right)\\
&\quad-c_3\partial_\epsilon\left[\sqrt{\epsilon}\left(1-e^{\frac{z_1}{v\cos\theta}(\lambda-x)}\right)\right]\\
&\quad-c_4\cos^2\theta\partial_\epsilon\left[\sqrt{\epsilon}v^2\left(1-e^{\frac{z_1}{v\cos\theta}(\lambda-x)}\right)\right]\\
&\quad+c_5\cos^2\theta\partial_\epsilon^2\left[\sqrt{\epsilon}v^2\left(1-e^{\frac{z_1}{v\cos\theta}(\lambda-x)}\right)\right]\Big].
\end{aligned}
\tag{E.5}
$$

An evaluation of the energy derivatives yields

$$
\partial_\epsilon\left[\sqrt{\epsilon}\left(1-e^{-\frac{z_1}{v\cos\theta}x}\right)\right]=\frac{1}{\sqrt{2m}v^2}\left[v\left(1-e^{-\frac{z_1}{v\cos\theta}x}\right)-\frac{z_1x}{\cos\theta}e^{-\frac{z_1}{v\cos\theta}x}\right],\tag{E.6}
$$

$$
\partial_\epsilon\left[\sqrt{\epsilon}v^2\left(1-e^{-\frac{z_1}{v\cos\theta}x}\right)\right]=\frac{1}{\sqrt{2m}}\left[3v\left(1-e^{-\frac{z_1}{v\cos\theta}x}\right)-\frac{z_1x}{\cos\theta}e^{-\frac{z_1}{v\cos\theta}x}\right],\tag{E.7}
$$

$$
\begin{aligned}
\partial_\epsilon^2\left[\sqrt{\epsilon}v^2\left(1-e^{-\frac{z_1}{v\cos\theta}x}\right)\right]= \\
&\frac{1}{\sqrt{2m}mv^3}\left[3v^2\left(1-e^{-\frac{z_1}{v\cos\theta}x}\right)-\frac{3vz_1x}{\cos\theta}e^{-\frac{z_1}{v\cos\theta}x}-\frac{z_1^2x^2}{\cos^2\theta}e^{-\frac{z_1}{v\cos\theta}x}\right].
\end{aligned}
\tag{E.8}
$$

The corresponding derivatives of $e^{\frac{z_1}{v\cos\theta}(\lambda-x)}$ are obtained by replacing $x\to(x-\lambda)$. The integration over ϕ is trivial and the integration over ϵ is carried out by approximating the derivative of the Fermi

function with a delta function

$$
\begin{aligned}
-\kappa\mu_{\mathrm{B}} \int \frac{d^3k}{(2\pi)^3}\, {}^{(1)}\tilde{g}^{\text{trans}}_{\vec{k}}(x) = \\
&- \frac{i\kappa\mu_{\mathrm{B}} z_2}{\pi\hbar^3 v_{\mathrm{F}}} \Bigg[\int_{-1}^{1} dt \Big(\left[-c_3 m + c_1 m^2 v_{\mathrm{F}}^2\right] + t^2 \left[3c_5 + m v_{\mathrm{F}}^2 \left(c_2 m v_{\mathrm{F}}^2 - 3c_4\right)\right] \Big) \\
&\quad + \left[-3c_5 - m v_{\mathrm{F}}^2 \left(c_2 m v_{\mathrm{F}}^2 - 3c_4\right)\right] \left(\int_{-1}^{0} dt\, t^2 e^{\frac{z_1}{v_{\mathrm{F}} t}(x-\lambda)} + \int_{0}^{1} dt\, t^2 e^{-\frac{z_1 x}{v_{\mathrm{F}} t}} \right) \\
&\quad + \frac{z_1}{v_{\mathrm{F}}} \left(c_4 m v_{\mathrm{F}}^2 - 3c_5\right) \left((x-\lambda) \int_{-1}^{0} dt\, t e^{\frac{z_1}{v_{\mathrm{F}} t}(\lambda - x)} + x \int_{0}^{1} dt\, t e^{-\frac{z_1 x}{v_{\mathrm{F}} t}} \right) \\
&\quad + \left[v_{\mathrm{F}}^{-2} \left(c_3 m v_{\mathrm{F}}^2 - c_1 m^2 v_{\mathrm{F}}^4 - c_5 z_1^2 (x-\lambda)^2 \right) \right] \int_{-1}^{0} dt\, e^{\frac{z_1}{v_{\mathrm{F}} t}(\lambda - x)} \\
&\quad + \left[v_{\mathrm{F}}^{-2} \left(c_3 m v_{\mathrm{F}}^2 - c_1 m^2 v_{\mathrm{F}}^4 - c_5 z_1^2 x^2 \right) \right] \int_{0}^{1} dt\, e^{-\frac{z_1 x}{v_{\mathrm{F}} t}} \\
&\quad + \left[\frac{c_3 m z_1 (x-\lambda)}{v_{\mathrm{F}}} \right] \int_{-1}^{0} dt\, \frac{1}{t} e^{\frac{z_1}{v_{\mathrm{F}} t}(\lambda - x)} + \left[\frac{c_3 m z_1 x}{v_{\mathrm{F}}} \right] \int_{0}^{1} dt\, \frac{1}{t} e^{-\frac{z_1 x}{v_{\mathrm{F}} t}} \Bigg],
\end{aligned}
\tag{E.9}
$$

where we substituted $\cos\theta = t$ for brevity.
The spatially independent part of the transverse conduction electron magnetization reads

$$
\begin{aligned}
\left\langle {}^{(1)}\hat{\sigma}^{\text{trans}} \right\rangle &= -\frac{i\kappa\mu_{\mathrm{B}} z_2}{\pi\hbar^3 v_{\mathrm{F}}} \left(2\left[-c_3 m + c_1 m^2 v_{\mathrm{F}}^2\right] + \frac{2}{3}\left[3c_5 + m v_{\mathrm{F}}^2 \left(c_2 m v_{\mathrm{F}}^2 - 3c_4\right)\right] \right) \\
&= -\frac{\mu_{\mathrm{B}}}{e\lambda} \frac{2ie^2 \tau_c^2 \tau_s \tau_{\mathrm{sf}}^2 v_{\mathrm{F}} \left(m v_{\mathrm{F}}^2 \tau_c \tau_{\mathrm{sd}} - 3\hbar\tau_s \right)}{3\hbar^3\pi \left(2\tau_c\tau_s^2 + \tau_{\mathrm{sf}}\left(\tau_s^2 - \tau_c^2\right)\right)\left(2\tau_c(\tau_{\mathrm{sd}} - 2i\tau_{\mathrm{sf}}) + \tau_{\mathrm{sf}}\tau_{\mathrm{sd}}\right)} E_x \\
&= -\frac{\mu_{\mathrm{B}}}{e\lambda} i\pi \frac{2e^2 \tau_c^2 \tau_s \tau_{\mathrm{sf}}^2 \left(n\tau_c\tau_{\mathrm{sd}} - \hbar N(\epsilon_{\mathrm{F}})\tau_s \right)}{m\left(2\tau_c\tau_s^2 + \tau_{\mathrm{sf}}\left(\tau_s^2 - \tau_c^2\right)\right)\left(2\tau_c(\tau_{\mathrm{sd}} - 2i\tau_{\mathrm{sf}}) + \tau_{\mathrm{sf}}\tau_{\mathrm{sd}}\right)} E_x \\
&= -\frac{\mu_{\mathrm{B}}}{e\lambda} i\pi \frac{2e^2 n \tau_c^2 \tau_s \tau_{\mathrm{sf}}^2 \tau_{\mathrm{sd}} \left(\tau_c - P\tau_s \right)}{m\left(2\tau_c\tau_s^2 + \tau_{\mathrm{sf}}\left(\tau_s^2 - \tau_c^2\right)\right)\left(2\tau_c(\tau_{\mathrm{sd}} - 2i\tau_{\mathrm{sf}}) + \tau_{\mathrm{sf}}\tau_{\mathrm{sd}}\right)} E_x.
\end{aligned}
\tag{E.10}
$$

Evaluation of the momentum integration yields for the spatially dependent part the result

$$
\begin{aligned}
&\langle {}^{(1)}\hat{\sigma}^{\text{trans}}(x)\rangle = \\
&-\frac{i\kappa\mu_{\text{B}}z_2}{\pi\hbar^3 v_{\text{F}}}\Bigg[\left[-3c_5 - mv_{\text{F}}^2\left(c_2 mv_{\text{F}}^2 - 3c_4\right)\right] \\
&\quad\Big[\frac{1}{6v_{\text{F}}^3}\Big(v_{\text{F}}e^{\frac{z_1(x-\lambda)}{v_{\text{F}}}}\left(2v_{\text{F}}^2 - v_{\text{F}}z_1(x-\lambda) + z_1^2(x-\lambda)^2\right) - z_1^3(x-\lambda)^3\,\Gamma(0,-\frac{z_1(x-\lambda)}{v_{\text{F}}})\Big)\Big] \\
&\quad+\frac{1}{6v_{\text{F}}^3}\Big(v_{\text{F}}e^{-\frac{z_1 x}{v_{\text{F}}}}\left(2v_{\text{F}}^2 - v_{\text{F}}z_1 x + z_1^2x^2\right) - z_1^3x^3\Gamma(0,\frac{z_1x}{v_{\text{F}}})\Big) \\
&\quad+\left[\frac{z_1}{v_{\text{F}}}\left(c_4 mv_{\text{F}}^2 - 3c_5\right)\right] \\
&\quad\Big[\frac{(x-\lambda)}{2v_{\text{F}}^2}\left(v_{\text{F}}e^{\frac{z_1(x-\lambda)}{v_{\text{F}}}}\left(v_{\text{F}} - z_1(x-\lambda)\right) + z_1^2(x-\lambda)^2\,\Gamma(0,-\frac{z_1(x-\lambda)}{v_{\text{F}}})\right) \\
&\quad+\frac{x}{2v_{\text{F}}^2}\left(v_{\text{F}}e^{-\frac{z_1x}{v_{\text{F}}}}\left(v_{\text{F}} - z_1x\right) + z_1^2x^2\Gamma(0,\frac{z_1x}{v_{\text{F}}})\right)\Big] \\
&\quad+v_{\text{F}}^{-2}\left(c_3 mv_{\text{F}}^2 - c_1m^2v_{\text{F}}^4 - c_5z_1^2(x-\lambda)^2\right)\Bigg[e^{\frac{z_1(x-\lambda)}{v_{\text{F}}}} + \frac{z_1(x-\lambda)}{v_{\text{F}}}\Gamma(0,-\frac{z_1(x-\lambda)}{v_{\text{F}}}) \\
&\quad\quad+\left[v_{\text{F}}^{-2}\left(c_3 mv_{\text{F}}^2 - c_1m^2v_{\text{F}}^4 - c_5z_1^2x^2\right)\right]\left[e^{-\frac{z_1x}{v_{\text{F}}}} - \frac{z_1x}{v_{\text{F}}}\Gamma(0,\frac{z_1x}{v_{\text{F}}})\right] \\
&\quad\quad+\left[\frac{c_3 mz_1}{v_{\text{F}}}\right]\left[(x-\lambda)\,\Gamma(0,-\frac{z_1(x-\lambda)}{v_{\text{F}}}) + x\Gamma(0,\frac{z_1x}{v_{\text{F}}})\right]\Bigg]\Bigg],
\end{aligned}
\tag{E.11}
$$

where the integral exponential function is defined as

$$
\text{Ei}(z) = \int_1^\infty dt\,\frac{e^{-zt}}{t}, \tag{E.12}
$$

and the incomplete Γ-function is given by

$$
\Gamma(a,z) = \int_z^\infty dt\,t^{a-1}e^{-t}. \tag{E.13}
$$

The complete result reads after some reordering

$$
\begin{aligned}
\langle {}^{(1)}\hat{\sigma}^{\text{trans}}_{\text{tot}}(x)\rangle &= \langle {}^{(1)}\hat{\sigma}^{\text{trans}}\rangle + \langle {}^{(1)}\hat{\sigma}^{\text{trans}}(x)\rangle \\
&= -\frac{i\kappa\mu_{\text{B}}z_2}{6\hbar^3\pi v_{\text{F}}^2} \\
&\quad \Big[2v_{\text{F}}\Big(3c_5 + m(-3c_3 + v_{\text{F}}^2(-3c_4 + 3c_1 m + c_2 m v_{\text{F}}^2))\Big) \\
&\qquad + e^{-\frac{z_1 x}{v_{\text{F}}}}\Big(- 6c_5 v_{\text{F}} + 6c_3 m v_{\text{F}} + 6c_4 m v_{\text{F}}^3 - 6c_1 m^2 v_{\text{F}}^3 \\
&\qquad\quad - 2c_2 m^2 v_{\text{F}}^5 - 6c_5 z_1 x + c_2 m^2 v_{\text{F}}^4 z_1 x - c_2 m^2 v_{\text{F}}^3 z_1^2 x^2\Big) \\
&\qquad + m^2 v_{\text{F}}^2 z_1 x\left(6c_1 + c_2 z_1^2 x^2\right)\,\text{Ei}(\frac{z_1 x}{v_{\text{F}}}) + (x \to (\lambda - x))\Big] E_x \\
&= -\frac{\mu_{\text{B}}}{e\lambda} i\pi \frac{e^2 n \tau_c^2 \tau_s \tau_{\text{sf}}}{2m\tau_{\text{sd}}\left(2\tau_c\tau_s^2 + \tau_{\text{sf}}\left(\tau_s^2 - \tau_c^2\right)\right)\left(2\tau_c(\tau_{\text{sd}} - 2i\tau_{\text{sf}}) + \tau_{\text{sf}}\tau_{\text{sd}}\right)} E_x \\
&\quad \Big[2\tau_{\text{sd}}\tau_{\text{sf}}\left(\frac{3\hbar\tau_s}{m v_{\text{F}}^2} - \tau_c\tau_{\text{sd}}\right) \\
&\qquad + e^{-\frac{\left(\frac{1}{2\tau_c} + \frac{1}{\tau_{\text{sf}}} - i\frac{2}{\tau_{\text{sd}}}\right)x}{v_{\text{F}}}}\Big[2\tau_{\text{sd}}\tau_{\text{sf}}\left(\tau_c\tau_{\text{sd}} - \frac{3\hbar\tau_s}{m v_{\text{F}}^2}\right) \\
&\qquad\quad - x\left(\frac{3\hbar^2\left(2\tau_c\left(\tau_{\text{sd}} - 2i\tau_{\text{sf}}\right) + \tau_{\text{sd}}\tau_{\text{sf}}\right)}{m^2 v_{\text{F}}^5 \tau_{\text{sd}}} + \frac{\tau_{\text{sd}}\left(2\tau_c\left(\tau_{\text{sd}} - 2i\tau_{\text{sf}}\right) + \tau_{\text{sd}}\tau_{\text{sf}}\right)}{2v_{\text{F}}}\right) \\
&\qquad\quad + x^2\left(\frac{\left(2\tau_c\left(\tau_{\text{sd}} - 2i\tau_{\text{sf}}\right) + \tau_{\text{sd}}\tau_{\text{sf}}\right)^2}{4v_{\text{F}}^2\tau_c\tau_{\text{sf}}}\right)\Big] \\
&\qquad + \text{Ei}(\left(\frac{1}{2\tau_c} + \frac{1}{\tau_{\text{sf}}} - i\frac{2}{\tau_{\text{sd}}}\right)\frac{x}{v_{\text{F}}})\Big[x\left(\frac{3\hbar\tau_s\left(2\tau_c + \tau_{\text{sf}}\right)\left(2\tau_c\left(\tau_{\text{sd}} - 2i\tau_{\text{sf}}\right) + \tau_{\text{sd}}\tau_{\text{sf}}\right)}{m v_{\text{F}}^3 \tau_c \tau_{\text{sf}}}\right) \\
&\qquad\quad - x^3\left(\frac{\left(2\tau_c\left(\tau_{\text{sd}} - 2i\tau_{\text{sf}}\right) + \tau_{\text{sd}}\tau_{\text{sf}}\right)^3}{8v_{\text{F}}^3\tau_c^2\tau_{\text{sd}}\tau_{\text{sf}}^2}\right)\Big] + (x \to (\lambda - x))\Big]. \qquad \text{(E.14)}
\end{aligned}
$$

The total torque is obtained by summing up the conduction electron magnetization (E.14) within the domain wall. Instead of directly integrating Eq. (E.14), it is more appropriate to interchange the order

of the spatial and the momentum integration. Thus, we perform first the spatial integration of Eq. (E.1)

$$
\begin{aligned}
\langle {}^{(1)}\hat{\sigma}_{\text{tot}}^{\text{trans}} \rangle &= \int_0^\lambda dx \, \langle {}^{(1)}\hat{\sigma}_{\text{tot}}^{\text{trans}}(x) \rangle \\
&= -\kappa\mu_{\text{B}} \int \frac{d^3k}{(2\pi)^3} \int_0^\lambda dx \, \tilde{g}_{\vec{k}}^{\text{trans}}(x) \\
&= 4\pi i \kappa \mu_{\text{B}} z_2 \int \frac{d^3k}{(2\pi)^3} \int_0^\lambda dx \, \Theta(v_x) 2 \left(1 - e^{-\frac{z_1 \lambda}{2 v_x}} \cosh \frac{z_1}{2 v_x} (2x - \lambda) \right) \\
&\quad \Big[\partial_\epsilon f^{\text{charge}}(\epsilon, J_{\text{sd}})(c_1 + c_2 v_x^2) \\
&\qquad + \partial_\epsilon^2 f^{\text{charge}}(\epsilon, J_{\text{sd}})(c_3 + c_4 v_x^2) \\
&\qquad + \partial_\epsilon^3 f^{\text{charge}}(\epsilon, J_{\text{sd}}) c_5 v_x^2 \Big] \\
&= 8\pi i \kappa \mu_{\text{B}} z_2 m^3 \int \frac{d^3v}{(2\pi\hbar)^3} \Theta(v_x) \left[\lambda - \frac{v_x}{z_1} \left(1 - e^{-\frac{z_1 \lambda}{v_x}} \right) \right] \\
&\quad \Big[\partial_\epsilon f^{\text{charge}}(\epsilon, J_{\text{sd}})(c_1 + c_2 v_x^2) \\
&\qquad + \partial_\epsilon^2 f^{\text{charge}}(\epsilon, J_{\text{sd}})(c_3 + c_4 v_x^2) \\
&\qquad + \partial_\epsilon^3 f^{\text{charge}}(\epsilon, J_{\text{sd}}) c_5 v_x^2 \Big]. \qquad \text{(E.15)}
\end{aligned}
$$

The velocity integration is carried out in spherical coordinates analogously as before, where the derivatives of the delta function are shifted by partial integrations. The result for the total transverse magnetization reads

$$
\begin{aligned}
\langle {}^{(1)}\hat{\sigma}_{\text{tot}}^{\text{trans}} \rangle = \frac{i \kappa \mu_{\text{B}} z_2}{12 \hbar^3 \pi v_{\text{F}}^2} \\
&\Big[\frac{6}{z_1} \left(1 - e^{\frac{z_1 \lambda}{v_{\text{F}}}} \right) v_{\text{F}}^2 \left(8 c_5 + m \left(-4 c_3 + v_{\text{F}}^2 \left(-4 c_4 + 2 c_1 m + c_2 m v_{\text{F}}^2 \right) \right) \right) \\
&- \lambda \Big[24 v_{\text{F}} \Big(c_5 \left(1 + e^{-\frac{z_1 \lambda}{v_{\text{F}}}} \right) \\
&\quad + \frac{m}{12} \left(-12 c_3 + v_{\text{F}}^2 \left(-12 c_4 + m \left(6 c_1 \left(2 - e^{-\frac{z_1 \lambda}{v_{\text{F}}}} \right) + c_2 \left(4 - e^{-\frac{z_1 \lambda}{v_{\text{F}}}} \right) v_{\text{F}}^2 \right) \right) \right) \Big) \Big] \\
&- \lambda^2 \left[m^2 v_{\text{F}}^2 z_1 \left(c_2 e^{-\frac{z_1 \lambda}{v_{\text{F}}}} v_{\text{F}}^2 + 12 c_1 \Gamma(0, \frac{z_1 \lambda}{v_{\text{F}}}) \right) \right] \\
&+ \lambda^3 \left[c_2 e^{-\frac{z_1 \lambda}{v_{\text{F}}}} m^2 v_{\text{F}}^3 z_1^2 \right] \\
&- \lambda^4 \left[(c_2 m^2 v_{\text{F}}^2 z_1^3 \Gamma(0, \frac{z_1 \lambda}{v_{\text{F}}}) \right] \Big]
\end{aligned}
$$

$$
\begin{aligned}
\langle {}^{(1)}\hat{\sigma}_{\text{tot}}^{\text{trans}} \rangle = \frac{\mu_{\text{B}}}{e\lambda} i\pi \frac{e^2 n \tau_c^2 \tau_s \tau_{\text{sf}}}{4m\tau_{\text{sd}} \left(2\tau_c \tau_s^2 + \tau_{\text{sf}} \left(\tau_s^2 - \tau_c^2\right)\right) \Lambda} E_x \\
\Big(\Big[-\frac{12}{m^2 v_{\text{F}}^3 \Lambda} \left(1 - e^{-\frac{z_1 \lambda}{v_{\text{F}}}}\right) \tau_c \tau_{\text{sd}} \tau_{\text{sf}} \\
\left(-4\hbar^2 \tau_c \tau_{\text{sf}} + m^2 v_{\text{F}}^4 \tau_c \tau_{\text{sd}}^2 \tau_{\text{sf}} + 2\hbar m v_{\text{F}}^2 \tau_s \tau_{\text{sd}} \left(2\tau_c - \tau_{\text{sf}}\right)\right) \Big] \\
+ \lambda \Big[\frac{2}{m^2 v_{\text{F}}^4} \Big(4m v_{\text{F}}^2 \tau_{\text{sd}} \tau_{\text{sf}} \left(-3\hbar\tau_s + m v_{\text{F}}^2 \tau_c \tau_{\text{sd}}\right) \\
+ e^{-\frac{z_1 \lambda}{v_{\text{F}}}} \left(-12\hbar^2 \tau_c \tau_{\text{sf}} - m^2 v_{\text{F}}^4 \tau_c \tau_{\text{sd}}^2 \tau_{\text{sf}} + 6\hbar m v_{\text{F}}^2 \tau_s \tau_{\text{sd}} \left(2\tau_c + \tau_{\text{sf}}\right)\right) \Big) \Big] \\
+ \lambda^2 \Big[\frac{\Lambda}{2m v_{\text{F}}^3 \tau_c \tau_{\text{sf}}} e^{-\frac{z_1 \lambda}{v_{\text{F}}}} \left(m v_{\text{F}}^2 \tau_c \tau_{\text{sd}} \tau_{\text{sf}} - 12 e^{\frac{z_1 \lambda}{v_{\text{F}}}} \hbar \tau_s \left(2\tau_c + \tau_{\text{sf}}\right) \Gamma(0, \frac{z_1 \lambda}{v_{\text{F}}}) \right) \Big] \\
- \lambda^3 \Big[\frac{\Lambda^2}{4 v_{\text{F}}^2 \tau_c \tau_{\text{sf}}} e^{-\frac{z_1 \lambda}{v_{\text{F}}}} \Big] \\
+ \lambda^4 \Big[\frac{\Lambda^3}{8 v_{\text{F}}^3 \tau_c^2 \tau_{\text{sd}} \tau_{\text{sf}}^2} \Gamma(0, \frac{z_1 \lambda}{v_{\text{F}}}) \Big] \Big).
\end{aligned}
\tag{E.16}
$$

Appendix F

Abbreviations for the second-order distribution

This appendix provides some abbreviations as employed in the second-order solution in section 5.5.5.3.

In Eq. (5.250) the derivative with respect to k_x of the first-order solution (5.248) contains the following abbreviations

$$
\begin{aligned}
z_1 &= \frac{1}{2\tau_c} + \frac{1}{\tau_{\text{sf}}} - i\frac{2}{\tau_{\text{sd}}}, \\
z_3 &= \frac{eE_x\hbar\tau_c\tau_s}{l_{\text{mfp}}m^2\tau_{\text{sd}}^2\left(2\tau_c\tau_s^2 + \tau_{\text{sf}}\left(\tau_s^2 - \tau_c^2\right)\right)\Lambda}, \\
d_1 &= \hbar x\tau_s\tau_{\text{sd}}\left(2\tau_c + \tau_{\text{sf}}\right)\Lambda, \\
d_2 &= -mx\tau_c\tau_{\text{sd}}^2\tau_{\text{sf}}\Lambda, \\
d_3 &= 4m\tau_c^2\tau_{\text{sd}}^3\tau_{\text{sf}}^2, \\
d_4 &= \hbar^2 x\tau_c\tau_{\text{sf}}\Lambda, \\
d_5 &= 2\hbar mx\tau_s\tau_{\text{sd}}\tau_c\Lambda, \\
d_6 &= -2\hbar m\tau_c\tau_s\tau_{\text{sd}}^2\tau_{\text{sf}}\left(6\tau_c + \tau_{\text{sf}}\right), \\
d_7 &= 2m^2\tau_c^2\tau_{\text{sd}}^3\tau_{\text{sf}}^2, \\
d_8 &= \hbar^2 mx\tau_c\tau_{\text{sf}}\Lambda, \\
d_9 &= -6\hbar^2 m\tau_c^2\tau_{\text{sd}}\tau_{\text{sf}}^2, \\
d_{10} &= -4\hbar m^2\tau_c^2\tau_s\tau_{\text{sd}}^2\tau_{\text{sf}}, \\
d_{11} &= -2\hbar^2 m^2\tau_c^2\tau_{\text{sd}}\tau_{\text{sf}}^2.
\end{aligned}
\tag{F.1}
$$

The explicit expressions as used in Eq. 5.251 read

$$\begin{aligned}
\Delta_1 &= \Im\left(\lim_{\tau_{\text{sf}}\to\infty} \partial_{k_x}\, {}^{(1)}\tilde{g}^{\text{trans}}_{\vec{k}}(x)\right) \\
&= \tilde{z}_2 e^{-\frac{x+\lambda}{2v_x\tau_c}}\Big[\partial_\epsilon f^{\text{charge}}(\epsilon, J_{\text{sd}})\left(\tilde{d}_1\mathcal{H}(x,\lambda,v_x)v_x^{-2} + \tilde{d}_2\mathcal{H}(x,\lambda,v_x) + \tilde{d}_3\mathcal{I}(x,\lambda,v_x)v_x\right) \\
&\quad + \partial_\epsilon^2 f^{\text{charge}}(\epsilon, J_{\text{sd}})\left(\tilde{d}_4\mathcal{H}(x,\lambda,v_x)v_x^{-2} + \tilde{d}_5\mathcal{I}(x,\lambda,v_x)v_x + \tilde{d}_6\mathcal{I}(x,\lambda,v_x)v_x^3\right) \\
&\quad + \partial_\epsilon^3 f^{\text{charge}}(\epsilon, J_{\text{sd}})\left(\tilde{d}_7\mathcal{H}(x,\lambda,v_x) + \tilde{d}_8\mathcal{I}(x,\lambda,v_x)v_x\right) \\
&\quad + \partial_\epsilon^4 f^{\text{charge}}(\epsilon, J_{\text{sd}})\tilde{d}_9\mathcal{I}(x,\lambda,v_x)v_x^3\Big],
\end{aligned} \tag{F.2}$$

$$\begin{aligned}
\Delta_2 &= \Im\left(\lim_{\tau_{\text{sf}}\to\infty} {}^{(1)}\tilde{g}^{\text{trans}}_{\vec{k}}(x)\right) \\
&= \tilde{z}_2 e^{-\frac{x+\lambda}{2v_x\tau_c}}\mathcal{G}(x,\lambda,v_x)\Big[\partial_\epsilon f^{\text{charge}}(\epsilon, J_{\text{sd}})\left(\tilde{c}_1 + \tilde{c}_2 v_x^2\right) \\
&\quad + \partial_\epsilon^2 f^{\text{charge}}(\epsilon, J_{\text{sd}})\tilde{c}_3 + \partial_\epsilon^3 f^{\text{charge}}(\epsilon, J_{\text{sd}})\tilde{c}_5 v_x^2\Big],
\end{aligned} \tag{F.3}$$

with the following definitions

$$\begin{aligned}
\tilde{z}_2 &= \frac{4\pi e\tau_c^2\tau_s E_x}{l_{\text{mfp}} m\left(\tau_c - \tau_s\right)\left(\tau_c + \tau_s\right)\tau_{\text{sd}}\left(16\tau_c^2 + \tau_{\text{sd}}^2\right)}, \\
\mathcal{G}(x,\lambda,v_x) &= e^{\frac{\lambda}{2v_x\tau_c}}\left(2\tau_{\text{sd}} e^{\frac{x}{2v_x\tau_c}} - \tau_{\text{sd}}\cos\frac{2x}{v_x\tau_{\text{sd}}} + 4\tau_c\sin\frac{2x}{v_x\tau_{\text{sd}}}\right) \\
&\quad - e^{\frac{x}{v_x\tau_c}}\left(\tau_{\text{sd}}\cos\frac{2(x-\lambda)}{v_x\tau_{\text{sd}}} + 4\tau_c\sin\frac{2(x-\lambda)}{v_x\tau_{\text{sd}}}\right), \\
\tilde{c}_1 &= \hbar\tau_{\text{sd}}\tau_s, \\
\tilde{c}_2 &= -m\tau_c\tau_{\text{sd}}^2, \\
\tilde{c}_3 &= \hbar^2\tau_c, \\
\tilde{c}_5 &= \hbar^2 m\tau_c, \\
\mathcal{H}(x,\lambda,v_x) &= x\, e^{\frac{\lambda}{2v_x\tau_c}}\cos\frac{2x}{v_x\tau_{\text{sd}}} + (x-\lambda)\, e^{\frac{x}{v_x\tau_c}}\cos\frac{2\left(x-\lambda\right)}{v_x\tau_{\text{sd}}}, \\
\mathcal{I}(x,\lambda,v_x) &= e^{\frac{\lambda}{2v_x\tau_c}}\left(\tau_{\text{sd}}\cos\frac{2x}{v_x\tau_{\text{sd}}} - 4\tau_c\sin\frac{2x}{v_x\tau_{\text{sd}}}\right) \\
&\quad - e^{\frac{x}{v_x\tau_c}}\left(\tau_{\text{sd}}\cos\frac{2\left(x-\lambda\right)}{v_x\tau_{\text{sd}}} + 4\tau_c\sin\frac{2\left(x-\lambda\right)}{v_x\tau_{\text{sd}}}\right),
\end{aligned}$$

$$
\begin{aligned}
\tilde{d}_1 &= -\frac{\hbar^2\tau_s\left((4\tau_c)^2+\tau_{\text{sd}}^2\right)}{2m\tau_c},\\
\tilde{d}_2 &= \frac{1}{2}\hbar\tau_{\text{sd}}\left((4\tau_c)^2+\tau_{\text{sd}}^2\right),\\
\tilde{d}_3 &= 2\hbar\tau_c\tau_{\text{sd}}^2,\\
\tilde{d}_4 &= -\frac{\hbar^3\left((4\tau_c)^2+\tau_{\text{sd}}^2\right)}{2m\tau_{\text{sd}}},\\
\tilde{d}_5 &= -\hbar^2\tau_s\tau_{\text{sd}},\\
\tilde{d}_6 &= \hbar m\tau_c\tau_{\text{sd}}^2,\\
\tilde{d}_7 &= -\frac{\hbar^3\left((4\tau_c)^2+\tau_{\text{sd}}^2\right)}{2\tau_{\text{sd}}},\\
\tilde{d}_8 &= -3\hbar^3\tau_c,\\
\tilde{d}_9 &= -\hbar^3 m\tau_c.
\end{aligned}
\tag{F.4}
$$

Acknowledgments

I would like to express my deep gratitude to all the people who contributed to this thesis in either way and without whom this work would not have been possible.

- First of all, I would like to thank my supervisor Prof. Dr. Daniela Pfannkuche for offering me the possibility of a PhD position in her group, for the numerous discussions that always taught me not to overlook the physics by the formalism and for all her support. In particular, she spent a lot of time and work in correcting our publications and this thesis.
- I would like to thank Prof. Dr. Ulrich Merkt for taking over the second report of this thesis and for his intensive support. He always found time to discuss results with me and helped me a lot concerning the illustration of my results. Without his and Dr. Katrin Buth's personal dedication the Graduiertenkolleg 1286 "Maßgeschneiderte Metall-Halbleiter-Hybridsysteme" would not have taken place in its present form.
- I would like to thank Prof. Dr. Michael Thorwart for his willingness to take over the second report of the disputation.
- I would like to thank Prof. Dr. Rembert Duine of the Utrecht University for refereeing this thesis.
- I am grateful to PD Dr. Alexander Chudnovskiy for valuable discussions.
- I am thankful to PD Dr. Guido Meier for the collaboration and his support.

My special thanks go out to all present and former group members of the I. Institut für Theoretische Physik for the nice and relaxed working atmosphere. In particular,

- Benjamin Krüger who was always willing to share his tremendous physical point of view with me, which helped me a lot,
- Dr. Peter Moraczewski for the great atmosphere in our office and for numerous discussions concerning physical as well as private content,
- Dr. Philipp Knake for his colleagueship and support, in particular in dealing with mathematical questions,
- Daniel Becker for our discussions about transport in general and his continuous help with Mathematica, in particular during the extensive analytical calculation of the domain-wall resistivity,

- Dr. Dirk-Sören Lühmann for his knowledge and support in technical details and beyond and
- Dr. Jacek Swiebodzinski for the enjoyable time during the diploma and doctoral thesis.

Furthermore,

- I appreciate Massoud Najafi and Bernd Güde for taking care of the good mood, their support with the figures and their tremendous help in proofreading of this thesis,
- I thank Dr. André Drews for his positive personality and a great time at conferences,
- I thank Dr. Karel Výborný of the FZU, Prague, for valuable discussions,
- I thank all the members of the Graduiertenkolleg 1286 "Maßgeschneiderte Metall-Halbleiter-Hybridsysteme" and the members of group N and group H for great conferences and status meetings,
- I am grateful to all my former colleagues for an enjoyable study: Christian Hambrock, Dr. Tobias Kasprzik, Dr. Tim Köppen, Dr. Marco Drewes, Benjamin Lutz and Dr. Nanda Wattimena,
- I would like to thank all my friends for their friendship, for being patient with me and for their sympathy with my lack of time during the writing of this thesis.

Finally, I am especially indebted to my parents and my family for their unconditional support and Steffi for sharing her life with me.

Bibliography

[1] W. Thomson, Proc. R. Soc. London **8**, 546 (1857).

[2] L. Berger, J. Appl. Phys. **55**, 1954 (1984).

[3] L. Berger, J. Appl. Phys. **49**, 2156 (1978).

[4] N. F. Mott and H. Jones, The Theory of the Properties of Metals and Alloys. Oxford, Oxford University Press, 1936.

[5] S. Zhang and Z. Li, Phys. Rev. Lett. **93**, 127204 (2004).

[6] S. A. Wolf, D. D. Awschalom, R. A. Buhrman, J. M. Daughton, S. von Molnár, M. L. Roukes, A. Y. Chtchelkanova, and D. M. Treger, Science **294**, 1488 (2001).

[7] G. A. Prinz, Science **282**, 1660 (1998).

[8] I. Žutić, J. Fabian, and S. Das Sarma, Rev. Mod. Phys. **76**, 323 (2004).

[9] R. Fiederling, M. Keim, G. Reuscher, W. Ossau, G. Schmidt, A. Waag, and L. W. Molenkamp, Nature **402**, 787 (1999).

[10] D. Atkinson, D. Allwood, G. Xiong, M. D. Cooke, C. C. Faulkner, and R. P. Cowburn, Nature Materials **2**, 85 (2003).

[11] C. Chappert, A. Fert, and F. V. Dau, Nature Materials **6**, 813 (2007).

[12] P. Weiss, J. Phys. **6**, 661 (1907).

[13] P. Weiss and G. Foex, Le Magnétism. Paris, Armand Colln, 1926.

[14] J. Slonczewski, J. Magn. Magn. Mater. **159**, L1 (1996).

[15] L. Berger, Phys. Rev. B **54**, 9353 (1996).

[16] C. H. Marrows, Adv. Phys. **54**, 585 (2005).

[17] M. N. Baibich, J. M. Broto, A. Fert, F. N. V. Dau, F. Petroff, P. Etienne, G. Creuzet, A. Friederich, and J. Chazelas, Phys. Rev. Lett. **61**, 2472 (1988).

[18] G. Binasch, P. Grünberg, F. Saurenbach, and W. Zinn, Phys. Rev. B **39**, 4828 (1989).

[19] S. S. P. Parkin, US Patent **309**, 6,834,005 (2004).

[20] S. S. P. Parkin, M. Hayashi, and L. Thomas, Science **320**, 190 (2008).

[21] M. Hayashi, L. Thomas, R. Moriya, C. Rettner, and S. S. S. P. Parkin, Science **320**, 209 (2008).

[22] A. Vanhaverbeke and M. Viret, Phys. Rev. B **75**, 024411 (2007).

[23] T. M. Maffitt, J. K. DeBrosse, J. A. Gabric, E. T. Gow, M. C. Lamorey, J. S. Parenteau, D. R. Willmott, M. A. Wood, and W. J. Gallagher, IBM J. Res. & Dev. **50**, 25 (2006).

[24] D. A. Allwood, G. Xiong, C. C. Faulkner, D. Atkinson, D. Petit, and R. P. Cowburn, Science **296**, 2003 (2002).

[25] J. J. Versluijs, M. A. Bari, and J. M. D. Coey, Phys. Rev. Lett. **87**, 026601 (2001).

[26] A. Yamaguchi, T. Ono, S. Nasu, K. Miyake, K. Mibu, and T. Shinjo, Phys. Rev. Lett. **92**, 077205 (2004).

[27] M. Yamanouchi, D. Chiba, F. Matsukura, and H. Ohno, Nature (London) **428**, 539 (2004).

[28] D. A. Allwood, G. Xiong, C. C. Faulkner, D. Atkinson, D. Petit, and R. P. Cowburn, Science **309**, 1688 (2005).

[29] J. He, Z. Li, and S. Zhang, Journal of Applied Physics **98**, 016108 (2005).

[30] R. P. Cowburn, Patent Application **309**, WO002004077451A1 (2004).

[31] A. Ney, C. Pampuch, R. Koch, and K. H. Ploog, Nature **425**, 485 (2003).

[32] Y. Saito and H. Sugiyama, Patent Application p. US 2005/0282379A1 (2005).

[33] D. Meyners, K. Rott, H. Brückl, G. Reiss, and J. Wecker, J. Appl. Phys. **99**, 023907 (2006).

[34] N. F. Mott, Advances in Physics **13**, 325 (1964).

[35] L. Berger, Phys. Lett. A **46**, 3 (1973).

[36] L. Berger, Phys. Rev. B **33**, 1572 (1986).

[37] L. Berger, J. Appl. Phys. **50**, 2137 (1979).

[38] L. Berger, J. Appl. Phys. **71**, 2721 (1992).

[39] J. S. Sun, J. Magn. Magn. Mater. **202**, 157 (1999).

[40] E. B. Myers, D. C. Ralph, J. A. Katine, R. N. Louie, and R. A. Buhrman, Science **285**, 867 (1999).

[41] J. A. Katine, F. J. Albert, R. A. Buhrman, E. B. Myers, and D. C. Ralph, Phys. Rev. Lett. **84**, 3149 (2000).

[42] J. Grollier, V. Cros, A. Hamzic, J. M. George, H. Jaffés, A. Fert, G. Faini, J. B. Youssef, and H. Legall, Appl. Phys. Lett. **78**, 33663 (2001).

[43] M. Tsoi, V. Tsoi, J. Bass, A. G. M. Jansen, and P. Wyder, Phys. Rev. Lett. **89**, 246803 (2002).

[44] S. I. Kiselev, J. C. Sankey, I. N. Krivorotov, N. C. Emley, R. J. Schoelkopf, R. A. Buhrman, and D. C. Ralph, Nature (London) **425**, 380 (2003).

[45] M. Tsoi, A. G. M. Jansen, J. Bass, W. C. Chiang, M. Seck, V. Tsoi, and P. Wyder, Phys. Rev. Lett. **80**, 4281 (1998).

[46] M. Tsoi, A. G. M. Jansen, J. Bass, W. C. Chiang, V. Tsoi, and P. Wyder, Nature **406**, 46 (2000).

[47] Y. B. Bazaliy, B. A. Jones, and S.-C. Zhang, Phys. Rev. B **57**, R3213 (1998).

[48] A. Thiaville, Y. Nakatani, J. Miltat, and Y. Suzuki, Europhys. Lett. **69**, 990 (2005).

[49] G. Tatara and H. Kohno, Phys. Rev. Lett. **92**, 086601 (2004).

[50] R. A. Duine, A. S. Núñez, and A. H. MacDonald, Phys. Rev. Lett. **98**, 056605 (2007).

[51] J. Fernández-Rossier, M. Braun, A. S. Núñez, and A. H. MacDonald, Phys. Rev. B **69**, 174412 (2004).

[52] A. Thiaville, Y. Nakatani, J. Miltat, and N. Vernier, J. Appl. Phys. **95**, 7049 (2004).

[53] Y. Tserkovnyak, H. J. Skadsem, A. Brataas, and G. E. W. Bauer, Phys. Rev. B **74**, 144405 (2006).

[54] H. Kohno, G. Tatara, and J. Shibata, J. Phys. Soc. Jap. **75**, 113706 (2006).

[55] R. A. Duine, A. S. Núñez, J. Sinova, and A. H. MacDonald, Phys. Rev. B **75**, 214420 (2007).

[56] J. Xiao, A. Zangwill, and M. Stiles, Phys. Rev. B **73**, 054428 (2006).

[57] H. Kohno and J. Shibata, J. Phys. Soc. Jap. **76**, 063710 (2007).

[58] G. Tatara, H. Kohno, and J. Shibata, J. Phys. Soc. Jap. **77**, 031003 (2008).

[59] G. Tatara, H. Kohno, J. Shibata, Y. Lemaho, and K.-J. Lee, J. Phys. Soc. Jap. **76**, 054707 (2007).

[60] G. Tatara and P. Entel, Phys. Rev. B **78**, 064429 (2008).

[61] W. Heisenberg, Z. Phys. **49**, 619 (1928).

[62] W. Pauli, Z. Phys. **43**, 601 (1927).

[63] P. M. Levy and S. Zhang, Phys. Rev. Lett. **79**, 5110 (1997).

[64] D. C. Langreth and J. W. Wilkins, Phys. Rev. B **6**, 3189 (1972).

[65] M. Fähnle, R. Singer, D. Steiauf, and V. P. Antropov, Phys. Rev. B **73**, 172408 (2006).

[66] E. C. Stoner, Rep. Prog. Phys. **11**, 43 (1946).

[67] D. C. Ralph and M. D. Stiles, J. Magn. Magn. Mater. **320**, 1190 (2008).

[68] C. Kittel, Quantum Theory of Solids, Wiley (1963).

[69] I. I. Mazin, Phys. Rev. Lett. **83**, 1427 (1999).

[70] J. W. Gadzuk, Phys. Rev. **182**, 416 (1969).

[71] G. Tatara, H. Kohno, and J. Shibata, Physics Reports **468**, 213 (2008).

[72] A. Hubert and R. Schäfer, Magnetic Domains, Springer-Verlag Berlin (1998).

[73] T. Jungwirth, J. Sinova, J. Mašek, J. Kučera, and A. H. MacDonald, Rev. Mod. Phys. **78**, 809 (2006).

[74] L. Landau and E. Lifshitz, Physik. Z. Sowjetunion **8**, 153 (1935).

[75] H. Barkhausen, Z. Phys. **20**, 401 (1919).

[76] N. W. Ashcroft and N. D. Mermin, Solid State Physics, (1976).

[77] F. Bloch, Z. Phys. **74**, 295 (1932).

[78] C. Kittel, Phys. Rev. **70**, 965 (1946).

[79] R. V. Coleman and G. G. Scott, Phys. Rev. **107**, 1276 (1957).

[80] T. G. Gilbert, Phys. Rev. **100**, 1243 (1955).

[81] T. L. Gilbert, IEEE Trans. Magn. **40**, 3443 (2004).

[82] H. J. Skadsem, Y. Tserkovnyak, A. Brataas, and G. E. W. Bauer, Phys. Rev. B **75**, 094416 (2007).

[83] W. S. Ament and G. T. Rado, Phys. Rev. **97**, 1558 (1955).

[84] B. Heinrich, D. Fraitová, and V. Kamberský, Phys. Status Solidi **23**, 501 (1967).

[85] V. Korenman and R. E. Prange, Phys. Rev. B **6**, 2769 (1972).

[86] V. S. Lutovinov and M. U. Reizer, Sov. Phys. JETP **50**, 355 (1979).

[87] A. Z. Solontsov and A. N. Vasil‘ev, Phys. Lett. B **177**, 362 (1993).

[88] H. Suhl, IEEE Trans. Magn. **34**, 1834 (1998).

[89] A. Y. Dobin and R. H. Victora, Phys. Rev. Lett. **90**, 167203 (2003).

[90] D. Steiauf and M. Fähnle, Phys. Rev. B **72**, 064450 (2005).

[91] K. Gilmore, Y. U. Idzerda, and M. D. Stiles, Phys. Rev. Lett. **99**, 027204 (2007).

[92] M. C. Hickey and J. S. Moodera, Phys. Rev. Lett. **102**, 137601 (2009).

[93] S. Zhang and S. S.-L. Zhang, Phys. Rev. Lett. **102**, 086601 (2009).

[94] Z. Li and S. Zhang, Phys. Rev. Lett. **92**, 207203 (2004).

[95] P. M. Haney, R. A. Duine, A. S. Núñez, and A. H. MacDonald, J. Magn. Magn. Mater. **320**, 1300 (2008).

[96] Z. Li and S. Zhang, Phys. Rev. B **70**, 024417 (2004).

[97] K. Capelle, G. Vignale, and B. L. Györffy, Phys. Rev. Lett. **87**, 206403 (2001).

[98] A. Fert, J.-L. Duvail, and T. Valet, Phys. Rev. B **52**, 6513 (1995).

[99] G. S. D. Beach, M. Tsoi, and J. L. Erskine, J. Magn. Magn. Mater. **320**, 1272 (2008).

[100] L. Berger, Phys. Rev. B **75**, 174401 (2007).

[101] S. E. Barnes and S. Maekawa, Phys. Rev. Lett. **95**, 107204 (2005).

[102] M. Hayashi, L. Thomas, Y. B. Bazaliy, C. Rettner, R. Moriya, X. Jiang, and S. S. P. Parkin, Phys. Rev. Lett. **96**, 197207 (2006).

[103] G. Meier, M. Bolte, R. Eiselt, B. Krüger, D.-H. Kim, and P. Fischer, Phys. Rev. Lett. **98**, 187202 (2007).

[104] L. Heyne, M. Kläui, D. Backes, T. A. Moore, S. Krzyk, U. Rüdiger, L. J. Heyderman, A. F. Rodríguez, F. Nolting, T. O. Mentes, et al., Phys. Rev. Lett. **100**, 066603 (2008).

[105] L. Thomas, M. Hayashi, X. Jiang, R. Moriya, C. Rettner, and S. S. P. Parkin, Nature **443**, 197 (2006).

[106] S. Lepadatu, M. C. Hickney, A. Potenza, H. Marchetto, T. R. Charlton, S. Langridge, S. S. Dhesi, and C. H. Marrows, Phys. Rev. B **79**, 094402 (2009).

[107] S. Lepadatu, A. Vanhaverbeke, D. Atkinson, R. Allenspach, and C. H. Marrows, Phys. Rev. Lett. **102**, 127203 (2009).

[108] M. Hayashi, L. Thomas, C. Rettner, R. Moriya, and S. S. P. Parkin, Appl. Phys. Lett. **92**, 162503 (2008).

[109] G. S. D. Beach, C. Knutson, C. Nistor, M. Tsoi, and J. L. Erskine, Physical Review Letters **97**, 057203 (2006).

[110] C. Burrowes, A. P. Mihai, D. Ravelosona, J.-V. Kim, C. Chappert, L. Vila, A. Marty, Y. Samson, F. Garcia-Sanchez, L. D. Buda-Prejbeanu, et al., Nature Physics **6**, 17 (2009).

[111] G. Tatara and H. Fukuyama, Phys. Rev. Lett. **78**, 3773 (1997).

[112] J. M. Ziman, Electrons and Phonons, Oxford Press (1960).

[113] P. Drude, Ann. Phys. (Leipzig) **3**, 369 (1900).

[114] D. K. Ferry and C. Jacoboni, Quantum transport in semiconductors, Plenum Press (1992).

[115] K. Fuchs, Proc. Cambridge Philos. Soc. **34**, 100 (1938).

[116] H. Sondheimer, Adv. Phys. **1**, 1 (1952).

[117] J. Jäckle, Einführung in die Transporttheorie, Vieweg (1978).

[118] S. Bohlens, B. Krüger, A. Drews, M. Bolte, G. Meier, and D. Pfannkuche, Applied Physics Letters **93**, 142508 (2008).

[119] O. A. Tretiakov, D. Clarke, G.-W. Chern, Y. B. Bazaliy, and O. Tchernyshyov, Phys. Rev. Lett. **100**, 127204 (2008).

[120] A. A. Thiele, J. Appl. Phys. **45**, 377 (1974).

[121] A. A. Thiele, Physical Review Letters **30**, 230 (1973).

[122] W. Döring, Z. Naturforsch. **3a**, 373 (1948).

[123] B. Krüger, A. Drews, M. Bolte, U. Merkt, D. Pfannkuche, and G. Meier, Phys. Rev. B **76**, 224426 (2007).

[124] K. Bussmann, G. A. Prinz, S.-F. Cheng, and D. Wang, Appl. Phys. Lett. **75**, 2476 (1999).

[125] B. Van Waeyenberge, A. Puzic, H. Stoll, K. W. Chou, T. Tylisczak, R. Hertel, M. Fähnle, H. Brückl, K. Rott, G. Reiss, et al., Nature **444**, 461 (2006).

[126] K. Yamada, S. Kasai, Y. Nakatani, K. Kobayashi, H. Kohno, A. Thiaville, and T. Ono, Nature Materials **6**, 270 (2007).

[127] R. Hertel, S. Gliga, M. Fähnle, and C. M. Schneider, Phys. Rev. Lett. **98**, 117201 (2007).

[128] V. P. Kravchuk, D. D. Sheka, Y. Gaididei, and F. G. Mertens, J. Appl. Phys. **102**, 043908 (2007).

[129] A. Wachowiak, J. Wiebe, M. Bode, O. Pietzsch, M. Morgenstern, and R. Wiesendanger, Science **298**, 577 (2002).

[130] O. Tretiakov and O. Tchernyshyov, Phys. Rev. B **75**, 012408 (2007).

[131] B. Krüger, A. Drews, M. Bolte, U. Merkt, D. Pfannkuche, and G. Meier, J. Appl. Phys. **103**, 07A501 (2008).

[132] M. Bolte, G. Meier, B. Krüger, A. Drews, R. Eiselt, L. Bocklage, S. Bohlens, T. Tyliszczak, A. Vansteenkiste, B. Van Waeyenberge, et al., Phys. Rev. Lett. **100**, 176601 (2008).

[133] J. Raabe, C. Quitmann, C. H. Back, F. Nolting, S. Johnson, and C. Buehler, Phys. Rev. Lett. **94**, 217204 (2005).

[134] K.-S. Lee and S.-K. Kim, Appl. Phys. Lett. **91**, 132511 (2007).

[135] S. Kasai, Y. Nakatani, K. Kobayashi, H. Kohno, and T. Ono, Phys. Rev. Lett. **97**, 107204 (2006).

[136] S.-B. Choe, Y. Acremann, A. Scholl, A. Bauer, A. Doran, J. Stöhr, and H. A. Padmore, Science **304**, 420 (2004).

[137] A. Drews, B. Krüger, M. Bolte, U. Merkt, and G. Meier, Phys. Rev. B **77**, 094413 (2008).

[138] S. K. Kim, Y. S. Choi, K. S. Lee, K. Y. Guslienko, and D. E. Jeong, Appl. Phys. Lett. **91**, 082506 (2007).

[139] K. Y. Guslienko, K.-S. Lee, and S.-K. Kim, Phys. Rev. Lett. **100**, 027203 (2008).

[140] K.-S. Lee, K. Y. Guslienko, J.-Y. Lee, and S.-K. Kim, Phys. Rev. B **76**, 174410 (2007).

[141] S.-K. Kim, K.-S. Lee, Y.-S. Yu, and Y.-S. Choi, Appl. Phys. Lett. **92**, 0022509 (2008).

[142] M. Curcic, B. V. Waeyenberge, A. Vansteenkiste, M. Weigand, V. Sackmann, H. Stoll, M. Fähnle, T. Tyliszczak, G. Woltersdorf, C. H. Back, et al., Physical Review Letters **101**, 197204 (2008).

[143] R. Moriya, L. Thomas, M. Hayashi, Y. B. Bazaliy, C. Rettner, and S. S. S. P. Parkin, Nature Materials **4**, 368 (2008).

[144] S. Kasai, K. Nakano, K. Kondou, N. Ohshima, K. Kobayashi, and T. Ono, Appl. Phys. Express **1**, 091302 (2008).

[145] P. Pavan, R. Bez, P. Olivo, and E. Zanoni, Proceedings of the IEEE **85**, 1248 (1997).

[146] The International Technology Roadmap for Semiconductors (2010).

[147] T. R. McGuire and R. I. Potter, IEEE Trans. Magn. **11**, 1018 (1975).

[148] R. I. Potter, Phys. Rev. B **10**, 4626 (1974).

[149] J. Smit, Physica **16**, 612 (1951).

[150] A. A. Kovalev, Y. Tserkovnyak, K. Výborný, and J. Sinova, Phys. Rev. B **79**, 195129 (2009).

[151] K. Výborný, A. A. Kovalev, J. Sinova, and T. Jungwirth, Phys. Rev. B **79**, 045427 (2009).

[152] T. Shinjo, T. Okuno, R. Hassdorf, K. Shigeto, and T. Ono, Science **289**, 930 (2000).

[153] J. Shibata, Y. Nakatani, G. Tatara, H. Kohno, and Y. Otani, Phys. Rev. B **73**, 020403(R) (2006).

[154] S.-K. Kim, K.-S. Lee, Y.-S. Yu, and Y.-S. Choi, Appl. Phys. Lett. **92**, 022509 (2008).

[155] Y. Tserkovnyak, A. Brataas, and G. E. W. Bauer, J. Magn. Magn. Mater. **320**, 1282 (2008).

[156] J.-i. Ohe and B. Kramer, Phys. Rev. Lett. **96**, 027204 (2006).

[157] William H. Press , Saul A. Teukolsky , William T. Vetterling , Brian P. Flannery, Numerical recipes in C (2nd ed.): the art of scientific computing, Cambridge University Press, New York, (1992).

[158] A. Newell, W. Williams, and D. Dunlop, J. Geo. Res. **98**, 9551 (1993).

[159] A. Abanov and V. L. Pokrovsky, Phys. Rev. B **58**, R8889 (1998).

[160] J. Nibarger, R. Lopusnik, and T. Silva, Appl. Phys. Lett. **82**, 2112 (2003).

[161] M. Schneider, T. Gerrits, A. Kos, and T. Silva, Appl. Phys. Lett. **87**, 072509 (2005).

[162] Z. Liu, F. Giesen, X. Zhu, R. D. Sydora, and M. R. Freeman, Phys. Rev. Lett. **98**, 087201 (2007).

[163] M. Hayashi, L. Thomas, Y. B. Bazaliy, C. Rettner, R. Moriya, X. Jiang, and S. S. P. Parkin, Phys. Rev. Lett. **96**, 197207 (2006).

[164] K. Y. Guslienko, Appl. Phys. Lett. **89**, 022510 (2006).

[165] B. Krüger, M. Najafi, S. Bohlens, R. Frömter, D. P. F. Möller, and D. Pfannkuche, Phys. Rev. Lett. **104**, 077201 (2010).

[166] B. Krüger, A. Drews, M. Bolte, U. Merkt, D. Pfannkuche, and G. Meier, J. Appl. Phys. **103**, 07A501 (2008).

[167] K. Y. Guslienko, B. A. Ivanov, V. Novosad, Y. Otani, H. Shima, and K. Fukamichi, J. Appl. Phys. **91**, 8037 (2002).

[168] S. Bohlens and D. Pfannkuche, Phys. Rev. Lett. **105**, 177201 (2010).

[169] I. A. Campbell and A. Fert, in *Ferromagnetic Materials*, edited by E. P. Wohlfahrt (North-Holland, Amsterdam, 1982).

[170] A. Kamenev, Many-body theory of non-equilibrium systems, in Nanophysics: Coherence and transport, edited by H. Bouchiat, Y. Gefen, S. Guéron, G. Montambaux, and J. Dalibard; pp 177-246, (Elsevier, Amsterdam, 2005).

[171] Y. Lyanda-Geller, I. L. Aleiner, and P. M. Goldbart, Phys. Rev. Lett. **81**, 3215 (1998).

[172] X. Waintal and M. Viret, Europhys. Lett. **65**, 427 (2004).

[173] M. D. Stiles and A. Zangwill, Phys. Rev. B **66**, 014407 (2002).

[174] A. Brataas, G. E. W. Bauer, and P. J. Kelly, Physics Reports **427**, 157 (2006).

[175] M. D. Stiles and A. Zangwill, J. Appl. Phys. **91**, 6812 (2002).

[176] C. Cohen-Tannoudji, B. Diu, and Franck Laloë, Quantum mechanics, de Gruyter (2002).

[177] A. Brataas, Y. V. Nazarov, and G. E. W. Bauer, Phys. Rev. Lett. **84**, 2481 (2000).

[178] N. F. Mott, Proc. Roy. Soc. London, Ser. A **153**, 699 (1936).

[179] N. F. Mott, Proc. Roy. Soc. London, Ser. A **156**, 368 (1936).

[180] A. Fert and I. A. Campbell, Phys. Rev. Lett. **21**, 1190 (1968).

[181] P. C. van Son, H. van Kempen, and P. Wyder, Phys. Rev. Lett. **58**, 2271 (1987).

[182] T. Valet and A. Fert, Phys. Rev. B **48**, 7099 (1993).

[183] R. P. van Gorkom, A. Brataas, and G. E. W. Bauer, Phys. Rev. Lett. **83**, 4401 (1999).

[184] M. B. Stearns, J. Magn. Magn. Mater. **5**, 167 (1977).

[185] E. Šimánek, Phys. Rev. B **63**, 224412 (2001).

[186] F. Piéchon and A. Thiaville, Phys. Rev. B **75**, 174414 (2007).

[187] D. Papaconstantopoulos, *Handbook of the Band Structure of Elemental Solids* (Plenum, New York, 1986).

[188] A. Matthiessen, Rep. Brit. Ass. **32**, 144 (1862).

[189] B. A. Gurney, V. S. Speriosu, J.-P. Nozieres, H. Lefakis, D. R. Wilhoit, and O. U. Need, Phys. Rev. Lett. **71**, 4023 (1993).

[190] S. Lepadatu, J. S. Claydon, C. J. Kinane, T. R. Charlton, S. Langridge, A. Potenza, S. S. Dhesi, P. S. Keatley, R. J. Hicken, B. J. Hickey, et al., Phys. Rev. B **81**, 020413 (2010).

[191] G. Tatara, T. Takayama, H. Kohno, J. Shibata, Y. Nakatani, and H. Fukuyama, J. Phys. Soc. Jap. **75**, 064708 (2006).

[192] M. Hayashi, L. Thomas, C. Rettner, R. Moriya, Y. B. Bazaliy, and S. S. S. P. Parkin, Phys. Rev. Lett. **98**, 037204 (2007).

[193] G. G. Cabrera and L. M. Falicov, Phys. Status Solidi B **61**, 539 (1974).

[194] G. G. Cabrera and L. M. Falicov, Phys. Status Solidi B **62**, 217 (1974).

[195] J. B. A. N. van Hoof, K. M. Schep, A. Brataas, G. E. W. Bauer, and P. J. Kelly, Phys. Rev. B **59**, 138 (1999).

[196] A. Brataas, G. Tatara, and G. E. W. Bauer, Phys. Rev. B **60**, 3406 (1999).

[197] E. Šimánek and A. Rebei, Phys. Rev. B **71**, 172405 (2005).

[198] F. S. Bergeret, A. F. Volkov, and K. B. Efetov, Phys. Rev. B **66**, 184403 (2002).

[199] V. K. Dugaev, J. Barnaś, A. Łusakowski, and L. A. Turski, Phys. Rev. B **65**, 224419 (2002).

[200] C. Wickles and W. Belzig, Phys. Rev. B **80**, 104435 (2009).

[201] J. F. Gregg, W. Allen, K. Ounadjela, M. Viret, M. Hehn, S. M. Thompson, and J. M. D. Coey, Phys. Rev. Lett. **77**, 1580 (1996).

[202] M. Viret, D. Vignoles, D. Cole, J. M. D. Coey, W. Allen, D. S. Daniel, and J. Gregg, Phys. Rev. B **53**, 8464 (1996).

[203] U. Rüdiger, J. Yu, L. Thomas, S. S. P. Parkin, and A. D. Kent, Phys. Rev. B **59**, 11914 (1999).

[204] K. M. Hong and N. Giordano, J. Phys. Condens. Matter **10**, L401 (1998).

[205] Y. Otani, S. G. Kim, K. Fukamichi, O. Kitakami, and Y. Shimada, IEEE Trans. Magn. **34**, 1096 (1998).

[206] A. D. Kent, U. Rüdiger, J. Yu, S. Zhang, P. Levy, Y. Zhong, and S. S. P. Parkin, IEEE Trans. Magn. **34**, 900 (1998).

[207] U. Rüdiger, J. Yu, S. Zhang, A. D. Kent, and S. S. P. Parkin, Phys. Rev. Lett. **80**, 5639 (1998).

[208] A. D. Kent, U. Rüdiger, J. Yu, L. Thomas, and S. S. P. Parkin, J. Appl. Phys. **85**, 5243 (1999).

[209] R. P. van Gorkom, J. Caro, S. J. C. H. Theeuwen, K. P. Wellock, N. N. Gribov, and S. Radelaar, Appl. Phys. Lett. **74**, 422 (1999).

[210] T. Taniyama, I. Nakatani, T. Namikawa, and Y. Yamazaki, Phys. Rev. Lett. **82**, 2780 (1999).

[211] R. Danneau, P. Warin, J. P. Attané, I. Petej, C. Beigné, C. Fermon, O. Klein, A. Marty, F. Ott, Y. Samson, et al., Phys. Rev. Lett. **88**, 157201 (2002).

[212] U. Ebels, A. Radulescu, Y. Henry, L. Piraux, and K. Ounadjela, Phys. Rev. Lett. **84**, 983 (2000).

[213] S. Lepadatu and Y. B. Xu, Phys. Rev. Lett. **92**, 127201 (2004).

[214] C. H. Marrows and B. C. Dalton, Phys. Rev. Lett. **92**, 097206 (2004).

[215] L. Klein, Y. Kats, A. F. Marshall, J. W. Reiner, T. H. Geballe, M. R. Beasley, and A. Kapitulnik, Phys. Rev. Lett. **84**, 6090 (2000).

[216] M. Viret, Y. Samson, P. Warin, A. Marty, F. Ott, E. Søndergård, O. Klein, and C. Fermon, Phys. Rev. Lett. **85**, 3962 (2000).

[217] T. Ono, H. Miyajima, K. Shigeto, K. Mibu, N. Hosoito, and T. Shinjo, Science **284**, 468 (1999).

[218] N. Kazantseva, R. Wieser, and U. Nowak, Phys. Rev. Lett. **94**, 037206 (2005).

[219] M. Franchin, T. Fischbacher, G. Bordignon, P. de Groot, and H. Fangohr, Phys. Rev. B **78**, 054447 (2008).

[220] P. Bruno, Phys. Rev. Lett. **83**, 2425 (1999).

[221] J. Kötzler, M. H. D. A. Garanin, and L. Jahn, Phys. Rev. Lett. **71**, 177 (1993).

[222] D. Ravelosona, D. Lacour, J. A. Katine, B. D. Terris, and C. Chappert, Phys. Rev. Lett. **95**, 117203 (2005).

[223] M. Feigenson, J. W. Reiner, and L. Klein, Phys. Rev. Lett. **98**, 247204 (2007).

[224] H. F. Fuke, S. Hashimoto, M. Takagishi, H. Iwasaki, S. Kawasaki, K. Miyake, and M. Sahashi, IEEE Trans. Magn. **43**, 2848 (2007).

[225] N. García, M. Muñoz, and Y.-W. Zhao, Phys. Rev. Lett. **82**, 2923 (1999).

[226] H. Imamura, N. Kobayashi, S. Takahashi, and S. Maekawa, Phys. Rev. Lett. **84**, 1003 (2000).

[227] G. R. Taylor, A. Isin, and R. V. Coleman, Phys. Rev. **165**, 621 (1968).

[228] P. A. E. Jonkers, S. J. Pickering, H. De Raedt, and G. Tatara, Phys. Rev. B **60**, 15970 (1999).

[229] P. Freitas and L. Berger, J. Appl. Phys. **57**, 1266 (1985).

[230] C. Y. Hung and L. Berger, J. Appl. Phys. **63**, 4276 (1988).

[231] E. B. Myers, D. C. Ralph, J. A. Katine, R. N. Louie, and R. A. Buhrman, Science **285**, 867 (1999).

[232] T. Taniguchi, J. Sato, and H. Imamura, Phys. Rev. B **79**, 212410 (2009).

[233] M. Thorwart and R. Egger, Phys. Rev. B **76**, 214418 (2007).

[234] F. C. Schwerer and J. Silcox, Phys. Rev. Lett. **20**, 101 (1996).

[235] E. H. Sondheimer, Advances in Physics **50**, 499 (2001).

[236] A. Stern, Phys. Rev. Lett. **68**, 1022 (1992).

[237] V. A. Gopar, D. Weinmann, R. A. Jalabert, and R. L. Stamps, Phys. Rev. B **69**, 014426 (2004).

[238] V. S. Rychkov, S. Borlenghi, H. Jaffres, A. Fert, and X. Waintal, Phys. Rev. Lett. **103**, 066602 (2009).

[239] M. Kläui, P.-O. Jubert, R. Allenspach, A. Bischof, J. A. C. Bland, G. Faini, U. Rüdiger, C. A. F. Vaz, L. Vila, and C. Vouille, Phys. Rev. Lett. **95**, 026601 (2005).

[240] J. Fabian and S. D. Sarma, J. Appl. Phys. **85**, 5075 (1999).

[241] I. Mertig, R. Zeller, and P. H. Dederichs, Phys. Rev. B **49**, 11767 (1994).

[242] P. Zahn, I. Mertig, M. Richter, and H. Eschrig, Phys. Rev. Lett. **75**, 2996 (1995).

[243] E. Saitoh, H. Miyajima, T. Yamaoka, and G. Tatara, Nature **432**, 203 (2004).

[244] I. M. Miron, P.-J. Zermatten, G. Gaudin, S. Auffret, B. Rodmacq, and A. Schuhl, Phys. Rev. Lett. **102**, 137202 (2009).

[245] S. Datta and B. Das, Applied Physics Letters **56**, 665 (1990).

[246] M. Bode, S. Heinze, A. Kubetzka, O. Pietzsch, X. Nie, G. Bihlmayer, S. Blügel, and R. Wiesendanger, Phys. Rev. Lett. **89**, 237205 (2002).

[247] R. A. Duine, Phys. Rev. B **79**, 014407 (2009).

[248] J. Shibata, G. Tatara, and H. Kohno, Phys. Rev. Lett. **94**, 076601 (2005).

[249] S. E. Barnes and S. Maekawa, Phys. Rev. Lett. **98**, 246601 (2007).

[250] S. A. Yang, G. S. D. Beach, C. Knutson, D. Xiao, Q. Niu, M. Tsoi, and J. L. Erskine, Phys. Rev. Lett. **102**, 067201 (2009).

[251] Y. Tserkovnyak and M. Mecklenburg, Phys. Rev. B **77**, 134407 (2008).

[252] R. A. Duine, Phys. Rev. B **77**, 014409 (2008).

[253] Y. Tserkovnyak and C. H. Wong, Phys. Rev. B **79**, 014402 (2009).

[254] K. Uchida1, S. Takahashi, K. Harii1, J. Ieda, W. Koshibae, K. Ando1, S. Maekawa, and E. Saitoh, Nature **455**, 778 (2008).

[255] A. A. Kovalev and Y. Tserkovnyak, Phys. Rev. B **80**, 100408 (2009).

[256] M. Yamanouchi, D. Chiba, F. Matsukura, T. Dietl, and H. Ohno, Phys. Rev. Lett. **96**, 096601 (2006).

[257] D. Chiba, M. Yamanouchi, F. Matsukura, T. Dietl, and H. Ohno, Phys. Rev. Lett. **96**, 096602 (2006).

[258] A. K. Nguyen, H. J. Skadsem, and A. Brataas, Phys. Rev. Lett. **98**, 146602 (2007).

[259] K. Obata and G. Tatara, Phys. Rev. B **77**, 214429 (2008).

[260] A. Machon and S. Zhang, Phys. Rev. B **79**, 094422 (2009).

[261] J. M. Luttinger, Phys. Rev. **102**, 1030 (1956).

[262] J. J. Sakurai, Modern Quantum Mechanics (revised edition), Addison Wesley (1993).

[263] E. H. Hall, Philos. Mag. **10**, 301 (1880).

[264] E. H. Hall, Philos. Mag. **12**, 157 (1881).

[265] R. Karplus and J. M. Luttinger, Phys. Rev. **95**, 1154 (1954).

[266] J. Smit, Physica **21**, 877 (1955).

[267] N. A. Sinitsyn, J. Phys.: Cond. Mat. **20**, 023201 (2008).

[268] M.-C. Chang and Q. Niu, Phys. Rev. Lett. **75**, 1348 (1995).

[269] M. V. Berry, Proc. R. Soc. Lond. A **392**, 45 (1984).

[270] E. N. Adams and E. I. Blount, J. Phys. Chem. Solids **10**, 286 (1957).

[271] G. Sundaram and Q. Niu, Phys. Rev. B **59**, 14915 (1999).

[272] J. M. Luttinger, Phys. Rev. **112**, 739 (1958).

[273] J. Smit, Physica **24**, 29 (1958).

[274] S. K. Lyo and T. Holstein, Phys. Rev. Lett. **29**, 423 (1972).

[275] L. Berger, Phys. Rev. B **2**, 4559 (1970).

[276] S. Murakami, N. Nagaosa, and S.-C. Zhang, Science **301**, 1348 (2003).

[277] Y. Yao, L. Kleinman, A. H. MacDonald, J. Sinova, T. Jungwirth, D. s. Wang, E. Wang, and Q. Niu, Phys. Rev. Lett. **92**, 37204 (2004).

[278] M.-C. Chang and Q. Niu, Phys. Rev. B **53**, 7010 (1996).

[279] P. Gosselin, F. Ménas, A. Bérard, and H. Mohrbach, Europhys. Lett. **76**, 651 (2006).

[280] D. Culcer, J. Sinova, N. A. Sinitsyn, T. Jungwirth, A. H. MacDonald, and Q. Niu, Phys. Rev. Lett. **93**, 046602 (2004).